Intracellular replication and persistence strategies of the Q Fever pathogen Coxiella burnetii

Mélanie Burette

THÈSE POUR OBTENIR LE GRADE DE DOCTEUR DE L'UNIVERSITÉ DE MONTPELLIER

En Biologie cellulaire

École doctorale Sciences Chimiques et Biologiques pour la Santé (CBS2)

Unité de recherche CNRS UMR 9004 - Université de Montpellier

Institut de Recherche en Infectiologie de Montpellier (IRIM)

Intracellular replication and persistence strategies of the Q fever pathogen *Coxiella burnetii*

Présentée par Mélanie BURETTE

Le 07 Décembre 2020

Sous la direction du Dr Matteo BONAZZI, directeur de thèse

Devant le jury composé de

Dr Agathe SUBTIL, Directrice de Recherche, Institut Pasteur de Paris	Présidente du jury
Dr Suzana SALCEDO, Chargée de Recherche, CNRS, IBCP Lyon	Rapportrice
Pr Serge MOSTOWY, Professeur, London School of Hygiene and Tropical Medicine	Rapporteur
Pr Jean-Louis MEGE, Professeur des Universités - Practicien Hospitalier, Aix-Marseille Université	Examinateur
Dr Anne KERIEL, Chargée de Recherche, INSERM, Université de Montpellier	Examinatrice
Dr Matteo BONAZZI, Directeur de Recherche, CNRS, Université de Montpellier	Directeur de thèse

UNIVERSITÉ DE MONTPELLIER

Acknowledgements

Après presque 4 ans passés à l'IRIM dont 3 années de thèse, il est temps pour moi de quitter la famille IRIMienne ! Je voudrais remercier ici toutes les personnes qui ont fait que ces années resteront inoubliables.

Tout d'abord, je tiens à remercier Matteo, mon directeur de thèse. Merci de m'avoir pris en stage alors que je ne connaissais rien de la paillasse (mais je pense m'être bien rattrapé depuis…). Merci de m'avoir accordé ta confiance et la possibilité de faire une thèse dans ton équipe ! Tu m'as aidé à développer mon esprit scientifique et à prendre confiance en moi pendant toutes ces années où mes journées comptaient 48 heures. Ton excellence scientifique, ta passion et ton dynamisme font que tu auras été un véritable moteur pour moi dans ces années de thèse, surtout quand les choses ont pu être un peu « tout floues » parfois. Je continue de penser que l'important dans une thèse, c'est aussi son chef, alors merci SuperChef pour ton soutien, ta disponibilité, ta bonne humeur mais aussi pour ces discussions scientifiques ou non que nous avons partagé autour d'un café (surtout quand j'arrivais avant toi le matin…). WW te laisse quelques datas (beaucoup peut-être ?), mais si besoin, tu sais que je ne serai jamais trop loin pour l'équipe.

Je remercie ensuite tous les membres de l'équipe avec qui j'ai partagé mes années de thèse, en particulier mon colocataire de bureau Jorge (aussi appelé JAGG ou George de la Grace) avec qui les pauses cafés/goûter/chocolat étaient rythmées de confidences et de nouveaux mots français essentiels à ton vocabulaire. Merci à Eric, Stephan, Safia, Véronique Alessandra et son mari Franck. C'était un vrai plaisir de vous croiser tous les jours et de partager des moments de détente, faits de rire et d'échanges. Vous me manquerez. Une mention spéciale pour un futur grand docteur qui m'a dit un jour « La vérité tu t'es bien démerdée. T'as eu des hauts, des bas mais c'est pas grave, l'important c'est que tu restes au milieu » signé A. Bienvenu. Alors merci pour tout Arthurito, pour tous ces moments partagés, ton soutien sans faille pendant mes derniers mois de thèse et pour nos fous rires. Je te passe le flambeau pour que tu fasses encore mieux que moi et je sais que tu y arriveras. N'oublie pas, tant que je n'ai pas cherché, c'est pas perdu, heureusement je reste dans le coin amigo !

Un grand merci à toi, Ghizlane, ma grande rencontre de cette thèse ! Pour ton soutien, ta bienveillance et ta gentillesse. Je n'oublierai pas tout ce que j'ai eu la chance de partager avec toi, comme des heures de galère avec ces manips en THP-1, à espérer voir un histogramme bouger au FACS, mais aussi ces pauses café et ces moments de complicités. Tu es une merveilleuse personne, un vrai exemple de motivation et de courage alors ne change surtout pas. Tu mérites que tes projets se concrétisent et je te le souhaite sincèrement du fond du cœur. Je garde tes conseils en tête pour la suite, ne te fais pas de soucis, de toute façon, on continuera de se voir !

Merci aux membres passés et présents du groupe de la pause de 17h, Arthur (toujours là celui-là…), Matthéo, Lucien, Paul, Nathalie et Leslie, pour ne pas m'avoir laissé seule avec mon psychopathe réglé comme une horloge… mais surtout pour les fous rires et les bons moments passés au labo. Merci aussi à Emma, Rayane et Baptiste pour leur gentillesse et les fous rires partagés au détour d'un couloir !

Je tiens aussi à adresser un grand merci à l'équipe support et en particulier à Pascale pour ta disponibilité, tes conseils et ces conversations au détour de ton bureau. Sans toi, rien n'est possible dans notre quotidien à la paillasse alors merci pour tout, tu es vraiment une personne en or.

Mes remerciements aussi à mon professeur de bactériologie, Robert Zumbihl, qui m'a insufflé sa passion pour les bactéries et les interactions hôte-pathogène. Je n'aurai jamais fait de thèse sans vos conseils et vos encouragements à continuer, merci de m'avoir mis sur la route de Matteo Bonazzi, ce fut de magnifiques années !

I would like to thank Prof. Hubert Hilbi and Dr. Stephane Bodin for agreeing to be in my thesis committee. It is of great value to me that you have taken this time to evaluate my thesis.

I am deeply grateful to all members of the jury, Dr Suzana Salcedo, Professor Serge Mostowy, Dr Agathe Subtil, Dr Anne Keriel and Professor Jean-Louis Mege, for agreeing to read the manuscript and to participate in the defense of this thesis.

Les derniers mais non les moindres :

Merci à mes Desperate PhD students, Yasamine et Monia pour ces moments de folies passés ensemble. A ces brunchs, ces conversations de groupes, ces voice notes (avec l'accent du sud…) et ces délires (de karaoké et de chocolat…), tard le soir pour souffler

pendant la rédaction de cette thèse en plein confinement. Merci pour tout votre soutien et tout votre amour quand j'ai décidé de prendre un grand virage dans ma vie. Vous êtes ma plus belle rencontre de ces années de fac. On a commencé cette aventure en même temps, on l'a conclu en beauté ensemble, je vous aime mes Desperate PhD.

Merci à ma sœur, ma meilleure amie, Kim, pour ton soutien, ta bienveillance, nos fous rires et nos weekends de GP. Peut-être tu n'as pas conscience de l'importance que tu as pour moi, mais tu es l'une des seules personnes qui reste quand tout s'écroule dans ma vie et ce, depuis bientôt 16 ans. Toi la seule qui me connait par cœur et sur qui je peux compter à n'importe quelle heure du jour ou de la nuit. Toi la seule qui trouve toujours les mots pour me faire rire, me consoler ou me conseiller. Sans toi, je ne serai pas qui je suis aujourd'hui, tu fais partie de moi, tu es ma sœur, ma famille à jamais. Merci aussi à Jessy Gottin, ingénieur informaticien, de prendre soin de toi car je suis trop loin de toi. Maintenant prochaine étape, des mini-nous, j'ai hâte GP !

Sovint penso en tot el que he aconseguit durant aquests tres anys, i mai hagués imaginat que tu series tant important, Eric. Vaig venir per una tesi, i marxo amb l'amor de la meva vida... Això és per tu, que has compartit els meus moments d'alegria però també de frustració i dubte, tant a la feina com a casa. Això és per tu, pel teu gran recolzament, mai sabré com agrair-te tot el que m'aportes cada dia. Tot i que a vegades dubto de mi mateixa, estic molt segura d'una cosa : tu ets el meu exemple, el meu amor, la meva meitat, i no necessito escriure més perquè se que estas llegint els meus pensaments...

Gracias a mis suegros por ser tan bueno conmigo. ¡A los buenos años por venir juntos!

Enfin, je ne saurai exprimer en quelques lignes tout mon amour pour vous, mes chers parents, Alain et Laurence. Je dirai simplement que c'est sans aucun doute grâce à vous que j'en suis arrivée là. Vous avez fait de moi une vraie compétitrice, une perfectionniste qui veut être meilleure dans tout ce qu'elle fait. Vous m'avez soutenue et encouragée dans les bons comme les mauvais moments mais surtout vous m'avez entourée de votre amour tout au long de cette aventure qui parfois a pu vous dépasser. J'espère vous rendre fiers, en tout cas, je suis fière de vous avoir comme parents, merci d'être comme vous êtes, merci d'être là, je vous aime plus que tout au monde…

A mes grands-parents, Danièle, Gilberte et Michel B., j'espère que de là où vous êtes, vous êtes fières de moi… A la vôtre !

Table of Contents

List of Figures

List of Tables

Abbreviations

ACCM-2 : Acidified citrate cysteine medium-2
AIM2 : Absent in melanoma 2
Akt : RAC-alpha serine/threonine-protein kinase
ALIX : Programmed cell death 6-interacting protein
AMP : adenosine monophosphate
AP-2 : adaptor protein-2
AP1 : Activator protein 1
Arf : ADP ribosylation factor
ATP : Adenosine tri-phosphate
Bad : BCL2 associated agonist of cell death
BAR : Bin, Amphiphysin and Rvs
BAX : Bcl-2-associated X protein
Bcl-2 : B-cell lymphoma protein-2
BlaM : β-lactamase
BMDM : Bone marrow-derived macrophages
BMP : Bis(monoacylglycerol)phosphate
bp : base pair
BSA : Bovine serum albumin
BSL-2 : Biosafety level-2
BSL-3 : Biosafety level-3
$CaCl_2$: Calcium dichloride
cAMP : cyclic adenosine monophosphate
CBQY : Chinese *C. burnetii* Qiyi strain
CCL : Chemokine ligand
CCV : *Coxiella*-containing vacuoles
CFT : Complement fixation test
ChIP : Chromatin immunoprecipitation
CHO : Chinese hamster ovary
CHOP : C/EBPζ-C/EBP homologous protein
CLR : C-type lectin receptor
CME : Clathrin-mediated endocytosis
CO : carbon monoxide
COP : Coat protein complex
CR3 : Complement receptor 3
CryoET : Electron cryotomography
Cvp : *Coxiella* vacuole protein
CXCL : Chemokine (C-X-C motif) ligand
CyaA : adenylate cyclase
DAG : Diacylglycerol
DC : Dendritic cell
DHCR24 : 24-Dehydrocholesterol Reductase
DMEM : Dulbecco's Modified Eagle Medium
DNA : Desoxyribonucleic acid
dNTP : Nucleoside triphosphates containing deoxyribose
Dot : Defect in organelle trafficking

DPBS : Dulbecco's phosphate buffer saline
dpi : days post-infection
DTT : Dithiothreitol
EDTA : Ethylenediaminetetraacetic acid
EE : Early endosome
ELISA : Enzyme-Linked Immunosorbent Assay
ER : Endoplasmic reticulum
Erk : Extracellular signal-regulated kinase
ESCRT : Endosomal sorting complex required for transport
EUGENs : Eukaryotic-like GENes
FCHO2 : FCH and mu domain containing endocytic adaptor 2
FCS : Foetal calf serum
Gal-3 : Galectin-3
GAP : GTPase activation protein
GDP : Guanosine di-phosphate
GE : Genome equivalent
GEF : Guanine nucleotide exchange factor
GFP : Green fluorescent protein
GM-CSF : Granulocyte-macrophage colony-stimulating factor
GM130 : Golgi stack marker 130
GPL : Glycerophospholipid
GSDMD : Gasdermin-D
GTP : Guanosine tri-phosphate
GUV : Giant unilamellar vesicle
h : hour
hAM : Human alveolar macrophages
HBSS : Hank's balanced salt solution
HEL : Human embryonic lung
HIV-1 : Human immunodeficiency virus -1
Hsp70 : Heat shock protein 70
Icm : Intracellular multiplication
IFA : Indirect immunofluorescence assay
IFN : Interferon
IgG : Immunoglobulin G
IgM : Immunoglobulin M
IGS lnc RNA : Intergenic spacer long non-coding RNA
IκBα : Nuclear factor kappa-light polypeptide gene enhancer in B cells inhibitor alpha
IL : Interleukin
ILV : Intraluminal vesicle
IM : Inner membrane
IRF : IFN regulatory factor
JNK : c-JUN N-terminal kinase
kb : kilobases
LAMP : Lysosomal-associated membrane protein
LB : Luria-Bertani
LBPA : Lysobisphosphatidic acid
LC3B : microtubule associated protein 1 light chain 3 beta
LCV : Large cell variant
LE : Late endosome
LED : *Legionella* effector domain
LLOMe : L-leucyl-L-leucine methyl ester
LPS : Lipopolysaccharide

LTA : Lipoteichoic acid
LUV : Large unilamellar vesicle
Lys : Lysosome
MAPK : Mitogen-activated protein kinase
MDM2 : Mouse double minute 2 homolog
$MgCl_2$: Magnesium dichloride
MH-S : Murine alveolar
MLS : Mitochondrial localisation signals
MOI : Multiplicity of infection
MOM : Mitochondrial outer membrane
MOPS : (3-(*N*-morpholino)propanesulphfonic acid)
MVB : multivesicular body
MyD88 : Myeloid differentiation primary response 88
NaCl : Sodium chloride
NF-κB : Nuclear factor kappa-light-chain-enhance of activated B cells
NK : Natural killer
NLR : Nucleotide-binding oligomerisation domain (NOD)-like receptor
NLS : Nuclear localisation signals
NMI : *C. burnetiiC. burnetii* Nine Mile Phase I
NMII : *C. burnetiiC. burnetii* Nine Mile Phase II
NOD-1 : Nucleotide-binding oligomerisation domain-containing protein -1
NoDS : Nucleolar detention signal
OM : Outer membrane
OMCC : Outer-membrane associated core complex
OmpA : Outer membrane protein A
ORP1L : Oxysterol-binding protein (OSBP)-related protein 1 long
P4C : PtdIns4P binding of SidC
P4M : PtdIns4P binding of SidM
PA : Phosphatidic acid
PAMP : Pathogen-associated molecular pattern
PBMC : Peripheral blood mononuclear cell
PCD : Programmed cell death
PCR : Polymerase chain reaction
PEI : Polyethylenimine
PI : Phosphoinositide
$PI(3,4,5)P_3$: Phosphatidylinositol 3,4,5-trisphosphate
$PI(3,4)P_2$: Phosphatidylinositol 3,4-bisphosphate
$PI(3,5)P_2$: Phosphatidylinositol 3,5-bisphosphate
PI(3)P : Phosphatidylinositol 3-phosphate
$PI(4,5)P_2$: Phosphatidylinositol 4,5-bisphosphate
PI(4)P : Phosphatidylinositol 4-phosphate
PI(5)P : Phosphatidylinositol 5-phosphate
PKA : cAMP-dependent kinase
PM : Plasma membrane
PMA : Phorbol 12-Myristate 12-Acetate
PRR : Pattern recognition receptor
PtdCho : Phosphatidylcholine
PtdEtn : Phosphatidylethanolamine
PtdGlc : Phosphatidylglucoside
PtdGro : Phosphatidylglycerol
PtdIns : Phosphatidylinositol
PtdSer / PS : Phosphatidylserine

PVDF : Polyvinylidene difluoride
PX : Phox homology
RAB : Ras-related proteins in brain
RanGAP : Ran GTPase activating protein
RbCl : Rubidium chloride
RCC : Regulation of Chromosome Condensation repeat
RFP : Red fluorescent protein
RhoA : Ras homolog family member A
RIP : RNA immunoprecipitation
RLR : Retinoid acid-inducible gene I (RIG-I)-like receptor
RNA : Ribonucleic acid
RPMI : Roswell Park Memorial Institute
S4TE : Searching Algorithm for Type-IV secretion system Effectors
Sar1 : Secretion-associated Ras related GTPase 1
SCID : Severe Combined ImmunoDeficient
SCV : Small cell variant
SDS : Sodium dodecyl sulfatesulphate
SEAP : Secreted embryonic alkaline phosphatase
SiRNA : Small interfering RNA
SLM : Short Linear Motif
SNARE : Soluble N-ethylmaleimide-sensitive factor attachment protein receptor
SNX : Sorting nexin
SPP1 : Secreted phosphoprotein 1
STX17 : Syntaxin-17
T1SS : Type I Secretion System
T2SS : Type II Secretion System
T3SS : Type III Secretion System
T4ASS : Type IVA Secretion System
T4BSS : Type IVB Secretion System
T4CP : Type IV coupling protein subcomplex
T4SS : Type IV Secretion System
TEMED : Tetramethylethylenediamine
TGF-β : Transforming growth factor-beta
TGN : Trans-Golgi Network
TLR : Toll-like receptor
Tn : Transposon
TNF-α : Tumour necrosis factor alpha
TRIF : Toll interleukin receptor (TIR) domain-cintaining containing adaptor inducing IFN-β
VAMP : Vesicle-associated membrane protein
VHL : Von Hippel-Lindau tumour suppressor
VPS : Vacuolar protein sorting
VPS4 : Vacuolar sorting-associated protein 4
WT : wild-type

Preface

Bacteria are prokaryotic organisms that are ubiquitous on Earth by colonising almost every surface (Whitman *et al.*, 1998). Interactions between bacteria and host organisms can be beneficial or deleterious, with three types of symbiotic relationships that have been described: commensalism, mutualism and parasitism (Steinert *et al.*, 2000). Commensalism is beneficial to the bacteria and is neutral to the host, while mutualism provides benefits to both partners (Steinert *et al.*, 2000). On the contrary, in parasitism, bacteria called "pathogens" are deleterious to the host by damaging its integrity and growing at its expense (Steinert *et al.*, 2000). Despite representing 1% of known bacteria, pathogenic bacteria are responsible for severe diseases including tuberculosis, pneumonia and foodborne illnesses, killing over 17 million people each year (WHO, 2018)[1]. Co-evolution of bacterial pathogens with their hosts resulted in the emergence of strategies aiming at ensuring their replication and persistence. Among these, intracellular lifestyle allows escaping the harsh extracellular environment where sheer stress and circulating antibody can lead to bacterial clearance (Case and Samuel, 2016). Some intracellular pathogens escape the internalisation vacuole to replicate within the cytosol of the host cell, while others remain within vacuolar compartments and generate their replicative niche by manipulating host membrane trafficking (Martinez *et al.*, 2018). Pathogenic bacteria use virulence factors, often mimicking host cell determinants, to subvert cellular processes. On the other hand, host cells have developed counter-strategies to sense the presence of aberrant, bacterial-containing compartments (Martinez *et al.*, 2018). Thus, host-pathogen interaction define the complex dialogue between bacterial virulence factors and host response mechanisms. Understanding the intimate details of the functional and molecular basis of these interactions is essential to understand bacterial pathogenesis and to identify novel microbial or host targets for the development of new antimicrobials.

[1]World Health Organisation (2018, May 24) The top 10 causes of death. https://www.who.int/en/news-room/fact-sheets/detail/the-top-10-causes-of-death

Introduction

1. The etiological agent of Q Fever

1.1 Historic perspective

Dr Edward Holbrook Derrick first described Q fever in 1935, following an outbreak of undiagnosed febrile disease observed among slaughterhouse workers in Brisbane, Queensland, Australia (Derrick, 1937). Unable to identify the causative agent, this fever of unknown origin was named Q (for « Query ») fever. It is only a few years later that Macfarlane Burnet and Mavis Freeman isolated the bacterium from infectious material sent by Derrick (Burnet and Freeman, 1937; Maurin and Raoult, 1999). In the meantime, a new infectious agent related to *Rickettsia* species was isolated from ticks by Drs. Herald Cox and Gordon Davis in the Nine Mile Valley, Montana, United States (Davis *et al.*, 1938). The Nine Mile agent was also responsible for symptoms closely related to Q fever after an accidental laboratory infection (Davis *et al.*, 1938). The two isolates were compared, and cross-immunity studies finally confirmed that the two newly identified infectious agents were indeed the same pathogen. Given its rickettsial features, the etiological agent of Q fever was firstly designated as *Rickettsia burnetii* (Derrick, 1939). A few years later, in 1948, *Rickettsia burnetii* was finally classified into a separate genus based on distinct phenotypic characters from rickettsial species and was renamed *Coxiella burnetii*, in honour of Cox and Burnet (Philip, 1948). It was only after phylogenetic studies based on its 16S rRNA sequence that *C. burnetii* was reclassified in the phylum *Proteobacteria*, class γ-*Proteobacteria*, order *Legionellales*, family *Coxiellaceae* (Weisburg *et al.*, 1989).

Since the identification of *C. burnetii* in the 1930s, Q fever outbreaks of zoonotic origin have been observed worldwide, except for New Zealand (Hilbink *et al.*, 1993). In the United States, two outbreaks of Q fever occurred among meatpacking plant employees in 1946 in Amarillo and Chicago (Topping *et al.*, 1947; Shepard, 1947). Concurrently, several outbreaks occurred in southern Europe during World War II, among Allied soldiers who slept on contaminated hay near infected cattle and sheep (Bobbins *et al.*, 1946). In 1955, Q fever outbreaks were reported in South America and Africa (Vanderburg *et al.*, 2014). Q fever cases have continued to be reported in France, the United Kingdom, Spain, Switzerland, Greece, Italy and Germany in the 1980s-1990s (Maurin and Raoult, 1999). However, the most significant Q fever outbreak was recently reported in the Netherlands between 2007 and 2011 with more than 4000 human cases, following a high number of spontaneous abortions in farm animals (Roest *et al.*, 2011). This outbreak demonstrated that *C. burnetii* represents a significant threat to the public health and economy.

C. burnetii has been included in biological weapons programs during the Cold War (Madariaga *et al.*, 2003). Indeed, *C. burnetii* has several features that are suitable for its use as a biological weapon, including airborne transmission, high infectivity and remarkable resistance to environmental stresses (Madariaga *et al.*, 2003). These characteristics will be discussed later in this thesis. During the Cold War, experiments aiming at the development of biological weapons were carried out in the United States on pathogens including *C. burnetii* (Noah *et al.*, 2002). Human trials were conducted on volunteers among members of the Seventh Day Adventist Church by the US military for the Project Whitecoat in order to determine the vulnerability of humans to pathogens (Christopher *et al.*, 1997; Anderson *et al.*, 2005). At the same time, the Soviet Union's biological weapons program was established to achieve the same intent with the weaponisation and stockpiling of toxins or pathogens including the Q fever agent (Madariaga *et al.*, 2003). Due to all these concerns, *C. burnetii* has been ever since classified as a potential category B biothreat (Oyston and Davies, 2011).

1.2 Microbiology of *Coxiella burnetii*

1.2.1 Morphological characteristics

C. burnetii is a Gram-negative obligate intracellular pleiomorphic bacterium that mainly targets monocytes, macrophages and trophoblasts. However, several cell types can be infected by *C. burnetii in vitro*, such as fibroblasts, epithelial and endothelial cells as well as myeloid cells (Dragan and Voth, 2020). This small coccobacillus measures 0.2 to 0.4 μm wide and 0.4 to 1 μm long with a complex biphasic developmental cycle involving two distinct morphological forms: the small cell variant (SCV) and the large cell variant (LCV) (McCaul and Williams, 1981; Coleman *et al.*, 2004). The two forms can be differentiated by growth rate, gene expression and structure of the bacterial cell wall. The SCV is the small and non-replicating form, which is metabolically inactive and extremely resistant to environmental stresses. Indeed, SCVs can survive nutrient limitation, desiccation, osmotic pressure and high temperatures (McCaul *et al.*, 1981). SCVs are also the forms encountered in the environment. The LCV, on the contrary, is the larger and strictly intracellular form of *C. burnetii*. LCVs are replicative and metabolically active. The SCV-to-LCV morphological transition occurs within the host cell, when bacteria reside into membrane-bound compartments called *Coxiella*- containing vacuoles (CCV) (discussed in chapter *2. "The infectious cycle of Coxiella burnetii"*). LCVs replicate in exponential phase over 4 days to finally reach the stationary phase at 6 days post-infection (d.p.i), when *C. burnetii* LCVs convert back to SCVs (Coleman *et al.*, 2004) (**Figure 1**).

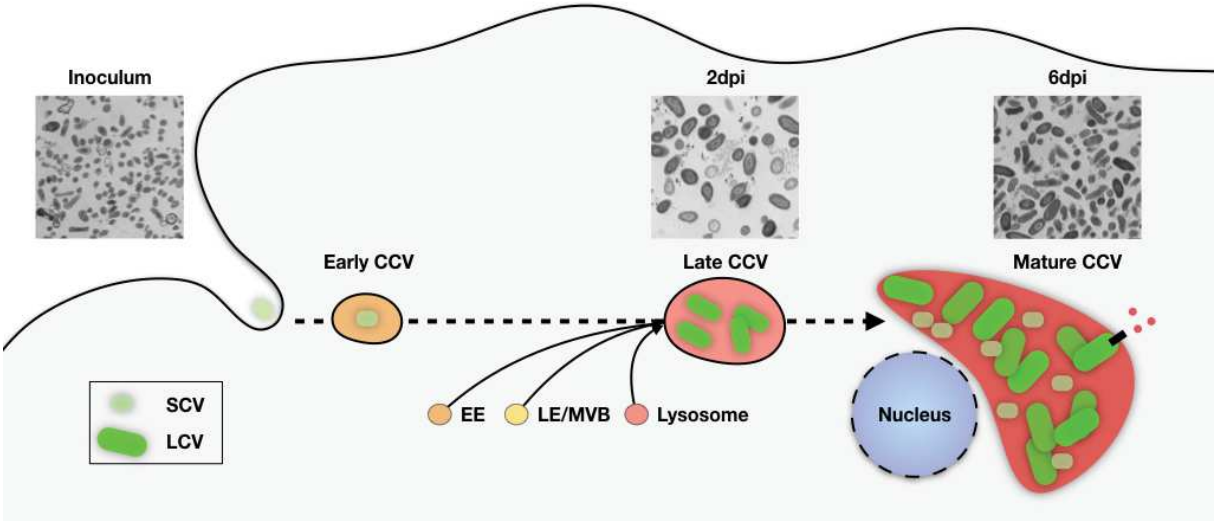

Figure 1. *C. burnetii* biphasic morphogenesis (adapted from Omsland *et al.*, 2009). *C. burnetii* enters cells in its non-replicative SCV form and resides in a membrane-bound compartment called *Coxiella*-containing vacuole (CCV). The transition between the non-replicative SCV and the replicative LCV form occurs during the first 2 d.p.i. (lag phase). Exponential bacterial replication occurs over the next 4 days. At 6 d.p.i., a mixed population of LCVs and SCVs are observed in mature CCVs (stationary phase).

1.2.2 Genomic features

Depending on *C. burnetii* isolates, the size of the chromosome varies between 1,989,565 and 2,214,254 base pairs (bp) (**Table 1**). Most *C. burnetii* isolates also possess a plasmid which varies in size between 37,000 and 55,000 bp. Comparative genome analysis allowed the classification of *C. burnetii* isolates into eight distinct genomic groups (from I to VIII) according to the genetic diversity of *C. burnetii* (Hendrix *et al.*, 1991; Hornstra *et al.*, 2011; Piñero *et al.*, 2015). It appears that isolates from a common genomic group are closely related to each other regarding genome content but also geographical location. Indeed, European isolates belong to Group I to IV, while North American isolates represent Group V and VI, and the other continents isolates are in Group IV (Hemsley *et al.*, 2019). Interestingly, genetic variability is also linked to clinical presentation. Indeed, isolates from genomic groups I, II and III were related to acute Q fever in humans, whereas genomic groups IV and V were associated with chronic Q fever (Maurin and Raoult, 1999). Some studies also suggest that clinical presentation is related to the sequence of the cryptic plasmid (Samuel *et al.*, 1985), whose genetic content might influence the acute or chronic outcome of the disease (Thiele and Willems, 1994). So far, 5 different plasmid types have been described in *C. burnetii* strains: QpH1, QpRS, QpDG, QpDV and an uncharacterised plasmid isolated from the

Chinese *C. burnetii* Qiyi (CBQY) strain (Ning *et al.*, 1992; Valková and Kazár, 1995; Lautenschläger *et al.*, 2000; Jäger *et al.*, 2002). A plasmidless *C. burnetii* strain was also identified; however, this strain contained a plasmidic DNA fragment integrated into its chromosome, suggesting the importance of plasmid sequences in *C. burnetii* (Willems *et al.*, 1997).

The diversity between *C. burnetii* isolates is not exclusively related to variations among plasmid types. Indeed, comparative genome analysis also showed that *C. burnetii* pathogenic potential depends on polymorphisms and variations among their lipopolysaccharide (LPS) composition (Hackstadt *et al.*, 1985; Hendrix *et al.*, 1991). At the genomic level, substantial rearrangements, including accumulation of pseudogenes and the presence of genetic insertions have been shown to influence strain-associated virulence (Beare *et al.*, 2009; Pearson *et al.*, 2013). Despite its isolation from ticks dates back in 1935, the first *C. burnetii* genome was sequenced only in 2003 from the Nine Mile isolate, which is thus considered as the reference strain (Seshadri *et al.*, 2003). Since then, seven new complete genomes have become available (Beare *et al.*, 2009; D'Amato *et al.*, 2014; D'Amato *et al.*, 2015; Millar *et al.*, 2017), allowing comparative virulence studies of *C. burnetii* strains (Long *et al.*, 2019). Interestingly, genome sequencing of the highly virulent Cb175 strain isolated in French Guiana revealed a substantial genome reduction compared to the Nine Mile Phase I reference strain (D'Amato *et al.*, 2015; Melenotte *et al.*, 2019) (**Table 1**). Conversely, the Dugway 5J108-111 strain isolated in the United States is considered avirulent, despite having the largest genome among all *C. burnetii* strains (Beare *et al.*, 2017), suggesting that there is no correlation between *C. burnetii* virulence and genome size.

Strain	Accession no.	Source	*In silico* MLVA	Genome (bp)	Plasmid type	References
NMRSA493[c]	NC_002971.3	Tick	NM	1,995,281	QpH1	Beare et al., 2009
Cb175[c]	HG825990.3	Human	NM	1,989,565	QpH1	D'Amato et al., 2015
Cb185[d]	NZ_CBTH000000000.1	–	NM	1,991,515	unknown	–
Z3055[c]	PRJEB1438	Sheep	*	1,995,463	QpH1	D'Amato et al., 2014
Cb109[d]	AKYP00000000	Human	CbNL01	2,030,000	QpH1	Rouli et al., 2012
EV-Cb_C13[d]	CCAM01000000	Ruminant	CbNL01	2,023,172	unknown	Sidi-Boumedine et al., 2014
NL-Limburg[d]	JZWL00000000	Human	CbNL01	2,214,254	QpH1	Hammerl et al., 2015
Cb_B1[d]	CCAH01000000	Ruminant	CbNL12	2,008,014	QpH1	Sidi-Boumedine et al., 2014
EV-Cb_BK10[d]	CCAL01000000	Ruminant	CbNL12	1,999,727	unknown	Sidi-Boumedine et al., 2014
Cb_B18[d]	CCAI01000000	Ruminant	CbNL12	2,008,445	unknown	Sidi-Boumedine et al., 2014
CbRSA331[c]	NC_010117.1	Human	CbRSA331	2,016,427	QpH1	–
Dugway[c]	NC_009727.1	Rodents	Dugway	2,158,758	QpDG	Beare et al., 2009
CbuG_Q212[c]	NC_011527.1	Human	CbuG_Q212	2,008,870	integrated	Beare et al., 2009
CbuK_Q154[c]	NC_011528.1	Human	CbuK_Q154	2,063,100	QpRS	Beare et al., 2009
Q321[d]	AAYJ01000000	Cattle	Q321	2,004,584	QpDV	Beare et al., 2006
Goat Q177[d]	NZ_AAUP00000000.2	Goat	Goat Q177	2,090,565	QpRS	–
Cb_O184[d]	CCAK01000000	Ruminant	Cb_O184	2,168,222	QpRS	Sidi-Boumedine et al., 2014
Namibia[d]	CP007555	Goat	Namibia	2,101,438	QpRS	Walter et al., 2014a
AuQ01[d]	JPVV00000000	Human	AuQ01	2,073,000	QpRS	Walter et al., 2014b

[c]*Complete genome sequence.*
[d]*Draft genome sequence.*
**In silico MLVA genotype more similar to NM genotype.*
–Information not available.

Table 1. List of sequenced *C. burnetii* strains genomes (adapted from Kuley *et al.*, 2017)

1.2.3 Phase variation

C. burnetii is characterised by a phase variation which is defined by the structure of the LPS, an important factor of *C. burnetii* virulence involved in the ability to cause acute or chronic disease (Hackstadt, 1990; Baca *et al.*, 1994). This variation is similar to the smooth-to-rough variation with virulent and avirulent forms observed in members of the family *Enterobacteriaceae* (Abnave *et al.*, 2017). Phase I bacteria display a full-length LPS and are related to the natural virulent forms observed in human and animal infections. Serial passages in embryonated eggs and cell cultures favour the transition to Phase II, which is characterised by a 26-kb (kilobases) deletion of a genomic region harbouring genes encoding enzymes involved in LPS biosynthesis. This event results in the biogenesis of a truncated LPS and loss-of virulence (Hackstadt *et al.*, 1985; Hoover *et al.*, 2002; Beare *et al.*, 2006; Beare *et al.*, 2018). As such, Phase I and Phase II LPS are morphologically indistinguishable, with the major difference lying in the sugar composition of the O-antigen. Phase I LPS contains L-virenose, dihydrohydroxystreptose and galactosamineuronyl-α-(1,6)-glucosamine, which are missing in Phase II LPS (**Figure 2**). Despite the lack of O-antigen in Phase II LPS, febrile responses have been observed in immunodeficient mice infected by *C. burnetii* Nine Mile phase II (or NMII) allowing to monitor clinical symptoms and evaluate infection (Ochoa-Repáraz *et al.*, 2007). Also, while all *C. burnetii* strains require manipulation in biosafety level-3 (BSL-3) confinement, the non-revertable, avirulent Phase II can be manipulated in biosafety level-2 (BSL-2) environments (Amano and Williams, 1984; Hackstadt, 1996). Importantly, loss-of-virulence of NMII has no impact on infection *in vitro* since both NMI and NMII strains efficiently replicate in cultured cells. Thus, the NMII strain represents a relevant model to study *C. burnetii* pathogenesis (Howe *et al.*, 2010).

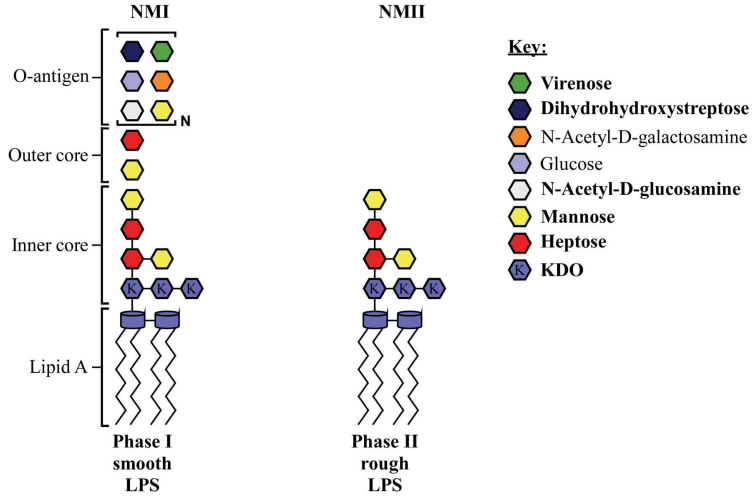

Figure 2. *C. burnetii* NMI and NMII LPS forms (adapted from Beare *et al.*, 2018).

1.2.4 Dot/Icm type 4B secretion system

1.2.4.1 Molecular structure and function of the Dot/Icm type 4B secretion system

Sequencing of the *C. burnetii* genome highlighted components of Type I, Type II and Type IV secretion systems (T1SS, T2SS and T4SS respectively) (Sexton and Vogel, 2002; Peabody *et al.*, 2003; Beare *et al.*, 2009). However, the role of T1SS and T2SS in *C. burnetii* pathogenesis remains unclear. It has been suggested that T1SS may play a role in bacterial internalisation by host cells as recently reported for *L. pneumophila* (Fuche *et al.*, 2015). To date, only the T4SS has been studied in the context of bacterial pathogenesis and infection.

T4SSs are bacterial multiprotein machineries embedded in the bacterial cell envelope and mediate the delivery of proteins and nucleic acids into host cells (Voth *et al.*, 2012; Guzmán-Herrador *et al.*, 2017). The T4SSs structure resembles a channel that allows the injection of material including DNA or bacterial proteins, directly in the host cell cytoplasm through the bacterial membrane. T4SSs are important virulence determinants with two main functions: the contribution in horizontal gene transfer involved in antibiotic resistance and the manipulation of eukaryotic host cells to establish a productive infection (Bleves *et al.*, 2020). T4SSs can be divided into two different types based on component number and structures: type IVA (T4ASS) and type IVB (T4BSS). Originally identified in the plant pathogen *Agrobacterium tumefaciens*, T4ASS are composed of a dozen of different proteins and are found in different bacterial pathogens such as *Brucella*, *Bartonella*, *Rickettsia* and *Anaplasma*. In contrast, T4BSS, also called Defect in organelle trafficking/Intracellular multiplication (Dot/Icm) system, is composed of 24-27 proteins and only found in *L. pneumophila* and *C. burnetii* (Voth *et al.*, 2012) (**Figure 3**).

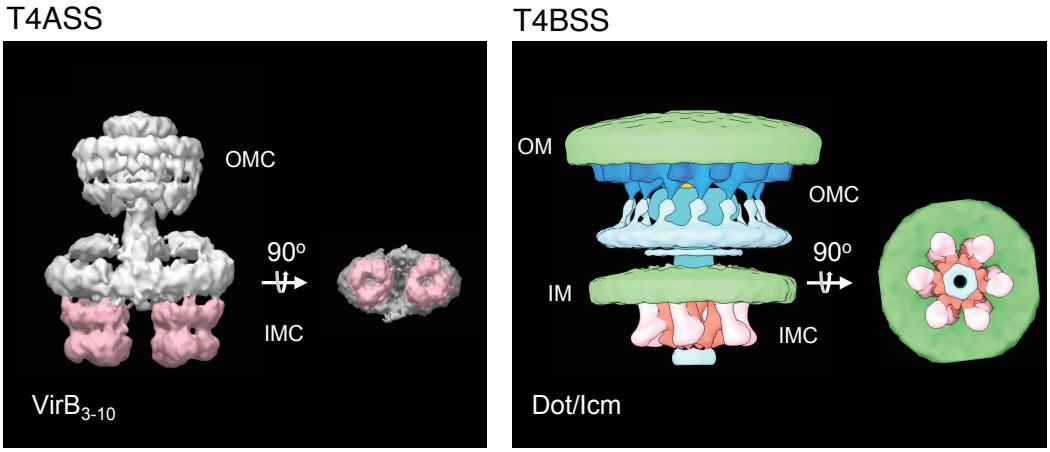

Figure 3. Structure of T4SSs (from Hu *et al.*, 2019). Side and bottom views of *E. coli* R388 VirB T4ASS reconstructed by single-particle negative-stain electron microscopy (left) and *L. pneumophila* Dot/Icm T4BSS obtained by in situ CryoET (electron cryotomography) (right).

The best characterised Dot/Icm Type 4B Secretion System is that of *L. pneumophila*, the causative agent of the severe pneumonia Legionnaires' disease. The *L. pneumophila* T4BSS is composed of 27 Dot and Icm proteins which can be divided in membrane and cytoplasmic components including an outer-membrane (OM) protein (DotH), OM lipoproteins (DotC, DotD, DotK), a periplasmic protein (IcmX), inner membrane (IM) proteins (DotA, DotE, DotF, DotG, DotI, DotJ, DotM, DotP, DotU, DotV, IcmF, IcmT, and IcmV), inner membrane (IM)-associated ATPases (DotB, DotL, DotO), and soluble cytosolic proteins (DotN, IcmQ, IcmR, IcmS, IcmW, and LvgA) (Nagai and Kubori, 2011; Chetrit *et al.*, 2018). These components can be grouped into several subcomplexes including the outer-membrane associated core complex (OMCC) consisting of five proteins (DotC, DotD, DotF, DotG, DotH) and the type IV coupling protein (T4CP) subcomplex consisting of six proteins (DotL, DotM, DotN, IcmS, IcmW, LvgA) (Vincent *et al.*, 2006; Kwak *et al.*, 2017) (**Figure 4**). The *C. burnetii* T4BSS is highly homologous to that of *L. pneumophila* and four *C. burnetii dot/icm* genes can complement corresponding *L. pneumophila* mutants (Zusman *et al.*, 2003; Zamboni *et al.*, 2003). This is not surprising given the fact that the two bacteria are phylogenetically close (Qiu and Luo, 2017). However, several differences exist between the two systems. *C. burnetii* T4BSS has 24 homologous components with the *L. pneumophila* T4BSS and lacks DotJ, DotV and IcmR. In addition to these differences, *C. burnetii* T4BSS is exclusively localised at one pole of the bacterial cell membrane while the *L. pneumophila* system is localised at both poles (Zusman *et al.*, 2003; Morgan *et al.*, 2010; Jeong *et al.*, 2017). Nevertheless, given the high degree of homology, it is assumed that *L. pneumophila* and *C. burnetii* T4BSS share the same structure and function.

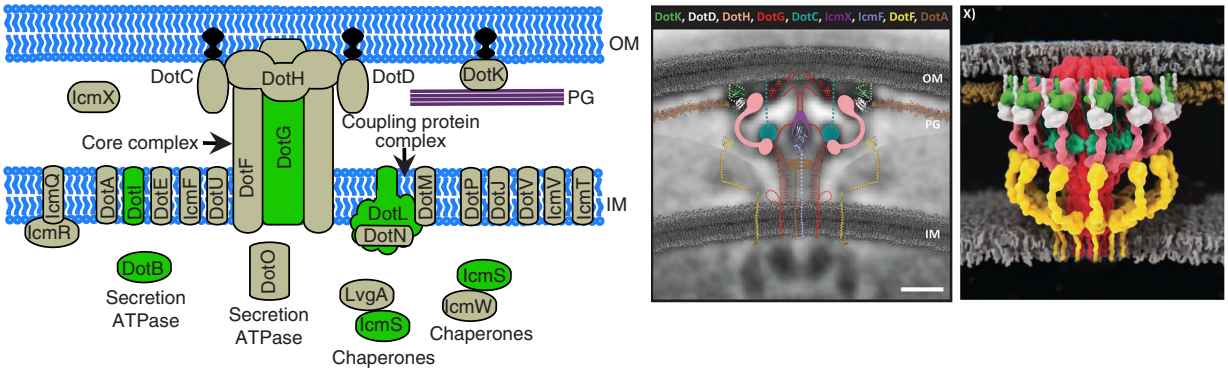

Figure 4. Type IVB secretion system of *L. pneumophila* (adapted from Chetrit *et al.*, 2018; Ghosal *et al.*, 2019). Schematic model of *L. pneumophila* T4BSS (left) and detailed representation of the periplasmic portion based on cryoelectron tomography (right) applicable to *C. burnetii.* The 3D model shows the secretion channel composed of DotG (red) surrounded by the secretion chamber consisting of DotH, DotD, DotK, and DotC (pink, green, white and cyan respectively) and wings composed of DotF (yellow).

The structure and the assembly of the *L. pneumophila* T4BSS have been recently characterised using cryoelectron tomography (Chetrit *et al.*, 2018; Ghosal *et al.*, 2019; Park *et al.*, 2020). The composition consists of an "outside-inside" assembly of five distinct structures from the outer membrane region to the inner membrane region (Park *et al.*, 2020). The OMCC and the IM protein structure assemble to span the bacterial cell envelope and the membrane of the replicative niche. The cytoplasmic ATPase DotO is recruited to the core complex and, once positioned, it recruits the second cytoplasmic ATPase DotB, essential for the translocation of Dot/Icm substrates into the host cell cytoplasm (Vogel *et al.*, 1998). The assembly of the DotO-DotB ATPases complex represents a crucial step in the T4BSS activation by inducing conformational changes that create a channel for direct bacterial secretion (Park *et al.*, 2020) (**Figure 5**). It has been demonstrated that the acidic pH and the degradative capacity of lysosomes are necessary for *C. burnetii* Dot/Icm secretion system function (Newton *et al.*, 2013; Newton *et al.*, 2020); however, the molecular mechanisms regulating these processes remain to be defined. Finally, a recent study also highlights the importance of the novel *C. burnetii* protein EirA (Essential for intracellular replication A) in Dot/Icm effector translocation. Mutation in *eirA* results in robust defect in *C. burnetii* replication, nevertheless EirA is not a T4BSS substrate and localises within the bacterial cytoplasm and inner membrane. The observation that the absence of EirA blocks Dot/Icm effector translocation suggests that EirA may functionally regulate the assembly of the T4BSS or its expression levels (Kuba *et al.*, 2020).

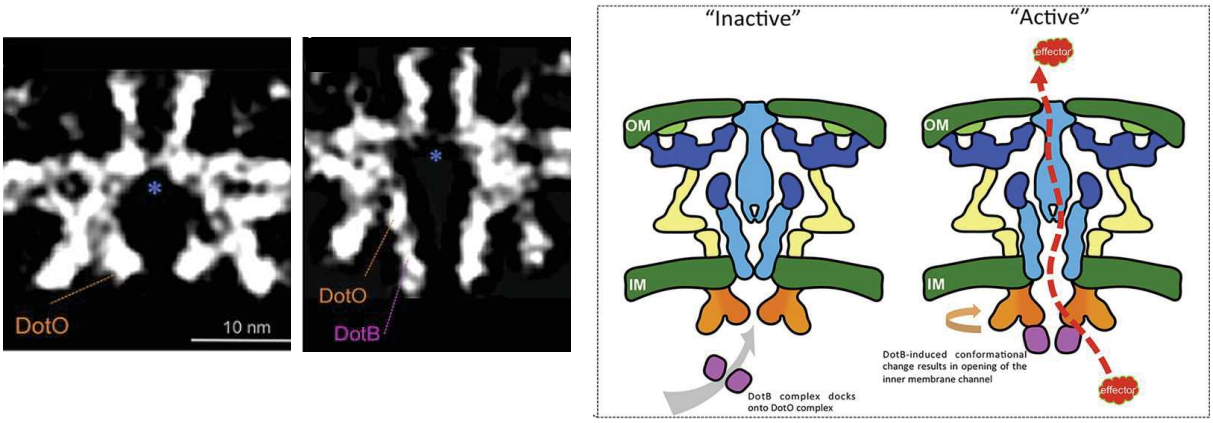

Figure 5. DotB-dependent conformational change activates the Dot/Icm secretion system (adapted from Park *et al.*, 2020). Proposed model of Dot/Icm secretion system activation with the DotB-free inactive structure and the DotB-bound active structure illustrated by central sections.

Components of the Dot/Icm secretion system play distinct and specific roles in the transport and translocation of bacterial effector proteins. Cytoplasmic chaperones including LvgA, IcmS and IcmW recruit effectors through the recognition of their C-terminal Dot/Icm translocation signal termed E-Block motif (detailed in part *1.2.4.2* "*Substrates of the Dot/Icm Type IVB Secretion System*"). Next, effector-bound chaperones interact with IM proteins and specifically with the T4CP subcomplex that links effectors to the bacterial IM. This allows the delivery of Dot/Icm substrates to the secretion chamber composed of DotG, DotF and DotH. This chamber allows the transport of effectors through the periplasmic space and across the outer membrane of bacteria. The Dot/Icm secretion system spans the membrane of the replicative niche allowing direct bacterial secretion into the host cell cytoplasm (Zamboni *et al.*, 2003). Interestingly, some Dot/Icm secretion system components also have a C-terminal translocation signal including IcmD, IcmX, DotA, DotC, DotD and DotH. However, only IcmX and DotA are secreted in a Dot/Icm-dependent manner during axenic growth of *C. burnetii* (Luedtke *et al.*, 2017). Interestingly, during infection of host cells, DotA localises to the CCV membrane and vesicles positive for CD63, a multivesicular bodies (MVBs) marker. The role of Dot/Icm secreted components remains unclear for the moment but it could be hypothesised that DotA and IcmX are involved in the transport of effectors across the CCV membrane (Luedtke *et al.*, 2017).

Finally, the importance of the Dot/Icm secretion system in *C. burnetii* pathogenesis has been demonstrated by analysing the phenotype of mutants in Dot/Icm genes. Indeed, deletion of *dotA* and *dotB* (Beare *et al.*, 2012) as well as transposon mutagenesis of *dotA*, *dotB*, *icmV*, *E*, *D*, *G*, *J*, *N*, *C*, *P*, *K*, *X* and *L1* prevent the development of the *C. burnetii* replicative niche and demonstrate that these genes are essential for bacterial replication (Carey *et al.*, 2011; Beare *et al.*, 2011; Martinez *et al.*, 2014).

1.2.4.2 Substrates of the Dot/Icm type 4B secretion system

The genetic intractability of *C. burnetii* and the high homology between the T4BSS of *L. pneumophila* and that of *C. burnetii* made *L. pneumophila* an ideal surrogate system to identify *C. burnetii* Dot/Icm effectors. The adenylate cyclase (CyaA) and β-lactamase (BlaM) reporter assays allowed the identification of more than 130 *C. burnetii* candidate effectors (Pan *et al.*, 2008; Chen *et al.*, 2010; Carey *et al.*, 2011; Weber *et al.*, 2013; Newton *et al.*, 2016), some of which have been recently validated in *C. burnetii* (Martinez *et al.*, 2016; Siadous *et al.*, 2020; Martinez *et al.*, 2020; Burette *et al.*, 2020). While the role of many *C. burnetii* effectors remains uncharacterised, some of these have been investigated. A

subclass of effectors localises to the CCV membrane and are thus called Cvps (for *Coxiella* vacuolar proteins) (Larson *et al.*, 2015). These are involved in CCV biogenesis and replication, through the manipulation of membrane trafficking mechanisms mediated by clathrin (Larson *et al.*, 2013; Latomanski *et al.*, 2016), RAB (Ras-related proteins in brain) GTPases ((Siadous *et al.*, 2020); **Appendix 1**) or host phosphoinositides (Martinez *et al.*, 2016). Other effectors manipulate host cell pathways including autophagy (Gutierrez *et al.*, 2005; Romano *et al.*, 2007; Newton *et al.*, 2014; Winchell *et al.*, 2018; Larson *et al.*, 2019; Siadous *et al.*, 2020), signal transduction (MacDonald *et al.*, 2012), gene transcription (Weber *et al.*, 2016), apoptosis (Lührmann and Roy, 2007; Vázquez and Colombo, 2010; Lührmann *et al.*, 2010; Klingenbeck *et al.*, 2013; Bisle *et al.*, 2016; Schäfer *et al.*, 2017) and innate immune response (Cunha *et al.*, 2015; Mahapatra *et al.*, 2016; Burette *et al.*, 2020) (**Figure 6**). Effectors involved in these processes will be further described in chapter *2. "The infectious cycle of Coxiella burnetii"*.

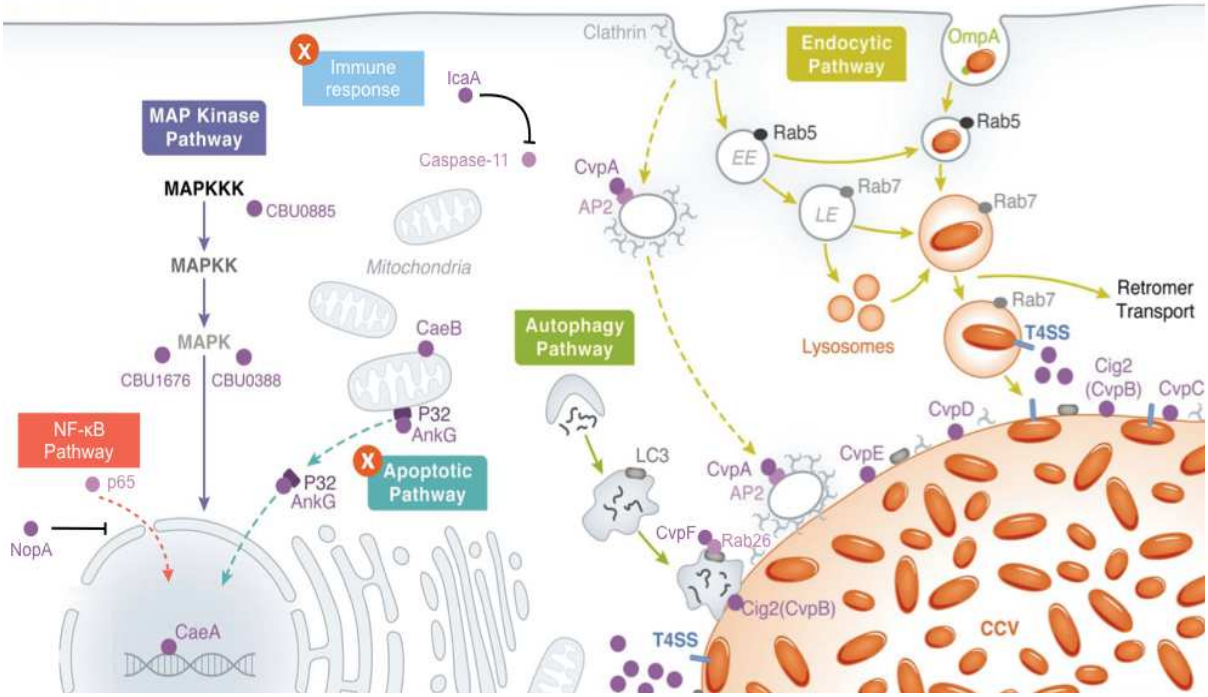

Figure 6. Manipulation of host signalling pathways by *C. burnetii* (adapted from Moffatt *et al.*, 2015). Following bacterial internalisation, the acidification of *Coxiella*-containing vesicles activates *C. burnetii* metabolism. This triggers the synthesis of the Dot/Icm secretion system and the secretion of effector proteins. Over 130 effectors are translocated through the Dot/Icm system into the host cytosol where they target specific eukaryotic processes leading to the remodelling of the CCV into a highly fusogenic vacuole that supports bacterial replication. It is known that the CCV fuses with clathrin-coated vesicles, autophagosomes and endolysosomal vesicles and effectors that may be involved in these processes are highlighted in purple. Furthermore, specific effectors manipulate signalling pathways by blocking the apoptotic processes at both mitochondrial and nuclear levels or the immune response by down-modulating the inflammasome signalling with IcaA (Inhibition of caspase activation A) or the NF-kB pathway with NopA.

Mutation of genes coding for effector proteins frequently led to bacterial replication defects or increased cytotoxicity, highlighting the non-redundant functions of these effectors during *C. burnetii* infectious cycle and pathogenesis (Weber *et al.*, 2013; Martinez *et al.*, 2014).

Bioinformatics approaches have been developed to facilitate the identification of bacterial effector proteins, based on a number of typical features. In the case of *C. burnetii* for example, it has been shown that the two-component system PmrA/B regulates the expression of Dot/Icm genes and a subset of effector-coding genes. The regulatory element recognised by PmrA is found in the predicted promoter region of these genes and consists of a tandem repeat sequence (cTTAATatT) located up to 100 bp upstream from the first ATG codon of genes (Zusman *et al.*, 2007; Chen *et al.*, 2010; Beare *et al.*, 2014). Recently, it has been shown that the *C. burnetii* PmrA/B transcriptional activity responds to breakdown products present in the CCV such as specific amino acids, leading to an up-regulated expression of genes required for the activity of the Dot/Icm secretion system (Newton *et al.*, 2020).

Amino acid sequence analysis of several effector proteins indicated that an enrichment in glutamic acid at their C-terminus was required for their efficient translocation by the Dot/Icm secretion system and defined a secretion signal called the E-block motif, consisting of 20 to 35 amino acid residues in the C-terminal of Dot/Icm substrates (Nagai *et al.*, 2005). This region exhibits a regular distribution of small, polar, charged and hydrophobic amino acids as well as glutamic acid residues (Nagai *et al.*, 2005; Huang *et al.*, 2011; Weber *et al.*, 2013; Lifshitz *et al.*, 2013).

Dot/Icm effectors can also be predicted based on the homology to known bacterial effectors or eukaryotic protein. Indeed, similar to other intracellular bacteria including *Legionella* and *Chlamydia*, *C. burnetii* encodes effector proteins containing domains or motifs that are typically found in eukaryotic proteins. These EUGENs (for EUkaryotic-like GENes) are likely acquired by horizontal gene transfer (De Felipe *et al.*, 2005) during co-evolution of bacteria with the host cells and are probably involved in pathogenic or symbiotic interactions, by mimicking eukaryotic host cell proteins (Duron *et al.*, 2015). Analysis of the *C. burnetii* genome revealed the presence of 56 potential EUGENs (Burette *et al.*, 2020), which can be classified depending on the eukaryotic-like domain they encode. EUGENs possess domains involved in protein-protein or protein-DNA interactions such as Ankyrin repeats domains (Pan *et al.*, 2008; Voth *et al.*, 2009), tetratricopeptide repeats (Bang *et al.*, 2016), short linear motifs (SLMs) (Larson *et al.*, 2013), Regulation of Chromosome Condensation repeats (RCC) (Burette *et al.*, 2020), Ser/Thr kinase domains ((Martinez *et al.*, 2020); **Appendix 2**), F-box motifs (Angot *et al.*, 2007) or acetyltransferases (Ma and Ma, 2016).

T4SS effectors may contain several of the above-mentioned features which, when combined, are strong predictors of T4SS effectors in a given bacterial genome. The bioinformatics tool S4TE (Searching Algorithm for Type-IV secretion system Effectors) has been recently developed to predict and classify putative T4BSS candidates in α- and γ-proteobacteria, by using a combination of 14 features. The S4TE algorithm analyses both nucleic and protein sequences by searching for promoter motifs, homologies to known T4SS effectors, eukaryotic-like features, the presence of localisation signals such as nuclear or mitochondrial localisation signals (NLS or MLS, respectively) and E-block motifs (Noroy *et al.*, 2019) (**Figure 7**). This powerful bioinformatics tool facilitates the identification of putative candidate effector proteins and was used in my PhD project for the identification of *C. burnetii* EUGENs and genes encoding lipid-binding effectors (discussed in chapter *III. "Results"*).

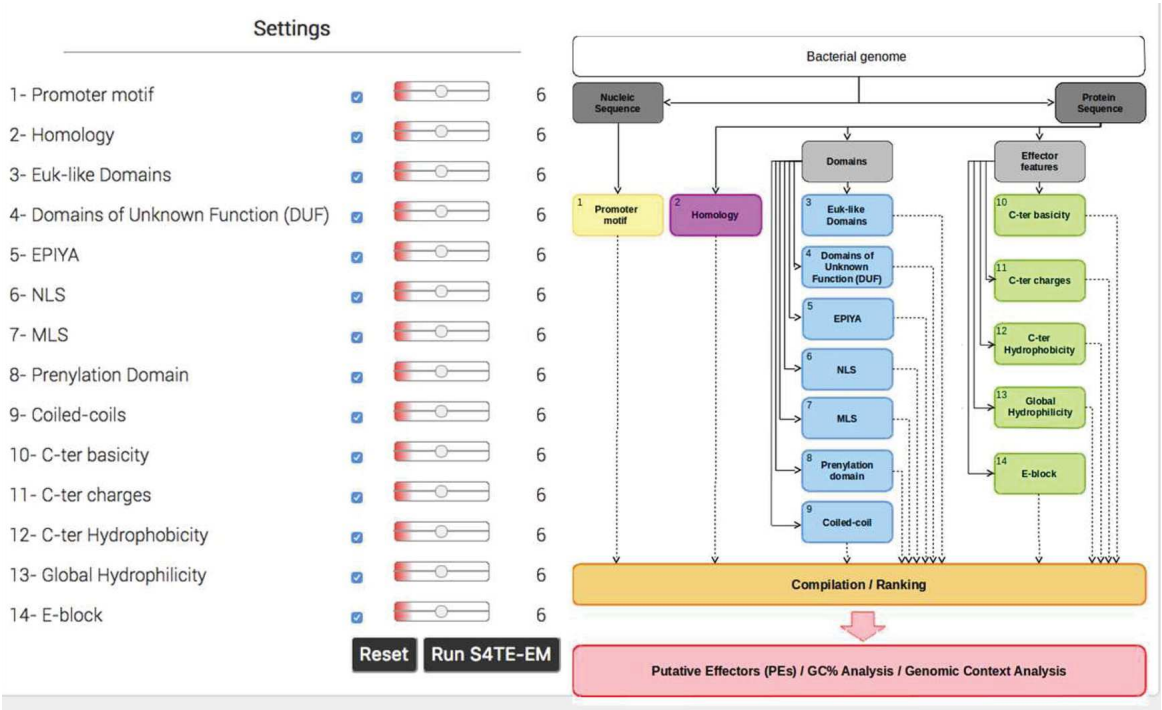

Figure 7. Prediction of T4SS effectors by the S4TE software (from Noroy *et al.*, 2019). This bioinformatics tool search for T4SS effector features in a given bacterial genome in order to identify and classify the putative T4SS effectors based on their combination of effector features to provide the best candidates for further characterisation. Euk-like: Eukaryotic-like, NLS: Nuclear Localisation Signal, MLS: Mitochondrial Localisation Signal, C-ter: C-terminal. https://sate.cirad.fr.

1.3 Q Fever

1.3.1 Infection

Human Q fever or animal coxiellosis is a worldwide zoonotic disease that affects humans and a broad range of animals. Among animals, the primary reservoirs for *C. burnetii* are domestic ruminants like cattle, sheep and goats (Eldin *et al.*, 2017). However, additional reservoirs exist in wild animals with reported isolation of *C. burnetii* from wild mammals (González-Barrio and Ruiz-Fons, 2019), reptiles (Stephen and Achyutha Rao, 1979) and birds (Babudieri and Moscovici, 1952) (**Figure 8**). *C. burnetii* is also detected in arthropods, and especially in several tick species (Glazunova *et al.*, 2005), however, their vector potential in disease transmission needs to be further investigated (Duron *et al.*, 2015b). In animals, *C. burnetii* infection is frequently asymptomatic and thus difficult to detect. In pregnant animals, *C. burnetii* accumulates in the placenta and leads to different reproductive disorders such as abortion, stillbirths, weak offspring or infertility (Tissot-Dupont and Raoult, 2008). Pregnant females shed the SCV form of *C. burnetii* into the environment through birth products including placenta and birth fluids, but also in bodily secretions such as urine, faeces, vaginal mucus and milk (Rodolakis, 2009). *C. burnetii* can persist into the environment for prolonged periods after bacterial shedding thus contributing to pathogen dissemination (Kersh *et al.*, 2013a). The main routes of animal infection are the airborne dispersal of contaminated particles between farms (Nusinovici *et al.*, 2017) and the introduction of infected animals into a herd.

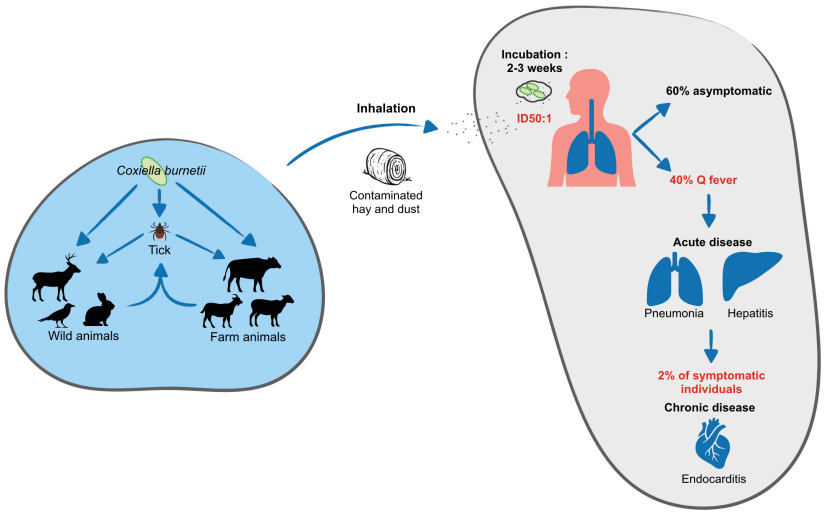

Figure 8. Overview of *C. burnetii* infection (adapted from Burette and Bonazzi, 2020)
C. burnetii is an obligate intracellular pathogen which infects wild and domesticated animals. Bacteria are shed in the environment with birth products and excretions, leading to the contamination of hay and dust. Symptoms occur 2–3 weeks after the inhalation of contaminated particles and the internalisation of *C. burnetii* by alveolar macrophages. Human Q fever remains asymptomatic in 60% of infected individuals, whereas 40% develop an acute, febrile disease, which can evolve into a chronic disease with more severe symptoms, including endocarditis.

Human infection mainly occurs through the inhalation of bacteria from contaminated hay or dust (Maurin and Raoult, 1999; Tissot-Dupont and Raoult, 2008) (**Figure 8**). Direct contact with infected animals or their products may also lead to human contamination, constituting a severe risk for people working in farms, slaughterhouses or laboratories (Eldin *et al.*, 2017). *C. burnetii* is extremely infectious as airborne exposure to 1 to 10 bacteria is sufficient to cause infection (Madariaga *et al.*, 2003; Brooke *et al.*, 2013). Moreover, airborne bacterial dispersal is promoted over long distances (up to 20 km) in favourable weather conditions (Tissot-Dupont *et al.*, 2004; Nusinovici *et al.*, 2015; Nusinovici *et al.*, 2017). To a lesser extent, the foodborne transmission also constitutes a route of infection through ingestion of dairy products from contaminated animals (Fishbein and Raoult, 1992; Miller *et al.*, 2020). Direct transmission from infected ticks to humans has not been proven; however, ticks play an important role in Q fever transmission by maintaining animal infection. Finally, anecdotal cases of human-to-human transmission of *C. burnetii* seem to suggest a potential route of nosocomial infection during delivery or autopsies (Weber and Rutala, 2001; Amit *et al.*, 2014), blood transfusion (Kersh *et al.*, 2013b), bone marrow transplantation (Kanfer *et al.*, 1988) and sexual transmission (Milazzo *et al.*, 2001). Human Q fever causes a broad spectrum of clinical presentations. Infections remain asymptomatic in the majority of cases, whereas 40% of infected individuals develop an acute form of the disease, leading to pneumonia, fever and flu-like symptoms with a mortality rate ranging between 1 and 2%. Patients may rarely present hepatitis, neurological or cardiac involvements. In 2% of symptomatic patients, Q fever can develop into a chronic disease, months to years after the initial infection. Chronic Q fever is associated with more severe symptoms such as endocarditis, vascular infections, septic arthritis and abortion with a mortality rate that reaches 65% (Eldin *et al.*, 2017) (**Figure 8**).

An annual incidence of 500 cases per million persons was observed in France, against 38 cases per million in Australia or 0.28 cases per million in the United States between 1978 and 2004 (Hartzell *et al.*, 2008). However, it is believed that a large number of human Q fever cases remaining unreported and/or underestimated due to asymptomatic infections and nonspecific symptoms for Q fever.

1.3.2 Diagnosis

Due to the obligate intracellular nature of *C. burnetii*, the diagnosis of Q fever cannot be performed using standard laboratory culture techniques. Thus, specific culture techniques employed to grow and detect the bacterium will be discussed in part *2.2.3* (*"Impact of technological advances on C. burnetii research"*). Consequently, indirect diagnostic tools have

been implemented based on serology, detection of *C. burnetii* DNA, cell culture and immunohistochemistry (Eldin *et al.*, 2017) (**Figure 9**). Suspected *C. burnetii* infection can be tested for IgG and IgM (Immunoglobulin G and M, respectively) antibodies response in the sera of patients using indirect immunofluorescence assay (IFA), which remains the most sensitive method during the early phases of infection. Complement fixation test (CFT) and Enzyme-Linked Immunosorbent Assay (ELISA) are also routinely used. In terms of serology, both acute and chronic forms of the disease induce the production of antibodies against phase I and phase II antigens. Anti-phase II antibodies predominate in acute Q fever while anti-phase I antibodies are mainly found during chronic infections. Ig antibody response begins with anti-phase II IgM antibodies, followed by anti-phase II IgG antibodies, anti-phase I IgM antibodies and finally anti-phase I IgG antibodies. Phase II IgG or IgM antibodies are detectable 2-3 weeks after the onset of acute disease and for the diagnosis, IgG II titer of ≥ 1:200 and/or IgM II titer of ≥ 1:50 are considered significant. Phase II antibodies decrease within 3-6 months, whereas chronic infection is associated with an elevated phase I IgG response (IgG I titer of ≥ 1:800) (Dupuis *et al.*, 1985; Eldin *et al.*, 2017) (**Figure 9**). Detection of *C. burnetii* DNA in the sera and the blood of patients by polymerase chain reaction (PCR) is also used for diagnosis. Unlike serology, it has the advantage of detecting *C. burnetii* within the first 2 weeks of infection. 16S-23S RNA, sequences from QpH1 or QpRS plasmids or chromosomal genes such as those coding for the outer membrane protein *com1*, the isocitrate-dehydrogenase *icd*, the superoxide dismutase *sod* or the IS1111 repetitive element are commonly targeted sequences for this approach, with the latter being the most sensitive by qPCR due to its multiple copies within *C. burnetii* genome (Klee *et al.*, 2006; de Bruin *et al.*, 2011). Cell culture and in particular shell-vial assay can be performed to isolate intracellular pathogens such as *C. burnetii* from clinical samples for diagnostic purposes. This technique is based on the inoculation of a clinical sample with monolayers of human embryonic lung (HEL) fibroblasts in shell vials. Inoculated shell vials are centrifuged to enhance attachment and internalisation of *C. burnetii* in the cells, and then incubated at 37°C, under 5% CO_2 atmosphere for 5-7 days. Detection of *C. burnetii* inside the cells is then performed by Gimenez or immunofluorescence staining (Gouriet *et al.*, 2005). Despite being less sensitive than PCR and requiring a BSL3 environment, this technique allows the detection of live bacteria. Finally, immunohistochemical analysis of tissue samples may help to detect *C. burnetii* in various organs; however, this approach has limited efficiency and can be only used in patients with chronic Q fever (Lepidi *et al.*, 2009).

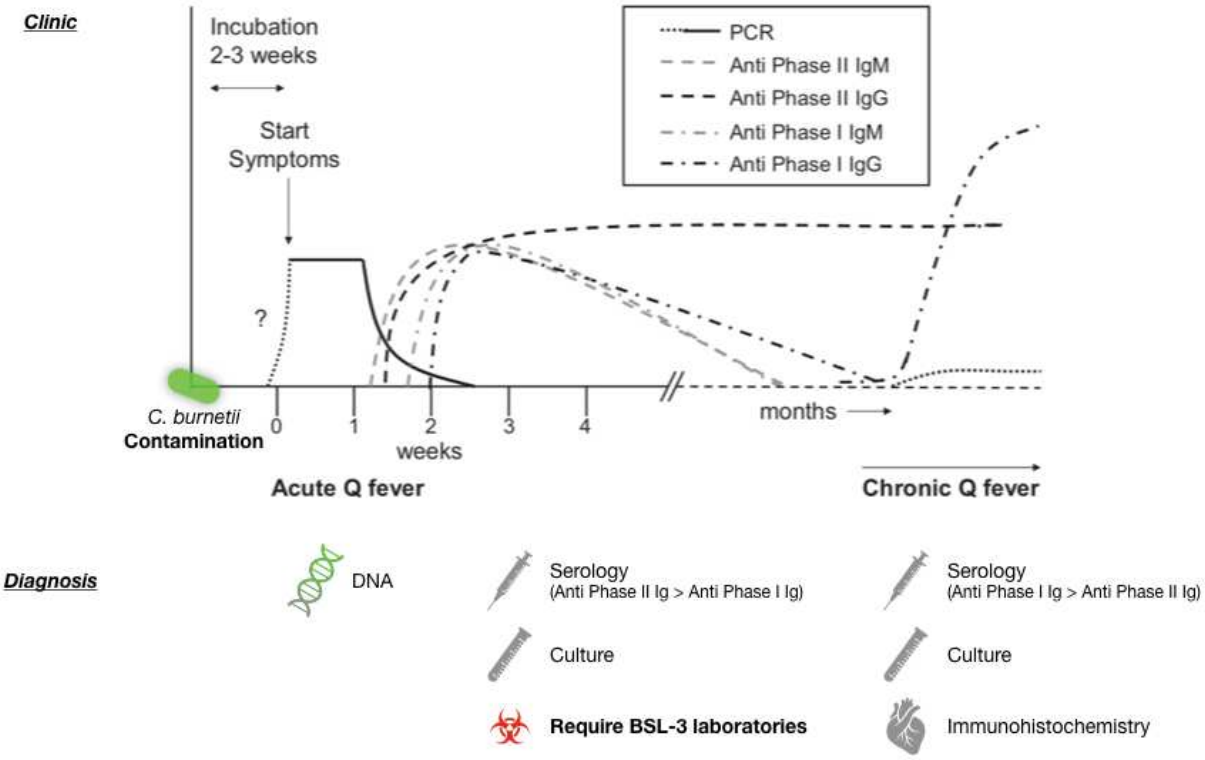

Figure 9. Clinical aspects and diagnosis tools in Q fever infection (adapted from Van Wijk *et al.*, 2011). Acute Q fever infections are mostly asymptomatic. Flu-like illness symptoms may occur after an incubation period of 2-3 weeks following contamination by *C. burnetii*. Patients with acute Q fever can develop a chronic form of the disease with more severe symptoms. Ig antibodies response begins 1-2 weeks after the onset of symptoms. Anti-phase II Ig are predominant during acute infections whereas chronic infections are associated with anti-phase I Ig. For Q fever diagnosis, *C. burnetii* infection can be detected by PCR, serological analysis, isolation or immunohistochemistry.

1.3.3 Treatment

Q fever is usually treated with antibiotics. Doxycycline over two weeks is the most recommended regimen to treat acute Q fever. Conversely, the most effective treatment for chronic Q fever combines doxycycline with hydroxychloroquine for up to 18 months and even for years to avoid relapse (Wiener-Well *et al.*, 2010). Given the unique intracellular adaptation of *C. burnetii* in an acidic phagolysosomal-like compartment (discussed in chapter *2. "The infectious cycle of Coxiella burnetii"*), the increase in lysosomal pH induced by the hydroxychloroquine improves the bactericidal activity of doxycycline, thus explaining the efficiency of this combined therapy (Maurin *et al.*, 1992; Smith *et al.*, 2019). It has been recently showed that lysosomal acidification to pH<4.8 is in fact detrimental to *C. burnetii* (Samanta *et al.*, 2019). Other antibiotics such as rifampin, macrolides, fluoroquinolones and trimethoprim/sulfamethoxazole have been proposed as alternative treatments but these were

never shown to be as efficient as the combined doxycycline/hydroxychloroquine treatment (Kersh, 2013). However, the emergence of a doxycycline-resistant strain in 2005 shows the importance to develop new antimicrobial therapies to treat Q fever (Rolain *et al.*, 2005). To date, Q-Vax produced from inactivated phase I *C. burnetii*, is the sole human vaccine available against Q fever (Marmion *et al.*, 1990). Q-Vax is highly efficient and has been used in Australia since 1989. However, the severe side effects developed by people already immune to *C. burnetii* has restricted its use. Pre-screening including a cutaneous test must be performed on each patient, prior to vaccination, making the large distribution of Q-Vax logistically difficult. Thus, Q-Vax is only recommended for people at-risk such as veterinarians, laboratory workers, farmers and slaughterhouse workers (Ruiz and Wolfe, 2014).

1.3.4 Animal models of *C. burnetii* infection

Animal models of infection play an important role in the study of bacterial virulence, pathogenesis and host-pathogen interactions. However, the development of appropriate animal models for Q fever remains challenging, as coxiellosis is mostly asymptomatic in animals. Several infection models are commonly used to study *C. burnetii* infections, including small mammals, non-human primates and invertebrates. Each of them present advantages and limitations that have to be taken into account (Metters *et al.*, 2019) (**Table 2**).

Small mammals such as mice and guinea pigs have been used to study Q fever. Mice are generally resistant to *C. burnetii* infections and usually clear the pathogen after infection (Metters *et al.*, 2019). However, Severe Combined ImmunoDeficient (SCID) mice have been used as a mammalian model to study infections by both virulent (NMI) and avirulent (NMII) *C. burnetii* strains. Both strains can be detected in multiple organs of infected mice allowing the study of dissemination defects. This model can also be used to determine the virulence potential and the relative fitness of individual *C. burnetii* mutant strains (Weber *et al.*, 2016b; van Schaik *et al.*, 2017). More recently, *MyD88*$^{-/-}$ mice have been presented as a new model to study determinants of chronicity and resolution in Q fever. The absence of MyD88 during *C. burnetii* infection led to impairment in inflammatory cytokines production, perturbation of granuloma formation and increase of spread and persistence of *C. burnetii* after intratracheal infection. In addition, the increased and prolonged bacterial burden in this model showed that *MyD88*$^{-/-}$ mice could constitute a suitable model to study chronic Q fever (Kohl *et al.*, 2019). *MyD88*$^{-/-}$ mice also possess a fully functional adaptive immune system, which gives a remarkable advantage over SCID mice. Contrary to mice, guinea pigs are more susceptible to *C. burnetii* infections, thus representing a better model to study acute Q fever (Metters *et al.*,

2019). Recently, the guinea pig model has been used in a comparative study to evaluate the virulence of multiple *C. burnetii* strains (Long *et al.*, 2019). However, the lack of genetic tools available and the costs of maintenance limit its use for *in vivo* studies.

Non-human primates such as Cynonomolgus and Rhesus monkeys are important models to evaluate antibiotics and vaccine efficacies which could potentially lead to favourable results for a Q fever vaccine (Waag *et al.*, 1999; Waag *et al.*, 2008). These models closely mimic human acute Q fever, however, ethical considerations and elevated maintenance costs make them minimally used as infection models (Metters *et al.*, 2019).

Invertebrates models also emerged as ideal tools to examine specific aspects of *C. burnetii* pathogenesis. Due to their small size and low maintenance cost, insects such as *Galleria mellonella*, *Drosophila melanogaster* and *Caenorhabditis elegans* are commonly used as infection models (Metters *et al.*, 2019). These models are susceptible to *C. burnetii* phase I and phase II infections, thus representing invaluable tools to identify *C. burnetii* virulence factors (Norville *et al.*, 2014; Martinez *et al.*, 2014; Martinez *et al.*, 2016; Bastos *et al.*, 2017) and determine the host tolerance to *C. burnetii* infection (Kohler *et al.*, 2016; Battisti *et al.*, 2017). These models also possess an innate immune response highly similar to that of vertebrates, allowing the investigation of host-pathogen interactions. However, due to their lack of adaptative immune response, they are less adapted to vaccine development studies.

	C. elegans	*D. melanogaster*	*G. mellonella*	Mouse	SCID mouse	*MyD88*$^{-/-}$ mouse	Guinea pig	Primates
Infection route	Feeding	Injection	Injection		Intraperitoneal (i.p.), intratracheal (i.t.), aerosol	i.p., i.t.	i.p., aerosol	Aerosol
Precise dosing	-	-/+	+	+	+	+	+	+
Survival at 37°C	-	-	+	+	+	+	+	+
Genetically tractable	+	+	-	+	+	+	-	-
Ethical considerations	-	-	-	+	+	+	+	+
Innate immunity representative of humans	-	+	+	+	+	+	+	+
Adaptive immunity	-	-	-	+	-	+	+	+
Susceptible to phase I and phase II strains *Phase I yet to be tested	Phase II*	Phase II*	+	Phase I	+	Phase II*	Phase I	Phase I
Signs of disease	• Reduced movement • Deformed anal region • Death	• Death	• Reduced movement • Melanization • Dehydration • Death	• No overt symptoms • Mild histopathological changes	• Ruffled fur • Hunchback appearance • Weight loss • Splenomegaly • Hepatitis • Endocarditis • Death	• No overt symptoms	• Fever • Lethargy • Weight loss • Pneumonia • Hepatitis	• Fever • Weight loss • Depression • Pneumonia • Hepatitis
Acute or chronic infection	Acute	Acute	Acute		Chronic	Chronic	Acute	Acute

Table 2. Summary of available animal models for *C. burnetii* infections (adapted from Kohl *et al.*, 2019; Metters *et al.*, 2019).

2. The infectious cycle of *Coxiella burnetii*

2.1 Adhesion and invasion

The ability to invade cells is essential for obligate intracellular bacteria. Bacterial adhesion and invasion of host cells are mediated by two distinct processes: the trigger and the zipper mechanisms. The trigger mechanism involves severe actin rearrangements which are induced by effector proteins translocated upon bacterial adhesion to host cells. In contrast, the zipper mechanism uses bacterial proteins to engage host surface receptors, leading to bacterial internalisation (Pizarro-Cerdá and Cossart, 2006) (**Figure 10**).

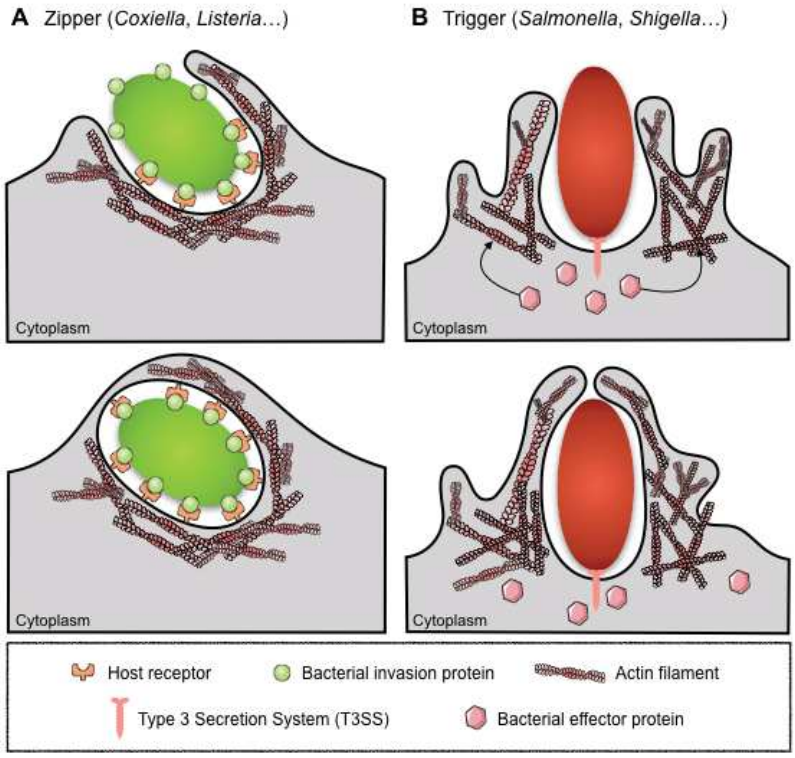

Figure 10. Zipper and trigger mechanisms of bacterial invasion (adapted from Zheng *et al.*, 2015). A. Zipper mechanism: bacterial invasion proteins interact with host cell membrane receptors to stimulate actin-rich membrane ruffles and then to internalise the pathogen. **B.** Trigger mechanism: Bacterial effector proteins secreted by the Type 3 Secretion System (T3SS) induce a dynamic actin remodelling to engulf the pathogen.

C. burnetii Phase I is passively internalised by alveolar macrophages through actin-dependent phagocytosis (Meconi *et al.*, 1998; Meconi *et al.*, 2001). *C. burnetii* entry is initiated by the interaction of lipid raft-associated $\alpha_v\beta_3$ integrins and an unknown bacterial ligand (Capo *et al.*, 1999). Following engagement of the $\alpha_v\beta_3$ integrin receptor, a remodeling of the host cell actin cytoskeleton regulated by the GTPases of the Rho family occurs, leading to membrane

ruffling (Salinas *et al.*, 2015) (**Figure 11**). Importantly, *C. burnetii* also invades non-phagocytic cells such as epithelial and endothelial cells. The internalisation is facilitated by the interaction of the *C. burnetii* invasin OmpA (Outer membrane protein A) with an unknown host cell receptor (Martinez *et al.*, 2014) (**Figures 11 and 12**) and, similar to what has been observed in phagocytic cells, actin cytoskeleton plays an important role in the entry (Rosales *et al.*, 2012). $\alpha_v\beta_3$ integrin is poorly expressed in epithelial cells, suggesting that *C. burnetii* invasion involves other receptors.

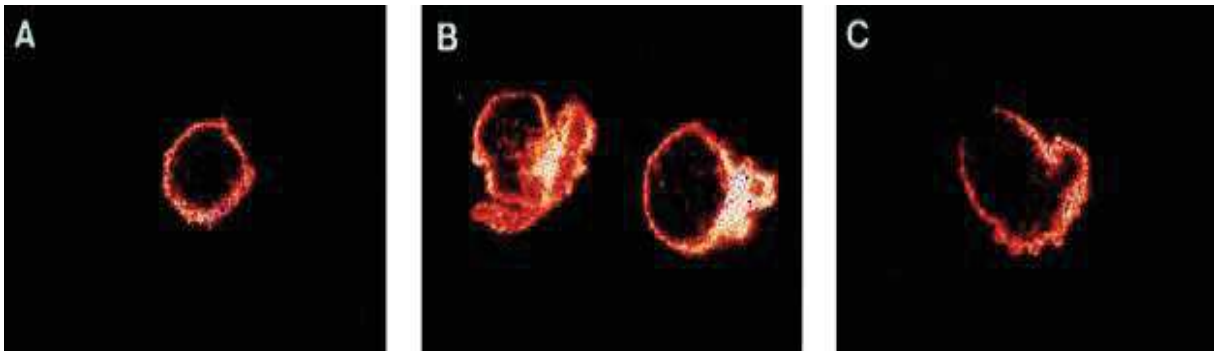

Figure 11. Actin reorganisation in *C. burnetii*-infected monocytes (adapted from Meconi *et al.*, 1998). Monocytes were non-infected (**A**) or infected with Phase I *C. burnetii* for 5 min (**B**) or 15 min (**C**) and examined by laser scanning confocal microscopy showing the membrane ruffling following *C. burnetii* infection.

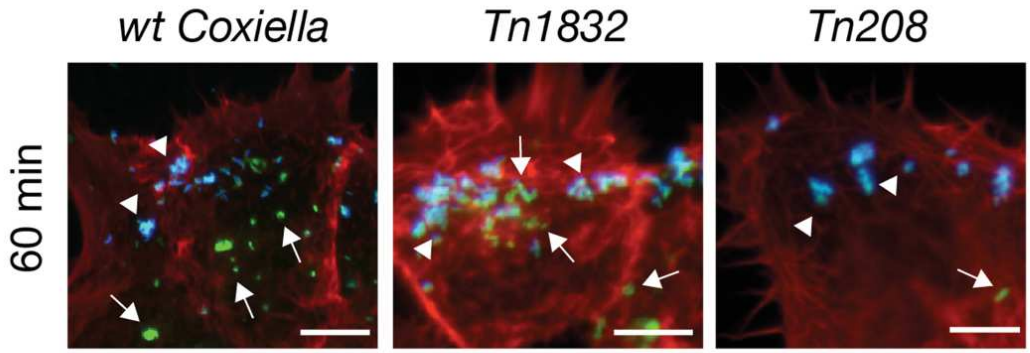

Figure 12. *C. burnetii* invasin OmpA is involved in host cell invasion (adapted from Martinez *et al.*, 2014). Non-phagocytic epithelial cells (A431) challenged with *wild-type (wt) Coxiella*, the control transposon mutant *Tn1832* or the OmpA mutant *Tn208*. 60 min after infection, cells were fixed and labelled for extracellular (blue) and total (green) bacteria. The internalisation of the OmpA mutant *Tn208* was strongly reduced as compared to *wt Coxiella* or *Tn1832*.

`

Similarly, it is conceivable that OmpA may play also a role in *C. burnetii* replication in macrophages as OmpA transposon mutants replicate less efficiently in macrophages (Martinez *et al.*, 2016).

Phase variation plays an important role in *C. burnetii* internalisation, as Phase II bacteria are more efficiently internalised than Phase I by both phagocytic and non-phagocytic cells. Indeed, the invasion of macrophages by Phase II *C. burnetii* engages the complement receptor 3 (CR3) as a co-receptor to $\alpha_v\beta_3$ integrin and in this case, no membrane ruffling is observed (Meconi *et al.*, 1998; Capo *et al.*, 1999). Thus, it has been proposed that Phase I *C. burnetii* LPS interferes with phagocytosis by excluding CR3 receptor from membrane ruffles leading to a less efficient internalisation (Capo *et al.*, 1999; Capo *et al.*, 2003; Honstettre *et al.*, 2004).

Following uptake by both phagocytic and non-phagocytic cells, *C. burnetii* generates a replicative niche called *Coxiella*-containing vacuole (CCV) that matures along the endocytic pathway by heterotypic fusion with early and late endosomes, lysosomes and autophagosomes (Voth and Heinzen, 2009b; Burette and Bonazzi, 2020) (**Figure 13**). These successive fusion events lead to the acquisition of several markers from early and late endosomes (small GTPases RAB5 and RAB7), autophagosomes (LC3B) and lysosomes (LAMP-1, LAMP-2) (Romano *et al.*, 2007). The acidic pH as well as the degradative environment within the *Coxiella*-containing phagolysosome triggers a genetic reprogramming followed by the morphological differentiation from SCV form to LCV (Coleman *et al.*, 2004; Newton *et al.*, 2020). Indeed, unlike many other intracellular bacteria such as *Legionella*, *Brucella*, *Anaplasma*, *Chlamydia* or *Ehrlichia,* which prevent lysosomal degradation (Martinez *et al.*, 2018), *C. burnetii* generates a unique intracellular acidic compartment (pH~5.2), containing active lysosomal hydrolases (Pareja *et al.*, 2017; Samanta *et al.*, 2019). In addition, the fusion of CCVs with lysosomes triggers the synthesis and assembly of the *C. burnetii* main virulence factor, the T4BSS (Newton *et al.*, 2013; Newton *et al.*, 2020). This system allows the translocation of bacterial effector proteins directly in the host cell cytoplasm where they manipulate a number of host signalling pathways to promote intracellular replication and persistence (**Figure 13**). Indeed, the biogenesis and maturation of a large and unique CCV requires an important supply of membranes and proteins, which may be provided by the manipulation of several vesicular trafficking by *C. burnetii* effector proteins. Bacterial persistence within these large, hybrid compartments also requires the subversion of apoptosis and the immune response, to avoid cell death and bacterial detection. To facilitate host cell subversion, *C. burnetii* effectors may facilitate, antagonise or even mimic the function of host proteins. In the following section, intracellular replication and persistence strategies will be discussed regarding the subversion of host vesicular trafficking involved in the CCV biogenesis and the control of host cell defence.

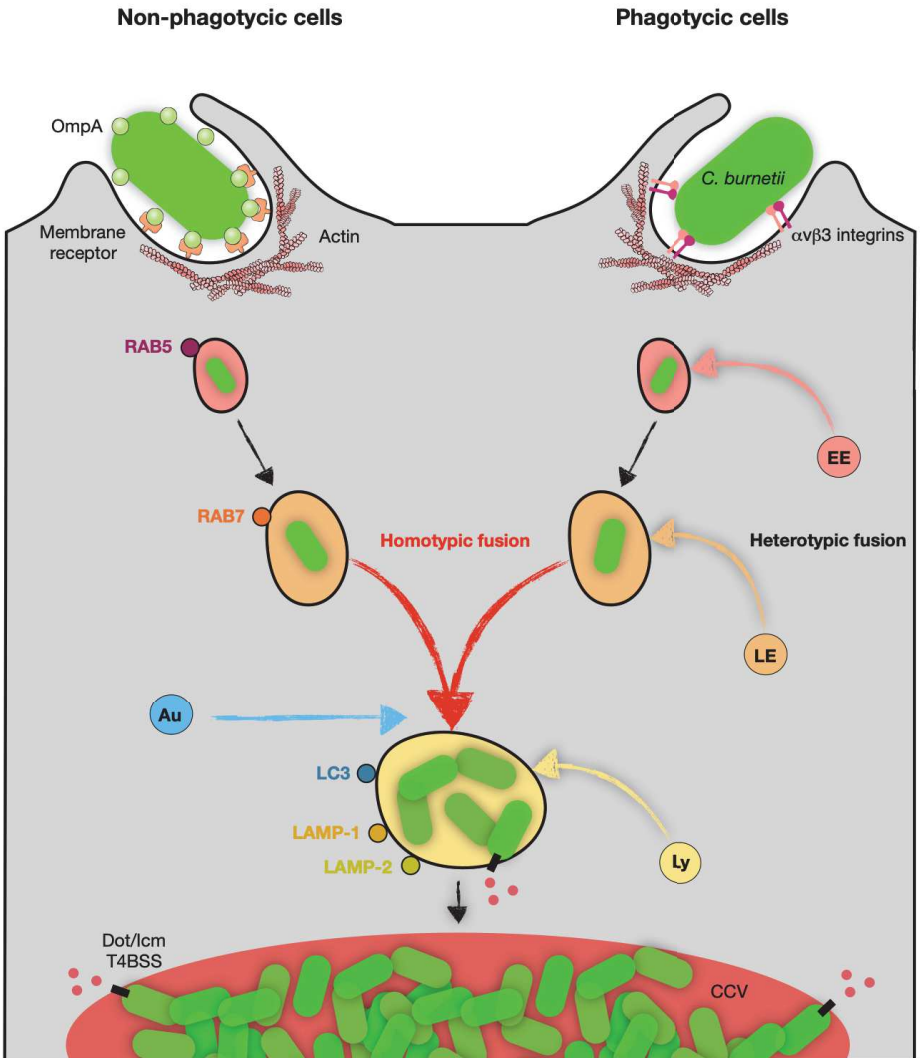

Figure 13. **Intracellular cycle of *C. burnetii*.** *C. burnetii* internalisation is facilitated by the interaction of the bacterial invasion OmpA with an unknown receptor. In macrophages, *C. burnetii* enters by phagocytosis through the interaction with $\alpha_v\beta_3$ integrins. In both cell types, early CCVs mature along the endocytic pathway by heterotypic fusion with early endosomes (EEs), late endosomes (LEs) and lysosomes (Lys) leading to the acquisition of several markers from these compartments. Acidification of the CCV activates bacterial metabolism and the translocation of bacterial effector proteins (red circles) by the Dot/Icm secretion system. This is required for homotypic fusion of multiples CCVs and the formation of a large CCV in which bacteria replicate in high numbers.

2.2 Biogenesis of the *Coxiella*-Containing Vacuole

2.2.1 Subversion of vesicular trafficking pathways

2.2.1.1 Endocytic and autophagy pathways

Endocytosis is a fundamental process in eukaryotic cells to monitor their environment and to control nutrient acquisition. The process involves the engulfment of extracellular particles or molecules that are subsequently transported to specific compartments in the cell. Cargo internalised by clathrin-dependent or -independent endocytosis transit to early endosomes, which serve as sorting platforms. There, cargo can undergo degradation in late endosomes and lysosomes, interact with the Trans-Golgi Network (TGN) or recycle back to the plasma membrane (Doherty and McMahon, 2009). The endocytic pathway is defined by fusion and fission events of internalised vesicles, which are largely controlled by the recruitment of RAB GTPases and by the lipid composition of vesicular membranes (discussed in part "*2.2.2.1 Lipids in eukaryotic cells"*) (Jean and Kiger, 2012). RAB GTPases are master regulators of vesicular trafficking and maturation events. RAB proteins cycle between a cytosolic, inactive, GDP-bound state and a membrane-anchored, active, GTP-bound state. The transition to the active state is mediated by a guanine nucleotide exchange factor (GEF), which promotes the exchange of GDP to GTP, whereas the inactivation is catalysed by a GTPase activating protein (GAP) which stimulates GTP hydrolysis (Hutagalung and Novick, 2011).

Many intracellular bacteria take control of the endocytic pathway to establish their intracellular niche. While intracellular bacteria such as *Legionella* or *Brucella* have evolved strategies to avoid lysosomal degradation, *C. burnetii* requires an acidified environment to efficiently replicate. Following uptake, the CCV matures through the endocytic pathway acquiring endocytic markers such as RAB5 and RAB7 in a Dot/Icm-independent manner. Small interfering RNA (siRNA)-mediated depletion of RAB5 and RAB7 showed that these endocytic trafficking regulators are important in CCV biogenesis and intracellular replication, even if they are passively recruited to CCVs (Howe *et al.*, 2003; McDonough *et al.*, 2013; Newton *et al.*, 2013).

If on the one hand membrane trafficking along the endocytic pathway is required to allow CCVs to fuse with lysosomes independently of *C. burnetii* effector proteins, some effectors have been shown to actively manipulate the endocytic pathway later on during the infection. Coxiella vacuolar protein A (CvpA) and co-regulated with *icm* genes 57 (Cig57), are capable of modulating the clathrin-dependent trafficking pathway by recruiting clathrin-coated vesicles to the CCV (Larson *et al.*, 2013; Latomanski *et al.*, 2016). CvpA and Cig57 contain

endocytic sorting motifs that are important for the interaction with clathrin-mediated endocytosis (CME)-related proteins: the adaptor protein-2 (AP-2) complex and the nucleator protein FCH and mu domain containing endocytic adaptor 2 (FCHO2), respectively (**Figure 14**). siRNA-mediated depletion of clathrin or mutations in either *cvpA* or *cig57* impact *C. burnetii* replication and CCV biogenesis, suggesting that the manipulation of clathrin-mediated membrane transport may promote membrane supply for CCV development (Larson *et al.*, 2013; Latomanski *et al.*, 2016). Additionally, clathrin has been shown to facilitate the fusion of autophagosomes with the CCV, indicating that its subversion during *C. burnetii* infections impacts different vesicular pathways (Latomanski and Newton, 2018). The role of autophagy during *C. burnetii* infections will be discussed further below.

The *C. burnetii* effector for intracellular replication A (CirA) stimulates the GTPase activity of Ras homolog family member A (RhoA) by acting as a GAP and favors CCV biogenesis. It has been suggested that CirA may promote cytoskeletal rearrangements and thus, the rerouting of host vesicles to the CCV (Aguilera *et al.*, 2009; Weber *et al.*, 2016) (**Figure 14**). More recently, the identification of arginine finger-like motifs and endosome-lysosome basolateral sorting signals within CirA seems to strengthen the hypothesis that the effector protein manipulates endocytic trafficking by facilitating heterotypic and homotypic vesicular fusion events (Weber *et al.*, 2018).

Homotypic fusion of CCVs also depends on Soluble N-ethylmaleimide-sensitive factor attachment protein receptors (SNARE) proteins which are key players in endocytosis. Indeed, syntaxin-17 (STX17), Vesicle-associated membrane protein 3, 7 and 8 (Vamp3, Vamp7 and Vamp8, respectively) are involved in CCV biogenesis and are manipulated in a Dot/Icm-dependent manner (**Figure 14**). Furthermore, siRNA-mediated depletion of either STX17 or Vamp7 results in a severe defect in homotypic fusion of CCVs suggesting that both proteins are involved in the regulation of this process (McDonough *et al.*, 2013; Campoy *et al.*, 2013). Given the role of STX17 in autophagosomes formation and the fusion of autophagosomes with lysosomes, additional studies were undertaken focusing on the role of autophagy during *C. burnetii* infection.

Macroautophagy (thereafter termed autophagy) is a fundamental process allowing eukaryotic cells to respond to starving conditions by delivering cytoplasmic components and organelles to the lysosome for degradation. Autophagy also represents an important mechanism in host cell defense against intracellular pathogens (Levine and Kroemer, 2008). Under starving conditions, cytoplasmic components are sequestered into double-membrane

vesicles called autophagosomes. Autophagosomes fuse with lysosomes thus generating a degradative compartment called autolysosome (Yu *et al.*, 2018).

Early studies demonstrated the presence of host autophagy proteins LC3B (microtubule associated protein 1 light chain 3 beta) and RAB24 at CCV membranes, suggesting a fusion of the CCV with autophagosomes in a Dot/Icm-dependent manner (Romano *et al.*, 2007) (**Figure 14**). The autophagy pathway has been shown as promoting CCV biogenesis (Gutierrez *et al.*, 2005; Romano *et al.*, 2007), intracellular replication (Larson *et al.*, 2019) and contributing to the repair of damaged CCVs (Mansilla Pareja *et al.*, 2017). The importance of autophagy in homotypic fusion of CCVs has been demonstrated through siRNA-mediated depletion of essential host autophagy genes (McDonough *et al.*, 2013; Newton *et al.*, 2014), resulting in a "multivacuolar" phenotype, where multiple, smaller CCVs were observed in infected cells. An identical phenotype was observed in cells infected with *C. burnetii* strains carrying transposon insertions in the gene encoding the effector protein CvpB (or Cig2) (Newton *et al.*, 2014; Martinez *et al.*, 2016). Indeed, CvpB promotes autophagy-mediated homotypic fusion of CCVs by interacting with cellular lipids (further discussed in part *2.2.2.2 "Subversion of host lipid metabolism by Coxiella burnetii"*) (Martinez *et al.*, 2016; Kohler *et al.*, 2016) (**Figure 14**). Besides CvpB, other T4BSS effectors hijack the autophagy machinery for an optimal CCV development as the recently characterised CvpF. We demonstrated that CvpF stimulates autophagy by subverting the function of the autophagy-related RAB GTPase RAB26 to promote CCV biogenesis and virulence (**Figure 14**). By interacting with RAB26 and recruiting it to CCVs, CvpF stimulates the anchoring of LC3B on CCVs, illustrating that autophagy is manipulated at different levels by *Coxiella* effectors to promote CCV biogenesis (Siadous *et al.*, 2020).

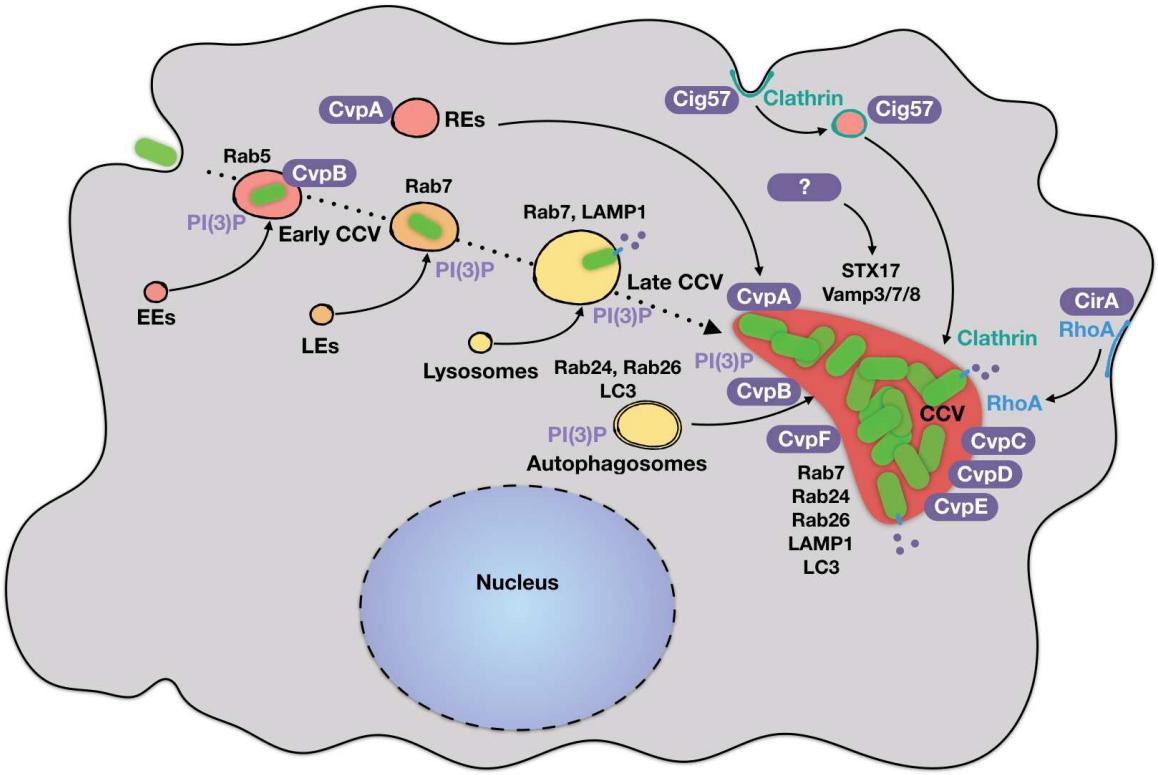

Figure 14. Subversion of endocytic and autophagy pathways by *C. burnetii*. Several effector proteins are collectively beneficial for the biogenesis of the mature CCV where bacterial replication occurs. These include the Cvp family (for *Coxiella* vacuolar protein) of effectors that localize at CCV membranes and manipulate host membrane trafficking pathways. CvpA interacts with the clathrin adaptor AP-2 at recycling endosomes (REs), re-routing these compartments to the forming CCV. CvpB binds PI(3)P at early endosomes and enriches this phospholipid at CCVs. In turn, this favors the autophagy-mediated homotypic fusion between CCVs. CvpF interacts with the autophagy-related RAB GTPase RAB26 to stimulate the anchoring of LC3B on CCVs. Cig57 interacts with the clathrin adaptor FCHO2 at clathrin-coated pits and re-routes clathrin-mediated membrane traffic to the CCV. CirA. stimulates the GTPase activity of RhoA which is recruited to the CCV to favor CCV biogenesis.

2.2.1.2 Secretory and retrograde pathways

The secretory and retrograde vesicular trafficking pathways represent a bidirectional transport that is essential in eukaryotic cells. The secretory pathway ensures the synthesis and the delivery of proteins and lipids (further described in part *2.2.2.1 "Lipids in eukaryotic cells"*) from the rough endoplasmic reticulum (ER) to the Golgi apparatus. The ER-to-Golgi transport is mediated by protein complexes called the Coat protein complex (COP) proteins. COPII proteins mediate cargo delivery from the ER to the Golgi through a Secretion-Associated Ras related GTPase 1 (Sar1)-GTPase-dependent activity. Conversely, COPI proteins are involved in cargo recycling from the Golgi to the ER and regulated by the activity of Arf (ADP ribosylation factor) GTPases (Duden, 2003). In the Golgi apparatus, glycosylated proteins and lipids are

finally packaged into transport vesicles addressed to the plasma membrane for exocytosis or to cellular compartments (Gomez-Navarro and Miller, 2016). The retrograde pathway is an important cellular mechanism involved in the trafficking of proteins and lipids from endosomes to the Golgi and the ER to ensure their recycling to the plasma membrane or maintain a steady-state localisation of proteins as well as lipid homeostasis (Johannes and Popoff, 2008).

Even if the CCV displays several autolysosomal features, it has been reported that *C. burnetii* hijacks both the secretory and retrograde pathways to promote CCV biogenesis and intracellular replication. Indeed, at later time points of infection, CCVs are decorated with the RAB GTPase RAB1B, which regulates ER-to-Golgi transport, suggesting the re-routing of the early secretory pathway (Campoy *et al.*, 2011) (**Figure 15**). In addition, either siRNA-mediated depletion of RAB1B or the chemically-induced disruption of the secretory pathway using brefeldin A affect the biogenesis of the CCV, thus showing the importance of the secretory pathway in this process (Campoy *et al.*, 2011). To date, at least 5 *C. burnetii* effectors have been identified as potentially interfering with the host secretory pathway. Indeed, ectopic expression of CBU0635, CBU1556 (also called CvpC), CBU1825, CBUA0019 and ElpA (ER-localising protein A) significantly reduces the secretion of host proteins, as determined by the secreted embryonic alkaline phosphatase (SEAP) reporter assay (Carey *et al.*, 2011; Weber *et al.*, 2013; Graham *et al.*, 2015) (**Figure 15**). In addition to the subversion of the secretory pathway, retrograde transport has also been demonstrated as important for intracellular replication of *C. burnetii*. Interestingly, siRNA-mediated depletion of key components of this pathway such as the retromer subunits Vacuolar Protein Sorting 29 and 35 (VPS29 and VPS35, respectively), as well as Sorting Nexins 2, 3, 5 and 6 (SNX2, SNX3, SNX5, SNX6, respectively) results in a strong intracellular replication defect (McDonough *et al.*, 2013). However, the mechanisms by which the pathogen modulates this pathway remain unclear (**Figure 15**).

Finally, it has been demonstrated that CCVs are transiently damaged during infections and *C. burnetii* actively manipulates both the endocytic and autophagy pathways to repair CCV membranes (Pareja *et al.*, 2017). Most galectins exert their functions extracellularly; however, intracellular activities including the recruitment of ESCRT components to damaged lysosomes have been reported (Jia *et al.*, 2020) as well as the monitoring of bacterial vacuole rupture (Paz *et al.*, 2010). The endosomal sorting complex required for transport (ESCRT) machinery is organised into several complexes designated ESCRT-0, -I, -II and -III combined to the ATPase activity of the vacuolar sorting-associated protein 4 (VPS4) and associated factors including the ALIX (Programmed cell death 6-interacting protein) protein (Hurley, 2015). The

ESCRT machinery is involved in many processes such as MVBs biogenesis, membrane bending and scission or repair of damaged endolysosomes (Skowyra *et al.*, 2018). During *C. burnetii* infections, both galectin-3 and the ESCRT machinery are transiently recruited to damaged CCVs, and their function is important for *C. burnetii* intracellular replication (Pareja *et al.*, 2017; Radulovic *et al.*, 2018).

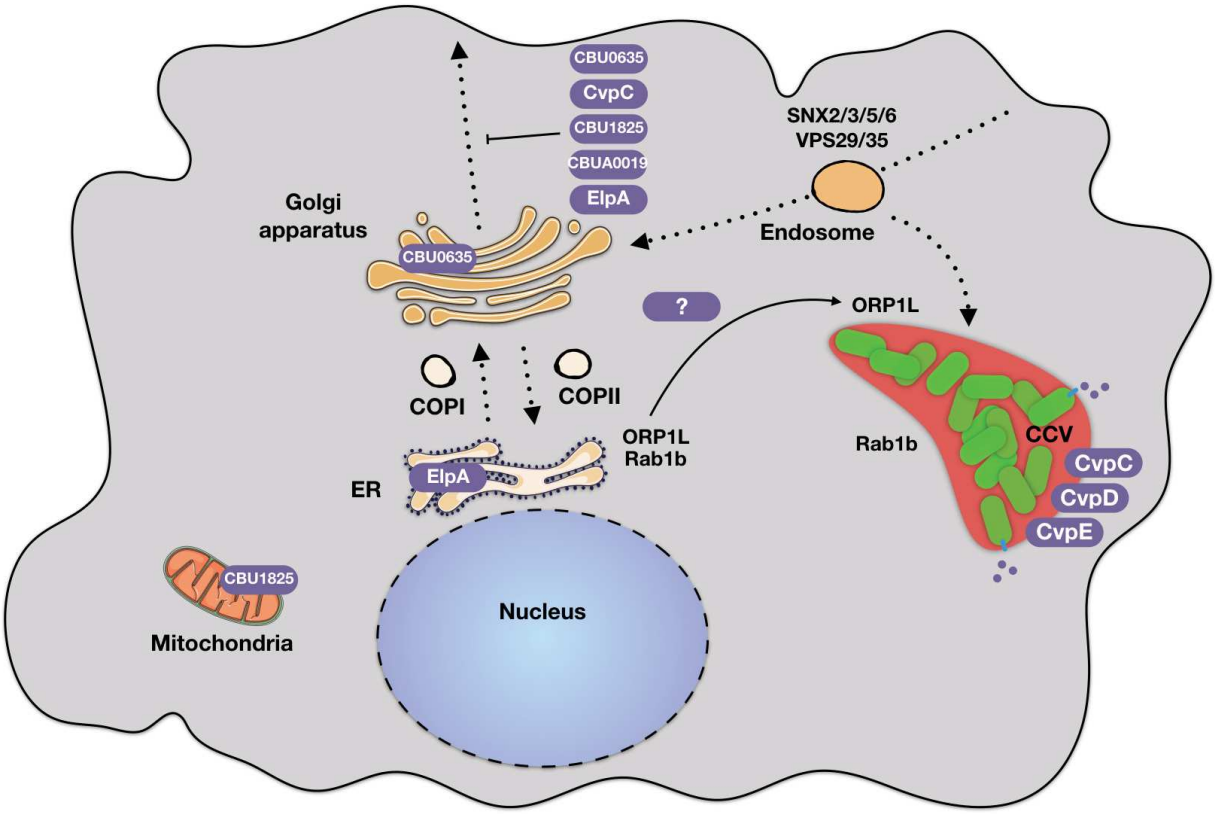

Figure 15. Subversion of secretory and retrograde pathways by *C. burnetii*. *C. burnetii* recruits the small GTPase RAB1b to CCV membranes to intercept ER-to-Golgi vesicle trafficking by an unknown Dot/Icm-dependent mechanism. ElpA and CBU0635 localise to the ER and the Golgi apparatus, respectively, and modulate the secretory pathway. Additionally, CvpC, CBU1825, CBUA0019 also disrupt the secretion of host proteins by an unknown mechanism.

2.2.2 Manipulation of lipid metabolism

2.2.2.1 Lipids in eukaryotic cells

(i) Lipid diversity and synthesis

In eukaryotic cells, lipids play many key roles in cells such as energy sources, membrane structural components, platforms for protein recruitment and signalling molecules (Van Meer *et al.*, 2008). Cellular membranes consist of lipids and proteins forming a barrier that protects the cell and the organelles from the extracellular environment. Cellular lipids are

classified in three main classes according to their chemical structures: glycerophospholipids, sphingolipids and sterols (Harayama and Riezman, 2018). Glycerophospholipids are the main constituents of membranes and consist of a glycerol backbone attached to two fatty acids and a modified phosphate head group. Depending on the headgroup nature, nine different glycerophospholipids can be found in eukaryotic membranes: phosphatidic acid (PA), phosphatidylcholine (PtdCho), phosphatidylethanolamine (PtdEtn), phosphatidylserine (PtdSer), phosphatidylinositol (PtdIns), phosphatidylglycerol (PtdGro), cardiolipin, lysobisphosphatidic acid (LBPA) also called bis(monoacylglycerol)phosphate (BMP) and phosphatidylglucoside (PtdGlc) (Harayama and Riezman, 2018) (**Figure 16**). Sphingolipids are the second most abundant lipids in membranes and contain a sphingoid base linked to a hydrophobic acyl chain as well as a phosphate head group. Similarly to glycerophospholipids, the headgroup type defines the sphingolipid name allowing to distinguish simple sphingolipids such as ceramides, from complex glycosphingolipids that includes sphingomyelins, the main component of myelin sheath in nerve cells (Hannun and Obeid, 2018) (**Figure 16**). Finally, sterols are structurally different from glycerophospholipids and sphingolipids as they possess four fused hydrocarbon rings linked to a hydroxyl group. In mammalian cells, the major sterol is cholesterol, an important lipid component that plays an essential role in membrane structure and function (Van Meer *et al.*, 2008) (**Figure 16**). Indeed, cholesterol influences the biophysical properties of membranes as rigidity and also clusters with sphingolipids to form membrane microdomains called lipid rafts (Ikonen, 2008). Lipid rafts function as signalling platforms for proteins and play a role in many cellular processes including endocytosis, signal transduction, protein sorting and intracellular membrane trafficking (Stüven *et al.*, 2003; Simons and Vaz, 2004; Yang *et al.*, 2016).

A GLYCERO-PHOSPHOLIPIDS

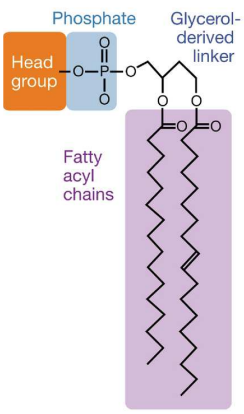

Glycero-phospholipids (GPLs)		Headgroup nature
Phosphatidic acid	PA	-
Phosphatidylcholine	PtdCho	Choline
Phosphatidylethanolamine	PtdEtn	Ethanolamine
Phosphatidylserine	PtdSer	Serine
Phosphatidylinositol	PtdIns	Inositol
Phosphatidylglycerol	PtdGro	Glycerol
Cardiolipin		Phosphatidylglycerol
Lysobisphosphatidic acid	LBPA	Lysophosphatidic acid
Phosphatidylglucoside	PtdGlc	Glucose

B SPHINGOLIPIDS

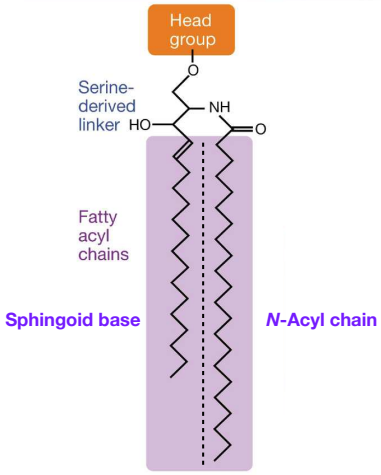

Sphingolipid		Headgroup nature
Ceramide	Cer	Hydroxyl
Sphingomyelin		Phosphocholine
Phosphatidylethanolamine	CerPE	Phosphoethanolamine
Phosphatidylserine	GlcCer	Glucose
Phosphatidylinositol	GalCer	Galactose
Complex glycosphigolipids	GSLs	Oligosaccharides
Ceramide-1-phosphate	C1P	Phosphate

C CHOLESTEROL

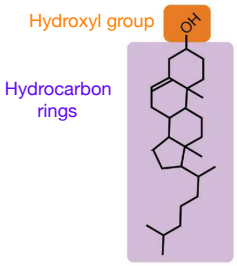

Figure 16. Chemical diversity of membrane lipids (adapted from Jacquemyn *et al.*, 2017; Harayama and Riezman, 2018). A. The structure of glycerophospholipid (GPL) consists of two fatty acyl chains, a glycerol backbone and a headgroup. The table section indicates the different headgroup nature that defines the lipid name (same for B). B. The structure of sphingolipids is defined by a sphingoid base, a N-acyl chain and a headgroup. C. The structure of the main sterol: cholesterol with four hydrocarbon rings fused to a hydroxyl group.

The biosynthesis of lipids mainly occurs in the endoplasmic reticulum ER which contains the enzymes that produce the majority of lipids (Jacquemyn *et al.*, 2017). However, some lipids can be synthesized in other organelles, such as LBPA in late endosomes and

lysosomes (Somerharju, 1979; Kobayashi *et al.*, 1998) cardiolipin in mitochondria (Gaspard and McMaster, 2015) and sphingolipids in the Golgi apparatus (Van Meer *et al.*, 2008). The ER is the major regulator of lipid levels within cells as it ensures the distribution of newly synthesised lipids to other organelles and to the plasma membrane (PM) via the secretory pathway and/or ER contact sites (Jain and Holthuis, 2017; Funato *et al.*, 2020). Indeed, lipid distribution occurs through a mechanism of vesicle budding and fusion as well as a non-vesicular lipid export through ER contact sites that probably involves lipid transfer proteins (Funato *et al.*, 2020).

(ii) Lipid composition of cellular membranes

The lipid composition of cellular membranes varies between organelles (Casares *et al.*, 2019), membrane leaflets (Ingólfsson *et al.*, 2014) and membrane subdomains (Ikonen, 2008). Lipid composition is important not only for the biophysical properties of membranes, such as curvature and bending stiffness but also for the regulation of membrane trafficking (Haucke and Di Paolo, 2007; Harayama and Riezman, 2018). In eukaryotic cells, the lipid composition of membranes is highly regulated, as observed in the endocytic pathway (Haucke and Di Paolo, 2007). Indeed, the plasma membrane and early endosomes are enriched in sphingolipids and sterols, with concentration decreasing with the maturation to late endosomes. Conversely, the concentration of LBPA increases from early to late endosomes to promote sphingolipid hydrolysis, fusion processes, lysosome stabilisation and MVB generation (Kobayashi *et al.*, 2002; Matsuo *et al.*, 2004; Kolter and Sandhoff, 2005; Kirkegaard *et al.*, 2010). Vesicular sorting is also mediated by the interplay between lipid phosphatases and kinases involved in the spatial and temporal distribution of another class of lipids, the phosphoinositides (PIs) (Kutateladze, 2010). PIs are the phosphorylated derivatives of PtdIns which are synthesised in the ER as well as within a mobile ER-derived PtdIns-synthesising compartment that ensures an active distribution of PtdIns to subcellular membranes (Agranoff *et al.*, 1970; Kim *et al.*, 2011). PIs are only present on the cytosolic side of membrane bilayers and consist of a phosphodiester linker that connects a diacylglycerol backbone and an inositol ring, which can be mono- or poly- phosphorylated in positions, 3, 4, and 5 (Kutateladze, 2010) (**Figure 17B**). Thus, seven different PI isoforms can be found in cell membranes, including monophosphorylated PIP (PI(3)P, PI(4)P and PI(5)P), bisphosphorylated PIP_2 ($PI(3,4)P_2$, $PI(3,5)P_2$ and $PI(4,5)P_2$) and trisphosphorylated PIP_3 ($PI(3,4,5)P_3$) (Kutateladze, 2010) (**Figure 17A**).

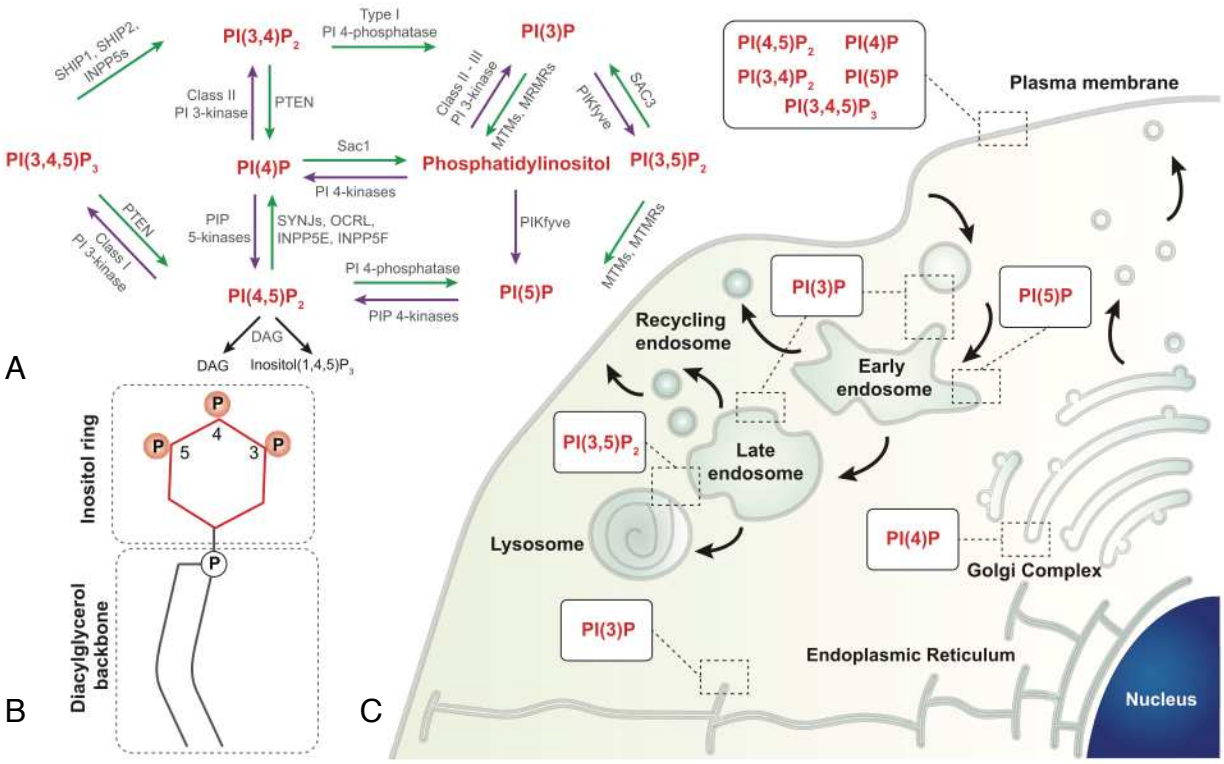

Figure 17. Phosphoinositide structure and metabolism in eukaryotic cells (adapted from Goud *et al.*, 2016). Phosphoinositides (PI) are mono- or poly-phosphorylated derivatives of phosphatidylinositol phospholipid which consist of a diacylglycerol backbone linked to an inositol ring by a phosphodiester linker (**B**). The inositol ring can be phosphorylated in positions 3, 4 and 5, thus giving raise to seven different phosphoinositide isoforms which are metabolised by different phosphatases and kinases (**A**). Each PI species is accumulated in specific membrane compartments according to its role in vesicular trafficking (**C**).

Despite representing less than 1% of total cell lipids, PIs are key players in signalling pathways through the regulation of multiple cellular processes such as membrane trafficking, signal transduction, cytoskeleton rearrangements or lipid transport (Balla *et al.*, 2009) (**Table 3**). The presence of distinct PIs on compartment membranes allows the intracellular trafficking machinery to discern an organelle from another (Behnia and Munro, 2005; Jean and Kiger, 2012) (**Figure 17C**). Phagosomes, early endosomes, late endosomes, MVBs and autophagosomes are enriched in phosphatidylinositol 3-phosphate (PI(3)P), a crucial lipid for the coordination of membrane trafficking along the endocytic pathway (Gillooly *et al.*, 2000; Funderburk *et al.*, 2010; Marat and Haucke, 2016) (**Table 3**). The presence of PI(3)P has also been reported within membranes of the Golgi apparatus and the ER, albeit to a lesser extent (Sarkes and Rameh, 2010). Late endosomes and MVBs are enriched in phosphatidylinositol 3,5-bisphosphate ($PI(3,5)P_2$), a lipid that is particularly found on lysosomes (Mccartney *et al.*, 2014) (**Table 3**). Despite its low abundance, $PI(3,5)P_2$ plays a crucial role in endosomal

trafficking homeostasis by regulating endosomal fusion and fission events as well as the retrograde pathway (Mccartney *et al.*, 2014). Phosphatidylinositol 4-phosphate (PI(4)P) and phosphatidylinositol 4,5-biphosphate ($PI(4,5)P_2$) are the most abundant PIs in mammalian cells (Di Paolo and De Camilli, 2006) (**Table 3**). PI(4)P is particularly enriched at the Golgi apparatus and at the PM (Di Paolo and De Camilli, 2006), where it plays an important role in the regulation of vesicular trafficking from the Golgi to the PM and endosomes, lipid metabolism and mitochondrial fission (D'Angelo *et al.*, 2008; Yamaji and Hanada, 2015; Mesmin *et al.*, 2017; Nagashima *et al.*, 2020) (**Table 3**). $PI(4,5)P_2$ is mainly found at the PM, although evidence for its presence within membranes of the ER, Golgi apparatus, endosomes and the nucleus has also been reported (Watt *et al.*, 2002; Tan *et al.*, 2015). $PI(4,5)P_2$ has multiple roles at the PM including endocytosis or actin rearrangements (Sun *et al.*, 2013).

Phosphoinositides (PI)	Total lipid content (%)	Main localization	Other localization	Function
PI	80 %	ER		Phosphorylated PI precursor
PI(3)P	0,5 - 1,5%	Endosomes, MVBs, autophagosomes	Golgi apparatus, ER	Endosomal trafficking, autophagy, cytokinesis, exocytosis and cell signaling
PI(4)P	10 %	Golgi apparatus	Plasma membrane, endosomes, autophagosomes, lysosomes, ER	Vesicular trafficking, lipid metabolism, mitochondrial fission
PI(5)P	0,1 - 0,5%	Plasma membrane, Golgi apparatus, ER, nucleus	Endosomes, autophagosomes	Actin rearrangements, vesicular trafficking, autophagy, gene expression
$PI(3,4)P_2$	0,1 - 1%	Plasme membrane, endosomes, ER	Lysosomes, MVBs	Endocytosis, cytoskeleton rearrangements
$PI(3,5)P_2$	0,1 - 1%	Endosomes, lysosomes	MVBs	Endosomal fission and fusion, retrograde transport
$PI(4,5)P_2$	10 %	Plasma membrane	Golgi apparatus, endosomes, ER, nucleus	Endocytosis, exocytosis, endosomal trafficking, phagocytosis, actin cytoskeleton assembly, polarization, adhesion, cell migration, PIP3 precursor
$PI(3,4,5)P_3$	0,1 - 1%	Plasma membrane	Nucleus	Cell survival, cell proliferation, actin cytoskeleton rearrangements, gene expression

Table 3. Phosphoinositides localisation and function (adapted from Viaud and Payrastre, 2015).

Interestingly, there is increasing evidence for a role of $PI(4,5)P_2$ in endolysosomal trafficking and recycling, as well as autophagy (Tan *et al.*, 2015). Phosphatidylinositol 3,4,5-triphosphate ($PI(3,4,5)P_3$) is found at low levels at the PM and its local concentration increases following the engagement of membrane receptors at the onset of phagocytosis (Salamon and Backer, 2013) (**Table 3**). PM is also enriched in phosphatidylinositol 3,4-biphosphate ($PI(3,4)P_2$), a lipid involved in endocytosis and present within membranes of endosomes, MVBs and lysosomes (Posor *et al.*, 2013; Xie *et al.*, 2013; Marat and Haucke, 2016). Finally, phosphatidylinositol 5-phosphate (PI(5)P) accumulates in the nuclear membrane as well as in

the PM under stress or infection by bacterial pathogens such as *Shigella flexneri* (Ramel *et al.*, 2011; Viaud *et al.*, 2014a; Viaud *et al.*, 2014b) (**Table 3**). PI(5)P is also found in low abundance in the ER, the Golgi apparatus, early endosomes and autophagosomes (Sarkes and Rameh, 2010; Vicinanza *et al.*, 2015). Interestingly, this lipid has recently been reported to play a role in gene expression (Vicinanza *et al.*, 2015; Hasegawa *et al.*, 2017).

(iii) Lipid-binding domains

Lipids are capable of interacting with proteins by means of dedicated lipid-binding domains with a wide range of affinities and specificities for lipid species (Lemmon, 2008). Lipid-binding domains are short sequence motifs that are often enriched in basic and aromatic residues (such as lysine and arginine), thus allowing proteins to bind negatively charged lipids (Saliba *et al.*, 2015). Lipid-binding domains can specifically recognise membrane lipids or sense biophysical properties of membranes such as charge, amphiphilicity or curvature (Lemmon, 2008). They include at least 17 different domains described in **Table 4**.

In contrast to eukaryotic lipid-binding domains, only few prokaryotic lipid-binding domains have been identified in bacterial proteins. Indeed, a handful of bacterial proteins have been reported to specifically bind lipids in eukaryotic cells without presenting canonical lipid-binding domains (Pizarro-Cerdá *et al.*, 2015; Martinez *et al.*, 2018). For example, the *C. burnetii* effector CvpB interacts with PI(3)P via its N-terminal domain, which does not display any known lipid-binding domain (Martinez *et al.*, 2016). Other effectors as the *Salmonella* typhimurium effectors SteA and SopA or the *Shigella flexneri* effector IpgB1 interact with PIs (Weigele *et al.*, 2017) and three non-canonical PI(3)P-binding domains have been recently identified in *L. pneumophila* effectors (*Legionella* effector domains LED006, LED027, LED035) (Nachmias *et al.*, 2019). Some of these effectors encode domains that share similarities with lipid-binding domains found in eukaryotes, such as short motifs enriched in basic residues.

Alternatively, other bacterial proteins mimic eukaryotic lipid-binding domains. For example, the *Vibrio parahaemolyticus* effector VopS displays a PX-like domain that interact with PI(4,5)P_2 at the PM (Salomon *et al.*, 2013) and the *Bacillus subtilis* membrane protein SpoVM that acts as a BAR domain-containing protein, capable of sensing membrane curvature (Ramamurthi *et al.*, 2006).

Interestingly, prokaryotic PI(4)P-binding domains have been also identified in *L. pneumophila* effectors (Del Campo *et al.*, 2014; Luo *et al.*, 2015) (**Table 4**). Three effectors (SidM, Lem4 and Lem28) bind PI(4)P through a P4M (PtdIns4P binding of SidM) domain (Brombacher *et al.*, 2009; Hubber *et al.*, 2014) and two homologous effectors (SidC and SdcA)

bind PI(4)P via a P4C (PtdIns4P binding of SidC) domain (Ragaz *et al.*, 2008; Schoebel *et al.*, 2010; Hsu *et al.*, 2014). Both types of domains display positively charged residues in a binding pocket, as often observed in eukaryotic lipid-binding domains. However, these PI-binding domains actually do not share any amino acid sequence or structural homology to known eukaryotic PI-binding proteins. This highlights the large diversity of lipid-binding domains that recognise membrane lipids with various affinity and often high specificity.

Domain	Typical size (in amino acids)	Lipid target	Dimerisation	Membrane curvature sensor
PH (Pleckstrin homology)	~120	PIs, PtdSer, PA, sphingolipids	Sometimes	No
FYVE (Fab1, YOTB, Vac1, and EEA1)	~80	PI(3)P	Most of cases	No
PX (Phox homology)	~100-140	PIs, but mostly PI(3)P	Most of cases	No
C1 (Conserved region-1)	~50	DAG	No	No
C2 (Conserved region-2)	~130-160	PtdSer, PtdCho, $PI(3,4,5)P_3$, $PI(4,5)P_2$	No	No
Tubby	~260	PI(3)P, PI(5)P	n/a	No
PHD (Plant homeodomain)	~50-80	PI(5)P	n/a	No
PROPPINs (β–propellers that bind phosphoinositides)	~500	$PI(3,5)P_2$, sometimes PI(3)P	No	No
GOLPH3 (Golgi phosphoprotein 3)	~260	PI(4)P	n/a	No
PTB (phosphotyrosine-binding)	~100-170	PI(4)P, $PI(4,5)P_2$	n/a	No
PDZ (PSD-95, Discs Large, and ZO-1)	~80-100	$PI(4,5)P_2$	n/a	No
GRAM (glucosyltransferases, RAB-like GTPase activators, and myotubularins)	~70	PI(5)P, $PI(3,5)P_2$	n/a	No
GLUE (GRAM-like ubiquitin-binding in EAP45)	~290	$PI(3,4,5)P_3$	n/a	No
FERM (4.1, ezrin, radixin, moesin)	~150	$PI(4,5)P_2$	n/a	No
ANTH (AP180 N-terminal homology)	~280	$PI(4,5)P_2$	Yes	Yes
ENTH (Epsin N-terminal homology)	~150	$PI(4,5)P_2$	No	No
BAR (Bin, Amphiphysin, and Rvs)	~240-320	Phospholipids, but mostly $PI(4,5)P_2$ and PtdSer	Yes	Yes
N-BAR (N-terminal helix BAR)	~240-320	Phospholipids	Yes	Yes, and promotes positive cuvature
F-BAR (extended Fes/CIP4 homology BAR)	~240-320	Phospholipids	Yes	Yes, and promotes positive cuvature
I-BAR (inverse-BAR)	~240-320	Phospholipids	Yes	Yes, and promotes negative cuvature
P4C (PtdIns4P binding of SidC)	~130	PI(4)P	n/a	No
P4M (PtdIns4P binding of SidM)	~130	PI(4)P	n/a	No

Table 4. Summary of eukaryotic and prokaryotic phospholipid-binding domains (adapted from Lemmon, 2008; Pemberton and Balla, 2019). n/a : not applicable

To investigate the spatial organisation and dynamics of lipids in living cells, a large panel of lipid biosensors interacting with PIs and other lipids including LBPA, PtdSer, PA, DAG (Diacylglycerol) or cholesterol (Wills *et al.*, 2018) are extensively used (Várnai *et al.*, 2017; Wills *et al.*, 2018). These can be divided into 4 categories : lipid-binding domains, toxin domains, antibodies and fluorophore-labeled lipids (Maekawa and Fairn, 2014; Wills *et al.*, 2018) (**Figure 18**) (**Table 5**).

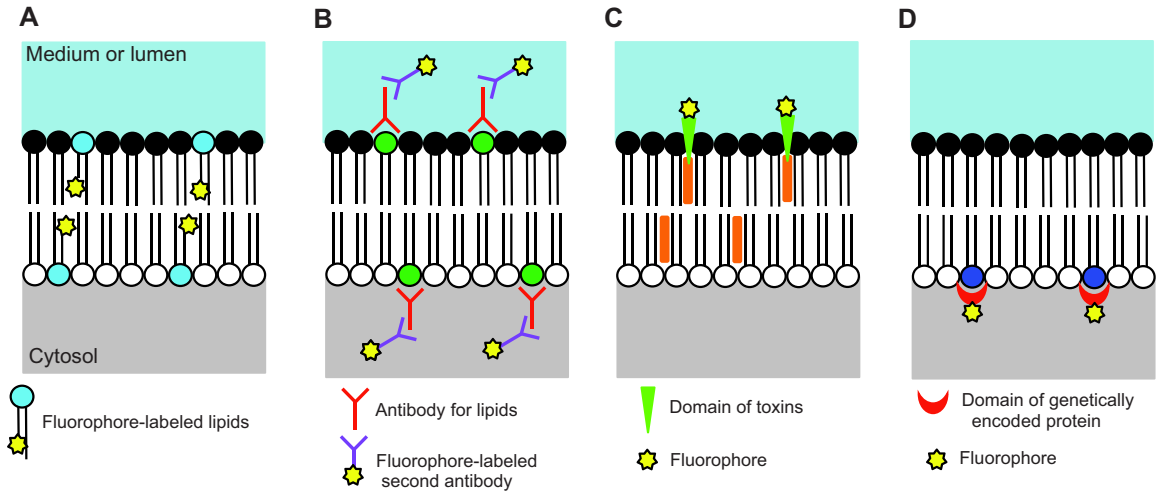

Figure 18. Schematic representation of the different types of lipid biosensors (from Maekawa and Fairn, 2014). (A-D) Schematics of the four different types of commonly used lipid biosensors : **A.** fluorophore-labeled lipids, **B.** antibodies, **C.** toxin domains and **D.** genetically encoded protein domains.

Lipid	Biosensor	Localization
Cholesterol	Filipin TopFluor-cholesterol Perfringolysin O-D4	PM, endosomes Endosomes, Golgi PM (outer)
SM	Lysenin	PM (exoplasmic)
LBPA	anti-LBPA antibody	LE, lysosomes
PS	Lact-C2 Anti-PS antibody	PM (inner), endosomes, TGN
PA	PASS/2xPABD (spo20p)	PM, ER
DAG	PKCδ-C1	Golgi, PM (inner); phagosomes
PI(3)P	2xFYVE-EEA1 PX-p40^{phox}	EE
PI(4)P	N-PH-ORP5 N-PH-ORP8 PH-OSBP PH-FAPP1 P4M-SidM P4C-SidC	PM Golgi, PM PM, Golgi, Endosomes
PI(5)P	3xPHD (ING2)	PM, nucleus
PI(3,4)P_2	PH-TAPP1-CT PH-Akt	PM PM, endosomes
PI(3,5)P_2	ML1-N2x2	EE, LE, lysosomes
PI(4,5)P_2	PH-PLCδ	PM
PI(3,4,5)P_3	PH-Akt PH-Btk	PM

Table 5. Commonly used lipid biosensors (adapted from Maekawa and Fairn, 2014; Wills et al., 2018).

2.2.2.2 Subversion of host lipid metabolism by *Coxiella burnetii*

Intracellular replication of vacuolar pathogens require the generation of a host-derived compartment. Thus host lipids are commonly manipulated by these bacteria to establish infections (van der Meer-Janssen *et al.*, 2010; Pizarro-Cerdá *et al.*, 2015). In the case of *C. burnetii*, several studies have demonstrated that the subversion of host cell lipids such as cholesterol and phosphoinositide metabolism, is crucial for CCV biogenesis and intracellular replication (Gilk *et al.*, 2013; Martinez *et al.*, 2016; Samanta *et al.*, 2017; Mulye *et al.*, 2017).

(i) Manipulation of cholesterol

Cholesterol is an important lipid required for both *C. burnetii* internalisation and CCV biogenesis. Indeed, DHCR24(24-Dehydrocholesterol Reductase)$^{-/-}$ cells, which are unable to synthesise endogenous cholesterol, fail to efficiently internalise *C. burnetii* (Gilk *et al.*, 2013). Similarly, the use of inhibitors of cholesterol metabolism severely impacts CCV biogenesis and intracellular replication (Howe and Heinzen, 2006). The CCV membrane is enriched in sterols, particularly in cholesterol, and contains the lipid raft-associated proteins flotillin-1 and -2, creating organised microdomains that may recruit important proteins involved in CCV biogenesis (Howe and Heinzen, 2006). Interestingly, *C. burnetii* increases host cell cholesterol content by up-regulating the expression of genes involved in cholesterol biosynthesis and exogenous cholesterol uptake (Gilk *et al.*, 2013) (**Figure 19**). However, *C. burnetii* does not appear to generate cholesterol itself and seems to actively manipulate the cholesterol metabolism of the host cell. Indeed, the *C. burnetii* genome encodes two eukaryotic-like sterol reductases, CBU1158 (a putative Δ7 sterol reductase) and CBU1206 (a putative Δ24 sterol reductase). (Seshadri *et al.*, 2003; Beare *et al.*, 2009) (**Figure 19**). However, only the enzymatic activity of CBU1206 has been experimentally demonstrated, suggesting that CBU1206 may act on the final stages of cholesterol biosynthesis in mammalian cells. The presence of cholesterol in CCVs could originate from its fusion with cholesterol-rich multivesicular bodies (Gilk *et al.*, 2013) as well as the bacterial re-routing of both endogenous and exogenous cholesterol trafficking pathways (Mulye *et al.*, 2017) (**Figure 19**). Recent studies also showed that lipid droplets (LDs), which are major cellular components for the storage of lipids and in particular cholesterol, is important for *C. burnetii* intracellular growth suggesting that *C. burnetii* uses multiple pathways to recruit cholesterol to CCVs (Mulye *et al.*, 2018). On the other hand, the alteration of cholesterol homoeostasis by increasing cholesterol levels affects CCV size and bacterial growth by further acidifying CCVs, thus indicating that

C. burnetii requires a well-controlled cholesterol homeostasis (Mulye *et al.*, 2017). To this aim, *C. burnetii* probably manipulates host mechanisms to control local concentrations of cholesterol. A recent study has investigated the role of oxysterol-binding protein (OSBP)-related protein 1, long (ORP1L) in CCV biogenesis, as this eukaryotic lipid-binding protein is involved in cholesterol-dependent endocytic trafficking as well as interactions between endosomes and the ER. ORP1L is indeed recruited to CCVs in a Dot/Icm-dependent manner, where it controls CCV membrane dynamics as well as CCV-ER interactions (Justis *et al.*, 2017) (**Figure 19**). Given the role of ORP1L in cholesterol dynamics, it has been suggested that *C. burnetii* may control cholesterol trafficking at CCVs by targeting ORP1L in order to maintain cholesterol homeostasis. This depends on the activity of the T4BSS, however, to date, the identification and the role of *C. burnetii* effectors manipulating host cholesterol metabolism remain elusive.

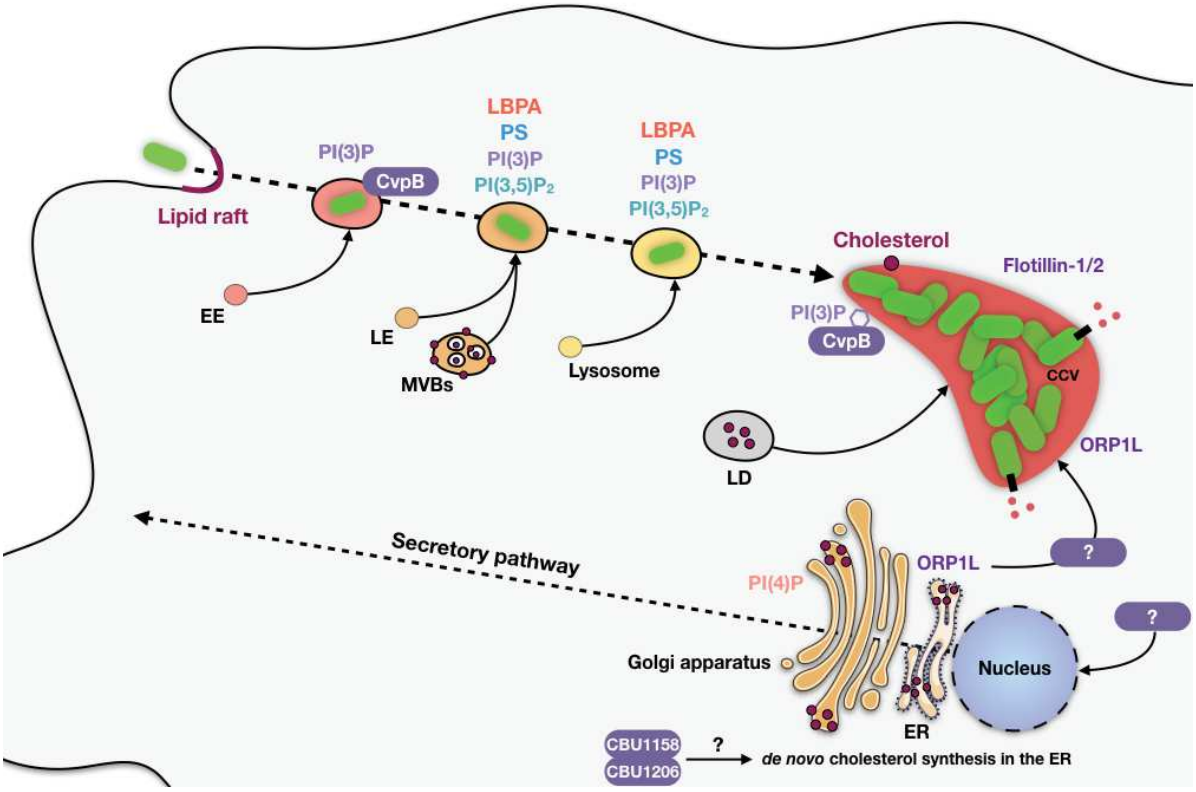

Figure 19. Manipulation of host lipid metabolism by *C. burnetii*. Cholesterol is a main factor in *C. burnetii* lifestyle in both internalisation via cholesterol-rich lipid rafts and CCV biogenesis. MVBs and lipid droplets traffic to the CCV and may serve as source of cholesterol in CCV membrane. CBU1158 and CBU1206 may act on the de novo cholesterol synthesis in the ER and an unknown *C. burnetii* effector targets the host gene expression to manipulate cholesterol homeostasis. PI(3)P metabolism is another host lipid metabolism hijacked by *C. burnetii*. CvpB binds PI(3)P at early endosomes and enriches this phospholipid at CCVs. This is required to favour the autophagy-mediated homotypic fusion between CCVs.

(ii) Manipulation of phosphoinositides

Given the important role of PIs in host cells, it is not surprising that intravacuolar bacteria have developed strategies to hijack PI metabolism, either for their uptake or for the biogenesis of their replicative compartment. To this aim, bacterial pathogens secrete effectors that directly bind PIs (Hilbi *et al.*, 2011) and/or modify their metabolism (Weber *et al.*, 2009). Several studies demonstrated that *C. burnetii* also has the capacity to hijack PI metabolism. Indeed, *C. burnetii* manipulates PI(3)P metabolism for an optimal development of its CCV through the action of CvpB (*Coxiella* vacuolar protein B, also called Cig2) (Newton *et al.*, 2014; Martinez *et al.*, 2016; Kohler *et al.*, 2016) (**Figure 19**). The effector localises at CCVs and early endosomes by interacting with PI(3)P and PS, and perturbs the recruitment of the PI 5-kinase PIKfyve thus preventing the phosphorylation of PI(3)P to PI(3,5)P_2. Thus, CvpB plays a dual role during *C. burnetii infection*. First, CvpB promotes homotypic fusion of CCVs by recruiting and stabilising the autophagosomal machinery at CCVs via PI(3)P-binding. Second, CvpB triggers enlargement and clustering of early endosomes, leading to the formation of large PI(3)P-positive compartments which fuse with CCVs for vacuole expansion (**Figure 20**). Mutation in *cvpB* leads to a multivacuolar phenotype, rescuable by gene complementation, thus showing the central role of CvpB in CCV homotypic fusion (**Figure 20**). The *in vivo* relevance of this process has been highlighted in the insect model *Galleria mellonella* (Martinez *et al.*, 2016) and SCID mice (van Schaik *et al.*, 2017). In both infection models, *cvpB*::Tn mutant displayed decreased colonisation and prolonged host survival, showing the importance of PI metabolism manipulation for CCV biogenesis and virulence. To date, only one *C. burnetii* T4BSS effector has been identified as manipulating PI metabolism. However, there is preliminary evidence that *C. burnetii* secretes other PI-binding effectors to promote membrane supply to the forming CCV upon infection.

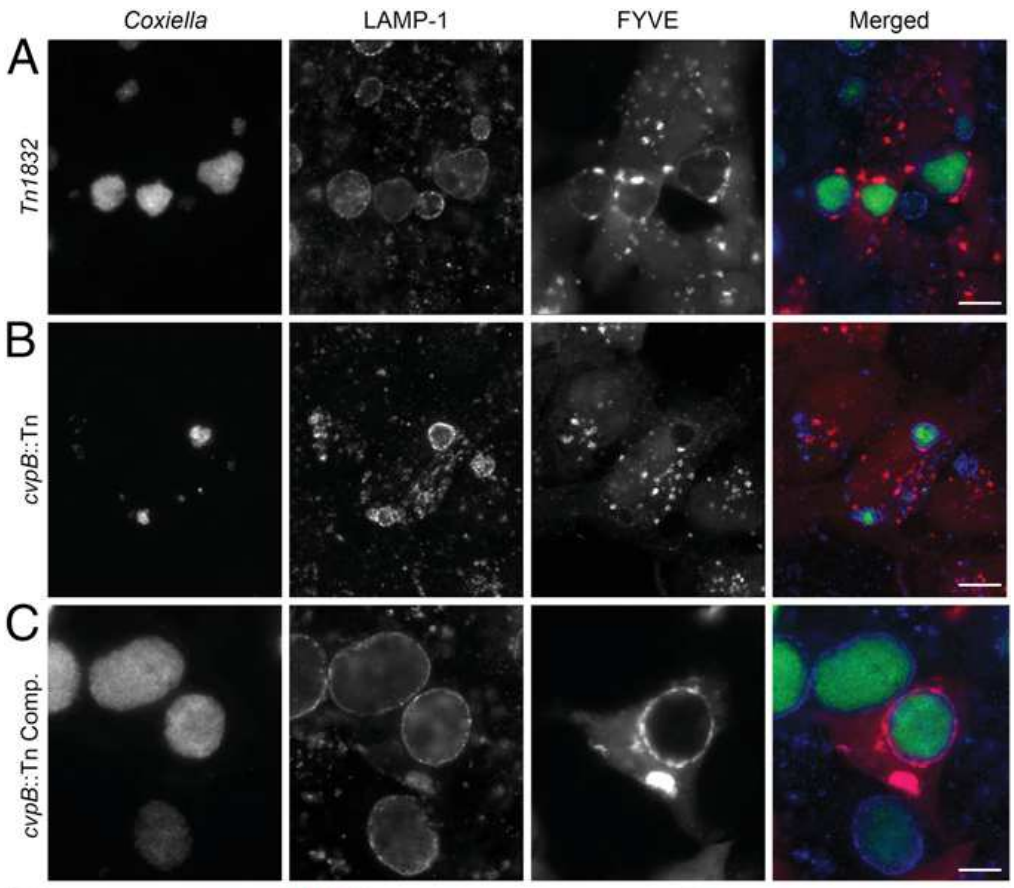

Figure 20. *C. burnetii* effector CvpB triggers the recruitment of PI(3)P at CCV membrane (from Martinez *et al.*, 2016). U2OS cells stably expressing the PI(3)P probe mCherry-2xFYVE (red) were infected with WT *C. burnetii* (Tn1832; **A**), the *cvpB*::Tn mutant (**B**) or the complemented strain (**C**) for 3 days. PI(3)P co-localises with LAMP1 (blue) at CCVs surrounding *C. burnetii* colonies (green) in a CvpB-dependent manner. (Scale bars: 10μm).

2.2.3 Impact of technological advances on *C. burnetii* research

In the following review article, we focus on how the major technological advances have impacted the study of host-pathogen interactions mediated by the zoonotic pathogen *Coxiella burnetii*. We first introduce *C. burnetii* infections to underline its unique intracellular adaptation. Next, we discuss how the development of an axenic culture medium in 2009 has dramatically accelerated the development and implementation of innovative tools to investigate the biogenesis of CCVs, from mutagenesis to screening approaches.

From neglected to dissected: How technological advances are leading the way to the study of *Coxiella burnetii* pathogenesis

Burette M and Bonazzi M. Cell Microbiol. 2020 Apr;22(4):13180..

Received: 10 October 2019 | Revised: 8 January 2020 | Accepted: 19 January 2020

DOI: 10.1111/cmi.13180

SPECIAL ISSUE - REVIEW

WILEY

From neglected to dissected: How technological advances are leading the way to the study of *Coxiella burnetii* pathogenesis

Melanie Burette | Matteo Bonazzi

IRIM, UMR 9004 CNRS, Université de Montpellier, Montpellier, France

Correspondence
Matteo Bonazzi, IRIM, UMR 9004 CNRS, Université de Montpellier, Montpellier, France.
Email: matteo.bonazzi@irim.cnrs.fr

Funding information
Agence Nationale de la Recherche, Grant/Award Numbers: ANR- 17-CE15-0021, ANR-13-IFEC-0003, ANR-14-CE14-0012-01

Abstract

Coxiella burnetii is an obligate intracellular bacterial pathogen responsible for severe worldwide outbreaks of the zoonosis Q fever. The remarkable resistance to environmental stress, extremely low infectious dose and ease of dissemination, contributed to the classification of *C. burnetii* as a class B biothreat. Unique among intracellular pathogens, *C. burnetii* escapes immune surveillance and replicates within large autophagolysosome-like compartments called *Coxiella*-containing vacuoles (CCVs). The biogenesis of these compartments depends on the subversion of several host signalling pathways. For years, the obligate intracellular nature of *C. burnetii* imposed significant experimental obstacles to the study of its pathogenic traits. With the development of an axenic culture medium in 2009, *C. burnetii* became genetically tractable, thus allowing the implementation of mutagenesis tools and screening approaches to identify its virulence determinants and investigate its complex interaction with host cells. Here, we review the key advances that have contributed to our knowledge of *C. burnetii* pathogenesis, leading to the rise of this once-neglected pathogen to an exceptional organism to study the intravacuolar lifestyle.

KEYWORDS

Coxiella burnetii, effector proteins, host-pathogen interactions, molecular genetics, phenotypic screening

1 | INTRODUCING *COXIELLA BURNETII*

Coxiella burnetii is a Gram negative obligate intracellular pathogen, and the causative agent of Q fever, a worldwide zoonotic disease (Eldin et al., 2017). Animal coxiellosis is mostly associated with abortion, stillbirths and weak offspring (Figure 1). Desiccation of placental materials, excretions of birthing fluids, urine, faeces and milk from infected animals contribute to shed *C. burnetii* into the environment (Eldin et al., 2017). Transmission to humans results from exposure to contaminated aerosols and dust (Figure 1). In humans, *C. burnetii* infections are often asymptomatic and self-limiting, however, 40% of individuals infected with *C. burnetii* develop an acute disease which is associated with a flu-like syndrome, pneumonia, hepatitis and chronic fatigue (Eldin et al., 2017) (Figure 1). Acute disease may convert into a chronic illness with severe complications, including endocarditis (Eldin et al., 2017). An important risk factor for Q fever outbreaks is the multiple zoonotic reservoirs of *C. burnetii*, which include domestic livestock and wild animals (mammals, reptiles, birds and ticks) (Eldin et al., 2017). *C. burnetii* is extremely infectious, with 1-to-10 bacteria being sufficient to cause disease (Brooke et al., 2013). The low infectious dose coupled to remarkable environmental stability contribute to the significant spreading of *C. burnetii* infections well away from the outbreak source and led to the classification of *C. burnetii* as a category B biothreat (Madariaga et al., 2003).

Coxiella burnetii is a stealth pathogen that actively escapes innate immune recognition by inhibiting the NF-κB pathway (Mahapatra et al., 2016) and inflammasome activation (Cunha et al., 2015). Infected cells are also protected from apoptosis, thereby preserving the bacterial replicative niche over long periods (Lührmann et al., 2017). *C. burnetii* enters macrophages by phagocytosis through the

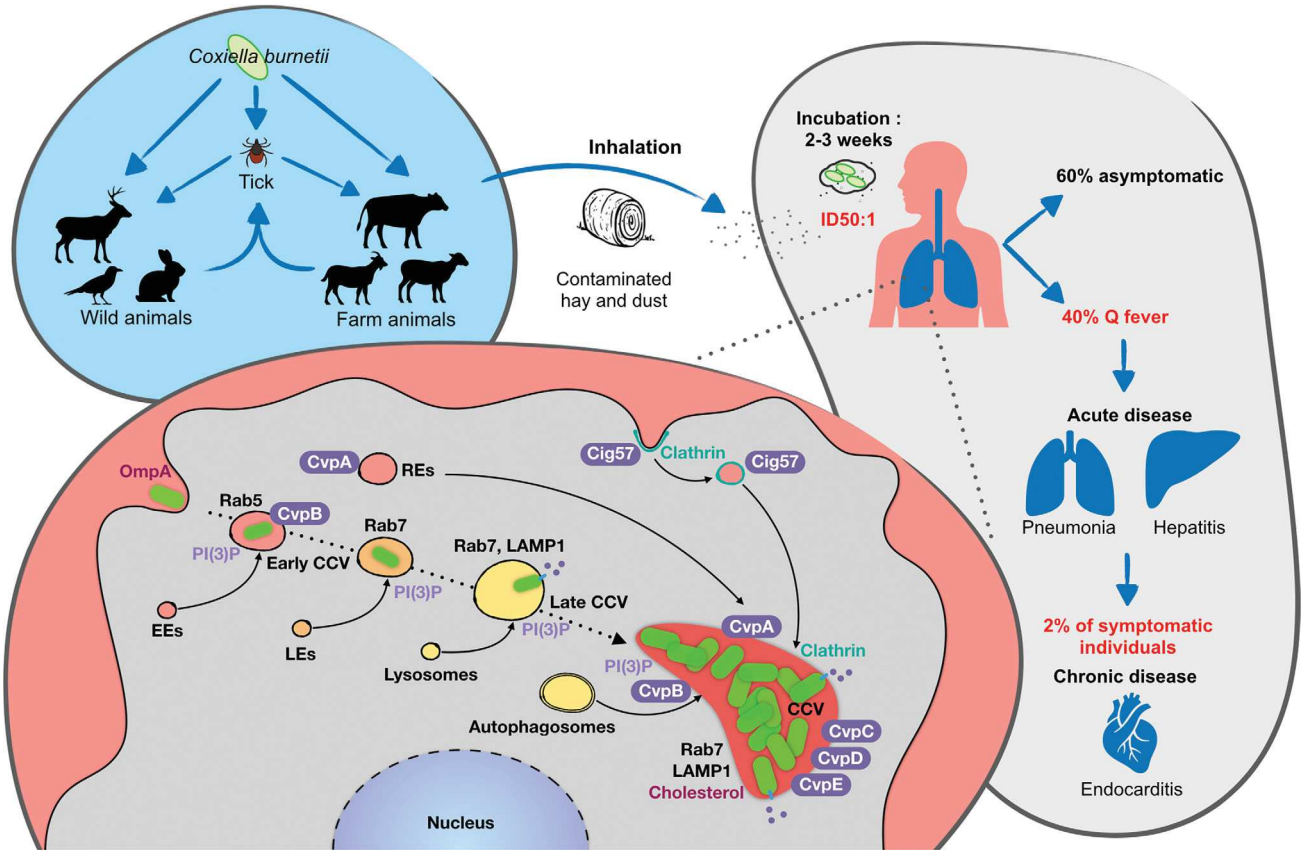

FIGURE 1 Overview of *C. burnetii* infections. *C. burnetii* is an obligate intracellular pathogen which infects wild and farm animals. Bacteria are shed in the environment with birth products and excretions leading to the contamination of hay and dust. Human infection occurs 2–3 weeks after the inhalation of contaminated particles, followed by the internalisation of *C. burnetii* by alveolar macrophages. Human Q fever remains asymptomatic in 60% of infected individuals, whereas 40% develop an acute, febrile disease, which can turn into a chronic disease with more severe symptoms including endocarditis. *C. burnetii* invades eukaryotic cell through phagocytosis, which is facilitated by the bacterial invasin OmpA. Early CCVs mature along the endocytic pathway by successive fusion events with early endosomes (EEs), late endosomes (LEs) and lysosomes. Acidification of the CCV activates bacterial metabolism and the translocation of bacterial effector proteins (purple circles and ovals) by the Dot/Icm secretion system. Several effector proteins are collectively beneficial for the biogenesis of the mature CCV where bacterial replication occurs. These include the Cvp family (for *Coxiella* vacuolar proteins) of effectors that localise at CCV membranes and manipulate host membrane trafficking pathways. CvpA interacts with the clathrin adaptor AP2 at recycling endosomes (REs), re-routing these compartments to the forming CCV. CvpB binds PI(3)P at early endosomes and enriches this phospholipid at CCVs. This is required to favour the autophagy-mediated homotypic fusion between CCVs. Although not a Cvp, Cig57 interacts with the clathrin adaptor FCHO2 at clathrin-coated pits and re-routes clathrin-mediated membrane traffic to the CCV

interaction with αVβ3 integrins (Capo et al., 1999). In contrast, in non-phagocytic cells, internalisation is facilitated by the invasin OmpA (Outer membrane protein A) (Martinez et al., 2014) (Figure 1). Following internalisation, bacteria reside within early endosomal compartments, also called early CCVs, that passively mature along the endocytic pathway by successive fusion events with early and late endosomes and lysosomes (Figure 1). Maturation is accompanied by the acidification of the CCV lumen (Heinzen et al., 1996), which is required to activate bacterial metabolism (Hackstadt and Williams, 1981) and the translocation of bacterial effector proteins by a Dot/Icm Type 4b Secretion System (T4SS) (Newton et al., 2013). Thus, by 48 h post-infection, cells display a single, large, mature CCV, where markers of multiple membrane compartments co-exist (Dragan and Voth, 2019), which is indicative of the capacity of *C. burnetii* to hijack multiple host membrane trafficking pathways (Figure 1). Importantly, the biogenesis of these remarkable compartments is a two-step process requiring both cellular and bacterial factors. This review will focus on the recent technological advances that fostered remarkable progress in our understanding of the complex host/pathogen interplay that controls the generation of the *C. burnetii* replicative niche.

2 | THE LONG AND WINDING ROAD (TO GENETIC MANIPULATION)

Together with its high infectivity, the obligate intracellular nature of *C. burnetii* has imposed severe constraints on the study of its pathogenesis. An important step towards the development of tools to investigate *C. burnetii* infection was the isolation of a Phase II variant

(NMII) of the Nine Mile Phase I strain (NMI), presenting a single deletion of 21 genes involved in lipopolysaccharide biosynthesis and displaying loss-of-virulence phenotype in animal models (Moos and Hackstadt, 1987; Hoover et al., 2002). Thus, NMII was allowed for manipulation in biosafety level-2 (BSL-2) environments (Figure 2D), as opposed to other *C. burnetii* strains that require manipulation in

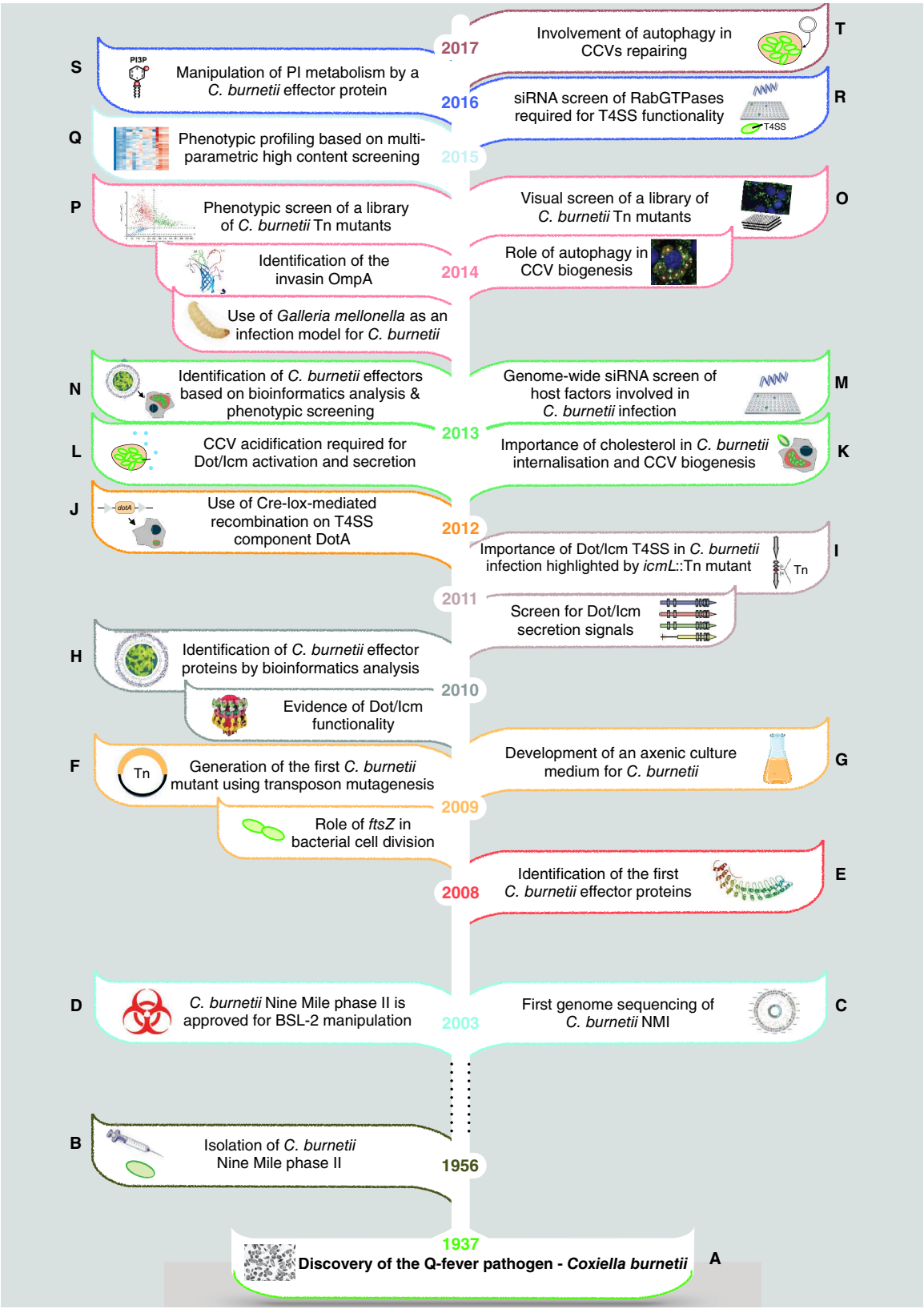

FIGURE 2 Milestone discoveries that have contributed to the knowledge of *C. burnetii* pathogenesis

biosafety level-3 (BSL-3) confinement. Importantly, loss-of-virulence of NMII has no impact either on intracellular growth kinetics or development of CCVs in cultured cells, making NMII a relevant model to study host-pathogen interactions (Howe et al., 2010).

Nevertheless, bacterial amplification of *C. burnetii* in embryonated eggs and/or cultured cells represented a real obstacle for its genetic manipulation. Indeed, transposon mutagenesis allowed the generation of *C. burnetii* mutants (Beare et al., 2009); however, amplification and isolation of these from infected cells ruled out the possibility of isolating mutations in virulence genes. Thus, until 2011, *ftsZ* was the only *C. burnetii* gene characterised using Himar1 transposon mutagenesis (Beare et al., 2009) (Figure 2F).

Whole-genome sequencing of *C. burnetii* NMI RSA493 in 2003 allowed the identification of typical features, including a Dot/Icm secretion system, which is highly homologous to that of *L. pneumophila* (Seshadri et al., 2003) (Figure 2C). This finding was pivotal to develop bioinformatics-based approaches to predict effector proteins-coding genes. These revealed that similar to *L. pneumophila*, effector proteins translocated by *C. burnetii* encode a C-terminal secretion signal called the E-block motif and are mostly under the control of a PmrA response regulator (Zusman et al., 2007). Due to the genetic intractability of *C. burnetii* at that time, candidate effector proteins were tested for secretion using *L. pneumophila* as a surrogate model, exploiting the homologies between the Dot/Icm secretion systems of the two pathogens. This approach allowed the Roy laboratory to validate the translocation of four *C. burnetii* effector proteins encoding ankyrin repeat homology domains (ARHDs) (Pan et al., 2008) (Figure 2E). Later work from the Samuel laboratory reported the first large-scale, bioinformatics-based identification of *C. burnetii* effector proteins and used the *L. pneumophila* system to validate the secretion of 32 new T4SS substrates (Chen et al., 2010) (Figure 2H). Moreover, using a shuttle plasmid system for the expression of recombinant proteins in *C. burnetii*, Chen and colleagues also demonstrated that the functionality of the Dot/Icm secretion system (Chen et al., 2010).

One year later, a genetic screen of *C. burnetii* proteins carrying C-terminal secretion signals led to the identification of additional effector proteins (Carey et al., 2011) (Figure 2I). For this study, wild type (wt) *L. pneumophila* or the T4SS-defective *ΔdotA* mutant were transformed with a library containing adenylate cyclase enzyme (CyaA)-tagged random fragments of *C. burnetii* genome, leading to the validation of seven additional *C. burnetii* effectors (Carey et al., 2011). These were further tested for their intracellular localization and function, which indicated a possible implication in the manipulation of host membrane trafficking. Of note, this is the first study to report a replication phenotype associated with a transposon insertion in the *C. burnetii* Dot/Icm gene *icmL* (*icmL*::Tn), thus demonstrating the importance of *C. burnetii* effector protein translocation for infection (Carey et al., 2011) (Figure 2I). Today, the development of tailored bioinformatics algorithms for the identification of T4SS effector proteins led to the identification of over 140 candidate *C. burnetii* T4SS effectors (Voth et al., 2009; Chen et al., 2010; Carey et al., 2011; Maturana et al., 2013; Weber et al., 2013). Recent genome comparison of the *C. burnetii* strains NMII RSA493, Henzerling RSA331, G Q212, K Q154 and Dugway 5J108-111, revealed that many genes encoding candidate effector proteins are either pseudogenised or missing altogether, leaving only 44 out of the 143 identified effector protein-coding genes intact across all strains (Larson et al., 2016). Despite these significant advances, functional analysis of *C. burnetii* genes involved in virulence was still limited by the genetic intractability of this pathogen.

A game-changer in the study of *C. burnetii* infections has been the development of a synthetic medium (ACCM for Acidified Citrate Cysteine Medium), followed by the development of ACCM-2, allowing the extracellular culture of this obligate intracellular bacterium (Omsland et al., 2009, 2011) (Figure 2G). ACCM-2 development stems from metabolic requirement studies using microarrays, genomic reconstruction of metabolic pathways and metabolite typing (Omsland et al., 2009, 2011). These studies highlighted that *C. burnetii* requires acid activation buffer (pH 4.75), to reproduce the CCV microenvironment (Heinzen et al., 1996) and increase its metabolic potential as well as low oxygen levels (2.5%) to facilitate the bacterial micro-aerophilic respiration (Omsland et al., 2009, 2011). This scientific milestone finally enabled genetic manipulation of *C. burnetii*, leading to a new era in our understanding of its pathogenesis (Figure 2).

3 | FROM GENES TO FUNCTION: CHARACTERISATION OF *C. BURNETII* EFFECTORS INVOLVED IN VACUOLE BIOGENESIS

With the development of axenic culture, targeted deletion of *C. burnetii* was formally achievable (albeit remaining extremely challenging), and the role of *C. burnetii* effector proteins in infection could be tested directly. The Heinzen laboratory first exploited axenic culture with the generation of a *dotA* deletion mutant (Beare et al., 2012) (Figure 2J) and with the identification and characterisation of CvpA (for *Coxiella* vacuolar protein A). This effector protein localises at CCVs and reroutes recycling endosomes to this compartment by interacting with the clathrin adaptor protein AP2 (Larson et al., 2013) (Figure 1). In a follow-up study, the Heinzen laboratory identified four additional members of what constitutes today the Cvp sub-class of *C. burnetii* effector proteins (CvpA, CvpB/Cig2 and CvpC-to-E, Figure 1) (Larson et al., 2015). Accordingly, targeted deletion of *C. burnetii* vacuolar proteins severely affects the biogenesis of CCVs (Larson et al., 2013, 2015).

If targeted deletion of *C. burnetii* genes remains challenging, *Himar1*-based transposon mutagenesis has been extensively applied to the generation of libraries of *C. burnetii* mutants. Thus, by 2013, the Samuel laboratory reported the first study that combined bioinformatics-mediated identification of candidate effector proteins with transposon mutagenesis (Weber et al., 2013) (Figure 2N). Searching the *C. burnetii* genome for T4SS features (PmrA consensus sequences, E-block motifs and homologies with known effectors), led to the identification of 234 genes encoding putative *C. burnetii*

effector proteins. β-lactamase translocation assay in *L. pneumophila* validated 53 T4SS substrates, most of which were never reported before. Transposon mutagenesis showed that 10 effector proteins were involved in the biogenesis of CCVs and bacterial replication (Weber et al., 2013) (Figure 2N).

The following year, two independent studies reported the large-scale identification of *C. burnetii* virulence determinants based on the generation of two libraries of *C. burnetii* transposon mutants (Martinez et al., 2014; Newton et al., 2014) (Figure 2O, (r)). The Bonazzi library consisted of 3,000 GFP-tagged mutants, among which over 1,000 were sequenced, annotated and screened using quantitative, multiparametric image analysis to identify bacterial factors involved in host cell invasion, intracellular replication and persistence (Martinez et al., 2014, 2015). This approach allowed to validate the function of 16 out of the 22 genes constituting the *C. burnetii* Dot/Icm secretion system, characterise the phenotype associated with transposon insertions in 31 genes encoding effector proteins and identify the first *C. burnetii* invasin OmpA (for Outer membrane protein A), which is necessary and sufficient to trigger internalisation by non-phagocytic cells (Martinez et al., 2014) (Figures 1 and 2P). This study was also the first to report the use of the insect model *Galleria mellonella* to investigate *C. burnetii* virulence in vivo (Martinez et al., 2014).

The Roy laboratory used a modified-Himar1 expressing mCherry fluorescent protein to generate over 3200 mutants. These were visually screened in HeLa cells to identify genes important in the biogenesis of CCVs and bacterial replication using the lysosomal marker LAMP-1 to visualise the membranes of the *C. burnetii* replicative compartment (Newton et al., 2014) (Figure 2O). This approach allowed the isolation of mutants characterised by different intracellular phenotypes, including defects in intracellular replication and homotypic fusion of independent CCVs or the appearance of filamentous bacteria. Of note, mutants carrying a transposon insertion in gene encoding *CBU1751* (*cig57*) displayed a severe vacuole biogenesis defect (Newton et al., 2014). The Newton laboratory has further characterised the role of this effector protein in the development of CCVs and intracellular replication, showing that Cig57 subverts clathrin-mediated traffic by interacting with FCHO2, an accessory protein of clathrin-coated pits (Latomanski et al., 2016) (Figure 1). More recently, CTLC (clathrin heavy chain) has been observed at CCVs, where it plays an essential role in vacuole expansion (Latomanski and Newton, 2018). Importantly, CTLC recruitment to the CCV is related to autophagy, and conversely, the fusion of autophagosomes with CCVs is dependent on CTLC (Latomanski and Newton, 2018). The Roy visual screen also highlighted a multivacuolar phenotype associated with transposon insertions in the gene CBU0021 (*cig2*), identical to that previously observed following the knockdown of autophagy-related genes (McDonough et al., 2013), suggesting a functional link between a bacterial effector protein and the manipulation of a specific host cell function (Figure 2O). This hypothesis was further investigated, demonstrating that Cig2 contributes to the recruitment of the autophagy machinery to CCVs (Figure 1), thus facilitating their homotypic fusion and contributing to an enhanced bacterial virulence in the *Galleria mellonella* infection model (Kohler et al., 2016).

4 | IT TAKES TWO TO TANGO: ROLE OF HOST CELL PATHWAYS IN *C. BURNETII* VACUOLE BIOGENESIS

If on one hand effector proteins translocation is critical for pathogenesis, host cell proteins, lipids and membrane trafficking pathways also play a significant role in *C. burnetii* infections. As mentioned above, the maturation of CCVs along the endocytic pathway is a pre-requisite for effector proteins translocation (Newton et al., 2013)-(Figure 2L); thus, Rab GTPases of the endocytic pathway play a key role in *C. burnetii* intracellular replication (Figure 1) (Beron et al., 2002; Romano et al., 2007; Campoy et al., 2011). Indeed, silencing of either Rab5 or Rab7 correlates with effector protein translocation defects (Newton et al., 2016) (Figure 2R).

A comprehensive characterisation of the host cell components required for the biogenesis of CCVs was provided for the first time by a genome-wide screen using siRNA targeting eukaryotic genes in *C. burnetii*-infected HeLa cells (McDonough et al., 2013) (Figure 2M). Host determinants required for *C. burnetii* infection were identified by the analysis of the number and size of CCVs, revealing the importance of several eukaryotic pathways in critical infection events. As expected, the silencing of genes encoding pH-regulating proteins CLN3 and CLCN5, as well as components of the vacuolar ATPase resulted in a defect in the biogenesis of CCVs (McDonough et al., 2013). Besides, the depletion of the retromer cargo complex VPS26-VPS29-VPS35 leads to defective in bacterial replication, revealing a role for retrograde membrane trafficking in *C. burnetii* infections (McDonough et al., 2013). Interestingly, seminal work from the Colombo laboratory in the past decade demonstrated that the induction of autophagy favours the biogenesis of CCVs and that *C. burnetii* actively manipulates autophagy during infections (Gutierrez et al., 2005; Romano et al., 2007). However, the precise role of autophagy in CCVs' development remained to be characterised. The genome-wide screening approach of the Roy laboratory revealed that knockdown of autophagy proteins syntaxin-17, ATG5 and ATG12 results in the formation of multiple CCVs of smaller size as compared to control cells (McDonough et al., 2013). It was later demonstrated that this multivacuolar phenotype is the result of the defective homotypic fusion of CCVs (Newton et al., 2014; Martinez et al., 2016).

The Voth and Heinzen laboratories have further explored the complex interplay between *C. burnetii* and autophagy by. The autophagy-associated cargo receptor p62 is actively recruited at CCVs, independently of LC3-interacting domains (Winchell et al., 2018). Interestingly, *C. burnetii* infections seem to preserve p62 from degradation upon induction of autophagy (Winchell et al., 2018). Accordingly, *C. burnetii* infections inhibit mTORC1, a master regulator of autophagy, by a non-canonical mechanism that does not result in accelerated autophagy, nor a block of the autophagic flux (Larson et al., 2019). Finally, autophagy is also involved in repairing the

membranes of CCVs during expansion, which are subject to transitory damage and loss-of-acidification (Mansilla Pareja et al., 2017) (Figure 2T).

Besides host cell proteins, lipids also play a significant role in the development of CCVs, which are rich in sterols (Gilk et al., 2010). Indeed, cholesterol homeostasis regulates CCVs biogenesis and intracellular survival of *C. burnetii* (Gilk et al., 2013; Mulye et al., 2017) (Figure 2K). Accordingly, *C. burnetii* actively manipulates cholesterol metabolism via a eukaryotic-like Δ24 sterol reductase (Gilk et al., 2010). Furthermore, an image-based supervised machine learning approach led to the identification of CvpB/Cig2 as the first *C. burnetii* effector protein to bind phosphoinositides and manipulate their metabolism (Martinez et al., 2016) (Figure 2S). Indeed, CvpB/Cig2 binds phosphatidylinositol-3-phosphate (PI[3]P) and phosphatidylserine (PS) and perturbs the activity of the PI3-kinase PIKFYVE. This inhibition results in an enrichment of PI(3)P at CCVs, which is essential for their homotypic fusion (Martinez et al., 2016). Importantly, despite the apparent defect in the biogenesis of CCVs, *cvpB* transposon mutants were unaffected in their capacity of replicating within infected cells. However, *cvpB* mutants are attenuated in the in vivo models *Galleria mellonella* (Martinez et al., 2016) and SCID mice (van Schaik et al., 2017), demonstrating that the biogenesis of CCVs can modulate *C. burnetii* virulence, independently of bacterial replication.

5 | TO INFINITY AND BEYOND (CONCLUSIONS)

As of today, *C. burnetii* stands as the sole example of an obligate intracellular bacterial pathogen for which a specific axenic culture medium has been developed. Consequently, research on this dangerous and complex pathogen has bloomed during this decade, with the development of genetic tools and phenotypic screening approaches to better understand the complex interactions established between *C. burnetii* and its host. The generation of libraries of *C. burnetii* transposon mutants combined with the development of multi-parametric screening approaches have allowed the rapid and unbiased identification of microbial genes involved in specific steps of the infectious process. This has been facilitated by the fact that the majority of *C. burnetii* transposon mutants isolated to date display a significant phenotype during infection (Martinez et al., 2014), suggesting a milder functional gene redundancy as compared to the closely related pathogen *L. pneumophila*. Accordingly, bioinformatics predicted ~150 effector proteins compared to the 300 translocated by *Legionella*.

Nevertheless, understanding how these newly identified virulence determinants manipulate host cell functions remains exceptionally challenging. Probably due to the complex nature of this compartment, a large proportion of the *C. burnetii* effector proteins identified and characterised to date are involved in the biogenesis of the CCV; however, proteins involved in the manipulation of other signalling pathways including apoptosis and inflammation have been identified and partially characterised. With the development of advanced bioinformatics approaches such as unsupervised machine learning, hierarchical clustering and Bayesian network analysis, we can now compare microbial-targeted and host-targeted phenotypic screens, to identify sets of bacterial and eukaryotic genes predicted to be involved in the same biological process during infection.

Despite the giant leaps taken since the development of axenic culture, many technical barriers still exist today. Directed mutagenesis remains challenging, limiting our studies to the mutants available in the transposon libraries hosted in the laboratories that undertook this endeavour. Nevertheless, our knowledge of this once-neglected pathogen is ever increasing. This will allow, in the near future, to address burning questions on *C. burnetii* pathogenesis, including a characterisation of the strategies used to evade immune recognition, cell-to-cell spread and, consequently, dissemination to distant organs (heart and liver) following infection of alveolar macrophages.

ACKNOWLEDGEMENTS

Work in our laboratory is supported by the Agence Nationale de la Recherche (ANR; ANR-14-CE14-0012-01, project AttaQ and ANR-17-CE15-0021, project QPID) and by the ERA-NET Infect-ERA (ANR-13-IFEC-0003, project EUGENPATH). We apologise to all colleagues whose work was not discussed in this review.

CONFLICT OF INTEREST

The authors declare no conflict of interest.

ORCID

Matteo Bonazzi https://orcid.org/0000-0001-5499-8759

REFERENCES

Beare, P. A., Larson, C. L., Gilk, S. D., & Heinzen, R. A. (2012). Two systems for targeted gene deletion in *Coxiella burnetii*. *Applied and Environmental Microbiology*, *78*, 4580–4589.

Beare, P. A., Howe, D., Cockrell, D. C., Omsland, A., Hansen, B., & Heinzen, R. A. (2009). Characterization of a *Coxiella burnetii* ftsZ mutant generated by Himar1 transposon mutagenesis. *Journal of Bacteriology*, *191*, 1369–1381.

Beron, W., Gutierrez, M. G., Rabinovitch, M., & Colombo, M. I. (2002). *Coxiella burnetii* localizes in a Rab7-labeled compartment with autophagic characteristics. *Infection and Immunity*, *70*, 5816–5821.

Brooke, R.J., Kretzschmar, M.E.E., Mutters, N.T., and Teunis, P.F. (2013) Human dose response relation for airborne exposure to *Coxiella burnetii*. *BMC Infectious Diseases 13*: 488 BMC Infectious Diseases.

Campoy, E. M., Zoppino, F. C. M., & Colombo, M. I. (2011). The early secretory pathway contributes to the growth of the Coxiella-replicative niche. *Infection and Immunity*, *79*, 402–413.

Capo, C., Lindberg, F. P., Meconi, S., Zaffran, Y., Tardei, G., Brown, E., … Mege, J. L. (1999). Subversion of monocyte functions by *Coxiella burnetii*: Impairment of the cross-talk between alphavbeta3 integrin and CR3. *Journal of Immunology*, *163*, 6078–6085.

Carey, K. L., Newton, H. J., Lührmann, A., & Roy, C. R. (2011). The *Coxiella burnetii* dot/Icm system delivers a unique repertoire of type IV effectors into host cells and is required for intracellular replication. *PLoS Pathogens*, *7*, e1002056.

Chen, C., Banga, S., Mertens, K., Weber, M. M., Gorbaslieva, I., Tan, Y., … Samuel, J. E. (2010). Large-scale identification and translocation of type IV secretion substrates by *Coxiella burnetii*. *Proceedings of the National Academy of Sciences*, *107*, 21755–21760.

Cunha, L. D., Ribeiro, J. M., Fernandes, T. D., Massis, L. M., Khoo, C. A., Moffatt, J. H., … Zamboni, D. S. (2015). Inhibition of inflammasome activation by *Coxiella burnetii* type IV secretion system effector IcaA. *Nature Communications*, *6*, 10205.

Dragan, A. L., & Voth, D. E. (2019). *Coxiella burnetii*: International pathogen of mystery. *Microbes and Infection*, 1–11.

Eldin, C., Mélenotte, C., Mediannikov, O., Ghigo, E., Million, M., Edouard, S., … Raoult, D. (2017). From Q fever to *Coxiella burnetii* infection: A paradigm change. *Clinical Microbiology Reviews*, *30*, 115–190.

Gilk, S. D., Beare, P. A., & Heinzen, R. A. (2010). *Coxiella burnetii* expresses a functional Δ24 sterol reductase. *Journal of Bacteriology*, *192*, 6154–6159.

Gilk, S. D., Cockrell, D. C., Luterbach, C., Hansen, B., Knodler, L. A., Ibarra, J. A., … Heinzen, R. A. (2013). Bacterial colonization of host cells in the absence of cholesterol. *PLoS Pathogens*, *9*, e1003107.

Gutierrez, M. G., Vázquez, C. L., Munafó, D. B., Zoppino, F. C. M., Berón, W., Rabinovitch, M., & Colombo, M. I. (2005). Autophagy induction favours the generation and maturation of the Coxiella-replicative vacuoles. *Cellular Microbiology*, *7*, 981–993.

Hackstadt, T., & Williams, J. C. (1981). Biochemical stratagem for obligate parasitism of eukaryotic cells by *Coxiella burnetii*. *Proceedings of the National Academy of Sciences*, *78*, 3240–3244.

Heinzen, R. A., Scidmore, M. A., Rockey, D. D., & Hackstadt, T. (1996). Differential interaction with endocytic and exocytic pathways distinguish parasitophorous vacuoles of *Coxiella burnetii* and *Chlamydia trachomatis*. *Infection and Immunity*, *64*, 796–809.

Hoover, T. A., Culp, D. W., Vodkin, M. H., Williams, J. C., & Thompson, H. A. (2002). Chromosomal DNA deletions explain phenotypic characteristics of two antigenic variants, phase II and RSA 514 (crazy), of the *Coxiella burnetii* nine mile strain. *Infection and Immunity*, *70*, 6726–6733.

Howe, D., Shannon, J. G., Winfree, S., Dorward, D. W., & Heinzen, R. A. (2010). *Coxiella burnetii* phase I and II variants replicate with similar kinetics in degradative phagolysosome-like compartments of human macrophages. *Infection and Immunity*, *78*, 3465–3474.

Kohler, L. J., Reed, S. R., Sarraf, S. A., Arteaga, D. D., Newton, H. J., & Roy, C. R. (2016). Effector protein Cig2 decreases host tolerance of infection by directing constitutive fusion of autophagosomes with the Coxiella-containing vacuole. *MBio*, *7*, 1–14.

Larson, C. L., Beare, P. A., Howe, D., & Heinzen, R. A. (2013). *Coxiella burnetii* effector protein subverts clathrin-mediated vesicular trafficking for pathogen vacuole biogenesis. *Proceedings of the National Academy of Sciences*, *110*, E4770–E4779.

Larson, C. L., Beare, P. A., Voth, D. E., Howe, D., Cockrell, D. C., Bastidas, R. J., … Heinzen, R. A. (2015). *Coxiella burnetii* effector proteins that localize to the Parasitophorous vacuole membrane promote intracellular replication. *Infection and Immunity*, *83*, 661–670.

Larson, C. L., Martinez, E., Beare, P. A., Jeffrey, B., Heinzen, R. A., & Bonazzi, M. (2016). Right on Q: Genetics begin to unravel *Coxiella burnetii* host cell interactions. *Future Microbiology*, *11*, 919–939.

Larson, C. L., Sandoz, K. M., Cockrell, D. C., & Heinzen, R. A. (2019). Non-canonical inhibition of mTORC1 by Coxiella burnetii promotes replication within a phagolysosome-like vacuole. *MBio*, *10*, 1–16.

Latomanski, E. A., & Newton, H. J. (2018). Interaction between autophagic vesicles and the Coxiella-containing vacuole requires CLTC (clathrin heavy chain). *Autophagy*, *14*, 1710–1725.

Latomanski, E. A., Newton, P., Khoo, C. A., & Newton, H. J. (2016). The effector Cig57 hijacks FCHO-mediated vesicular trafficking to facilitate intracellular replication of *Coxiella burnetii*. *PLoS Pathogens*, *12*, 1–24.

Lührmann, A., Newton, H. J., & Bonazzi, M. (2017). Beginning to understand the role of the type IV secretion system effector proteins in *Coxiella burnetii* pathogenesis. *Current Topics in Microbiology and Immunology*, *413*, 243–268.

Madariaga, M. G., Rezai, K., Trenholme, G. M., & Weinstein, R. A. (2003). Q fever: A biological weapon in your backyard. *The Lancet Infectious Diseases*, *3*, 709–721.

Mahapatra, S., Gallaher, B., Smith, S. C., Graham, J. G., Voth, D. E., & Shaw, E. I. (2016). *Coxiella burnetii* employs the dot/Icm type IV secretion system to modulate host NF-κB/RelA activation. *Frontiers in Cellular and Infection Microbiology*, *6*, 1–13.

Mansilla Pareja, M. E., Bongiovanni, A., Lafont, F., & Colombo, M. I. (2017). Alterations of the *Coxiella burnetii* replicative vacuole membrane integrity and interplay with the autophagy pathway. *Frontiers in Cellular and Infection Microbiology*, *7*, 1–17.

Martinez, E., Allombert, J., Cantet, F., Lakhani, A., Yandrapalli, N., Neyret, A., … Bonazzi, M. (2016). *Coxiella burnetii* effector CvpB modulates phosphoinositide metabolism for optimal vacuole development. *Proceedings of the National Academy of Sciences*, *113*, E3260–E3269.

Martinez, E., Cantet, F., & Bonazzi, M. (2015). Generation and multi-phenotypic high-content screening of *Coxiella burnetii* transposon mutants. *Journal of Visualized Experiments*, *2015*, 1–11.

Martinez, E., Cantet, F., Fava, L., Norville, I., & Bonazzi, M. (2014). Identification of OmpA, a *Coxiella burnetii* protein involved in host cell invasion, by multi-phenotypic high-content screening. *PLoS Pathogens*, *10*, e1004013.

Maturana, P., Graham, J. G., Sharma, U. M., & Voth, D. E. (2013). Refining the plasmid-encoded type IV secretion system substrate repertoire of *Coxiella burnetii*. *Journal of Bacteriology*, *195*, 3269–3276.

McDonough, J. A., Newton, H. J., Klum, S., Swiss, R., Agaisse, H., & Roy, C. R. (2013). Host pathways important for *Coxiella burnetii* infection revealed by genome-wide RNA interference screening. *MBio*, *4*, 1–13.

Moos, A., & Hackstadt, T. (1987). Comparative virulence of intra- and interstrain lipopolysaccharide variants of *Coxiella burnetii* in the Guinea pig model. *Infection and Immunity*, *55*, 1144–1150.

Mulye, M., Samanta, D., Winfree, S., Heinzen, R. A., & Gilk, S. D. (2017). Elevated cholesterol in the *Coxiella burnetii* intracellular niche is bacteriolytic. *MBio*, *8*, 1–18.

Newton, H. J., Kohler, L. J., McDonough, J. A., Temoche-Diaz, M., Crabill, E., Hartland, E. L., & Roy, C. R. (2014). A screen of *Coxiella burnetii* mutants reveals important roles for dot/Icm effectors and host autophagy in vacuole biogenesis. *PLoS Pathogens*, *10*, e1004286.

Newton, H. J., McDonough, J. A., & Roy, C. R. (2013). Effector protein translocation by the *Coxiella burnetii* dot/Icm type IV secretion system requires Endocytic maturation of the pathogen-occupied vacuole. *PLoS One*, *8*, e54566.

Newton, P., Latomanski, E. A., & Newton, H. J. (2016). Applying fluorescence resonance energy transfer (FRET) to examine effector translocation efficiency by *Coxiella burnetii* during siRNA silencing. *Journal of Visualised Experiments*, *113*, 54210.

Omsland, A., Beare, P. A., Hill, J., Cockrell, D. C., Howe, D., Hansen, B., … Heinzen, R. A. (2011). Isolation from animal tissue and genetic transformation of *Coxiella burnetii* are facilitated by an improved axenic growth medium. *Applied and Environmental Microbiology*, *77*, 3720–3725.

Omsland, A., Cockrell, D. C., Howe, D., Fischer, E. R., Virtaneva, K., Sturdevant, D. E., … Heinzen, R. A. (2009). Host cell-free growth of the Q fever bacterium *Coxiella burnetii*. *Proceedings of the National Academy of Sciences*, *106*, 4430–4434.

Pan, X., Lührmann, A., Satoh, A., Laskowski-Arce, M.A., and Roy, C.R. (2008) Ankyrin repeat proteins comprise a diverse family of bacterial type IV effectors. *Science* (80-) *320*: 1651–1654.

Romano, P. S., Gutierrez, M. G., Berón, W., Rabinovitch, M., & Colombo, M. I. (2007). The autophagic pathway is actively modulated by phase II *Coxiella burnetii* to efficiently replicate in the host cell. *Cellular Microbiology*, *9*, 891–909.

van Schaik, E. J., Case, E. D., Martinez, E., Bonazzi, M., & Samuel, J. E. (2017). The SCID mouse model for identifying virulence determinants

in *Coxiella burnetii*. *Frontiers in Cellular and Infection Microbiology*, *7*, 1–10.

Seshadri, R., Paulsen, I. T., Eisen, J. A., Read, T. D., Nelson, K. E., Nelson, W. C., … Heidelberg, J. F. (2003). Complete genome sequence of the Q-fever pathogen *Coxiella burnetii*. *Proceedings of the National Academy of Sciences*, *100*, 5455–5460.

Voth, D. E., Howe, D., Beare, P. A., Vogel, J. P., Unsworth, N., Samuel, J. E., & Heinzen, R. A. (2009). The *Coxiella burnetii* ankyrin repeat domain-containing protein family is heterogeneous, with C-terminal truncations that influence dot/Icm-mediated secretion. *Journal of Bacteriology*, *191*, 4232–4242.

Weber, M. M., Chen, C., Rowin, K., Mertens, K., Galvan, G., Zhi, H., … Samuel, J. E. (2013). Identification of *Coxiella burnetii* type IV secretion substrates required for intracellular replication and Coxiella-containing vacuole formation. *Journal of Bacteriology*, *195*, 3914–3924.

Winchell, C. G., Dragan, A. L., Brann, K. R., Onyilagha, F. I., Kurten, R. C., & Voth, D. E. (2018). *Coxiella burnetii* subverts p62/Sequestosome 1 and activates Nrf2 Signaling in human macrophages. *Infection and Immunity*, *86*, 1–12.

Zusman, T., Aloni, G., Halperin, E., Kotzer, H., Degtyar, E., Feldman, M., & Segal, G. (2007). The response regulator PmrA is a major regulator of the icm/dot type IV secretion system in *Legionella pneumophila* and *Coxiella burnetii*. *Molecular Microbiology*, *63*, 1508–1523.

How to cite this article: Burette M, Bonazzi M. From neglected to dissected: How technological advances are leading the way to the study of *Coxiella burnetii* pathogenesis. *Cellular Microbiology*. 2020;22:e13180. https://doi.org/10.1111/cmi.13180

2.3 Manipulation of host cell defences

Host cells have developed a number of strategies to counter bacterial infections. Indeed, the detection of bacterial infection triggers several responses including ER stress, inflammatory responses or autophagy, collectively leading to cell death and bacterial clearance (Ashida *et al.*, 2011).

Apoptosis is a form of programmed cell death (PCD) that allows the clearance of damaged or infected cells without inducing inflammation. It is characterised by typical morphological changes such as membrane blebbing, cell shrinkage, nuclear condensation and fragmentation into membrane-bound apoptotic bodies which are rapidly phagocytosed. Apoptosis can be initiated by the intrinsic or the extrinsic pathways and these involve key apoptotic molecules such as the Bcl-2 (B-cell lymphoma protein-2) family of proteins and caspases (cysteine-aspartic proteases). The intrinsic pathway involves the activation of Bcl-2 proteins leading to mitochondrial membrane permeabilisation and subsequent release of cytochrome *c* into the cytoplasm while the extrinsic pathway is mediated by activated caspases following ligand binding to death receptors (Nagata, 2018).

The immune system include an innate and an adaptative response that act in a complementary way against foreign threats (Medzhitov and Janeway C., 2000). Innate immunity is an early and nonspecific reaction whereas adaptive immunity provides a specific but non immediate reaction (Medzhitov and Janeway C., 2000).

As a stealth pathogen, *C. burnetii* evades innate immune recognition and persist in infected cells. Although the precise mechanisms involved in the inhibition of apoptosis and innate immunity are not fully understood, some effector proteins involved in these processes have been identified and characterised.

2.3.1 Inhibition of apoptosis

To prevent premature host cell death, *C. burnetii* interferes with intrinsic and extrinsic apoptotic pathways, either by promoting anti-apoptotic transcription activity (Voth *et al.*, 2007) or by preventing the release of cytochrome *c* (Lührmann and Roy, 2007). The role of *C. burnetii* effector proteins in the inhibition of apoptosis has been highlighted with the identification of 3 anti-apoptotic effectors. The first identified anti-apoptotic *C. burnetii* effector is the eukaryotic-like protein AnkG which displays 2 ankyrin repeats (Lührmann *et al.*, 2010). AnkG inhibits intrinsic apoptosis by interfering with the pro-apoptotic activity of the mitochondrial-associated

protein p32 (Eckart *et al.*, 2014). Indeed, AnkG localises to mitochondria but migrates to the nucleus by interacting with p32 and importin-α1, a host cell protein involved in the nucleocytoplasmic transport of proteins. It has been suggested that AnkG probably localises to mitochondria in order to sense apoptosis and then, interacts with p32 and importin-α1 to relocalise to the nucleus where it can prevent apoptosis by an unknown mechanism (Schäfer *et al.*, 2017) (**Figure 21**).

Another *C. burnetii* anti-apoptotic effector is CaeB (*C. burnetii* anti-apoptotic effector B), which robustly inhibits the intrinsic apoptosis (Klingenbeck *et al.*, 2013). Similarly to AnkG, CaeB localises to mitochondria (Carey *et al.*, 2011); however, an ER localisation has also been described (Rodríguez-Escudero *et al.*, 2016). CaeB blocks the mitochondrial apoptotic pathway without preventing the activation or the mitochondrial insertion of the pro-apoptotic protein Bax (Bcl-2-associated X protein). In fact, CaeB interferes with the permeabilisation of the mitochondrial outer membrane (MOM) (Klingenbeck *et al.*, 2013), which triggers the intrinsic apoptosis (Peña-Blanco and García-Sáez, 2018) (**Figure 21**).

Finally, *C. burnetii* also secretes CaeA (*C. burnetii* anti-apoptotic effector A), a nuclear effector protein which prevents both intrinsic and extrinsic apoptosis by acting in the late steps of the apoptotic pathway (Klingenbeck *et al.*, 2013). Indeed, CaeA does not repress the activation of caspase 9 but rather targets caspase 7 by preventing its cleavage. Interestingly, a recent study highlights the importance of the EK (glutamic acid/lysine) repetition motif for the anti-apoptotic activity of CaeA (Bisle *et al.*, 2016) (**Figure 21**). Nevertheless, little is known about the anti-apoptotic activity of CaeA showing that further investigations are required to determine how CaeA prevents this process in the nucleus of infected cells.

Additionally, *C. burnetii* also prevents apoptosis by regulating the activity of pro-survival host signaling proteins including Akt (RAC-alpha serine/threonine-protein kinase), Erk1/2 (Extracellular signal-regulated kinases 1/2), p38 and cAMP-dependent kinase (PKA) (Voth and Heinzen, 2009a; Macdonald *et al.*, 2014; Cherla *et al.*, 2018) (**Figure 21**). During the infection, Akt and PKA inhibit the activity of the pro-apoptotic protein Bad (BCL2 associated agonist of cell death) via its phosphorylation, thus promoting macrophage survival (Macdonald *et al.*, 2014) (**Figure 21**). Furthermore, *C. burnetii* also inhibits apoptosis through an autophagy-dependent manner by favouring the interaction between the autophagy-related protein Beclin 1 and Bcl-2 at the CCV (Vázquez and Colombo, 2010). Recently, it has been shown that *C. burnetii* also antagonises the ER stress-induced apoptosis by preventing the nuclear translocation of the pro-apoptotic transcriptional factor CHOP (C/EBPζ-C/EBP homologous protein) (Brann *et al.*, 2020) (**Figure 21**). These processes depend on a functional T4BSS, however, the bacterial effectors involved remain to be identified.

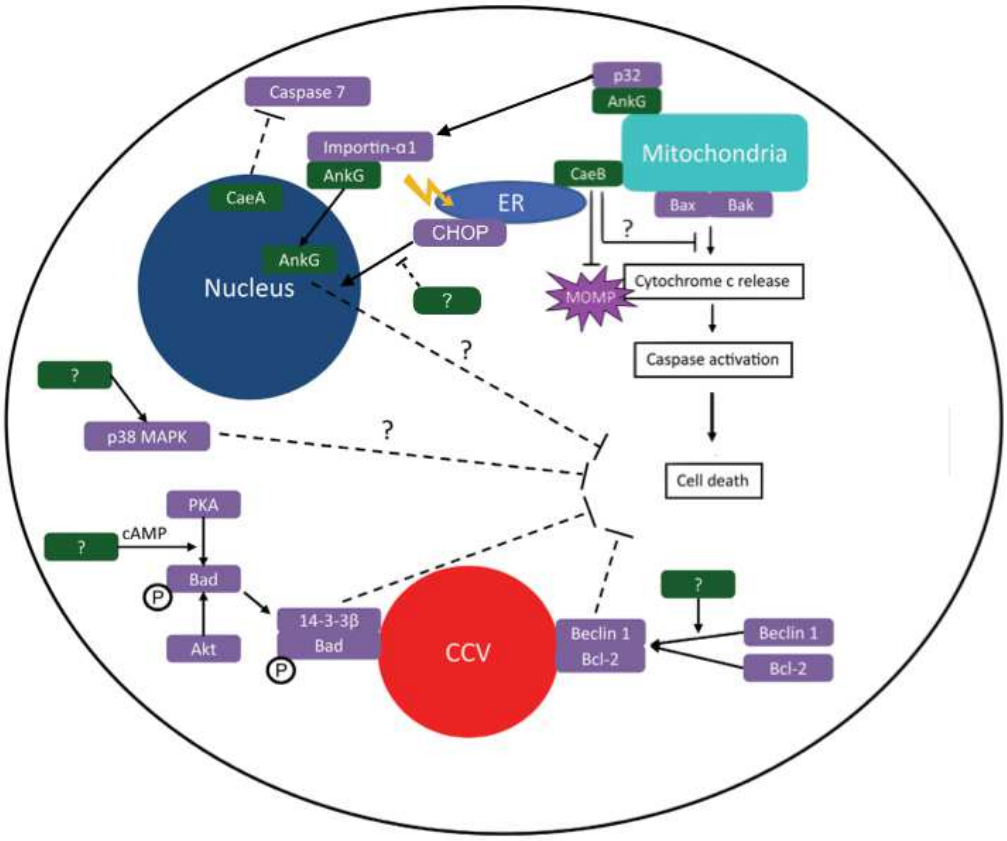

Figure 21. Cell death pathways affected by *C. burnetii* (adapted from Cordsmeier *et al.*, 2019). *C. burnetii* prevents apoptosis by regulating the activity of pro-survival host signaling proteins including Akt, Erk1/2, p38 and cAMP-dependent kinase (PKA). Furthermore, *C. burnetii* inhibits apoptosis by favouring the interaction between Beclin-1 and Bcl-2. Recently, it has been that *C. burnetii* also antagonizes the ER stress-induced apoptosis. Three *C. burnetii* effector proteins have been identified with an anti-apoptotic activity. AnkG prevents apoptosis by interfering with p32 activity through an unknown mechanism. CaeA inhibits the activation of Caspase-7 by preventing its cleavage. Finally, CaeB blocks apoptosis by inhibiting the mitochondrial pathway and the MOMP. Green boxes: *C. burnetii* effector proteins; purple boxes: eukaryotic proteins.

2.3.2 Modulation of the innate immune response

2.3.2.1 Innate immunity in eukaryotic cells

(i) Innate immune defences

During the early phases of infection, pathogen activates innate immune cells such as antigen-presenting dendritic cells (DCs), phagocytic macrophages and cytotoxic natural killer (NK) cells as well as humoral factors such as the complement system (Netea *et al.*, 2017) (**Figure 22**). Macrophages are known to play a critical role in innate immunity through the phagocytosis of pathogens but also the stimulation of the immune response by recruiting other immune cells (Wynn *et al.*, 2013). In response to external stimuli, macrophages rapidly respond by polarising into two types of activated macrophages, the classical M1 phenotype and the alternative M2 phenotype (Mantovani *et al.*, 2004). M1 macrophages are characterised by the production of proinflammatory cytokines that recruits other immune cells such as lymphocytes and NK cells to coordinate an immune response for pathogen elimination, whereas M2 macrophages are associated to immunoregulatory activities (Mantovani *et al.*, 2004). In addition to macrophages and NK cells, DCs initiate specific immune responses through antigen processing and presentation to cells of the adaptive immune response such as T and B lymphocytes (Kapsenberg, 2003).

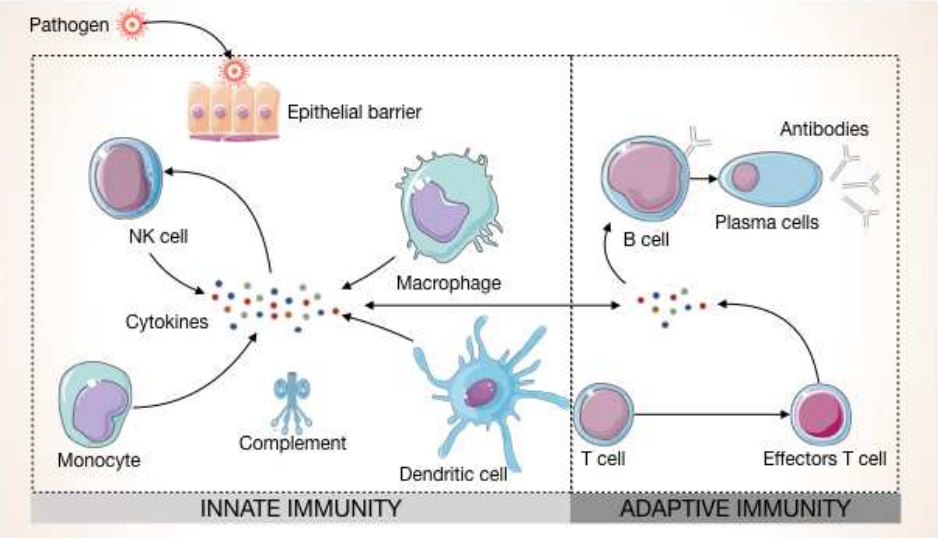

Figure 22. Main mechanisms of innate and adaptive immunity. The epithelial barrier constitutes the first line of defence against pathogens. Pathogen activates innate immune cells including macrophages, dendritic cells (DCs) and natural killer (NK) cells as well as humoral factors as complement system. Activated cells secrete cytokines that ensure the immune response. Adaptive immunity develops later and requires cross-talking events between antigen-presenting cells (DCs and macrophages) and lymphocytes, which leads to pathogen elimination.

Microbial detection is crucial to ensure the elimination of pathogens. The host receptors dedicated to pathogen recognition are called pattern recognition receptors (PRRs). These can sense a broad range of pathogen-specific molecules termed pathogen-associated molecular patterns (PAMPs), at the host cell surface as well as in the cytosol (Medzhitov and Janeway, 2002). PRRs are present in several resident tissue cells as well as effector cells and can be divided into three main classes : membrane-bound Toll-like receptors (TLRs), C-type lectin receptors (CLRs) and the cytosolic sensing receptors, which include retinoid acid-inducible gene I (RIG-I)-like receptors (RLRs) and nucleotide-binding oligomerisation domain (NOD)-like receptors (NLRs) (Mogensen, 2009) (**Figure 23**).

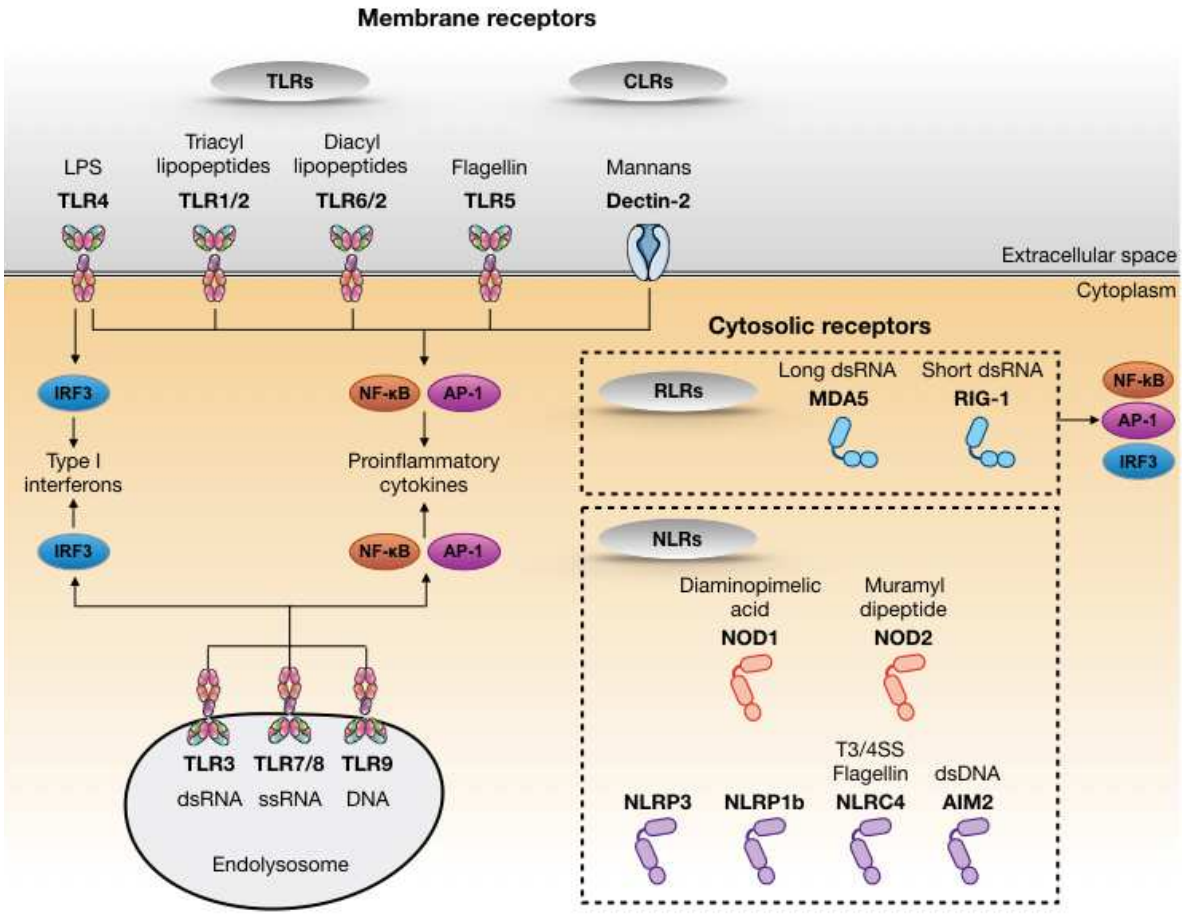

Figure 23. Major classes of pattern-recognition receptors (PRRs) and their most important ligands.

(ii) Surface sensors

The TLR family is the most characterised class of PRRs. These are expressed in most cell types including epithelial cells as well as macrophages, DCs and lymphocytes (Iwasaki and Medshitov, 2004). 10 human TLRs have been described that recognise multiple PAMPs originating from bacteria, viruses, protozoa and fungi (Akira *et al.*, 2006). TLR1, 2, 4, 5, 6 and 10 are expressed at the cell surface and mostly detect bacterial products (Mogensen, 2009). In contrast, TLR3, 7, 8 and 9 are present in intracellular compartments, including endosomes and lysosomes (Barton and Kagan, 2009) and are specialised in the recognition of nucleic acids (Heil *et al.*, 2004). Gram-negative bacteria are detected by TLR4 through their LPS while both Gram-negative and -positive bacteria are recognised by TLR2 via lipoproteins, peptidoglycan and lipoteichoic acid (LTA) (Poltorak *et al.*, 1998; Schwandner *et al.*, 1999). Additionally, TLR5 is activated by flagellin, which is the main constituent of the motility apparatus of flagellated bacteria (Hayashi *et al.*, 2001). Converserly, TLR3, 7, 8 and 9 are activated by foreign nucleic acids including double and single-stranded RNA produced during viral replication as well as unmethylated CpG DNA derived from both viral and bacterial genomes (Hemmi *et al.*, 2000; Hayashi *et al.*, 2001; Heil *et al.*, 2004) (**Figure 23**).

Pathogen recognition triggers TLRs dimerisation and the recruitment of the adaptor proteins MyD88 or TIR domain-containing adaptor inducing IFN-β (TRIF), which in turn activates immune signaling pathways (Akira and Takeda, 2004; O'Neill and Bowie, 2007). Three main immune signaling pathways exist, including the nuclear factor-kappa B (NF-κB), the mitogen-activated protein kinases (MAPKs) p38 and JNK (c-JUN N-terminal kinases), and the IFN regulatory factors (IRFs), whose activation results in the nuclear translocation of NF-κB, activator protein 1 (AP1) or IRF3/7 transcription factors, respectively (Akira and Takeda, 2004) (**Figure 23**). In unstimulated cells, the interaction with the nuclear factor kappa-light polypeptide gene enhancer in B cells inhibitor alpha (IκBα) retains NF-κB in the cytoplasm. Stressful stimuli, including recognition of the tumor necrosis factor alpha (TNF-α) by the TNF receptor or LPS by TLR4, trigger the phosphorylation and the proteasomal degradation of IκBα. This liberates NF-κB and unmasks its NLS. This is then recognised by importin-α and members of the importin-β family, which mediate nuclear translocation of NF-κB. In the nucleus, NF-κB interacts with specific gene promoters in order to stimulate the expression of proinflammatory genes (Lawrence, 2009) (**Figure 24**). Energy for nuclear transport of NLS-containing proteins is provided by intracellular gradients of the small GTPase Ras-related nuclear protein (Ran), which interacts with the importin complexes. GDP-bound Ran is largely

cytoplasmic and nuclear translocation triggers the conversion to the GTP-bound form by means of the Ran GEF RCC1 (regulator of chromosome condensation-1). In its GTP-bound form, Ran triggers the dissociation of importins from the cargo and importin complexes recycle back to the cytoplasm. There, Ran GTPase activating protein (RanGAP) stimulates the GTPase activity of Ran to generate Ran-GDP, which dissociates from importin complexes (Stewart, 2007) (**Figure 23**).

Similar mechanisms regulate the MAPK and IRF signalling pathways allowing NF-κB and AP1 to induce the production of proinflammatory cytokines including TNF-α, interleukin-6 (IL-6), IL-12 and the pro-forms of IL-1α and IL-1β while IRF3/7 is involved in the synthesis of type I interferons IFNα and IFNβ (Akira and Takeda, 2004). Through the expression of multiple crucial genes involved in the immune response, these proinflammatory signalling pathways play pivotal roles in both inflammation and innate immunity (Iwasaki and Medzhitov, 2004).

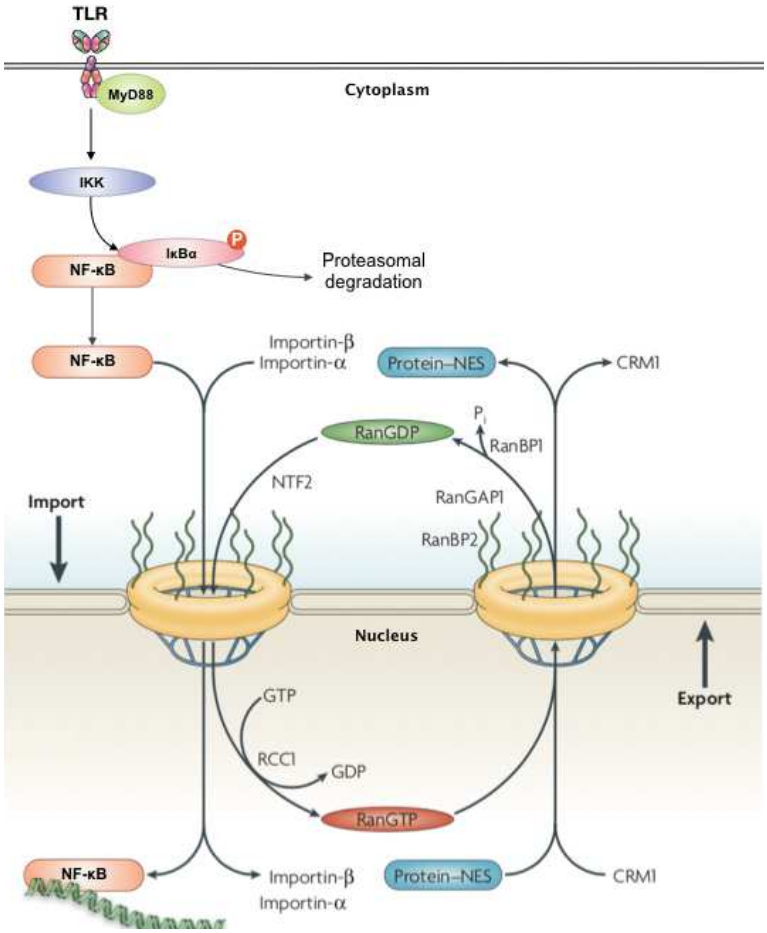

Figure 24. Nucleocytoplasmic transport of NF-κB (adapted from Clarke and Zhang, 2008). Host sensing of microbial components by TLRs triggers the NF-κB signaling pathways. The recruitment of the adaptor protein MyD88 activates the IKK complex which in turn phosphorylates IκBα allowing thus its ubiquitination for proteasomal degradation. IκBα degradation releases the p50/p65 NF-κB heterodimer, which translocates into the nucleus in a Ran-dependent manner to finally activates transcription of proinflammatory cytokines. P: phosphorylation.

(iii) Cytosolic sensors

In addition to surface sensors, cells also display cytosolic sensors including RLRs and NLRs, to recognise intracellular pathogens. RLRs sense viral RNA which lead to the production of proinflammatory cytokines and type I interferons (Dixit and Kagan, 2013). NLRs detect both viral and bacterial components inducing either the activation of proinflammatory gene and/or caspases (Kanneganti *et al.*, 2007). The best characterised NLR family members are the NLRC receptors NOD-1 and -2 (Nucleotide-binding oligomerisation domain-containing protein -1 and -2, respectively) and the inflammasome-inducing NLRP receptors (Franchi *et al.*, 2009) (**Figure 23**). The former sense bacterial peptidoglycan-derived molecules while the latter detect several ligands including bacterial DNA, flagellin, T3SS structural proteins as well as viral RNA (Broz, 2019; da Costa *et al.*, 2019). Inflammasomes are multiprotein complexes which can be formed from five different cytosolic proteins sensors among the NLR family including NLRP1, NLRP3, NLRC4, AIM2 (absent in melanoma 2) and pyrin (Broz, 2019) (**Figure 23**). These proteins induce caspase-1 activation which promote IL-1β, IL-18 and IL-1α release, membrane permeabilisation and finally cause a form of cell death known as pyroptosis (Martinon *et al.*, 2002; Bergsbaken *et al.*, 2009). These represent canonical inflammasomes that differ from the noncanonical inflammasome pathway, which activates caspase-11 in mouse cells and caspase-4 and -5 in human cells following LPS recognition (Kayagaki *et al.*, 2011; Baker *et al.*, 2015).

Pathogen recognition mediated by surface and cytosolic sensors finally constitute an important barrier to many pathogens-derived molecules in host cells. However, some pathogens, including *C. burnetii*, have evolved strategies to evade one or more of these sensors to allow intracellular persistence.

2.3.2.2 Immune evasion by *Coxiella burnetii*

While some pathogens exploit inflammation to their own advantages, others, such as *C. burnetii*, prevent the recognition by the innate immune system to promote their survival (Asrat *et al.*, 2015). Studies on the manipulation of host innate immunity by *C. burnetii* appear controversial as they report diverging results according to bacterial strains and host cells used. The ability of *C. burnetii* to alter the immune response has nevertheless been demonstrated in many ways, showing the importance to investigate how the pathogen subverts host defenses to allow intracellular persistence.

(i) *Manipulation of host sensing*

C. burnetii preferentially targets lung monocytes and macrophages which represent the first line of defense against inhaled pathogens. As previously described in part *2.3.2.1 "Innate immunity in eukaryotic cells"*, pathogen detection usually results in stimulation of pattern recognition receptors such as TLRs, which are critical for an optimal immune response. Little is known about the role of TLRs in *C. burnetii* recognition, but a recent study showed that different *C. burnetii* strains can be detected by TLR1, 2 and 6, leading to cytokines production. Surprisingly, the cytosolic sensor NOD-2 has also been involved in *C. burnetii* recognition (Ammerdorffer *et al.*, 2015). However, *C. burnetii* can invade cells without stimulating TLR2 or TLR4, depending on the LPS structure, which may partly explain the distinct immune responses to *C. burnetii* NMI or NMII. Indeed, TLR2 is differently activated by *C. burnetii* NMI and NMII. It has been proposed that the full length LPS produced by *C. burnetii* acts as a shield to prevent bacterial recognition by TLR2 in human DC (Shannon *et al.*, 2005) (**Table 6**). However, this shielding potential is only observed in DCs as it does not prevent recognition in human peripheral blood mononuclear cells (PBMCs) (Ammerdorffer *et al.*, 2015) (**Table 6**). In addition to what is observed in human PBMCs, LPS from *C. burnetii* NMI or NMII activates TLR2 but not TLR4 in the epithelial Chinese hamster ovary (CHO) cell line (Zamboni *et al.*, 2004) (**Table 6**). The same phenotype was observed in bone marrow-derived macrophages (BMDMs) from TLR2 deficient mice ($TLR2^{-/-}$) infected with *C. burnetii* NMII. Indeed, impaired cytokines production and high permissivity to *C. burnetii* NMII infections were reported, suggesting that TLR2 activation is crucial for host defense by limiting *C. burnetii* replication (Zamboni *et al.*, 2004). It has been demonstrated that NMI LPS, but not NMII LPS, recognition by TLR4 mediates bacterial uptake, actin reorganisation and production of pro-inflammatory cytokines in murine macrophages (Honstettre *et al.*, 2004). A parallel study revealed that *C. burnetii* NMI LPS does not stimulate TLR4 and acts as an antagonist in human PBMCs (Zamboni *et al.*, 2004) (**Table 6**). In BMDMs, this antagonistic engagement of TLR4 by NMI LPS actually blocks the activation of p38α-MAPK pathway which is involved in the production of pro-inflammatory cytokines (Conti *et al.*, 2014) (**Table 6**). In support of this finding, it has been also reported that TLR4 has no role in cytokine production in human PBMCs infected with *C. burnetii* NMI (Ammerdorffer *et al.*, 2015), while both TLR2 and TLR4 mediate cytokine production in response to NMII infection in BMDMs (Bradley *et al.*, 2016) (**Table 6**). Collectively, these results reveal the complexity of the immune response against *C. burnetii* infection.

Following host cell internalisation, *C. burnetii* alters the microbicidal activity of macrophages by modulating their activation profiles and their polarisation into an anti-inflammatory M2-like phenotype. Indeed, *C. burnetii* stimulates the phenotypic switch from M1 polarisation to an atypical M2 macrophage with M2-typical properties but secreting pro-inflammatory cytokines such as interleukin 6 and 8 (IL-6 and IL-8, respectively), that are rather associated with M1-polarised macrophages (Benoit *et al.*, 2008). This suggests that *C. burnetii* may attempt to convert macrophages to a less hostile intracellular environment, by reprogramming macrophages towards an anti-inflammatory phenotype. This may facilitate *C. burnetii* persistence and replication within the host cell, without alerting the immune system.

	***C. burnetii* phase I**		***C. burnetii* phase II**	
	TLR2	**TLR4**	**TLR2**	**TLR4**
Human dendritic cells (DCs)	X	n/a	n/a	X
Human peripheral blood mononuclear cells (PBMCs)	✓	X	✓	n/a
Murine bone marrow derived-macrophages (BMDMs)	✓	X	✓	X
Epithelial chinese hamster ovary (CHO)	n/a	✓	✓	✓

Table 6. Differences in *C. burnetii* phase I and phase II detection depending on cell types. n/a : not applicable

(ii) Manipulation of innate immune signaling pathways

As highlighted in the context of pathogen detection, cytokine production in response to *C. burnetii* infection also widely differs according to bacterial strains and host cells used. Following pathogen detection, TLR signaling ultimately leads to the activation of MAPKs, NF-κB and IRF3, thus triggering the expression of genes encoding immunoregulatory/inflammatory cytokines and interferon. Infection of human alveolar macrophages (hAMs) by either NMI and NMII *C. burnetii* stimulates TNF-α, IL-6 and IL-10 production (Graham *et al.*, 2013) (**Table 7**). *C. burnetii* also slightly increases the expression of type I IFN-regulated genes, either in human macrophages stimulated with NMI LPS or in BMDMs infected with the NMII strain (Bradley *et al.*, 2016; Hedges *et al.*, 2016) (**Table 7**). The role of type I IFN during infection remains unclear as it can either counter or promote *C. burnetii* replication (Hedges *et al.*, 2016). In term of cytokine responses, NMII triggers increased cytokine production. Contrary to NMI, NMII infections induce IL-1β secretion in hAMs, increase p38α-MAPK activation and stimulate IL-12 and TNF-α production in human DCs (Shannon *et al.*, 2005). Interestingly, infection of murine RAW264.7 macrophages by *Coxiella* NMII induces

the production of TNF-α, IL-6, IFN-γ and GM-CSF (Granulocyte-Macrophage Colony-Stimulating Factor) but not the production of IL-12 (**Table 7**). Conversely, NMII-infected peritoneal murine macrophages produce TNF-α, IFN-γ, IL-12 and to a lesser extent IL-10 and GM-CSF. However, neither RAW264.7 nor peritoneal murine macrophages produce IL-1α, IL-1β and TGF-β (Transforming Growth Factor-beta) following NMII infection (Ochoa-Repáraz *et al.*, 2007). The secretion of TNF-α, IL-6 and IL-10 is also observed in BMDMs infected with NMII and clearly depends on the TLR adapter protein MyD88 (Bradley *et al.*, 2016; Kohl *et al.*, 2019). These results suggest that NMI and NMII trigger different but slightly overlapping cytokine responses in mouse and human macrophages. Nevertheless, few studies clearly demonstrate that *C. burnetii* has the ability to attenuate the innate immune responses by modulating cytokine signaling. Indeed, it has been reported that *C. burnetii* NMII suppresses IL8, CCL2 (Chemokine ligand 2), CXCL1 (Chemokine (C-X-C motif) ligant 1) and SPP1 (Secreted phosphoprotein 1) expression to evade the host innate immune response in THP-1 cells (**Table 7**). In this case, *C. burnetii* protein synthesis is required, suggesting that Dot/Icm activity and the translocation of bacterial effectors are involved in this process (Mahapatra *et al.*, 2010). Similarly, PBMCs exposed to heat-killed NMI organisms produce more TNF-α, IL-1β, IL-6, and IL-10 as compared to cells challenged with live bacteria, but equal amounts of IFN-γ, IL-17, and IL-22 (Jansen *et al.*, 2018) (**Table 7**). The same phenotype is observed in murine alveolar (MH-S) macrophages infected with the NMII strain as compared to cells infected with the T4BSS-deficient *dotA* mutant strain. Indeed, *C. burnetii* blocks the IL-17 signaling in a Dot/Icm-dependent manner by down-regulating the expression of genes encoding proinflammatory cytokines and chemokines such as IL-1α, IL-1β, TNF-α, CXCL2 and CCL5 (Clemente *et al.*, 2018). Interestingly, NMII Dot/Icm activity modulates the production of proinflammatory cytokines in murine alveolar macrophages but not in BMDMs, showing once again that *C. burnetii* elicits distinct immune responses according to cell types (Bradley *et al.*, 2016).

	***C. burnetii* phase I**	***C. burnetii* phase II**
Human alveolar macrophages (hAMs)	✓	✓
Human dendritic cells (DCs)	X	✓
Human peripheral blood mononuclear cells (PBMCs)	✓	✓
Human monocytic THP-1 cells	n/a	X
Murine alveolar macrophages (MH-S)	n/a	X
Murine bone marrow derived-macrophages (BMDMs)	n/a	✓
Murine peritoneal macrophages	n/a	✓
Murine RAW264.7 macrophages	n/a	✓

Table 7. Differences in cytokine production in response to *C. burnetii* phase I and phase II. n/a : not applicable

C. burnetii also evades the host immune response by modulating the pro-inflammatory NF-κB signalling pathway (Mahapatra *et al.*, 2016). It has been reported that *C. burnetii* activates NF-κB via the canonical pathway by phosphorylating the NF-κB subunit p65 (RelA). In THP-1 infected cells, a down-modulation of NF-κB is observed during the early and mid phases of infection. To determine whether this down-modulation is Dot/Icm-dependent, NF-κB activation was analysed by measuring p65 phosphorylation and nuclear localisation in cells infected with either *C. burnetii* NMII or the T4BSS-deficient *dotA* mutant. This revealed higher levels of p65 phosphorylation and nuclear translocation in cells infected with the *ΔdotA* mutant, strongly suggesting that *C. burnetii* secretes bacterial effectors that modulate NF-κB signaling (Mahapatra *et al.*, 2016). To date however, only one *C. burnetii* effector has been shown to modulate the host innate immune response. Indeed, the Dot/Icm effector IcaA (Inhibition of caspase activation A) inhibits the non-canonical inflammasome pathway and pyroptotic cell death in BMDMs, thus contributing to *C. burnetii* persistence (Cunha *et al.*, 2015). IcaA inhibits caspase-11 activation which is involved in the non-canonical activation of the NLRP3 inflammasome. Consequently, IcaA inhibits caspase-1 activation, which leads to an impaired IL-1β production and inflammasome activation in BMDMs-infected cells (Cunha *et al.*, 2015; Bradley *et al.*, 2016). However, inflammasome modulation by *C. burnetii* differs in hAMs, as *C. burnetii* infection triggers increased expression of inflammasome-related genes and IL-1β production in hAMs without eliciting elevated caspase-1 activity or pyroptosis (Graham *et al.*, 2013; Mahapatra *et al.*, 2016). This could be due to the fact that humans possess two homologs to murine caspase-11 (caspase-4 and -5). It is thus possible that IcaA may target and prevent the activity of caspase-4 but fails to block caspase-5 activity in hAMs-infected cells. This may explain why IcaA inhibits caspase-1 activation in BMDMs and not in hAMs. However, *C. burnetii* infections do not elicit pyroptosis suggesting that other unidentified effectors may modulate inflammasome activation.

All these findings clearly illustrate how *C. burnetii* has evolved distinct immune evasion strategies including avoidance of TLR recognition, modulation of inflammatory responses or inhibition of pyroptosis to promote its persistence. However, much remains to be done to unravel the complexity of the innate immune response against *C. burnetii*.

3. Aim of the thesis

Coxiella burnetii, the agent of Q fever, subverts host cell functions to modulate innate immune response and generate a replicative niche called CCV, characterised by a unique protein and lipid composition. Key to *C. burnetii* successful infection is the Dot/Icm-dependent secretion of bacterial effector proteins; however, for years, the obligate intracellular nature of *C. burnetii* imposed significant experimental obstacles to the study of its pathogenic features. With the development of an axenic culture medium in 2009, *C. burnetii* became genetically tractable, thus allowing to investigate its complex interaction with host cells. Technological advances strongly contribute to the highlighting of *C. burnetii* virulence determinants involved in the manipulation of membrane trafficking pathways or other signalling pathways including apoptosis and inflammation. The activity of the *C. burnetii* Dot/Icm secretion system is necessary to inhibit the NF-κB pathway during infections; however, the effector proteins involved in this process remained unknown (Mahapatra *et al.*, 2016). In the same way, our team showed that *C. burnetii* subverts PI(3)P metabolism for an optimal development of its CCV through the action of CvpB (Martinez *et al.*, 2016), suggesting that *C. burnetii* manipulates other lipid metabolism for CCV biogenesis.

During my PhD, I had the opportunity to study host/pathogen interactions underlying the persistence and intracellular replication of *C. burnetii*. In the first part of my results, I caracterised a *Coxiella burnetii* effector involved in silencing the innate immune response, while in the second part of my results, I determined the lipid composition of CCV and identified two *C. burnetii* effectors (CBU0635 and CBU2007) potentially involved in *C. burnetii*/host lipids interactions.

Material and Methods

1. Materials

1.1 Chemicals

Unless otherwise stated, all chemicals were purchased from Sigma (Sigma-Aldrich Chemie GmbH, Germany).

1.2 Strains

Strains used in this study are listed in **Table 8**.

1.2.1 *Escherichia coli*

All bacteria were cultured in Luria-Bertani (LB) broth or on LB agar supplemented with ampicillin (100 µg/ml), kanamycin (50 µg/ml) or chloramphenicol (30 µg/ml) as required.

1.2.2 *Coxiella burnetii*

All bacteria were cultured in 1x ACCM-2 (13.4 mM citric acid, 16.1 mM sodium citrate, 3.67 mM potassium phosphate, 1 mM magnesium chloride, 0.02 mM calcium chloride, 0.01 mM iron sulfate, 125.4 mM sodium chloride, 1.5 mM L-cysteine, 0.1 g/L Bacto Neopeptone, 2.5 g/L casamino acids, 1 g/L methyl beta cyclodextrin, 125 ml/L RPMI, pH 4.75) or on 2x ACCM-2 plates supplemented with chloramphenicol (3 µg/ml) and/or kanamycin (375 µg/ml) as required. Bacterial liquid cultures were inoculated into 1x ACCM-2 medium and incubated for 7 days in a humidified atmosphere of 5% CO_2 and 2.5% O_2 at 37°C. Solid ACCM-2 plates were composed of two layers created in petri dishes by mixing 10ml of pre-warmed 2x ACCM-2 with 10ml of 0.5% of melted Ultra-pure Agarose (Invitrogen). The bacterial inoculum was added to the top agarose solution poured on top of the solidified bottom agarose. Plates were cooled for 20 min, refrigerated at 4°C for 30 min to aid agarose solidification and then placed to air dry in a microbial safety cabinet for 20 min. Plates were incubated for 7 days in a humidified atmosphere of 5% CO_2 and 2.5% O_2 at 37°C.

To quantify bacterial suspension, 50µl of bacterial suspension was added to 5µl 10% Triton-X100 in a black, clear-bottomed, 96-well plates and incubated for 10 min at room temperature on a plate shaker. The dsDNA quantitation reagent was diluted at 1:200 in 1x Tris-EDTA (TE) buffer and added to the bacterial samples at a ratio of 1:1 and incubated 2 to 5 min at room temperature, in the dark. An Infinite 200 pro microplate reader (TECAN) was used to measure fluorescence. Flurorescence of dsDNA standard samples (2 µg/ml to 2 ng/ml)

at standard fluorescein wavelengths (excitation ~480 nm, emission ~520 nm) was assessed in parallel, to plot a standard curve and determine the concentration of unknown samples. All measurements were performed in duplicate. To obtain bacterial concentration, DNA concentration is divided by the mass of *C. burnetii* genome and express in genome equivalent (GE)/ml.

1.3 Cell lines

Human bone osteosarcoma epithelial U2OS and human monocytic leukaemia THP-1 cell lines were routinely maintained according to standard protocols. All media and supplements were obtained from Gibco-BRL and Sigma. U2OS cells were cultured in high glucose (4.5 g/l) Dulbecco's Modified Eagle Medium (DMEM) while THP-1 cells were cultured in Roswell Park Memorial Institute (RPMI) medium. Culture media were supplemented with 10% heat inactivated foetal calf serum (FCS). FCS was heat inactivated for 30 min at 56°C prior to use, aliquoted and stored at -20°C. Cells were cultured statically at 37°C in a humidified atmosphere of 5% CO_2.

U2OS cells were sub-cultured every four days by removal of the spent medium, followed by treatment of the confluent cells. Confluent cells were washed with 5 ml Dulbecco's Phosphate Buffer Saline (DPBS) followed by treatment with trypsin-EDTA (ethylenediaminetetraacetic acid) 0.25% (Gibco). Cells were harvested after 5 minutes, followed by the addition of 8 ml of fresh DMEM of which 1 ml was sub-cultured in a final volume of 5 ml (equivalent of 1 passage). U2OS cells were discarded after 18 passages. THP-1 cells were sub-cultured by centrifugation of the cell suspension at 1,500 rpm for 5 minutes. After discarding the supernantant, cells were resuspended at a density of 5.0 x 10^5 cells/ml in fresh medium + 10% FCS. THP-1 cell culture was maintained at a high density (2.0 x 10^6 cells/ml) with media being refreshed every 5-7 days for a period of 1 month.

THP-1 cells were differentiated into macrophages-like with Phorbol 12-Myristate 12-Acetate (PMA, Invivogen) at a concentration of 200 ng/ml in RPMI + 10% FCS for 48h. Following differentiation, fresh RPMI medium supplemented with 10% FCS was added for 24h, prior to infection experiments.

1.4 Plasmids

Plasmids used in this study are listed in **Table 9**.

1.5 Oligonucleotide primers

All synthetic primers used in polymerase chain reactions (PCR) were synthesised by Sigma-Aldrich GmbH (Germany). Primers used in this study are listed in **Table 10**. Oligonucleotide primers were used at a final concentration of 10 pmol/µl.

1.6 Antibodies

Antibodies used in this study are listed in **Table 11**.

2. DNA manipulation

2.1 Polymerase Chain Reaction conditions

PCR reactions were performed in 1X Phusion polymerase buffer using 50 ng of template DNA, 1 pmol/µl of each primer, 0.25 mM of each dNTP and 2U/µl of Phusion High-Fidelity DNA polymerase (Thermo Fisher Scientific). PCR was performed in a final volume of 50 µl in 200 µl PCR tubes using the T100 thermal cycler (Bio-RAD) with the following cycle: initial denaturation for 30 seconds at 98°C; 35 cycles of denaturation at 98°C for 30 sec, annealing at X°C for 30 sec, elongation at 72°C for Y min; final elongation at 72°C for 10 min. X was optimised for each PCR reaction, with a value ranging from 50 to 70°C. Y was calculated according to the estimated size of the DNA fragment to amplify and the polymerisation speed of the DNA polymerase (30 sec per kb on average).

2.2 Agarose gel electrophoresis

Following PCR-amplification, DNA was resolved by horizontal electrophoresis. Gels were cast using 1% to 2% agarose gels, and a 1:10000 dilution of SYBR Safe DNA gel stain (Invitrogen) to aid visualisation. Prior to gel loading, DNA samples were mixed with 6X loading buffer (2.5% Ficoll®-400, 10 mM EDTA, 3.3 mM Tris-HCl, 0.08% SDS, 0.02% pink/red dye 1, 0.001% blue dye 2). Gels were run in 1x TAE buffer (40 mM Tris-acetate, 1 mM EDTA) using a constant voltage of 130 V. DNA bands were visualised using a Safe Imager blue light transilluminator (Invitrogen). DNA fragment size was estimated using a GeneRuler 1 kb Plus DNA ladder (Thermo Fisher Scientific).

2.3 Restriction endonuclease digestion

DNA restriction digest was performed overnight at 37°C (according to the optimal temperature for enzymatic activity) in a final volume of 50 µl with DNA template, 5 U of each

restriction enzyme (NEB), 5 µl of restriction buffer (selected according to the enzyme(s) used, NEB). Digested DNA products were run on agarose gels and purified using a NucleoSpin Gel and PCR clean-up gel extraction kit (Macherey Nagel).

2.4 Purification of DNA

PCR-amplified and digested DNA was run on agarose gels and visualised using a Safe ImagerTM blue light transilluminator (Invitrogen). The agarose plug containing the DNA was removed using a scalpel and DNA was purified using a NucleoSpin Gel and PCR clean-up gel extraction kit (Macherey Nagel) according to manufacturer's protocols. Briefly, the agarose plug was melted at 55°C in a high salt-containing buffer and DNA was purified on silica-membranes columns to remove contaminants. DNA was eluted in 30 µl of sterile deionised water and processed for ligation or stored at -20°C.

2.5 Ligation of DNA fragments

Digested PCR fragments were ligated into digested plasmids using T4 DNA ligase and the supplied buffer (NEB). Ligation reactions were performed overnight at room temperature in a final volume of 20 µl. This comprised 1X ligation buffer (50 mM Tris-HCl pH 7.5, 10 mM $MgCl_2$, 10 mM DTT, 1 mM ATP), 40 U/µl T4 DNA ligase, and digested plasmid and insert DNA used at a typical vector:insert molar ratio of 1:3.

2.6 PCR colony

PCR colony was performed in 1X GoTaq® buffer using bacterial colonies as DNA template, 1 pmol/µl of each primer, 0.25 mM of each dNTP, 1.5mM of $MgCl_2$ and 2U/µl of GoTaq® G2 Flexi DNA polymerase (ProMega). PCR was performed in a final volume of 25 µl in 200 µl PCR tubes using the T100 thermal cycler (Bio-RAD) with the following cycle: initial denaturation for 5 min at 94°C; 35 cycles of denaturation at 94°C for 30 sec, annealing at X°C for 45 sec, elongation at 72°C for Y min; final elongation at 72°C for 10 min. X was optimised for each PCR reaction, with a value ranging from 50 to 70°C. Y was calculated according to the estimated size of the DNA fragment to amplify and the polymerisation speed of the DNA polymerase (1 min per kb on average). PCR-colony amplified was run on agarose gels and successful construct was selected for inoculating overnight liquid culture.

2.7 Plasmid DNA purification

Small scale, purified plasmid DNA was prepared from 5 ml of overnight liquid cultures using GenElute Plasmid Miniprep kit according to the manufacturer's protocols (Sigma). Large scale, purified plasmid DNA was prepared from 300 ml of overnight liquid cultures using NucleoBond Xtra Maxi Plus purification kit according to the manufacturer's protocols (Macherey Nagel). Briefly, bacteria were harvested and resuspended in an alkaline solution containing sodium dodecyl sulphate (SDS) and RNase. These conditions provoke the lysis of bacteria as well as the denaturation of genomic and plasmid DNA. Neutralisation of the solution led to re-annealing of plasmid DNA and precipitation of genomic DNA. Bacterial debris and precipitated DNA were then aggregated by centrifugation. Plasmid DNA was then purified and concentrated on silica-membranes columns. Following a washing step with 70% ethanol, plasmid DNA was eluted in sterile water.

2.8 DNA sequencing

DNA was sequenced using primers corresponding to the flanking regions of the DNA fragment of interest. Sequencing was performed by Eurofins Genomics (Ebersberg, Germany) using 100 ng/µl and 10pmol of primers. Sequences were analysed using SerialCloner alignment function.

3. Transformation of bacteria

3.1 Heat shock

For preparation of chemically competent *E. coli*, an overnight bacterial culture was inoculated into LB medium at a dilution of 1:100 and incubated with shaking at 200 rpm at 37°C until the culture reached mid-log phase (OD_{600} = 0.45-0.55). Following a 15 min incubation on ice, the bacterial culture was centrifuged at 3000 rpm at 4°C for 10 minutes. The supernatant was discarded and the bacteria were resuspended in 0.1 volumes (compared to the original culture volume) of ice-cold RF1 buffer (100 mM RbCl, 50 mM $MnCl_2$, 30 mM potassium acetate, 10 mM $CaCl_2$, 15% (v/v) glycerol, pH 5.8). Following 10 min of incubation on ice, the bacteria were pelleted by centrifugation as described above. The supernatant was discarded and the bacterial pellet was resuspended in 0.01 volumes (compared to the original culture volume) of ice-cold RF2 buffer (10 mM MOPS, 10 mM RbCl, 75 mM CaCl2, 15% (v/v) glycerol, pH 6.5). 200 µl aliquots were stored at -80°C.

For each heat shock transformation, 50 µl of competent bacteria were thawed on ice before addition of DNA (5 µg of plasmid DNA or 10 µl of ligation reaction). Bacteria were then incubated for 30 min on ice before being heat shocked for 1 min at 42°C. Following addition of 600 µl of LB medium, the transformation mix was then incubated shaking at 37°C with shaking at 200 rpm for 1 h. Bacteria were then plated on LB agar plates containing the appropriate antibiotic and incubated at 37°C overnight.

3.2 Electroporation

For preparation of electrocompetent *C. burnetii*, 2.10^6 GE/ml was inoculated into 100 ml of 1x ACCM-2 and incubated for 7 days at 37°C. Following 7 days of culture, bacteria were pelleted at 4,500 rpm for 30 min at 4°C. The bacterial pellet was resuspended in 30 ml of sterile ice-cold 10% glycerol and centrifuged as described above. The bacterial pellet was resuspended in 2 ml of sterile ice-cold 10% glycerol before being aliquoted and stored at -80°C.

For each electroporation reaction, 50 µl of electrocompetent bacteria were thawed on ice before addition of 10 to 20 µg plasmid DNA. Bacteria were transferred to an ice-cold electroporation cuvette. Electroporation was performed using a BioRad gene pulser programmed to the following settings: 500 Ω, 25 µF, 1,8 kV. Following addition of 950 µl of RPMI medium, 200 µl of the transformation mix was inoculated into 3 ml of 1x ACCM-2 supplemented with 1% FCS and incubated for 24 h in a humidified atmosphere of 5% CO_2 and 2.5% O_2 at 37°C. The following day, 1x ACCM-2 was supplemented with chloramphenicol (3 µg/ml) and/or kanamycin (375 µg/ml) as required and transformed bacteria were incubated 3 more days in a humidified atmosphere of 5% CO_2 and 2.5% O_2 at 37°C. Bacteria were then plated on 2x ACCM-2 plates containing the appropriate antibiotics as described in section **A.2.2** and incubated for 7 days in a humidified atmosphere of 5% CO_2 and 2.5% O_2 at 37°C

4. Protein analysis

4.1 Quantification of protein concentration

Protein concentration was estimated using the BCA (bicinchonic acid) protein assay (Pierce) according to the manufacturer's protocol. Briefly, the proteins samples were added to the BCA reagent at a ratio of 1:20 and incubated for 30 min at 37°C. A Sunrise plate reader (TECAN) was used to measure absorbance at A_{562}. Absorbance of bovine serum albumin (BSA) standard samples (0 to 2000 µg/ml BSA) at A_{562} was assessed in parallel, to plot a

standard curve and determine the concentration of unknown samples. All measurements were performed in duplicate.

4.2 Sodium dodecyl sulphate-polyacrylamide gel electrophoresis (SDS/PAGE)

Resolving gels were made using 8% to 12% acrylamide in a Tris-HCl/SDS buffer (0.375 M Tris- HCl, pH 8.8, 0.1% SDS) and stacking gels were made using 4% acrylamide in a Tris-HCl/SDS buffer (0.125 M Tris-HCl, pH 6.8, 0.1% SDS). Polymerisation of acrylamide was generated using 0.1% (w/v) ammonium persulfate and 0.1% (v/v) TEMED. After polymerisation, gels were positioned in a gel electrophoresis tank (Biorad) with 1x running buffer (3 g/l Tris, 14.4 g/l glycine, 0.1% SDS). Samples were mixed with 4x Laemmli buffer (160 mM Tris-HCl, pH 6.8, 8% SDS, 30% glycerol, 40 mM EDTA, 4% β-mercaptoethanol, 0.08% Bromophenol blue) prior to loading. Gels were run at 90 V for 10 min and then at 200V until the blue dye front reached the bottom of the gel. The molecular weight of the samples was compared to a PageRuler plus prestained protein ladder (Thermo Fisher Scientific).

4.3 Silver staining of SDS-PAGE

Silver was used to stain proteins separated by SDS-PAGE using the silver stain kit (Pierce) according to the manufacturer's protocol. Briefly, gels were fixed in 30% (v/v) ethanol and 10% (v/v) acetic acid solution two times for 15 min. Gels were washed two times with 10% (v/v) ethanol for 5 min and two times with ultrapure water for 5 minutes. Gels were then sensitised for 1 min and stained for 30 min. Gels were finally developed until the protein bands could be visualised and the reaction was stopped with 5% acetic acid for 10 minutes.

4.4 Western blotting

Proteins resolved by SDS-PAGE were transferred to a Polyvinylidene difluoride (PVDF) membrane (Thermo Fisher Scientific) using a wet electroblotting system (Biorad). Briefly, SDS-PAGE, PVDF membrane and Whatman papers were soaked in wet transfer buffer (25 mM Tris, 192 mM glycine, 15% (v/v) methanol) and stacked on the blotting apparatus. Proteins were transferred under constant voltage (routinely 100 V, 400 mA) for 1h to 1.5h at 4°C. PVDF membranes were then blocked at room temperature in 5% (w/v) skimmed milk in Phosphate buffer saline (PBS) containing 0.1% (v/v) Tween-20 (PBST) for 1 h on a rocking platform. Blocking buffer was then replaced with primary antibody (listed in Appendix 4) diluted in 5% skimmed milk in PBST. Membranes were incubated on a rocking platform for 1 h before being washed thoroughly 3 times in PBST. Anti-mouse and anti-rabbit Horse radish peroxydase

(HRP)-conjugated secondary antibodies (Sigma) were diluted (1:2000) in PBST/5% skimmed milk and added to the membranes. After 60 min incubation as previously described, membranes were washed thoroughly 3 times in PBST. Western blots were developed using the Enhanced ChemiLuminescence (ECL) SuperSignal West Femto Maximum Sensitivity Substrate (Thermo Fisher Scientific) and visualised using a ChemiDoc imaging system (Biorad).

4.5 Densitometry

Regions of Interest (ROIs) were obtained from each band of interest and the intensity was measured using ImageJ. For each band, the same ROI was used for background calculation and removal from areas adjacent to each band. The intensity of bands from samples were normalised for the intensity of the corresponding control sample.

5. Infection

U2OS or THP-1 cells were infected with the appropriate *C. burnetii* strain (MOI of 100) in DMEM and RPMI medium respectively, centrifuged at 400 x g for 10 min at room temperature to synchronise infection and then incubated at 37°C in a humidified atmosphere of 5% CO_2.

6. Secretion assay

For *C. burnetii* effector translocation assays, U2OS cells were cultured in black, clear-bottomed, 96-well plates and infected with the appropriate *C. burnetii* strain (MOI of 100) for 6, 12, 24, 48 and 72 h. *C. burnetii* expressing BLAM alone or BLAM-tagged CBU0021 (CvpB) were used as negative and positive controls, respectively. Cell monolayers were loaded with the fluorescent substrate CCF4/AM (LiveBLAzer-FRET B/G loading kit; Invitrogen) in a solution containing 20 mM HEPES, 15 mM probenecid (Sigma) pH 7.3, in Hank's Balanced Salt Solution (HBSS). Cells were incubated in the dark for 2 h at room temperature and imaged using an EVOS inverted fluorescence microscope. Images were acquired using DAPI and GFP filter cubes. The image analysis software CellProfiler was used to segment and count total cells and positive cells in the sample using the 520-nm and 450-nm emission channels, respectively, and to calculate the intensity of fluorescence in each channel. Following background fluorescence subtraction using negative control samples, the percentage of positive cells was then calculated and used to evaluate effector translocation. A threshold of

20% of positive cells was applied to determine efficient translocation of bacterial effector proteins.

7. Protein-lipid overlay assay

7.1 Pulldown of lipid-binding proteins

C. burnetii NMII strain was grown in 1x ACCM-2 medium for 7 days and harvested at 1,000 x *g* for 45 min at 4°C, washed once in cold W-buffer (10 mM HEPES (pH 7.4), 150 mM NaCl) supplemented with 0.25% Nonidet P-40 (NP-40). Bacteria were sonicated using a Branson Sonifier S-450 for 20 seconds every 30 seconds for 15 min and centrifuged at 10,000 x *g* for 5 min at 4°C. The amount of soluble protein was estimated using the BCA assay as described in section **4.1.**

For pulldown assays, 1 ml of lysate containing 10 – 30 ug of total proteins was incubated 2 h at 4°C with 50 µl of lipid-coated agarose beads (10 pM of lipids / µl slurry; Echelon). The beads were washed five times in W-buffer supplemented with 0.25% NP-40. Bound proteins were eluted by adding 20 µl of Laemmli buffer (5 min, 95 °C) and analysed by SDS-PAGE/Silver staining.

7.2 PIP strips

Purified His-tagged *C. burnetii* proteins were incubated with PIP Strips (Echelon) following the manufacturer's recommendations. Briefly, Tris buffered saline + BSA (TBS-T/BSA) (10 mM Tris·HCl, pH 8, 150 mM NaCl, 0.1% Tween 20, 3% (wt/vol) BSA) was used throughout the assay. PIP Strips were first blocked for 1 h in TBS-T/BSA before being incubated with 1 µg/mL of purified proteins at 4 °C overnight. Membranes were washed three times with TBS-T/BSA and immunoblotted with anti-His HRP-conjugated antibodies for 1 h at room temperature. Following three washes with TBS-T/BSA, the membranes were probed with ECL for signal detection and visualised using a ChemiDoc imaging system (Biorad).

8. Eukaryotic cells methods

8.1 Cell transfection

U2OS cells were grown to 70% confluence on glass cover slips in 24-well plates (Falcon) and transfected with Polyethylenimine (PEI, tebu-bio) according to the manufacturer's indications. Briefly, U2OS cells were incubated in 500 µl of fresh DMEM + 10% FCS. For 1 well in a 24-well plate, 1µg of plasmid DNA and 2 µl of PEI were diluted in 100 µl of sterile

150mM NaCl and were incubated at room temperature for 10 min. The transfection mix was then added to the cells and the plates were gently swirled and incubated at 37°C in a humidified atmosphere of 5% CO_2 for 12 to 24 h.

8.2 Tripartite split-GFP assay

For the interaction assay, U2OS cells were grown to 90% confluence on glass cover slips in 24-well plates (Falcon) and transfected with Lipofectamine 2000 (Invitrogen) according to the manufacturer's indications. For 1 well in a 24-well plate, 1 µg of plasmids encoding for GFP1-9, GFP10 and GFP11 fusions were diluted with 2 µl of Lipofectamine 2000 in 100 µl of DMEM without FCS and were incubated at room temperature for 20 min. The transfection mix was then added to the cells and the plates were gently swirled and incubated at 37°C in a humidified atmosphere of 5% CO_2 for 24 h.

At 24 h post-transfection, cells were fixed in 4% paraformaldehyde in PBS solution and processed for immunofluorescence. Protein/protein interactions were scored by calculating the percentage of GFP-positive cells over the total number of cells positive for the anti-GFP antibody.

8.3 Cell fractionation

U2OS cells were grown in 100-mm Petri dishes before being infected with *C. burnetii* strains used in this study or transfected as described above with 10 µg of plasmid DNA and 20 µl of PEI in 500 µl of sterile 150 mM NaCl. Transfected or infected cells were washed 2 times with DPBS and centrifuged at 1500 rpm at 4°C for 10 minutes. Cell pellets were then subjected to cell fractionation to isolate cytoplasmic, nuclear, and chromatin fractions. As described in Prokop *et al.*, 2017, cells were resuspended in 3 volumes of buffer A (20 mM HEPES, pH 7, 0.15 mM EDTA, 0.15 mM EGTA, 10 mM KCl, 0.5 mM spermine and 0.15 mM spermidine protease inhibitors (Complete, Roche)) at 4°C. Cells were lysed in 1% NP-40 by vortexing for 20 s at 4°C. Lysates were mixed with 8/9 volumes of buffer SR (50 mM HEPES, pH 7, 0.25 mM EDTA, 10 mM KCl, 70% [wt/vol] sucrose, 0.5 mM spermine and 0.15 mM spermidine, protease inhibitors (Complete, Roche)). Cell lysates were centrifuged at 2,000 g for 5 min at 4°C to recover the nuclear fraction. Supernatants were centrifuged at 20,000 *g* for 20 min at 4°C to collect the cytoplasmic fraction. Nuclei were washed in 3 volumes of buffer B (10 mM HEPES, pH 7, 0.1 mM EDTA, 100 mM NaCl, 25% [wt/vol] glycerol, 0.5 mM spermine and 0.15 mM spermidine, protease inhibitors (Complete, Roche)) and then centrifuged at 2,000 × *g* for 5 min at 4°C. Pellets were resuspended in 2 volumes of sucrose buffer (20 mM

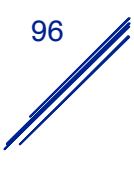

Tris, pH 7.65, 60 mM NaCl, 15 mM KCl, 0.34 M sucrose, 0.5 mM spermine, and 0.15 mM spermidine, protease inhibitors (Complete, Roche)). High-salt buffer (20 mM Tris, pH 7.65, 0.2 mM EDTA, 25% glycerol, 900 mM NaCl, 1.5 mM $MgCl_2$, 0.5 mM spermine and 0.15 mM spermidine, supplemented with protease inhibitor) was added drop by drop while vortexing, to reach a final concentration of 300 nM. Nuclei were incubated on ice for 30 min and homogenised every 5 min. Following the incubation, 1/3 volumes of sucrose buffer was added, and nuclear extract cell lysates were centrifuged for 10 min at 10,000 × *g* to collect soluble nuclear fractions. Pellets were then resuspended in 2 volumes of sucrose buffer followed by the addition of 0.0025 U/µl micrococcal nuclease and 1 mM $CaCl_2$ prior to incubation for 15 min at 37°C to digest DNA. 4 mM EDTA was added to stop DNA digestion and samples were sonicated using a Bioruptor Pico (Diagenode) for 30 s every minute for 10 min. Samples were finally centrifuged at 13,000 *g* to collect chromatin fractions.

Where appropriate, cytoplasmic, nuclear, and chromatin fractions were subjected to immunoprecipitation using 40 µL of anti-HA magnetic beads (Sigma) for 2 h at 4 °C with rotation. Bound proteins were eluted using 80 µL of 100 µg/mL^{-1} HA-peptide (Sigma) and then resuspended in 4x Laemmli buffer for Western blot analysis as described in section **4**.

8.4 Co-immunoprecipitation

U2OS cells were grown to 60% confluence in 100-mm Petri dishes before being transfected as described above with 10 µg of plasmid DNA and 20 µl of PEI in 500 µl of sterile 150 mM NaCl. 24h post-transfection, cells were washed 2 times with DPBS and lysed in 500 µl of lysis buffer (10 mM Tris-HCl, pH 7.5, 150 mM NaCl, 0.5mM EDTA, 1% NP40, protease inhibitors (Complete, Roche)). The lysate was transferred to a pre-chilled eppendorf tube and centrifuged at 14,000 rpm for 10 minutes at 4°C. The cleared lysate was transferred to a fresh pre-chilled eppendorf tube containing 25 µl of pre-equilibrated GFP-Trap magnetic beads (Chromotek) and incubated on a spinning wheel for 2 h at 4°C. The beads were washed 3 times with wash buffer (10 mM Tris-HCl, pH 7.5, 150 mM NaCl, 0.5mM EDTA, protease inhibitors (Complete, Roche)) and then resuspended in 4x Laemmli buffer. Analysis of the samples was performed by Western blot as described in section **4.4**

8.5 Ran activation assay

U2OS cells were either infected or transfected and lysed with lysis buffer (25 mM HEPES, pH 7.5, 150 mM NaCl, 1% NP-40, 10 mM $MgCl_2$, 1 mM EDTA, 2% glycerol, protease inhibitors (Complete, Roche)). Cell lysates were then centrifuged for 10 min at 14,000 × g at 4

°C. For Ran-GTP immunoprecipitation, 40 µL of RanBP1 (Ran-specific binding protein 1) beads (Cell Biolabs, Inc.) were incubated with cell lysates for 1 h at 4 °C on a spinning wheel, and then washed three times with lysis buffer. The beads were resuspended in 4x Laemmli buffer and then analysed by Western blot as described in section **4.4**. GTP-bound Ran levels were determined by calculating the signal ratio of GTP-bound Ran over the total amount of Ran.

8.6 NF-κB / IRF-3 translocation assay

To analyse NF-κB nuclear translocation, U2OS cells were grown to 60% confluence before being transfected as previously described. At 24 h post-transfection, cells were incubated with media containing 10 ng/mL TNF-α (Peprotech) to activate the NF-κB pathway, for 30 min at 37 °C. Alternatively, cells were preincubated with media containing 5 nM leptomycin B (LMB, LC laboratories) to block nuclear export, for 4 h at 37 °C, followed by a TNF-α treatment as indicated above where needed. For *C. burnetii* infection assays, cells were infected with *C. burnetii* and incubated at 37 °C for 1 to 3 days. Cells were then fixed in 4% paraformaldehyde in PBS solution and processed for NF-κB immunostaining. The image analysis software CellProfiler was used to segment all nuclei using the Hoechst staining and cell contours using nuclei as seeds and p65 labeling. Cytoplasm was segmented by subtracting nuclei from cell objects. Next, mCherry signal was used to identify and isolate the subpopulation of transfected cells and single cell measurements of the ratio of the mean p65 fluorescence in the nucleus versus cytoplasm were calculated for each condition. For infection assays, CellProfiler was used to identify and isolate the population of infected cells based on the GFP fluorescence associated with the strains of *C. burnetii* used in this study and nuclear p65 fluorescence was specifically measured as described above in the subpopulation of infected cells. To analyse IRF-3 translocation, U2OS cells expressing FLAG-IRF-3 were were transfected as described above. At 24 h post-transfection, cells were infected with a defective-interfering H4 Sendai virus, used at 50 hemagglutination units (HAU)/mL to activate the IRF-3 pathway, for 18 h at 37 °C. Cells were then fixed in 4% paraformaldehyde in PBS solution and processed for FLAG immunostaining. IRF3 nuclear translocation was measured as described above for p65.

8.7 Immunofluorescence staining

U2OS cells were fixed in 4% (wt/vol) paraformaldehyde in PBS solution at room temperature for 20 min. Samples were then rinsed in PBS solution and incubated in blocking solution (0.5% BSA, 50 mM NH_4Cl in PBS solution, pH 7.4). Cells were then incubated with

the primary antibodies diluted in blocking solution for 1 h at room temperature, rinsed five times in PBS solution and further incubated for 1 h with the secondary antibodies diluted in the blocking solution. Where appropriate, phalloidin coupled to Alexa Fluor 647 (Life technologies) was added to the secondary antibody solution for actin staining. To visualise nuclear proteins, cells were fixed as previously described in 4% (wt/vol) paraformaldehyde in PBS solution. Cells were permeabilised with 0.5% Triton X-100 in PBS solution for 3 min at room temperature. Sample were then rinsed in PBS solution and incubated with blocking solution (0.1% Triton X-100, 5% [wt/vol] milk in PBS solution) for 1 h at room temperature. Cells were then incubated with the primary antibodies diluted in blocking solution for 1 h at 37 °C, rinsed five times in PBS solution and incubated with the secondary antibodies for 1 h at room temperature. For all conditions, coverslips were mounted by using Fluoromount mounting medium (Sigma) supplemented with Hoechst 33258 (Sigma) for DNA staining.

8.8 Microscopy and image analysis

Samples were imaged with a Zeiss Axio Imager Z1 epifluorescence microscope (Carl Zeiss) connected to a CoolSNAP HQ^2 charge-coupled device (CCD) camera (Photometrics). Images were acquired alternatively with 100×, 63×, or 40× oil immersion objectives and processed with MetaMorph (Universal Imaging). ImageJ and CellProfiler softwares were used for image analysis and quantifications.

Confocal microscopy was performed using a TCS SP8 HyVolution microscope (Leica) connected to an SP5-SMD microscope (Leica). Images were acquired with a 63x oil immersion objective and processed with LAS-AF (Leica). 3D reconstruction was performed using IMARIS software.

Simultaneous multicolor confocal image acquisition was performed in live with the Opera phenix system (Perkin Elmer). Images were acquired with a 63x oil immersion objective and analysed using Icy software.

8.9 Flow cytometry

For intracellular human TNF-α/IFN-α4 staining, 5×10^4 THP-1 cells differentiated for 2 days in PMA (200 ng/mL) and seeded in 24-well plates were infected with the indicated *C. burnetii* strain for 72 and 96 h. Cells were then treated with 1 µg/mL of Brefeldin A (BFA, Biolegend) for the last 24 h to inhibit protein secretion. The following day, cells were fixed using 2% paraformaldehyde in PBS solution for 20 min at 4 °C. After washing with fluorescence-

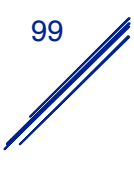

activated cell sorting (FACS) buffer (1% BSA in PBS solution), cells were permeabilised in FACS buffer supplemented with 0.1% saponin for 30 min at 4 °C and then stained with anti-TNF-α-PE and IFN-α-PE antibodies for 1 h at 4 °C. Infected cells were analysed based on the GFP fluorescence associated with the strains of *C. burnetii* used in this study. Flow cytometry analyses were performed on a BD FACSCalibur flow cytometer (BD Biosciences) using flow cytometry (CellQuest software, BD Biosciences). FlowJo software (Tree Star) was used to analyse data.

9. Statistical analysis

Statistical analyses of data were performed using Prism software (GraphPad,). For experiments requiring statistical analysis, an adapted statistical test was performed.

Strain	Description	Origin
WT *C. burnetii*	*C. burnetii* RSA 439 Nine Mile II	Robert Heinzen
GFP-tagged WT *C. burnetii*	*C. burnetii* RSA 439 Nine Mile II carrying a transposon insertion between *cbu1847b* and *cbu1849*	(Martinez *et al.*, 2014)
C. burnetii Tn227	*C. burnetii* RSA 439 Nine Mile II carrying a transposon insertion GFP-CAT in *cbu1217* (*nopA*)	(Martinez *et al.*, 2014)
C. burnetii Tn1898	*C. burnetii* RSA 439 Nine Mile II carrying a transposon insertion GFP-CAT in *cbu0635*	(Martinez *et al.*, 2014)
C. burnetii Tn1577	*C. burnetii* RSA 439 Nine Mile II carrying a transposon insertion GFP-CAT in *cbu2007*	Unpublished data
C. burnetii Tn292	*C. burnetii* RSA 439 Nine Mile II carrying a transposon GFP-CAT in *cbu1648* (*dotA*)	(Martinez *et al.*, 2014)
***nopA::Tn* Comp.**	*C. burnetii* RSA 439 Nine Mile II *Tn227* transformed with a pUC18R6K-miniTn7T-Kan-promNopA-4HA-NopA plasmid encoding 4HA-*nopA* under the control of the endogenous promoter	This study
SeV-DI-H4	Replication-defective Sendaï Virus	D. Garcin

Table 8. List of pathogen strains used in this study

Name	Description	Origin
pXDC61K	IPTG-inducible expression vector for N-terminal fusion of Beta-lactamase enzyme in *C. burnetii*, Kanamycin resistance	Julie Allombert
pXDC61K-CBU0021	IPTG-inducible expression of BLAM-CBU0021 (CvpB)	(Martinez *et al.* 2016)
pXDC61K-CBU0072	IPTG-inducible expression of BLAM-CBU0072 (AnkA)	Julie Allombert
pXDC61K-CBU0175	IPTG-inducible expression of BLAM-CBU0175	Julie Allombert
pXDC61K-CBU0295	IPTG-inducible expression of BLAM-CBU0295 (CstK)	Julie Allombert
pXDC61K-CBU0447	IPTG-inducible expression of BLAM-CBU0447 (AnkF)	Julie Allombert
pXDC61K-CBU0635	IPTG-inducible expression of BLAM-CBU0635	This study
pXDC61K-CBU0781	IPTG-inducible expression of BLAM-CBU0781 (AnkG)	Julie Allombert
pXDC61K-CBU1217	IPTG-inducible expression of BLAM-CBU1217 (NopA)	Julie Allombert
pXDC61K-CBU2007	IPTG-inducible expression of BLAM-CBU2007	This study
pLVX-mCherry-N2	CMV expression vector expressing a C-terminal mCherry tag	(Martinez *et al.* 2016)
pLVX-mCherry-C1	CMV expression vector expressing a N-terminal mCherry tag	Clontech
mCherry2-C1	CMV expression vector expressing a N-terminal mCherry tag	Addgene
pLVX-NopA-mCherry	CMV expression vector expressing NopA (CBU1217) fused to a C-terminal mCherry tag	Julie Allombert
pLVX-NopA$_{Nter}$-mCherry	CMV expression vector expressing the N-terminal domain of CBU1217 (aa1-195) fused to a C-terminal mCherry tag	Julie Allombert
pLVX-NopA$_{Cter}$-mCherry	CMV expression vector expressing the C-terminal domain of CBU1217 (aa196-497) fused to a C-terminal mCherry tag	Julie Allombert
pLVX-CvpB$_{opt}$-mCherry	CMV expression vector expressing CvpB (codon optimised) with C-terminal fusion of mCherry tag	(Martinez *et al.* 2016)
pLVX-CBU0635$_{1-61}$-mCherry	CMV expression vector expressing CBU0635$_{1-61}$ (aa1-61) fused to a C-terminal mCherry tag	This study
pLVX-CBU0635$_{138-313}$-mCherry	CMV expression vector expressing CBU0635$_{138-313}$ (aa138-313) fused to a C-terminal mCherry tag	This study
pLVX-CBU1576-mCherry	CMV expression vector expressing CBU1576 fused to a C-terminal mCherry tag	This study
pLVX-CBU1639-mCherry	CMV expression vector expressing CBU1639 fused to a C-terminal mCherry tag	This study
pLVX-CBU1686-mCherry	CMV expression vector expressing CBU1686 fused to a C-terminal mCherry tag	This study
pLVX-CBU2007-mCherry	CMV expression vector expressing CBU2007 fused to a C-terminal mCherry tag	This study
pCL-Neo-mCherry-2xFYVE	Encodes mCherry-2xFYVE (PI3P probe)	(Martinez *et al.* 2016)
mCh2-C1-OSBP-PH	Encodes mCherry-OSBP-PH(PI4P probe)	This study
mCh2-C1-FAPP1-PH	Encodes mCherry-FAPP1-PH-mCherry (PI4P probe)	This study
mCh2-C1-P4C_SidC	Encodes mCherry-P4C_SidC (PI4P probe)	This study
P4M_SidM-mCherry	Encodes mCherry-P4M_SidM (PI4P probe)	Rossella Venditti
mCherry-PHD2X	Encodes mCherry-PHD2X (PI5P probe)	Bernard Payrastre
pLVX-mCherry-AKT-PH	Encodes mCherry-AKT-PH (PI3,4P_2 probe)	This study
NES-mCherry-TAPP1-cPHx3	Encodes mCherry-TAPP1-cPHx3 (PI3,4P_2 probe)	Addgene
mCh2-C1-ML1N-PH	Encodes mCherry-ML1N-PH (PI3,5P_2 probe)	This study
pLVX-PLCδ-2xPH-mCherry	Encodes PLCδ-2xPH-mCherry (PI4,5P_2 probe)	This study
pLVX-mCherry-Gab2-PH	Encodes mCherry-Gab2-PH (PI3,4,5P_3 probe)	This study
pLVX-BTK-PH-mCherry	Encodes mCherry-BTK-PH (PI3,4,5P_3 probe)	This study
mRFP-Lactadherin-C2	Encodes RFP-Lactadherin-C2 (PS probe)	Addgene

Name	Description	Origin
mCh2-C1-PKCɣ-PH	Encodes mCherry-PKCɣ-PH (DAG probe)	This study
Spo2op1-DsRed	Encodes spo2op1-DsRed (PA probe)	Nicolas Vitale
Spo2op2-RFP	Encodes spo2op2-RFP (PA probe)	Nicolas Vitale
pRK5-HA	CMV expression vector for N-terminal fusion of HA tag	(Martinez *et al.* 2016)
pRK5-HA-NopA	CMV expression vector for N-terminal HA-tagged full length NopA (CBU1217)	Julie Allombert
pRK5-HA-NopA$_{Nter}$	CMV expression vector for HA-tagged NopA (CBU1217) N-terminal domain (aa1-195)	Julie Allombert
pRK5-HA-NopA$_{Cter}$	CMV expression vector for HA-tagged NopA (CBU1217) C-terminal domain (aa196-497)	Julie Allombert
pRK5-HA-NopA$_{RCC1}$	CMV expression vector for HA-tagged NopA (CBU1217) C-terminal domain (aa196-243)	This study
pRK5-HA-NopA$_{RCC1-2}$	CMV expression vector for HA-tagged NopA (CBU1217) C-terminal domain (aa196-310)	This study
pRK5-HA-NopA$_{RCC1-2-3}$	CMV expression vector for HA-tagged NopA (CBU1217) C-terminal domain (aa196-368)	This study
pRK5-HA-NopA$_{RCC4}$	CMV expression vector for HA-tagged NopA (CBU1217) C-terminal domain (aa429-497)	This study
pRK5-HA-NopA$_{RCC3-4}$	CMV expression vector for HA-tagged NopA (CBU1217) C-terminal domain (aa314-497)	This study
pRK5-HA-NopA$_{RCC2-3-4}$	CMV expression vector for HA-tagged NopA (CBU1217) C-terminal domain (aa251-497)	This study
pRK5-HA-CvpB	pCMV expression vector expressing CvpB with N-terminal fusion of HA tag	(Martinez *et al.* 2016)
pRK5-HA-CvpF	pCMV expression vector expressing CvpF with N-terminal fusion of HA tag	(Siadous et al., 2020)
pRK5-HA-CBU0635	pCMV expression vector expressing CBU0635 with N-terminal fusion of HA tag	This study
pRK5-HA-CBU0635$_{1-61}$	CMV expression vector expressing CBU0635$_{1-61}$ (aa1-61) with N-terminal of HA tag	This study
pRK5-HA-CBU0635$_{138-313}$	CMV expression vector expressing CBU0635$_{138-313}$ (aa138-313) with N-terminal of HA tag	This study
pRK5-HA-CBU0635$_{C133A}$	CMV expression vector expressing CBU0635$_{C133A}$ with N-terminal of HA tag	This study
pRK5-HA-CBU0635$_{R139A}$	CMV expression vector expressing CBU0635$_{R139A}$ with N-terminal of HA tag	This study
pRK5-HA-CBU1576	pCMV expression vector expressing CBU1576 with N-terminal fusion of HA tag	This study
pRK5-HA-CBU1576$_{Nter}$	pCMV expression vector expressing the N-terminal domain of CBU1576 (aa1-588) with N-terminal fusion of HA tag	This study
pRK5-HA-CBU1576$_{Cter}$	pCMV expression vector expressing the C-terminal domain of CBU1576 (aa589-839) with N-terminal fusion of HA tag	This study
pRK5-HA-CBU2007	pCMV expression vector expressing CBU2007 with N-terminal fusion of HA tag	This study
pRK5-HA-CBU2007$_{1-213}$	pCMV expression vector expressing the N-terminal domain of CBU2007$_{1-213}$ (aa1-213) with N-terminal fusion of HA tag	This study
pRK5-HA-CBU2007$_{214-395}$	pCMV expression vector expressing the C-terminal domain of CBU2007$_{214-395}$ (aa214-395) with N-terminal fusion of HA tag	This study
pRK5-HA-CBU2007$_{214-345}$	pCMV expression vector expressing the C-terminal domain of CBU2007$_{214-345}$ (aa214-345) with N-terminal fusion of HA tag	This study
pcDNA3-IRF-3-3xFLAG- SmNLuc	T7 expression vector encoding IRF-3 with C-terminal fusion of 3FLAG tag	Sebastien Nisole
pcDNA-CHMP4B-Flag	Encodes human CHMP4B with C-terminal fusion of Flag tag	(Morita *et al.*, 2007)
pCMV_GFP1-9-OPT	T7 expression vector encoding GFP1-9	(Cabantous *et al.* 2013)

Name	Description	Origin
pcDNA3-GFP10-zipper-GFP11	T7 expression vector encoding GFP10-GFP11	(Cabantous *et al.* 2013)
pcDNA3-GFP10-zipper	T7 expression vector for N-terminal fusion of GFP10	(Cabantous *et al.* 2013)
pcDNA3-GFP10-zipper-Ran	T7 expression vector expressing Ran with N-terminal fusion of GFP10 tag	This study
pcDNA3-zipper-GFP11	T7 expression vector for C-terminal fusion of GFP11	(Cabantous *et al.* 2013)
pcDNA3-NopA-zipper-GFP11	T7 expression vector expressing NopA with C-terminal fusion of GFP11 tag	This study
pcDNA3-RCC1-zipper-GFP11	T7 expression vector expressing RCC1 with C-terminal fusion of GFP11 tag	This study
pcDNA3-Fibrillarin-zipper-GFP11	T7 expression vector expressing Fibrillarin with C-terminal fusion of GFP11 tag	This study
pGBKT7-Ran$_{WT}$	T7 expression vector encoding RanWT	Aymelt Itzen
pGBKT7-Ran$_{T24N}$	T7 expression vector encoding RanT24N	Aymelt Itzen
pGBKT7-Ran$_{Q69L}$	T7 expression vector encoding RanQ69L	Aymelt Itzen
pGBKT7-Ran$_{N122I}$	T7 expression vector encoding RanN122I	Aymelt Itzen
pLVX-GFP-N2	CMV expression vector for C-terminal fusion of GFP	Eric Martinez
pLVX-Ran$_{WT}$-GFP-N2	CMV expression vector expressing Ran$_{WT}$ with C-terminal fusion of GFP tag	This study
pLVX-Ran$_{T24N}$-GFP-N2	CMV expression vector expressing Ran$_{T24N}$ with C-terminal fusion of GFP tag	This study
pLVX-Ran$_{Q69L}$-GFP-N2	CMV expression vector expressing Ran$_{Q69L}$ with C-terminal fusion of GFP tag	This study
pLVX-Ran$_{N122I}$-GFP-N2	CMV expression vector expressing Ran$_{N122I}$ with C-terminal fusion of GFP tag	This study
pEGFP-2xFYVE	Encodes GFP-2xFYVE (PI3P probe)	Scot Ouellette
GFP-OSBP-PH	Encodes GFP-OSBP-PH (PI4P probe)	Addgene
FAPP1-PH-GFP	Encodes FAPP1-PH-GFP (PI4P probe)	Rossella Venditti
P4C_SidC-GFP	Encodes P4C_SidC-GFP (PI4P probe)	Rossella Venditti
P4M_SidM-GFP	Encodes P4M_SidM-GFP (PI4P probe)	Rossella Venditti
eGFP-PHD2X	Encodes GFP-PHD2X (PI5P probe)	Bernard Payrastre
GFP-C1-AKT-PH	Encodes AKT-PH-GFP (PI3,4P_2 probe)	Addgene
NES-GFP-TAPP1-cPHx2	Encodes GFP-TAPP1-cPHx2 (PI3,4P_2 probe)	Addgene
pEGFP-C1-ML1N-PH	Encodes GFP-ML1N-PH (PI3,5P_2 probe)	Addgene
PLCδ-2xPH-GFP	Encodes PLCδ-2xPH-GFP (PI4,5P_2 probe)	Addgene
Gab2-PH-GFP	Encodes mCherry-Gab2-PH (PI3,4,5P_3 probe)	Addgene
BTK-PH-GFP	Encodes mCherry-BTK-PH (PI3,4,5P_3 probe)	Addgene
peGFP-Lactadherin-C2	Encodes GFP-Lactadherin-C2 (PS probe)	Addgene
GFP-C1-PKCɣ-PH	Encodes GFP-PKCɣ-PH (DAG probe)	Addgene
GFP Spo2op1	Encodes GFP-spo2op1 (PA probe)	Nicolas Vitale
GFP Spo2op2	Encodes GFP-spo2op2 (PA probe)	Nicolas Vitale
peGFP-RAB5	Encodes human RAB5 with N-terminal fusion of GFP tag	Addgene
peGFP-RAB7	Encodes human RAB7 with N-terminal fusion of GFP tag	Addgene
peGFP-RAB7$_{T22N}$	Encodes human RAB7$_{T22N}$ with N-terminal fusion of GFP tag	Addgene
peGFP-RAB7$_{Q67L}$	Encodes human RAB7$_{Q67L}$ with N-terminal fusion of GFP tag	Addgene
pGFP-M6PR	Encodes human M6PR with C-terminal fusion of GFP tag	(Polishchuk *et al.*, 2006)
pcDNA-GFP-TSG101	Encodes human TSG101 with N-terminal fusion of GFP tag	(Morita *et al.*, 2007)
peGFP-VPS4A	Encodes human VPS4A with N-terminal fusion of GFP tag	(Morita *et al.*, 2007)

Name	Description	Origin
peGFP-VPS4A$_{K178Q}$	Encodes human VPS4A$_{K178Q}$ with N-terminal fusion of GFP tag	Delphine Muriaux
peGFP-VPS4A$_{E225Q}$	Encodes human VPS4A$_{E225Q}$ with N-terminal fusion of GFP tag	Delphine Muriaux
Sac1$_{K2A}$-GFP	CMV expression vector expressing Sac1$_{K2A}$ with C-terminal fusion of GFP tag	Seth Field
pUC18R6K-miniTn7T-Kan	miniTn7 transposon with kanamycin resistance cassette	Robert Heinzen
pUC18R6K-miniTn7T-Kan-promNopA-4HA-NopA	miniTn7 transposon with kanamycin resistance cassette expressing 4HA-NopA under the control of the endogenous promoter	This study
pUC18R6K-miniTn7T-Kan-prom-CBU0634-4HA-CBU0635	miniTn7 transposon with kanamycin resistance cassette expressing 4HA-CBU0635 under the control of the endogenous promoter	This study
pUC18R6K-miniTn7T-Kan-prom-CBU0634-4HA-CBU0635-CBU0636	miniTn7 transposon with kanamycin resistance cassette expressing 4HA-CBU0635 under the control of the endogenous promoter	This study
pUC18R6K-miniTn7T-Kan-pmrA-4HA-CBU2007	miniTn7 transposon with kanamycin resistance cassette expressing 4HA-CBU2007 under the control of the endogenous promoter	This study
pUC18R6K-miniTn7T-Kan-pmrA-4HA-CBU2007-CBU2006-CBU2005-CBU2004	miniTn7 transposon with kanamycin resistance cassette expressing 4HA-CBU2007 under the control of the endogenous promoter	This study

Table 9. List of plasmids used in this study

Primer Name	Sequence
BLAM Translocation Assay	
Generation of pXDC61K-BLAM derivatives	
CBU0635-KpnI-Fw	CCAGGTACCATGCGAGAGGAAAAAGAGG
CBU0635-BamHI-Rev	CCAGGATCCCTAAACTAATGTCATTAAACGGTTATC
CBU1576-BamHI-Fw	CCAGGATCCATGCGTCCAGAACATAAAAAACCAATC
CBU1576-XbaI-rev	CCATCTAGACTAATGTTTCATCGAATACACCAC
CBU2007-BamHI	AGGGGATCCATGACAGTTTATTCCCGATATGA
CBU2007-XbaI-rev	AGGTCTAGACTAAAGGGTCCGGTATTTGAAG
Ectopic Expression	
Generation of pLVX-mCherry-N2 derivatives	
CBU1217-MluI	AGGACGCGTATGAGAACTTCGCATCAAAATCAA
CBU1217-NotI-rev	AGGGCGGCCGCCTTTCTGGAAAAAGGGGCGTA
CBU1217-Nter-NotI-rev	AGGGCGGCCGCTTTCTGTGAGTATGAATGCATG
CBU1217-Cter-start-MluI	AGGACGCGTATGGAAGGAGGAATTTATGGCTGG
PH-PLCd-MluI	AGGACGCGTATGGACTCGGGCCGG
PH-PLCd-NotI-rev	AGGGCGGCCGCTCGCATCCATGGAGCCTGAGTGGTG
PH-Btk-MluI	AGGACGCGTATGCAGAAAGAAGAAGCTATGGCC
PH-Btk-NotI-rev	AGGGCGGCCGCTCGAGGTTTTAAGCTTCCATTCCTGTT
CBU635-MluI	AGGACGCGTGCCACCATGCGAGAGGAAAAAGAGGAGG
CBU635-NotI-rev	AGGGCGGCCGCAAACTAATGTCATTAAACGGTTATCAG
CBU635(138-313)-MluI-Fw	AGGACGCGTGCCACCATGCATAGGCTTGTTAAGCA
CBU635(0-61)-NotI-Rv	GTTCGGCCGCAGATTTTTGCTTTCACGGATTGC
CBU635(0-313)-NotI-Rv	GTTGCGGCCGCGAATTTTATTTACCCATTCACGATCG
CBU1576-MluI	AGGACGCGTGCCACCATGCGTCCAGAACATAAAAAACCAATC
CBU1576-NotI-rev	AGGGCGGCCGCAATGTTTCATCGAATACACCACAA
CBU1639-MluI	AGGACGCGTGCCACCATGATGAGTCAAGTGCCTTTC
CBU1639-NotI-rev	AGGGCGGCCGCATCGGCTCACCCTTCGAC
CBU1686-MluI	AGGACGCGTGCCACCATGCCCTCTAGTTCTAAAGATTTAAG
CBU1686-NotI-rev	AGGGCGGCCGCAGGGTTGATATCCGTTTGTTGGTTC
CBU2007-MluI	AGGACGCGTGCCACCATGACAGTTTATTCCCGATATGAAT
CBU2007-NotI-rev	AGGGCGGCCGCAAAGGGTCCGGTATTTGAAGGG
Generation of pLVX-mCherry-C1 derivatives	
AKT-PH-EcoRI	AGGGAATTCAAACGACGTAGCCATTGTGAAG
AKT-PH-BamHI-rev	AGGGGATCCCTATGAATTCCATGGTCACACGG
PH-Gab2-EcoRI	AGGGAATTCAATGAGCGGCGGCGGC
PH-Gab2-BamHI-rev	AGGGGATCCTTAGAAGCCGCAGATCTGGC
Generation of mCherry2-C1 derivatives	
OSBP-PH-HindIII	AAGCTTCATCGGCTCGAGAGGG
OSBP-PH-XmaI-rev	CCCGGGTCACGAATTCTTCTTCACAGCT
FAPP1-PH-XhoI-Fw	CTCGAGGCATGGAGGGGGTGTTGTAC
FAPP1-PH-XmaI-Rev	CCCGGGTCAAGTCCTTGTATCAGTC
P4C-SidC-XhoI-Fw	CTCGAGGCAAGCCATTATTGGATGTGG
P4C-SidC-XmaI-rev	CCCGGGTCATTCCAGAGAGATGATTTCATC
ML1N-XhoI	CTCGAGGGTACTCTGACCTGACTATGGCAACAC
ML1N-XmaI-rev	AGGTCTAGATTAATTATCCAGGTCAGGGGGG
PKCg-XhoI	CTCGAGCTCACAAGTTCACCGCTCG
PKCgamma-HpaI-rev	GTTAACCTAGATCCGGTGGATCCC
Generation of pLVX-GFP-N2 derivatives	
Ran-EcoRI	AGGGAATTCCATGGCTGCGCAGGGAGAGC
Ran-BamHI-rev	AGGGGATCCCTACAGGTCATCATCCTCATC
Generation of pRK5-HA derivatives	
CBU1217-BamHI	AGAGGATCCAGAACTTCGCATCAAAATCAACC
CBU1217-EcoRI-rev	AGAGAATTCGTTCGAATCCCGCCCTCTC
CBU1217Nter-stop-EcoRI-rev	AGGGAATTCTTATTCTGTGAGTATGAATGCATGTC
CBU1217Cter-start-BamHI	AGGGGATCCATGGAAGGAGGAATTTATGGCTGG
CBU1217-1RCC-BamHI	AGGGGATCCCAAGGGTATATTTACGCCTGG

CBU1217-2RCC-BamHI	AGGGGATCCGGTTACATTTATGCTTGGGGTAA
CBU1217-3RCC-BamHI	AGGGGATCCGCACGGACAGCACAAGGACAT
RCC1-EcoRI-rev	CCGGAATTCTTAACGGTCCGCGAAATTAAGTTGG
RCC1-2-EcoRI-rev	CCGGAATTCTTATAGTTGAGTAAGTGCCAAGGTATGTC
RCC1-2-3-EcoRI-rev	CCGGAATTCTTATTCTGTTCGCGCGAGAGAAC
635-BamHI-Fw	CCAGGATCCCGAGAGGAAAAAGAGGAGG
635-EcoRI-rev	GCTGAATTCCTAAACTAATGTCATTAAACGGTTATCAG
CBU635(138-313)-BamHI-Fw	CCAGGATCCCATAGGCTTGTTAAGCATTGGAATG
CBU635(0-61)-EcoRI-Rv	GCTGAATTCCTAGATTTTTGCTTTCACGGATTG
CBU635(0-313)-EcoRI-Rv	GCTGAATTCCTAAATTTTATTTACCCATTCACGATC
635-C133A-Fw	CTACATTACCATATCTGGTTTGGCTGTATTTGCTTGCCATAGGCTTG
635-C133A-rev	CAAGCCTATGGCAAGCAAATACAGCCAAACCAGATATGGTAATGTAG
635-R139A-Fw	GTTTGTGTGTATTTGCTTGCCATGCGCTTGTTAAGCATTGGAATGCC
635-R139A-Rev	GGCATTCCAATGCTTAACAAGCGCATGGCAAGCAAATACACACAAAC
CBU1576-BamHI-Fw	CCAGGATCCCGTCCAGAACATAAAAAACCAA
CBU1576-HindIII-rev	GCTAAGCTTCTAATGTTTCATCGAATACACCACAA
CBU1576-Nter-HindIII-rev	GCTAAGCTTCTAAATGTCCTGCGAAAGCT
CBU1576-Cter-BamHI-Fw	CCAGGATCCTATCTCCGATACAAATTCCGA
CBU2007-BamHI-Fw	CCAGGATCCACAGTTTATTCCCGATATGAATTTC
CBU2007-HindIII-rev	GCTAAGCTTCTAAAGGGTCCGGTATTTGAAG
2007(214-395)-BamHI-Fw	CCAGGATCCATGAAAGTTCAGAATTATGTTCGGTC
2007(1-213)-HindIII-rev	GCTAAGCTTCTAAGTTTCTTCAGGAACAAAATAGGTG
2007(214-345)-HindIII-Rev	GCTAAGCTTCTATTCTGGGTTAGTTTTTATTGAATCAATTTTAG
Generation of vectors for tripartite GFP assay	
Ran-BspEI	TCCTCCGGAATGGCTGCGCAGGGAGA
Ran-XbaI-rev	CTAGTCTAGACTACAGGTCATCATCCTCATCCG
NopA-NotI	AAGGAAAAAAGCGGCCGCACCATGAGAACTTCGCATCAAAATCAA
NopA-ClaI-rev	CCCATCGATCTTTCTGGAAAAAGGGGCGTA
RCC1-NotI	AAGGAAAAAAGCGGCCGCACCATGTCACCCAAGCGC
RCC1-ClaI-rev	CCCATCGATGCTCTGTTCTTTGTCCTTGAC
FBL-NotI	AAGGAAAAAAGCGGCCGCACCATGAAGCCAGGATTCAGTCC
FBL-ClaI-rev	CCCATCGATGTTCTTCACCTTGGGGGG
***nopA*::Tn Complementation**	
NheI-prom1217-fw	CTAGCTAGCAGCGTGGTTTTATGAGAAAT
PstI-prom1217-Rev	CCAATGCATTGGTTCTGCAGTTCTTAGTTCTCCGTTTTAAGG
***cbu0635*::Tn Complementation**	
Prom0634-NheI-Fw	CTAGCTAGCGGATTTTGACTTTCTATTCGAC
Prom0634-PstI-Rv	TGGCTGCAGATTTATCTCCTTCTCTAATTAGAATAG
0635-XmaI-Fw	CTACCCGGGCTATGCGAGAGGAAAAAGAG
0635-BamHI-Rv	TGGGGATCCCTAAACTAATGTCATTAAACGG
0635-0636-BamHI-Rv	TGGGGATCCCTATATTAATTTTTTTCGTAGAAGC
***cbu2007*::Tn Complementation**	
Prom2007-Nhe1-Fw	CTAGCTAGCTTCAGTCTTTCAATCGCTTGG
Prom2007-PstI-Rv	TGGCTGCAGAGTTAAATCATAACTTCCTAAGG
2007-XmaI-Fw	CTACCCGGGATATGACAGTTTATTCCCGATATG
2007-BamHI-Rv	TGGGGATCCCTAAAGGGTCCGGTATTTG
2007-2004-BamHI-Rv	TGGGGATCCTCAACCAGACTTAGAAAATAACTC

Table 10. List of primers used in this study

Antibody	Dilution			Source
	Western blot	Immunofluorescence	Flow cytometry	
R α-NMII	1/5000e	1/500e		Covalab
R α-HA	1/2000e	1/200e		Proteintech
M α-HA	1/2000e	1/200e		Proteintech
M α-Ran	1/4000e			Sigma
M α-FLAG		1/200e		Sigma
M α-β-tubulin	1/2000e			Sigma
R α-GFP	1/2000e			Thermo Fisher Scientific
R α-Fibrillarin	1/2000e	1/200e		Abcam
R α-RAB26	1/1000e			Abcam
R α-PML		1/100e		Abcam
M α-DRP1	1/1000e			Abcam
M α-GAPDH	1/2000e			Life Technologies
R α-NF-κB p65	1/1000e	1/100e		Cell Signaling
M α-IκBα	1/1000e			Cell Signaling
R α-LAMP1		1/500e		Sigma
R α-GM130		1/200e		Abcam
R α-TGN46		1/100e		Proteintech
R α-LC3B		1/100e		Sigma
M α-LBPA		1/100e		Echelon
M α-ALIX		1/100e		Abcam
M α-6xHIS HRP	1/1000e			Sigma
H α-TNF-α			1/50e	Miltenyi
H α-IFN-α			1/50e	Miltenyi
α-M 488, 555, 647		1/1000e		Invitrogen
α-R 488, 555, 647		1/1000e		Invitrogen
α-R HRP	1/2000e			Sigma
α-M HRP	1/2000e			Sigma

Table 11. List of antibodies used in this study

Results

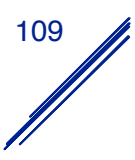

1. Modulation of innate immune signalling by a *Coxiella burnetii* eukaryotic-like effector protein

As illustrated above, the NF-kB pathway is inhibited by a Dot/Icm-mediated mechanism during *C. burnetii* infections; however, the effector protein/s involved in this process remained unknown (Mahapatra *et al.*, 2016). By investigating *C. burnetti* effector proteins containing eukaryotic-like domains, my thesis work allowed to demonstrate that NopA (Nucleolar protein A) is involved in the suppression of the NF-kB pathway by disrupting nucleocytoplasmic transport in infected cells. NopA displays 4 regulation of chromatin condensation (RCC) domains, which are found in the eukaryotic Ran GEF RCC1. Similar to RCC1, NopA localises at the nucleus of infected or transfected cells, it is found in the chromatin nuclear fraction, and uses the RCC domains to interact with Ran, a GTPase involved in the nucleocytoplasmic transport. Differently from RCC1 however, NopA accumulates at nucleoli, where it sequesters Ran, thus disrupting the Ran GDP-GTP gradient required for the nucleocytoplasmic transport of proteins. This leands to a defect in the nuclear import of the NF-kB subunit p65. Accordingly, qRT-PCR and flow cytometry analysis on a panel of cytokines has shown that cells exposed to the *Coxiella nopA::Tn* or *dotA*::Tn mutant strains present a functional innate immune response, as opposed to cells exposed to wt *C. burnetii* or the corresponding *nopA* complemented strain. Thus, NopA is an important regulator of the innate immune response allowing *C. burnetii* to behave as a stealth pathogen.

Modulation of innate immune signalling by a *Coxiella burnetii* eukaryotic-like effector protein

Burette M*, Allombert J*, Lambou K, Maarifi G, Nisole S, Di Russo Case E, Blanchet FP, Hassen-Khodja C, Cabantous S, Samuel S, Martinez E, Bonazzi M. Proc Natl Acad Sci U S A. 2020 Jun 16;117(24):13708-18.

Modulation of innate immune signaling by a *Coxiella burnetii* eukaryotic-like effector protein

Melanie Burette[a,1], Julie Allombert[a,1], Karine Lambou[a], Ghizlane Maarifi[a], Sébastien Nisole[a], Elizabeth Di Russo Case[b], Fabien P. Blanchet[a], Cedric Hassen-Khodja[c], Stéphanie Cabantous[d], James Samuel[b], Eric Martinez[a], and Matteo Bonazzi[a,2]

[a]Institut de Recherche en Infectiologie de Montpellier (IRIM) UMR 9004, CNRS, Université de Montpellier, 34293 Montpellier, France; [b]Department of Microbial and Molecular Pathogenesis, Texas A&M Health Science Center College of Medicine, Bryan, TX 77807–3260; [c]Montpellier Ressources Imagerie (MRI), BioCampus Montpellier, CNRS, INSERM, Université de Montpellier, 34293 Montpellier, France; and [d]Centre de Recherche en Cancérologie de Toulouse, INSERM, Université Paul Sabatier-Toulouse III, CNRS, 31037 Toulouse, France

Edited by Ralph R. Isberg, Tufts University School of Medicine, Boston, MA, and approved April 21, 2020 (received for review August 27, 2019)

The Q fever agent *Coxiella burnetii* uses a defect in organelle trafficking/intracellular multiplication (Dot/Icm) type 4b secretion system (T4SS) to silence the host innate immune response during infection. By investigating *C. burnetii* effector proteins containing eukaryotic-like domains, here we identify NopA (nucleolar protein A), which displays four regulator of chromosome condensation (RCC) repeats, homologous to those found in the eukaryotic Ras-related nuclear protein (Ran) guanine nucleotide exchange factor (GEF) RCC1. Accordingly, NopA is found associated with the chromatin nuclear fraction of cells and uses the RCC-like domain to interact with Ran. Interestingly, NopA triggers an accumulation of Ran-GTP, which accumulates at nucleoli of transfected or infected cells, thus perturbing the nuclear import of transcription factors of the innate immune signaling pathway. Accordingly, qRT-PCR analysis on a panel of cytokines shows that cells exposed to the *C. burnetii nopA*::Tn or a Dot/Icm-defective *dotA*::Tn mutant strain present a functional innate immune response, as opposed to cells exposed to wild-type *C. burnetii* or the corresponding *nopA* complemented strain. Thus, NopA is an important regulator of the innate immune response allowing *Coxiella* to behave as a stealth pathogen.

Coxiella burnetii | effector proteins | innate immune sensing | host/pathogen interactions | nucleocytoplasmic transport

The nuclear factor kappa-light-chain-enhancer of activated B cells (NF-κB) family of transcription factors regulates the expression of genes associated with diverse cellular functions and plays a central role in regulating the innate and acquired host immune response to bacterial infections (1, 2). Under physiological conditions, the transcription factors of the NF-κB family are sequestered in the cytoplasm by specific interactions with nuclear factor kappa-light polypeptide gene enhancer in B cells inhibitor alpha (IκBα), which mask the nuclear localization signal (NLS) on transcription factors. Exogenous signals, including recognition of the tumor necrosis factor (TNF) by TNF receptor or the bacterial lipopolysaccharide (LPS) by toll-like receptor 4 (TLR4), activate the NF-κB signaling pathway by triggering the phosphorylation and proteasomal degradation of IκBα, thus unmasking the NLS on transcription factors. The signal is then recognized by importin-α and members of the importin-β family, which mediate the translocation of transcription factors to the nucleus through nuclear pore complexes (1). Energy for nuclear transport of NLS-containing proteins is provided by intracellular gradients of the small GTPase Ras-related nuclear protein (Ran), which interacts with the importin complexes upon nuclear import. GDP-bound Ran is largely cytoplasmic and nuclear translocation triggers the conversion to the GTP-bound form by means of the Ran guanine nucleotide exchange factor (GEF) RCC-1 (regulator of chromosome condensation-1). In its GTP-bound form, Ran triggers the dissociation of importins from the cargo and importin complexes recycle back to the cytoplasm. There, Ran GTPase activating protein (RanGAP) generates Ran-GDP, which dissociates from importin complexes (3).

Given its pivotal role in the antimicrobial response, it is not surprising to observe that a considerable number of bacterial pathogens deploy effector proteins that modulate the NF-κB signaling pathway (1, 2). These are mostly involved in phosphorylation, ubiquitination, and proteasomal degradation of components of the NF-κB complex, whereas others modulate NF-κB-mediated transcription (1, 2). Interestingly, it has recently been reported that *Salmonella* and *Orientia tsutsugamushi* effector proteins can interfere with nucleocytoplasmic transport, thereby inhibiting nuclear translocation of the p65/RelA transcription factor (4, 5).

The Q fever pathogen *Coxiella burnetii* is an obligate intracellular bacterium that relies on the translocation of effector proteins by a defect in organelle trafficking/intracellular multiplication (Dot/Icm) type 4b secretion system (T4SS) to replicate within large autolysosomal-like compartments inside infected cells (6, 7). Bioinformatics analysis identified over 140 *C. burnetii* genes encoding candidate effector proteins (7); however, the majority of these remain underinvestigated due to the technical constraints associated with the genetic manipulation of this organism. A subset of effector proteins is involved in the biogenesis of *Coxiella*-containing vacuoles (CCVs), by rerouting membrane traffic to the bacterial replicative niche, while other effectors manipulate the

Significance

***Coxiella burnetii* is a stealth pathogen that evades innate immune recognition by inhibiting the NF-κB signaling pathway. This process is mediated by the bacterial Dot/Icm secretion system; however, the bacterial effector/s, as well as the molecular mechanism involved in this process have remained unknown to date. Here, by investigating *C. burnetii* proteins with eukaryotic-like features (EUGENs), we discovered a new effector protein, NopA (nucleolar protein A), which localizes at nucleoli of infected cells and perturbs nucleocytoplasmic transport by manipulating the intracellular gradients of the GTPase Ran. In doing so, NopA reduces the nuclear levels of transcription factors involved in the innate immune sensing of pathogens and single-handedly down-modulates the expression of a panel of cytokines.**

Author contributions: M. Burette, J.A., G.M., S.N., E.D.R.C., J.S., E.M., and M. Bonazzi designed research; M. Burette, J.A., K.L., G.M., S.N., E.D.R.C., and E.M. performed research; G.M., S.N., E.D.R.C., F.P.B., C.H.-K., and S.C. contributed new reagents/analytic tools; M. Burette, J.A., G.M., S.N., E.D.R.C., F.P.B., C.H.-K., J.S., E.M., and M. Bonazzi analyzed data; and M. Burette, E.M., and M. Bonazzi wrote the paper.

The authors declare no competing interest.

This article is a PNAS Direct Submission.

[1]M. Burette and J.A. contributed equally to this work.

[2]To whom correspondence may be addressed. Email: matteo.bonazzi@irim.cnrs.fr.

This article contains supporting information online at https://www.pnas.org/lookup/suppl/doi:10.1073/pnas.1914892117/-/DCSupplemental.

apoptotic and inflammatory pathways to ensure intracellular persistence (6). Importantly, *C. burnetii* behaves as a stealth pathogen, evading the host innate immune response by down-modulating the NF-κB and the inflammasome signaling pathways (8, 9). The *C. burnetii* effector protein IcaA (inhibition of caspase activation A) inhibits NOD-like receptor family pyrin domain containing 3 (NLRP3)-mediated inflammasome activation induced by caspase-11 (8), whereas the NF-κB signaling pathway is down-modulated in a Dot/Icm-dependent manner, by perturbing the nuclear translocation of the p65/RelA subunit, without affecting the overall cellular levels of p65 (9). However, the bacterial effector/s involved in this process remains uncharacterized (9). We have previously reported the large-scale phenotypic characterization of the *C. burnetii* transposon mutant library, which led to gaining important insights into the function of the Dot/Icm secretion system, and which highlight an important set of virulence determinants (10–12). Importantly, several genes involved in intracellular replication of *C. burnetii* encode proteins with predicted eukaryotic-like domains, which prompted us to investigate eukaryotic-like genes (EUGENs) on a genome-wide scale. Here, we identify and validate the Dot/Icm-mediated translocation of seven *C. burnetii* EUGENs. Among these, NopA (nucleolar protein A) displays four regulation of chromosome condensation (RCC) repeats, which are partially homologous to the seven repeats found in the bladed β-propeller structure of the Ran GEF RCC1 (13–15). Similarly to RCC1, NopA also localizes at the nucleus of infected or transfected cells; it is found associated with the chromatin nuclear fraction; and it uses the RCC-like domain to interact with Ran. Differently from RCC1, however, NopA accumulates at nucleoli and sequesters Ran, thus perturbing nucleocytoplasmic transport. Indeed, NopA perturbs nuclear translocation of p65 upon cell treatment with TNF-α or challenge with *C. burnetii*. Conversely, transposon insertions in the *nopA* gene restore nuclear translocation of p65 during infections, to levels that are similar to those observed with the Dot/Icm-deficient *C. burnetii dotA* mutant. Accordingly, myeloid cells challenged with the *C. burnetii nopA* or *dotA* mutant strains present a functional innate immune response, as opposed to myeloid cells exposed to wild-type (WT) *C. burnetii* or the *nopA* complemented strain.

Results

Identification of *C. burnetii* EUGENS. The searching algorithm for type IV effector proteins (S4TE) 2.0 (16) was used to identify *C. burnetii* eukaryotic-like genes (EUGENs) encoding candidate effector proteins. This allowed the identification of 56 genes, which were validated using the Protein families database (PFAM), Simple Modular Architecture Research Tool (SMART), Conserved Domain Database (CDD), and Eukaryotic Linear Motif (ELM) databases (*SI Appendix*, Table S1). Of these, 20 candidate EUGENS were retained for further analysis (*SI Appendix*, Table S2), based on the S4TE score (16), the eukaryotic-like domain encoded, and the presence of corresponding transposon mutants in our library (10). *cbu0072* (*ankA*), *cbu0201* (*ankC*), *cbu0447* (*ankF*), *cbu0781* (*ankG*), and *cbu1213* (*ankI*) encode ankyrin repeats (17, 18); *cbu0295*, *cbu0547*, and *cbu1457* (*cig43*) encode tetratricopeptide repeats; *cbu0175* and *cbu1379a* encode predicted Ser/Thr kinases; *cbu0801* (*rimI*), *cbu0505* (*cig14*), and *cbu1799* encode acetyltransferases; *cbu0096* encodes a predicted phospholipase D; *cbu0519* (*dedA*) encodes a SNARE-like domain-containing protein; *cbu1206* encodes a predicted sterol reductase; *cbu1217* encodes a protein with four regulation of chromosome condensation (RCC) repeats; *cbu1724* encodes a predicted F-box protein; *cbu1366* (*cig40*) encodes a coiled-coil domain-containing protein; and *cbu0542* (*ligA*) encodes a predicted DNA ligase (*SI Appendix*, Table S2). Of note, Dot/Icm-dependent translocation of proteins encoded by 8 of these genes has been previously validated using *Legionella pneumophila* as a surrogate system (17, 19, 20) (*SI Appendix*, Table S2). Selected genes were cloned into pXDC61K-*blaM* vector, thus generating N-terminal fusions with β-lactamase, and transformed into *C. burnetii* Nine Mile II (NMII) RSA439. The expression of 16 out of 20 chimeric proteins was validated by Western blot using an anti-β-lactamase antibody (*SI Appendix*, Fig. S1*A*). Candidate effector protein translocation was assessed at 6, 12, 24, 48, and 72 h postinfection using the β-lactamase assay. *C. burnetii* expressing β-lactamase alone or β-lactamase-tagged CvpB (CBU0021) (12) were used as negative and positive controls, respectively. CvpB, CBU0295, and CBU1217 were efficiently translocated from 12 h postinfection, whereas AnkA, F, and G were translocated from 24 h postinfection (Fig. 1 *A* and *B*). Finally, AnkC, CBU0175, and CBU1724 were also translocated, albeit less efficiently, at later time points of infection (Fig. 1 *A* and *B*). Plasmids encoding translocated effectors were then transformed into the *C. burnetii dotA*::Tn strain to validate their Dot/Icm-dependent secretion at 72 h postinfection. The expression of 6 chimeric proteins was validated by Western blot using an anti-β-lactamase antibody (*SI Appendix*, Fig. S1*B*). None of the effector proteins were secreted by the Dot/Icm-defective mutant as expected (Fig. 1*A*). Next, *cbu0072* (*ankA*), *cbu0295*, *cbu0447* (*ankF*), *cbu0781* (*ankG*), and *cbu1217* were cloned into a pLVX-mCherry vector to tag effector proteins at their N-terminal domain and their localization was investigated in noninfected and *C. burnetii*-infected U2OS cells (Fig. 1*C*). AnkA and CBU0295 were mostly diffuse in the cytoplasm and did not localize at CCVs in infected cells. AnkF displayed a punctate pattern in the cytoplasm, which partially colocalized with the lysosomal marker LAMP1 in noninfected and infected cells alike (Fig. 1*C*). Differently from previous reports, indicating a translocation of AnkG from mitochondria to the nucleus of transfected cells following staurosporine treatment (21), in our hands, this effector protein displayed nuclear localization even in the absence of staurosporine, in both infected and noninfected cells (Fig. 1*C*). Of note, CBU1217 was exclusively localized at subnuclear structures in over 90% of either infected or noninfected cells (Fig. 1*C*).

The Effector Protein CBU1217 Localizes at Nucleoli in Infected and Transfected Cells. The localization of CBU1217 was further investigated by cloning the gene into a pJA-LacO-4HA plasmid, to express the effector protein carrying an N-terminal 4×HA tag in *C. burnetii*, under the control of an isopropyl β-D-1-thiogalactopyranoside (IPTG) promoter, and monitor its localization during infection. GFP-expressing WT *C. burnetii* or the *dot/icm* mutant *dotA*::Tn (10) were transformed either with pJA-LacO-4HA or with pJA-LacO-4HA-*cbu1217*. Expression of 4HA-CBU1217 was validated by Western blot using an anti-HA antibody (*SI Appendix*, Fig. S1*C*). U2OS cells were challenged with the transformed *C. burnetii* strains and NopA localization was assessed, in the presence or absence of IPTG, using anti-HA and anti-fibrillarin antibodies, and Hoechst dye. Infections by *C. burnetii* transformed with pJA-LacO-4HA-*cbu1217* in the absence of IPTG did not show specific HA labeling (Fig. 2*A*). Addition of 1 mM IPTG triggered 4HA-CBU1217 expression, which colocalized with fibrillarin in over 90% of HA-positive cells (Fig. 2*B*). The intracellular localization of 4HA-CBU1217 was lost when cells were infected with the *dotA*::Tn mutant transformed with pJA-LacO-4HA-*cbu1217* in the presence of IPTG (Fig. 2*D*), confirming that CBU1217 is a Dot/Icm substrate. Induction of the expression of the HA tag alone did not show specific localization (Fig. 2*C*). We thus named the new *C. burnetii* EUGEN NopA, for nucleolar protein A.

As mentioned above, NopA encodes four RCC repeats in its C-terminal domain (Fig. 2*E*). In the eukaryotic protein RCC1, seven repeats are arranged in a seven-bladed propeller, which associates with nuclear chromatin and acts as a GEF for Ran, thus regulating nucleocytoplasmic protein transport (3). To determine the role of the RCC-like domain in NopA localization and function, the effector protein was cloned into a pRK5-HA plasmid to generate HA-tagged NopA. U2OS cells transfected with pRK5-HA-NopA were processed for immunofluorescence using Hoechst dye and anti-HA and anti-fibrillarin antibodies. In parallel, HA-NopA localization was investigated by Western blot using U2OS cells transfected as above and lysed and separated into cytoplasmic, nuclear, and chromatin fractions. Full-length NopA ($NopA_{FL}$) localized at nucleoli in over 90% of transfected cells, confirming our observations in the context of *C. burnetii* infections (Fig. 2*E*). Western blot analysis confirmed that NopA is excluded from the cytoplasmic fraction and localized at the soluble and chromatin nuclear fractions (Fig. 2*E*). Next, we generated HA-tagged NopA deletions to exclude ($NopA_{N\text{-}ter}$; amino acids [aa] 1 to 195, Fig. 2*F*) or include ($NopA_{C\text{-}ter}$; aa 196 to 497, Fig. 2*G*) the RCC repeats. Ectopically expressed HA-$NopA_{N\text{-}ter}$ was

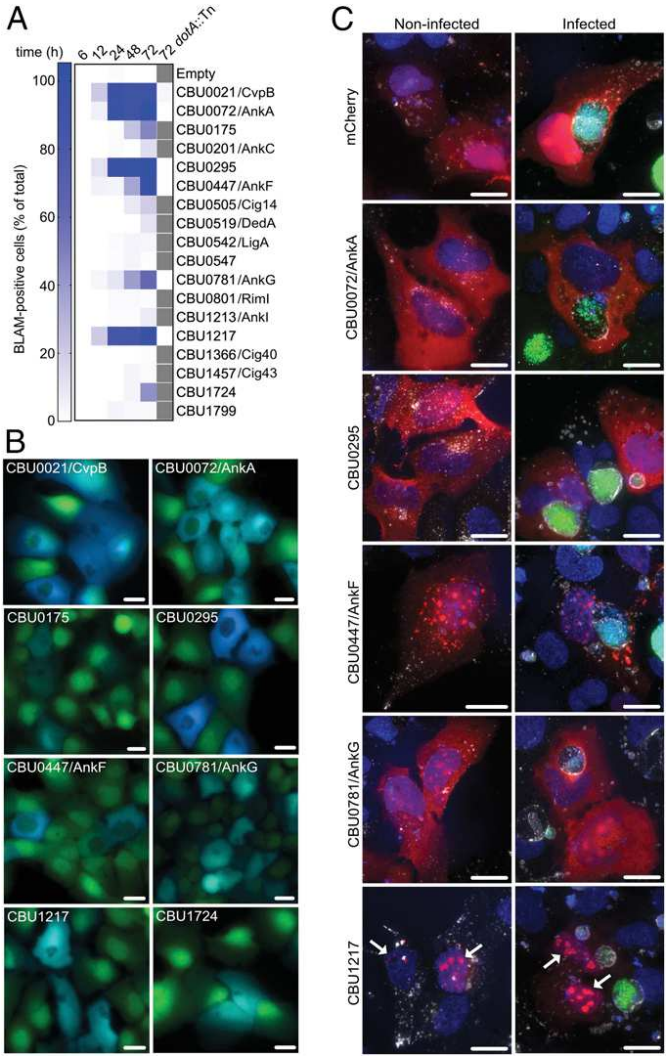

Fig. 1. Identification of *C. burnetii* EUGENs. (*A*) U2OS cells were challenged with *C. burnetii* strains expressing BLAM-tagged versions of candidate EUGENs for 6, 12, 24, 48, and 72 h. The percentage of BLAM-positive, infected cells was automatically calculated using CellProfiler over the total number of infected cells per each condition. Empty, BLAM empty vector. The Dot/Icm-dependent translocation of the effectors that were efficiently secreted was validated in the *dotA*::Tn mutant strain at 72 h postchallenge. (*B*) Representative images of positive (blue) cells treated as in *A*. (*C*) Noninfected or GFP-expressing *C. burnetii*-infected U2OS cells were transfected with plasmids encoding N-terminally tagged mCherry versions of the effector proteins validated in *A* (red). At 24 h after transfection, cells were fixed and labeled with Hoechst (blue) and an anti-LAMP1 antibody (white). White arrows point at CBU1217 subnuclear localization. (Scale bars, 10 μm.)

excluded from nuclei and remained diffuse in the cytoplasm (Fig. 2*F*), whereas HA-NopA$_{C\text{-}ter}$ retained the nucleolar localization (Fig. 2*G*). Cell fractionation confirmed the cytoplasmic localization of HA-NopA$_{N\text{-}ter}$ and the nuclear localization of HA-NopA$_{C\text{-}ter}$, as well as the association with the chromatin fraction (Fig. 2 *F* and *G*). Thus, despite the lack of typical nuclear or nucleolar localization signals, the C-terminal domain of NopA encoding the RCC-like domain, is necessary and sufficient for the nucleolar targeting of the effector protein. The role of the RCC repeats in the intracellular localization of NopA was further dissected by generating increasing deletions of single RCC repeats (numbered from 1 to 4 from the N-terminal) from either the N-terminal or C-terminal ends of HA-NopA$_{C\text{-}ter}$ (*SI Appendix*, Fig. S2*A*). The intracellular localization of each construct was tested by immunofluorescence and cell fractionation following ectopic expression in U2OS cells. Interestingly, this revealed that the first RCC repeat is critical for targeting NopA to the nucleus as removal of this repeat from NopA$_{C\text{-}ter}$ displaces the protein to the cytoplasm (*SI Appendix*, Fig. S2 *B* and *C*). The first two RCC repeats (RCC12; aa 196 to 310) alone localize within the nucleus but are excluded from nucleoli (*SI Appendix*, Fig. S2*E*) and instead localize at promyelocytic leukemia (PML) bodies (*SI Appendix*,

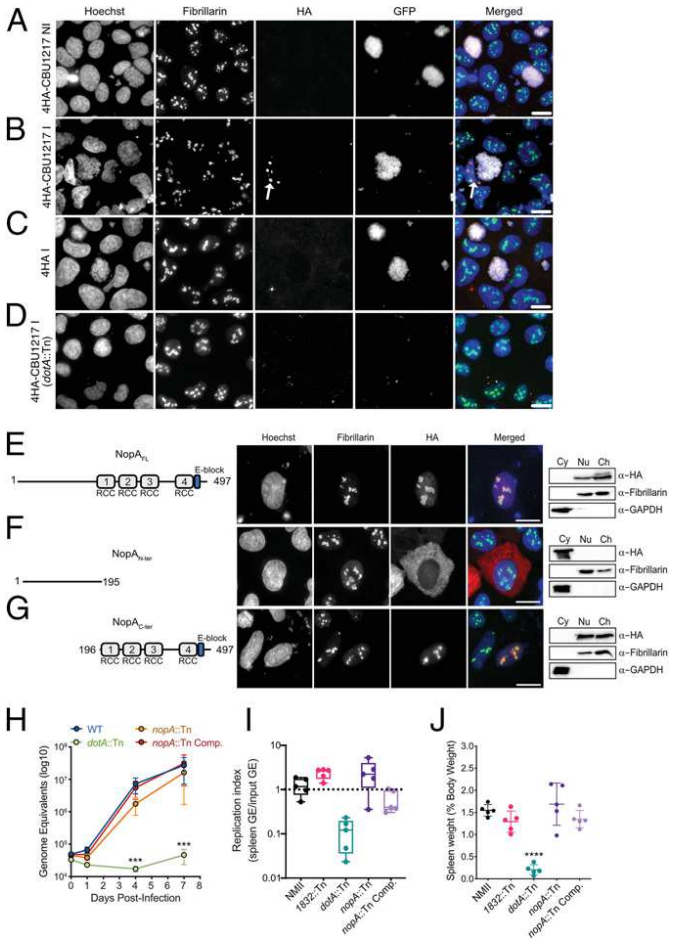

Fig. 2. Intracellular localization of CBU1217/NopA and role in *C. burnetii* replication during infection. U2OS cells were challenged either with WT GFP-tagged *C. burnetii* (white) transformed with plasmids encoding 4HA-tagged CBU1217/NopA (*A* and *B*, red) or the 4HA tag alone (*C*, red), or with the GFP-tagged *dotA*::Tn mutant (*D*, white), transformed with plasmids encoding 4HA-tagged CBU1217/NopA, all under the control of an IPTG-inducible promoter. At 72 h postinfection, cells were fixed and labeled with Hoechst (blue) and anti-fibrillarin antibodies (green). I, IPTG-induced; NI, noninduced. Arrow points at 4HA-CBU1217/NopA localization in infected cell. U2OS cells were transfected with plasmids encoding HA-tagged versions of either full-length (*E*) or the indicated deletion mutants (*F* and *G*) of HA-tagged NopA. At 24 h after transfection, cells were either fixed and labeled with Hoechst (blue), an anti-fibrillarin antibody (green) and an anti-HA antibody (red, *Center*), or lysed and processed for cell fractionation (*Right*). Cell fractions were analyzed by Western blotting using anti-fibrillarin and anti-GAPDH antibodies as nuclear and chromatin (Nu and Ch) and cytoplasmic (Cy) markers, respectively, and anti-HA antibodies to reveal NopA localization. (Scale bars, 10 μm.) (*H*) Genome equivalents (GEs) calculated using TaqMan real-time PCR with DNA purified from infected spleens of 5 SCID mice per group on day 14 after challenge with 1×10^6 GEs of the strains shown. (*I*) Replication index calculated as the ratio between spleen GE at the time of necropsy and the input GE of the strains listed in the figure legend. (*J*) Spleen weight as a percentage of total body weight at the time of necropsy on day 14 after infection with 1×10^6 GEs of the strains listed in the figure legend. Values are the mean of three independent infections, with error bars indicating SDs from the mean. ****$P < 0.0001$, ***$P < 0.001$, two-way ANOVA (*H*) and one-way ANOVA (*J*), Dunnett's multiple comparisons test.

Fig. S2*G*). This localization remains unchanged with the addition of the third RCC repeat (*SI Appendix*, Fig. S2 *D* and *F*), and it is only with the addition of the complete $NopA_{C\text{-}ter}$ that the protein localizes at nucleoli (Fig. 2*G*), suggesting the presence of a nucleolar-targeting motif in the fourth RCC repeat. Unfortunately, we were unable to express detectable amounts of single RCC repeats (RCC1 and RCC4, *SI Appendix*, Fig. S2*A*).

NopA Is Not Involved in *C. burnetii* Intracellular Replication. Given the early translocation of NopA observed using the β-lactamase assay, we determined the time course of NopA production during infection. To this aim, we have complemented the *nopA* mutation, using a mini Tn7 transposon to integrate a WT copy of HA-tagged *nopA*, under the regulation of its predicted endogenous promoter, in the chromosome of the *C. burnetii Tn227* strain, which carries the transposon insertion closest to the *nopA* start codon (10). Protein expression was then monitored by Western blot, using an anti-HA antibody, from cells challenged with the complemented *nopA*::Tn strain for 12, 24, 48, and 72 h. By this approach, detectable amounts of NopA were observed from 12 h postinfection (*SI Appendix*, Fig. S1*D*).

We previously reported that transposon insertions in *nopA* do not affect bacterial replication in Vero cells (10). To further investigate the role of NopA in *C. burnetii* infections, bacterial replication and virulence of the wild-type, *dotA*::Tn, *nopA*::Tn, and the *nopA*::Tn complemented strain (*nopA*::Tn Comp.) described above, were tested using either bone marrow-derived macrophages (BMDMs) or a severe combined immunodeficiency (SCID) mouse model of infection. Confirming our initial observations, transposon insertions in *nopA* do not affect *C. burnetii* replication (Fig. 2 *H* and *I*) or virulence (as determined here by splenomegaly measurements, Fig. 2*J*).

NopA Interacts with the Small GTPase Ran. Given that NopA localizes at nucleoli and presents four out of the seven RCC repeats present in the eukaryotic Ran-GEF RCC1, we investigated whether NopA can interact with Ran. To this aim, U2OS cells incubated either with the *nopA*::Tn mutant or the complemented strain expressing 4HA-tagged NopA under the control of the predicted endogenous promoter (*nopA*::Tn Comp.). Twenty-four hours postinfection, cells were lysed, separated into cytoplasmic, nuclear, and chromatin fractions, and NopA was immunocaptured from cell fractions using an anti-HA antibody. As expected, NopA was not detected in cells infected with the *nopA*::Tn mutant strain, whereas it was efficiently isolated from the nuclear and chromatin fractions of cells challenged with the complemented strain (Fig. 3*A*). Of note, whole cell lysates of cells incubated with the complemented strain also presented an accumulation of Ran in the chromatin fraction, which was not observed in cells challenged with the *nopA*::Tn mutant strain (Fig. 3*A*). Importantly, Ran was efficiently detected, together with NopA, in immunoprecipitates from the nuclear and chromatin fractions of cells challenged with the *nopA*::Tn complemented strain, indicating indeed an interaction with the *C. burnetii* effector protein (Fig. 3*A*). The NopA/Ran interaction was further investigated in U2OS cells, following the ectopic expression of either HA-tagged $NopA_{N\text{-}ter}$, $NopA_{C\text{-}ter}$, or the *C. burnetii* effector protein CvpF as negative control (22). Unfortunately, under these conditions, we were unable to immunoprecipitate full-length NopA from transfected cells. Similarly to infected cells, 24 h posttransfection, cells were lysed,

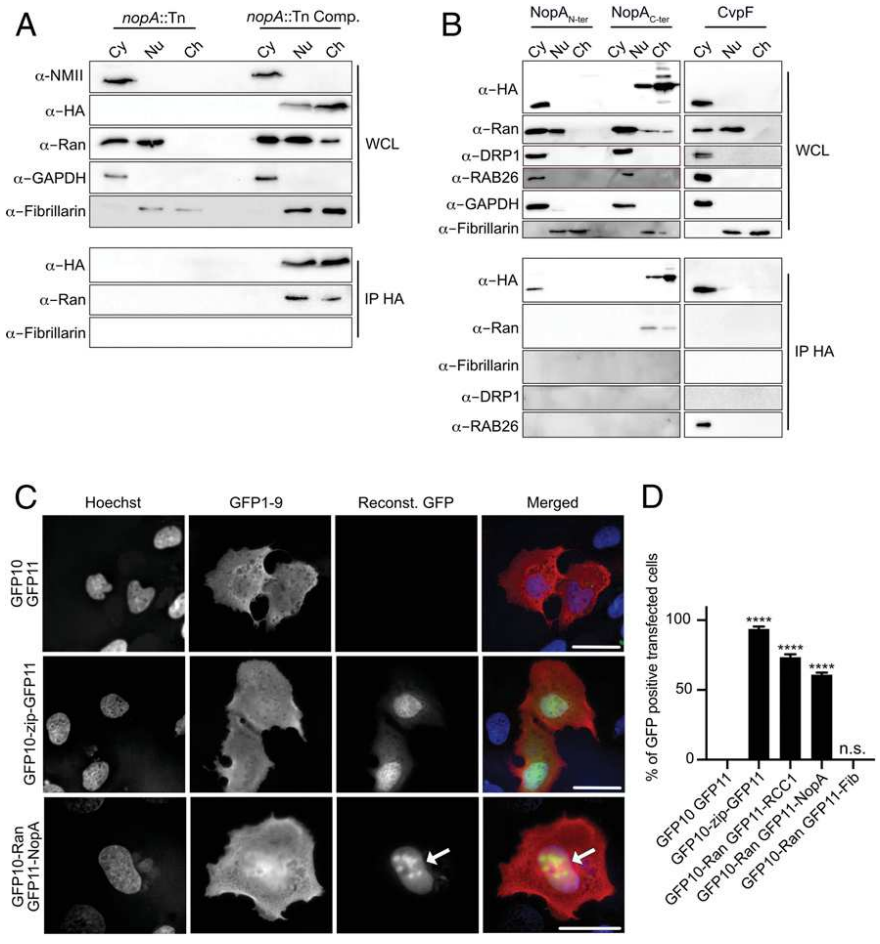

Fig. 3. NopA interacts with the small GTPase Ran. (*A*) U2OS cells challenged for 24 h with either the *C. burnetii nopA* transposon mutant (*nopA*::Tn) or the corresponding complemented strain (*nopA*::Tn Comp.) were lysed and processed for cell fractionation. Whole cell lysates (WCLs) were probed with the indicated antibodies, as well as anti-GAPDH and anti-fibrillarin antibodies as cytoplasmic (Cy), and nuclear/chromatin (Nu/Ch) markers, respectively. Following immunoprecipitation with anti-HA-coated magnetic beads, the presence of Ran and that of fibrillarin (as a negative control) was assessed using specific antibodies (IP HA). (*B*) U2OS cells transfected with HA-tagged versions of either the N-terminal domain ($NopA_{N\text{-}ter}$), the C-terminal domain ($NopA_{C\text{-}ter}$) of NopA, or CvpF as negative control were lysed and processed for cell fractionation. WCLs were probed with the indicated antibodies, as well as anti-GAPDH and anti-fibrillarin antibodies as cytoplasmic (Cy), nuclear/chromatin (Nu/Ch) markers, respectively. Following immunoprecipitation with anti-HA-coated magnetic beads, the presence of candidate interacting proteins was assessed using specific antibodies (IP HA). (*C*) U2OS cells were transfected with plasmids encoding GFP1-9 in combination with plasmids encoding either the GFP10 and GFP11 tags alone as negative control (*Top* row), GFP10 and GFP11 linked by a leucine zipper motif (GFP10-zip-GFP11) as positive control (*Middle* row), or GFP10-Ran and GFP11-NopA (*Bottom* row). At 24 h after transfection, cells were fixed and labeled with Hoechst (blue) and anti-GFP antibodies (red) to reveal nuclei and the expression of GFP1-9, respectively. Protein/protein interaction was assessed following the reconstitution of GFP (Reconst. GFP, green). Arrows point at nuclei in which Ran and NopA interact. (*D*) The percentage of cells presenting GFP reconstitution over the total number of GFP1-9-positive cells was calculated. Values are means ± SD from two independent experiments. Asterisks indicate statistically significant variations (n.s., nonsignificant, ****$P < 0.0001$, one-way ANOVA, Dunnett's multiple comparison test). (Scale bars, 20 μm.)

separated into cytoplasmic, nuclear, and chromatin fractions, and NopA truncations and CvpF were immunocaptured from cell fractions using an anti-HA antibody. As expected, $NopA_{N\text{-}ter}$ and CvpF were efficiently isolated from the cytoplasmic fractions, whereas $NopA_{C\text{-}ter}$ was isolated from the nuclear and cytoplasmic fractions (Fig. 3*B*). In agreement with what we observed in infected cells, the ectopic expression of $NopA_{C\text{-}ter}$ triggered an accumulation of Ran to the chromatin fractions (Fig. 3*B*). Moreover, Ran was specifically detected in the nuclear and chromatin fractions upon immunocapturing of $NopA_{C\text{-}ter}$, confirming an interaction between the two proteins (Fig. 3*B*). Of note, no interaction was detected between Ran and $NopA_{N\text{-}ter}$, despite their shared cytoplasmic localization (Fig. 3*B*). Furthermore, $NopA_{C\text{-}ter}$ did not interact with other small GTPases such as DRP1 or RAB26, nor with the nucleolar marker fibrillarin (Fig. 3*B*). Conversely, the *C. burnetii* effector protein CvpF (22), was readily immunocaptured from the cytoplasm of transfected cells and interacted with RAB26 as reported (22) (Fig. 3*B*).

Finally, the direct interaction between NopA and Ran was further investigated using the tripartite split-GFP interaction sensor (23). Briefly, the assay is based on a tripartite association between two GFP β-strands (GFP10 and GFP11), fused to proteins of interest, and the complementary GFP1-9 detector. If proteins interact, GFP10 and GFP11 self-associate with GFP1-9 to reconstitute a functional GFP. pCDNA3-zipper-GFP10 and pCDNA3-zipper-GFP11 were used as negative control, whereas a plasmid encoding GFP10 and GFP11 linked by a zipper motif (GFP10-zip-GFP11) was used as positive control (23). *ran* cDNA was cloned into the pCDNA3-GFP10-zipper plasmid to generate the GFP10-Ran, whereas *nopA*, *rcc1*, and *fbl* (the gene encoding fibrillarin) were cloned into the pCDNA3-zipper-GFP11 plasmid to generate the corresponding GFP11 fusion proteins. Combinations of the above-mentioned constructs with a pCMV plasmid encoding GFP1-9 were used for triple transfections in U2OS cells. After fixation, an anti-GFP antibody was used to identify cells expressing GFP1-9 (which is not fluorescent) and protein interactions were analyzed by monitoring GFP reconstitution. As expected, coexpression of GFP1-9 with GFP10 and GFP11 did not result in the reconstitution of GFP (Fig. 3 *C*, *Top* row, and 3*D*). The coexpression of GFP1-9 with GFP10-zip-GFP11 led to the reconstitution of GFP fluorescence in over 93% of transfected cells, demonstrating the functionality of the assay (Fig. 3 *C*, *Center* row, and 3*D*). Importantly, over 60% of cells expressing GFP1-9 in combination with GFP10-Ran and GFP11-NopA showed reconstitution of GFP, with a fluorescent signal detected at nuclei, with a strong accumulation at nucleoli (Fig. 3 *C*, *Bottom* row, and 3*D*). On the contrary, the expression of GFP1-9 in combination with GFP10-Ran and GFP11-RCC1 allowed reconstitution of GFP fluorescence, which was homogeneously detected in the nucleus in over 73% of transfected cells (*SI Appendix*, Fig. S3 *A* and *D*). Lack of GFP reconstitution upon expression of GFP1-9 in combination with GFP10-Ran and GFP11-fibrillarin indicated that the shared nucleolar localization was not sufficient for GFP reconstitution (*SI Appendix*, Fig. S3 *A* and *D*).

Ectopic expression of either mCherry-$NopA_{FL}$ or mCherry-$NopA_{C\text{-}ter}$ in combination with GFP-Ran in U2OS cells also confirmed the colocalization of both proteins at nucleolar structures labeled with the anti-fibrillarin antibody (*SI Appendix*, Fig. S3*B*), Conversely, Ran-GFP accumulation at nucleoli was lost when the small GTPase was ectopically expressed in U2OS cells in combination either with mCherry alone or mCherry-$NopA_{N\text{-}ter}$ (*SI Appendix*, Fig. S3*B*). Collectively, these observations indicate that NopA specifically interacts with Ran and may sequester it at nucleoli.

NopA Preferentially Interacts with GDP-Bound Ran and Triggers an Increase in Ran-GTP. To determine whether NopA displays preferential binding to Ran in its GDP- versus GTP-bound form, a GFP-trap assay was carried out on U2OS cells cotransfected with plasmids encoding HA-$NopA_{C\text{-}ter}$ in combination with either GFP alone, GFP-Ran, GFP-Ran_{T24N} (GDP-locked), GFP-Ran_{Q69L} (GTP-locked), or GFP-Ran_{N122I} (nucleotide-free form). Similar to RCC1, NopA displayed preferential binding to either GDP-locked Ran_{T24N} or the nucleotide-free form Ran_{N122I} (Fig. 4*A*).

Next, we investigated whether NopA binding to Ran can affect the Ran GDP/GTP ratio that is required to fuel nucleocytoplasmic transport. U2OS cells were challenged either with WT *C. burnetii*, the *dotA*::Tn, *nopA*::Tn, or the *nopA*::Tn complemented strains.

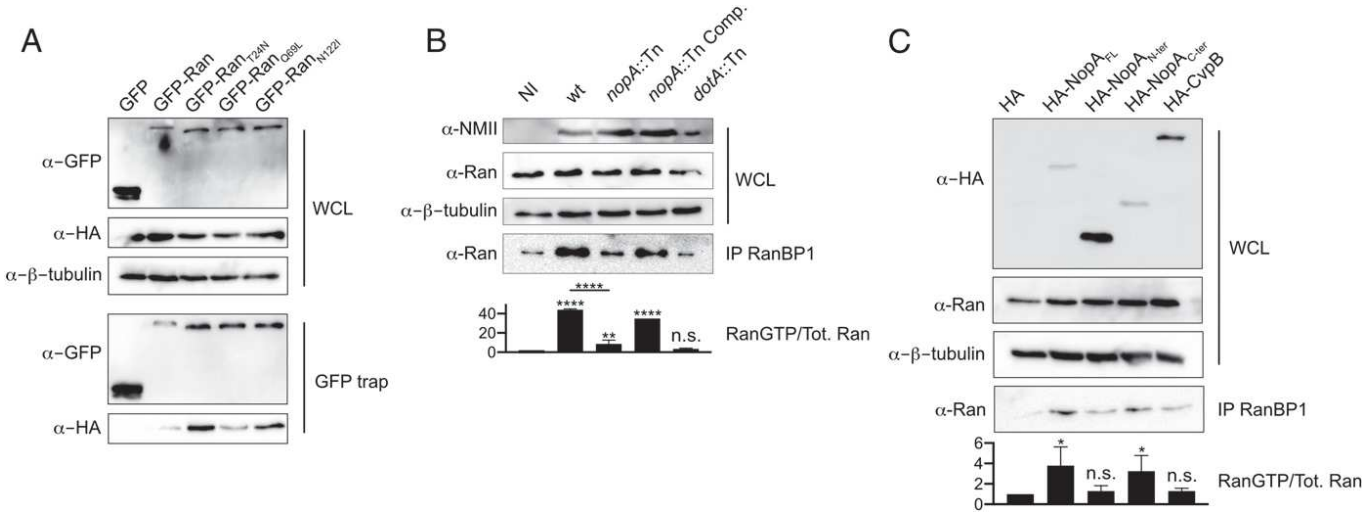

Fig. 4. NopA increases the intracellular levels of Ran-GTP. (*A*) The GFP-trap assay was carried out in U2OS cells expressing HA-tagged $NopA_{C\text{-}ter}$ in combination with either GFP alone, GFP-Ran, GFP-Ran_{T24N} (GDP-locked), GFP-Ran_{Q69L} (GTP-locked), or GFP-Ran_{N122I} (guanosine-free). WCLs (*Upper*) were probed with anti-GFP and anti-HA antibodies to assess the expression of the GFP-tagged proteins and HA-tagged $NopA_{C\text{-}ter}$, and anti-tubulin antibodies as loading control. Protein/protein interactions were assessed using anti-GFP and anti-HA antibodies following GFP capture (GFP-trap, *Lower*). (*B*) GTP-bound Ran was pulled down using RanBP1-coated beads from cell lysates of U2OS cells challenged for 24 h with either WT *C. burnetii* (WT), a *nopA* transposon mutant (*nopA*::Tn), the corresponding complemented strain (*nopA*::Tn Comp.), or the Dot/Icm-defective mutant (*dotA*::Tn). Noninfected cells (NI) were used as control. WCLs were probed with anti-*C. burnetii* (NMII), anti-Ran, and anti-β-tubulin antibodies. GTP-bound Ran was revealed using an anti-Ran antibody (IP RanBP1). (*C*) GTP-bound Ran was pulled down using RanBP1-coated beads from cell lysates of U2OS cells expressing either the HA tag alone, HA-tagged versions of either full-length ($NopA_{FL}$), the N-terminal domain ($NopA_{N\text{-}ter}$), the C-terminal domain ($NopA_{C\text{-}ter}$) of NopA, or CvpB. WCLs were probed with anti-HA antibodies to assess the expression of the HA-tagged versions of NopA and anti-Ran and anti-tubulin antibodies as loading controls. GTP-bound Ran was revealed using an anti-Ran antibody (IP RanBP1). The signal ratio of GTP-bound Ran over the total amount of Ran is indicated for experiments illustrated in *B* and *C*. Values are mean ± SD from three independent experiments. n.s., nonsignificant, $****P < 0.0001$, $**P < 0.007$, $*P < 0.02$, one-way ANOVA, Dunnett's multiple comparison test.

Noninfected cells were used as control. Twenty-four hours post-infection, cells were lysed and incubated with agarose beads coated with the Ran effector Ran-binding protein 1 (RanBP1), to specifically pull down the GTP-bound form of Ran. Indeed, infection with WT *C. burnetii* triggered a 40-fold increase in the intracellular levels of Ran-GTP, as compared to noninfected cells (Fig. 4*B*). This phenotype was lost in cells challenged with the *dotA*::Tn mutant strain and only an 8.5-fold increase was observed in cells challenged with the *nopA*::Tn mutant strain. Increased levels of Ran-GTP were largely restored (35-fold increase) in cells exposed to the complemented strain (*nopA*::Tn Comp., Fig. 4*B*). The effects of NopA on the intracellular levels of Ran-GTP were further investigated in U2OS cells transfected with plasmids encoding either HA alone, HA-NopA, HA-$NopA_{N\text{-}ter}$, HA-$NopA_{C\text{-}ter}$, or the *C. burnetii* effector protein CvpB (12) used here as negative control. A threefold increase in the intracellular levels of Ran-GTP was observed in cells expressing either HA-NopA or HA-$NopA_{C\text{-}ter}$, as compared to cells transfected with HA alone or HA-$NopA_{N\text{-}ter}$ (Fig. 4*C*). As expected, ectopic expression of CvpB had negligible impact on the intracellular levels of Ran-GTP (Fig. 4*C*). These observations suggest that NopA sequestration of Ran at nucleoli leads to an increase in the intracellular levels of Ran-GTP, which may negatively regulate nuclear import (24).

NopA Perturbs Protein Translocation to the Nucleus. Given the role of Ran in nucleocytoplasmic traffic, and the previously reported observation that *C. burnetii* infections modulate nuclear translocation of p65 by a Dot/Icm-dependent mechanism (9), we investigated whether NopA affects the nuclear localization of p65, which follows the activation of the NF-κB signaling pathway. U2OS cells transfected with plasmids encoding either HA- or mCherry-tagged versions of NopA were either left untreated or challenged with 10 ng/mL TNF-α for 30 min, and the nuclear translocation of p65 was monitored using an anti-p65 antibody either by fluorescence microscopy or Western blot following cell fractionation. Cells expressing either HA- or mCherry-tagged CvpB or the tags alone were used as controls. TNF-α treatment efficiently activated the NF-κB pathway, as indicated by the significant degradation of IκBα (Fig. 5*A*). Accordingly, p65 was readily relocalized to the nucleus of cells expressing either the HA or mCherry tags alone or tagged versions of the *C. burnetii* effector CvpB (Fig. 5 *B–D*). However, p65 translocation was largely inhibited in cells expressing either HA-NopA or mCherry-NopA (Fig. 5 *B–D*). In all cases, the intracellular levels of p65 remained largely unaltered. To determine whether NopA modulates the intracellular levels of p65 by perturbing its nuclear import or by accelerating its nuclear export, U2OS cells expressing either mCherry-NopA, mCherry-CvpB, or mCherry alone as controls, were incubated for 4 h with 5 nM leptomycin B (LMB), a fungal metabolite that blocks nuclear export by covalently binding to exportin 1. As p65 shuttles continuously between the nucleus and the cytoplasm, treatment with LMB in mCherry or mCherry-CvpB expressing cells led to an accumulation of the transcription factor in the nucleus (Fig. 5*D* and *SI Appendix*, Fig. S4). Interestingly however, ectopic expression of mCherry-NopA significantly prevented p65 nuclear accumulation in response to LMB treatment (Fig. 5*D* and *SI Appendix*, Fig. S4). A similar phenotype was observed in cells treated with LMB for 4 h, followed by a 30-min incubation with TNF-α (Fig. 5*D* and *SI Appendix*, Fig. S4). These data indicate that indeed, NopA perturbs nuclear import.

Next, we tested whether the perturbation of nuclear import triggered by NopA was specific to p65 and *C. burnetii* infections. The nuclear translocation of the transcription factor IRF3 was monitored in U2OS cells cotransfected with 3FLAG-tagged IRF3 in combination with either mCherry alone, mCherry-NopA, or mCherry-CvpB, and infected with the Sendai virus for 18 h. Noninfected cells were used as control (*SI Appendix*, Fig. S5*A*). Similar to what we reported for p65, IRF3 was readily translocated to the nuclei of cells expressing either mCherry alone or mCherry-CvpB but remained largely cytoplasmic in cells expressing mCherry-NopA (*SI Appendix*, Fig. S5 *A* and *B*).

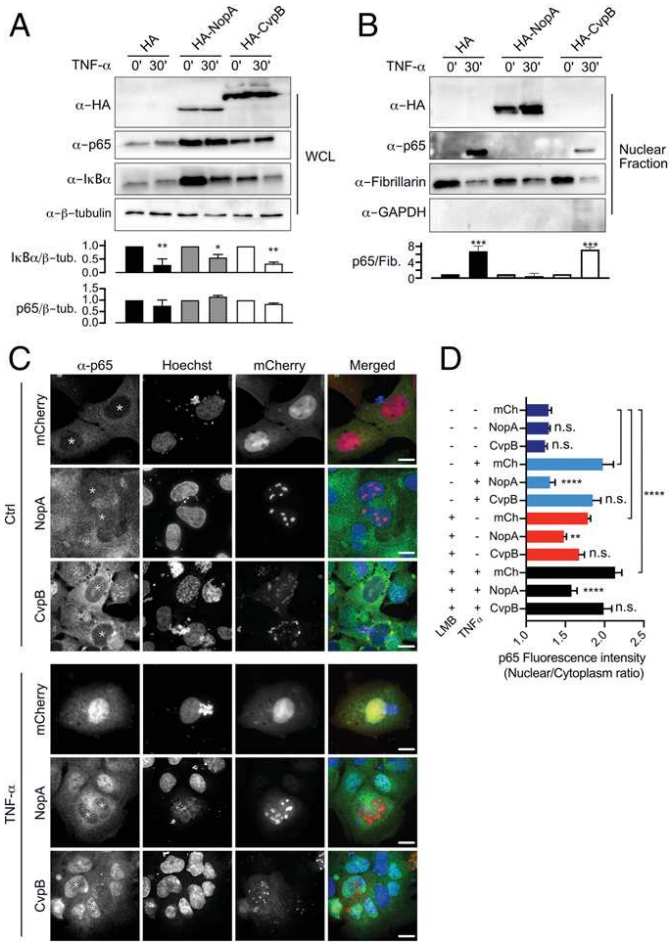

Fig. 5. Overexpression of NopA interferes with the nuclear translocation of p65. Representative Western blot of U2OS cells expressing either the HA tag alone, HA-NopA, or HA-CvpB left untreated or incubated with 10 ng/mL TNF-α for 30 min, lysed, and processed for cell fractionation. Whole cell lysates (*A*, WCLs) were used to assess the overall levels of p65 and IκBα and nuclear fractions (*B*) to monitor p65 translocation to the nucleus (nuclear fraction). The signal ratio of p65 over tubulin or fibrillarin and of IκBα over tubulin is indicated for experiments illustrated in *A* and *B*. Values are mean ± SD from three independent experiments. (*C*) Representative images of U2OS cells expressing mCherry-NopA or mCherry-CvpB and treated as in *A*. The localization of p65 was monitored using an anti-p65 antibody and Hoechst staining of nuclei. Asterisks indicate transfected cells. (*D*) CellProfiler was used to identify mCherry-expressing U2OS cells and to measure the median of the ratios of p65 fluorescence intensity at nuclei versus cytoplasm. Values are means ± SEM from two independent experiments where a minimum of 200 nuclei were measured per condition. Asterisks indicate statistically significant variations [n.s., nonsignificant, $****P < 0.0001$, $***P < 0.001$, $**P < 0.01$, $*P < 0.1$, one-way ANOVA, Dunnett's (*A* and *B*) and Bonferroni (*D*) multiple comparison test]. (Scale bars, 10 μm.)

NopA Is Involved in the Silencing of the Innate Immune Response during *C. burnetii* Infections. p65 nuclear translocation was further monitored in U2OS cells noninfected or challenged either with 10 ng/mL TNF-α for 30 min, WT *C. burnetii*, the Dot/Icm-defective mutant *dotA*::Tn, the *nopA*::Tn, or the complemented strain (*nopA*::Tn Comp.), for 24, 48, and 72 h by fluorescence microscopy and, for the 72 h time point, by Western blot following cell fractionation. IκBα was significantly degraded in all conditions as compared to noninfected cells, indicating an efficient activation of the NF-κB pathway (Fig. 6*A*). Translocation of p65 to the nucleus was readily detected in cells treated with TNF-α, either by Western blotting (Fig. 6*B*) or by immunofluorescence (Fig. 6 *C* and *D*). Cells challenged with WT *C. burnetii* or the *nopA*::Tn complemented

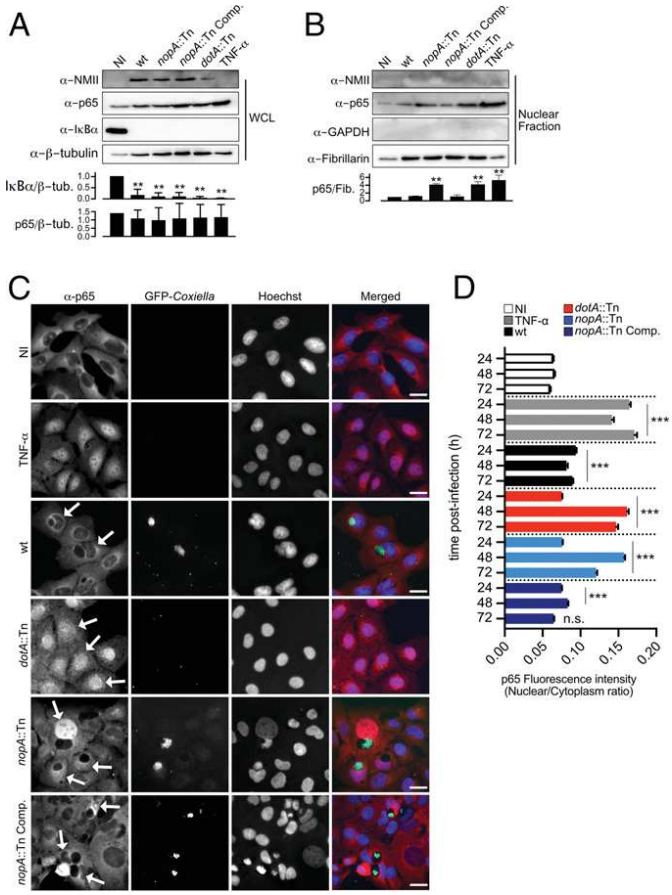

Fig. 6. NopA interferes with the nuclear translocation of p65 during *C. burnetii* infections. Representative Western blot of U2OS cells challenged for 72 h with GFP-tagged strains of WT *C. burnetii* (WT), the Dot/Icm-defective *dotA* transposon mutant (*dotA*::Tn), the *nopA* transposon mutant (*nopA*::Tn), or the corresponding complemented strain (*nopA*::Tn Comp.). Noninfected cells (NI) and cells treated with 10 ng/mL TNF-α (TNF-α) for 30 min were used as negative and positive controls, respectively. Cells were lysed and fractionated to isolate nuclear fractions. Whole cell lysates (*A*, WCLs) were used to assess the overall levels of p65 and IκBα and nuclear fractions (*B*) to monitor p65 translocation to the nucleus (nuclear fraction). Normalized densitometry of indicated protein ratios was calculated. Values are means ± SD from two independent experiments. (*C*) Representative images of U2OS cells treated as in *A*. The localization of p65 (red) was monitored using an anti-p65 antibody and Hoechst staining of nuclei (blue). White arrows indicate nuclei of infected cells. (*D*) U2OS cells were treated as in *A* for 24, 48, and 72 h. CellProfiler was used to identify infected and total U2OS cells and to measure the median of the ratios of p65 fluorescence intensity at nuclei versus cytoplasm. Values are means ± SEM from two independent experiments where a minimum of 400 nuclei were measured per condition. In all cases, n.s., nonsignificant, ***$P < 0.0001$, one-way ANOVA, Dunnett's multiple comparison test. (Scale bars, 10 μm.)

strain showed a small but significant increase in nuclear p65 fluorescence as compared to noninfected, untreated cells (Fig. 6 *B–D*). However, incubation with either the *dotA*::Tn or the *nopA*::Tn mutants triggered an accumulation of p65 to the nucleus which was comparable to the TNF-α treatment (Fig. 6 *B–D*). Measurement of p65 nuclear translocation by immunofluorescence, which was specifically measured in infected cells, resulted in a stronger phenotype as compared to Western blot analysis, which was carried out on the total cell population.

To investigate the downstream effects of perturbing the nuclear translocation of transcription factors involved in the immune response to *C. burnetii* infections, differentiated THP-1 macrophages were exposed to either WT *C. burnetii*, the Dot/Icm-deficient *dotA*::Tn mutant, the *nopA*::Tn mutant, or the corresponding complemented strain (*nopA*::Tn Comp.) for 24, 48, and 72 h. Total RNA was extracted from cell lysates and qRT-PCR analysis was used to monitor the expression of a panel of cytokines (Fig. 7*A* and *SI Appendix*, Fig. S6*A*). A slight increase in the mRNA expression levels of all tested cytokines was observed in cells exposed to WT *C. burnetii* or the *nopA*::Tn complemented strain, as compared to noninfected cells. Interestingly however, cells exposed to either the *dotA*::Tn mutant or the *nopA*::Tn mutant displayed a comparable, significant increase in the production of the majority of the cytokines tested, ranging from a 2-fold increase to a 100-fold increase for IL8 (Fig. 7*A* and *SI Appendix*, Figs. S6*A* and S7). Down-modulation of the innate immune response was further confirmed by monitoring TNF-α and IFN-α production in THP-1 macrophages infected as above for 72 and 96 h. As *C. burnetii* effectors are known to perturb the secretory pathway of infected cells (20, 25), THP-1 cells were treated with brefeldin A (BFA) 24 h prior to fixation and the intracellular levels of TNF-α and IFN-α were assessed by flow cytometry (Fig. 7 *B* and *C*), following the application of a specific gating to isolate the population of infected cells (*SI Appendix*, Fig. S6*B*). A significant increase in the intracellular levels of both cytokines was observed in cells infected either with the *nopA*::Tn or the *dotA*::Tn strains as compared to cells infected with WT *C. burnetii* or the *nopA*::Tn complemented strain (Fig. 7 *B* and *C*). Overall, our data indicate that *C. burnetii* uses the Dot/Icm secretion system to down-modulate the NF-κB signaling pathway as previously reported (9), and that NopA is a key effector for this process.

Discussion

Intracellular bacterial pathogens and symbionts establish intimate interactions with their eukaryotic hosts, which have evolved by co-evolution over time. Part of their adaptation to their intracellular niches has been mediated by transkingdom acquisition and functional integration of eukaryotic genes in bacterial genomes (26). Indeed, EUGENs represent a hallmark of intracellular bacteria, and are rarely observed in free-living bacteria. Importantly, many EUGENs from intracellular bacteria produce candidate or validated effector proteins that are translocated into host cells through dedicated type III or type IV secretion systems (27). Thus, EUGENs are predicted to play an important role in the establishment of parasitic or symbiotic bacterial lifestyles.

In this study, bioinformatics analysis combined with translocation assays led to the identification of seven *C. burnetii* effector proteins encoding eukaryotic-like domains involved in protein/protein interactions, protein/chromatin interactions, and posttranslational modifications. CBU0447 and CBU0175 are conserved among *C. burnetii* strains, whereas the remaining five EUGENS present some degree of polymorphism (7). Upon ectopic expression in epithelial cells of translocated ankyrin repeat-containing proteins, AnkA (CBU0072) was largely cytoplasmic, whereas AnkF (CBU0447) seemed to associate with membranes that partially colocalized with the lysosomal marker LAMP1. AnkG (CBU0781), which was previously reported to localize at mitochondria and translocate to the nucleus upon staurosporine treatment of transfected cells (21), partially localized to the nucleus even in the absence of staurosporine in our hands. It is thus possible that other Ank proteins modify their intracellular localization at different stages of infection.

Here, we have focused our study on CBU1217, which encodes four RCC repeats in its C-terminal domain (aa 196 to 497). RCC repeats are found in the regulation of chromosome condensation 1 (RCC1) eukaryotic protein (28). In eukaryotes, the RCC domain consists of seven homologous repeats of 51 to 68 amino acid residues, arranged in a β-propeller fold (15). A single RCC domain constitutes the majority of the protein in the case of the RCC1 subgroup of the RCC1 superfamily, whereas multiple RCC domains can be found, either alone or in combination with other functional domains of the other subgroups of the superfamily (13). As such, RCCs are versatile domains that can be involved in protein/protein or protein/chromatin interactions, guanine nucleotide exchange factor (GEF), and posttranslational modifications including ubiquitination and phosphorylation (13). RCC1 is primarily found in association with histones H2A and H2B on chromatin (29) and acts as a GEF for the small GTPase Ran, a master regulator of nucleocytoplasmic

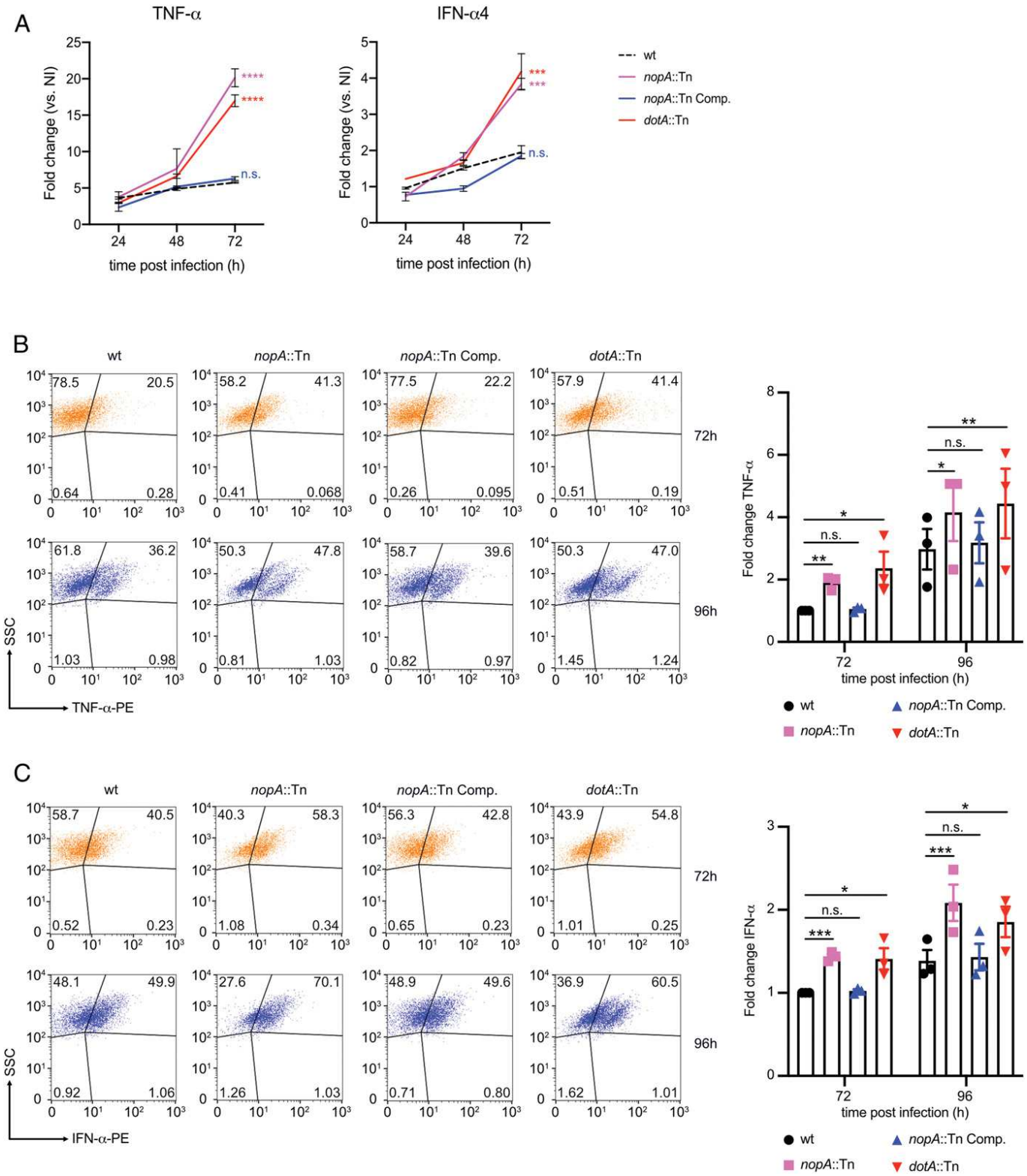

Fig. 7. NopA inhibits cytokines production. (*A*) Differentiated THP-1 cells were challenged either with GFP-expressing WT *C. burnetii* (WT), the Dot/Icm-defective *dotA* transposon mutant (*dotA*::Tn), the *nopA* transposon mutant (*nopA*::Tn), or the corresponding complemented strain (*nopA*::Tn Comp.) for 24, 48, 72, and 96 h. The expression of TNF-α and IFN-α4 cytokines was assessed by RT-qPCR for the indicated time points. Dot plots from a representative experiment showing intracellular staining of TNF-α (*B*) and IFN-α (*C*) in cells infected for 72 and 96 h and treated with BFA for the last 24 h. Infected cells were first gated on the GFP$^+$ population and the percentage of cells expressing TNF-α and IFN-α was assessed. Flow cytometry data are presented on graphs as fold relative to WT. Values are means ± SD from three independent experiments. n.s., nonsignificant, ****$P < 0.0001$, ***$P < 0.001$, **$P < 0.01$, *$P < 0.1$. Full statistical analysis for the 72-h time point illustrated in *A* is available in *SI Appendix*, Fig. S7.

transport during interphase and mitotic spindle assembly during mitosis (30).

Among vacuolar bacterial pathogens, the *L. pneumophila* effector protein LegG1 encodes an RCC-like domain (RLD) consisting of three out of the seven RCC repeats typically found in eukaryotes (31). Of note, LegG1 localizes at *Legionella*-containing vacuoles (LCVs) where it recruits and activates Ran to promote microtubule polymerization and LCV mobility (32). Differently from LegG1, *C. burnetii* NopA encodes an additional RCC repeat and, despite the lack of typical nuclear or nucleolar localization signals, exclusively localizes at nuclei with a strong enrichment in the chromatin fraction, which is consistent with RCC1 localization. NopA RCC repeats are necessary and sufficient to target the protein to nucleoli and exert its functions. Moreover, the first RCC repeat seems to be critical for targeting NopA to the nucleus, as removal of this repeat from $NopA_{C\text{-}term}$ displaces the protein to the cytoplasm. Interestingly, the first two RCC repeats (aa 196–310) alone localize at PML bodies. This localization remains unchanged with the addition of the third RCC repeat and it is only the expression of the complete $NopA_{C\text{-}term}$ that triggers protein localization at nucleoli, suggesting the presence of a nucleolar-targeting motif in the fourth RCC repeat.

Similarly to the eukaryotic protein RCC1, NopA interacts with Ran, with preferential affinity for the GDP-bound form and promotes the activation of Ran. Differently from RCC1, however, NopA also triggers a nucleolar accumulation of Ran. Thus, the observed increase in the intracellular levels of GTP-bound Ran may result from either GEF activity of NopA (which has been reported for RCC1), or via the observed sequestration of Ran at nucleoli, which would prevent GTP-bound Ran to recycle back to the cytoplasm, where Ran GTPase-activating proteins (GAPs) stimulate GTP to GDP conversion. As we were unable to purify sufficient amounts of either full-length NopA or $NopA_{C\text{-}ter}$, we could not assess for the moment whether NopA has intrinsic GEF activity. Interestingly, a residual increase in the intracellular levels of Ran-GTP was still observed in cells challenged with the *nopA*::Tn mutant strain, as compared to infections with the Dot/Icm-defective *dotA*::Tn strain. This may suggest that other *C. burnetii* effectors may have a role in the modulation of Ran activity.

Of note, mutations in *nopA* do not affect *C. burnetii* intracellular replication (10). However, increasing the intracellular levels of Ran-GTP results in a global alteration in the nucleocytoplasmic transport of proteins (24). It has been reported that during infections, *C. burnetii* requires Dot/Icm activity to down-modulate the NF-κB pathway by perturbing the nuclear translocation of the p65 transcription factor (9). Here we demonstrate that NopA is one of the effector proteins involved in this process, as indicated by the strong inhibition of nuclear translocation of p65 upon treatment of cells with TNF-α or infection. The modulation of the NF-κB signaling pathway has been reported for a number of bacterial pathogens and viruses (1, 2). In most cases, bacteria interfere with the degradation of IκBα and the release of p65 or by triggering the proteasomal degradation of p65 itself. Other bacteria, including *L. pneumophila* and *Shigella flexneri* may also inhibit the innate immune response downstream of p65 nuclear translocation, at the level of transcription and mRNA processing, respectively (2). Finally, an emerging number of bacterial effectors inhibit NF-κB activation by modulating the nuclear translocation and/or accumulation of p65, by interfering with nucleocytoplasmic protein transport. The *Salmonella* SPI-2 T3SS effector protein SpvD accumulates importin-α in the nucleus by binding exportin Xpo2, thereby preventing p65 nuclear import (4). *O. tsutsugamushi* uses ankyrin repeat-containing effector proteins Ank1 and 6 by coopting the function of both importin-β and exportin 1, thus accelerating p65 nuclear export (5). Here we show that the NF-κB pathway is readily activated upon *C. burnetii* infections as shown by efficient IκBα degradation. However, NopA perturbs nuclear accumulation of p65 by triggering the nuclear accumulation of GTP-bound Ran, resulting in an imbalanced Ran gradient across cells. In turn, this leads to a defective nuclear import of proteins, as also demonstrated by challenging cells ectopically expressing NopA with leptomycin B to block nuclear export.

Considering that these bacterial effectors manipulate common adaptors and GTPases involved in nucleocytoplasmic transport, it would be of interest to monitor their effect on a broader panel of proteins and investigate how infected cells respond to these perturbations. For example, other *C. burnetii* effector proteins have been described to localize at the nucleus of infected cells (21, 33, 34). In this perspective, it is important to note that nuclear translocation of p65 is not completely ablated during *C. burnetii* infections, and that the strongest phenotypes are observed at 48 and 72 h post-infection, which is compatible with a reduced, but still detectable translocation of protein to the nucleus at earlier time points. Here we show that indeed the perturbation of nuclear import by NopA affects a broader class of proteins, also outside the context of *C. burnetii* infections, as indicated by the perturbation of nuclear translocation of IRF3 in response to Sendai virus infection, in cells ectopically expressing NopA.

To monitor the downstream effects of inhibiting the nuclear accumulation of transcription factors involved in immune sensing, we challenged differentiated THP-1 cells with WT *C. burnetii* or strains carrying mutations either in the Dot/Icm secretion system or in *nopA*. As expected, infections by the WT strain elicited a minor response in the expression of a panel of cytokines, including TNF-α, interleukins, and interferons, in agreement with the observation that *C. burnetii* is a stealth pathogen. Evasion of the innate immune response was unmasked by infections with the Dot/Icm-defective strain *dotA*::Tn, which triggered a significant cytokine response. Interestingly, infections by the *nopA*::Tn mutant strain largely phenocopied the *dotA*::Tn mutation, suggesting that NopA is critical for the down-modulation of the innate immune response.

Together, this work highlighted a number of *C. burnetii* eukaryotic-like effector proteins and showed that one of them, NopA, is responsible for evading the host innate immune response by interfering with nucleocytoplasmic transport.

Materials and Methods

Antibodies, reagents, bacterial strains, cell lines, and growth conditions used in this study are listed in *SI Appendix*.

Plasmids. Plasmids used in this study are listed in *SI Appendix*, Table S4. DNA sequences were amplified by PCR using Phusion polymerase (New England Biolabs) and gene-specific primers (Sigma).

Plasmid Design for Secretion Assay in *C. burnetii*. Selected genes from *SI Appendix*, Table S2 were amplified from *C. burnetii* RSA439 NMII genomic DNA using primer pairs indicated in *SI Appendix*, Table S5. PCR products were cloned into the pXDC61-BLAM plasmid to generate N-terminal-tagged fusion version of all candidate effector proteins.

Plasmid Design for Mammalian Cells Transfection. Effector-coding genes were amplified from *C. burnetii* RSA439 NMII genomic DNA using primer pairs indicated in *SI Appendix*, Table S5. PCR products were cloned either into pLVX-mCherry-N2 or pRK5-HA plasmids to generate N-terminal-tagged mCherry or HA fusion versions of all effector proteins, respectively. For cloning of Ran in pcDNA3-GFP10-zipper, Ran was amplified using forward primers Ran-*Bsp*EI and reverse primers Ran-*Xba*I-rev. For cloning of NopA, RCC1, and fibrillarin in pcDNA3-zipper-GFP11, genes were amplified using forward primers NopA-*Not*I, RCC1-*Not*I, or FBL-*Not*I and reverse primers NopA-*Cla*I-rev, RCC1-*Cla*I-rev, or FBL-*Cla*I-rev. pGBKT7-containing eukaryotic sequence of Ran WT, RanT24N/Q69L/N122I mutants were kindly provided by Aymelt Itzen, Zentrum für Experimentelle Medizin Institut für Biochemie und Signaltransduktion, Hamburg, Germany. Ran WT and mutants were amplified from pGBKT7-Ran-WT, pGBKT7-Ran-T24N, pGBKT7-Ran-Q69L, and pGBKT7-Ran-N122I using primers pairs *Xho*I-Ran-F and Ran-*Xma*I-rev, and the PCR products were cloned into pLVX-GFP-N2.

Plasmid Design for *nopA* Complementation in *C. burnetii*. For *nopA* complementation, the *nopA* putative promoter and *nopA* sequences were amplified using the primer pairs *Nhe*I-prom1217-fw/*Pst*I-prom1217-Rev and CBU1217-BamHI/CBU1217-EcoRI-rev, respectively (*SI Appendix*, Table S5). The PCR products were cloned into pUCR6K-miniTn7-Kan-tetRA-4HA. Plasmids were electroporated in the *nopA*::Tn mutant strain *Tn227* (10).

Beta-Lactamase Translocation Assay. For *C. burnetii* effector translocation assays, cells were cultured in black, clear-bottomed, 96-well plates and infected with the appropriate *C. burnetii* strain (multiplicity of infection [MOI] of 100) for 24 and 48 h. *C. burnetii*-expressing BLAM alone or BLAM-tagged CBU0021 were used as negative and positive controls, respectively. Cell monolayers were loaded with the fluorescent substrate CCF4/AM (LiveBLAzer-FRET B/G loading kit; Invitrogen) in a solution containing 20 mM Hepes, 15 mM probenecid (Sigma) pH 7.3, in Hank's balanced salt solution (HBSS). Cells were incubated in the dark for 1 h at room temperature and imaged using an EVOS inverted fluorescence microscope. Images were acquired using DAPI and GFP filter cubes. The image analysis software CellProfiler was used to segment and count total cells and positive cells in the sample using the 520-nm and 450-nm emission channels, respectively, and to calculate the intensity of fluorescence in each channel. Following background fluorescence subtraction using negative control samples, the percentage of positive cells was then calculated and used to evaluate effector translocation. A threshold of 20% of positive cells was applied to determine efficient translocation of bacterial effector proteins.

Immunofluorescence Staining and Microscopy. Cells were fixed in 4% (wt/vol) paraformaldehyde in phosphate-buffered saline (PBS) solution at room temperature for 20 min. Samples were then rinsed in PBS solution and incubated in blocking solution (0.5% bovine serum albumine [BSA], 50 mM NH_4Cl in PBS solution, pH 7.4). Cells were then incubated with the primary antibodies diluted in blocking solution for 1 h at room temperature, rinsed five times in PBS solution, and further incubated for 1 h with the secondary antibodies diluted in the blocking solution. To visualize HA-tagged NopA or nuclear/nucleolar proteins, cells were fixed as previously described in 4% (wt/vol) paraformaldehyde in PBS solution. Then, cells were permeabilized with 0.5% Triton X-100 in PBS solution for 3 min at room temperature. Sample were then rinsed in PBS solution and incubated with blocking solution (0.1% Triton X-100, 5% [wt/vol] milk in PBS solution) for 1 h at room temperature. Cells were then incubated with the primary antibodies diluted in blocking solution for 1 h at 37 °C, rinsed five times in PBS solution, and incubated with the secondary antibodies for 1 h at room temperature. For all conditions, coverslips were mounted by using Fluoromount mounting medium (Sigma) supplemented with Hoechst 33258 for DNA staining. Samples were imaged with a Zeiss Axio Imager Z1 epifluorescence microscope (Carl Zeiss) connected to a CoolSNAP HQ^2 charge-coupled device (CCD) camera (Photometrics). Images were acquired alternatively with 100×, 63×, or 40× oil immersion objectives and processed with MetaMorph (Universal Imaging). ImageJ and CellProfiler software were used for image analysis and quantifications.

Immunoprecipitations and Pull-Down Assays. For coimmunoprecipitation experiments, pLVX-GFP-N2-tagged WT Ran, RanT24N/Q69L/N122I mutants, or vector control were cotransfected with pRK5-HA-$NopA_{C\text{-}ter}$ in U2OS cells. At 24 h posttransfection, cells were lysed in lysis buffer (10 mM Tris HCl, pH 7.5, 150 mM NaCl, 0.5 mM ethylenediaminetetraacetic acid [EDTA] 1% Nonidet P-40) supplemented with a protease inhibitor tablet (Complete; Roche) and incubated with 25 μL of GFP-Trap magnetic beads (Chromotek) for 2 h at 4 °C with rotation. The beads were then washed three times with wash buffer (10 mM Tris HCl, pH 7.5, 150 mM NaCl, 0.5 mM EDTA), resuspended in Laemmli buffer 4×, and analyzed by Western blot.

Tripartite Split-GFP Assay. U2OS were grown in Dulbecco's modified Eagle medium (DMEM) supplemented in 10% (vol/vol) fetal calf serum (FCS) at 37 °C and 5% CO_2. For the interaction assay, U2OS cells were cotransfected with Lipofectamine 2000 (Gibco, Invitrogen) with plasmids encoding for GFP1-9, GFP10, and GFP11 fusions. At 24 h posttransfection, cells were fixed in 4% paraformaldehyde in PBS solution and processed for immunofluorescence. Protein/protein interactions were scored by calculating the percentage of GFP-positive cells over the total number of cells positive for the anti-GFP antibody.

Cell Fractionation. U2OS cells were grown to 60% confluence in 100-mm Petri dishes before being transfected with 10 μg of pRK5-HA-$NopA_{N\text{-}ter}$ or pRK5-HA-$NopA_{C\text{-}ter}$ in JetPEI reagent (Polyplus-Transfection) according to the manufacturer's recommendations. At 24 h after transfection, cells were washed in PBS and pelleted at 4 °C. U2OS cells cultured in 100-mm dishes were infected with the *nopA*::Tn mutant or the corresponding complemented strain (*nopA*::Tn Comp.) expressing a 4HA-tagged version of NopA. After 24 h of infection, cells were washed in PBS and pelleted at 4 °C. Transfected or infected cell pellets were subjected to cell fractionation as previously described (35). Where appropriate, cytoplasmic, nuclear, and chromatin fractions were subjected to immunoprecipitation using 40 μL of anti-HA magnetic beads (Sigma) for 2 h at 4 °C with rotation. Bound proteins were eluted using 80 μL of 100 $\mu g/mL^{-1}$ HA-peptide (Sigma) and then resuspended in Laemmli buffer 4× and analyzed by Western blot.

Ran Activation Assay. For the analysis of enzymatic activity of NopA, U2OS cells were either infected or transfected and lysed with lysis buffer (25 mM Hepes, pH 7.5, 150 mM NaCl, 1% Nonidet P-40, 10 mM $MgCl_2$, 1 mM EDTA, 2% glycerol) containing a protease inhibitor tablet (Complete; Roche). Cell lysates were then centrifuged for 10 min at 14,000 × *g* at 4 °C. For Ran-GTP immunoprecipitation, 40 μL of RanBP1 beads (Cell Biolabs, Inc.) were incubated with cell lysates for 1 h at 4 °C, and then washed three times with lysis buffer, subjected to sodium dodecyl sulfate-polyacrylamide gel electrophoresis (SDS/PAGE), and visualized by Western blotting using an anti-Ran antibody (1:4,000, Sigma). GTP-bound Ran levels were determined by calculating the signal ratio of GTP-bound Ran over the total amount of Ran.

NF-κB/IRF3 Translocation Assays. To analyze NF-κB translocation, U2OS cells were grown to 60% confluence before being transfected as previously described. At 24 h posttransfection, cells were incubated with media containing 10 ng/mL TNF-α for 30 min at 37 °C. Alternatively, cells were preincubated with media containing 5 nM LMB for 4 h at 37 °C, followed by a TNF-α treatment as indicated above where needed. For *C. burnetii* infection assays, cells were infected with *C. burnetii* and incubated at 37 °C for 1 to 3 d. Cells were then fixed in 4% paraformaldehyde in PBS solution and processed for NF-κB immunostaining. The image analysis software CellProfiler was used to segment all nuclei using the Hoechst staining and cell contours using nuclei as seeds and p65 labeling. Cytoplasm was segmented by subtracting nuclei from cell objects. Next, mCherry signal was used to identify and isolate the subpopulation of transfected cells, and single cell measurements of the ratio of the mean p65 fluorescence in the nucleus versus cytoplasm were calculated for each condition. For infection assays, CellProfiler was used to identify and isolate the population of infected cells based on the GFP fluorescence associated with the strains of *C. burnetii* used in this study and nuclear p65 fluorescence was specifically measured as described above in the subpopulation of infected cells. To analyze IRF3 translocation, pLVX-mCherry-N2-tagged NopA, CvpB, or empty vector were cotransfected with pcDNA3-3×FLAG-tagged IRF-3 in U2OS cells. At 24 h posttransfection, cells were infected with a defective-interfering H4 Sendai virus (36) provided by D. Garcin, Department of Microbiology and Molecular Medicine, University of Geneva, Geneva Switzerland, and used at 50 hemagglutination units (HAU)/mL for 18 h at 37 °C. Cells were then fixed in 4% paraformaldehyde in PBS solution and processed for FLAG immunostaining. IRF3 nuclear translocation was measured as described above for p65.

Densitometry. Regions of Interest (ROIs) were obtained from each band of interest and the intensity was measured using ImageJ. For each band, the same ROI was used for background calculation and removal from areas adjacent to each band. For the experiments illustrated in Fig. 5, the intensity of bands from samples treated with TNF-α were normalized for the intensity of the corresponding untreated sample. For the experiments illustrated in Fig. 6, the intensity of bands from samples challenged with *C. burnetii* or treated with TNF-α were normalized for the intensity of the noninfected (NI) sample.

qRT-PCR Analysis of Cytokine mRNA. Total RNA was extracted from THP-1 cells using the RNeasy Micro kit and submitted to DNase treatment (Qiagen), following manufacturer's instructions. RNA concentration and purity were evaluated by spectrophotometry (NanoDrop 2000c, Thermo Fisher Scientific). A total of 500 ng of RNA was reverse transcribed with both oligo-dT and random primers, using PrimeScript RT Reagent Kit (Perfect Real Time, Takara) in a 10-mL reaction. Real-time PCR reactions were performed in duplicates using Takyon ROX SYBR MasterMix blue dTTP (Eurogentec) on an Applied Biosystems QuantStudio 5, using the following program: 3 min at 95 °C followed by 40 cycles of 15 s at 95 °C, 20 s at 60 °C, and 20 s at 72 °C. Cycle threshold (Ct) values for each transcript were normalized to the geometric mean of the expression of RPL13A, B2M, and ACTB (i.e., reference genes) and the fold changes were determined by using the $2^{-\Delta\Delta Ct}$ method. Primers used for quantification of transcripts by real-time quantitative PCR are indicated in *SI Appendix*, Table S5.

SCID Mouse Infections. SCID (C.B-17/LcrHsd-Prkdcscid) mice were purchased from Envigo and housed in the Texas A&M Health Science Center (TAMHSC) animal facility. All animal procedures were done in compliance with Texas A&M University Institutional Animal Care and Use Committee (Animal Use Protocol, AUP 2016–0370). Infections were performed as described previously (37). Briefly, 6- to 8-wk-old female mice (SCID or C57BL/6) were infected with 1×10^6 viable *C. burnetii* phase II strain via intraperitoneal (i.p.) injection. Inoculum concentrations were confirmed by serial dilution spot plating on acidified citrate cysteine medium-2-defined (ACCM-D) agarose as described previously (38).

Mouse Tissue Collection, Processing, and DNA Purification. At 10 d (competitive infections) or 14 d postinfection (single infections), the mouse spleens were removed and weighed at necropsy to determine splenomegaly (spleen weight/body weight). Each spleen was added to 1 mL PBS and homogenized using an Omni tissue homogenizer equipped with plastic tips. A total of 100 μL of homogenate was added to 400 μL of TriZol LS (Invitrogen) for RNA extraction. For DNA extraction, 100 μL of homogenate was added to 900 μL tissue lysis buffer (Roche) plus 100 μL of proteinase K and incubated at 55 °C overnight. The following day 100 μL of 10% SDS (wt/vol) was added and incubated at room temperature for 1 h. Lysed tissue samples were then processed using the Roche High Pure PCR template preparation kit according to the manufacturer's instructions.

Enumeration of *Coxiella* in Mouse Spleens. DNA purified from infected organs was used as template for TaqMan real-time PCR using primers and probe for *com1* or primers and probe of *IS1111* as described previously (37). Quantitative PCR was performed in 20-μL reactions with ABI TaqMan universal PCR mastermix run on an ABI StepOne Plus machine. The replication index reported for each mouse was calculated by dividing the number of genome copies recovered from spleens by the number of genome copies in the original inoculum.

Flow Cytometry. For intracellular human TNF-α/IFN-α4 staining, 5×10^4 THP-1 cells differentiated in phorbol 12-myristate 13-acetate (PMA) (200 ng/mL) for 2 d seeded in 24-well plates were infected with the indicated *C. burnetii* strain for 72 and 96 h. Cells were then treated with 1 μg/mL of BFA for the last 24 h. The following day, cells were fixed using 2% paraformaldehyde in PBS solution for 20 min at 4 °C. After washing with fluorescence-activated cell sorting (FACS) buffer (1% BSA in PBS solution), cells were permeabilized in FACS buffer supplemented with 0.1% saponin for 30 min at 4 °C and then stained with anti-TNF-α-PE and IFN-α-PE antibodies for 1 h at 4 °C. Infected cells were analyzed based on the GFP fluorescence associated with the strains of *C. burnetii*. Flow cytometry analyses were performed on a BD FACSCalibur flow cytometer using flow cytometry (CellQuest software, BD Biosciences). FlowJo software (Tree Star) was used to analyze data.

Data Availability. All data discussed in the paper are available to readers either in the manuscript or in *SI Appendix*.

ACKNOWLEDGMENTS. This work was supported by the European Research Area Net (ERA-NET) Infect-ERA (ANR-13-IFEC-0003), the French National Research Agency (ANR; ANR-14-CE14-0012-01, ANR-10-LABX-12-01). G.M. is the recipient of a fellowship from the Agence National de la Recherche sur le SIDA et les Hépatites virales. We acknowledge the imaging facility MRI, member of the national infrastructure France-BioImaging supported by the French National Research Agency (ANR-10-INBS-04, "Investments for the Future"). We thank Dr. Caroline Goujon, Dr. Marylene Mougel (IRIM), Prof. Hubert Hilbi and Leoni Swart (University of Zurich), and Prof. Aymelt Itzen (University of Hamburg) for scientific advice and for sharing materials.

1. M. M. Rahman, G. McFadden, Modulation of NF-κB signalling by microbial pathogens. *Nat. Rev. Microbiol.* **9**, 291–306 (2011).
2. S. Asrat, K. M. Davis, R. R. Isberg, Modulation of the host innate immune and inflammatory response by translocated bacterial proteins. *Cell. Microbiol.* **17**, 785–795 (2015).
3. M. Stewart, Molecular mechanism of the nuclear protein import cycle. *Nat. Rev. Mol. Cell Biol.* **8**, 195–208 (2007).
4. N. Rolhion *et al*., Inhibition of nuclear transport of NF-κB p65 by the *Salmonella* type III secretion system effector SpvD. *PLoS Pathog.* **12**, e1005653 (2016).
5. S. M. Evans, K. G. Rodino, H. E. Adcox, J. A. Carlyon, *Orientia tsutsugamushi* uses two Ank effectors to modulate NF-κB p65 nuclear transport and inhibit NF-κB transcriptional activation. *PLoS Pathog.* **14**, e1007023 (2018).
6. A. Lührmann, H. J. Newton, M. Bonazzi, Beginning to understand the role of the Type IV secretion system effector proteins in *Coxiella burnetii* pathogenesis. *Curr. Top. Microbiol. Immunol.* **413**, 243–268 (2017).
7. C. L. Larson *et al*., Right on Q: Genetics begin to unravel *Coxiella burnetii* host cell interactions. *Future Microbiol.* **11**, 919–939 (2016).
8. L. D. Cunha *et al*., Inhibition of inflammasome activation by *Coxiella burnetii* type IV secretion system effector IcaA. *Nat. Commun.* **6**, 10205 (2015).
9. S. Mahapatra *et al*., *Coxiella burnetii* employs the Dot/Icm type IV secretion system to modulate host NF-κB/RelA activation. *Front. Cell. Infect. Microbiol.* **6**, 188 (2016).
10. E. Martinez, F. Cantet, L. Fava, I. Norville, M. Bonazzi, Identification of OmpA, a *Coxiella burnetii* protein involved in host cell invasion, by multi-phenotypic high-content screening. *PLoS Pathog.* **10**, e1004013 (2014).
11. E. Martinez, F. Cantet, M. Bonazzi, Generation and multi-phenotypic high-content screening of *Coxiella burnetii* transposon mutants. *J. Vis. Exp.* **2015**, e52851 (2015).
12. E. Martinez *et al*., *Coxiella burnetii* effector CvpB modulates phosphoinositide metabolism for optimal vacuole development. *Proc. Natl. Acad. Sci. U.S.A.* **113**, E3260–E3269 (2016).
13. O. Hadjebi, E. Casas-Terradellas, F. R. Garcia-Gonzalo, J. L. Rosa, The RCC1 superfamily: From genes, to function, to disease. *Biochim. Biophys. Acta* **1783**, 1467–1479 (2008).
14. T. Seki, N. Hayashi, T. Nishimoto, RCC1 in the Ran pathway. *J. Biochem.* **120**, 207–214 (1996).
15. L. Renault *et al*., The 1.7 A crystal structure of the regulator of chromosome condensation (RCC1) reveals a seven-bladed propeller. *Nature* **392**, 97–101 (1998).
16. C. Noroy, T. Lefrançois, D. F. Meyer, Searching algorithm for Type IV effector proteins (S4TE) 2.0: Improved tools for Type IV effector prediction, analysis and comparison in proteobacteria. *PLOS Comput. Biol.* **15**, e1006847 (2019).
17. X. Pan, A. Lührmann, A. Satoh, M. A. Laskowski-Arce, C. R. Roy, Ankyrin repeat proteins comprise a diverse family of bacterial type IV effectors. *Science* **320**, 1651–1654 (2008).
18. D. E. Voth *et al*., The *Coxiella burnetii* ankyrin repeat domain-containing protein family is heterogeneous, with C-terminal truncations that influence Dot/Icm-mediated secretion. *J. Bacteriol.* **191**, 4232–4242 (2009).
19. C. Chen *et al*., Large-scale identification and translocation of type IV secretion substrates by *Coxiella burnetii*. *Proc. Natl. Acad. Sci. U.S.A.* **107**, 21755–21760 (2010).
20. K. L. Carey, H. J. Newton, A. Lührmann, C. R. Roy, The *Coxiella burnetii* Dot/Icm system delivers a unique repertoire of type IV effectors into host cells and is required for intracellular replication. *PLoS Pathog.* **7**, e1002056 (2011).
21. R. A. Eckart *et al*., Antiapoptotic activity of *Coxiella burnetii* effector protein AnkG is controlled by p32-dependent trafficking. *Infect. Immun.* **82**, 2763–2771 (2014).
22. F. Ayenoue Siadous *et al*., *Coxiella* effector protein CvpF subverts RAB26-dependent autophagy to promote vacuole biogenesis and virulence. *Autophagy*, 10.1080/15548627.2020.1728098 (2020).
23. S. Cabantous *et al*., A new protein-protein interaction sensor based on tripartite split-GFP association. *Sci. Rep.* **3**, 2854 (2013).
24. I. Palacios, K. Weis, C. Klebe, I. W. Mattaj, C. Dingwall, RAN/TC4 mutants identify a common requirement for snRNP and protein import into the nucleus. *J. Cell Biol.* **133**, 485–494 (1996).
25. E. M. Campoy, F. C. M. Zoppino, M. I. Colombo, The early secretory pathway contributes to the growth of the *Coxiella*-replicative niche. *Infect. Immun.* **79**, 402–413 (2011).
26. K. S. de Felipe *et al*., Evidence for acquisition of Legionella type IV secretion substrates via interdomain horizontal gene transfer. *J. Bacteriol.* **187**, 7716–7726 (2005).
27. K. S. de Felipe *et al*., Legionella eukaryotic-like type IV substrates interfere with organelle trafficking. *PLoS Pathog.* **4**, e1000117 (2008).
28. M. Ohtsubo, H. Okazaki, T. Nishimoto, The RCC1 protein, a regulator for the onset of chromosome condensation locates in the nucleus and binds to DNA. *J. Cell Biol.* **109**, 1389–1397 (1989).
29. I. G. Macara, M. E. Nemergut, C. A. Mizzen, T. Stukenberg, C. D. Allis, Chromatin docking and exchange activity enhancement of RCCl by histones H2A and H2B. **292**, 1540–1543 (2001).
30. P. R. Clarke, C. Zhang, Spatial and temporal coordination of mitosis by Ran GTPase. *Nat. Rev. Mol. Cell Biol.* **9**, 464–477 (2008).
31. S. Ninio, J. Celli, C. R. Roy, A Legionella pneumophila effector protein encoded in a region of genomic plasticity binds to Dot/Icm-modified vacuoles. *PLoS Pathog.* **5**, e1000278 (2009).
32. E. Rothmeier *et al*., Activation of Ran GTPase by a Legionella effector promotes microtubule polymerization, pathogen vacuole motility and infection. *PLoS Pathog.* **9**, e1003598 (2013).
33. W. Schäfer *et al*., Nuclear trafficking of the anti-apoptotic *Coxiella burnetii* effector protein AnkG requires binding to p32 and Importin-α1. *Cell. Microbiol.* **19**, e12634 (2017).
34. M. M. Weber *et al*., Modulation of the host transcriptome by *Coxiella burnetii* nuclear effector Cbu1314. *Microbes Infect.* **18**, 336–345 (2016).
35. A. Prokop *et al*., Orfx, a nucleomodulin required for Listeria monocytogenes virulence. *MBio* **8**, e01550-17 (2017).
36. L. Strahle, D. Garcin, D. Kolakofsky, Sendai virus defective-interfering genomes and the activation of interferon-beta. *Virology* **351**, 101–111 (2006).
37. E. J. van Schaik, E. D. Case, E. Martinez, M. Bonazzi, J. E. Samuel, The SCID mouse model for identifying virulence determinants in *Coxiella burnetii*. *Front. Cell. Infect. Microbiol.* **7**, 25 (2017).
38. K. M. Sandoz, P. A. Beare, D. C. Cockrell, R. A. Heinzen, Correction for Sandoz et al., Complementation of Arginine Auxotrophy for Genetic Transformation of *Coxiella burnetii* by Use of a Defined Axenic Medium. *Appl. Environ. Microbiol.* **82**, 3695 (2016).

SUPPORTING INFORMATION

Supporting Methods

Antibodies and reagents

Polyclonal anti-*C. burnetii* (NMII) was produced by Covalab. Hoechst 33258, anti-mouse and anti-rabbit HRP-conjugated, monoclonal antibodies anti-HA, Ran, FLAG and β-tubulin were purchased from Sigma. Polyclonal anti-GFP was from Thermo Fisher Scientific. Polyclonal anti-Fibrillarin, RAB26, PML and monoclonal anti-DRP1 antibodies were from Abcam. Monoclonal anti-GAPDH was from Life Technologies. Polyclonal anti-HA antibody was from Proteintech. 4% paraformaldehyde in PBS solution were from Santa Cruz. Polyclonal anti-NF-κB p65 and monoclonal anti- IκBα antibodies were from Cell Signalling. Mouse and rabbit IgG conjugated to Alexa Fluor 488, 555 or 647 were purchased from Invitrogen. Human anti-TNF-α and human anti-IFN-α were from Miltenyi. Brefeldin A Solution (BFA, 420601) was purchased from BioLegend. TNF-α (300-01A) was purchased from PeproTech. Phorbol 12-myristate 13-acetate (PMA, Invivogen) and leptomycin B (LMB, LC Laboratories) were kindly provided by Dr. Caroline Goujon and Dr. Marylene Mougel, respectively.

Bacterial strains, cell lines and growth conditions.

Strains used in this study are listed in Table S3. *Coxiella burnetii* NMII and transposon mutants were grown in ACCM-2 supplemented with kanamycin (340 μg/ml) and/or chloramphenicol (3 μg/ml) as appropriate in a humidified atmosphere of 5% CO_2 and 2.5% O_2 at 37 °C. Cells were routinely maintained in RPMI (THP-1) or DMEM (U2OS), supplemented with 10% foetal calf serum (FCS) in a humidified atmosphere of 5% CO_2 at 37 °C. Where appropriate, THP1 cells were seeded at 200,000 per well in 24-well plates in RPMI medium supplemented with 10% FCS and treated with 200 ng/ml PMA for 48 h to allow the differentiation into macrophages. Fresh medium supplemented with 10% FCS was added 48h post-differentiation.

The following day, cells were challenged with *C. burnetii* for 1 to 4 d. Total RNA were collected at 24h intervals during the time course of the experiment. Primary bone marrow derived macrophages (BMDM) were prepared from C57BL/6 (Envigo, Houston, TX) as previously described (1). To infect BMDM with *C. burnetii*, bacterial stocks from ACCM-D cultures were enumerated by TaqMan qPCR using primers and probe directed against the *com1* gene sequence (2) and applied to the cells on ice at a multiplicity of infection (MOI) of 10. The inoculated BMDM were centrifuged at 500x*g* for 10 minutes at 4°C, and then shifted to a water bath at 37 °C, 5% CO_2 to synchronize bacterial uptake. After one hour, the cells were washed 3 times with warm DMEM to remove excess inoculum. The medium was replaced with complete macrophage medium (DMEM supplemented with 10% FBS, and 10% L929-conditioned medium), and returned to the incubator for a total of 7 days. The culture medium was replaced daily. For bacterial growth curves, infected cells were collected in triplicate wells at 0, 1, 4, and 7 days post-infection for genomic DNA isolation and enumeration of bacteria by TaqMan qPCR (2).

Cell transfection.

For the ectopic expression of proteins in mammalian cells, cells were grown to 60% confluence and transfected with JetPEI cationic polymer transfection reagent (Polyplus Transfection) or Lipofectamine 2000, according to the manufacturer's recommendations. Cells were assayed 12–24 h post transfection.

Supporting information references

1. A. Chong, *et al*., The early phagosomal stage of Francisella tularensis determines optimal phagosomal escape and Francisella pathogenicity island protein expression. *Infect. Immun.* (2008) https:/doi.org/10.1128/IAI.00682-08.
2. E. J. van Schaik, E. D. Case, E. Martinez, M. Bonazzi, J. E. Samuel, The SCID mouse model for identifying virulence determinants in Coxiella burnetii. *Front. Cell. Infect. Microbiol.* **7**, 1–10 (2017).

Supporting Figures

Figure S1

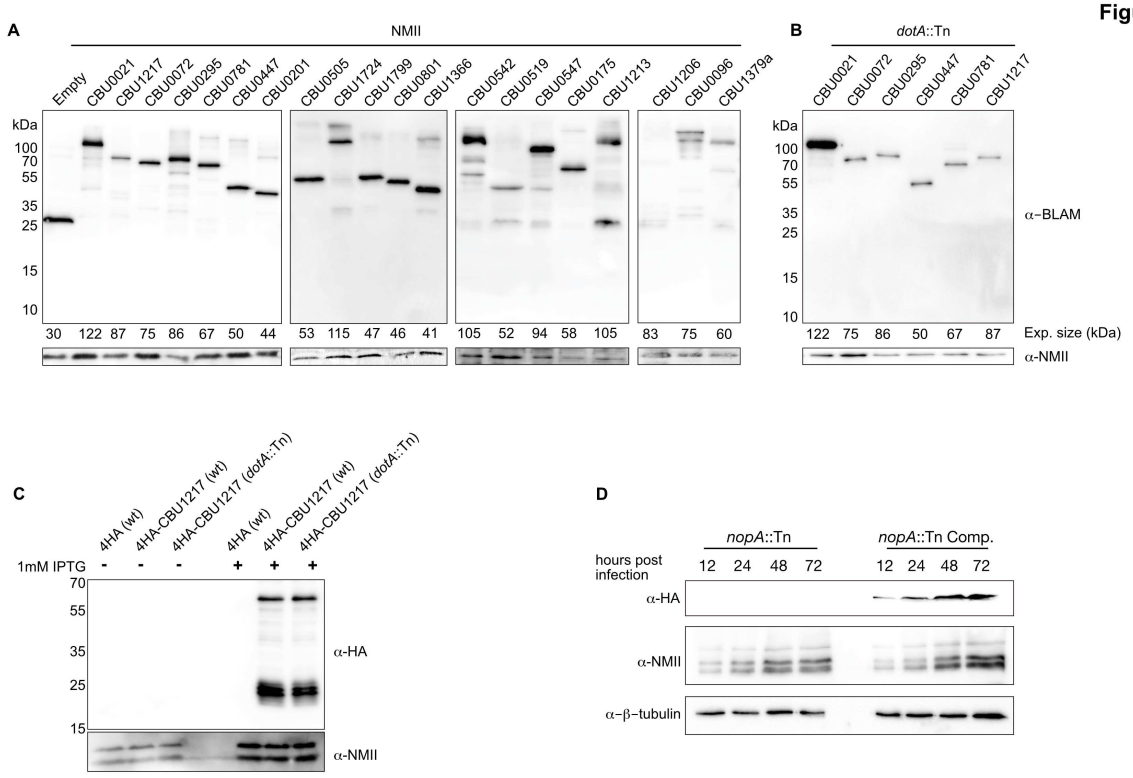

Figure S2

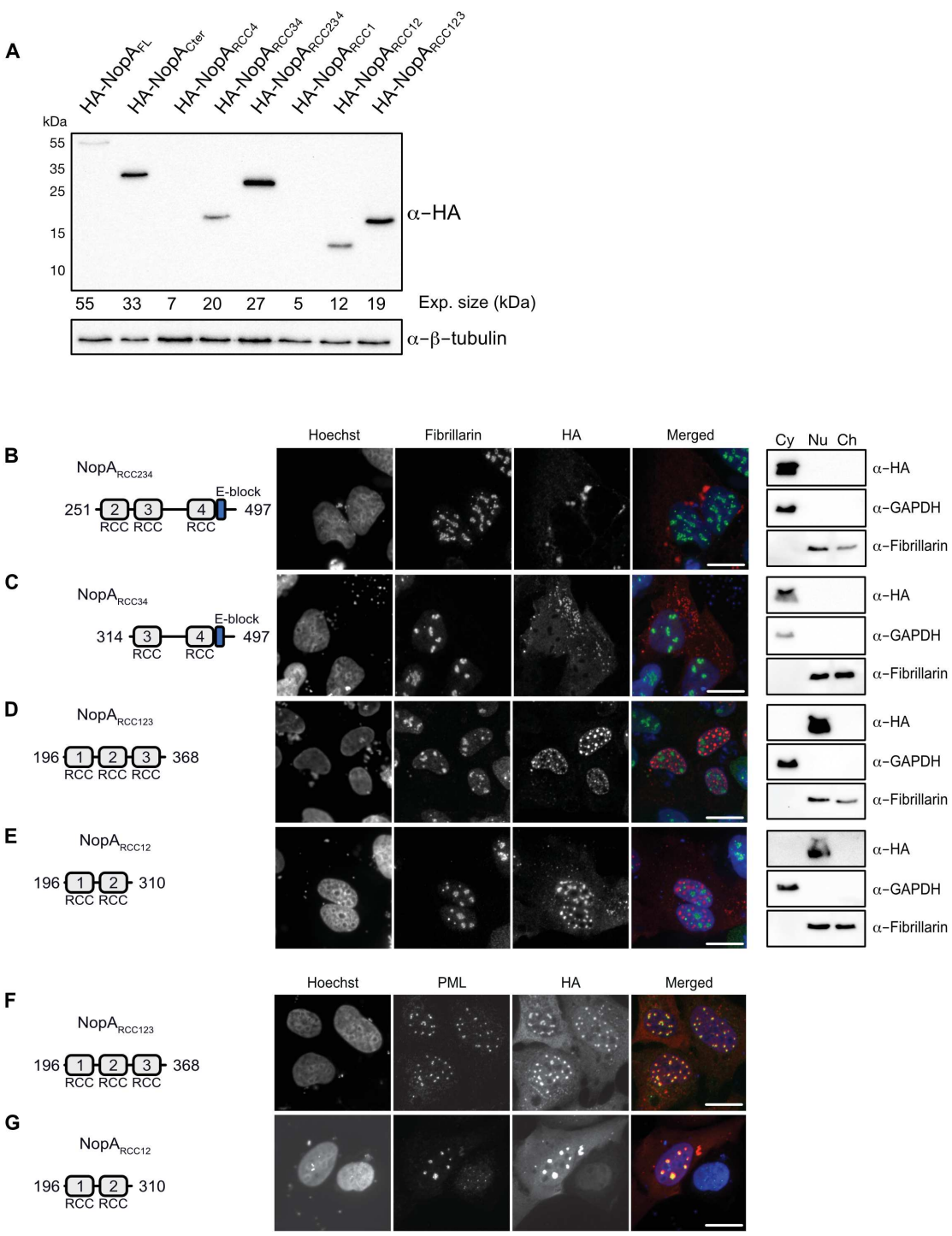
A
HA-NopA$_{FL}$
HA-NopA$_{Cter}$
HA-NopA$_{RCC4}$
HA-NopA$_{RCC34}$
HA-NopA$_{RCC234}$
HA-NopA$_{RCC1}$
HA-NopA$_{RCC12}$
HA-NopA$_{RCC123}$
kDa
55
35
25
15
10
α-HA
55 33 7 20 27 5 12 19
Exp. size (kDa)
α-β-tubulin
B
NopA$_{RCC234}$
251 2 3 4 497
E-block
RCC RCC RCC
C
NopA$_{RCC34}$
314 3 4 497
E-block
RCC RCC
D
NopA$_{RCC123}$
196 1 2 3 368
RCC RCC RCC
E
NopA$_{RCC12}$
196 1 2 310
RCC RCC
Hoechst
Fibrillarin
HA
Merged
Cy Nu Ch
α-HA
α-GAPDH
α-Fibrillarin
F
NopA$_{RCC123}$
196 1 2 3 368
RCC RCC RCC
G
NopA$_{RCC12}$
196 1 2 310
RCC RCC
Hoechst
PML
HA
Merged

Figure S3

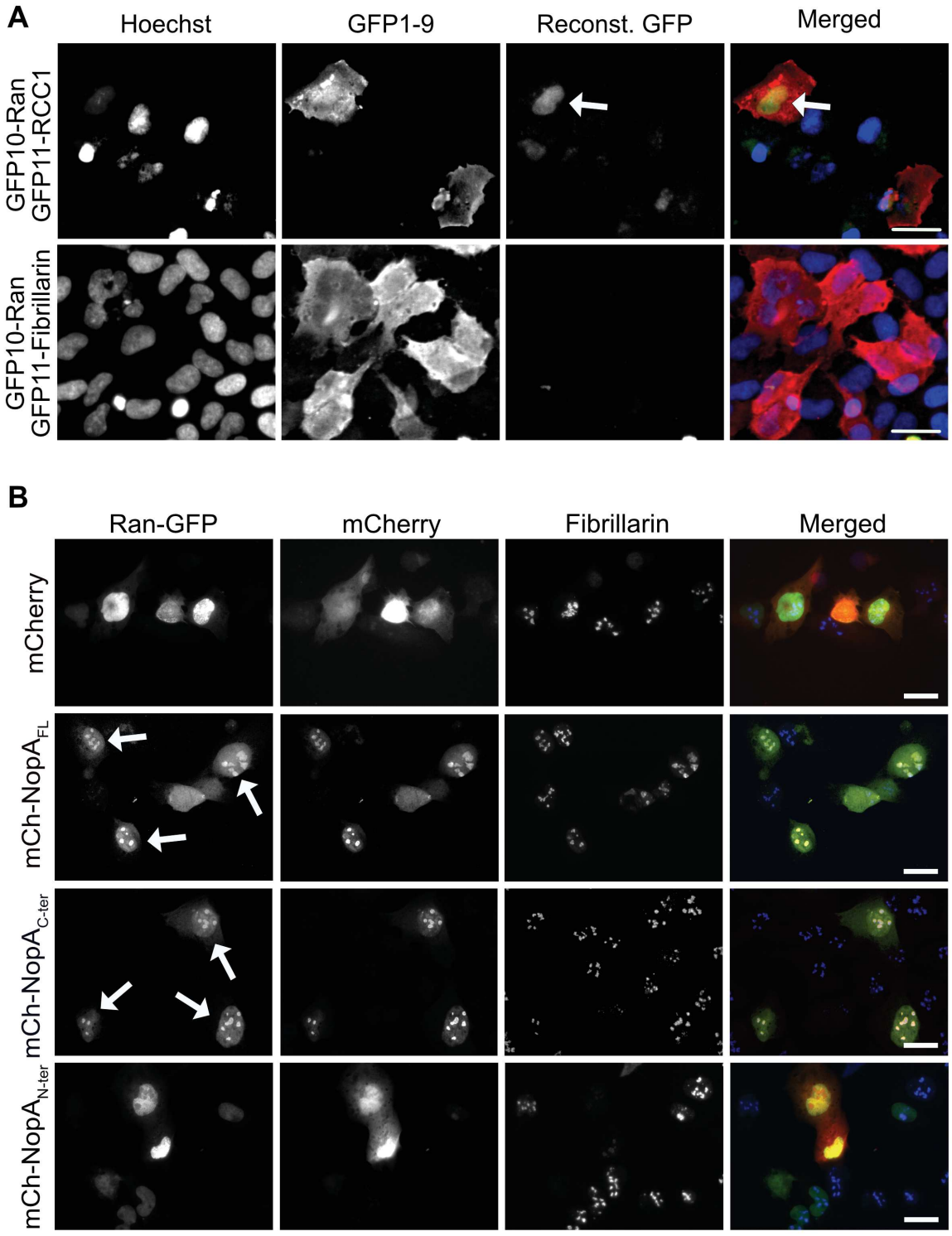
A
Hoechst
GFP1-9
Reconst. GFP
Merged
GFP10-Ran
GFP11-RCC1
GFP10-Ran
GFP11-Fibrillarin
B
Ran-GFP
mCherry
Fibrillarin
Merged
mCherry
mCh-NopA$_{FL}$
mCh-NopA$_{C\text{-}ter}$
mCh-NopA$_{N\text{-}ter}$

Figure S4

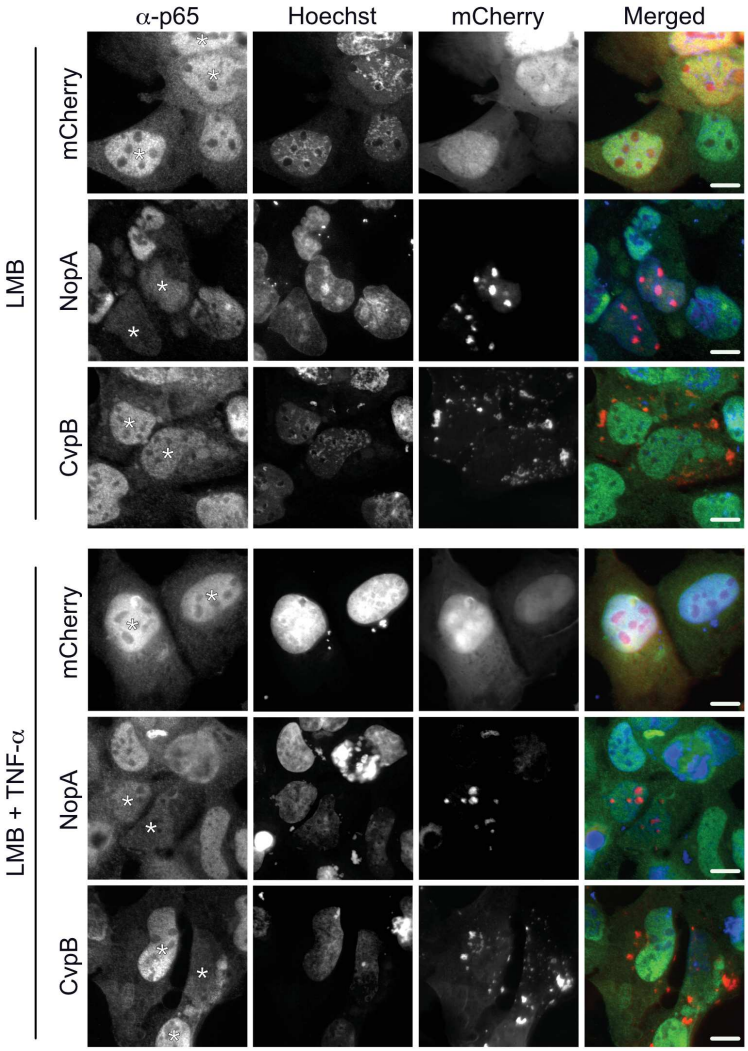
α-p65
Hoechst
mCherry
Merged
LMB
mCherry
NopA
CvpB
LMB + TNF-α
mCherry
NopA
CvpB

Figure S5

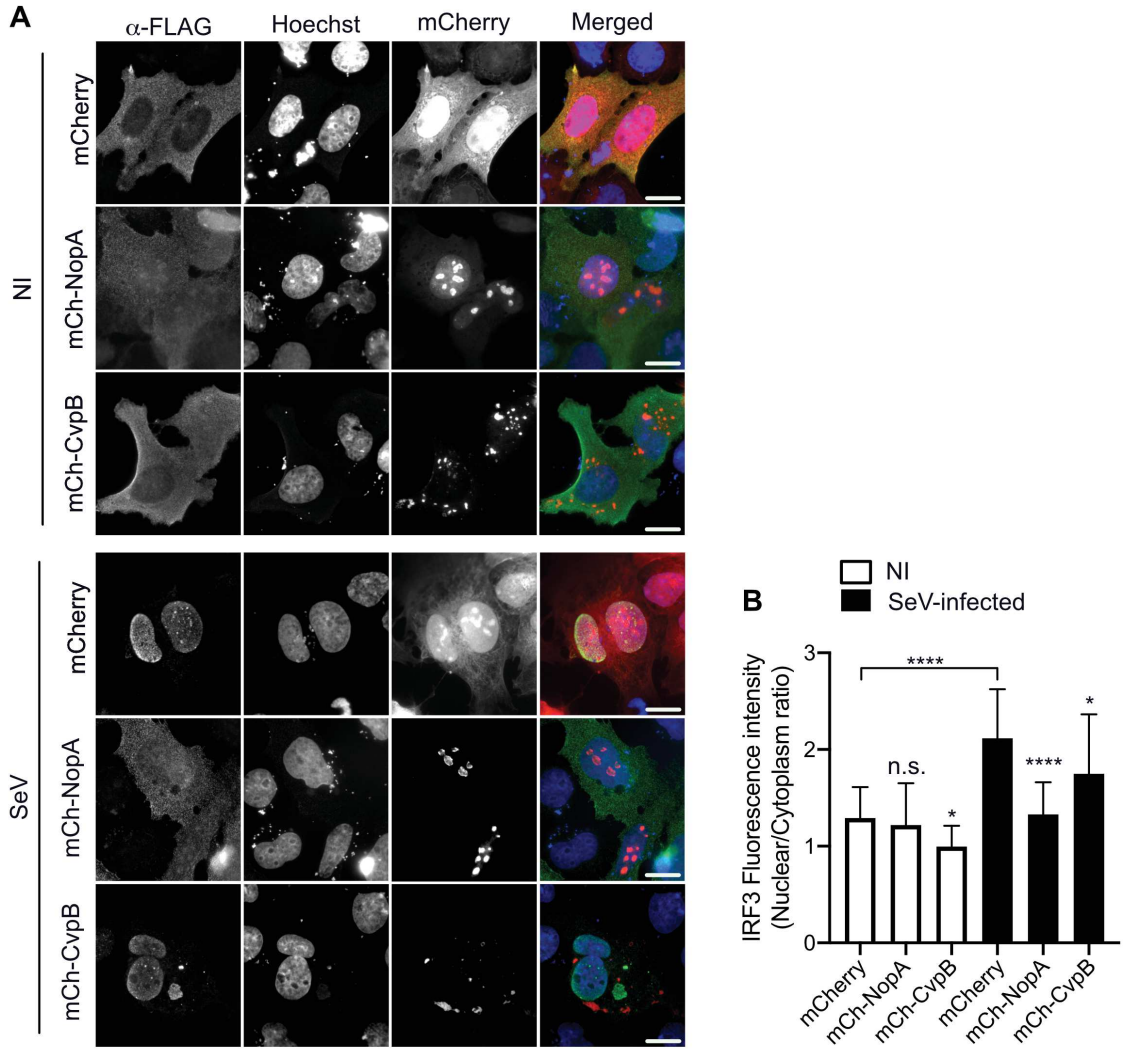
A
α-FLAG
Hoechst
mCherry
Merged
NI
SeV
mCherry
mCh-NopA
mCh-CvpB
B
NI
SeV-infected
IRF3 Fluorescence intensity (Nuclear/Cytoplasm ratio)
n.s.
****
*

Figure S6

A

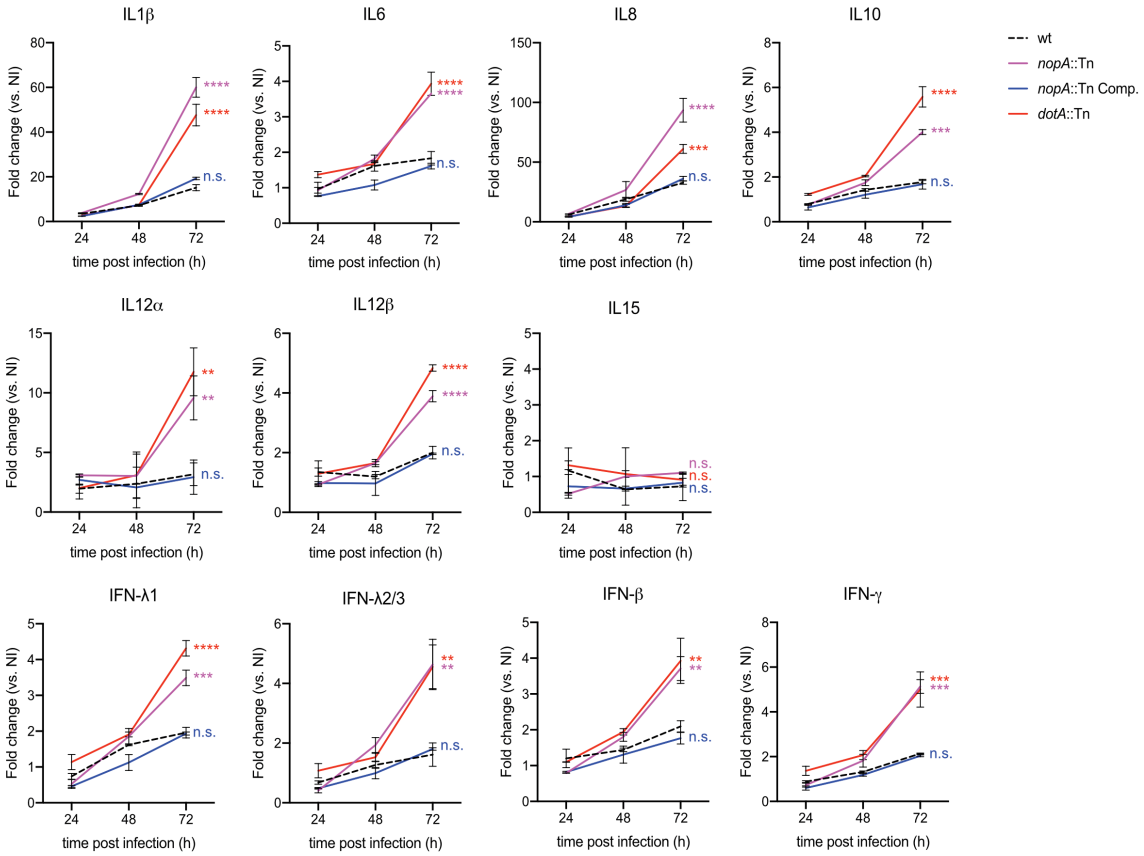
IL1β
IL6
IL8
IL10
IL12α
IL12β
IL15
IFN-λ1
IFN-λ2/3
IFN-β
IFN-γ
Fold change (vs. NI)
time post infection (h)
n.s.
wt
nopA::Tn
nopA::Tn Comp.
dotA::Tn

B

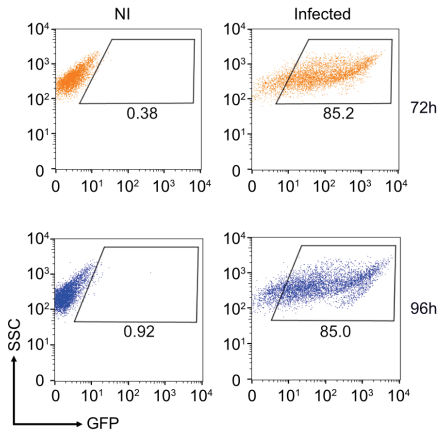
NI
Infected
0.38
85.2
72h
0.92
85.0
96h
SSC
GFP

IL1β

	Nil	wt	*dotA*::Tn	*nopA*::Tn	*nopA*::Tn Comp.
Nil	-	0.0156	2E-04	1E-04	0.0069
wt		-	7E-04	2E-04	n.s.
dotA::Tn			-	0.0181	0.0011
nopA::Tn				-	3E-04
nopA::Tn Comp.					-

IL6

	Nil	wt	*dotA*::Tn	*nopA*::Tn	*nopA*::Tn Comp.
Nil	-	0.0209	1E-04	2E-04	n.s.
wt		-	5E-04	7E-04	n.s.
dotA::Tn			-	n.s.	4E-04
nopA::Tn				-	5E-04
nopA::Tn Comp.					-

IL8

	Nil	wt	*dotA*::Tn	*nopA*::Tn	*nopA*::Tn Comp.
Nil	-	0.0058	5E-04	1E-04	0.0048
wt		-	0.0064	5E-04	n.s.
dotA::Tn			-	0.0058	0.0074
nopA::Tn				-	5E-04
nopA::Tn Comp.					-

IL10

	Nil	wt	*dotA*::Tn	*nopA*::Tn	*nopA*::Tn Comp.
Nil	-	n.s.	1E-04	3E-04	n.s.
wt		-	1E-04	0.001	n.s.
dotA::Tn			-	0.0044	1E-04
nopA::Tn				-	0.001
nopA::Tn Comp.					-

IL12α

	Nil	wt	*dotA*::Tn	*nopA*::Tn	*nopA*::Tn Comp.
Nil	-	n.s.	0.0073	0.0163	n.s.
wt		-	0.0163	0.0368	n.s.
dotA::Tn			-	n.s.	0.0162
nopA::Tn				-	0.0368
nopA::Tn Comp.					-

IL12β

	Nil	wt	*dotA*::Tn	*nopA*::Tn	*nopA*::Tn Comp.
Nil	-	0.0042	0	1E-04	0.0042
wt		-	1E-04	3E-04	n.s.
dotA::Tn			-	0.0042	1E-04
nopA::Tn				-	3E-04
nopA::Tn Comp.					-

IL15

	Nil	wt	*dotA*::Tn	*nopA*::Tn	*nopA*::Tn Comp.
Nil	-	n.s	n.s	n.s	n.s
wt		-	n.s	n.s	n.s
dotA::Tn			-	n.s	n.s
nopA::Tn				-	n.s
nopA::Tn Comp.					-

TNF-α

	Nil	wt	*dotA*::Tn	*nopA*::Tn	*nopA*::Tn Comp.
Nil	-	0.0026	0	0	0.002
wt		-	1E-04	0	n.s.
dotA::Tn			-	0.0104	1E-04
nopA::Tn				-	0
nopA::Tn Comp.					-

IFN-λ1

	Nil	wt	*dotA*::Tn	*nopA*::Tn	*nopA*::Tn Comp.
Nil	-	0.0066	0	2E-04	0.0066
wt		-	2E-04	0.001	n.s.
dotA::Tn			-	0.0066	2E-04
nopA::Tn				-	0.001
nopA::Tn Comp.					-

IFN-L2-3

	Nil	wt	*dotA*::Tn	*nopA*::Tn	*nopA*::Tn Comp.
Nil	-	n.s.	0.0103	0.0103	n.s.
wt		-	0.019	0.019	n.s.
dotA::Tn			-	n.s.	0.019
nopA::Tn				-	0.019
nopA::Tn Comp.					-

IFN-α4

	Nil	wt	*dotA*::Tn	*nopA*::Tn	*nopA*::Tn Comp.
Nil	-	0.049	5E-04	8E-04	n.s.
wt		-	0.002	0.0032	n.s.
dotA::Tn			-	n.s.	0.0019
nopA::Tn				-	0.003
nopA::Tn Comp.					-

IFN-β

	Nil	wt	*dotA*::Tn	*nopA*::Tn	*nopA*::Tn Comp.
Nil	-	n.s.	0.0033	0.0043	n.s.
wt		-	0.017	0.0243	n.s.
dotA::Tn			-	n.s.	0.0108
nopA::Tn				-	0.0152
nopA::Tn Comp.					-

IFN-γ

	Nil	wt	*dotA*::Tn	*nopA*::Tn	*nopA*::Tn Comp.
Nil	-	n.s.	0.0013	0.0012	n.s.
wt		-	0.0039	0.0039	n.s.
dotA::Tn			-	n.s.	0.0039
nopA::Tn				-	0.0038
nopA::Tn Comp.					-

Supporting Figures legends

Figure S1. A, B, Lysates of *C. burnetii* wt (NMII) or *dotA*::Tn strains transformed with pXDC61K plasmids encoding BLAM-tagged versions of the indicated genes were analysed by Western blotting using anti-BLAM and an anti-*C. burnetii* (NMII) antibodies. The expected size of BLAM-tagged proteins is indicated below the first blot. **C**, Lysates of *C. burnetii* transformed with pJA-LacO plasmids encoding 4HA-tagged NopA under the control of an IPTG inducible promoter were probed with anti-HA and anti-*C. burnetii* (NMII) antibodies. **D**, U2OS cells challenged with the *C. burnetii nopA*::Tn mutant or the corresponding complemented strain (*nopA*::Tn Comp.) for the indicated times were lysed and NopA expression was assessed using an anti-HA antibody. Anti-NMII and anti-β-tubulin antibodies were used to validate the presence of *C. burnetii* and as loading control, respectively.

Figure S2. A, U2OS cells were transfected with plasmids encoding the HA-tagged NopA truncations indicated and protein expression was tested using an anti-HA antibody and anti-β-tubulin antibody as loading control. **B**-**E**, U2OS cells were transfected with plasmids encoding the HA-tagged NopA truncations indicated in the left panels. 24 hours after transfection cells were either fixed and labelled with Hoechst (blue), an anti-fibrillarin antibody (green) and an anti-HA antibody (red, centre panels) or lysed and processed for cell fractionation (right panels). Cell fractions were analysed by Western blotting using anti-fibrillarin and anti-GAPDH antibodies as nuclear and chromatin (Nu, Ch) and cytoplasmic (Cy) markers, respectively, and anti-HA antibodies to reveal NopA localisation. **F, G** U2OS cells treated as in **D** and **E** were fixed and labelled with Hoechst (blue), an anti-PML antibody (green) and an anti-HA antibody (red). Scale bars are 10 μm.

Figure S3. A, U2OS cells were transfected with plasmids encoding GFP1-9 in combination with plasmids encoding either GFP10-Ran and GFP11-RCC1 (top row) or GFP10-Ran and GFP11-Fibrillarin (bottom row). 24 hours after transfection cells were fixed and labelled with Hoechst (blue) and an anti-GFP antibody (red) to reveal nuclei and the expression of GFP1-9, respectively. Protein-protein interaction was assessed following the reconstitution of GFP (Reconst. GFP, green). Scale bars are 20 μm. **B,** U2OS cells expressing Ran-GFP (green) in combination either with mCherry alone or mCherry-tagged versions of either full length ($NopA_{FL}$), the C-terminal domain ($NopA_{C\text{-}ter}$) or the N-terminal domain ($NopA_{N\text{-}ter}$) of NopA (red) were fixed 24 hours post-transfection and labelled with anti-fibrillarin antibodies (blue). Scale bars are 10 μm.

Figure S4. Representative images of U2OS cells expressing mCherry, mCherry-NopA or mCherry-CvpB (red) and treated with leptomycin B (LMB) alone for 4 hours (upper panels) or pre-treated with LMB followed by a 30 min incubation with TNFα (lower panels). The localisation of p65 was monitored using an anti-p65 antibody (green) and Hoechst staining of nuclei (blue). Scale bars are 10 μm.

Figure S5. A, Representative images of U2OS cells co-transfected with 3FLAG-tagged IRF3 in combination with either mCherry alone, mCherry-NopA or mCherry-CvpB (red) infected with Sendai Virus (SeV) for 18 hours. Following fixation, the localisation of IRF3 was monitored using an anti-FLAG antibody (green) and Hoechst staining of nuclei (blue). Non-infected (NI) U2OS cells were used as control. **B**, CellProfiler was used to identify mCherry transfected U2OS cells from **A** and measure the median of the ratios of 3FLAG-IRF3 fluorescence intensity at nuclei versus cytoplasm. Values are means ± SEM from 2 independent experiments where a minimum of 200 nuclei were measured per condition. n.s. = non-

significant, **** = P<0.0001, * = P<0.1, one-way ANOVA, Bonferroni multiple comparison test. Scale bars are 10 μm.

Figure S6. A, Differentiated THP-1 cells were challenged either with GFP-expressing wt *C. burnetii* (wt), the Dot/Icm-defective *dotA* transposon mutant (*dotA*::Tn), the *nopA* transposon mutant (*nopA*::Tn) or the corresponding complemented strain (*nopA*::Tn Comp.) for 24, 48, 72 and 96 hours and the expression of the indicated cytokines was assessed by RT-qPCR and normalised for non-infected (NI) cells. Values are means ± SD from 3 experiments. n.s. = non-significant, **** = P<0.0001, *** = P<0.001, ** = P<0.01. Full statistical analysis for the 72 hours post infection time point is available at Figure S7. **B**, GFP expression was quantified by flow cytometry at 72 and 96 hours post-infection. GFP+ cells were analysed for cytokines production following brefeldin A (BFA) treatment for the last 24h. Dot plots from a representative experiment are shown (related to Figure 7).

Figure S7. Statistical analysis for the charts illustrated in Figure 7. Statistical analysis was performed using the R software version 3.6.0. An upper triangular matrix was created to display the P-value between two conditions. For these matrices, a pairwise comparison of means using T-tests with pooled SD were used. P-values < 0,05 were significant. n.s. = non-significant.

Supporting Tables

Supporting Table 1

CDS	Gene	S4TE Score	S4TE Motif/Domain	Predicted Role	PFAM	SMART	NCBI CDD	TMHMM	ELM	Tn mutants in library	Secretion (*L. pneumophila*)
CBU_0053	*enhA.1*	37	Transpeptidase catalytic domain	Protein-protein interactions	YkuD domain (124-247) (E-value = 1,5x10^-11)		YkuD domain (124-247) (E-value = 1,48x10^-9)		Signal Peptide (1-31) YkuD domain (124-247)	*Tn2059*	N/A
CBU_0072	*ankA*	279	Ankyrin Repeat	Protein-protein interactions	Ank (1-93) (E-value = 1,5x10^-7)		Ank (3-110) (E-value = 4,12 x 10^-11)			*Tn326; Tn932; Tn1165; Tn1197; Tn1219*	Yes (Pan et al. 2008)
CBU_0096	*cls*	27	Cardiolipin synthetase	Membrane stability	PLDc domain (32-193) (E-value = 4,3x10^-16) PLDc domain (231-358) (E-value = 1,9x10^-19)	PLDc domain (133-160) (E-value =1,21x10^-4) PLDc domain (304-330) (E-value = 5,88x10^-3)	PLDc domain(217-385) (E-value =2,5x10^-71) PLDc domain (23-194) (E-value =3,36x10^-66)		PLDc domain (133-160) PLDc domain (304-330)	*Tn1825*	N/A
CBU_0175		203	Protein kinase	Protein phosphorylation	Pkinase (26-175) (E-value = 9,7x10^-14)		STKc (Ser/Thr Kinase) (25-175) (E-value = 2,26x10^-13)		Pkinase (26-176)		Yes (Chen et al. 2010)
CBU_0201	*ankC*	247	Ankyrin Repeat	Protein-protein interactions	Ank (25-128) (E-value =2,8x10^-17)	Ank (30-59) (E-value = 42,3) Ank (64-93) (E-value = 0,759) Ank (97-127) (E-value = 29,9)	Ank (38-117) (E-value =5,86x10^-17)		Ank domain (30-59) Ank (64-93) Ank (97-127)		No (Pan et al. 2008)
CBU_0295		221	Tetratricopeptide Repeat	Protein-protein interactions		Sel1 (84-119) (E-value =4,39x10^-2) Sel1 (120-151) (E-value = 45,4) Sel1 (152-183) (E-value = 47,8)	Sel1 (49-234) (E-value = 2,53x10^-8)		Sel1 (84-119) Sel1 (120-151) Sel1 (152-183)		Yes (Carey et al. 2011)
CBU_0335		10	Acid Phosphatase	Protein de-phosphorylation	Acid phosphatase (9-221) (E-value = 8,9x10^-39)		HAD-like domain (40-221) (E-value = 2,65x10^-45)				N/A
CBU_0381		16	Phosphatase	Protein de-phosphorylation	GrpB (16-179) (E-value = 1,9x10^-57)		GrpB domain (16-179) (E-value = 3,81x10^-74)		LIG-PP2a-1 (43-47) (E-value = 1,69x10^-5)	*Tn135*	N/A
CBU_0447	*ankF*	247	Ankyrin Repeat	Protein-protein interactions	Ank (14-107) (E-value = 9,5x10^-12)	Ank (42-71) (E-value = 0,218) Ank (73-102) (E-value = 6,759) Ank (108-138) (E-value = 78,8)	Ank (41-163) (E-value = 4,44x10^-18)		Ank domain (42-71) Ank (73-102) Ank (108-138)	*Tn1897*	Yes (Pan et al. 2008)
CBU_0485		10	Phosphatase	Protein de-phosphorylation	Metallophosphoesterase (7-210) (E-value = 1,1x10^-10)	PP2Ac domain (3-231) (E-value = 1,28)	MPP-PPP domain (10-227) (E-value = 7,78x10^-45)		PP2Ac (3-231)	*Tn300; Tn2261; Tn2505*	N/A
CBU_0505		114	Acetyltransferase	Lipid modification	Acetyltransferase (19-157) (E-value = 8,7x10^-28)		Acetyltransferase (80-156) (E-value = 7,29x10^-11)			*Tn625*	N/A
CBU_0519	*dedA*	130	SNARE-associated Golgi protein	Vesicular fusion	SNARE associated domain (34-160) (E-value = 2,3x10^-19)	Transmembrane Fragments (12-34) (54-76) (139-161) (171-193)	SNARE associated domain (1-164) (E-value = 3,19x10^-37)	Transmembrane Fragments (12-34) (54-76) (139-161) (171-193	Transmembrane Fragments (12-34) (54-76) (139-161) (171-193)		N/A
CBU_0530		16	Tetratricopeptide Repeat	Protein-protein interactions		TPR (109-142) (E-value = 71,1) TPR (181-214) (E-value = 3,27) TPR (215-248) (E-value = 0,876)	TPR (41-137) (E-value = 1,29x10^-4) TPR (186-281) (E-value = 9,82x10^-7)		TPR (109-142) TPR (181-214) TPR (215-248) Signal peptide (1-16)	*Tn2313*	N/A
CBU_0542	*ligA*	105			NAD-dependent DNA ligase adenylation (8-324) (E-value = 9,7x10^-124) NAD-dependent DNA ligase OB fold (326-407) (E-value=8,9x10^-34) NAD-dependent DNA ligase zinc finger (413-440) (E-value = 5,6x10^-10) HHH (Helix-hairpin-helix) (516-579) (E-value = 4,2x10^-24) BRCT (598-671) (E-value = 2,2x10^-15)	LIGANc (9-454) (E-value = 3,26x10^-260) HhH1 (452-471) (E-value = 136) HhH (486-505) (E-value = 5,71) HhH (518-537) (E-value = 114) HhH (550-569) (E-value = 1,76) BRCT (597-673) (E-value = 1,94x10^-11)	LIGANc (12-323) (E-value = 3,75x10^-164) DNA ligase OB fold (326-408) (E-value = 2,21x10^-39) DNA ligase Zinc Binding domain (413-440) (E-value = 9,17x10^-8) HHH5 (448-508) (E-value = 7,37x10^-4) HHH2 (516-579) (E-value = 5,18x10^-25) BRCT (602-672) (E-value = 3,07x10^-14)			N/A
CBU_0547		97	Tetratricopeptide Repeat	Protein-protein interactions	TRP (68-135) (E-value =3,6x10^-16) TRP (138-203) (E-value = 1,3x10^-10) TRP (204-271) (E-value = 2,9x10^-16) TRP (271-338) (E-value = 6,4x10^-15) Truncated methyltransferase domain (403-555) (E-value = 2,5x10^-11)	TPR (2-35) (E-value = 18,7) TPR(36-69) (E-value = 4,84x10^-3) TPR (70-103) (E-value = 2,59x10^-3) TPR (104-137) (E-value = 6,09x10^-3) TPR (138-171) (E-value = 24,3) TPR (172-205) (E-value = 3,9x10^-7) TPR (206-239) (E-value = 1,43x10^-5) TPR (240-273) (E-value = 3,99x10^-4) TPR (274-306) (E-value = 2,67x10^-5) TPR (307-340) (E-value = 1,15x10^-4)	TPR (38-136) (E-value = 5,41x10^-15) TPR (106-204) (E-value = 2,78x10^-15) TPR (174-272) (E-value = 2,7x10^-17) TPR (244-339) (E-value = 1,83x10^-15) adenosylmeth_methyltransf. dom. (407-504) (E-value = 2,98x10^-10)		TPR (2-35) TPR (36-69) TPR (70-103) TPR (104-137) TPR (138-171) TPR (172-205) TPR (206-239) TPR (240-273) TPR (274-306) TPR (307-340) Methyltransferase domain (409-500)	*Tn2450*	N/A
CBU_0607	*mvaD*	10	Diphosphomevalonate decarboxylase	Lipid metabolism	GHMP kinase N domain (105-165) (E-value = 2x10^-8) NUDIX domain (359-495) (E-value = 8x10^-20)		GHMP kinase N domain (23-308) (E-value = 1,84x10^-53) IPP isomerase (332-497) (E-value = 7,83x10^-67)		NUDIX domain (359-495)		N/A
CBU_0608	*mvaK*	21	Phosphomevalonate kinase	Protein phosphorylation	GHMP kinase N domain (85-152) (E-value = 3,7x10^-18) GHMP kinase C domain (215-310) (E-value = 3x10^-20)		GHMP-kinase (85-152) (E-value = 1,07x10^-16) GHMP-kinase (215-278) (E-value = 2,61x10^-6)				N/A
CBU_0609		35	Mevalonate kinase	Protein phosphorylation	GHMP kinase N domain (119-186) (E-value = 9,7x10^-16) GHMP kinase C domain (244-301) (E-value = 1,6x10^-4)		GHMP-kinase (119-186) (E-value =5,93x10^-17)		MOD-CAAXbox (337-340) (E-value =2,201x10^-6)		N/A
CBU_0610	*hmgA*	39	CoA reductase	Lipid metabolism	HMG-CoA reductase (12-350) (E-value = 2x10^-93)		HMG-CoA reductase (15-350) (E-value = 3,02x10^-131)		LIG-OCRL-FandH (292-304) (E-value = 9,772x10^-6)		N/A
CBU_0684		11	F-box	Ubiquitin-related process	domain sulfotransfer (102-361) (E-value = 3x10^-8)		domaine sulfotransferase tronque (203-352) (E-value = 3,43x10^-4)		Sulfotransfer (102-361) DOC-AGC9-PIF-2 (72-77) (E-value = 3,267x10^-6)		N/A
CBU_0752		16	Phospholipase	Membrane lipid interactions	αβhydrolase domain (70-301) (E-value =3,9x10^-13)	Transmembrane Fragments (12-34)	αβhydrolase domain (70-294) (E-value =1,74x10^-13)	Transmembrane Fragments (12-34)	Transmembrane Fragments (12-34)		N/A
CBU_0781	*ankG*	330	Ankyrin Repeat	Protein-protein interactions	Ank (54-156) (E-value =2x10^-12)	Ank (92-124) (E-value = 9,21) Ank (125^154) (E-value =5,71x10^-2) Coiled coil (198-242)	Ank (54-164) (E-value =2,33x10^-14)		Ank domain (92-124) Ank domain (125-154) Coiled-coil (198-242)		Yes (Pan et al. 2008)
CBU_0795	*folE*	26	Tetratricopeptide Repeat	Protein-protein interactions	GTP cyclohydrolase (9-187) (E-value = 2,4x10^-76)		GTP-cyclohydrolase domain (9-187) (E-value = 6,69x10^-108)		GTP cyclohydrolase domain (8-187)		N/A
CBU_0801	*rimI*	218	Acetyltransferase	Lipid modification	Acetyltransferase (44-119) (E-value = 1,7x10^-18)		Acetyltransferase (42-102) (E-value = 4,3x10^-13)				Yes (Chen et al. 2010)
CBU_0870		21	Tetratricopeptide Repeat	Protein-protein interactions	Sdh5 (6-78) (E-value = 4,8x10^-26)		Sdh5 (8-78) (E-value = 3,57x10^-24)				N/A
CBU_0886		16	Leucine rich repeat	Protein-protein interactions	Flavoprotein domain (5-133) (E-value = 5,5x10^-36) DPP (184-382) (E-value =2x10^-84)		DPP domain (184-361) (E-value = 3,92x10^-89)			*Tn46*	N/A
CBU_0898		16	Thyroglobulin type-1 repeat	Hormone biosynthesis	TY (25-97) (E-value = 5,8x10^-16)	Transmembrane Fragments (4-21) TY (52-101) (E-value = 5,26x10^-13)	TY (3-92) (E-value = 1,91x10^-17)	Transmembrane Fragments (4-21)	Signal peptide (1-18) Transmembrane Fragments (4-21) TY domain (52-101)		N/A
CBU_1136	*enhC*	168	Tetratricopeptide Repeat	Protein-protein interactions	Sel1 (49-84) (E-value = 5,3x10^-6) Sel1 (85-117) (E-value = 5,4x10^-4) Sel1 (118-152) (E-value = 1,9x10^-3) Sel1 (154-188) (E-value = 2,5) Sel1 (190-225) (E-value = 1,5x10^-8) Sel1 (363-398) (E-value = 2,1x10^-9) Sel1 (399-434) (E-value = 2,1x10^-9) Sel1 (435-473) (E-value = 9,5) Sel1 (592-624) (E-value = 0,22) Sel1 (695-730) (E-value = 2,9x10^-8) Sel1 (731-766) (E-value = 1x10^-3) Sel1 (768-799) (E-value = 18) Sel1 (800-835) (E-value = 2,6x10^-9) Sel1 (836-871) (E-value = 2x10^-3) Sel1 (872-907 (E-value = 9,3x10^-5) Sel1 (908-943) (E-value = 8,3x10^-5)	Sel1 (49-84) (E-value = 1,95x10^-8) Sel1 (85-117) (E-value = 6,96x10^-3) Sel1 (118-153) (E-value = 1,49x10^-4) Sel1 (154-188) (E-value = 6,08) Sel1 (190-225) (E-value = 8,97x10^-8) Sel1 (363-398) (E-value = 2,74x10^-12) Sel1 (399-434) (E-value = 1,16x10^-10) Sel1 (435-476) (E-value = 11,2) Sel1 (477-520) (E-value = 1,15x10^-5) Sel1 (556-591) (E-value = 7,39x10^-5) Sel1 (592-624) (E-value = 8,19x10^-2) Sel1 (659-694) (E-value = 240) Sel1 (695-730) (E-value = 2,16x10^-10) Sel1 (731-766) (E-value = 5,87x10^-12) Sel1 (767-799) (E-value = 12,1) Sel1 (800-835) (E-value = 5,19x10^-13) Sel1 (836-871) (E-value = 4,16x10^-3) Sel1 (872-907) (E-value = 3,25x10^-5)	Sel1 (49-84) (E-value = 1,09x10^-4) Sel1 (190-225) (E-value = 2,79x10^-4) Sel1 (363-398) (E-value = 1,17x10^-7) Sel1 (400-434) (E-value = 2,86x10^-6) Sel1 (695-730) (E-value = 3,2x10^-6) Sel1 (731-766) (E-value = 2,92x10^-7) Sel1 (800-834) (E-value = 2,27x10^-8) Sel1 (908-943) (E-value = 1,86x10^-3)		Signal peptide(1-19) Sel1 (49-84) Sel1 (85-117) Sel1 (118-153) Sel1 (154-188) Sel1 (190-225) Sel1 (363-398) Sel1 (399-434) Sel1 (435-476) Sel1 (477-520) Sel1 (556-591) Sel1 (592-624) Sel1 (659-694) Sel1 (695-730) Sel1 (731-766) Sel1 (767-799) Sel1 (800-835) Sel1 (836-871) Sel1 (872-907) Sel1 (908-943)		N/A
CBU_1158		16	Sterol reductase	Cholesterol metabolism	ERG4-ERG24 domain (22-440) (E-value = 5,3x10^-77)	Transmembrane Fragments (13-35) (75-93) (114-136) (146-165) (230-252) (267-289) (296-318) (379-401)	PEMT domain (57-440) (E-value = 2,91x10^-69)	Transmembrane Fragments (13-35) (75-93) (114-136) (146-165) (230-252) (267-289) (296-318) (379-401)	Transmembrane Fragments (13-35) (75-93) (114-136) (146-165) (230-252) (267-289) (296-318) (379-401)		N/A
CBU_1160		27	Tetratricopeptide Repeat	Protein-protein interactions	TPR (311-341) (E-value = 2,1x10^-3) TPR (345-376) (E-value = 2,9x10^-6)		TPR (311-384) (E-value = 7,6x10^-8)		LIG-OCRL-FandH-1 (289-281) (E-value = 9,722x10^-6)		N/A
CBU_1206		27	Sterol reductase	Cholesterol metabolism	ERG4-ERG24 (23-459) (E-value = 2,5x10^-129)	Transmembrane Fragments (29-51) (55-77) (90-112) (132-154) (161-183) (221-243) (283-305) (315-332) (396-418)	PEMT domain (28-420) (E-value = 4,07x10^-132)	Transmembrane Fragments (29-51) (55-77) (90-112) (132-154) (161-183) (221-243) (283-305) (315-332) (396-418)	Transmembrane Fragments (29-51) (55-77) (90-112) (132-154) (161-183) (221-243) (283-305) (315-332) (396-418) LIG-OCRL-FandH (369-381) (E-value = 9,772x10^-6)	*Tn1234*	N/A
CBU_1213	*ankI*	277	Ankyrin Repeat	Protein-protein interactions	Ank (372-456) (E-value = 3,4x10^-8)	Ank (367-404) (E-value =850) Ank (405-437) (E-value =0,407) Ank (441-472) (E-value =59,8) Ank (480-509) (E-value = 2,83)	Ank (362-497)(E-value =2,50x10^-17)		Ank domain (367-404) Ank (405-437) Ank (441-472) Ank (480-509)		No (Pan et al. 2008)
CBU_1217		215	F-box + RCC	Ubiquitin-related process Nuclear GTPase activity	RCC1 (255-310) (E-value 1,5,10^-10) RCC1 (314-368) (E-value = 2,4,10^-6) RCC1 (429-469) (E-value = 3,7 10^-6)	F-box (E-value non significative)	RCC1 (196-241) (E-value = 3,4x10^-4) RCC1 (256-310) (E-value = 3,10x10^-8) RCC1 (314-368) (E-value = 1,36x10^-5) RCC1 (430-457) (E-value = 6,83x10^-6)			*Tn227; Tn2438*	Yes (Chen et al. 2010)
CBU_1234		10	Tetratricopeptide Repeat	Protein-protein interactions	AAA domain (43-169) (E-value = 2,3x10^-31)		AAA domain (ATPase) (44-169) (E-value = 2,34x10^-35)				N/A
CBU_1237		16	Protein kinase	Protein phosphorylation	PIN domain (5-122) (E-value = 1,8x10^-10)	PINc (3-118) (E-value = 0,841)	PIN (6-127) (E-value = 3,45x10^-26)		PINc (3-118)		N/A
CBU_1261		21	Protein kinase	Protein phosphorylation	Peptidase (54-285) (E-value = 1,7x10^-76) PBP5c (304-395) (E-value = 5,1x10^-21)	Fragment transmembranaire (7-29) PBP5-C domain (304-395) (E-value = 2,7x10^-25)	Peptidase domain (63-285) (E-value = 1,58x10^-87) PBP5-C domain (304-395) (E-value = 9,67x10^-27)	Transmembrane Fragments (7-29)	Signal peptide (1-29) Transmembrane Fragments (7-29) Peptidase (54-285) PBP5c (304-395)		N/A
CBU_1292	*ankK*	240	Ankyrin Repeat	Protein-protein interactions	Ank (5-95) (E-value = 2,7x10^-14)	Ank (31-60) (E-value =2,47) Ank (64-93) (E-value =7,24x10^-7)	Ank (7-99) (E-value = 5x10^-16)		Ank domain (31-60) Ank (64-93)	*Tn943; Tn1327; Tn2003*	No (Pan et al. 2008)
CBU_1335		16		Cyclin domain-containing protein	Cyclin (47-161) (5.1x10^-18)		Cyclin (10-148) (5.91x10^-46)				N/A
CBU_1366		111	Coiled-coil	Protein-protein interactions	FixA domain (17-107) (E-value =6,6x10^-6)	coiled-coil (61-110)				*Tn1232*	No (Chen et al. 2010)
CBU_1379a		186	Protein kinase	Protein phosphorylation						*Tn100; Tn472; Tn555*	No (Chen et al. 2010)
CBU_1457		335	Tetratricopeptide Repeat	Protein-protein interactions	Sel1 (64-91) (E-value = 9,4) Sel1 (113-147) (E-value = 9,2x10-8) Sel1 (148-183) (E-value = 6,7x10^-8) Sel1 (184-223) (E-value = 5x10^-5)	Sel1 (112-147) (E-value = 8,24x10^-7) Sel1 (148-183) (E-value = 7,28x10^-8) Sel1 (184-224) (E-value = 7,13) Coiled coil (240-265)	Sel1 (115-146) (E-value = 2,99x10^-6) Sel1 (148-183) (E-value =5,97x10^-7)		Sel1 (112-147) Sel1 (148-183) Sel1 (184-224) Coiled coil (240-265)	*Tn1376*	Yes (Chen et al. 2010)
CBU_1472		16	Phosphatase	Protein de-phosphorylation					LIG-BRCT-MDC1-1 (62-68) (E-value =2,634x10^-6)		N/A
CBU_1482		71	Stomatin/Prohibitin homolog	Lipid raft-associated protein	PHB domain (21-192) (E-value = 3,3x10^-32)	PHB domain (prohibitin homologue) (18-175) (E-value = 1,44x10^-60)	Stomatin/prohibitin homologue (17-233) (E-value = 2,03x10^-48)	Transmembrane Fragments (5-22)	Transmembrane Fragments (3-22) PHB domain (19-175)		N/A
CBU_1485		27		Cyclin domain-containing protein	Cyclin (44-161) (3.4x10^-26)	Cyclin (77-159) (0.303)	Cyclin (43-165) (1.31x10^-28)				N/A
CBU_1489		16	Phosphatase	Protein de-phosphorylation	Metallophosphoesterase (1-223) (E-value = 1,3x10^-12)		MPP-YbbF domain (5-219) (E-value = 5,15x10^-56)		Metallophosphoesterase (2-199)		N/A
CBU_1678		59	Acetyltransferase	Lipid modification	Acetyltransferase (2-137) (7.8x10^-21)		NAT-SF (1-163) (2.18x10^-72)				N/A
CBU_1724		263	F-box	Ubiquitin-related process			Ankyrine domaine (168-265) (E-value = 4,24x10^-4)			*Tn587*	N/A
CBU_1730		10	Phosphatase	Protein de-phosphorylation	HAD domain (15-184) (E-value = 1,3x10^-15)		HAD-like domain (14-186) (E-value =6,78x10^-7)		Hydrolase (12-187)	*Tn240*	N/A
CBU_1744		10	Phosphatase	Protein de-phosphorylation	BON domain (52-116) (E-value = 5x10^-12) BON domain (130-189) (E-value = 9,9x10^-16)	Transmembrane fragment (15-37)	BON domain (69-116) (E-value = 1,33x10^-5) BON domain (141-185) (E-value = 1,51x10^-7)	Transmembrane Fragments (15-37)	Signal peptide (1-19) Transmembrane Fragments (15-37) BON domain (52-116) BON (130-189)	*Tn1074; Tn2197; Tn1306*	N/A
CBU_1780		93	Tetratricopeptide	Protein-protein interactions						*Tn137*	No (Carey et al. 2011)
CBU_1799		71	Acetyltransferase	Lipid modification	Acetyltransferase (2-80) (E-value = 4,0x10^-13)		NAT-SF (53-110) (E-value = 2,1x10^-9)				N/A
CBU_1987	*apaH*	26	Phosphatase	Protein de-phosphorylation	Metallophosphoesterase (19-248) (E-value = 1,1x10^-11)		MPP-ApaH domain (20-275) (E-value = 1,46x10^-13)		Metallophosphoesterase (19-248)	*Tn2282*	N/A
CBUA_0032		170	Phosphatase	Protein de-phosphorylation	Metallophosphoesterase (6-195) (E-value = 1,4x10^-20)		MPP-GpdQ (7-237) (E-value =1,51x10^-72)		Metallophosphoesterase (6-195)	*Tn2167*	N/A
CBUA_0012		50	Phospholipase	Membrane lipid interactions							N/A
CBUA_0014		45	F-box	Ubiquitin-related process							Yes (Chen et al. 2010)
CBUA_0024		42	Tetratricopeptide Repeat	Protein-protein interactions							N/A

Supporting table 2

CDS	Gene	S4TE Score	S4TE Motif/Domain	Predicted Role	PFAM	SMART	NCBI CDD	TMHMM	ELM	Tn mutants in library	Secretion by *L. pneumophila*	Secretion by *C. burnetii* (this study)
CBU_0072	*ankA*	279	**Ankyrin Repeat**	Protein-protein interactions	Ank (1-93) (E-value = 1,5x10^-7)		Ank (3-110) (E-value = 4,12 x 10^-11)			*Tn326; Tn532; Tn1165; Tn1197; Tn1219*	Yes (Pan et al. 2008)	Yes
CBU_0201	*ankC*	247			Ank (25-128) (E-value =2,8x10^-17)	Ank (30-59) (E-value = 42,3) Ank (64-93) (E-value = 0,759) Ank (97-127) (E-value = 29,9)	Ank (38-117) (E-value =5,86x10^-17)		Ank domain (30-59) Ank (64-93) Ank (97-127)		No (Pan et al. 2008)	No
CBU_0447	*ankF*	247			Ank (14-107) (E-value = 9,5x10^-12)	Ank (42-71) (E-value = 0,218) Ank (73-102) (E-value = 0,759) Ank (108-138) (E-value = 78,9)	Ank (41-163) (E-value = 4,44x10^-18)		Ank domain (42-71) Ank (73-102) Ank (108-138)	*Tn1897*	Yes (Pan et al. 2008)	Yes
CBU_0781	*ankG*	330			Ank (54-156) (E-value =2x10^-12)	Ank (82-124) (E-value = 9,21) Ank (127-154) (E-value =5,71x10^-2) Coiled coil (198-242)	Ank (54-164) (E-value =2,33x10^-14)		Ank domain (82-124) Ank domain (125-154) Coiled-coil (198-242)		Yes (Pan et al. 2008)	Yes
CBU_1213	*ankI*	277			Ank (372-456) (E-value = 3,4x10^-9)	Ank (357-404) (E-value =850) Ank (405-437) (E-value =0,407) Ank (441-472) (E-value =59,8) Ank (483-509) (E-value = 2,83)	Ank (362-497)(E-value =2,50x10^-17)		Ank domain (357-404) Ank (405-437) Ank (441-472) Ank (483-509)		No (Pan et al. 2008)	No
CBU_0295		221	**Tetratricopeptide Repeat**	Protein-protein interactions		Sel1 (84-119) (E-value =4,39x10^-2) Sel1 (120-151) (E-value = 45,4) Sel1 (152-183) (E-value = 47,8)	Sel1 (49-234) (E-value = 2,53x10^-8)		Sel1 (84-119) Sel1 (120-151) Sel1 (152-183)		Yes (Carey et al. 2011)	Yes
CBU_0547		97			TPR (68-135) (E-value =3,6x10^-16) TPR (138-203) (E-value = 1,3x10^-10) TPR (204-277) (E-value = 2,9x10^-16) TPR (277-338) (E-value = 6,4x10^-15) Truncated methyltransferase domain (403-555) (E-value = 2,5x10^-11)	TPR (2-35) (E-value = 18,7) TPR(36-69) (E-value = 4,84x10^-3) TPR (70-103) (E-value = 2,59x10^-3) TPR (104-137) (E-value = 6,08x10^-9) TPR (138-171) (E-value = 24,3) TPR (172-205) (E-value = 3,9x10^-7) TPR (206-239) (E-value = 1,43x10^-5) TPR (240-273) (E-value = 3,98x10^-4) TPR (274-306) (E-value = 2,67x10^-5) TPR (307-340) (E-value = 1,15x10^-4)	TPR (38-136) (E-value = 5,41x10^-15) TPR (106-204) (E-value = 2,78x10^-15) TPR (174-272) (E-value = 2,7x10^-17) TPR (244-338) (E-value = 1,83x10^-15) adenosylmeth, methyltransf, dom, (407-504) (E-value = 2,98x10^-10)		TPR (2-35) TPR (36-69) TPR (70-103) TPR (104-137) TPR (138-171) TPR (172-205) TPR (206-239) TPR (240-273) TPR (274-306) TPR (307-340) Methyltransferase domain (409-500)	*Tn2450*	N/A	No
CBU_1457		335			Sel1 (64-91) (E-value = 9,4) Sel1 (113-147) (E-value = 9,2x10-8) Sel1 (148-183) (E-value = 6,7x10^-8) Sel1 (184-223) (E-value = 5x10^-5)	Sel1 (112-147) (E-value = 8,24x10^-7) Sel1 (148-183) (E-value = 7,93x10^-9) Sel1 (184-224) (E-value = 7,13) Coiled coil (240-265)	Sel1 (115-146) (E-value = 2,99x10^-6) Sel1 (148-183) (E-value =5,97x10^-7)		Sel1 (112-147) Sel1 (148-183) Sel1 (184-224) Coiled coil (240-265)	*Tn1376*	Yes (Chen et al. 2010)	No
CBU_0175		203	**Protein kinase**	Protein phosphorylation	Pkinase (35-175) (E-value = 9,7x10^-14)		STKc (Ser/Thr Kinase) (25-175) (E-value = 2,26x10^-13)		Pkinase (25-176)		Yes (Chen et al. 2010)	Yes
CBU_1379a		186								*Tn100; Tn472; Tn555*	No (Chen et al. 2010)	N/A
CBU_0505		114	**Acetyltransferase**	Lipid modification	Acetyltransferase (19-157) (E-value = 8,7x10^-28)		Acetyltransferase (80-156) (E-value = 7,29x10^-11)			*Tn625*	N/A	No
CBU_0801	*nmt*	218			Acetyltransferase (44-119) (E-value = 1,7x10^-18)		Acetyltransferase (42-102) (E-value = 4,3x10^-13)				Yes (Chen et al. 2010)	No
CBU_1799		71			Acetyltransferase (2-80) (E-value = 4,0x10^-13)		NAT-SF (53-110) (E-value = 2,1x10^-9)				N/A	No
CBU_0096	*cls*	27	**Cardiolipin synthetase**	Membrane stability	PLDc domain (32-193) (E-value = 4,3x10^-16) PLDc domain (231-358) (E-value = 1,9x10^-19)	PLDc domain (133-160) (E-value =1,21x10^-4) PLDc domain (304-330) (E-value = 5,88x10^-3)	PLDc domain(217-385) (E-value =2,5x10^-71) PLDc domain (23-194) (E-value =3,39x10^-56)		PLDc domain (133-160) PLDc domain (304-330)	*Tn1825*	N/A	N/A
CBU_0519	*dedA*	130	**SNARE-associated Golgi protein**	Vesicular fusion	SNARE associated domain (34-160) (E-value = 2,3x10^-19)	Transmembrane Fragments (12-34) (54-76) (139-161) (171-193)	SNARE associated domain (1-164) (E-value = 3,19x10^-37)	Transmembrane Fragments (12-34) (54-76) (139-161) (171-193)	Transmembrane Fragments (12-34) (54-76) (139-161) (171-193)		N/A	No
CBU_0542	*lipA*	105			NAD-dependent DNA ligase adenylation (8-324) (E-value = 9,7x10^-124) NAD-dependent DNA ligase OB fold (326-407) (E-value=8,9x10^-34) NAD-dependent DNA ligase zinc finger (413-440) (E-value = 5,5x10^-10) HHH (Helix-hairpin-helix) (516-579) (E-value = 4,2x10^-24) BRCT (598-671) (E-value = 2,2x10^-15)	LIGANc (9-454) (E-value = 3,26x10^-260) HHH (482-471) (E-value = 136) HHH (486-555) (E-value = 5,71) HHH (518-537) (E-value = 114) HHH (550-569) (E-value = 1,76) BRCT (597-673) (E-value = 1,94x10^-11)	LIGANc (12-323) (E-value = 3,75x10^-164) DNA ligase OB fold (326-406) (E-value = 2,21x10^-38) DNA ligase Zinc Binding domain (413-440) (E-value = 9,17x10^-8) HHH5 (448-508) (E-value = 7,37x10^-4) HHH2 (516-579) (E-value = 5,15x10^-25) BRCT (632-672) (E-value = 3,07x10^-14)				N/A	No
CBU_1206		27	**Sterol reductase**	Cholesterol metabolism	ERG4-ERG24 (23-459) (E-value = 2,5x10^-129)	Transmembrane Fragments (29-51) (55-77) (90-112) (132-154) (161-183) (221-243) (283-305) (315-332) (366-418)	PEMT domain (28-420) (E-value = 4,07x10^-132)	Transmembrane Fragments (29-51) (55-77) (90-112) (132-154) (161-183) (221-243) (283-305) (315-332) (366-418)	Transmembrane Fragments (29-51) (55-77) (90-112) (132-154) (161-183) (221-243) (283-305) (315-332) (366-381) (E-value = 9,772x10^-6)	*Tn1234*	N/A	N/A
CBU_1217		215	**F-box + RCC**	Ubiquitin-related process Nuclear GTPase activity	RCC1 (255-310) (E-value 1,5.10^-10) RCC1 (314-368) (E-value = 2,4.10^-6) RCC1 (629-469) (E-value = 3,7.10^-6)	F-box (E-value non significative)	RCC1 (196-241) (E-value = 3,4x10^-4) RCC1 (256-310) (E-value = 3,15x10^-8) RCC1 (314-368) (E-value = 1,36x10^-5) RCC1 (430-457) (E-value = 6,83x10^-4)			*Tn227; Tn2438*	Yes (Chen et al. 2010)	Yes
CBU_1366		111	**Coiled-coil**	Protein-protein interactions	FlaA domain (17-107) (E-value =5,6x10^-6)	coiled-coil (61-110)				*Tn1232*	No (Chen et al. 2010)	No
CBU_1724		263	**F-box**	Ubiquitin-related process			Ankyrine domaine (168-265) (E-value = 4,24x10^-4)			*Tn587*	N/A	Yes

Supporting table 3

Strain	Description	Origin
GFP-expressing *C. burnetii*	*C. burnetii* RSA 439 Nine Mile II carrying a transposon insertion between CBU_1847b and CBU_1849 (*Tn1832*)	Martinez *et al.* 2014
nopA::Tn	*C. burnetii* RSA 439 Nine Mile II carrying a transposon insertion in CBU_1217 (*Tn227*)	Martinez *et al.* 2014
4HA	*C. burnetii* RSA 439 Nine Mile II *Tn1832* transformed with a pJA-LacO-4HA plasmid encoding the 2HA tag alone, under the control of an IPTG-inducible promoter	This study
4HA-NopA	*C. burnetii* RSA 439 Nine Mile II *Tn1832* transformed with a pJA-LacO-4HA plasmid encoding 4HA-*nopA* under the control of an IPTG-inducible promoter	This study
4HA-NopA (*dotA*::Tn)	*C. burnetii* RSA 439 Nine Mile II *Tn292* transformed with a pJA-LacO-4HA plasmid encoding 4HA-NopA under the control of an IPTG-inducible promoter	This study
***nopA::Tn* Comp.**	*C. burnetii* RSA 439 Nine Mile II *Tn227* transformed with a pUC18R6K-miniTn7T-Kan plasmid encoding 4HA-*nopA* under the control of the endogenous promoter	This study
dotA::Tn	*Coxiella burnetii* RSA 439 Nine Mile II carrying a transposon GFP-CAT in CBU_1648 (*dotA; Tn292*)	Martinez *et al.* 2014

Supporting table 4

Name	Description	Origin
pXDC61	IPTG-inducible expression vector for N-terminal fusion of Beta-lactamase enzyme in *C. burnetii*, Chloramphenicol resistance	(De Felipe *et al.*, 2008)
pXDC61K	IPTG-inducible expression vector for N-terminal fusion of Beta-lactamase enzyme in *C. burnetii*, Kanamycin resistance	This study
pXDC61K-CBU0021	IPTG-inducible expression of BLAM-CBU0021 (CvpB)	This study
pXDC61K-CBU0072	IPTG-inducible expression of BLAM-CBU0072 (AnkA)	This study
pXDC61K-CBU0096	IPTG-inducible expression of BLAM-CBU0096	This study
pXDC61K-CBU0175	IPTG-inducible expression of BLAM-CBU0175	This study
pXDC61K-CBU0201	IPTG-inducible expression of BLAM-CBU0201 (AnkC)	This study
pXDC61K-CBU0295	IPTG-inducible expression of BLAM-CBU0295	This study
pXDC61K-CBU0447	IPTG-inducible expression of BLAM-CBU0447 (AnkF)	This study
pXDC61K-CBU0505	IPTG-inducible expression of BLAM-CBU0505 (Cig14)	This study
pXDC61K-CBU0519	IPTG-inducible expression of BLAM-CBU0519	This study
pXDC61K-CBU0542	IPTG-inducible expression of BLAM-CBU0542 (LigA)	This study
pXDC61K-CBU0547	IPTG-inducible expression of BLAM-CBU0547	This study
pXDC61K-CBU0781	IPTG-inducible expression of BLAM-CBU0781 (AnkG)	This study
pXDC61K-CBU0801	IPTG-inducible expression of BLAM-CBU0801 (PanB)	This study
pXDC61K-CBU1206	IPTG-inducible expression of BLAM-CBU1206	This study
pXDC61K-CBU1213	IPTG-inducible expression of BLAM-CBU1213	This study
pXDC61K-CBU1217	IPTG-inducible expression of BLAM-CBU1217 (NopA)	This study
pXDC61K-CBU1366	IPTG-inducible expression of BLAM-CBU1366 (Cig40)	This study
pXDC61K-CBU1379a	IPTG-inducible expression of BLAM-CBU1379a	This study
pXDC61K-CBU1724	IPTG-inducible expression of BLAM-CBU1724	This study
pXDC61K-CBU1799	IPTG-inducible expression of BLAM-CBU1799	This study
pLVX-mCherry-N2	CMV expression vector expressing a C-terminal mCherry tag	This study
pLVX-CBU0072-mCherry	CMV expression vector expressing CBU0072 fused to a C-terminal mCherry tag	This study
pLVX-CBU0295-mCherry	CMV expression vector expressing CBU0295 fused to a C-terminal mCherry tag	This study
pLVX-CBU0447-mCherry	CMV expression vector expressing CBU0447 fused to a C-terminal mCherry tag	This study
pLVX-CBU0781-mCherry	CMV expression vector expressing CBU0781 fused to a C-terminal mCherry tag	This study
pLVX-CBU1217/NopA-mCherry	CMV expression vector expressing CBU1217 fused to a C-terminal mCherry tag	This study
pLVX-NopA$_{Nter}$-mCherry	CMV expression vector expressing the N-terminal domain of CBU1217 (aa1-195) fused to a C-terminal mCherry tag	This study
pLVX-NopA$_{Cter}$-mCherry	CMV expression vector expressing the C-terminal domain of CBU1217 (aa196-497) fused to a C-terminal mCherry tag	This study
pLVX-CvpBopt-mCherry	CMV expression vector expressing CvpB (codon optimised) with C-terminal fusion of mCherry tag	(Martinez *et al.*, 2016)
pRK5-HA	CMV expression vector for N-terminal fusion of HA tag	(Martinez *et al.*, 2016)
pRK5-HA-NopA	CMV expression vector for N-terminal HA-tagged full length NopA (CBU1217)	This study
pRK5-HA-NopA$_{Nter}$	CMV expression vector for HA-tagged NopA (CBU1217) N-terminal domain (aa1-195)	This study
pRK5-HA-NopA$_{Cter}$	CMV expression vector for HA-tagged NopA (CBU1217) C-terminal domain (aa196-497)	This study
pRK5-HA-NopA$_{RCC1}$	CMV expression vector for HA-tagged NopA (CBU1217) C-terminal domain (aa196-243)	This study
pRK5-HA-NopA$_{RCC1-2}$	CMV expression vector for HA-tagged NopA (CBU1217) C-terminal domain (aa196-310)	This study
pRK5-HA-NopA$_{RCC1-2-3}$	CMV expression vector for HA-tagged NopA (CBU1217) C-terminal domain (aa196-368)	This study

Name	Description	Origin
pRK5-HA-NopA$_{RCC4}$	CMV expression vector for HA-tagged NopA (CBU1217) C-terminal domain (aa429-497)	This study
pRK5-HA-NopA$_{RCC3-4}$	CMV expression vector for HA-tagged NopA (CBU1217) C-terminal domain (aa314-497)	This study
pRK5-HA-NopA$_{RCC2-3-4}$	CMV expression vector for HA-tagged NopA (CBU1217) C-terminal domain (aa251-497)	This study
pRK5-HA-CvpB	pCMV expression vector expressing CvpB with N-terminal fusion of HA tag	(Martinez *et al.*, 2016)
pRK5-HA-CvpF	pCMV expression vector expressing CvpF with N-terminal fusion of HA tag	(Siadous *et al.*, 2020)
pcDNA3-IRF-3-3xFLAG-SmNLuc	T7 expression vector encoding IRF-3 with C-terminal fusion of 3FLAG tag	Sebastien Nisole
pJA-LacO-2HA	pXDC61K derivative where BLAM gene has been replaced by 2HA tag	This study
pJA-LacO-4HA-NopA	pXDC61K derivative where BLAM gene has been replaced by 4HA-NopA (CBU1217)	This study
pCMV_GFP1-9-OPT	T7 expression vector encoding GFP1-9	(Cabantous *et al.* 2013)
pcDNA3-GFP10-zipper-GFP11	T7 expression vector encoding GFP10-GFP11	(Cabantous *et al.* 2013)
pcDNA3-GFP10-zipper	T7 expression vector for N-terminal fusion of GFP10	(Cabantous *et al.* 2013)
pcDNA3-GFP10-zipper-Ran	T7 expression vector expressing Ran with N-terminal fusion of GFP10 tag	This study
pcDNA3-zipper-GFP11	T7 expression vector for C-terminal fusion of GFP11	(Cabantous *et al.* 2013)
pcDNA3-NopA-zipper-GFP11	T7 expression vector expressing NopA with C-terminal fusion of GFP11 tag	This study
pcDNA3-RCC1-zipper-GFP11	T7 expression vector expressing RCC1 with C-terminal fusion of GFP11 tag	This study
pcDNA3-Fibrillarin-zipper-GFP11	T7 expression vector expressing Fibrillarin with C-terminal fusion of GFP11 tag	This study
pGBKT7-Ran$_{WT}$	T7 expression vector encoding RanWT	Aymelt Itzen
pGBKT7-Ran$_{T24N}$	T7 expression vector encoding RanT24N	Aymelt Itzen
pGBKT7-Ran$_{Q69L}$	T7 expression vector encoding RanQ69L	Aymelt Itzen
pGBKT7-Ran$_{N122I}$	T7 expression vector encoding RanN122I	Aymelt Itzen
pLVX-GFP-N2	CMV expression vector for C-terminal fusion of GFP	Eric Martinez
pLVX-RanWT-GFP-N2	CMV expression vector expressing RanWT with C-terminal fusion of GFP tag	This study
pLVX-Ran$_{T24N}$-GFP-N2	CMV expression vector expressing RanT24N with C-terminal fusion of GFP tag	This study
pLVX-Ran$_{Q69L}$-GFP-N2	CMV expression vector expressing RanQ69L with C-terminal fusion of GFP tag	This study
pLVX-Ran$_{N122I}$-GFP-N2	CMV expression vector expressing RanN122I with C-terminal fusion of GFP tag	This study
pUC18R6K-miniTn7T-Kan	miniTn7 transposon with kanamycin resistance cassette	Robert Heinzen
pUC18R6K-miniTn7T-Kan-promNopA-4HA-NopA	miniTn7 transposon with kanamycin resistance cassette expressing 4HA-NopA under the control of the endogenous promoter	This study

Supporting table 5

Primer Name	Sequence
BLAM Translocation Assay	
Generation of pXDC61K-BLAM	
P1169-KanR-HindIII	CATGCAAGCTTTTATCAGAAGAA
P1169-KanR-SnaBI-rev	AGGTACGTAGCTTATGGCTTCGTTTCGCAG
Generation of pXDC61K-BLAM derivatives	
CBU0021-XmaI	AGGCCCGGGTGAGCAGACAGCCATCATTGA
CBU0021-XmaI-rev	AGGCCCGGGGTATTTAAGCGGTCAATAAAAAATT
CBU0072-KpnI	AGGGGTACCTTGCAGTTGGCAGCCCGTGA
CBU0072-XbaI-rev	AGGTCTAGAGCGAAATACGGGATTTGTTTTTAT
CBU0096-KpnI	AGGGGTACCATTAAAAAAAAAGGTATTATGGAAAGT
CBU0096-BamHI-rev	AGGGGATCCTATCCAGTACTTAATATAAAG
CBU0175-KpnI	AGGGGTACCGGCGGGGCGACGGGCTAT
CBU0175-HindIII-rev	AGGGGATCCTAATTAATCCCATTCAATATTTTCTAA
CBU0201-KpnI	AGGGGTACCATGTTAATCCCGAGCCTCCAA
CBU0201-BamHI-rev	AGGGGATCCTACGGGCTACGCGTTATTGC
CBU0295-KpnI	AGGGGTACCTTGAGGTACAAGCGACACATG
CBU0295-BamHI-rev	AGGGGATCCGTTGGAGTTGCCCTTTTAAAAAG
CBU0447-KpnI	AGGGGTACCATGAGACAGCGTGAAATTAATGA
CBU0447-BamHI-rev	AGGGGATCCGCTACTTAGCGGACTACCGC
CBU0505-KpnI	AGGGGTACCATGCTTAATGCTTTTTATAGTTCAA
CBU0505-BamHI-rev	AGGGGATCCCTTGCCACTGAAGGTTCATAAG
CBU0519-KpnI	AGGGGTACCCTCAACATTGATTTGATTCATCTA
CBU0519-BamHI-rev	AGGGGATCCAGGCAATCGGATTAGGGTGAC
CBU0542-KpnI	AGGGGTACCGTGAATGGTGTGGAAGTTCCT
CBU0542-BamHI-rev	AGGGGATCCTTTCATCAAAAAACTCCCTTACG
CBU0547-KpnI	AGGGGTACCATGACCAACAAACTCCTTGAAC
CBU0547-BamHI-rev	AGGGGATCCCCCCCACCACTCACAGCCC
CBU0781-KpnI	AGGGGTACCATGAGTAGACGTGAGACTCCC
CBU0781-BamHI-rev	AGGGGATCCCACCCCTCATCTTTTTCACCG
CBU0801-KpnI	AGGGGTACCGTGAAAATTCGAAACTGGATTAAG
CBU0801-BamHI-rev	AGGGGATCCGATAAATACATTTGTCCATTTTCTAA
CBU1206-KpnI	AGGGGTACCCCTAATCGGGAGATAAAAATGAC
CBU1206-BamHI-rev	AGGGGATCCGAGAGTTTATTTAAAAAATAAACGGA
CBU1213-BamHI	AGGGGATCCATGAGAGAATCATCAGAAAATCAA
CBU1213-HindIII-rev	AGGAAGCTTGATAGGATAGTCTTTTATTGCTTC
CBU1217-KpnI	AGGGGTACCAGAACTTCGCATCAAAATCAACC
CBU1217-BamHI-rev	AGGGGATCCTAAAATCACTTTCTGGAAAAAGGG
CBU1366-KpnI	AGGGGTACCATGAAAAAATGGTCATTGATCGTA
CBU1366-BamHI-rev	AGGGGATCCACCGATTTATTCAAAATTATTTAATC
CBU1379a-KpnI	AGGGGTACCATGGAGCGAAGCGAAATACGG
CBU1379a-BamHI-rev	AGGGGATCCCTTCATGTTTCAAACGGTTATCTG
CBU1724-KpnI	AGGGGTACCATGACTCGGCAGATCAATTTCT
CBU1724-BamHI-rev	AGGGGATCCGCAGTTAACGAACGTACTATTTC
CBU1799-KpnI	AGGGGTACCATGAAAAATTATTATTTTTCAAATTCAA
CBU1799-BamHI-rev	AGGGGATCCCCGTATTCAGCCTAAATTTCCG
Ectopic Expression	
Generation of pLVX-mCherry-N2 derivatives	
CBU0072-MluI	AGGACGCGTTTGCAGTTGGCAGCCCGTGA

CBU0072-NotI-rev	AGGGCGGCCGCAAAACAGTCCGGGGCCTGAATA
CBU0295-MluI	AGGACGCGTTTGAGGTACAAGCGACACATG
CBU0295-NotI-rev	AGGGCGGCCGCAAAAAGTAAAGGATTGTTTAGAGTG
CBU0447-MluI	AGGACGCGTATGAGACAGCGTGAAATTAATGA
CBU0447-NotI-rev	AGGGCGGCCGCACCGCTGGAAGCCGCGATT
CBU0781-MluI	AGGACGCGTATGAGTAGACGTGAGACTCCC
CBU0781-NotI-rev	AGGGCGGCCGCACCGAGGACTAGACAGACAAG
CBU1217-MluI	AGGACGCGTATGAGAACTTCGCATCAAAATCAA
CBU1217-NotI-rev	AGGGCGGCCGCCTTTCTGGAAAAAGGGGCGTA
Generation of pRK5-HA derivatives	
CBU1217-BamHI	AGAGGATCCAGAACTTCGCATCAAAATCAACC
CBU1217-EcoRI-rev	AGAGAATTCGTTCGAATCCCGCCCTCTC
CBU1217Nter-stop-EcoRI-rev	AGGGAATTCTTATTCTGTGAGTATGAATGCATGTC
CBU1217Cter-start-BamHI	AGGGGATCCATGGAAGGAGGAATTTATGGCTGG
CBU1217-1RCC-BamHI	AGGGGATCCCAAGGGTATATTTACGCCTGG
CBU1217-2RCC-BamHI	AGGGGATCCGGTTACATTTATGCTTGGGGTAA
CBU1217-3RCC-BamHI	AGGGGATCCGCACGGACAGCACAAGGACAT
CBU1217-Cter-start-BamHI	AGGGGATCCATGGAAGGAGGAATTTATGGCTGG
RCC1-EcoRI-rev	CCGGAATTCTTAACGGTCCGCGAAATTAAGTTGG
RCC1-2-EcoRI-rev	CCGGAATTCTTATAGTTGAGTAAGTGCCAAGGTATGTC
RCC1-2-3-EcoRI-rev	CCGGAATTCTTATTCTGTTCGCGCGAGAGAAC
Generation of vectors for tripartite GFP assay	
Ran-BspEI	TCCTCCGGAATGGCTGCGCAGGGAGA
Ran-XbaI-rev	CTAGTCTAGACTACAGGTCATCATCCTCATCCG
NopA-NotI	AAGGAAAAAAGCGGCCGCACCATGAGAACTTCGCATCAAAATCAA
NopA-ClaI-rev	CCCATCGATCTTTCTGGAAAAAGGGGCGTA
RCC1-NotI	AAGGAAAAAAGCGGCCGCACCATGTCACCCAAGCGC
RCC1-ClaI-rev	CCCATCGATGCTCTGTTCTTTGTCCTTGAC
FBL-NotI	AAGGAAAAAAGCGGCCGCACCATGAAGCCAGGATTCAGTCC
FBL-ClaI-rev	CCCATCGATGTTCTTCACCTTGGGGGG
***nopA* Complementation**	
NheI-prom1217-fw	CTAGCTAGCAGCGTGGTTTTATGAGAAAT
PstI-prom1217-Rev	CCAATGCATTGGTTCTGCAGTTCTTAGTTCTCCGTTTTAAGG
qRT-PCR	
RPL13A-fw	AACAGCTCATGAGGCTACGG
RPL13A-rev	TGGGTCTTGAGGACCTCTGT
B2M-fw	TGCTGTCTCCATGTTTGATGTATCT
B2M-rev	TCTCTGCTCCCCACCTCTAAGT
ACTB-fw	CTGGAACGGTGAAGGTGACA
ACTB-rev	AAGGGACTTCCTGTAACAATGCA
IL1β-fw	CCAGCTACGAATCTCCGACC
IL1β-rev	TCTCCTGGAAGGTCTGTGGG
IL6-fw	TAACCACCCCTGACCCAACC
IL6-rev	ATTTGCCGAAGAGCCCTCAG
IL8-fw	AAGGGCCAAGAGAATATCCGAA
IL8-rev	ACTAGGGTTGCCAGATTTAACA
IL10-fw	GGGCTTGGGGCTTCCTAACT
IL10-rev	GCTGGCCACAGCTTTCAAGA
IL12α-fw	TCAGCAACATGCTCCAGAAG

IL12α-rev	GGTAAACAGGCCTCCACTGT
IFN-α4-fw	CCCACAGCCTGGGTAATAGGA
IFN-α4-rev	CAGCAGATGAGTCCTCTGTGC
IFN-β-fw	TGCTCTCCTGTTGTGCTTCTC
IFN-β-rev	CAAGCCTCCCATTCAATTGCC
IFN-γ-fw	TTCCAAGCCCACCACAACTG
IFN-γ-rev	GTGACTCTTCCAAGGCGTCC
IFN-λ1-fw	TTCCAAGCCCACCACAACTG
IFN-λ1-rev	GTGACTCTTCCAAGGCGTCC
TNF-α-fw	GGCGTGGAGCTGAGAGATAAC
TNF-α-rev	GGTGTGGGTGAGGAGCACAT

2. Role of lipids in the biogenesis of *Coxiella*-containing vacuoles

Among cellular targets for intracellular bacteria, host lipids and their metabolism are manipulated to establish infection (Hilbi, 2006; Pizarro-Cerdá *et al.*, 2015). The recent demonstration that *C. burnetii* uses the effector protein CvpB to modulate PI(3)P metabolism for an optimal development of CCVs (Martinez *et al.*, 2016), prompted us to further investigate the role of lipids upon *C. burnetii* infections. To this aim, this part of the PhD project is articulated in two tasks. The first aims at defining the lipid signature of CCVs at different stages of infection and will be carried out using an mCherry-tagged catalogue of lipid-binding probes in infected cells. The second task aims at the identification and caracterisation of *C. burnetii* lipid-binding effector proteins (LIEs). To this aim, *C. burnetii* lysates are incubated with agarose beads coated with specific lipids to pull-down candidate LIEs prior to their caracterisation.

2.1 *C. burnetii* actively re-routes PI(3)P, PI(4)P and LBPA at CCVs

To determine the lipid composition of CCVs, we established a library of well-characterised lipid-binding probes (**Table 12, Figure 25**) and cloned them into mCherry- or RFP-expressing vectors.

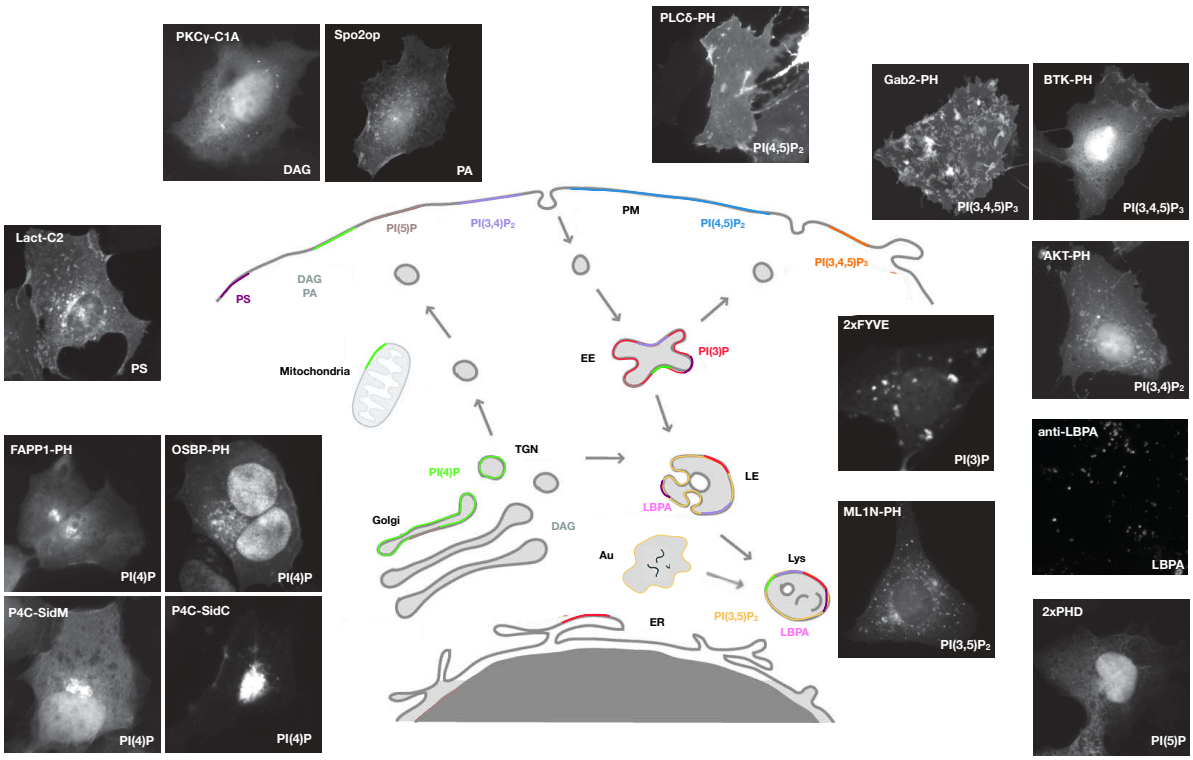

Figure 25. Subcellular distribution of lipids visualised by fluorescent lipid probes. Schematic diagram of the intracellular distribution of lipids in cellular membranes using lipid-binding probes or antibodies, illustrated by representative images of cells either transfected or labelled. (Scale bars, 10 µm.) PI(3)P, highlighted in red. PI(4)P, highlighted in green. PI(5)P, highlighted in brown. $PI(3,4)P_2$, highlighted in light purple. $PI(3,5)P_2$, highlighted in yellow. $PI(4,5)P_2$, highlighted in blue. $PI(3,4,5)P_3$, highlighted in orange. Diacylglycerol (DAG) and phosphatidic acid (PA), highlighted in gray. Lysobisphosphatidic acid (LBPA), highlighted in pink. Phosphatidylserine (PS), highlighted in dark purple. PM : plasma membrane; EE: early endosome; LE : late endosome; Lys : lysosome; Au : autophagosome; TGN : trans-golgi network; ER : endoplasmic reticulum.

Probe	Lipid	Predicted	Observed
2xFYVE	PI(3)P	EE, ER	spots/vesicles
OSBP-PH	PI(4)P	Golgi, PM, endosomes, lysosomes, mitochondria, peroxisomes	Golgi
FAPP1-PH	PI(4)P	Golgi, PM, endosomes, lysosomes, mitochondria, peroxisomes	Golgi
P4M-SidM (*L. pneumophila*)	PI(4)P	Golgi, PM, endosomes, lysosomes, mitochondria, peroxisomes	Golgi/PM
P4C-SidC (*L. pneumophila*)	PI(4)P	Golgi, PM, endosomes, lysosomes, mitochondria, peroxisomes	Golgi/PM
2xPHD	PI(5)P	Nucleus, PM, endosomes	Nucleus/cytoplasm
Akt-PH	$PI(3,4)P_2$/ $PI(3,4,5)P_3$	Membrane ruffles, endosomes, lysosomes	PM/ruffles/vesicles
ML1N-PH	$PI(3,5)P_2$	LE/Lysosomes	spots/PM
2xPLCδ-PH	$PI(4,5)P_2$	PM inner	PM
BTK-PH	$PI(3,4,5)P_3$	Membrane ruffles	cytoplasm/PM/ruffles
Gab2-PH	$PI(3,4,5)P_3$	Membrane ruffles	PM/ruffles
Lact-C2	PS	PM inner, endosomes, lysosomes	PM/vesicles
PKCγ-C1A	DAG	Golgi, PM, phagosomes	spots
PABD-Raf1	PA	PM	PM/cytoplasm
Spo1op / Spo2op	PA	PM	PM/cytoplasm
Filipin	Cholesterol	PM, endosomes	PM
anti-LBPA	LBPA	LE / Lysosomes	LE / Lysosomes

Table 12. Library of lipid-binding probes used in this study

These were used to monitor lipid localisation by automated confocal live cell imaging in U2OS cells infected with GFP-tagged WT *C. burnetii* over 2, 4 and 6 days. Due to the lack of specific probes, the localisation of LBPA was monitored in fixed cells using an anti-LBPA antibody. The accumulation of each monitored lipid at CCVs was visually scored from an

average of 100 cells per condition (**Figure 26A**). As expected, CCV membranes were labelled by PI(3,5)P_2 and PS, which are typical markers of late endosomes/lysosomes (Yeung *et al.*, 2009; Ebner *et al.*, 2019) (**Figure 26A** and **B**). Furthermore, PI(3)P was enriched at CCV membranes at all time points of infection (**Figure 26A** and **B**), confirming our previous observations (Martinez *et al.*, 2016). Interestingly, CCVs were also enriched in PI(4)P and LBPA (**Figure 26A** and **B**), which are typical lipids of the secretory pathway and multivesicular bodies, respectively.

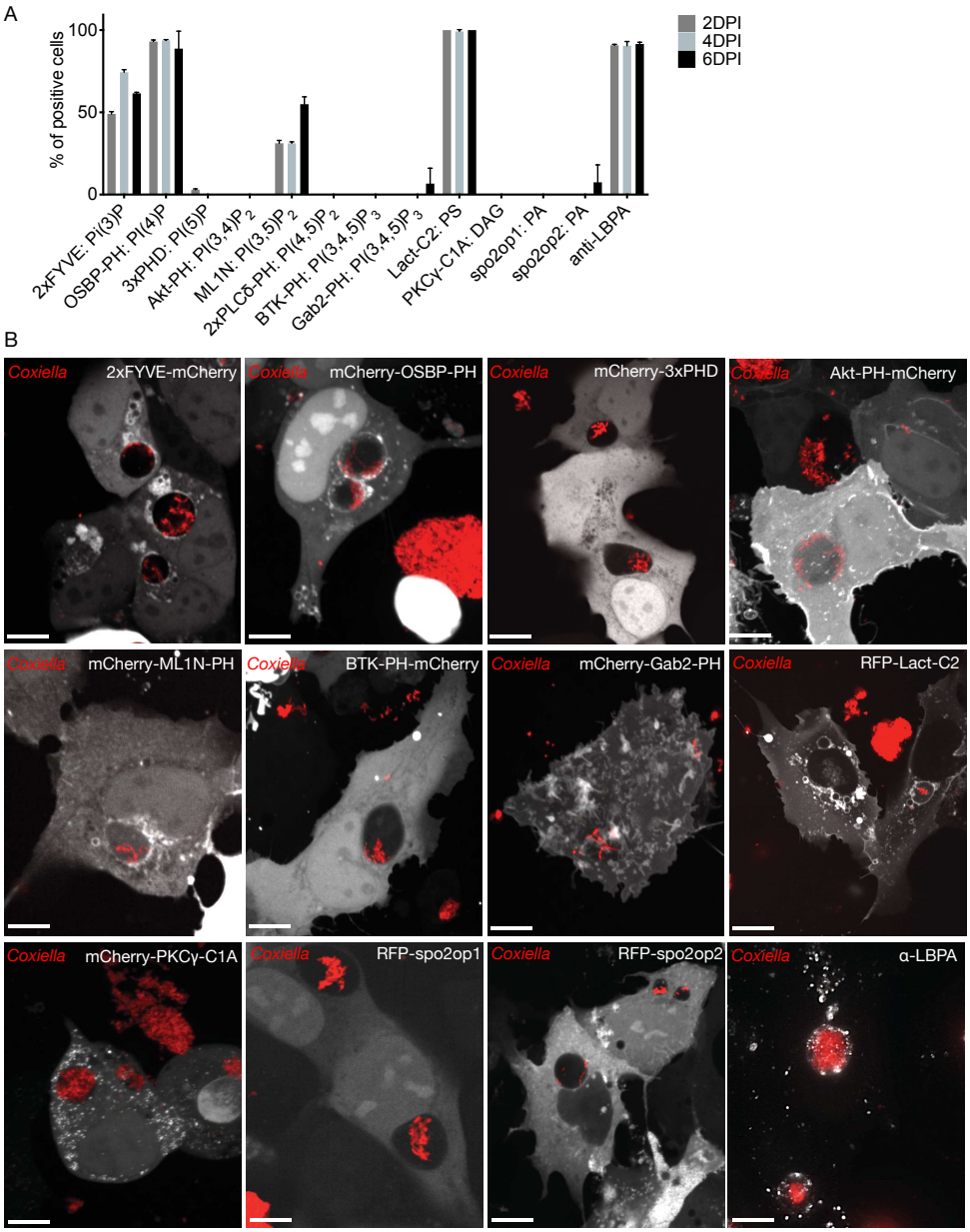

Figure 26. Caracterisation of the lipid signature of CCVs at different stages of infection. (A-B) U2OS cells were infected with *C. burnetii* WT GFP (red) and transiently transfected with an mCherry/RFP-tagged catalogue of lipid-binding probes (white). The percentage of lipid-positive CCV was calculated at 2, 4 and 6 days post-infection (dpi) revealing the presence of PI(3)P, PI(4)P, PI(3,5)P_2, PS and LBPA at WT CCVs. (Scale bars, 10 µm).

To determine whether *C. burnetii* actively controls lipid trafficking by means of effector proteins, we assessed the localisation of $PI(3,5)P_2$, PS, PI(3)P, PI(4)P and LBPA in cells infected with the Dot/Icm defective *dotA*::Tn mutant for 4 days. As expected, $PI(3,5)P_2$ and PS were still enriched at vacuoles containing the *dotA*::Tn mutant, whereas PI(3)P, whose recruitment depends on the translocation of the effector protein CvpB (Martinez *et al.*, 2016) was absent (**Figure 27**). Interestingly, both PI(4)P and LBPA were absent from vacuoles containing the *dotA*::Tn mutant (**Figure 27**), indicating that their recruitment to CCV membranes is Dot/Icm-dependent.

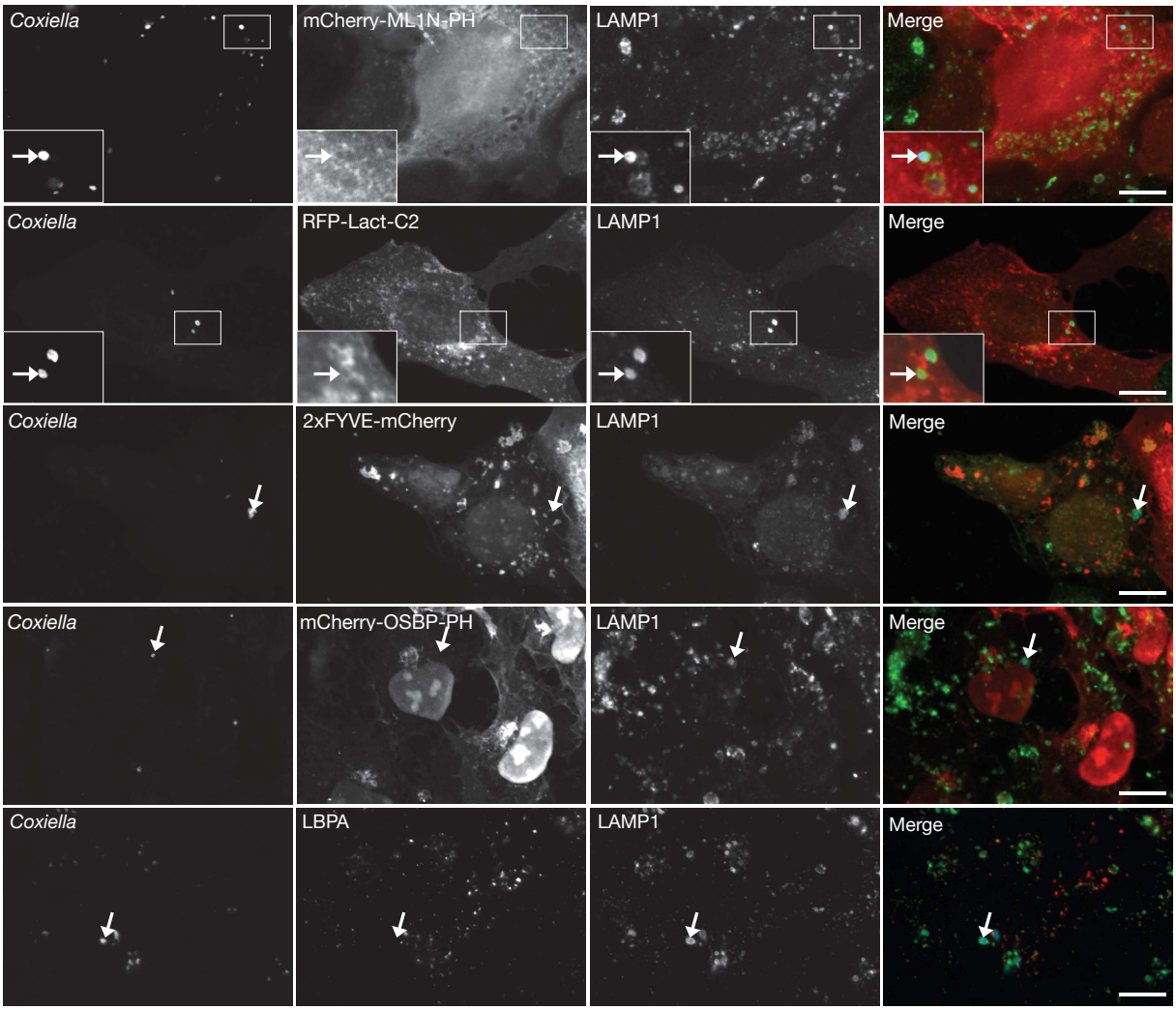

Figure 27. PI(3)P, PI(4)P and LBPA are actively recruited on CCVs. U2OS cells were challenged for 4 days with the Dot/Icm defective *dotA*::Tn mutant (blue) and transfected with either mCherry-ML1N-PH, RFP-Lact-C2, 2xFYVE-mCherry, mCherry-OSBP-PH or labelled with an anti-LBPA antibody (red). Cells were fixed and stained with an anti-LAMP1 antibody (green). White arrows indicate *C. burnetii* colonies. (Scale bars, 10 µm).

2.2 *C. burnetii* re-routes the Golgi pools of PI(4)P at CCV membranes

The unexpected enrichment of PI(4)P on CCV membranes prompted us to determine whether *C. burnetii* re-routes the secretory pathway to the CCV. The most abundant pools of PI(4)P appear to be at the Golgi apparatus and the plasma membrane (D'Angelo *et al.*, 2008). To test whether the PI(4)P detected at CCVs originates from the Golgi-associated pool, we used a mutant of the PI-4 phosphatase Sac1 (Sac1-K2A), which is retained at the Golgi apparatus where it constitutively dephosphorylates PI(4)P, without affecting other PI pools (Rohde *et al.*, 2003). U2OS cells were co-transfected with plasmids encoding the PI(4)P probe mCherry-OSBP-PH either in combination with either GFP alone or GFP-Sac1-K2A. 12 h post transfection, cells were infected with the *C. burnetii* NMII strain for 48 h prior to fixation. Non-infected U2OS cells were used as controls and labelled with an anti-GM130 antibody to visualise the Golgi apparatus and validate the depletion of the Golgi-associated PI(4)P pool. mCherry-OSBP-PH was found at the Golgi apparatus in GFP-expressing cells (**Figure 28A**), whereas in cells expressing GFP-Sac1-K2A, mCherry-OSBP-PH was diffuse in the cytoplasm (**Figure 28B**). As previously observed, PI(4)P was enriched at CCV membranes labelled by an anti-LAMP1 antibody in infected U2OS cells expressing GFP alone (**Figure 28C**). Interestingly, PI(4)P was absent from CCVs in cells expressing GFP-Sac1-K2A (**Figure 28D**), suggesting that indeed, the PI(4)P observed at CCVs originates from the Golgi complex. Moreover, the size of CCVs was smaller in cells depleted of PI(4)P, as compared to cells expressing GFP alone (**Figure 28D**), indicating that PI(4)P is important in early steps of CCV biogenesis to generate a large replicative compartment.

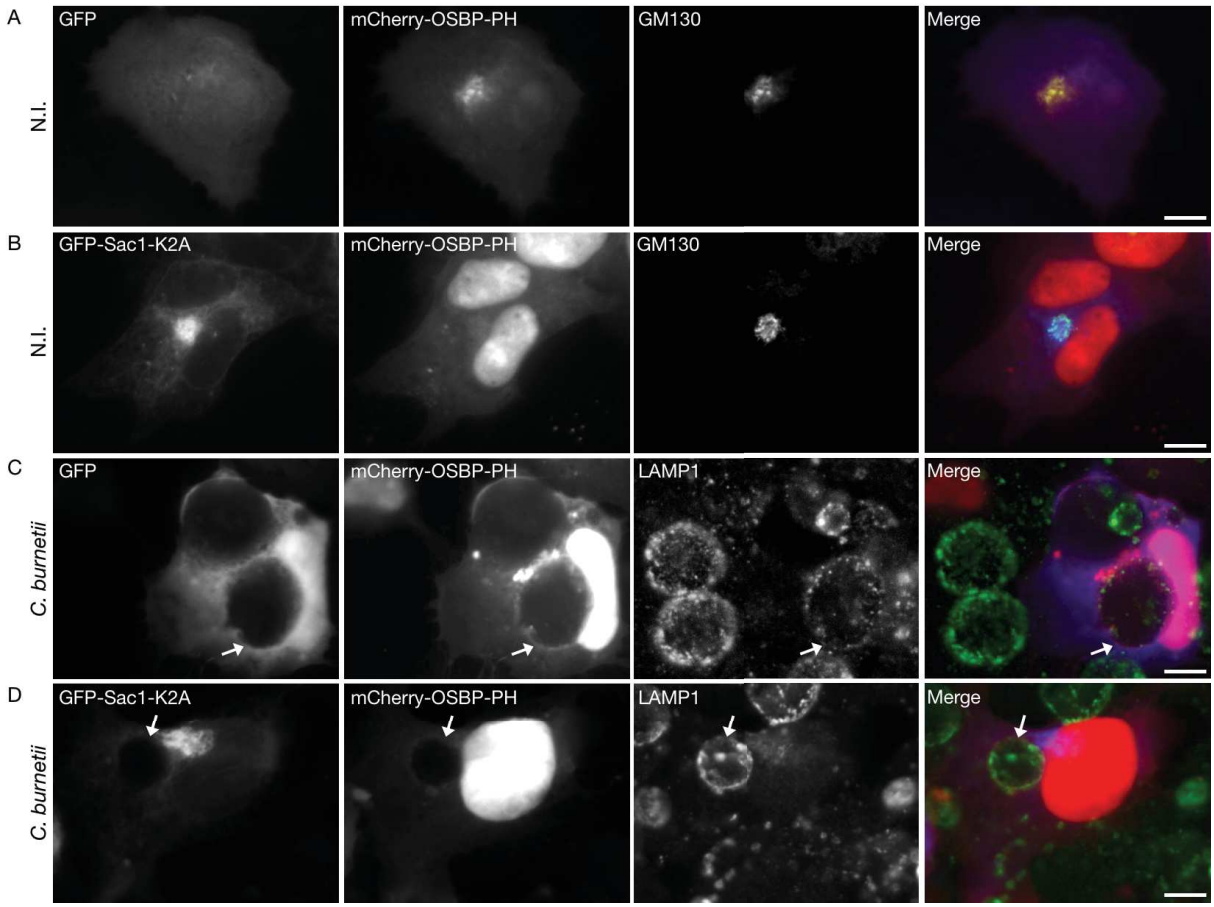

Figure 28. Golgi pools of PI(4)P are involved in PI(4)P incoming at CCV membranes. U2OS cells were transfected either with GFP alone (A) or GFP-Sac1-K2A (B) (blue) in combination with the PI(4)P probe mCherry-OSBP-PH (red). Cells were fixed cells 24 h post-transfection and stained with an anti-GM130 (green). (C) U2OS cells infected with *C. burnetii* NMII were transfected with mCherry-OSBP-PH (red) either in combination with GFP alone (C) or GFP-Sac1-K2A (D) (blue). Two days post infection, cells were fixed and labelled with an anti-LAMP1 (green). White arrows indicate CCVs. (Scale bars, 10 µm).

2.3 Identification of *C. burnetii* candidate lipid-binding effectors

We recently reported that PI(3)P is specifically recognised and recruited on CCVs by the Dot/Icm substrate CvpB (Martinez *et al.*, 2016). To investigate the possibility that additional lipid-binding proteins are translocated by *C. burnetii* during infection, we performed pulldown assays using lysates of *C. burnetii* NMII strain, incubated with a panel of 20 agarose beads coated with individual lipids. Following SDS-PAGE electrophoresis, eluates were silver stained revealing a number of candidate lipid-binding proteins (**Figure 29**): a PS-binding candidate (~140 kDa), an LBPA-binding candidate (~30kDa), two PI-binding candidates (~130 kDa and ~80 kDa) a PI(4)P-binding candidate (~50 kDa), 2 sphingosine-binding candidates (~100 kDa and ~30 kDa), and a cholesterol-binding candidate (~40 kDa) (**Figure 29**).

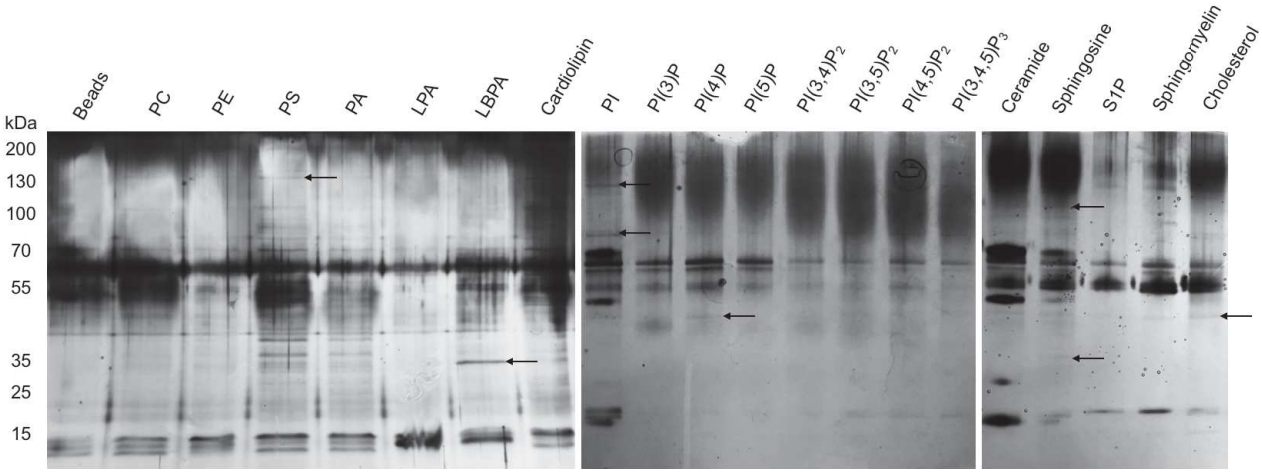

Figure 29. Identification of *C. burnetii* candidate lipid-binding effectors. Lipid-pulldown assay was carried out by incubating *Coxiella* lysates with a panel of lipid-coated beads. Eluates were analysed by silver staining to identify candidate lipid-binding effectors.

Unfortunately, the identification of these proteins by mass spectrometry was unsuccessful. Regardless, we carried out a bioinformatics analysis by cross-referencing the apparent molecular mass (± 10%) of proteins eluted from lipid-coated beads with the predicted molecular mass of *C. burnetii* hypothetical proteins. This allowed the identification of 67 protein-coding genes (**Table 13**), 5 of which were retained for further analysis based on literature analysis, the prediction of effector proteins using the S4TE algorithm (Noroy *et al.*, 2019) and the presence of putative lipid-related features identified using Protein Homology/analogy Recognition Engine V 2.0 (Phyre2), RaptorX (**Table 14**). Among these, *cbu0635* is a PI(4)P-binding candidate, previously shown to be translocated during infections, localise to the Golgi apparatus and interfere with the secretory pathway (Carey *et al.*, 2011).

Importantly, bioinformatics analysis revealed that *cbu0635* encodes a candidate PH and a candidate C2 domain (**Table 14**). *cbu1576* is a PI/PS-binding candidate encoding a putative PH domain (**Table 14**). *cbu1639* and *cbu686* are LBPA/sphingosine-binding and PI/PS-binding candidates, respectively, and are predicted as lipid binding proteins (**Table 14**). *cbu2007* is a LBPA/sphingosine-binding candidate that encodes for a putative F-BAR domain and is related to the *Legionella* effector SidF, a PI 3-phosphatase that hydrolyses PI(3,4)P_2 and PI(3,4,5)P_3 (Hsu *et al.*, 2012) (**Table 14**).

CDS	Gene	Molecular weight (kDa)	S4TE Score	Product	Predicted lipid-binding	Tn mutants in library	Secretion (*L. pneumophila*)	Localisation
CBU_0038		36.408	30	3-oxoacyl-ACP synthase	LBPA / Sphingosine	*Tn454*	N/A	N/A
CBU_0096	*cls*	43.512	29	Cardiolipin synthetase	LBPA / Sphingosine	*Tn80*	N/A	N/A
CBU_0119		50.949	91	Hypothetical protein	PI(4)P	*Tn392*	N/A	N/A
CBU_0184		42.957	47	Hypothetical protein	LBPA / Sphingosine	*Tn2862*	N/A	N/A
CBU_0193		44.844	49	Hypothetical protein	LBPA / Sphingosine	*Tn1548*	N/A	N/A
CBU_0295		54.39	136	Tetratricopeptide repeat-containing protein	PI(4)P	*Tn512*	Yes (Carey et al. 2011)	Cytoplasmic
CBU_0388		154.623	206	Hypothetical protein	PS	*Tn1589*	Yes (Weber et al. 2013)	Nuclear
CBU_0425	*cirB*	50.616	178	Hypothetical protein	PI(4)P	*Tn505*	Yes (Carey et al. 2011; Weber et al. 2013)	Cytoplasmic
CBU_0489		38.295	23	Phospholipase A1	LBPA / Sphingosine		N/A	N/A
CBU_0492		38.184	10	Glycerol-3-phosphate acyltransferase PlsX	LBPA / Sphingosine		N/A	N/A
CBU_0498		41.181	17	Hypothetical protein	LBPA / Sphingosine	*Tn1966*	N/A	N/A
CBU_0507		38.517	46	Hypothetical protein	LBPA / Sphingosine	*Tn928*	N/A	N/A
CBU_0530		43.29	56	Tetratricopeptide repeat-containing protein	LBPA / Sphingosine	*Tn1674*	N/A	N/A
CBU_0534		44.289	22	Hypothetical protein	LBPA / Sphingosine	*Tn2142*	N/A	N/A
CBU_0560		45.621	29	Hypothetical protein	LBPA / Sphingosine	*Tn225*	N/A	N/A
CBU_0609		37.851	36	Mevalonate kinase	LBPA / Sphingosine		N/A	N/A
CBU_0611		89.244	55	Hypothetical protein	PI / PS		N/A	N/A
CBU_0635		55.167	22	Hypothetical protein	PI(4)P	*Tn1898*	Yes (Carey et al. 2011)	Golgi apparatus / Vesicles
CBU_0685		123.543	71	Hypothetical protein	PI / Sphingosine / PS		N/A	N/A
CBU_0695		50.949	29	Hypothetical protein	PI(4)P		N/A	N/A
CBU_0698		43.29	17	Hypothetical protein	LBPA / Sphingosine	*Tn1690*	N/A	N/A
CBU_0781	*ankG*	37.629	131	Ankyrin repeat-containing protein	LBPA / Sphingosine		Yes (Pan et al. 2008)	N/A
CBU_0782		51.393	32	Hypothetical protein	PI(4)P		N/A	N/A
CBU_0786		43.401	17	CoA-transferase III protein	LBPA / Sphingosine	*Tn1913*	N/A	N/A
CBU_0794		51.615	210	Hypothetical protein	PI(4)P		Yes (Weber et al. 2013)	Nuclear
CBU_0837		54.945	55	Hypothetical protein	PI(4)P		N/A	N/A
CBU_0874		39.183	37	Chorismate synthase	LBPA / Sphingosine		N/A	N/A
CBU_0880		51.282	49	Hypothetical protein	PI(4)P		N/A	N/A
CBU_0885		43.179	164	Hypothetical protein	LBPA / Sphingosine		Yes (Weber et al. 2013)	Cytoplasmic
CBU_0914		41.292	N/A	Hypothetical protein	LBPA / Sphingosine	*Tn528*	N/A	N/A
CBU_0920		41.292	37	Fatty acid desaturase	LBPA / Sphingosine	*Tn992*	N/A	N/A
CBU_0923		41.847	111	Hypothetical protein	LBPA / Sphingosine	*Tn458*	N/A	N/A
CBU_0937	*cirC*	53.724	111	Hypothetical protein	PI(4)P	*Tn694*	Yes (Weber et al. 2013)	Cytoplasmic
CBU_0970		39.072	42	Hypothetical protein	LBPA / Sphingosine		N/A	N/A
CBU_0973		43.068	29	Isovaleryl-CoA dehydrogenase	LBPA / Sphingosine		N/A	N/A
CBU_0974		43.845	10	Acetyl-CoA acetyltransferase	LBPA / Sphingosine	*Tn1459*	N/A	N/A
CBU_1061a		40.959	20	Hypothetical protein	LBPA / Sphingosine		N/A	N/A
CBU_1063		52.059	180	Hypothetical protein	PI(4)P		N/A	N/A
CBU_1136	*enhC*	115.995	171	Tetratricopeptide repeat-containing protein	PI / Sphingosine / PS		N/A	N/A
CBU_1178		41.958	79	Hypothetical protein	LBPA / Sphingosine	*Tn1073*	N/A	N/A
CBU_1194		53.169	17	Hypothetical protein	PI(4)P	*Tn153*	N/A	N/A
CBU_1219		41.403	20	Hypothetical protein	LBPA / Sphingosine		N/A	N/A
CBU_1266		35.076	22	Lipoyl synthase	LBPA / Sphingosine		N/A	N/A
CBU_1292		51.726	154	Ankyrin repeat-containing protein	PI(4)P	*Tn943*	N/A	N/A
CBU_1311		90.354	17	Hypothetical protein	PI / PS	*Tn731*	N/A	N/A
CBU_1334		41.958	29	Hypothetical protein	LBPA / Sphingosine	*Tn2025*	N/A	N/A
CBU_1468		128.094	25	Hypothetical protein	PI / Sphingosine / PS		N/A	N/A
CBU_1510		35.187	17	Acetyl-CoA carboxylase carboxyltransferase subunit alpha	LBPA / Sphingosine		N/A	N/A
CBU_1576		93.24	149	Hypothetical protein	PI / PS		Yes (Weber et al. 2013)	Endoplasmic reticulum
CBU_1636		43.512	180	Hypothetical protein	LBPA / Sphingosine	*Tn2767*	Yes (Weber et al. 2013)	Nuclear
CBU_1639		44.289	168	Hypothetical protein	LBPA / Sphingosine	*Tn1226*	Yes (Weber et al. 2013)	Cytoplasmic
CBU_1658		40.182	17	Hypothetical protein	LBPA / Sphingosine		N/A	N/A

CBU_1686		85.914	173	Hypothetical protein	PI / PS		N/A	N/A
CBU_1701		52.059	20	Hypothetical protein	PI(4)P	*Tn1462*	N/A	N/A
CBU_1735		42.402	13	Hypothetical protein	LBPA / Sphingosine	*Tn687*	N/A	N/A
CBU_1741		44.067	17	Lipoprotein	LBPA / Sphingosine	*Tn538*	N/A	N/A
CBU_1752		45.843	10	Hypothetical protein	LBPA / Sphingosine	*Tn84*	N/A	N/A
CBU_1782		44.955	10	Phosphoglycerate kinase	LBPA / Sphingosine		N/A	N/A
CBU_1818		53.502	29	Hypothetical protein	PI(4)P	*Tn2670*	N/A	N/A
CBU_1819		41.958	29	Hypothetical protein	LBPA / Sphingosine		N/A	N/A
CBU_1823		38.85	191	Hypothetical protein	LBPA / Sphingosine		Yes (Carey et al. 2011)	Cytoplasmic
CBU_1831		53.613	17	Hypothetical protein	PI(4)P		N/A	N/A
CBU_1852		51.615	29	Hypothetical protein	PI(4)P		N/A	N/A
CBU_2007		43.956	233	Hypothetical protein	LBPA / Sphingosine	*Tn1577*	Yes (Weber et al. 2013)	Cytoplasmic
CBU_2013		40.626	131	Hypothetical protein	LBPA / Sphingosine	*Tn980*	Yes (Weber et al. 2013)	Cytoplasmic

Table 13. *C. burnetii* candidate lipid-binding effectors (LIEs)

CDS	Molecular weight (kDa)	S4TE Score	Predicted lipid-binding	Tn mutants in library	Localisation	S4TE motif/ domain	Bioinformatic screen
CBU_0635	55.167	22	PI(4)P	*Tn1898*	Golgi / Vesicles	E-block	C2 domain (12-38) PH domain (258 - 268) 6 transmembrane domains
CBU_1576	93.24	149	PI / PS		ER	PmrA ; E-block	PH domain (589 - 621)
CBU_1639	44.289	168	LBPA / Sphingosine	*Tn1226*	Cytoplasmic	PmrA ; E-block	Lipid binding protein
CBU_1686	85.914	173	PI / PS		N/A	E-block	Lipid binding protein
CBU_2007	43.956	233	LBPA / Sphingosine	*Tn1577*	Cytoplasmic	PmrA ; E-block	F-BAR domain (218-341) PI 3-phosphatase

Table 14. Selected *C. burnetii* candidate lipid-binding effectors (LIEs)

cbu0635, *cbu1576*, *cbu1639*, *cbu1686* and *cbu2007* were thus cloned into a pLVX-mCherry vector to tag proteins at their C-terminal domain and their localisation was investigated in non-infected and GFP-tagged WT *C. burnetii*-infected U2OS cells (**Figure 30**). CBU0635 localised to vesicular structures in the perinuclear area of cells, which may correspond to the Golgi apparatus, and in infected cells, the protein localised to CCVs (**Figure 30**). CBU1576 partially co-localised with the lysosomal marker LAMP1 in non-infected cells and at CCVs in infected cells (Figure 30). CBU1639 and CBU1686 were largely cytoplasmic with partial localisation at nuclear compartments in both infected and non-infected cells (**Figure 30**). CBU2007 localised at vesicles and plasma membrane in both infected and non-infected cells (**Figure 30**). Interestingly, ectopic expression of CBU2007 triggered the formation of a large LAMP1-positive compartment reminiscent of CCVs in non-infected cells (**Figure 30**).

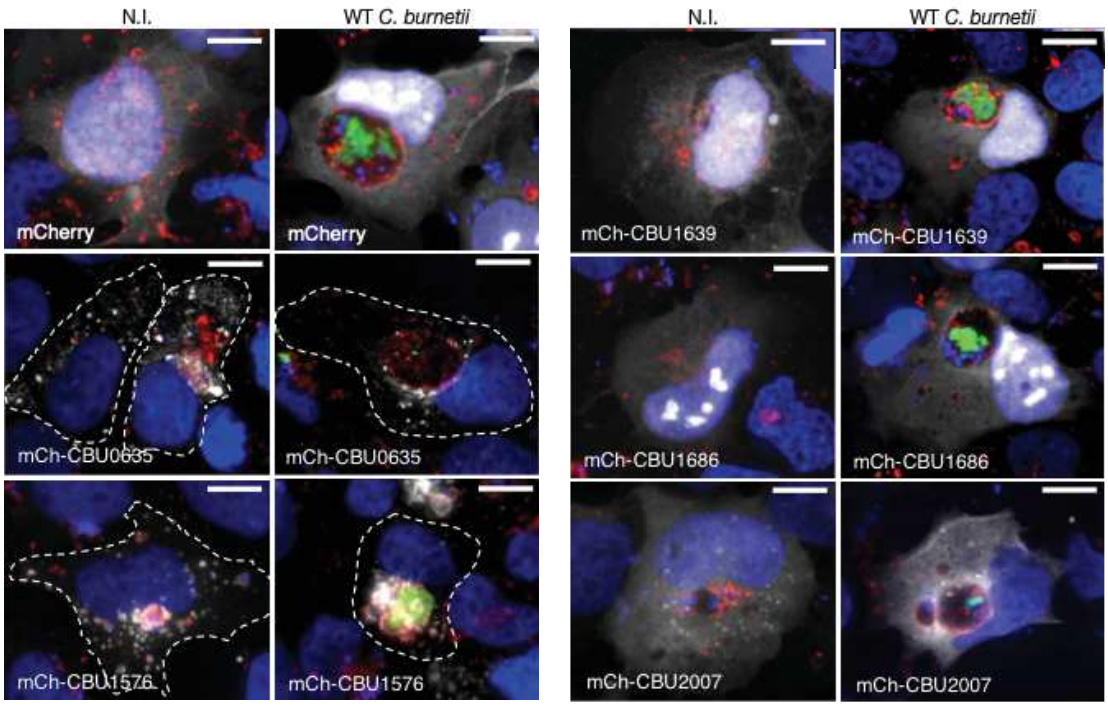

Figure 30. Intracellular localisation of selected *C. burnetii* candidate lipid-binding effectors. Non-infected or GFP-expressing *C. burnetii*-infected U2OS cells were transfected with plasmids encoding N-terminally tagged mCherry versions of the selected candidate lipid-binding proteins (**Table 13** and **14**, white). Cells were fixed 24 h after transfection and labelled with Hoechst (blue) and an anti-LAMP1 antibody (red). (Scale bars, 10 µm).

Given their original localisation which may be consistent with a potential lipid interaction, here we have focused our analysis on CBU0635, CBU1576 and CBU2007. Dot/Icm-dependent translocation of CBU0635 and CBU2007 has been previously reported using *Legionella pneumophila* as a surrogate system (Carey *et al.*, 2011; Weber *et al.*, 2013). To validate protein translocation in *C. burnetii*, CBU0635, CBU1576 and CBU2007 were cloned into the pXDC61K-BlaM vector, thus generating N-terminal fusions with β-lactamase, and transformed either into GFP-tagged *C. burnetii* (WT) or the Dot/Icm-defective *dotA*::Tn mutant strain. The expression of all β-lactamase-tagged constructs was validated by Western blot using an anti β-lactamase antibody (**Figure 31A**). Effector translocation was then assessed at 24, 48 and 72 h post-infection by means of a β-lactamase secretion assay on U2OS cells. *C. burnetii* expressing β-lactamase alone or β-lactamase-tagged CvpB (Martinez *et al.*, 2016) were used as negative and positive controls, respectively. All candidates were efficiently translocated at all time points of infection (**Figure 31B** and **C**), whereas none of the proteins were translocated by the Dot/Icm-defective mutant strain (**Figure 31B** and **C**), indicating that CBU0635, CBU1576 and CBU2007 are indeed Dot/Icm substrates. Due to the presence of corresponding transposon mutants in our library (Martinez *et al.*, 2014), we privileged the characterisation of CBU0635 and CBU2007.

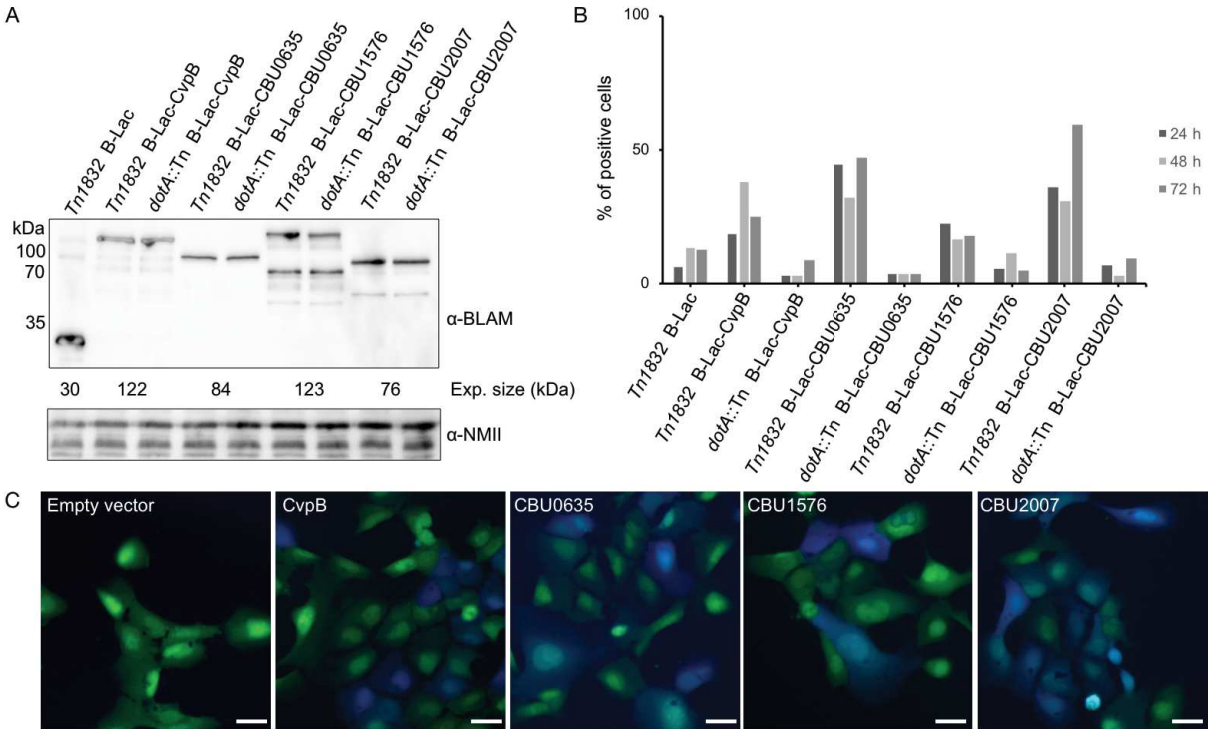

Figure 31. CBU0635, CBU1576 and CBU2007 are Dot/Icm substrates of *C. burnetii*. (A) Lysates of *C. burnetii* strains transformed with pXDC61K plasmids encoding BLAM-tagged versions of the indicated genes were analysed by Western blotting using anti-BLAM and an anti-*C. burnetii* (NMII) antibodies. The expected size of BLAM-tagged proteins is indicated below the top blot. (B) U2OS cells were challenged with *C. burnetii* strains expressing BLAM-tagged versions of candidate lipid-binding effectors for 24, 48, and 72 h. The percentage of BLAM-positive, infected cells was automatically calculated using CellProfiler over the total number of infected cells per each condition. The Dot/Icm-dependent translocation of the effectors that were efficiently secreted was validated in the dotA::Tn mutant strain at 24, 48 and 72 h postchallenge. (C) Representative images of positive (blue) cells treated as in B. (Scale bars, 10 μm).

2.3.1 Characterisation of the *C. burnetii* effector CBU0635

2.3.1.1 CBU0635 localises at the Trans-Golgi Network and targets PI(3,4)P_2 metabolism

CBU0635 was identified in our screening of *C. burnetii* effector proteins as a putative PI(4)P interactor. Bioinformatics analysis indicated that *cbu0635* is part of an operon, including *cbu0634* and *cbu0636*. It encodes a predicted a C-terminal E-Block motif, typically found in Dot/Icm effectors (Lifshitz *et al.*, 2013), 6 transmembrane domains and 2 putative lipid-binding domains (PH and C2) (**Figure 32A**). Unfortunately, we were unable to purify CBU0635 to test its direct interaction with lipids. Thus, we further investigated the potential interaction of the *C. burnetii* effector with host lipids indirectly. Intracellular localisation of CBU0635 was further investigated by cloning the gene into a pRK5-HA vector to generate HA-tagged CBU0635. HA-CBU0635 was thus expressed in U2OS cells either in combination with the PI(4)P probe GFP-OSBP-PH or a panel of antibodies and markers for intracellular compartments. In line with the previously reported localisation of CBU0635 at a perinuclear position close to the Golgi apparatus (Carey *et al.*, 2011), we observed that ectopically expressed HA-CBU0635 specifically localised at the TGN (revealed with an anti TGN46 antibody), whereas little overlap was observed with the Golgi stack marker GM130. According to the shared perinuclear localisation, partial overlap was observed between CBU0635 and PI(4)P (**Figure 32B**). Interestingly, we also observed that ectopic expression of CBU0635 led to an apparent condensation of the Golgi apparatus as compared with cells expressing HA alone (**Figure 32C** and **D**). Of note, the morphology of endosomes (**Figure 32E** and **F**), lysosomes (**Figure 32G**) and autophagosomes (**Figure 32H**) was unaffected by the ectopic expression of CBU0635, indicating that the effector protein specifically targets the Golgi apparatus.

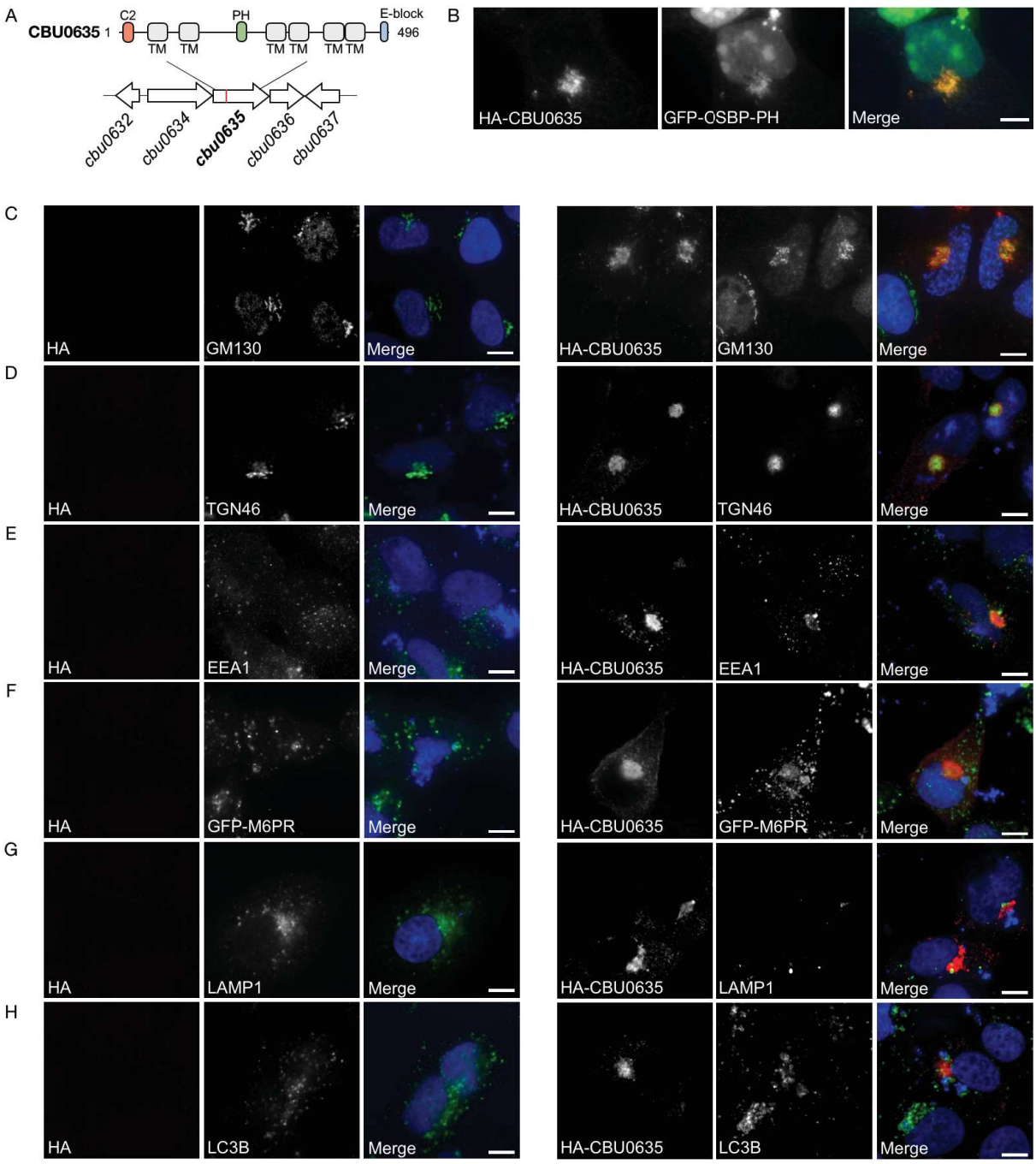

Figure 32. CBU0635 localises to PI(4)P-enriched compartment and triggers Golgi condensation. (A) Schematic representation of the CBU0635 sequence and the associated genomic context. The red bar represents the site of transposon insertion of the *cbu0635*::Tn mutant (*Tn1898*). CBU0635 contains putative C2 (orange) and PH (green) lipid-binding domains, 6 transmembrane domains (grey) and a putative E-block motif (blue). (B) U2OS cells were transfected with HA-CBU0635 (red) in combination with the PI(4)P probe GFP-OSBP-PH and labeled with Hoechst (blue). U2OS cells (C–H) were transfected either with HA alone (left panels) or HA-CBU0635 (right panels) in combination with GFP-M6PR (F). We fixed cells 24 h post-transfection and labelled with Hoechst (blue) and an anti-HA (red) in combination with either anti-GM130 (C), anti-TGN46 (D), anti-EEA1 (E), anti-LAMP1 (G) or anti-LC3B (H). (Scale bars, 10 µm).

To determine whether CBU0635 may use PI(4)P to localise at the TGN, we depleted the Golgi pool of PI(4)P by means of the Sac1-K2A mutant in cells expressing HA alone or HA-CBU0635. U2OS cells expressing the PI(4)P probe mCherry-OSBP-PH were used as control of the PI(4)P depletion. As previously described, expression of Sac1-K2A resulted in the complete loss of PI(4)P at the Golgi apparatus (**Figure 33A**). Despite the depletion of PI(4)P, the Golgi apparatus remained intact labelled with an anti-TGN46 antibody (**Figure 33A** and **B**). Regardless, CBU0635 was still observed at the TGN (**Figure 33C**), suggesting that CBU0635 targeting may depend on the interaction with Golgi-resident proteins or other lipids.

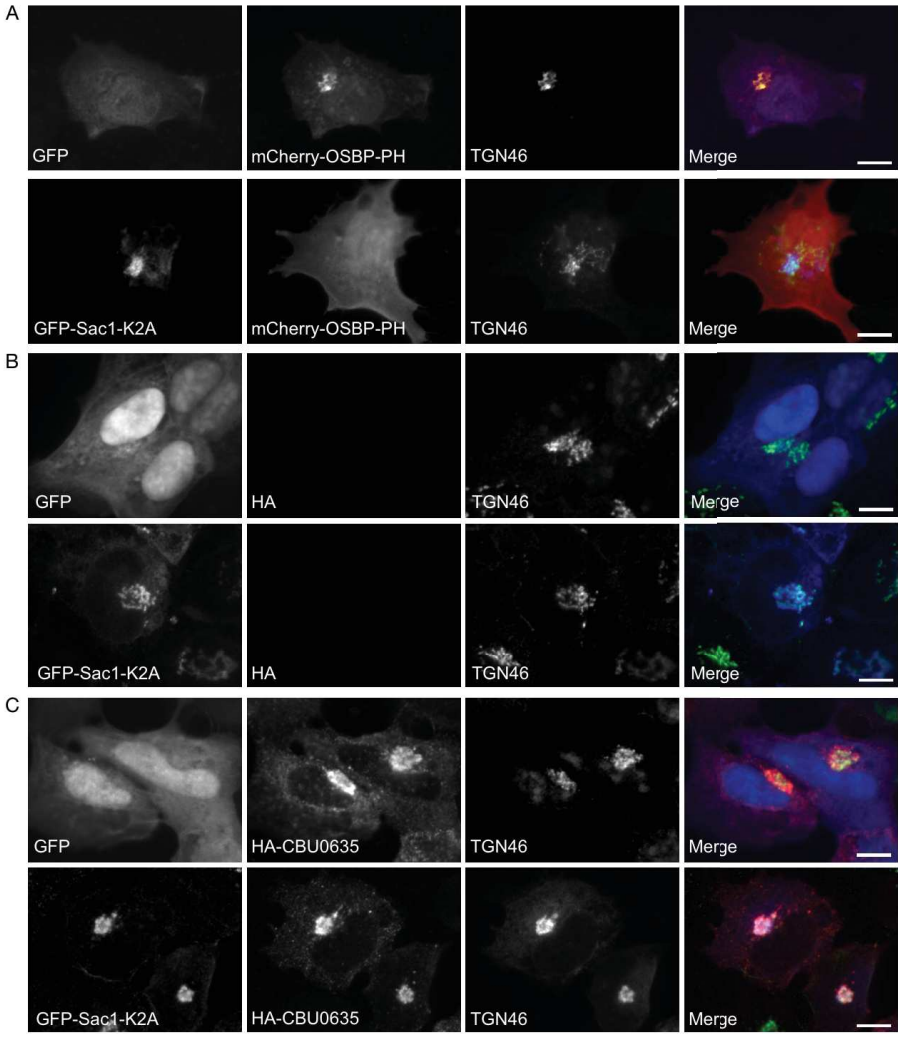

Figure 33. Absence of PI(4)P does not modify CBU0635 localisation. (A) U2OS cells were transfected with either GFP alone (top panels) or GFP-Sac1-K2A (bottom panels) (blue) in combination with the PI(4)P probe mCherry-OSBP-PH (red). We fixed cells 24 h post-transfection and stained with an anti-TGN46 (green). (B) U2OS cells were transfected with pRK5-HA in combination with either GFP alone (top panels) or GFP-Sac1-K2A (bottom panels) (blue) in combination with the PI(4)P probe mCherry-OSBP-PH (red). We fixed cells 24 h post-transfection and stained with an anti-TGN46 (green). (C) U2OS cells were transfected with pRK5-HA in combination with either GFP alone (top panels) or GFP-Sac1-K2A (bottom panels) (blue) in combination with the PI(4)P probe mCherry-OSBP-PH (red). We fixed cells 24 h post-transfection and stained with an anti-TGN46 (green). (Scale bars, 10 μm).

To assess the functionality of the predicted lipid-binding domains of CBU0635, we carried out a mutational analysis of the effector protein. U2OS cells were transfected with HA-tagged versions of CBU0635 deletions and we assessed the localisation of the bacterial effector fragments with respect to the Trans-Golgi marker TGN46. As previously observed, full length CBU0635 ($CBU0635_{FL}$) localised to the TGN (**Figure 34A**). The ectopic expression of a N-terminal domain alone, which includes both the predicted C2 and PH domains ($CBU0635_{1-313}$), was sufficient for TGN targeting (**Figure 34B**). We thus further dissected the N-terminal domain by generating deletion mutants expressing either the C2 domain ($CBU0635_{1-61}$) or the PH domain ($CBU0635_{138-313}$) alone. The C2 domain failed to localise at cellular membranes and remained diffuse in the cytoplasm (**Figure 34C**), suggesting that this putative lipid-binding domain is not functional. Interestingly, the PH domain-containing mutant $CBU0635_{138-313}$ lost its TGN localisation, however, the truncated protein remained associated with vesicles (**Figure 34D**) suggesting that the region containing the putative PH domain is relevant for CBU0635 localisation/function.

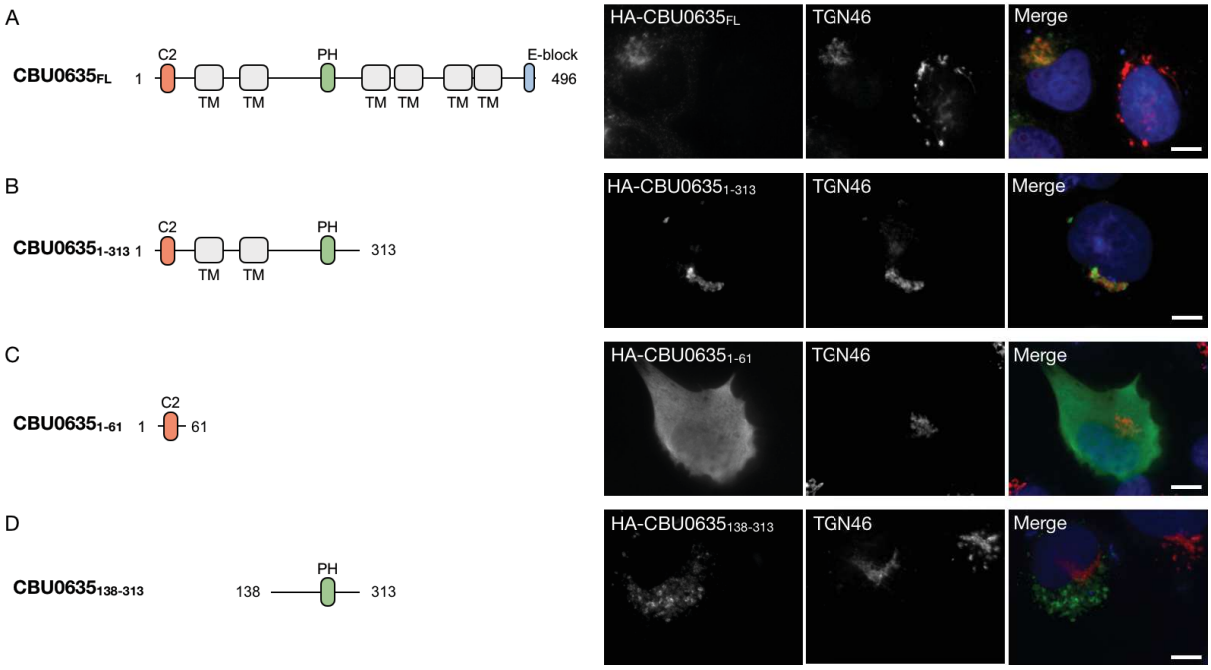

Figure 34. The putative PH domain of CBU0635 is functionally important. (A) U2OS cells were transfected with plasmids encoding HA-tagged versions of either full-length (A) or the indicated deletion mutants (B-D) of HA-tagged CBU0635. We fixed cells 24 h post-transfection and labelled with Hoechst (blue) and anti-TGN46 antibody (red, right). (Scale bars, 10 µm).

Given that PH domains from different proteins recognise multiple lipids (including PI(4)P) (Pemberton and Balla, 2019), the nature of CBU0635$_{138\text{-}313}$-labeled vesicles was further investigated by ectopically expressing the HA-tagged truncated protein in combination with a selection of GFP-tagged lipid-binding probes that localise to intracellular compartments. HA-CBU0635$_{138\text{-}313}$ partially co-localised with the PI(3,4)P_2 probe Akt-PH-GFP (**Figure 35**).

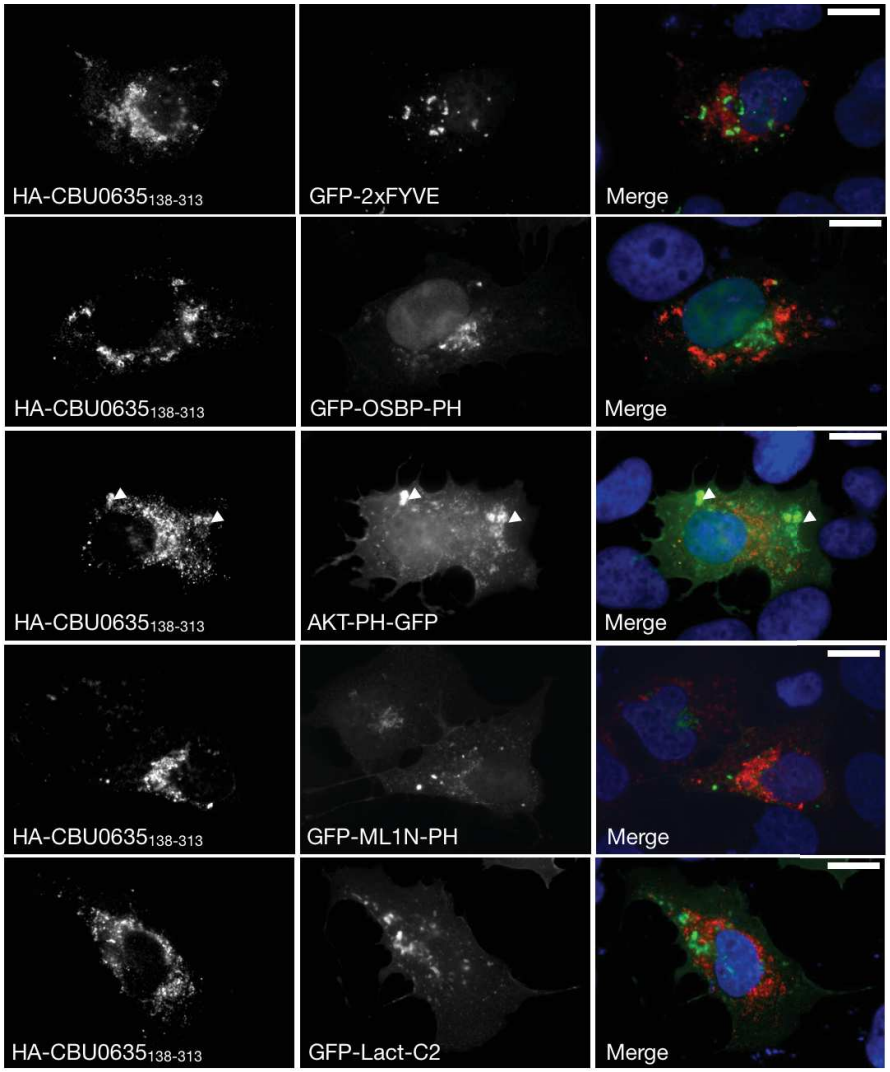

Figure 35. CBU0635$_{138\text{-}313}$ localises to PI(3,4)P_2-positive vesicles. U2OS cells were transfected with HA-CBU0635$_{138\text{-}313}$ in combination with either GFP-2xFYVE, GFP-OSBP-PH, AKT-PH-GFP, GFP-ML1N-GFP or GFP-Lact-C2. We fixed cells 24 h post-transfection and labelled with Hoechst (blue) and an anti-HA (red). White arrows indicate regions where CBU0635$_{138\text{-}313}$ and PI(3,4)P_2-positive vesicles localise. (Scale bars, 10 µm).

Interestingly, CBU0635$_{138-313}$ expression also triggered an increase in the size of PI(3,4)P_2-positive compartments compared with cells expressing the HA tag alone (**Figure 36**). More importantly, ectopic expression of HA-CBU0635$_{FL}$ led to the complete disappearance of PI(3,4)P_2-positive vesicles from transfected cells (**Figure 36**), suggesting that CBU0635 may act as a PI-phosphatase.

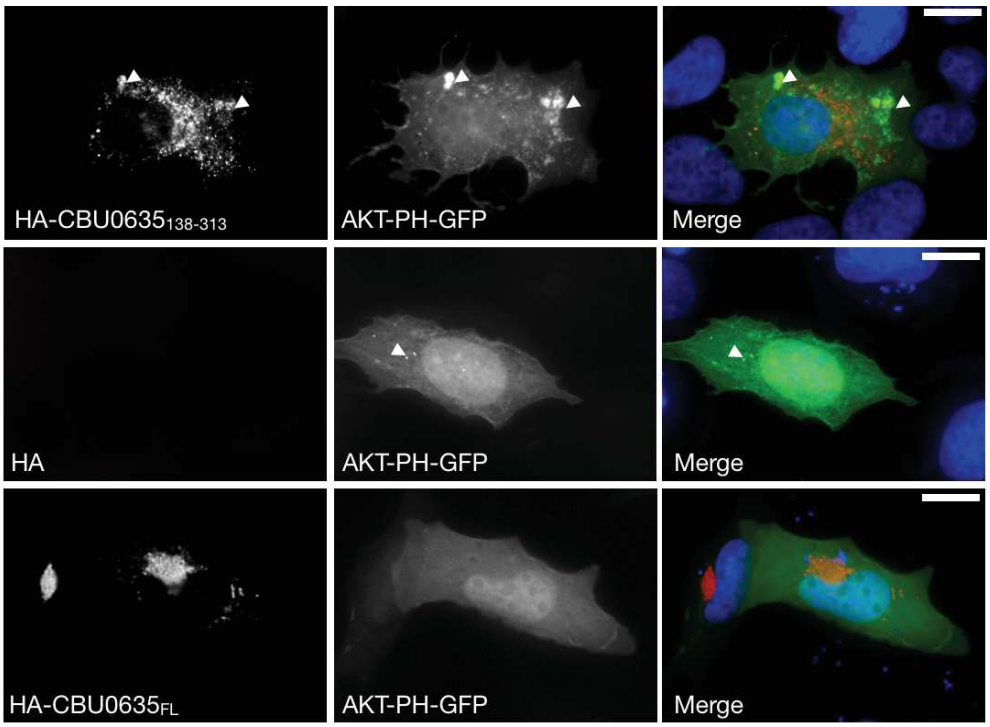

Figure 36. CBU0635 targets PI(3,4)P_2 metabolism. U2OS cells were transfected with either HA alone (top panels) or HA-CBU0635 (bottom panels) in combination with AKT-PH-GFP. We fixed cells 24 h post-transfection and stained with Hoescht (blue). White arrows indicate PI(3,4)P_2-positive vesicles. (Scale bars, 10 µm).

2.3.1.2 CBU0635 is a putative PI phosphatase

To further investigate a putative catalytic activity of CBU0635, we searched its aminoacidic sequence for CX_5R motifs, a signature sequence of the catalytic residues in PI phosphatases (Norris *et al.*, 1998). Indeed, bioinformatics analysis revealed the presence of a putative CX_5R motif (CVFACHR, aa 133-139) upstream of the putative PH lipid-binding domain (**Figure 37A**). We thus generated cysteine and arginine mutants of this motif to validate its functionality. HA, HA-CBU0635, HA-CBU0635$_{C133A}$ or HA-CBU0635$_{R139A}$ were thus ectopically expressed in U2OS cells in combination with the PI(3,4)P2 probe AKT-PH-GFP. As previously observed, ectopic expression of wt CBU0635 completely depleted PI(3,4)P_2-positive structures as compared to cells expressing the HA tag alone (**Figure 37B**). Interestingly, a significant number of PI(3,4)P2-positive vesicles remained visible in the cytoplasm of cells expressing

either the C133A or the R139A mutant (**Figure 37B**), suggesting that indeed, the CX_5R motif in CBU0635 may be functional and that the effector protein might regulate intracellular levels of $PI(3,4)P_2$. Further biochemical assays are required to determine whether CBU0635 can catalyse the dephosphorylation of $PI(3,4)P_2$ to either PI(4)P or PI(3)P.

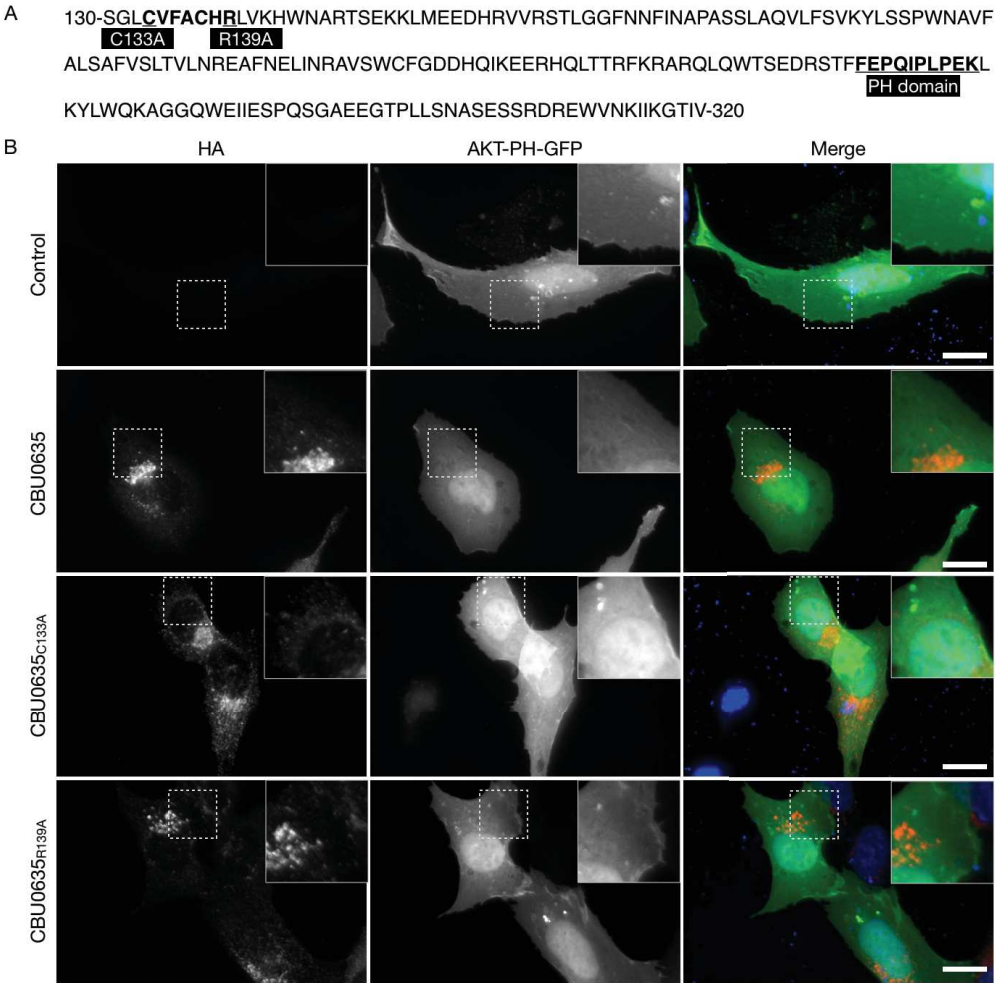

Figure 37. CBU0635 is a putative PI phosphatase. (A) Schematic representation of CBU0635 domain comprising amino acids 130 to 320. Putative PH lipid-binding domain and catalytic residue CX_5R are in bold and mutated residues are underlined. U2OS cells were transfected with the $PI(3,4)P_2$ probe AKT-PH-GFP in combination either HA alone, HA-CBU0635, HA-$CBU0635_{C133A}$ or HA-$CBU0635_{R139A}$ (red). Cells were fixed 24 h post-transfection and stained with Hoechst (blue). Inset shows the presence or not of $PI(3,4)P_2$-positive vesicles. (Scale bars, 10 µm).

2.3.1.3 CBU0635 is important for CCV biogenesis

To determine whether CBU0365 is involved in CCV biogenesis, we infected U2OS or PMA-treated THP-1 with a transposon insertion mutant in *cbu0635* (*Tn1898*), which was previously isolated in our laboratory (Martinez *et al.*, 2014). Southern blot analysis confirmed

the presence of a single transposon insertion in the genome of the mutant strain (**Figure 38A**). Cells were challenged either with GFP-tagged *C. burnetii* (WT) or the CBU0635 mutant *Tn1898* (hereafter referred to as *cbu0635*::Tn) for 6 days, fixed and labelled with an anti-LAMP1 antibody to visualise CCVs. Cells infected with WT *C. burnetii* displayed a large and unique LAMP1-positive vacuole (**Figure 38B** and **C**, top panels), whereas cells infected with the *cbu0635*::Tn mutant strain formed smaller CCVs in both cell types (**Figure 38B** and **C**, bottom panels), suggesting a potential role of CBU0635 in CCV biogenesis. Complementation of the *cbu0635*::Tn strain is in progress either by expressing *cbu0635* alone or the full *cbu0634-cbu0635-cbu0636* operon under the control of the endogenous promoter.

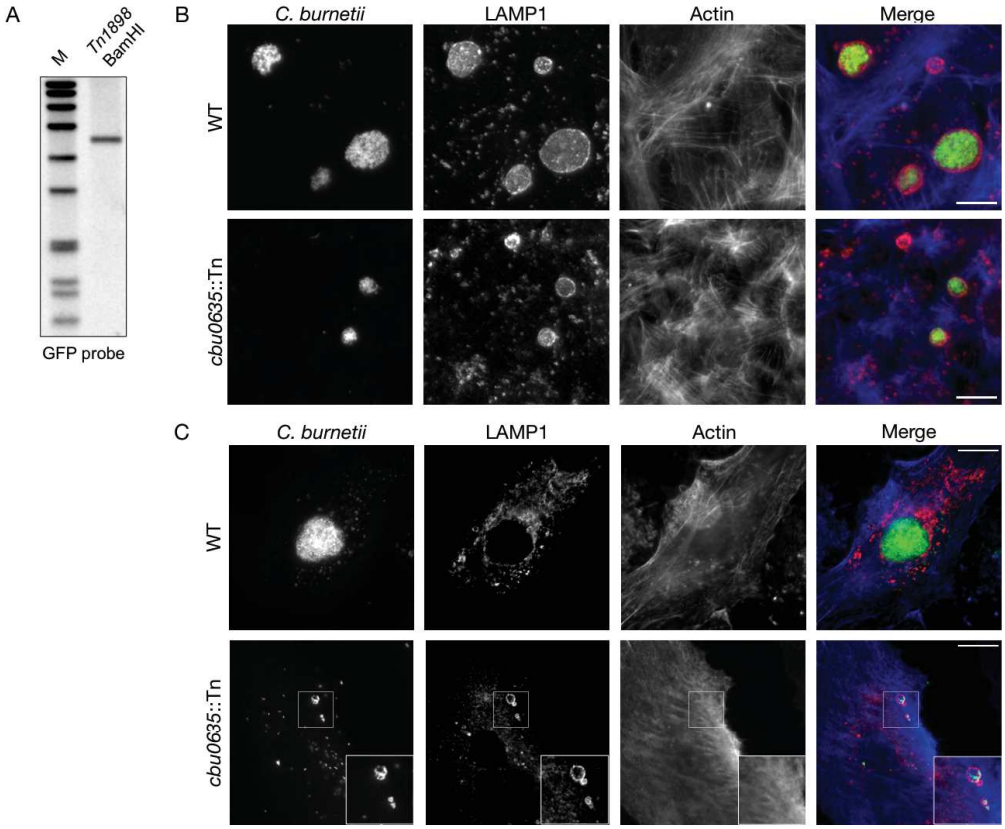

Figure 38. CBU0635 is a Dot/Icm T4BSS effector protein required for CCV biogenesis. (A) *cbu0635*::Tn mutant *Tn1898* genomic DNA was digested with the restriction enzyme BamHI (*Tn1898* BamHI), prior to migration on agarose gel and Southern blot analysis using a fluorescent GFP probe. The unique band observed confirms the unique insertion of the transposon in *cbu0635*. U2OS (B) or PMA-treated THP-1 (C) cells were infected with either *C. burnetii* WT GFP (top panels) or *cbu0635*::Tn (bottom panels) strains. Six days post-infection, cells were fixed and stained with anti-LAMP1 (red) and phalloidin (blue). (Scale bars, 10 µm).

Finally, we investigated a possible correlation between the putative PI phosphatase activity of CBU0635 and its role in CCV biogenesis by monitoring the localisation of PI(3,4)P_2 at CCVs generated by WT *C. burnetii* or the *cbu0635*::Tn mutant strain. In agreement with

what we have previously observed, CCVs generated by WT bacteria were negative for $PI(3,4)P_2$, and positive for PI(3)P and PI(4)P. However, the overall lipid composition remain unaltered for CCVs generated by the *cbu0635*::Tn mutant strain (**Figure 39A**, **B** and **C**).

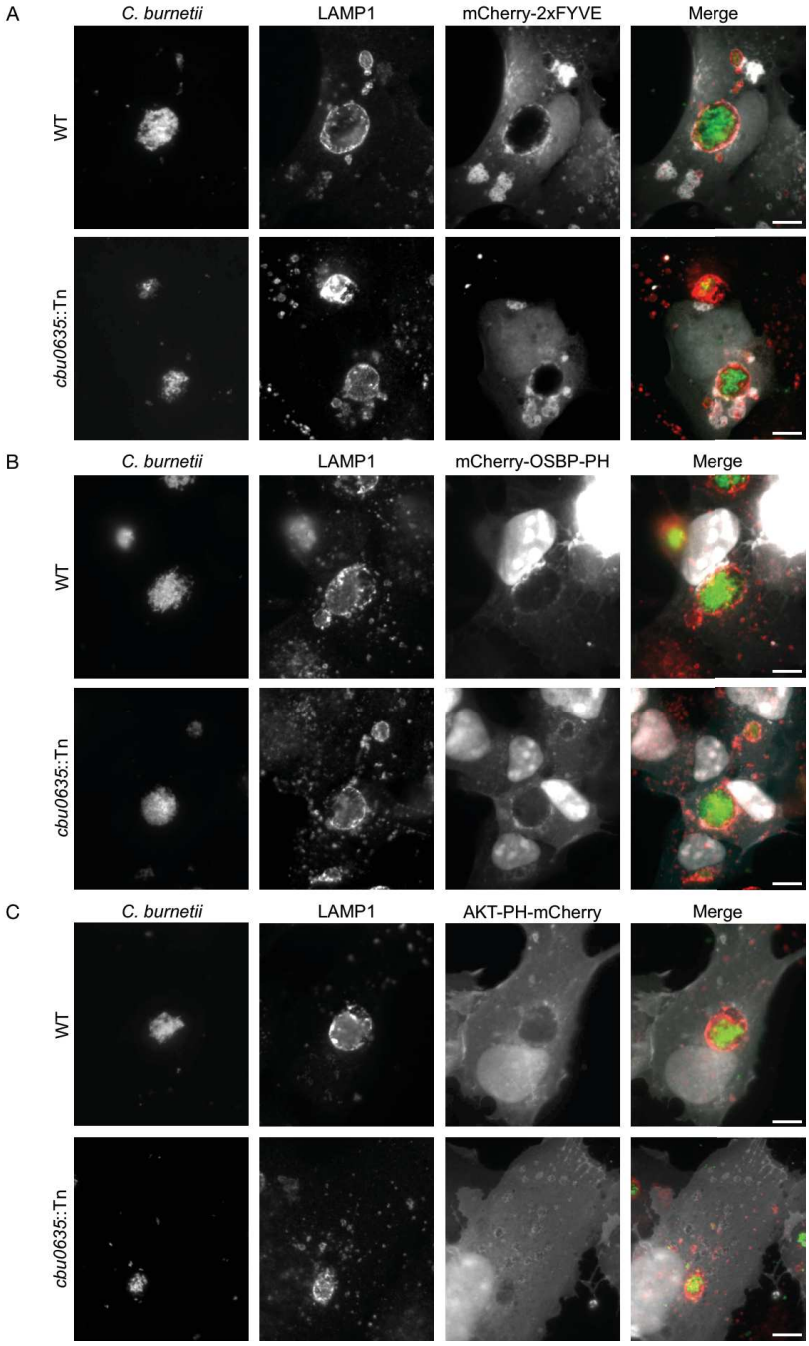

Figure 39. CBU0635 does not participate in the recruitment of PI(3)P, PI(4)P or $PI(3,4)P_2$ to CCVs. U2OS cells were infected with either *C. burnetii* WT GFP (top panels) or *cbu0635*::Tn (bottom panels) and transfected with either mCherry-2xFYVE (A), mCherry-OSBP-PH (B) or AKT-PH-mCherry (C) for 3 d. We fixed cells 24 h post-transfection and labelled with an anti-LAMP1 (pseudo-colored gray). (Scale bars, 10 µm).

2.3.2 Characterisation of the *C. burnetii* effector CBU2007

2.3.2.1 CBU2007 recruits LBPA on CCVs and is important for their biogenesis

CBU2007 was identified in our screening of *C. burnetii* effector proteins as a putative LBPA interactor. Bioinformatics analysis indicated that *cbu2007* is part of a PmrA-regulated operon together with *cbu2006*, *cbu2005* and *cbu2004*. It also encodes a putative C-terminal E-Block (Lifshitz *et al.*, 2013) (**Figure 40A**) and a putative F-BAR domain, a lipid-binding domain that induces and senses membrane curvature (Qualmann *et al.*, 2011) (**Figure 40A**). Given that LBPA is actively recruited at CCVs during infection, we investigated the possibility that CBU2007 is involved in this process. A transposon mutant in *cbu2007* (*Tn1577*) was previously isolated from our *C. burnetii* mutant library and recent Southern blot analysis validated the presence of a single transposon insertion in the genome of *Tn1577* (**Figure 40B**).

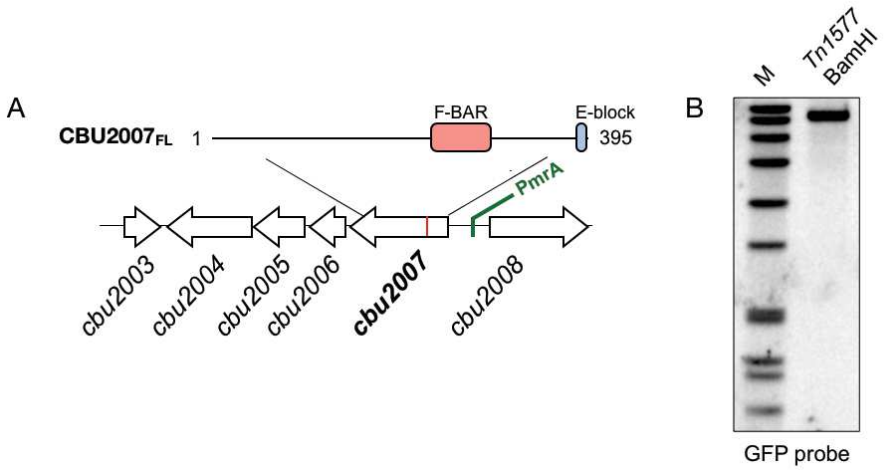

Figure 40. Genomic context of *cbu2007* and Southern blot analysis of *cbu2007*::Tn mutant strain. (A) Schematic representation of the CBU2007 sequence and the associated genomic context. The red bar represents the site of transposon insertion of an independently isolated mutant (*Tn1577*). The predicted PmrA sequence is indicated in green. CBU2007 contains a putative F-BAR lipid-binding domain (pink) and a putative E-block motif (blue). (B) *cbu2007*::Tn mutant *Tn1577* genomic DNA was digested with the restriction enzyme BamHI (*Tn1577* BamHI) prior to migration on agarose gel and Southern blot analysis using a fluorescent GFP probe. The unique band observed confirms the unique insertion of the transposon in *cbu2007*.

U2OS cells were thus challenged either with GFP-tagged *C. burnetii* (WT), the CBU2007 mutant *Tn1577* (hereafter referred to as *cbu2007*::Tn) or the *dotA*::Tn mutant for 6 days, fixed, and immuno-labelled with anti-LAMP1 and anti-LBPA antibodies to visualise CCVs and LBPA, respectively. In all conditions, LAMP1 and LBPA largely co-localised at vesicles in the cytoplasm of both infected and non-infected cells. LAMP1 decorated the whole external

membrane of CCVs harbouring WT bacteria as well as vesicles inside its lumen. In these conditions, LBPA co-localised with LAMP1 within isolated domains at the vacuole membrane. Interestingly however, a large number of LBPA-positive but LAMP1-negative vesicles were also observed in the lumen of the CCVs (**Figure 41A**). LAMP1 labelling of CCVs generated by the *cbu2007*::Tn mutant revealed highly convoluted membranes with protrusions extending both inside the lumen of the vacuole and projecting out of the external membrane (**Figure 41B**). Interestingly, LBPA was largely absent from these vacuoles. Finally, LAMP1 labelled vacuoles containing *dotA*::Tn mutants as expected. LBPA was also present within these vacuoles but remained segregated in a separate sub-compartment (**Figure 41C**). These results indicate that CBU2007 is involved in the biogenesis of CCV and in the recruitment of LBPA at these compartments.

Complementation of the *cbu2007*::Tn strain is in progress either by expressing *cbu2007* alone or the full *cbu2007-cbu2006-cbu2005-cbu2004* operon under the control of the endogenous PmrA promoter.

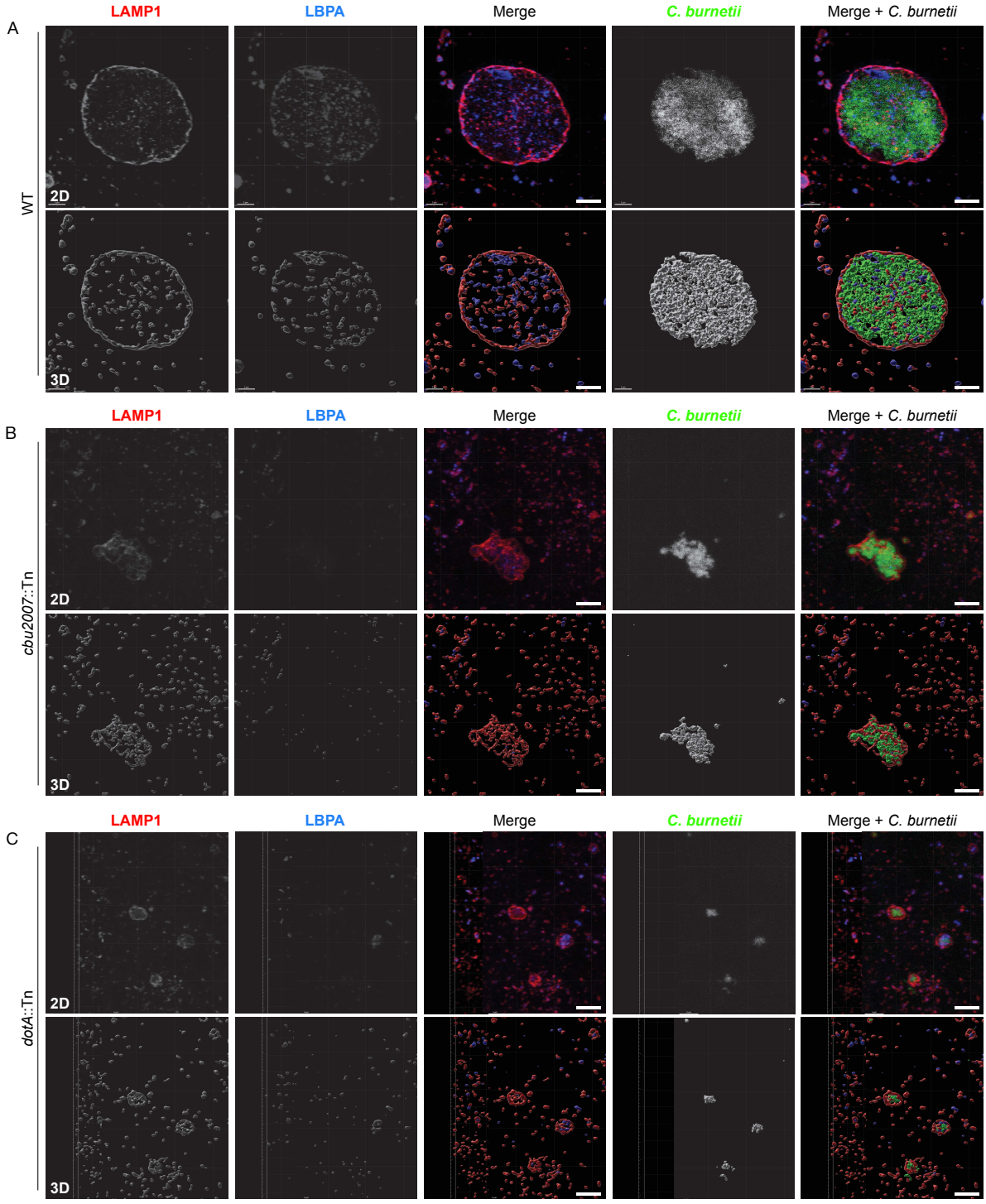

Figure 41. CBU2007 participates in LBPA recruitment to CCVs. (A-C) Representative 2D (top panels) and 3D (bottom panels) image reconstruction of confocal sections illustrating surface rendering of LAMP1 (red) and LBPA (blue) surrounding *C. burnetii* WT GFP (A), *cbu2007*::Tn (B) or *dotA*::Tn (C) colonies (green) in U2OS cells infected for 6 days. (Scale bars, 10 µm).

2.3.2.2 CBU2007 is a lipid-binding protein that manipulates lipid metabolism

Recombinant His-tagged CBU2007 was successfully obtained in collaboration with the Architecture et Fonction des Macromolécules Biologiques (AFMB) platform in Marseille (France), and was used to investigate the lipid-binding properties of CBU2007. PIP Strips were overlayed with recombinant His-CBU2007 and labelled with an anti-His antibody, revealing and interaction of His-CBU2007 with PS and, to a lesser extent, with monophosphorylated PIs [with a preferential binding to PI(3)P and PI(5)P] (**Figure 42**). Unfortunately, commercially available PIP Strips do not include LBPA, therefore, specific assays are currently being developed in our laboratory.

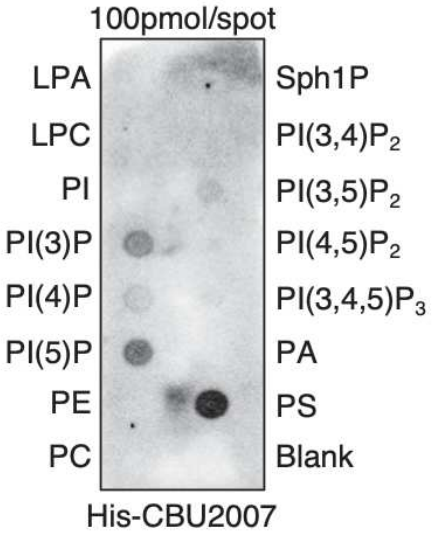

Figure 42. CBU2007 mainly interacts with PS. Representative protein/lipid overlay assays performed by incubating His-CBU2007 with PIP Strips spotted with 100 pmol lipid/spot.

The localisation of CBU2007 was further investigated by cloning the gene into a pRK5-HA vector to generate HA-tagged CBU2007 and ectopically express the effector protein in U2OS cells. First, PIP Strips experiments were validated by co-transfecting U2OS cells with HA-tagged CBU2007 in combination with lipid-binding probes of interest. Alternatively, HA-CBU2007 expressing cells were fixed and labelled with an anti-LBPA antibody to further investigate their putative interaction. As mentioned earlier, ectopic expression of CBU2007 in non-infected cells results in the appearance of a large, LAMP1-positive compartment, that is highly reminiscent of CCVs. This compartment was negative for the PI(3)P probe GFP-2xFYVE (**Figure 43A**), the PI(4)P probe GFP-OSBP-PH (**Figure 43B**) and the PI(5)P probe GFP-PHD2X (**Figure 43C**). Regardless, ectopic expression of CBU2007 seemed to trigger clustering and enlargement of PI(3)P-positive vesicles (**Figure 43A**). On the contrary,

CBU2007-induced vacuoles were positive for the PS probe GFP-Lact-C2 and LBPA (**Figure 43D** and **E**). In addition, CBU2007 expression triggered a significant increase in the size of LBPA-positive vesicles compared with cells expressing HA alone (**Figure 43E**), possibly correlating with our previous observations of LBPA enrichment to the CCV membrane in a CBU2007-dependent manner.

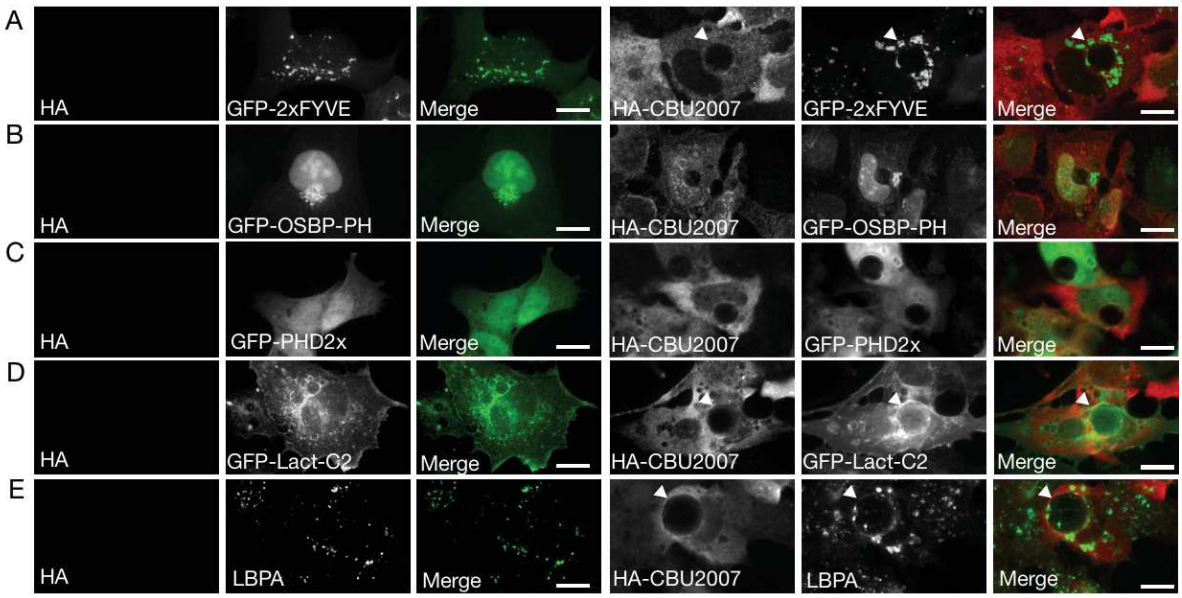

Figure 43. CBU2007 alters PI(3)P- and LBPA-positive vesicles size and clustering. U2OS cells (A–E) were transfected either with HA alone (left panels) or HA-CBU2007 (right panels) in combination with either GFP-2xFYVE (A), GFP-OSBP-PH (B), GFP-PHD2x (C) GFP-Lact-C2 (D) or labelled with an anti-LBPA antibody (E). We fixed cells 24 h post-transfection and labelled with an anti-HA (red). (Scale bars, 10 µm).

Next, we aimed at determining the role of the putative lipid-binding domain in CBU2007 by generating HA-tagged deletion mutants of CBU2007 to exclude ($CBU2007_{1-213}$; **Figure 44A**) or include the putative F-BAR domain ($CBU2007_{214-395}$; **Figure 44B**). U2OS cells were transfected with HA-tagged versions of CBU2007 deletions to assess 1) the localisation of the bacterial effector fragments 2) the formation of CBU2007-induced vacuoles and 3) the intracellular localisation of the lipid-binding probes GFP-2xFYVE, GFP-Lact-C2 and LBPA. CBU2007 deletions failed to trigger the formation of the large vacuole observed in cells expressing full length CBU2007 (**Figure 44A** and **B**), suggesting that, even if functional, the putative F-BAR domain requires the N-terminal part of the protein to exert its function. Similarly, the size of PI(3)P-, LBPA- or PS-positive compartments was unaltered by the ectopic expression of either deletion mutant. However, we observed a clustered perinuclear localisation of LBPA- and PS- positive vesicles in presence of $CBU2007_{214-395}$ (**Figure 44B**),

suggesting that in the context of infection, the putative F-BAR domain may play a role in the re-routing of endo/lysosomal vesicles to the CCV.

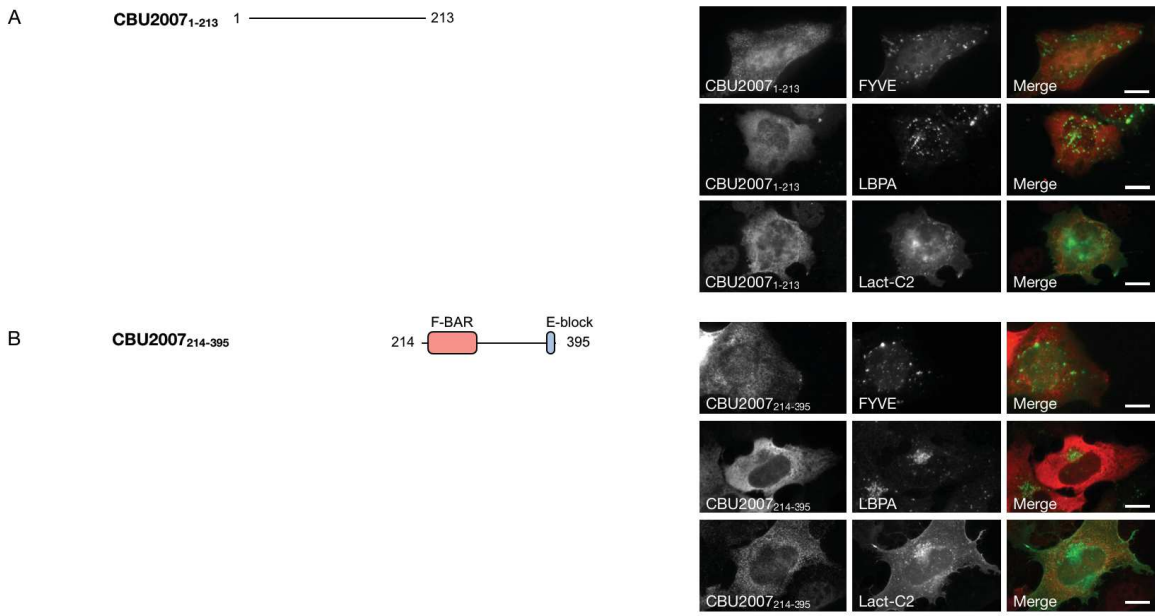

Figure 44. CBU2007$_{214-395}$ is sufficient to trigger PI(3)P- and LBPA-positive vesicles clustering. U2OS cells were transfected with plasmids encoding HA-tagged versions of the indicated deletion mutants (A and B) of HA-tagged CBU2007 (red) in combination with either GFP-2xFYVE or GFP-Lact-C2 or labelled with an anti-LBPA antibody (green). (Scale bars, 10 µm).

2.3.2.3 CBU2007 recruits the ESCRT machinery to the CCV

The ESCRT-III-associated protein ALIX is the only reported interactor of LBPA (Matsuo *et al.*, 2004). Interestingly, It has been previously reported that *C. burnetii* infections induce reversible ESCRT recruitment to the CCV (Radulovic *et al.*, 2018). We thus investigated whether CBU2007 interacts with the ESCRT machinery. U2OS cells were transfected either with plasmids encoding the HA tag alone or HA-CBU2007, in combination with plasmids encoding markers of the ESCRT machinery such as GFP-TSG101, GFP-VPS4A and FLAG-CHMP4B, or labeled by an anti-ALIX antibody. ALIX was efficiently recruited to CBU2007-induced vacuoles (**Figure 45A**), whereas the localisation of TSG101, CHMP4B and VPS4A remained largely unaffected (**Figure 45B**, **C** and **D**). These findings suggest that CBU2007-induced vacuoles may derive from MVBs.

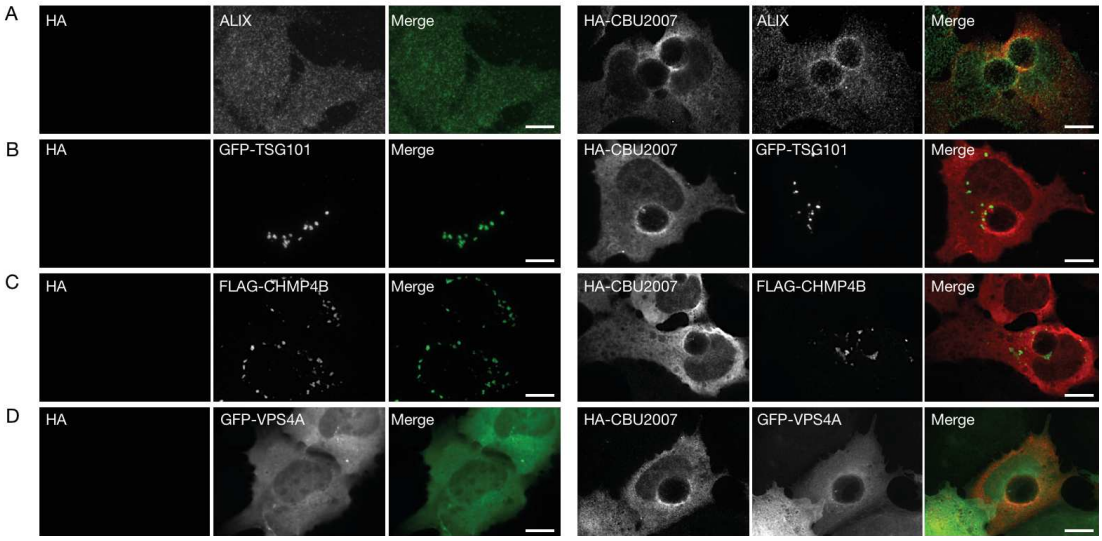

Figure 45. CBU2007 recruits the ESCRT machinery. U2OS cells (A-D) were transfected with either HA alone (left panels) or HA-CBU2007 (right panels) in combination with either GFP-TSG101 (B), FLAG-CHMP4B (C) or GFP-VPS4A (D) or labelled with an anti-ALIX (A) (green). We fixed cells 24 h post-transfection and labelled with anti-HA (red). (Scale bars, 10 µm).

Given the important role of VPS4A in MVB biogenesis, we were interested in determining whether the catalytic activity of VPS4A was important for the activity of CBU2007. U2OS cells we co-transfected either with plasmids encoding the HA tag alone or HA-CBU2007 in combination with plasmids encoding two inactive forms of VPS4A : GFP-VPS4A^{K178Q} and GFP-VPS4A^{E225Q}, which are unable to bind or hydrolyse ATP, respectively (Bishop and Woodman, 2000). Co-expression of either mutants with HA-CBU2007 did not affect the formation of the CBU2007-induced vacuole (**Figure 46**). However, membrane targeting of GFP-VPS4A^{K178Q} was reduced in cells expressing HA-CBU2007 as compared to cells expressing the HA tag alone (**Figure 46**), suggesting that CBU2007 may block VPS4A membrane binding and thus ATPase activity to inhibit fission events involved in MVB biogenesis.

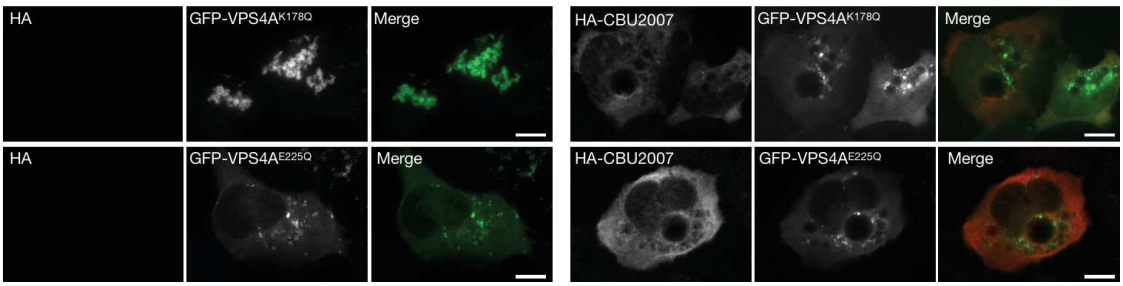

Figure 46. CBU2007 inhibits VPS4A membrane binding. U2OS cells were transiently transfected with either HA alone (left panels) or HA-CBU2007 (right panels) (red) in combination with GFP-VPS4A^{K178Q} or GFP-VPS4A^{E225Q}. We fixed cells 24 h post-transfection and labelled with anti-HA (red). (Scale bars, 10 µm).

To determine whether CBU2007 preferentially interacts with MVBs destined to degradation or recycling, U2OS cells were transfected with HA-tagged CBU2007 and the presence of intracellular markers at CBU2007-induced vacuoles was assessed. Vacuoles were negative for the autophagy marker LC3B (**Figure 47A**) and the early endosomal marker RAB5 (**Figure 47B**). On the contrary, CBU2007-induced compartments were positive for the late endosomal/MVB markers RAB7 (**Figure 47C**) and CD63 (**Figure 47D**), and the lysosomal/late endosomal protein LAMP1 (**Figure 47E**). Interestingly however, vacuoles were not acidic, as shown by the lack of LysoTracker accumulation (**Figure 47F**). Moreover, co-expression of GFP-RAB7 and HA-CBU2007 increased membrane targeting of CBU2007 (**Figure 47C**).

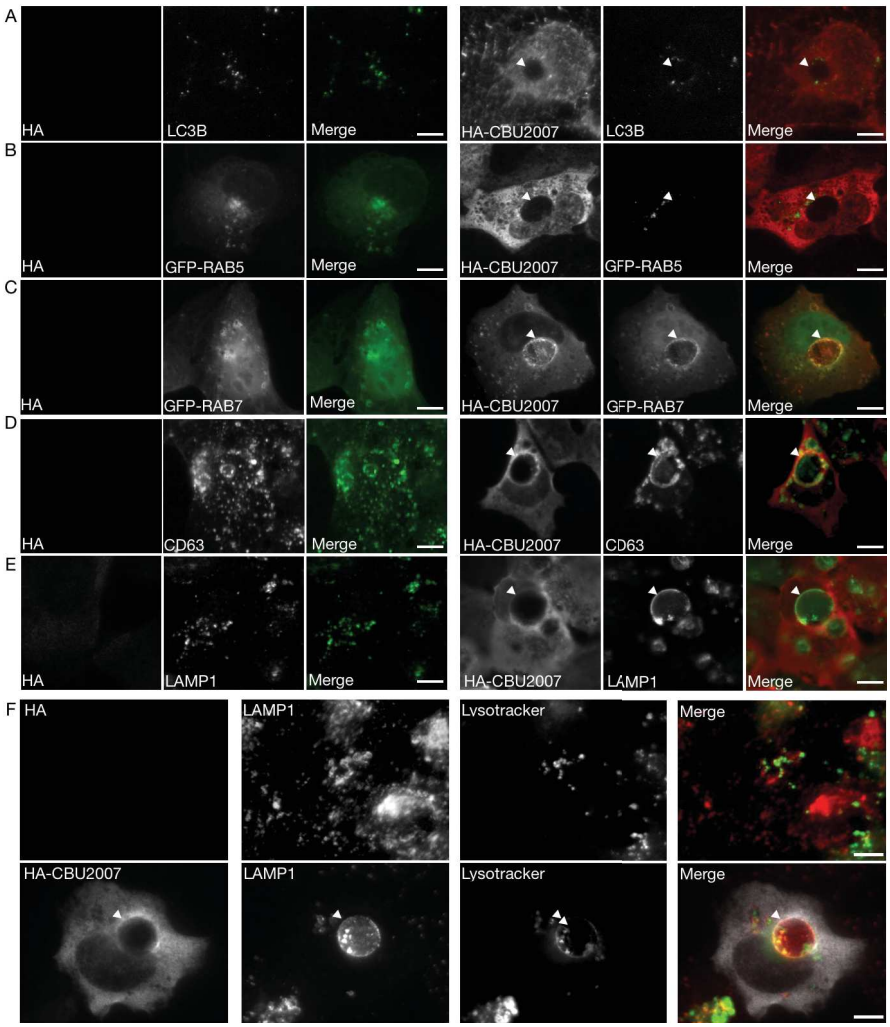

Figure 47. CBU2007 triggers LEs/MVBs enlargement. U2OS cells (A–E) were transfected either with HA alone (left panels) or HA-CBU2007 (right panels) in combination with either GFP-RAB5 (B) or GFP-RAB7 (C) or labelled with either anti-LC3B (A), anti-CD63 (D) or anti-LAMP1 (E) antibodies (green). We fixed cells 24 h post-transfection and labelled with an anti-HA (red). (F) U2OS cells were transfected with either HA alone (top panels) or HA-CBU2007 (bottom panels). We labelled cells with LysoTracker dye (green) 24 h post-transfection prior to fixation and staining with an anti-LAMP1 (red). (Scale bars, 10 μm).

Given the role of RAB7 in membrane fusion of endocytic vesicles (Vanlandingham and Ceresa, 2009) and its localisation at CBU2007-induced vacuoles, we investigated whether the small GTPase is involved in the biogenesis of this compartment. U2OS cells were transfected with HA-CBU2007 in combination either with GFP-RAB7^{Q67L} (dominant-positive) or GFP-RAB7^{T22N} (dominant-negative) to investigate the respective localisation of the two proteins and monitor the formation of CBU2007-induced vacuoles. As observed with the ectopic expression of WT RAB7, co-expression of GFP-RAB7^{Q67L} with HA-CBU2007 resulted in the targeting of both proteins to the large vacuole (**Figure 48**). Conversely, ectopic expression of GFP-RAB7^{T22N} reduced CBU2007 targeting to cellular membranes and results in the appearance of multiple, smaller vacuoles that fail to merge into the single one observed in cells expressing either WT RAB7 or GFP-RAB7^{Q67L} in combination with HA-CBU2007 (**Figure 48**). These data suggest that RAB7 is indeed involved in the formation of CBU2007-induced vacuoles. Immunoprecipitation of HA-CBU2007 will allow to investigate a potential interaction with RAB7.

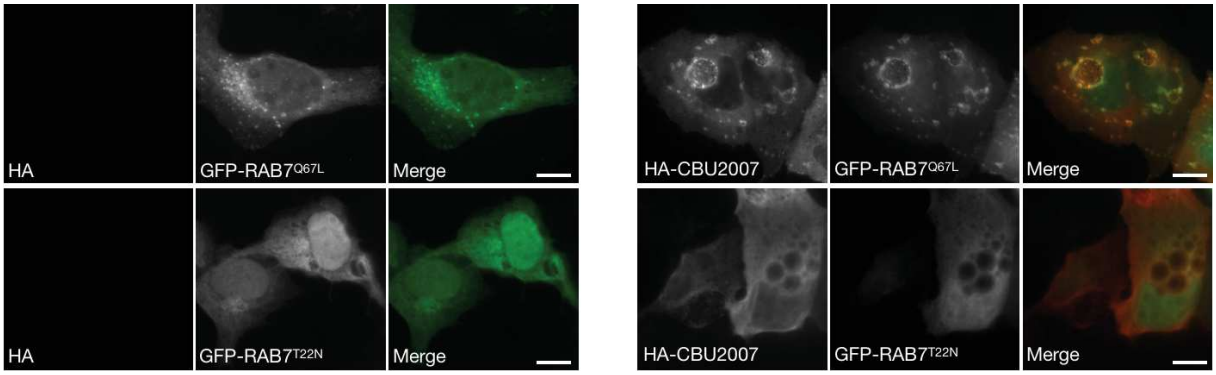

Figure 48. RAB7 is involved in the formation of CBU2007-induced vacuoles. U2OS cells were transiently transfected with either HA alone or HA-CBU2007 (red) in combination with GFP-RAB7^{Q67L} or GFP-RAB7^{T22N}. We fixed cells 24 h post-transfection and labelled with an anti-HA (red). (Scale bars, 10 µm).

Finally, to determine whether CBU2007 is involved in the recruitment of the ESCRT machinery at CCVs, U2OS cells were infected either with GFP-tagged *C. burnetii* (WT), the *cbu2007*::Tn or the *dotA*::Tn mutant strains for 3 days, fixed and labeled by an anti-ALIX and an anti-LBPA antibodies (**Figure 49**). Indeed, ALIX was recruited at CCVs generated by the WT *C. burnetii* while it remained diffused in cells infected either with the *cbu2007*::Tn or the *dotA*::Tn mutant strains (**Figure 49**), indicating that CBU2007 is involved in the recruitment of ALIX to the CCV.

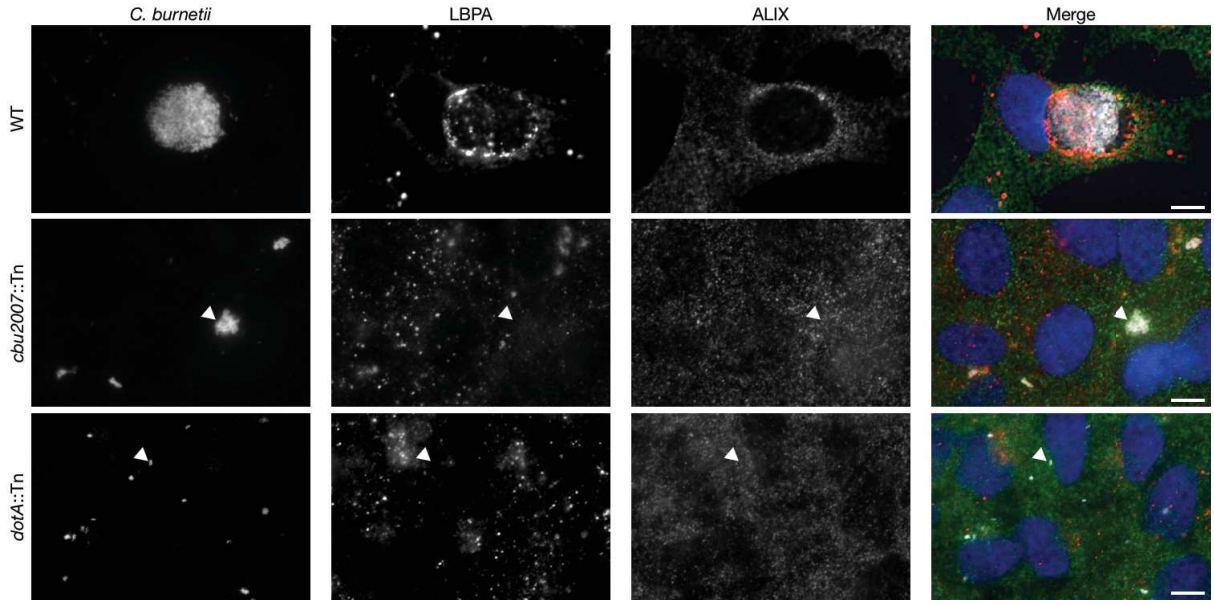

Figure 49. CBU2007 recruits the ESCRT machinery to CCVs. U2OS cells were infected with either *C. burnetii* WT GFP (top panels), *cbu2007*::Tn (middle panels) or *dotA*::Tn (bottom panels) (pseudo-colored gray) for 3 days, fixed, labelled with Hoechst (blue), anti-LBPA (red) and anti-ALIX (green). White arrows indicate *C. burnetii* colonies. (Scale bars, 10 µm).

Discussion

A fundamental step for the replication and persistence of intravacuolar bacterial pathogens is the establishment of a replicative niche inside host cells. This relies on the secretion of bacterial effector proteins in the cytoplasm of the infected cells by specialised secretion systems. Most intracellular bacterial pathogens use effector proteins to manipulate eukaryotic proteins and lipids, thus altering host signaling pathways and vesicular trafficking for successful infection (Martinez *et al.*, 2018). Among them, *C. burnetii* replicates within an unique, acidic and degradative compartment called the *Coxiella*-containing vacuole (CCV) and escapes immune surveillance (Burette and Bonazzi, 2020). My work has allowed to further characterise two aspects of the *C. burnetii* infectious cycle namely replicative niche biogenesis and persistence in host cells. The results obtained describe how *C. burnetii* persists as a stealth pathogen in host cells through the modulation of the innate immune signaling and how the manipulation of lipid metabolism is important for CCV biogenesis.

A common strategy of persistent bacterial pathogens is to evade immune clearance by overcoming cellular functions. Some bacterial effector proteins are secreted to promote persistence by modulating host innate immune responses and interfering with host detection mechanisms, signaling pathways or host transcription and translation (Asrat *et al.*, 2015). Indeed, previous studies have shown that *C. burnetii* evades the innate immune response by perturbing TLR signaling (Conti *et al.*, 2014), blocking pro-inflammatory pathways such as the non-canonical inflammasome (Cunha *et al.*, 2015) and modulating the NF-κB signaling pathway (Mahapatra *et al.*, 2010; Mahapatra *et al.*, 2016). Here, we have identified the eukaryotic-like protein NopA as a new bacterial effector that downmodulates the NF-κB signaling pathway by perturbing the nuclear translocation of the p65 subunit (Burette *et al.*, 2020) (**Figure 50**). Interestingly, multiple bacterial pathogens inhibit the NF-κB signaling pathway at several levels, but only a few perturb the nucleocytoplasmic transport of NF-κB (Asrat *et al.*, 2015) (**Figure 51**). For example, the *Salmonella typhimurium* effector SpvD prevents p65 nuclear import by interacting with the exportin

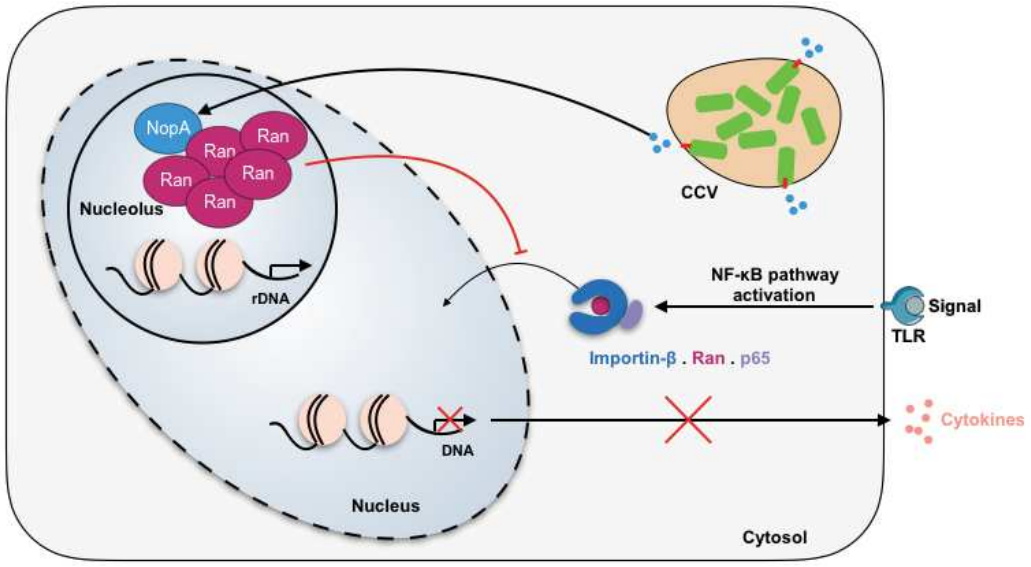

Figure 50. Schematic representation of the role of NopA upon *C. burnetii* infections. NopA localises at nucleoli of infected cells. By interacting with Ran, NopA triggers an imbalance in its nucleocytoplasmic gradient through the accumulation of GTP-bound Ran, thereby perturbing the nuclear import of eukaryotic proteins and the expression of pro-inflammatory cytokines.

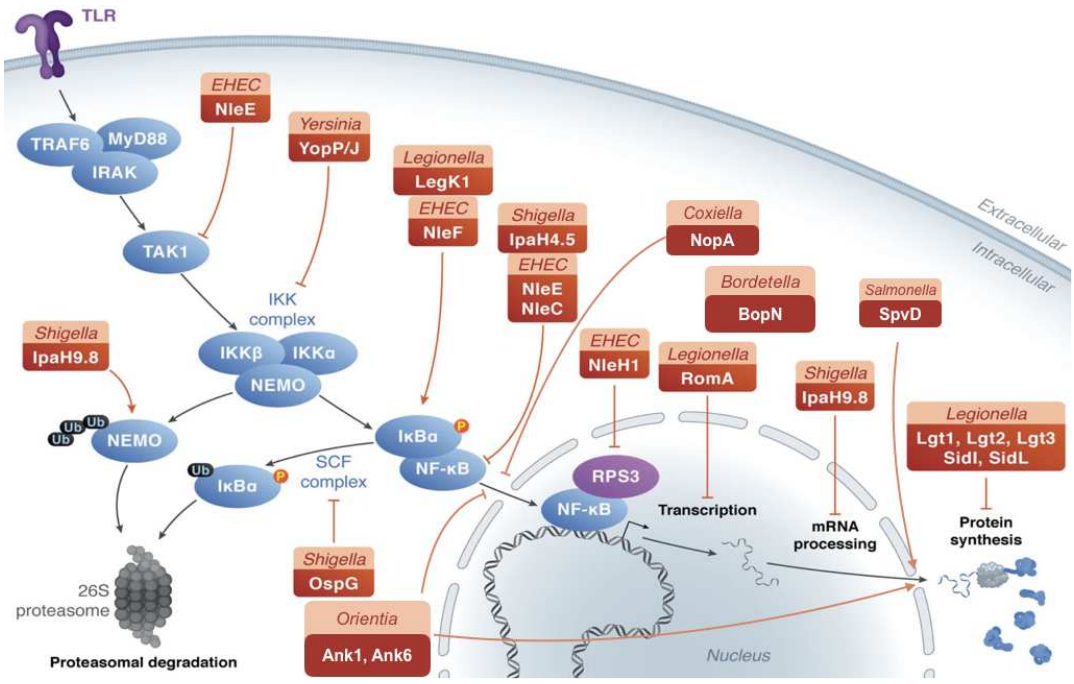

Figure 51. Bacterial proteins target the NF-κB pathway (adapted from Asrat *et al.*, 2015). The NF-κB signaling pathway can be modulated at several levels to stimulate (dotted arrows) or inhibit (dotted –l) host innate immunes responses. Bacterial proteins (oranges boxes: species (top) and bacterial protein (bottom)) are involved in phosphorylation (P), ubiquitination (Ub) and proteasomal degradation of components of the NF-κB complex, whereas other modulate the NF-κB-mediated transcription. Some of them are able to interfere in the nuclear import of the NF-κB subunit p65 as the *S. typhimurium* effector SpvD (Rolhion et al., 2016), the two *O. tsutsugamushi* proteins Ank1 and Ank6 (Evans et al., 2018), the *B. pertussis* effector BopN (Nagamatsu et al., 2009) and the recently identified *C. burnetii* effector NopA (Burette et al., 2020).

Xpo2, thereby inducing the nuclear accumulation of importin-α (Rolhion *et al.*, 2016) (**Figure 51**). Two *Orientia tsutsugamushi* effector proteins Ank1 and Ank6 subvert both importin and exportin activities, thus accelerating p65 nuclear export (Evans *et al.*, 2018) (**Figure 51**). The *Bordetella pertussis* effector BopN perturbs the nuclear translocation of p65 following IκBα degradation by manipulating the nuclear export (Nagamatsu *et al.*, 2009) (**Figure 51**).

Here, we have shown that the *C. burnetii* eukaryotic-like effector NopA sequesters Ran at nucleoli via its RCC-like domain, triggering s an imbalance in the nucleocytoplasmic gradient of the GTPase, thereby perturbing the nuclear import of eukaryotic proteins, including the p65 subunit of NF-κB. During infections, this results in a reduced expression of pro-inflammatory cytokines. Interestingly, the four RCC repeats found in NopA are homologous to those present in the eukaryotic Ran GEF RCC1. RCC1 is primarily found in association with chromatin and triggers the generation of GTP-bound Ran required for nucleocytoplasmic transport (Clarke and Zhang, 2008). Similar to the Ran GEF RCC1, NopA is found associated with the chromatin fraction, suggesting a potential interaction with DNA or RNA. and uses its RCC-like domain to interact with Ran. Differently from RCC1, however, NopA accumulates at host cell nucleoli and sequesters Ran, thus perturbing the shuttling of nuclear proteins. To date, very few bacterial effectors are able to localise to the nucleolus where they have distinct functions. The *L. pneumophila* effector LegAS4 is a histone methyltransferase that targets histone 3 lysine 4 (H3K4) (Li *et al.*, 2013). This leads to an increase of the transcription of ribosomal RNA genes (rRNA genes) which is the main function of the nucleolus (Boisvert *et al.*, 2007). *Bordetella bronchipseptica* and *Burkholderia thailandensis* also secrete nucleolar histone methyltransferase effectors, BtSET and BbSET respectively, to control rRNA synthesis in an epigenetic-dependent manner (Li *et al.*, 2013). LegAS4, BtSET and BbSET harbor a SET-domain, which is typically found in eukaryotic proteins with a methyltransferase activity (Cheng *et al.*, 2005). Another example of nucleolar bacterial protein is the *Escherichia coli* effector EspF that disrupts several nucleolar factors that are important for ribosomal biogenesis (Dean *et al.*, 2010). Whether NopA also plays a role as an epigenetic factor influencing gene expression remains to be investigated, given its putative interaction with DNA or RNA.

The modulation of nucleocytoplasmic transport by NopA deserves further investigation. Despite the clear impact of NopA on nucleocytoplasmic transport, shuttling of nuclear proteins is not completely suppressed during *C. burnetii* infections as cells challenged with the WT strain or the *nopA*::Tn complemented strains showed a small increase in nuclear p65 fluorescence as compared to cells infected with the *nopA*::Tn or the *dotA*::Tn strains. Interestingly, it has been shown that NF-κB-mediated anti-apoptotic genes such as *a1/bfl-1* and *c-iap2* are upregulated during *C. burnetii* infections (Voth *et al.*, 2007). Thus, NopA may

tightly modulate the nuclear translocation of p65 by allowing moderate NF-κB activation, thus reducing cytokines production and allowing the activity of anti-apoptotic pathways. Furthermore, the nuclear localisation of several *C. burnetii* effector proteins is not prevented by the expression and secretion of NopA (Eckart *et al.*, 2014; Weber *et al.*, 2016a; Schäfer *et al.*, 2017). However, NopA perturbs the nuclear translocation of IRF3, a transcriptional factor required to protect the host from viral infections by inducing type I IFN responses (Tamura *et al.*, 2008). Interestingly, this shows that NopA elicits a general impairment of the nucleocytoplasmic transport by affecting a broader class of proteins and also outside the context of *C. burnetii* infection. In this context, a recent study showed that *C. burnetii* selectively inhibits the nuclear translocation of the pro-apoptotic protein CHOP, to inhibit the ER-stress-induced apoptosis, whereas the nuclear import of the transcription factor ATF4 remains unaffected (Brann *et al.*, 2020). As NopA manipulates the nucleocytoplasmic transport in host cells, NopA may also interfere with the nuclear translocation of CHOP suggesting that NopA is important not only for the down-modulation of the innate immune response, but also for other processes such as apoptosis.

Among intracellular pathogens, *L. pneumophila* secretes 3 RCC1 repeat proteins LegG1, PpgA and PieG that are important for intracellular replication in host cells (Rothmeier *et al.*, 2013; Swart *et al.*, 2020). Similar to NopA, the 3 *L. pneumophila* RCC1 repeat effectors increase the intracellular levels of Ran-GTP by targeting distinct components of the Ran GTPase cycle. However, LegG1, PpgA and PieG localise to the cytoplasm where they stabilise microtubules in a Ran-dependent manner to promote the intracellular motility of LCVs (Rothmeier *et al.*, 2013; Swart *et al.*, 2020). Interestingly, the residual increase in the intracellular levels of Ran-GTP in cells infected with the *nopA*::Tn mutant suggest that other *C. burnetii* effectors may promote Ran activation as strain showed. Indeed, the gene *cbu0814* encodes for a hypothetical protein that displays one RCC repeat and may be secreted (Chen *et al.*, 2010).

Despite the emerging role of lipids in bacterial infection (van der Meer-Janssen *et al.*, 2010; Pizarro-Cerdá *et al.*, 2015), a systematic analysis of the interplay between bacterial effector proteins and host lipids has never been attempted. Building on the previous identification of CvpB as a *C. burnetii* effector that binds phosphoinositides and manipulate their metabolism (Martinez *et al.*, 2016), here we have further characterised the role of host lipids in *C. burnetii* infections, first by determining the lipid composition of CCVs during the course of infection and then by identifying two *C. burnetii* putative lipid-binding effector proteins. By using a wide array of lipid probes and confocal live cell imaging, PI(3)P, PI(4)P, PI(3,5)P_2, PS and LBPA were

found to be present on CCV membranes, however, only the recruitment of PI(3)P, PI(4)P and LBPA required a functional Dot/Icm T4SS (Figure 52). CCVs were originally defined as expanded autolysosomes. However, their lipid composition appeared far more complex than expected as the presence of the typical marker of early endosomes PI(3)P on CCVs was described (Martinez *et al.*, 2016). The presence of PI(4)P and LBPA to CCVs actually shows that several membrane trafficking pathways of the infected cell are subverted for the biogenesis of these compartments. Differently from other intracellular bacteria, which replicate in multiple but relatively small compartments, CCVs are extremely large and fusogenic, which leads to the generation of a single replicative niche per infected cell (Larson *et al.*, 2016). This may explain why *C. burnetii* requires to intercept multiple pathways such as endocytic, autophagy, secretory and recycling pathways for CCV biogenesis (Berón *et al.*, 2002; Campoy *et al.*, 2011; Larson *et al.*, 2013).

PI(4)P is essential for the secretory pathway by regulating the exit of cargo from the Golgi complex (Mayinger, 2009). As several studies have demonstrated that *C. burnetii* hijacks the secretory pathway (Campoy *et al.*, 2011; Carey *et al.*, 2011; Weber *et al.*, 2013; Graham *et al.*, 2015), we investigated if PI(4)P-positive secretory vesicles are re-routed to the forming CCVs. We showed that depleting the Golgi-associated pool of PI(4)P results in an absence of PI(4)P on CCVs that affects the early steps of CCV biogenesis. Similarly to *Legionella*-containing vacuoles, accumulation of PI(4)P on CCVs may promote the recruitment of secretory vesicles to favor CCV biogenesis (Ragaz *et al.*, 2008). For example, the *Legionella* effector SidF displays a PI-3 phosphatase activity and accumulates PI(4)P on *Legionella*-containing vacuoles by dephosphorylating $PI(3,4)P_2$ (Hsu *et al.*, 2012). The enrichment of PI(4)P on CCV membranes may thus be achieved by an unknown *C. burnetii* effector protein and/or via the activity of a host cell kinase. To date, however, we fail to identify *C. burnetii* transposon mutants generating PI(4)P-free vacuoles in our library.

Interestingly, the *C. burnetii* effector CBU0635 was identified in our screening of *C. burnetii* lipid-binding proteins as a putative PI(4)P interactor (Figure 53). Despite the fact that CBU0635 localises to and condenses the TGN, our data indicate that PI(4)P is not required for CBU0635 localisation at the TGN. As we were unable to purify either full-length CBU0635 or $CBU0635_{138-313}$ containing the putative PH domain, we could not assess the direct interaction of CBU0635 with lipids for the moment. Additional experiments are required to assess the functionality of the CBU0635 putative PH lipid-binding domain and whether protein targeting to membranes depends on the interaction with other lipids. Intracellular pathogens commonly manipulate lipid metabolism for the establishment of their replicative compartment (Weber *et al.*, 2009; Pizarro-Cerdá *et al.*, 2015). Bacterial effectors can bind host lipids to alter membrane targeting (Hilbi

et al., 2011) but can also modify PI metabolism (Weber *et al.*, 2009; Pizarro-Cerdá *et al.*, 2015). Indeed, several studies have reported bacterial PI phosphatases that share sequence similarities with the active CX_5R signature motif of eukaryotic PI phosphatases (Norris *et al.*, 1998). For example, *Legionella pneumophila* (Hsu *et al.*, 2012; Toulabi *et al.*, 2013) and *Mycobacterium tuberculosis* (Vergne *et al.*, 2005; Beresford *et al.*, 2007) secrete effectors with PI-3 phosphatase activity to clear PI(3)P from their vacuoles to arrest phagosome maturation. Similarly, the *Listeria monocytogenes* effector LipA has a lipid phosphatase activity for PI(3)P, PI(5)P and $PI(3,5)P_2$ and plays an important role in *Listeria* virulence. The enteric pathogens *Salmonella typhimurium* and *Shigella flexneri* use secreted PI-4 phosphatases during the course of infection (Mallo *et al.*, 2008; Viaud *et al.*, 2014b). The *S. typhimurium* effector SopB hydrolyses $PI(3,4)P_2$ to maintain high levels of PI(3)P at *Salmonella*-containing vacuoles and favor their biogenesis (Mallo *et al.*, 2008). Conversely, the *S. flexneri* effector IpgD hydrolyses $PI(4,5)P_2$ into PI(5)P to cause membrane ruffling and thus favor the bacterial invasion (Viaud *et al.*, 2014b). Interestingly, our data seem to indicate that CBU0635 may act as a PI phosphatase by manipulating $PI(3,4)P_2$ metabolism. Indeed, bioinformatics analysis of the aminoacid sequence of CBU0635 led to the identification of a putative CX_5R motif, correlating with our observation on the absence of $PI(3,4)P_2$-positive vesicles in CBU0635-expressing cells. More importantly, mutation of either the cysteine or the arginine residue in the putative motif restores the presence of $PI(3,4)P_2$-positive vesicles, which is indeed indicative of a PI phosphatase activity of CBU0635. This raises the possibility that CBU0635 may have dual functions during *C. burnetii* infection by manipulating lipid metabolism and by promoting membrane supply for CCV development. On the one hand, CBU0635 may localise to the TGN to re-route secretory vesicles to the forming CCV, correlating with the defective vacuole biogenesis phenotype observed with the *cbu0635::*Tn transposon mutant (**Figure 52**). Moreover, this hypothesis would be in agreement with a previous study showing that CBU0635 disturbs the secretory pathway (Carey *et al.*, 2011). On the other hand, CBU0635 may act as a PI-3 phosphatase that hydrolyses $PI(3,4)P_2$ to enrich cells in PI(4)P (**Figure 52**). However, this hypothesis remains to be experimentally validated as we cannot exclude a PI-4 phosphatase activity.

LBPA is a typical lipid of late endocytic multivesicular compartments and lysosomes (Kobayashi *et al.*, 1998). LBPA plays an essential role in the regulation of the transport of cholesterol (Kobayashi *et al.*, 1999) and the control of endosomal cholesterol levels (Chevallier *et al.*, 2008), which is another host-derived lipid recruited to CCVs (Howe and Heinzen, 2006). Cholesterol is an important component of membranes regulating membrane rigidity and fluidity (Ikonen, 2008). Here, we showed that the recruitment of LBPA at CCVs during infection

depends on the secreted effector CBU2007 (**Figure 52**). Indeed, most of CCVs generated by the *cbu2007*::Tn mutant present highly convoluted membranes devoid of LBPA. As LBPA levels are correlated with endosomal cholesterol levels (Chevallier *et al.*, 2008), our results may suggest that CBU2007 favor CCV biogenesis by influencing physical properties of CCV membranes. By recruiting LBPA to CCVs, CBU2007 may increase cholesterol levels in CCV membranes to stabilise their curvature and inner volume. Moreover, the formation of LBPA-rich micro domains on the CCV membrane suggests that CBU2007 may control the fusion and the fission of vesicles with the CCV membrane, thus contributing to CCV expansion (Bissig and Gruenberg, 2013).

The presence of LBPA on CCVs also suggests the direct fusion of MVBs with CCVs during the course of CCV biogenesis. The re-routing of MVBs to CCVs could thus be a strategy for *C. burnetii* to access essential host-derived components or to promote membrane supply as observed during *Chlamydia trachomatis* infections (Beatty, 2006; Beatty, 2008). Indeed, MVBs are lipid-rich, late endocytic compartments that are crucial in the transport of lipids and proteins (Piper and Katzmann, 2007). MVBs are defined by the presence of intraluminal vesicles (ILVs) that bud from the membrane of late endosomes into their lumen (Piper and Katzmann, 2007). This requires the activity of the ESCRT machinery, a multiproteic complex that participates in many processes involving membrane invagination (Hurley, 2015). The recruitment of the ESCRT machinery to endosomes depends on the ESCRT-associated protein ALIX, that also interacts with LBPA (Bissig and Gruenberg, 2013). Interestingly, several studies have shown that intracellular pathogens such as *C. burnetii*, *M. tuberculosis* and *S. enterica*, accumulate components of the ESCRT system on phagosomes to repair damage on these membranes (Mittal *et al.*, 2018; Radulovic *et al.*, 2018; Göser *et al.*, 2020). Our data show that CBU2007 regulates the activity of the ESCRT machinery by recruiting ALIX to the CCV. Indeed, CCVs generated by the *cbu2007*::Tn mutant are devoid of the ESCRT-associated protein ALIX, suggesting that CBU2007 might promote the repair of transient CCV damages by recruiting the ESCRT machinery.

Ectopically expressed CBU2007 strongly remodels the endosomal network by triggering the clustering of early and late endosomal vesicles, which probably participates in the biogenesis of large CBU2007-induced vacuoles. Importantly, CBU2007 encodes a putative F-BAR lipid-binding domain, potentially involved in the interaction of CBU2007 with PS. The reported intracellular distribution of PS at plasma membrane and endocytic vesicles (Yeung *et al.*, 2009; Leventis and Grinstein, 2010) correlated with our results on the subcellular localisation of CBU2007, suggesting that CBU2007 may use PS for membrane anchoring, by means of its putative F-BAR domain. As BAR domains play an important role in endocytosis

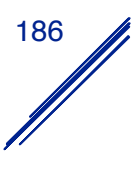

by sensing and inducing membrane curvature (Qualmann *et al.*, 2011), CBU2007 may similarly sense and induce membrane curvature to promote endocytosis and thus the biogenesis of CBU2007-induced vacuoles (**Figure 52**). In the context of infection, this may contribute to the expansion of CCVs.

Upon ectopic expression in non-infected cells, CBU2007 triggers the biogenesis of vacuoles that are positive for typical lipids and intracellular markers of MVBs including LBPA, LAMP1, CD63 and RAB7. We observed that overexpression of RAB7 increases membrane targeting of CBU2007 to the large CBU2007-induced vacuole. Similar to *C. burnetii* effectors CirA and CvpF that modulate the activity of RhoA and RAB26 GTPases, respectively (Weber *et al.*, 2016b; Weber *et al.*, 2018; Siadous *et al.*, 2020), CBU2007 may stimulate the GTPase activity of RAB7 to manipulate endocytic trafficking and facilitate heterotypic and homotypic vesicular fusion events. Besides its role in membrane fusion, RAB7 participates in cholesterol-dependent endosomal trafficking (Rocha *et al.*, 2009) and MVB formation (Kobuna *et al.*, 2010) by interacting with the protein ORP1L. Prior studies have shown that RAB7 is required for CCV biogenesis and expansion (Berón *et al.*, 2002; Newton *et al.*, 2013) and that ORP1L is actively recruited to the CCV to promote CCV expansion (Justis *et al.*, 2017). This raises the possibility that CBU2007 could be the effector involved in the recruitment of ORP1L to the CCV.

Our data have shown that the ESCRT-associated protein ALIX is efficiently recruited to the CBU2007-induced vacuole. Interestingly, CBU2007 seems to decrease the binding of the VPS4A complex, that terminates membrane scission (Schmidt and Teis, 2012). These observations raise the possibility that CBU2007 could block the formation of ILVs to generate a large and unique CCV by inhibiting VPS4A-dependent fission events (**Figure 52**).

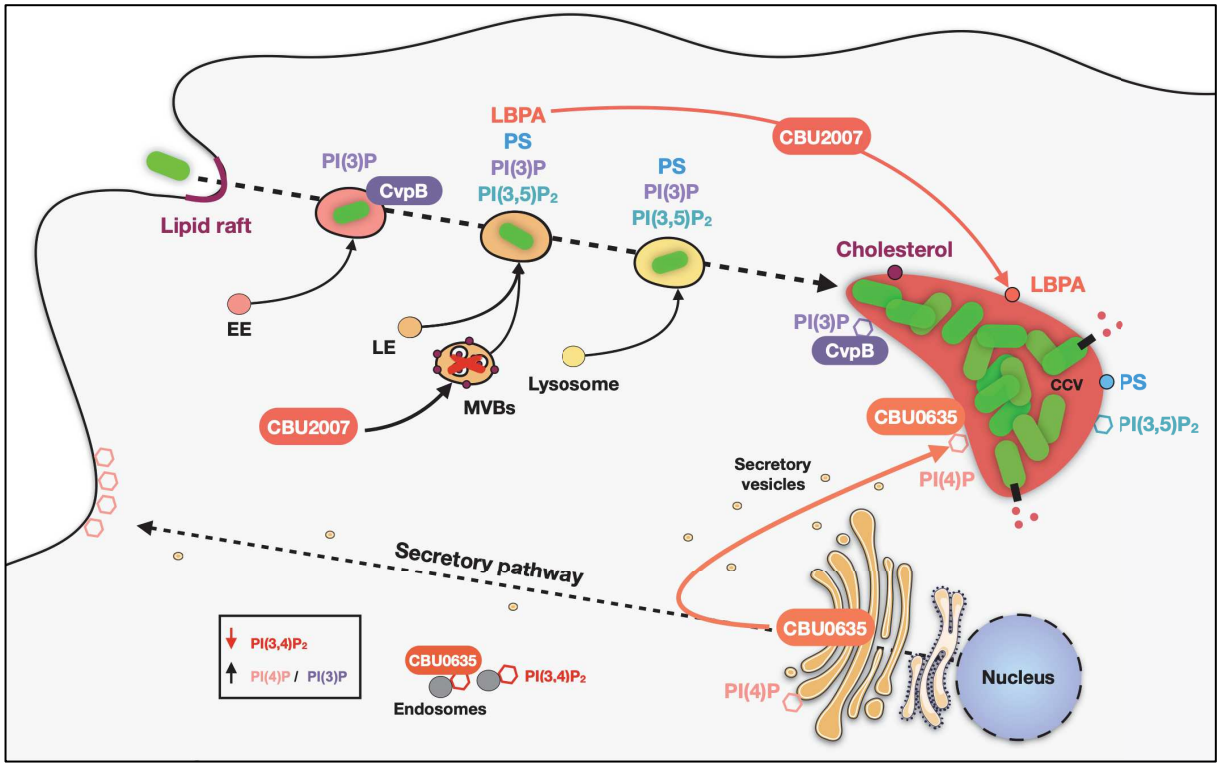

Figure 52. Hypothetical model of the role of CBU0635 and CBU2007 in the manipulation of lipid metabolism in the context of *C. burnetii* infections. CCVs membranes are enriched in PI(3)P and cholesterol. The newly characterisation of the lipid composition also highlighted the presence of $PI(3,5)P_2$, PS and interestingly, PI(4)P and LBPA at CCVs and these last two are actively recruited by *C. burnetii*. Screening of candidate lipid-binding effectors (LIEs) led to the identification of CBU0635, a putative PI(4)P interactor, and CBU2007, a putative LBPA interactor. CBU0635 localises to and condenses the TGN and may act as a PI phosphatase targeting $PI(3,4)P_2$ to enrich cells in either PI(3)P or PI(4)P. By affecting the Golgi shape and function, CBU0635 may re-route secretory vesicles to promote membrane supply to the forming CCV. CBU2007 contributes to CCV biogenesis probably by promoting the fusion of late endosomes while inhibiting fission events involved in the biogenesis of MVBs. CBU2007 mediates LBPA enrichment at CCVs and recruits the ESCRT machinery to the CCV and may be involved in membrane repair.

To conclude, this work has revealed new important strategies for *C. burnetii* to persist and replicate in host cells. On one hand, the function of the newly identified *C. burnetii* effector NopA was characterised showing how this protein modulates the innate immune signaling in infected cells. On the other hand, the role of lipid metabolism in the establishment of the CCV was investigated leading to the identification of two lipid-binding candidates among *C. burnetii* effector proteins. CBU0635 is a putative PI phosphatase that diverts the secretory pathway to the forming CCV while CBU2007 manipulates LBPA metabolism to recruit the ESCRT machinery and block the biogenesis of MVBs.

Interestingly, there is increasing evidence for an interplay between the immune response and vesicular trafficking. Recent evidence suggests that both lipid metabolism and the membrane-remodeling ESCRT-III machinery directly influence the activation of the

inflammasome, thereby coupling components of the vesicular trafficking to innate immune signaling. The activation of the NLRP3 inflammasome is characterised by gasdermin-D (GSDMD) pore formation in the plasma membrane that cause a type of cell death known as pyroptosis. Following activation, caspase-1 processes IL-1β and IL-18 cytokines and promote their release from cells (Broz, 2019). A recent study has shown that the ESCRT-III machinery has an anti-inflammatory effect by repairing membranes damaged by GSDMD pores, which limits pyroptosis and cytokine release (Rühl *et al.*, 2018). Otherwise, an alteration in cholesterol trafficking through a lysosomal accumulation dampens the activation of the NLRP3 inflammasome (de la Roche *et al.*, 2018). Another example is the targeting of NLRP3 to PI(4)P-enriched TGN, which is required for NLRP3 activation following its stimulation. Indeed, NLRP3 stimuli induce the disassembly of the TGN, which serves as a scaffold for NLRP3 to aggregate and induce ASC polymerisation and caspase-1 activation (Chen and Chen, 2018). Regarding the established crosstalk between innate immunity and vesicular trafficking, persistence is defined not only by the pathogen's ability to evade immune defenses, but also by its ability to hijack multiple functions of host cell factors. This finally highlights how two different aspects of the *C. burnetii* infectious cycle, such as intracellular replication and persistence, may be closely related during host cell infection.

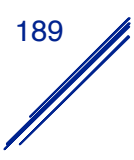

Future directions

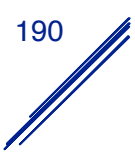

The aim of this thesis was to further characterise two aspects of the infectious cycle of *C. burnetii* as intracellular replication and persistence within the host. Several observations were made to direct future research in these projects.

We have characterised the role of NopA in the modulation of innate immune signalling upon *C. burnetii* infection, however, additional aspects of NopA function remain to be investigated. We have shown that NopA localises to nucleoli, however bioinformatics analysis failed to identify any nuclear or nucleolar localisation signals in NopA sequence. The minimum requirement for this localisation can be limited to the fourth RCC repeat, suggesting the presence of a nucleolar-targeting motif in this repeat. Interestingly, sequence analysis allowed the identification of NoDS motif (Nucleolar Detention Signals) in the NopA sequence. NoDS are typical of a set of host nucleolar factors as VHL (Von Hippel-Lindau tumor suppressor), Hsp70 (Heat shock protein 70) and MDM2 (Mouse Double Minute 2 homolog), that are captured and retained at nucleoli under stress conditions, by means of interactions with IGS long non-coding RNAs (IGS lnc RNAs) (Audas *et al.*, 2012; Jacob *et al.*, 2013). Targeted point mutations in NopA showed that this motif might indeed be functional. The interaction with IGS long non-coding RNA could be further investigated by RNA immunoprecipitation (RIP). Conversely, if NopA is not a NoDS-containing protein, one explanation of how NopA localises to nucleoli is a piggyback mechanism by binding to either importins or any host or *C. burnetii* nuclear proteins, which contains a classical NLS. To investigate this, it could be interesting to identify NopA interactors by immunoprecipitation using $NopA_{FL}$, $NopA_{N\text{-}ter}$ and $NopA_{C\text{-}ter}$ to identify proteins involved in the nuclear import of NopA.

In order to further explore the role of NopA, it will be interesting to determine whether NopA interacts with and also modifies the function of DNA or RNA within the host cells. This requires purifying NopA in order to perform chromatin immunoprecipitation (ChIP) or RIP. In parallel, NopA also encodes a putative F-box domain, which is another eukaryotic-like domain in addition to the 4 RCC-like repeats. This raises the possibility that NopA may also modulate host ubiquitination pathways, which is a strategy shared by multiple bacterial pathogens as *L. pneumophila* (Lomma *et al.*, 2010), *Shigella* spp (Singer *et al.*, 2008) or *Salmonella* typhimurium (Gulati *et al.*, 2019). Finally, we have shown that NopA interacts with Ran, with preferential affinity for the GDP-bound form and promotes its activation. The purification of NopA will be also useful to assess whether NopA activates Ran directly or indirectly via the Ran GEF RCC1 using an *in vitro* GEF assay. Given the role of Ran in spindle assembly during mitosis (Clarke and Zhang, 2008), it could be interesting to examine the impact of NopA on microtubules polymerisation. To test this, I propose to treat cells with taxol or nocodazole for

microtubule polymerisation or depolymerisation respectively, upon ectopic expression of NopA.

The role of NopA during *C. burnetii* infections suggest that the effector protein could be used as a new tool to perturb nuclear import and potentially regulate a vast number of host cell signaling pathways in health and disease. Indeed, multiple Gram-negative bacteria representing major public health issues including enteroinvasive *E. coli* (EIEC), *Shigella* spp, *Pseudomonas aeruginosa* cause infections characterised by a hyperinflammation (Schroeder and Hilbi, 2008; Wine *et al.*, 2010; Ciszek-Lenda *et al.*, 2019). With the emergence of multi-resistant bacterial strains, it becomes urgent to develop alternative approaches to fight infectious diseases. In this context, NopA could be used as a modulating agent of hyperinflammatory responses induced by bacterial infections. The effect of NopA may be investigated in *in vivo* models to evaluate their susceptibility to EIEC, *Shigella* spp or *P. aeruginosa* infections. Moreover, hyperinflammatory responses are also observed in cancers and autoimmune diseases suggesting the use of NopA outside the context of infectious diseases. Indeed, it has been shown that inhibiting the activity of the NF-κB signaling pathway in tumor cells stop their proliferation and make them more sensitive to anti-tumoral molecules (Escárcega *et al.*, 2007). Likewise, it has been reported that certain autoimmune diseases including Crohn's disease or rheumatoid arthritis induce an overproduction of pro-inflammatory cytokines through the deregulation of the NF-κB signaling pathway (Liu *et al.*, 2017; Han *et al.*, 2017; Xia *et al.*, 2018). In this context, NopA could thus be tested as a new immunomodulatory agent by manipulating the nuclear import of NF-κB or other transcription factors whose aberrant activity cause various diseases in humans (Bushweller, 2019).

Finally, NopA could be also tested for its capacity to interfere with the nuclear import of viral genomes and accessory proteins to counter viral infections. Indeed, infections by DNA viruses and some RNA viruses rely on nuclear import to replicate inside infected cells (Fay and Panté, 2015). I thus propose to study the effect of NopA on the translocation of viral DNA during infection by viruses.

We have gained new insights into the role of lipids upon *C. burnetii* infection that remains to be further characterised. We have better defined the lipid signature of CCVs at different stages of infection showing that PI(3)P, PI(4)P and LBPA are actively recruited to the CCV membrane. These results could then be exploited to determine the specific role of a given lipid and of its downstream signaling pathways in CCV biogenesis. To test this, inhibitors of targeted lipid metabolism could be used in non-infected and *C. burnetii*-infected cells to investigate the localisation and dynamics of lipids of interest upon treatment. If results are relevant, the effects

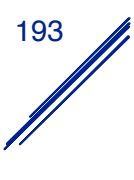

of the selected inhibitors of lipid metabolism on *C. burnetii* virulence could be evaluated *in vivo* using the SCID mouse model. Mice will be challenged with the WT *C. burnetii* to assess two traits relevant to virulence as the ability to replicate within the spleen by calculating bacterial genome equivalents and the ability to cause splenomegaly.

Similar to other intracellular pathogens, *C. burnetii* uses effectors to manipulate lipid metabolism during infection. In addition to CvpB (Martinez *et al.*, 2016), lipid pull-down assay revealed that other *C. burnetii* proteins may interact with lipids including PI, PI(4)P, PS, LBPA, cholesterol and sphingosine. In addition to the effector proteins CBU0635 and CBU2007 described here, this work paves the way for further analysis of *C. burnetii* lipid-binding candidates thus contributing to a better understanding of CCV biogenesis and *C. burnetii* intracellular replication.

Additional experiments are needed to further characterise the function of CBU0635 and CBU2007 during *C. burnetii* infections. In order to confirm the defective CCV biogenesis phenotype observed in cells challenged with the *cbu0635*::Tn or *cbu2007*::Tn mutants, it will be crucial to complement both strains. It will be then interesting to evaluate the *in vivo* relevance of these mutations using the SCID mouse model (van Schaik *et al.*, 2017).

Previous studies have reported the presence of the secretory pathway marker RAB1b on CCVs showing that CCVs intercept with the secretory pathway (Campoy *et al.*, 2011). In the context of infection, a potential function for CBU0635 could be to favour the re-routing of secretory vesicles to the forming CCV. To explore this hypothesis, we could assess the presence of the secretory pathway markers RAB1b or RAB6 on CCVs generated by either WT, *cbu0635*::Tn and *dotA*::Tn strains.

In order to further investigate this hypothesis, it could be interesting to investigate whether CBU0635 acts on the GOLPH3 pathway, which is known to regulate the Golgi shape and function in cells (Buschman *et al.*, 2015). Indeed, GOLPH3 is a PI(4)P-binding protein that localises to the Golgi apparatus and plays a critical role in the secretory pathway. Perturbation of the GOLPH3 pathway results in the alteration of both Golgi morphology and trafficking of secretory vesicles to the plasma membrane (Buschman *et al.*, 2015). As ectopic expression of CBU0635 triggers Golgi condensation and disturbs the secretory pathway, I then propose to investigate the intracellular localisation and levels of GOLPH3 in presence of CBU0635.

We have shown that CBU0635 encodes for a putative catalytic motif suggesting a PI-phosphatase activity. Further characterisation of CBU0635 activity requires its purification to assess its enzymatic activity using the malachite green-based assay *in vitro*. Because $CBU0635_{C133A}$ and $_{R139A}$ mutants seems to lose their putative enzymatic activity, the PI substrate specificity of purified WT, C133A and R139A mutants CBU0635 could be evaluated

by quantifying the amount of released phosphates. Purified CBU0635 will also allow to validate lipid interaction by incubating the recombinant protein with PIP Strips.

Purified recombinant CBU2007 was used in a PIP Strip assay showing that CBU2007 preferentially binds PS, however, LBPA-binding could not be assessed. To test this, I propose to perform protein/lipid overlay by spotting LBPA at decreasing concentrations on a PVDF membrane. Similar to what has been done for the characterisation of CvpB (Martinez *et al.*, 2016), large and giant unilamellar vesicles (LUVs and GUVs, respectively) of specific lipid composition could be used to confirm and characterise the specificity of both CBU0635 and CBU2007 interaction with lipids. Recombinant CBU2007 could also be incubated with LUVs of specific lipid composition and concentration matching those observed in either plasma membrane or endosomes, to investigate a preferential binding to either compartment. Finally, purified recombinant CBU0635 and CBU2007 could be used to identify their respective interactors by affinity purification technique to isolate either CBU0635- or CBU2007-containing protein complexes.

As BAR domain proteins are able to sense and induce membrane curvature, the functionality of the putative F-BAR domain in CBU2007 sequence could be tested using well-defined *in vitro* assays. Flat membrane sheets may be used with a plasma membrane-like composition containing 5-20% PS (Itoh *et al.*, 2005; Picas *et al.*, 2014) to investigate a possible role of CBU2007 in the remodeling of PS-containing membranes. Appearance of dynamic lipid tubules emanating from flat sheets would be indicative of a membrane remodeling activity of the bacterial effector protein. To characterise this activity, CBU2007$_{N\text{-}ter}$ and $_{C\text{-}ter}$ could be also purified to further investigate the functionality of the putative F-BAR domain.

We have shown that CBU2007 recruits the ESCRT machinery to the CCV and may inhibit fission events involved in MVB biogenesis. Beyond MVB biogenesis, the ESCRT machinery has important function in eukaryotic cell abscission and viral budding. The ESCRT machinery is typically hijacked by enveloped viruses, including HIV-1, to promote the release of viral particles from the host cell membrane by exocytosis (Votteler and Sundquist, 2013). To explore a potential inhibition of the ESCRT fission machinery by CBU2007, it could be interesting to see whether CBU2007 modulates HIV-1 viral particles release. Depending on the outcome of the experiment, CBU2007 could be used outside of the context of *C. burnetii* infections, as a new tool to inhibit the release of virus-like particles. Finally, the recruitment of the ESCRT machinery by CBU2007 suggest that the effector may be involved in repairing damaged lysosomes. A recent publication reported that galectin-3 (Gal-3) coordinates the lysosomal repair with the ESCRT component ALIX upon endomembrane damages (Jia *et al.*, 2020). To evaluate the role of CBU2007 in ESCRT-dependent membrane repair, membrane damage

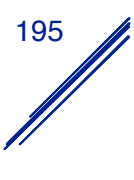

could be artificially induced by means of LLOMe (L-leucyl-L-leucine methyl ester) and Gal-3 recruitment could be monitored to assess membrane damage. It could be then interesting to observe whether the LLOMe treatment affects the formation of CBU2007-induced vacuoles as well as the localisation of membrane repair markers as ESCRT machinery components and Galectin-3.

To conclude, this work provides new insights on *C. burnetii* pathogenesis by investigating mechanisms adopted to evade the innate immunity and to manipulate lipid metabolism. If additional questions remain open, this work paves the way for the development of new antimicrobials targeting lipid metabolism and for the use of bacterial effector proteins outside of the context of *C. burnetii* infections.

Thesis summary in french

Au cours de l'évolution, les bactéries pathogènes ont développé une grande variété de stratégies pour survivre et se développer aux dépens de leur hôte. Les pathogènes bactériens intracellulaires se sont adaptés pour pouvoir constituer leur niche réplicative en détournant les mécanismes de l'hôte et en évitant les mécanismes de défense qui pourraient entraver la colonisation de leur hôte. Avec l'augmentation de la résistance aux antibiotiques, il est essentiel de mieux connaître les interactions hôte/pathogène qui permettent la biogenèse de leurs compartiments réplicatifs pour mieux comprendre les processus d'infection et concevoir de nouvelles molécules antimicrobiennes qui cibleraient spécifiquement les facteurs de l'hôte ou de la bactérie pour lutter efficacement contre les infections. *Coxiella burnetii* est l'agent causal de la coxiellose animale et de la fièvre Q humaine, considérée comme l'une des zoonoses réémergentes les plus préoccupantes en Europe (Quaglio *et al.*, 2012). Les principaux réservoirs de *C. burnetii* sont des animaux domestiques et d'élevage, chez lesquels les infections sont souvent asymptomatiques, donc difficiles à détecter. *C. burnetii* s'accumule principalement dans le placenta des animaux infectés et les bactéries sont dispersées dans l'environnement lors d'avortements ou de mises-bas précoces. Les humains sont des hôtes accidentels et sont infectés par inhalation d'aérosols contaminés (Maurin and Raoult, 1999). La fièvre Q se manifeste sous une forme aiguë ou chronique. La fièvre Q aiguë entraîne une pneumonie et une fièvre élevée avec un taux de mortalité de 2%, tandis que la fièvre Q chronique peut avoir des complications fatales comme l'endocardite et l'hépatite avec un taux de mortalité atteignant 65% (Madariaga *et al.*, 2003). La récente épidémie de fièvre Q aux Pays-Bas, avec 4000 cas de fièvre Q humaine, démontre la sévère virulence de ce pathogène (Roest *et al.*, 2011). En effet, avec une dose infectieuse minimale de 1 bactérie, *C. burnetii* est l'organisme le plus infectieux connu à ce jour. Sa haute résistance au stress environnementaux et sa propagation aérienne ont contribué à classer *C. burnetii* parmi les agents infectieux pouvant être employés à des fins bioterroristes. Il est important de noter qu'aucun vaccin contre la fièvre Q n'est actuellement commercialisé et que le traitement antibiotique complexe nécessite plusieurs mois de traitement, avec des cas de résistance / rechute observés (Morguet *et al.*, 2007).

Après inhalation, *C. burnetii* peut être internalisée par des cellules phagocytaires et non phagocytaires, ce qui est facilité par l'invasine bactérienne OmpA (Martinez *et al.*, 2014). Les bactéries se retrouvent alors dans des vacuoles contenant *Coxiella* (ou CCV), qui suivent la voie endocytaire, acquérant progressivement des marqueurs typiques des endosomes précoces (tels que EEA1), des endosomes tardifs et des lysosomes (tels que LAMP1). La baisse du pH vacuolaire et l'environnement dégradatif qui accompagne la maturation des CCV

active le système bactérien de sécrétion de type 4B Dot / Icm (T4SS) nécessaire pour transloquer les protéines effectrices dans le cytoplasme de la cellule hôte. Ce principal facteur de virulence permet à *C. burnetii* d'acquérir du matériel de la cellule hôte par fusion hétérotypique d'endosomes, d'autophagosomes et de lysosomes avec la CCV jusqu'à occuper la majeure partie du cytoplasme des cellules hôtes (Burette and Bonazzi, 2020). Une analyse bioinformatique combinée à des tests de sécrétion chez *C. burnetii* ou son modèle de substitution *Legionella pneumophila* ont permis d'identifier plus de 143 protéines effectrices potentielles chez *C. burnetii* (Larson *et al.*, 2016). Parmi ces effecteurs candidats, il a été démontré qu'un groupe de protéines inhibe l'apoptose et l'inflammation au cours de l'infection par *C. burnetii*, permettant ainsi la survie des cellules au cours de son long cycle infectieux, tandis qu'un autre groupe détourne le trafic des membranes intracellulaires et servent à générer une vacuole parasitophore hautement fusogènique, dans laquelle la bactérie se réplique en très grand nombre. Toutefois, très peu de partenaires cellulaires ont été identifiés pour ces effecteurs et leur rôle précis dans la réplication intracellulaire et la persistance de la bactérie reste très peu caractérisé. Pendant des années, la nature intracellulaire obligatoire de *C. burnetii* a cependant imposé des contraintes expérimentales importantes pour l'étude de sa pathogenèse. Avec le développement d'un milieu de culture axénique en 2009, *C. burnetii* est devenu génétiquement manipulable, ce qui a permis d'identifier des facteurs de virulence essentiels dans la manipulation du trafic vésiculaire, de l'apoptose (Lührmann *et al.*, 2010; Klingenbeck *et al.*, 2013) ou de l'inflammation (Cunha *et al.*, 2015) au cours de l'infection. Pour poursuivre la compréhension des mécanismes favorisant la virulence de *C. burnetii*, mes travaux de thèse se sont focalisés sur les interactions hôte/pathogène notamment impliquées dans deux aspects du cycle infectieux de la bactérie, à savoir la réplication intracellulaire et la persistance dans les cellules hôtes infectées.

Coxiella burnetii a un long cycle infectieux et peut persister dans les cellules pendant de longues périodes. La bactérie a développé des stratégies spécifiques pour atténuer la réponse inflammatoire des cellules hôtes et les protéger du stress induit par son invasion et sa réplication. Outre la sécrétion d'effecteurs bactériens de type 4 essentiels à la biogenèse de la CCV (Voth and Heinzen, 2007; Newton *et al.*, 2014), la bactérie sécrète des effecteurs qui inhibent l'apoptose et l'inflammation des cellules infectées (Van Schaik *et al.*, 2013; Mahapatra *et al.*, 2016). À ce jour, il a été démontré que trois protéines effectrices de *Coxiella* (CaeA, CaeB et AnkG) inhibent l'apoptose intrinsèque et extrinsèque (Cordsmeier *et al.*, 2019), tandis que l'effecteur IcaA inhibe l'activation de la voie inflammatoire non canonique (Cunha *et al.*, 2015). *C. burnetii* est également capable d'inhiber l'activation de la voie de

signalisation du facteur de transcription nucléaire kappa B (NF-κB), qui est le principal médiateur de l'inflammation (Mahapatra *et al.*, 2016). Cependant, la protéine effectrice bactérienne impliquée dans ce mécanisme restait inconnue à ce jour.

L'analyse bioinformatique du génome et du protéome de *Coxiella* a conduit à l'identification de potentielles protéines effectrices bactériennes contenant des domaines de type eucaryote, reflétant l'intime interaction qui existe entre cette bactérie et ses hôtes. Ces domaines sont pour la plupart impliqués dans des interactions protéine/protéine ou sont responsables de modifications post-traductionnelles, permettant ainsi de mimer ou déstabiliser des fonctions cellulaires essentielles au développement de la bactérie. En étudiant les protéines effectrices de *C. burnetii* contenant des domaines de type eucaryote, nous avons ici identifié NopA (pour protéine nucléolaire A), qui possède 4 répétitions RCC (régulateur de condensation chromosomique), homologues à celles retrouvées dans la protéine nucléaire eucaryote Ran Guanosine Exchange Factor (GEF) RCC1. Au cours de l'infection, NopA est retrouvé associé à la fraction nucléaire chromatinique des cellules et utilise son domaine de type RCC pour interagir avec Ran. De plus, NopA stimule l'accumulation de Ran-GTP au niveau des nucléoles des cellules transfectées ou infectées, perturbant ainsi l'import nucléaire des facteurs de transcription des voies de signalisation de l'immunité innée tels que NF-κB ou IRF3 (pour facteur régulateur de l'interféron 3). Ainsi, l'analyse par qRT-PCR d'un panel de cytokines a montré que les cellules infectées par les mutants *nopA*::Tn ou *dotA*::Tn (la souche déficiente pour la sécrétion d'effecteurs) présentent une réponse immunitaire innée fonctionnelle, contrairement aux cellules infectées par *C. burnetii* sauvage ou la souche *nopA*::Tn complémentée avec *nopA*. En conclusion, la première partie de mon travail de thèse a montré que l'effecteur NopA est un régulateur important de la réponse immunitaire innée permettant à *Coxiella* de se comporter comme un pathogène furtif (Burette *et al.*, 2020).

Une étape fondamentale pour la survie et la réplication des agents pathogènes bactériens intravacuolaires est l'établissement d'une niche réplicative à l'intérieur des cellules hôtes. Ces compartiments dérivés des membranes de l'hôte ont une composition unique en protéines et en lipides. Pour cela, les protéines effectrices bactériennes interagissent avec les protéines et les lipides eucaryotes pour manipuler le trafic vésiculaire de l'hôte, permettant ainsi aux bactéries d'échapper à la voie de dégradation de l'hôte et de faire converger les nutriments nécessaires à la réplication intracellulaire des bactéries (Martinez *et al.*, 2018). En plus de leur rôle structurale dans les membranes, les lipides sont des acteurs clés de la signalisation cellulaire en contrôlant directement ou indirectement de multiples fonctions telles que le trafic vésiculaire ou les réarrangements du cytosquelette (Goud *et al.*, 2016). De ce fait,

la manipulation des lipides apparait comme un mécanisme essentiel pour la biogenèse de la CCV et la réplication intracellulaire de *C. burnetii*. En effet, le métabolisme du phosphatidylinositol 3-phosphate (PI(3)P), un lipide particulièrement enrichi aux endosomes précoces et aux vésicules autophagiques, est manipulé par la protéine effectrice CvpB (pour protéine vacuolaire de *Coxiella* B) pour un développement optimal de la CCV, avec des conséquences importantes dans la virulence (Martinez *et al.*, 2016).

Cette découverte nous a incité à réaliser une analyse globale des interactions entre les protéines effectrices de *C. burnetii* et les lipides de l'hôte afin de comprendre le rôle des lipides dans la survie et la réplication intracellulaire de *C. burnetii.* En utilisant un panel de sondes fluorescentes couplés à des domaines de liaison aux lipides, nous avons tout d'abord déterminé la composition lipidique des CCVs au cours de l'infection, par microscopie confocale. Comme attendu pour un compartiment de type autolysosomal, la membrane de la CCV est enrichie en $PI(3,5)P_2$ et en phosphatidylsérine (PS), deux marqueurs typiques des endosomes tardifs et des lysosomes (Yeung *et al.*, 2009). L'analyse a également confirmé que *C. burnetii* recrute activement du PI(3)P et de manière intéressante, du LBPA et du PI(4)P à la CCV, deux lipides typiques des endosomes multivésiculaires et de la voie sécrétoire respectivement.

Nous avons ensuite cherché à identifier et caractériser de potentiels candidats effecteurs liant les lipides au cours de l'infection. A l'aide d'un panel de billes d'agarose recouvertes de lipides spécifiques, nous avons validé l'existence d'autres interactions entre les lipides eucaryotes et des protéines de *C. burnetii*, par co-précipitation. Combinée à une analyse bioinformatique, cette étude a conduit à l'identification de 5 protéines effectrices bactériennes potentielles contenant de possibles domaines de liaison aux lipides. Parmi elles, nous avons identifié la protéine effectrice CBU0635 comme un potentiel candidat liant le PI(4)P. CBU0635 possède deux potentiels domaines de liaison aux lipides, dont un domaine PH (pour domaine homologue de la pleckstrine) important pour sa localisation. Exprimée de manière ectopique, CBU0635 localise à des compartiments enrichis en PI(4)P et au réseau trans-golgien. CBU0635 provoque également une compaction de l'appareil de Golgi et interfère dans la voie sécrétoire, suggérant que la protéine pourrait détourner les vésicules sécrétoires vers la CCV afin d'en favoriser la biogenèse. CBU0635 possède également un potentiel site catalytique CX_5R, homologue à ceux présents dans les phosphatases de lipides (Norris *et al.*, 1998). CBU0635 pourrait ainsi être la première phosphatase de lipide de *C. burnetii*, qui déphosphorylerait le $PI(3,4)P_2$ pour enrichir les cellules en PI(3)P ou en PI(4)P. Pour finir, nous avons identifié CBU2007 comme un potentiel candidat liant le LBPA. CBU2007 possède un potentiel domaine F-BAR pouvant permettre la liaison aux lipides mais aussi

d'induire des courbures à la membrane. Au cours de l'infection, CBU2007 est impliqué dans le recrutement du LBPA et de la machinerie ESCRT à la CCV. L'importance de la manipulation du métabolisme du LBPA est mise en évidence par des mutations dans *cbu2007* résultant en un phénotype de CCV à la membrane déformée, indiquant un défaut dans la biogenèse des CCVs. L'expression ectopique de CBU2007 provoque l'élargissement et l'agrégation des vésicules positives au PI(3)P et au LBPA autour d'un large compartiment induit par CBU2007 et ayant tous les marqueurs des endosomes multivésiculaires. CBU2007 empêche le recrutement de l'ATPase VPS4A à ce compartiment, pourtant indispensable à la formation de vésicules intraluminales dans les endosomes multivésiculaires, suggérant que CBU2007 inhibe les évènements de fission à l'origine des endosomes multivésiculaires. En conclusion, la seconde partie de mon travail de thèse a montré que CBU0635 et CBU2007 sont des protéines effectrices bactériennes manipulant le métabolisme du $PI(3,4)P_2$ et du LBPA pour favoriser la biogenèse de la CCV et donc la réplication intracellulaire de *C. burnetii*.

Pour conclure sur les stratégies de réplication intracellulaire et de persistance de *C. burnetii*, ce travail de thèse a permis de mieux comprendre deux étapes cruciales du cycle infectieux de la bactérie. En effet, nous avons acquis de nouvelles connaissances sur la pathogenèse de *C. burnetii* en étudiant les mécanismes adoptés pour échapper à l'immunité innée et pour manipuler le métabolisme des lipides. Des questions supplémentaires subsistent, mais ce travail ouvre la voie au développement de nouveaux antimicrobiens et à l'utilisation de protéines effectrices bactériennes en dehors du contexte des infections à *C. burnetii*.

Bibliography

Abnave, P., Muracciole, X., & Ghigo, E. (2017). *Coxiella burnetii* lipopolysaccharide: What do we know? In *International Journal of Molecular Sciences* (Vol. 18, Issue 12). MDPI AG.

Agranoff, B. W., Benjamin, J. A., & Hajra, A. K. (1970). Biosynthesis of Phosphatidylinositol. *Annals of the New York Academy of Sciences*, *165*(2 New Dimension), 755–760.

Aguilera, M., Salinas, R., Rosales, E., Carminati, S., Colombo, M. I., & Berón, W. (2009). Actin dynamics and Rho GTPases regulate the size and formation of parasitophorous vacuoles containing Coxiella burnetii. *Infection and Immunity*, *77*(10), 4609–4620.

Akira, S., & Takeda, K. (2004). Toll-like receptor signalling. In *Nature Reviews Immunology* (Vol. 4, Issue 7, pp. 499–511). Nature Publishing Group.

Akira, S., Uematsu, S., & Takeuchi, O. (2006). Pathogen recognition and innate immunity. In *Cell* (Vol. 124, Issue 4, pp. 783–801). Cell.

Amano, K. I., & Williams, J. C. (1984). Chemical and immunological characterization of lipopolysaccharides from phase I and phase II *Coxiella burnetii*. *Journal of Bacteriology*, *160*(3), 994–1002.

Amit, S., Shinar, S., Halutz, O., Atiya-Nasagi, Y., & Giladi, M. (2014). Suspected person-to-person transmission of Q fever among hospitalized pregnant women. *Clinical Infectious Diseases*, *58*(11).

Ammerdorffer, A., Schoffelen, T., Gresnigt, M. S., Oosting, M., Den Brok, M. H., Abdollahi-Roodsaz, S., Kanneganti, T. D., De Jong, D. J., Van Deuren, M., Roest, H. J., Rebel, J. M., Netea, M. G., Joosten, L. A. B., & Sprong, T. (2015). Recognition of *Coxiella burnetii* by toll-like receptors and nucleotide-binding oligomerization domain-like receptors. *Journal of Infectious Diseases*, *211*(6), 978–987.

Anderson, A. D., Smoak, B., Shuping, E., Ockenhouse, C., & Petruccelli, B. (2005). Q fever and the US military [7]. In *Emerging Infectious Diseases* (Vol. 11, Issue 8, pp. 1320–1322). Centers for Disease Control and Prevention (CDC).

Angot, A., Vergunst, A., Genin, S., & Peeters, N. (2007). Exploitation of eukaryotic ubiquitin signaling pathways by effectors translocated by bacterial type III and type IV secretion systems. In *PLoS Pathogens* (Vol. 3, Issue 1, pp. 0001–0013). Public Library of Science.

Ashida, H., Mimuro, H., Ogawa, M., Kobayashi, T., Sanada, T., Kim, M., & Sasakawa, C. (2011). Cell death and infection: A double-edged sword for host and pathogen survival. In *Journal of Cell Biology* (Vol. 195, Issue 6, pp. 931–942). The Rockefeller University Press.

Asrat, S., Davis, K. M., & Isberg, R. R. (2015). Modulation of the host innate immune and inflammatory response by translocated bacterial proteins. *Cellular Microbiology*, *17*(6), 785–795.

Audas, T. E., Jacob, M. D., & Lee, S. (2012). Immobilization of Proteins in the Nucleolus by

Ribosomal Intergenic Spacer Noncoding RNA. *Molecular Cell*, *45*(2), 147–157.

Babudieri, B., & Moscovici, C. (1952). Experimental and natural infection of birds by *Coxiella burnetii*. *Nature*, *169*(4292), 195–196.

Baca, O. G., Li, Y. P., & Kumar, H. (1994). Survival of the Q fever agent *Coxiella burnetii* in the phagolysosome. *Trends in Microbiology*, *2*(12), 476–480.

Baker, P. J., Boucher, D., Bierschenk, D., Tebartz, C., Whitney, P. G., D'Silva, D. B., Tanzer, M. C., Monteleone, M., Robertson, A. A. B., Cooper, M. A., Alvarez-Diaz, S., Herold, M. J., Bedoui, S., Schroder, K., & Masters, S. L. (2015). NLRP3 inflammasome activation downstream of cytoplasmic LPS recognition by both caspase-4 and caspase-5. *European Journal of Immunology*, *45*(10), 2918–2926.

Balla, T., Szentpetery, Z., & Kim, Y. J. (2009). Phosphoinositide signaling: new tools and insights. In *Physiology* (Vol. 24, Issue 4, pp. 231–244).

Bang, S., Min, C. K., Ha, N. Y., Choi, M. S., Kim, I. S., Kim, Y. S., & Cho, N. H. (2016). Inhibition of eukaryotic translation by tetratricopeptide-repeat proteins of *Orientia tsutsugamushi*. *Journal of Microbiology*, *54*(2), 136–144.

Barton, G. M., & Kagan, J. C. (2009). A cell biological view of toll-like receptor function: Regulation through compartmentalization. In *Nature Reviews Immunology* (Vol. 9, Issue 8, pp. 535–541). Nat Rev Immunol.

Bastos, R. G., Howard, Z. P., Hiroyasu, A., & Goodman, A. G. (2017). Host and bacterial factors control susceptibility of *Drosophila melanogaster* to *Coxiella burnetii* infection. *Infection and Immunity*, *85*(7).

Battisti, J. M., Watson, L. A., Naung, M. T., Drobish, A. M., Voronina, E., & Minnick, M. F. (2017). Analysis of the *Caenorhabditis elegans* innate immune response to *Coxiella burnetii*. *Innate Immunity*, *23*(2), 111–127.

Beare, P. A., Gilk, S. D., Larson, C. L., Hill, J., Stead, C. M., Omsland, A., Cockrell, D. C., Howe, D., Voth, D. E., & Heinzen, R. A. (2011). Dot/Icm type IVB secretion system requirements for *Coxiella burnetii* growth in human macrophages. *MBio*, *2*(4).

Beare, P. A., Jeffrey, B. M., Long, C. M., Martens, C. M., & Heinzen, R. A. (2018). Genetic mechanisms of *Coxiella burnetii* lipopolysaccharide phase variation. *PLoS Pathogens*, *14*(2), 1–31.

Beare, P. A., Jeffrey, B. M., Martens, C. A., & Heinzen, R. A. (2017). Draft genome sequences of the avirulent *Coxiella burnetii* Dugway 7D77-80 and Dugway 7E65-68 strains isolated from rodents in Dugway, Utah. *Genome Announcements*, *5*(39).

Beare, P. A., Larson, C. L., Gilk, S. D., & Heinzen, R. A. (2012). Two systems for targeted gene deletion in *Coxiella burnetii*. *Applied and Environmental Microbiology*, *78*(13), 4580–4589.

Beare, P. A., Samuel, J. E., Howe, D., Virtaneva, K., Porcella, S. F., & Heinzen, R. A. (2006).

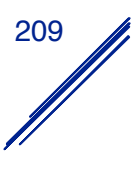

Genetic diversity of the Q fever agent, *Coxiella burnetii*, assessed by microarray-based whole-genome comparisons. *Journal of Bacteriology*, *188*(7), 2309–2324.

Beare, P. A., Sandoz, K. M., Larson, C. L., Howe, D., Kronmiller, B., & Heinzen, R. A. (2014). Essential role for the response regulator PmrA in *Coxiella burnetii* type 4B secretion and colonization of mammalian host cells. *Journal of Bacteriology*, *196*(11), 1925–1940.

Beare, P. A., Unsworth, N., Andoh, M., Voth, D. E., Omsland, A., Gilk, S. D., Williams, K. P., Sobral, B. W., Kupko, J. J., Porcella, S. F., Samuel, J. E., & Heinzen, R. A. (2009). Comparative genomics reveal extensive transposon-mediated genomic plasticity and diversity among potential effector proteins within the genus *Coxiella*. *Infection and Immunity*, *77*(2), 642–656.

Beatty, W. L. (2006). Trafficking from CD63-positive late endocytic multivesicular bodies is essential for intracellular development of *Chlamydia trachomatis*. *Journal of Cell Science*, *119*(2), 350–359.

Beatty, W. L. (2008). Late endocytic multivesicular bodies intersect the chlamydial inclusion in the absence of CD63. *Infection and Immunity*, *76*(7), 2872–2881.

Behnia, R., & Munro, S. (2005). Organelle identity and the signposts for membrane traffic. In *Nature* (Vol. 438, Issue 7068, pp. 597–604). Nature Publishing Group.

Benoit, M., Barbarat, B., Bernard, A., Olive, D., & Mege, J. L. (2008). *Coxiella burnetii*, the agent of Q fever, stimulates an atypical M2 activation program in human macrophages. *European Journal of Immunology*, *38*(4), 1065–1070.

Beresford, N., Patel, S., Armstrong, J., Szöor, B., Fordham-Skelton, A. P. A. P., & Tabernero, L. (2007). MptpB, a virulence factor from *Mycobacterium tuberculosis*, exhibits triple-specificity phosphatase activity. *Biochemical Journal*, *406*(3), 527–527.

Bergsbaken, T., Fink, S. L., & Cookson, B. T. (2009). Pyroptosis: Host cell death and inflammation. In *Nature Reviews Microbiology* (Vol. 7, Issue 2, pp. 99–109). Nature Publishing Group.

Berón, W., Gutierrez, M. G., Rabinovitch, M., & Colombo, M. I. (2002). *Coxiella burnetii* localizes in a Rab7-labeled compartment with autophagic characteristics. *Infection and Immunity*, *70*(10), 5816–5821.

Bishop, N., & Woodman, P. (2000). ATPase-defective mammalian VPS4 localizes to aberrant endosomes and impairs cholesterol trafficking. *Molecular Biology of the Cell*, *11*(1), 227–239.

Bisle, S., Klingenbeck, L., Borges, V., Sobotta, K., Schulze-Luehrmann, J., Menge, C., Heydel, C., Gomes, J. P., & Lührmann, A. (2016). The inhibition of the apoptosis pathway by the *Coxiella burnetii* effector protein CaeA requires the EK repetition motif, but is independent of survivin. *Virulence*, *7*(4), 400–412.

Bissig, C., & Gruenberg, J. (2013). Lipid sorting and multivesicular endosome biogenesis. *Cold*

Spring Harbor Perspectives in Biology, *5*(10), 1–18.

Bleves, S., Galán, J. E., & Llosa, M. (2020). Bacterial injection machines: Evolutionary diverse but functionally convergent. *Cellular Microbiology*, *22*(5).

Bobbins, F. C., Gauld, R. L., & Warner, F. B. (1946). Q fever in the mediterranean area: Report of its occurrence in allied troops: II. Epidemiology. *American Journal of Epidemiology*, *44*(1), 23–50.

Boisvert, F. M., Van Koningsbruggen, S., Navascués, J., & Lamond, A. I. (2007). The multifunctional nucleolus. In *Nature Reviews Molecular Cell Biology* (Vol. 8, Issue 7, pp. 574–585). Nature Publishing Group.

Bradley, W. P., Boyer, M. A., Nguyen, H. T., Birdwell, L. D., Yu, J., Ribeiro, J. M., Weiss, S. R., Zamboni, D. S., Roy, C. R., & Shin, S. (2016). Primary role for Toll-like receptor-driven tumor necrosis factor rather than cytosolic immune detection in restricting *Coxiella burnetii* phase II replication within mouse macrophages. *Infection and Immunity*, *84*(4), 998–1015.

Brann, K. R., Fullerton, M. S., & Voth, D. E. (2020). *Coxiella burnetii* requires host eukaryotic initiation factor 2α activity for efficient intracellular replication. *Infection and Immunity*, *88*(7).

Brombacher, E., Urwyler, S., Ragaz, C., Weber, S. S., Kami, K., Overduin, M., & Hilbi, H. (2009). Rab1 guanine nucleotide exchange factor SidM is a major phosphatidylinositol 4-phosphate-binding effector protein of *Legionella pneumophila*. *Journal of Biological Chemistry*, *284*(8), 4846–4856.

Brooke, R. J., Kretzschmar, M. E. E., Mutters, N. T., & Teunis, P. F. (2013). Human dose response relation for airborne exposure to *Coxiella burnetii*. *BMC Infectious Diseases*, *13*(1), 488.

Broz, P. (2019). Recognition of Intracellular Bacteria by Inflammasomes. *Bacteria and Intracellularity*, *7*(2), 301–313.

Burette, M., Allombert, J., Lambou, K., Maarifi, G., Nisole, S., Di Russo Case, E., Blanchet, F. P., Hassen-Khodja, C., Cabantous, S., Samuel, J., Martinez, E., & Bonazzi, M. (2020). Modulation of innate immune signaling by a *Coxiella burnetii* eukaryotic-like effector protein. *Proceedings of the National Academy of Sciences of the United States of America*, *117*(24), 13708–13718.

Burette, M., & Bonazzi, M. (2020). From neglected to dissected: How technological advances are leading the way to the study of *Coxiella burnetii* pathogenesis. *Cellular Microbiology*, *22*(4).

Burnet, F. M., & Freeman, M. (1937). Experimental Studies on the Virus of “Q” Fever. *Medical Journal of Australia*, *2*(8), 299–305.

Buschman, M. D., Xing, M., & Field, S. J. (2015). The GOLPH3 pathway regulates Golgi shape

and function and is activated by DNA damage. *Frontiers in Neuroscience*, *9*(OCT), 362.

Bushweller, J. H. (2019). Targeting transcription factors in cancer — from undruggable to reality. In *Nature Reviews Cancer* (Vol. 19, Issue 11, pp. 611–624). Nature Publishing Group.

Campoy, E. M., Mansilla, M. E., & Colombo, M. I. (2013). Endocytic SNAREs are involved in optimal *Coxiella burnetii* vacuole development. *Cellular Microbiology*, *15*(6), 922–941.

Campoy, E. M., Martín Zoppino, F. C., & Colombo, M. I. (2011). The early secretory pathway contributes to the growth of the *Coxiella*-replicative niche. *Infection and Immunity*, *79*(1), 402–413.

Capo, C, Lindberg, F. P., Meconi, S., Zaffran, Y., Tardei, G., Brown, E. J., Raoult, D., & Mege, J. L. (1999). Subversion of monocyte functions by *Coxiella burnetii*: impairment of the cross-talk between alphavbeta3 integrin and CR3. *Journal of Immunology (Baltimore, Md. : 1950)*, *163*(11), 6078–6085.

Capo, Christian, Moynault, A., Collette, Y., Olive, D., Brown, E. J., Raoult, D., & Mege, J.-L. (2003). *Coxiella burnetii* Avoids Macrophage Phagocytosis by Interfering with Spatial Distribution of Complement Receptor 3 . *The Journal of Immunology*, *170*(8), 4217–4225.

Carey, K. L., Newton, H. J., Lührmann, A., & Roy, C. R. (2011). The *Coxiella burnetii* Dot/Icm system delivers a unique repertoire of type IV effectors into host cells and is required for intracellular replication. *PLoS Pathogens*, *7*(5).

Casares, D., Escribá, P. V., & Rosselló, C. A. (2019). Membrane lipid composition: Effect on membrane and organelle structure, function and compartmentalization and therapeutic avenues. *International Journal of Molecular Sciences*, *20*(9).

Case, E. D. R., & Samuel, J. E. (2016). Contrasting Lifestyles Within the Host Cell. *Microbiology Spectrum*, *4*(1).

Chen, C., Banga, S., Mertens, K., Weber, M. M., Gorbaslieva, I., Tan, Y., Luo, Z. Q., & Samuel, J. E. (2010). Large-scale identification and translocation of type IV secretion substrates by *Coxiella burnetii*. *Proceedings of the National Academy of Sciences of the United States of America*, *107*(50), 21755–21760.

Chen, J., & Chen, Z. J. (2018). PtdIns4P on dispersed trans-Golgi network mediates NLRP3 inflammasome activation. *Nature*, *564*(7734), 71–76.

Cheng, X., Collins, R. E., & Zhang, X. (2005). Structural and sequence motifs of protein (histone) methylation enzymes. In *Annual Review of Biophysics and Biomolecular Structure* (Vol. 34, pp. 267–294). NIH Public Access.

Cherla, R., Zhang, Y., Ledbetter, L., & Zhang, G. (2018). *Coxiella burnetii* inhibits neutrophil apoptosis by exploiting survival pathways and antiapoptotic protein Mcl-1. *Infection and Immunity*, *86*(4), e00504-17.

Chetrit, D., Hu, B., Christie, P. J., Roy, C. R., & Liu, J. (2018). A unique cytoplasmic ATPase

complex defines the *Legionella pneumophila* type IV secretion channel. *Nature Microbiology*, *3*(6), 678–686.

Chevallier, J., Chamoun, Z., Jiang, G., Prestwich, G., Sakai, N., Matile, S., Parton, R. G., & Gruenberg, J. (2008). Lysobisphosphatidic acid controls endosomal cholesterol levels. *Journal of Biological Chemistry*, *283*(41), 27871–27880.

Christopher, G. W., Cieslak, T. J., Pavlin, J. A., & Eitzen, E. M. (1997). Biological warfare: A historical perspective. *Journal of the American Medical Association*, *278*(5), 412–417.

Ciszek-Lenda, M., Strus, M., Walczewska, M., Majka, G., Machul-Żwirbla, A., Mikołajczyk, D., Górska, S., Gamian, A., Chain, B., & Marcinkiewicz, J. (2019). *Pseudomonas aeruginosa* biofilm is a potent inducer of phagocyte hyperinflammation. *Inflammation Research*, *68*(5), 397–413.

Clarke, P. R., & Zhang, C. (2008). Spatial and temporal coordination of mitosis by Ran GTPase. *Nature Reviews Molecular Cell Biology*, *9*(6), 464–477.

Clemente, T. M., Mulye, M., Justis, A. V., Nallandhighal, S., Tran, T. M., & Gilk, S. D. (2018). *Coxiella burnetii* blocks intracellular interleukin-17 signaling in macrophages. *Infection and Immunity*, *86*(10), 1–15.

Coleman, S. A., Fischer, E. R., Howe, D., Mead, D. J., & Heinzen, R. A. (2004). Temporal analysis of *Coxiella burnetii* morphological differentiation. *Journal of Bacteriology*, *186*(21), 7344–7352.

Conti, F., Boucherit, N., Baldassarre, V., Trouplin, V., Toman, R., Mottola, G., Mege, J. L., & Ghigo, E. (2014). *Coxiella burnetii* lipopolysaccharide blocks p38a- MAPK activation through the disruption of TLR-2 and TLR-4 association. *Frontiers in Cellular and Infection Microbiology*, *4*(DEC), 182.

Cordsmeier, A., Wagner, N., Lührmann, A., & Berens, C. (2019). Defying death – how *Coxiella burnetii* copes with intentional host cell suicide. In *Yale Journal of Biology and Medicine* (Vol. 92, Issue 4, pp. 619–628). Yale Journal of Biology and Medicine Inc.

Cunha, L. D., Ribeiro, J. M., Fernandes, T. D., Massis, L. M., Khoo, C. A., Moffatt, J. H., Newton, H. J., Roy, C. R., & Zamboni, D. S. (2015). Inhibition of inflammasome activation by *Coxiella burnetii* type IV secretion system effector IcaA. *Nature Communications*, *6*.

D'Amato, F., Eldin, C., Georgiades, K., Edouard, S., Delerce, J., Labas, N., & Raoult, D. (2015). Loss of TSS1 in hypervirulent *Coxiella burnetii* 175, the causative agent of Q fever in French Guiana. *Comparative Immunology, Microbiology and Infectious Diseases*, *41*, 35–41.

D'Amato, F., Rouli, L., Edouard, S., Tyczka, J., Million, M., Robert, C., Nguyen, T. T., & Raoult, D. (2014). The genome of *Coxiella burnetii* Z3055, a clone linked to the Netherlands Q fever outbreaks, provides evidence for the role of drift in the emergence of epidemic clones. *Comparative Immunology, Microbiology and Infectious Diseases*, *37*(5–6), 281–

288.

D'Angelo, G., Vicinanza, M., Di Campli, A., & De Matteis, M. A. (2008). The multiple roles of PtdIns(4)P - Not just the precursor of PtdIns(4,5)P2. *Journal of Cell Science*, *121*(12), 1955–1963.

da Costa, L. S., Outlioua, A., Anginot, A., Akarid, K., & Arnoult, D. (2019). RNA viruses promote activation of the NLRP3 inflammasome through cytopathogenic effect-induced potassium efflux. *Cell Death and Disease*, *10*(5), 1–15.

Davis, G. E., Cox, H. R., Parker, R. R., & Dyer, R. E. (1938). A Filter-Passing Infectious Agent Isolated from Ticks. *Public Health Reports (1896-1970)*, *53*(52), 2259.

de Bruin, A., de Groot, A., de Heer, L., Bok, J., Wielinga, P. R., Hamans, M., van Rotterdam, B. J., & Janse, I. (2011). Detection of *Coxiella burnetii* in complex matrices by using multiplex quantitative PCR during a major Q fever outbreak in the Netherlands. *Applied and Environmental Microbiology*, *77*(18), 6516–6523.

De Felipe, K. S., Pampou, S., Jovanovic, O. S., Pericone, C. D., Ye, S. F., Kalachikov, S., & Shuman, H. A. (2005). Evidence for acquisition of *Legionella* type IV secretion substrates via interdomain horizontal gene transfer. *Journal of Bacteriology*, *187*(22), 7716–7726.

de la Roche, M., Hamilton, C., Mortensen, R., Jeyaprakash, A. A., Ghosh, S., & Anand, P. K. (2018). Trafficking of cholesterol to the ER is required for NLRP3 inflammasome activation. *Journal of Cell Biology*, *217*(10), 3560–3576.

Dean, P., Scott, J. A., Knox, A. A., Quitard, S., Watkins, N. J., & Kenny, B. (2010). The enteropathogenic *E. coli* effector EspF targets and disrupts the nucleolus by a process regulated by mitochondrial dysfunction. *PLoS Pathogens*, *6*(6), e1000961.

Del Campo, C. M., Mishra, A. K., Wang, Y. H., Roy, C. R., Janmey, P. A., & Lambright, D. G. (2014). Structural basis for PI(4)P-specific membrane recruitment of the *Legionella pneumophila* effector DrrA/SidM. *Structure*, *22*(3), 397–408.

Derrick, E. (1939). *Rickettsia burneti*: the Cause of" Q" Fever. *Medical Journal of Australia*, *1*(14).

Derrick, E. H. (1937). "Q" Fever, a New Fever Entity: Clinical Features, Diagnosis and Laboratory Investigation. *Medical Journal of Australia*, *2*(8), 281–299.

Di Paolo, G., & De Camilli, P. (2006). Phosphoinositides in cell regulation and membrane dynamics. In *Nature* (Vol. 443, Issue 7112, pp. 651–657). Nature Publishing Group.

Dixit, E., & Kagan, J. C. (2013). Intracellular Pathogen Detection by RIG-I-Like Receptors. In *Advances in Immunology* (Vol. 117, pp. 99–125). Academic Press Inc.

Doherty, G. J., & McMahon, H. T. (2009). Mechanisms of endocytosis. *Annual Review of Biochemistry*, *78*(1), 857–902.

Dragan, A. L., & Voth, D. E. (2020). *Coxiella burnetii*: international pathogen of mystery. In *Microbes and Infection* (Vol. 22, Issue 3, pp. 100–110). Elsevier Masson SAS.

Duden, R. (2003). ER-to-Golgi transport: COP I and COP II function. In *Molecular Membrane Biology* (Vol. 20, Issue 3, pp. 197–207). Taylor & Francis.

Dupuis, G., Peter, O., Peacock, M., Burgdorfer, W., & Haller, E. (1985). Immunoglobulin responses in acute Q fever. *Journal of Clinical Microbiology*, *22*(4), 484–487.

Duron, O., Noël, V., McCoy, K. D., Bonazzi, M., Sidi-Boumedine, K., Morel, O., Vavre, F., Zenner, L., Jourdain, E., Durand, P., Arnathau, C., Renaud, F., Trape, J. F., Biguezoton, A. S., Cremaschi, J., Dietrich, M., Léger, E., Appelgren, A., Dupraz, M., … Chevillon, C. (2015). The Recent Evolution of a Maternally-Inherited Endosymbiont of Ticks Led to the Emergence of the Q Fever Pathogen, *Coxiella burnetii. PLoS Pathogens*, *11*(5), 1–23.

Duron, O., Sidi-Boumedine, K., Rousset, E., Moutailler, S., & Jourdain, E. (2015). The Importance of Ticks in Q Fever Transmission: What Has (and Has Not) Been Demonstrated? In *Trends in Parasitology* (Vol. 31, Issue 11, pp. 536–552). Elsevier Ltd.

Ebner, M., Koch, P. A., & Haucke, V. (2019). Phosphoinositides in the control of lysosome function and homeostasis. *Biochemical Society Transactions*, *47*(4), 1173–1185.

Eckart, R. A., Bisle, S., Schulze-Luehrmann, J., Wittmann, I., Jantsch, J., Schmid, B., Berens, C., & Lührmann, A. (2014). Antiapoptotic activity of *Coxiella burnetii* effector protein AnkG is controlled by p32-dependent trafficking. *Infection and Immunity*, *82*(7), 2763–2771.

Eldin, C., Mélenotte, C., Mediannikov, O., Ghigo, E., Million, M., Edouard, S., Mege, J. L., Maurin, M., & Raoult, D. (2017). From Q fever to *Coxiella burnetii* infection: A paradigm change. In *Clinical Microbiology Reviews* (Vol. 30, Issue 1, pp. 115–190). American Society for Microbiology.

Escárcega, R. O., Fuentes-Alexandro, S., García-Carrasco, M., Gatica, A., & Zamora, A. (2007). The Transcription Factor Nuclear Factor-kappa B and Cancer. *Clinical Oncology*, *19*(2), 154–161.

Evans, S. M., Rodino, K. G., Adcox, H. E., & Carlyon, J. A. (2018). *Orientia tsutsugamushi* uses two Ank effectors to modulate NF-κB p65 nuclear transport and inhibit NF-κB transcriptional activation. *PLoS Pathogens*, *14*(5), e1007023.

Fay, N., & Panté, N. (2015). Nuclear entry of DNA viruses. In *Frontiers in Microbiology* (Vol. 6, Issue MAY). Frontiers Media S.A.

Fishbein, D. B., & Raoult, D. (1992). A cluster of *Coxiella burnetii* infections associated with exposure to vaccinated goats and their unpasteurized dairy products. *American Journal of Tropical Medicine and Hygiene*, *47*(1 II SUPPL.), 35–40.

Franchi, L., Warner, N., Viani, K., & Nuñez, G. (2009). Function of Nod-like receptors in microbial recognition and host defense. In *Immunological Reviews* (Vol. 227, Issue 1, pp. 106–128). Immunol Rev.

Fuche, F., Vianney, A., Andrea, C., Doublet, P., & Gilbert, C. (2015). Functional type 1 secretion system involved in *Legionella pneumophila* virulence. *Journal of Bacteriology*,

197(3), 563–571.

Funato, K., Riezman, H., & Muñiz, M. (2020). Vesicular and non-vesicular lipid export from the ER to the secretory pathway. In *Biochimica et Biophysica Acta - Molecular and Cell Biology of Lipids* (Vol. 1865, Issue 1, p. 158453). Elsevier B.V.

Funderburk, S. F., Wang, Q. J., & Yue, Z. (2010). The Beclin 1-VPS34 complex - at the crossroads of autophagy and beyond. In *Trends in Cell Biology* (Vol. 20, Issue 6, pp. 355–362). Trends Cell Biol.

Gaspard, G. J., & McMaster, C. R. (2015). Cardiolipin metabolism and its causal role in the etiology of the inherited cardiomyopathy Barth syndrome. In *Chemistry and Physics of Lipids* (Vol. 193, pp. 1–10). Elsevier Ireland Ltd.

Ghosal, D., Jeong, K. C., Chang, Y. W., Gyore, J., Teng, L., Gardner, A., Vogel, J. P., & Jensen, G. J. (2019). Molecular architecture, polar targeting and biogenesis of the Legionella Dot/Icm T4SS. *Nature Microbiology*, *4*(7), 1173–1182.

Gilk, S. D., Cockrell, D. C., Luterbach, C., Hansen, B., Knodler, L. A., Ibarra, J. A., Steele-Mortimer, O., & Heinzen, R. A. (2013). Bacterial Colonization of Host Cells in the Absence of Cholesterol. *PLoS Pathogens*, *9*(1).

Gillooly, D. J., Morrow, I. C., Lindsay, M., Gould, R., Bryant, N. J., Gaullier, J. M., Parton, R. G., & Stenmark, H. (2000). Localization of phosphatidylinositol 3-phosphate in yeast and mammalian cells. *EMBO Journal*, *19*(17), 4577–4588.

Glazunova, O., Roux, V., Freylikman, O., Sekeyova, Z., Fournous, G., Tyczka, J., Tokarevich, N., Kovacava, E., Marrie, T. J., & Raoult, D. (2005). *Coxiella burnetii* genotyping. *Emerging Infectious Diseases*, *11*(8), 1211–1217.

Gomez-Navarro, N., & Miller, E. (2016). Protein sorting at the ER-Golgi interface. *Journal of Cell Biology*, *215*(6), 769–778.

González-Barrio, D., & Ruiz-Fons, F. (2019). *Coxiella burnetii* in wild mammals: A systematic review. In *Transboundary and Emerging Diseases* (Vol. 66, Issue 2, pp. 662–671). Blackwell Publishing Ltd.

Göser, V., Kehl, A., Röder, J., & Hensel, M. (2020). Role of the ESCRT-III complex in controlling integrity of the *Salmonella*-containing vacuole. *Cellular Microbiology*, *22*(6).

Goud, B., Picas, L., & Gaits-Iacovoni, F. (2016). The emerging role of phosphoinositide clustering in intracellular trafficking and signal transduction. *F1000Research*, *5*(0), 422.

Gouriet, F., Fenollar, F., Patrice, J. Y., Drancourt, M., & Raoult, D. (2005). Use of shell-vial cell culture assay for isolation of bacteria from clinical specimens: 13 Years of experience. *Journal of Clinical Microbiology*, *43*(10), 4993–5002.

Graham, J. G., Macdonald, L. J., Hussain, S. K., Sharma, U. M., Kurten, R. C., & Voth, D. E. (2013). Virulent *Coxiella burnetii* pathotypes productively infect primary human alveolar macrophages. *Cellular Microbiology*, *15*(6), 1012–1025.

Graham, J. G., Winchell, C. G., Sharma, U. M., & Voth, D. E. (2015). Identification of ElpA, a *Coxiella burnetii* pathotype-specific Dot/Icm type IV secretion system substrate. *Infection and Immunity*, *83*(3), 1190–1198.

Gulati, A., Shukla, R., & Mukhopadhaya, A. (2019). *Salmonella* Effector SteA Suppresses Proinflammatory Responses of the Host by Interfering With IκB Degradation. *Frontiers in Immunology*, *10*.

Gutierrez, M. G., Vázquez, C. L., Munafó, D. B., Zoppino, F. C. M., Berón, W., Rabinovitch, M., & Colombo, M. I. (2005). Autophagy induction favours the generation and maturation of the *Coxiella*-replicative vacuoles. *Cellular Microbiology*, *7*(7), 981–993.

Guzmán-Herrador, D. L., Steiner, S., Alperi, A., González-Prieto, C., Roy, C. R., & Llosa, M. (2017). DNA delivery and genomic integration into mammalian target cells through Type IV A and B secretion systems of human pathogens. *Frontiers in Microbiology*, *8*(AUG), 1503.

Hackstadt, T. (1996). Biosafety concerns and *Coxiella burnetii*. *Trends in Microbiology*, *4*(9), 341–342.

Hackstadt, T., Peacock, M. G., Hitchcock, P. J., & Cole, R. L. (1985). Lipopolysaccharide variation in *Coxiella burnetii:* Intrastrain heterogeneity in structure and antigenicity. *Infection and Immunity*, *48*(2), 359–365.

Hackstadt, Ted. (1990). The Role of Lipopolysaccharides in the Virulence of *Coxiella burnetii. Annals of the New York Academy of Sciences*, *590*(1), 27–32.

Han, Y. M., Koh, J., Kim, J. W., Lee, C., Koh, S. J., Kim, B. G., Lee, K. L., Im, J. P., & Kim, J. S. (2017). NF-kappa B activation correlates with disease phenotype in Crohn's disease. *PLoS ONE*, *12*(7).

Hannun, Y. A., & Obeid, L. M. (2018). Sphingolipids and their metabolism in physiology and disease. In *Nature Reviews Molecular Cell Biology* (Vol. 19, Issue 3, pp. 175–191). Nature Publishing Group.

Harayama, T., & Riezman, H. (2018). Understanding the diversity of membrane lipid composition. *Nature Reviews Molecular Cell Biology*, *19*(5), 281–296.

Hartzell, J. D., Wood-Morris, R. N., Martinez, L. J., & Trotta, R. F. (2008). Q fever: Epidemiology, diagnosis, and treatment. In *Mayo Clinic Proceedings* (Vol. 83, Issue 5, pp. 574–579). Elsevier Ltd.

Hasegawa, J., Strunk, B. S., & Weisman, L. S. (2017). PI5P and PI(3,5)P2: Minor, but essential phosphoinositides. *Cell Structure and Function*, *42*(1), 49–60.

Haucke, V., & Di Paolo, G. (2007). Lipids and lipid modifications in the regulation of membrane traffic. In *Current Opinion in Cell Biology* (Vol. 19, Issue 4, pp. 426–435). NIH Public Access.

Hayashi, F., Smith, K. D., Ozinsky, A., Hawn, T. R., Yi, E. C., Goodlett, D. R., Eng, J. K., Akira,

S., Underhill, D. M., & Aderem, A. (2001). The innate immune response to bacterial flagellin is mediated by Toll-like receptor 5. *Nature*, *410*(6832), 1099–1103.

Hedges, J. F., Robison, A., Kimmel, E., Christensen, K., Lucas, E., Ramstead, A., & Jutila, M. A. (2016). Type I interferon counters or promotes *Coxiella burnetii* replication dependent on tissue. *Infection and Immunity*, *84*(6), 1815–1825.

Heil, F., Hemmi, H., Hochrein, H., Ampenberger, F., Kirschning, C., Akira, S., Lipford, G., Wagner, H., & Bauer, S. (2004). Species-Specific Recognition of Single-Stranded RNA via Till-like Receptor 7 and 8. *Science*, *303*(5663), 1526–1529.

Hemmi, H., Takeuchi, O., Kawai, T., Kaisho, T., Sato, S., Sanjo, H., Matsumoto, M., Hoshino, K., Wagner, H., Takeda, K., & Akira, S. (2000). A Toll-like receptor recognizes bacterial DNA. *Nature*, *408*(6813), 740–745.

Hemsley, C. M., O'Neill, P. A., Essex-Lopresti, A., Norville, I. H., Atkins, T. P., & Titball, R. W. (2019). Extensive genome analysis of *Coxiella burnetii* reveals limited evolution within genomic groups. *BMC Genomics*, *20*(1), 441.

Hendrix, L. R., Samuel, J. E., & Mallavia, L. P. (1991). Differentiation of *Coxiella burnetii* isolates by analysis of restriction-endonuclease-digested DNA separated by SDS-PAGE. In *Journal of General Microbiology* (Vol. 137, Issue 2).

Hilbi, H. (2006). Modulation of phosphoinositide metabolism by pathogenic bacteria. *Cellular Microbiology*, *8*(11), 1697–1706.

Hilbi, H., Weber, S., & Finsel, I. (2011). Anchors for effectors: Subversion of phosphoinositide lipids by *Legionella*. *Frontiers in Microbiology*, *2*(APR).

Hilbink, F., Penrose, M., Ko Vacova, E., & Kazar, J. (1993). Q fever is absent from new zealand. In *International Journal of Epidemiology* (Vol. 22, Issue 5).

Honstettre, A., Ghigo, E., Moynault, A., Capo, C., Toman, R., Akira, S., Takeuchi, O., Lepidi, H., Raoult, D., & Mege, J.-L. (2004). Lipopolysaccharide from *Coxiella burnetii* Is Involved in Bacterial Phagocytosis, Filamentous Actin Reorganization, and Inflammatory Responses through Toll-Like Receptor 4 . *The Journal of Immunology*, *172*(6), 3695–3703.

Hoover, T. A., Culp, D. W., Vodkin, M. H., Williams, J. C., & Thompson, H. A. (2002). Chromosomal DNA deletions explain phenotypic characteristics of two antigenic variants, phase II and RSA 514 (crazy), of the *Coxiella burnetii* Nine Mile strain. *Infection and Immunity*, *70*(12), 6726–6733.

Hornstra, H. M., Priestley, R. A., Georgia, S. M., Kachur, S., Birdsell, D. N., Hilsabeck, R., Gates, L. T., Samuel, J. E., Heinzen, R. A., Kersh, G. J., Keim, P., Massung, R. F., & Pearson, T. (2011). Rapid typing of *Coxiella burnetii*. *PLoS ONE*, *6*(11), e26201–e26201.

Howe, D., & Heinzen, R. A. (2006). *Coxiella burnetii* inhabits a cholesterol-rich vacuole and influences cellular cholesterol metabolism. *Cellular Microbiology*, *8*(3), 496–507.

Howe, D., Melnicáková, J., Barák, I., & Heinzen, R. A. (2003). Maturation of *Coxiella burnetii* parasitophorous vacuole requires bacterial protein synthesis but not replication. *Cellular Microbiology*, *5*(7), 469–480.

Howe, D., Shannon, J. G., Winfree, S., Dorward, D. W., & Heinzen, R. A. (2010). *Coxiella burnetii* phase I and II variants replicate with similar kinetics in degradative phagolysosome-like compartments of human macrophages. *Infection and Immunity*, *78*(8), 3465–3474.

Hsu, F. S., Luo, X., Qiu, J., Teng, Y. Bin, Jin, J., Smolka, M. B., Luo, Z. Q., & Mao, Y. (2014). The *Legionella* effector SidC defines a unique family of ubiquitin ligases important for bacterial phagosomal remodeling. *Proceedings of the National Academy of Sciences of the United States of America*, *111*(29), 10538–10543.

Hsu, F. S., Zhu, W., Brennan, L., Tao, L., Luo, Z. Q., & Mao, Y. (2012). Structural basis for substrate recognition by a unique *Legionella* phosphoinositide phosphatase. *Proceedings of the National Academy of Sciences of the United States of America*, *109*(34), 13567–13572.

Hu, B., Khara, P., Song, L., Lin, A. S., Frick-Cheng, A. E., Harvey, M. L., Cover, T. L., & Christie, P. J. (2019). In situ molecular architecture of the *Helicobacter pylori* cag type IV secretion system. *MBio*, *10*(3).

Huang, L., Boyd, D., Amyot, W. M., Hempstead, A. D., Luo, Z. Q., O'Connor, T. J., Chen, C., Machner, M., Montminy, T., & Isberg, R. R. (2011). The E Block motif is associated with *Legionella pneumophila* translocated substrates. *Cellular Microbiology*, *13*(2), 227–245.

Hubber, A., Arasaki, K., Nakatsu, F., Hardiman, C., Lambright, D., De Camilli, P., Nagai, H., & Roy, C. R. (2014). The Machinery at Endoplasmic Reticulum-Plasma Membrane Contact Sites Contributes to Spatial Regulation of Multiple *Legionella* Effector Proteins. *PLoS Pathogens*, *10*(7).

Hurley, J. H. (2015). ESCRT s are everywhere . *The EMBO Journal*, *34*(19), 2398–2407.

Hutagalung, A. H., & Novick, P. J. (2011). Role of Rab GTPases in membrane traffic and cell physiology. *Physiological Reviews*, *91*(1), 119–149.

Ikonen, E. (2008). Cellular cholesterol trafficking and compartmentalization. In *Nature Reviews Molecular Cell Biology* (Vol. 9, Issue 2, pp. 125–138). Nature Publishing Group.

Ingólfsson, H. I., Melo, M. N., Van Eerden, F. J., Arnarez, C., Lopez, C. A., Wassenaar, T. A., Periole, X., De Vries, A. H., Tieleman, D. P., & Marrink, S. J. (2014). Lipid organization of the plasma membrane. *Journal of the American Chemical Society*, *136*(41), 14554–14559.

Itoh, T., Erdmann, K. S., Roux, A., Habermann, B., Werner, H., & De Camilli, P. (2005). Dynamin and the actin cytoskeleton cooperatively regulate plasma membrane invagination by BAR and F-BAR proteins. *Developmental Cell*, *9*(6), 791–804.

Iwasaki, A., & Medzhitov, R. (2004). Toll-like receptor control of the adaptive immune responses. In *Nature Immunology* (Vol. 5, Issue 10, pp. 987–995). Nat Immunol.

Jacob, M. D., Audas, T. E., Uniacke, J., Trinkle-Mulcahy, L., & Lee, S. (2013). Environmental cues induce a long noncoding RNA-dependent remodeling of the nucleolus. *Molecular Biology of the Cell*, *24*(18), 2943–2953.

Jacquemyn, J., Cascalho, A., & Goodchild, R. E. (2017). The ins and outs of endoplasmic reticulum-controlled lipid biosynthesis. *EMBO Reports*, *18*(11), 1905–1921.

Jäger, C., Lautenschläger, S., Willems, H., & Baljer, G. (2002). *Coxiella burnetii* plasmid types QpDG and QpH1 are closely related and likely identical. *Veterinary Microbiology*, *89*(2–3), 161–166.

Jain, A., & Holthuis, J. C. M. (2017). Membrane contact sites, ancient and central hubs of cellular lipid logistics. In *Biochimica et Biophysica Acta - Molecular Cell Research* (Vol. 1864, Issue 9, pp. 1450–1458). Elsevier B.V.

Jansen, A. F. M., Dinkla, A., Roest, H. J., Bleeker-Rovers, C. P., Schoffelen, T., Joosten, L. A. B., Wever, P. C., Van Deuren, M., & Koets, A. P. (2018). Viable *Coxiella burnetii* induces differential cytokine responses in chronic Q fever patients compared to Heat-Killed Coxiella burnetii. *Infection and Immunity*, *86*(10).

Jean, S., & Kiger, A. A. (2012). Coordination between RAB GTPase and phosphoinositide regulation and functions. In *Nature Reviews Molecular Cell Biology* (Vol. 13, Issue 7, pp. 463–470). Nature Publishing Group.

Jeong, K. C., Ghosal, D., Chang, Y. W., Jensen, G. J., & Vogel, J. P. (2017). Polar delivery of *Legionella* type IV secretion system substrates is essential for virulence. *Proceedings of the National Academy of Sciences of the United States of America*, *114*(30), 8077–8082.

Jia, J., Claude-Taupin, A., Gu, Y., Choi, S. W., Peters, R., Bissa, B., Mudd, M. H., Allers, L., Pallikkuth, S., Lidke, K. A., Salemi, M., Phinney, B., Mari, M., Reggiori, F., & Deretic, V. (2020). Galectin-3 Coordinates a Cellular System for Lysosomal Repair and Removal. *Developmental Cell*, *52*(1), 69-87.e8.

Johannes, L., & Popoff, V. (2008). Tracing the Retrograde Route in Protein Trafficking. In *Cell* (Vol. 135, Issue 7, pp. 1175–1187). Elsevier.

Justis, A. V., Hansen, B., Beare, P. A., King, K. B., Heinzen, R. A., & Gilk, S. D. (2017). Interactions between the *Coxiella burnetii* parasitophorous vacuole and the endoplasmic reticulum involve the host protein ORP1L. *Cellular Microbiology*, *19*(1), e12637.

Kanfer, E., Farrag, N., Price, C., MacDonald, D., Coleman, J., & Barrett, A. J. (1988). Q fever following bone marrow transplantation. *Bone Marrow Transplantation*, *3*(2), 165–166.

Kanneganti, T. D., Lamkanfi, M., & Núñez, G. (2007). Intracellular NOD-like Receptors in Host Defense and Disease. In *Immunity* (Vol. 27, Issue 4, pp. 549–559). Immunity.

Kapsenberg, M. L. (2003). Dendritic-cell control of pathogen-driven T-cell polarization. In

Nature Reviews Immunology (Vol. 3, Issue 12, pp. 984–993). European Association for Cardio-Thoracic Surgery.

Kayagaki, N., Warming, S., Lamkanfi, M., Walle, L. Vande, Louie, S., Dong, J., Newton, K., Qu, Y., Liu, J., Heldens, S., Zhang, J., Lee, W. P., Roose-Girma, M., & Dixit, V. M. (2011). Non-canonical inflammasome activation targets caspase-11. *Nature*, *479*(7371), 117–121.

Kersh, G. J. (2013). Antimicrobial therapies for Q fever. In *Expert Review of Anti-Infective Therapy* (Vol. 11, Issue 11, pp. 1207–1214). Taylor & Francis.

Kersh, G. J., Fitzpatrick, K. A., Self, J. S., Priestley, R. A., Kelly, A. J., Ryan Lash, R., Marsden-Haug, N., Nett, R. J., Bjork, A., Massung, R. F., & Andersona, A. D. (2013). Presence and Persistence of *Coxiella burnetii* in the environments of goat farms associated with a Q fever outbreak. *Applied and Environmental Microbiology*, *79*(5), 1697–1703.

Kersh, G. J., Priestley, R., & Massung, R. F. (2013). Stability of *Coxiella burnetii* in stored human blood. *Transfusion*, *53*(7), 1493–1496.

Kim, Y. J., Guzman-Hernandez, M. L., & Balla, T. (2011). A highly dynamic ER-derived phosphatidylinositol-synthesizing organelle supplies phosphoinositides to cellular membranes. *Developmental Cell*, *21*(5), 813–824.

Kirkegaard, T., Roth, A. G., Petersen, N. H. T., Mahalka, A. K., Olsen, O. D., Moilanen, I., Zylicz, A., Knudsen, J., Sandhoff, K., Arenz, C., Kinnunen, P. K. J., Nylandsted, J., & Jäättelä, M. (2010). Hsp70 stabilizes lysosomes and reverts Niemann-Pick disease-associated lysosomal pathology. *Nature*, *463*(7280), 549–553.

Klee, S. R., Ellerbrok, H., Tyczka, J., Franz, T., & Appel, B. (2006). Evaluation of a real-time PCR assay to detect *Coxiella burnetii*. *Annals of the New York Academy of Sciences*, *1078*, 563–565.

Klingenbeck, L., Eckart, R. A., Berens, C., & Lührmann, A. (2013). The *Coxiella burnetii* type IV secretion system substrate CaeB inhibits intrinsic apoptosis at the mitochondrial level. *Cellular Microbiology*, *15*(4), 675–687.

Kobayashi, T., Beuchat, M. H., Chevallier, J., Makino, A., Mayran, N., Escola, J. M., Lebrand, C., Cosson, P., Kobayashi, T., & Gruenberg, J. (2002). Separation and characterization of late endosomal membrane domains. *Journal of Biological Chemistry*, *277*(35), 32157–32164.

Kobayashi, T., Beuchat, M. H., Lindsay, M., Frias, S., Palmiter, R. D., Sakuraba, H., Parton, R. G., & Gruenberg, J. (1999). Late endosomal membranes rich in lysobisphosphatidic acid regulate cholesterol transport. *Nature Cell Biology*, *1*(2), 113–118.

Kobayashi, T., Stang, E., Fang, K. S., De Moerloose, P., Parton, R. G., & Gruenberg, J. (1998). A lipid associated with the antiphospholipid syndrome regulates endosome structure and function. *Nature*, *392*(6672), 193–197.

Kobuna, H., Inoue, T., Shibata, M., Gengyo-Ando, K., Yamamoto, A., Mitani, S., & Arai, H. (2010). Multivesicular body formation requires OSBP-related proteins and cholesterol. *PLoS Genetics*, *6*(8), e1001055.

Kohl, L., Hayek, I., Daniel, C., Schulze-Lührmann, J., Bodendorfer, B., Lührmann, A., & Lang, R. (2019). MyD88 Is Required for Efficient Control of *Coxiella burnetii* Infection and Dissemination. *Frontiers in Immunology*, *10*(FEB), 1–11.

Kohler, L. J., Reed, S. R., Sarraf, S. A., Arteaga, D. D., Newton, H. J., & Roy, C. R. (2016). Effector protein cig2 decreases host tolerance of infection by directing constitutive fusion of autophagosomes with the *Coxiella*-containing vacuole. *MBio*, *7*(4).

Kolter, T., & Sandhoff, K. (2005). Principles of lysosomal membrane digestion: Stimulation of sphingolipid degradation by sphingolipid activator proteins and anionic lysosomal lipids. *Annual Review of Cell and Developmental Biology*, *21*(1), 81–103.

Kuba, M., Neha, N., Newton, P., Lee, Y. W., Bennett-Wood, V., Hachani, A., De Souza, D. P., Nijagal, B., Dayalan, S., Tull, D., McConville, M. J., Sansom, F. M., & Newton, H. J. (2020). Eira is a novel protein essential for intracellular replication of Coxiella burnetii. *Infection and Immunity*, *88*(6).

Kuley, R., Kuijt, E., Smits, M. A., Roest, H. I. J., Smith, H. E., & Bossers, A. (2017). Genome plasticity and polymorphisms in critical genes correlate with increased virulence of Dutch outbreak-related *Coxiella burnetii* strains. *Frontiers in Microbiology*, *8*(AUG), 1–17.

Kutateladze, T. G. (2010). Translation of the phosphoinositide code by PI effectors. *Nature Chemical Biology*, *6*(7), 507–513.

Kwak, M. J., Kim, J. D., Kim, H., Kim, C., Bowman, J. W., Kim, S., Joo, K., Lee, J., Jin, K. S., Kim, Y. G., Lee, N. K., Jung, J. U., & Oh, B. H. (2017). Architecture of the type IV coupling protein complex of *Legionella pneumophila*. *Nature Microbiology*, *2*, 17114.

Larson, C. L., Beare, P. A., Heinzen, R. A., Martinez, E., Bonazzi, M., & Jeffrey, B. (2016). Right on Q: Genetics Begin to Unravel *Coxiella burnetii* Host Cell Interactions. *Future Microbiology*, *11*(7), 919–939.

Larson, C. L., Beare, P. A., Howe, D., & Heinzen, R. A. (2013). *Coxiella burnetii* effector protein subverts clathrinmediated vesicular trafficking for pathogen vacuole biogenesis. *Proceedings of the National Academy of Sciences of the United States of America*, *110*(49), E4770–E4779.

Larson, C. L., Beare, P. A., Voth, D. E., Howe, D., Cockrell, D. C., Bastidas, R. J., Valdivia, R. H., & Heinzen, R. A. (2015). *Coxiella burnetii* effector proteins that localize to the parasitophorous vacuole membrane promote intracellular replication. *Infection and Immunity*, *83*(2), 661–670.

Larson, C. L., Sandoz, K. M., Cockrell, D. C., & Heinzen, R. A. (2019). Noncanonical inhibition of mTORC1 by *Coxiella burnetii* promotes replication within a phagolysosome-like

vacuole. *MBio*, *10*(1).

Latomanski, E. A., & Newton, H. J. (2018). Interaction between autophagic vesicles and the Coxiella-containing vacuole requires CLTC (clathrin heavy chain). *Autophagy*, *14*(10), 1710–1725.

Latomanski, E. A., Newton, P., Khoo, C. A., & Newton, H. J. (2016). The Effector Cig57 Hijacks FCHO-Mediated Vesicular Trafficking to Facilitate Intracellular Replication of Coxiella burnetii. *PLoS Pathogens*, *12*(12).

Lautenschläger, S., Willems, H., Jäger, C., & Baljer, G. (2000). Sequencing and characterization of the cryptic plasmid QpRS from *Coxiella burnetii*. *Plasmid*, *44*(1), 85–88.

Lawrence, T. (2009). The nuclear factor NF-kappaB pathway in inflammation. In *Cold Spring Harbor perspectives in biology* (Vol. 1, Issue 6). Cold Spring Harbor Laboratory Press.

Lemmon, M. A. (2008). Membrane recognition by phospholipid-binding domains. In *Nature Reviews Molecular Cell Biology* (Vol. 9, Issue 2, pp. 99–111). Nat Rev Mol Cell Biol.

Lepidi, H., Gouriet, F., & Raoult, D. (2009). Immunohistochemical detection of *Coxiella burnetii* in chronic Q fever hepatitis. *Clinical Microbiology and Infection*, *15*(SUPPL. 2), 169–170.

Leventis, P. A., & Grinstein, S. (2010). The distribution and function of phosphatidylserine in cellular membranes. In *Annual Review of Biophysics* (Vol. 39, Issue 1, pp. 407–427). Annu Rev Biophys.

Levine, B., & Kroemer, G. (2008). Autophagy in the Pathogenesis of Disease. In *Cell* (Vol. 132, Issue 1, pp. 27–42). Cell.

Li, T., Lu, Q., Wang, G., Xu, H., Huang, H., Cai, T., Kan, B., Ge, J., & Shao, F. (2013). SET-domain bacterial effectors target heterochromatin protein 1 to activate host rDNA transcription. *EMBO Reports*, *14*(8), 733–740.

Lifshitz, Z., Burstein, D., Peeri, M., Zusman, T., Schwartz, K., Shuman, H. A., Pupko, T., & Segal, G. (2013). Computational modeling and experimental validation of the Legionella and *Coxiella* virulence-related type-IVB secretion signal. *Proceedings of the National Academy of Sciences of the United States of America*, *110*(8).

Liu, T., Zhang, L., Joo, D., & Sun, S. C. (2017). NF-κB signaling in inflammation. *Signal Transduction and Targeted Therapy*, *2*(March), 17023.

Lomma, M., Dervins-Ravault, D., Rolando, M., Nora, T., Newton, H. J., Sansom, F. M., Sahr, T., Gomez-Valero, L., Jules, M., Hartland, E. L., & Buchrieser, C. (2010). The Legionella pneumophila F-box protein Lpp2082 (AnkB) modulates ubiquitination of the host protein parvin B and promotes intracellular replication. *Cellular Microbiology*, *12*(9), 1272–1291.

Long, C. M., Beare, P. A., Cockrell, D. C., Larson, C. L., & Heinzen, R. A. (2019). Comparative virulence of diverse *Coxiella burnetii* strains. *Virulence*, *10*(1), 133–150.

Luedtke, B. E., Mahapatra, S., Lutter, E. I., & Shaw, E. I. (2017). The *Coxiella burnetii* type IVB

secretion system (T4BSS) component DotA is released/secreted during infection of host cells and during in vitro growth in a T4BSS-dependent manner. *Pathogens and Disease*, *75*(4), 1–11.

Lührmann, A., Nogueira, C. V., Carey, K. L., & Roy, C. R. (2010). Inhibition of pathogen-induced apoptosis by a *Coxiella burnetii* type IV effector protein. *Proceedings of the National Academy of Sciences of the United States of America*, *107*(44), 18997–19001.

Lührmann, A., & Roy, C. R. (2007). *Coxiella burnetii* inhibits activation of host cell apoptosis through a mechanism that involves preventing cytochrome c release from mitochondria. *Infection and Immunity*, *75*(11), 5282–5289.

Luo, X., Wasilko, D. J., Liu, Y., Sun, J., Wu, X., Luo, Z. Q., & Mao, Y. (2015). Structure of the *Legionella* Virulence Factor, SidC Reveals a Unique PI(4)P-Specific Binding Domain Essential for Its Targeting to the Bacterial Phagosome. *PLoS Pathogens*, *11*(6), e1004965.

Ma, K.-W., & Ma, W. (2016). YopJ Family Effectors Promote Bacterial Infection through a Unique Acetyltransferase Activity. *Microbiology and Molecular Biology Reviews*, *80*(4), 1011–1027.

Macdonald, L. J., Graham, J. G., Kurten, R. C., & Voth, D. E. (2014). *Coxiella burnetii* exploits host cAMP-dependent protein kinase signalling to promote macrophage survival. *Cellular Microbiology*, *16*(1), 146–159.

MacDonald, L. J., Kurten, R. C., & Voth, D. E. (2012). *Coxiella burnetii* alters cyclic AMP-Dependent protein kinase signaling during growth in macrophages. *Infection and Immunity*, *80*(6), 1980–1986.

Madariaga, M. G., Rezai, K., Trenholme, G. M., & Weinstein, R. A. (2003). Q fever: A biological weapon in your backyard. *Lancet Infectious Diseases*, *3*(11), 709–721.

Maekawa, M., & Fairn, G. D. (2014). Molecular probes to visualize the location, organization and dynamics of lipids. *Journal of Cell Science*, *127*(22), 4801–4812.

Mahapatra, S., Ayoubi, P., & Shaw, E. I. (2010). *Coxiella burnetii* Nine Mile II proteins modulate gene expression of monocytic host cells during infection. *BMC Microbiology*, *10*, 1–14.

Mahapatra, S., Gallaher, B., Smith, S. C., Graham, J. G., Voth, D. E., & Shaw, E. I. (2016). *Coxiella burnetii* employs the Dot/Icm type IV secretion system to modulate host NF-κB/RelA activation. *Frontiers in Cellular and Infection Microbiology*, *6*(DEC).

Mallo, G. V., Espina, M., Smith, A. C., Terebiznik, M. R., Alemán, A., Finlay, B. B., Rameh, L. E., Grinstein, S., & Brumell, J. H. (2008). SopB promotes phosphatidylinositol 3-phosphate formation on *Salmonella* vacuoles by recruiting Rab5 and Vps34. *Journal of Cell Biology*, *182*(4), 741–752.

Mantovani, A., Sica, A., Sozzani, S., Allavena, P., Vecchi, A., & Locati, M. (2004). The chemokine system in diverse forms of macrophage activation and polarization. In *Trends*

in Immunology (Vol. 25, Issue 12, pp. 677–686). Elsevier.

Marat, A. L., & Haucke, V. (2016). Phosphatidylinositol 3-phosphates—at the interface between cell signalling and membrane traffic. *The EMBO Journal*, *35*(6), 561–579.

Marmion, B. P., Ormsbee, R. A., Kyrkou, M., Wright, J., Worswick, D. A., Izzo, A. A., Esterman, A., Feery, B., & Shapiro, R. A. (1990). Vaccine prophylaxis of abattoir-associated Q fever: Eight years' experience in Australian abattoirs. *Epidemiology and Infection*, *104*(2), 275–287.

Martinez, E., Allombert, J., Cantet, F., Lakhani, A., Yandrapalli, N., Neyret, A., Norville, I. H., Favard, C., Muriaux, D., & Bonazzi, M. (2016). *Coxiella burnetii* effector CvpB modulates phosphoinositide metabolism for optimal vacuole development. *Proceedings of the National Academy of Sciences of the United States of America*, *113*(23), E3260–E3269.

Martinez, E., Cantet, F., Fava, L., Norville, I., & Bonazzi, M. (2014). Identification of OmpA, a *Coxiella burnetii* Protein Involved in Host Cell Invasion, by Multi-Phenotypic High-Content Screening. *PLoS Pathogens*, *10*(3), e1004013.

Martinez, E., Huc-Brandt, S., Brelle, S., Allombert, J., Cantet, F., Gannoun-Zaki, L., Burette, M., Martin, M., Letourneur, F., Bonazzi, M., & Molle, V. (2020). The secreted protein kinase CstK from *Coxiella burnetii* influences vacuole development and interacts with the GTPase-activating host protein TBC1D5. *Journal of Biological Chemistry*, *295*(21), 7391–7403.

Martinez, E., Siadous, F. A., & Bonazzi, M. (2018). Tiny architects: Biogenesis of intracellular replicative niches by bacterial pathogens. *FEMS Microbiology Reviews*, *42*(4), 425–447.

Martinon, F., Burns, K., & Tschopp, J. (2002). The Inflammasome: A molecular platform triggering activation of inflammatory caspases and processing of proIL-β. *Molecular Cell*, *10*(2), 417–426.

Matsuo, H., Chevallier, J., Mayran, N., Le Blanc, I., Ferguson, C., Fauré, J., Blanc, N. S., Matile, S., Dubochet, J., Sadoul, R., Parton, R. G., Vilbois, F., & Gruenberg, J. (2004). Role of LBPA and Alix in Multivesicular Liposome Formation and Endosome Organization. *Science*, *303*(5657), 531–534.

Maurin, M., & Raoult, D. (1999). Q fever. In *Clinical Microbiology Reviews* (Vol. 12, Issue 4, pp. 518–553). American Society for Microbiology (ASM).

Maurin, Max, Benoliel, A. M., Bongrand, P., & Raoult, D. (1992). Phagolysosomal alkalinization and the bactericidal effect of antibiotics: The *Coxiella burnetii* Paradigm. *Journal of Infectious Diseases*, *166*(5), 1097–1102.

Mayinger, P. (2009). Regulation of Golgi function via phosphoinositide lipids. In *Seminars in Cell and Developmental Biology* (Vol. 20, Issue 7, pp. 793–800). Elsevier Ltd.

Mccartney, A. J., Zhang, Y., & Weisman, L. S. (2014). Phosphatidylinositol 3,5-bisphosphate: Low abundance, high significance. *BioEssays*, *36*(1), 52–64.

McCaul, T. F., Hackstadt, T., & Williams, J. C. (1981). Ultrastructural and biological aspects of *Coxiella burnetii* under physical disruptions. In *Rickettsiae and Rickettsial Diseases*.

McCaul, T. F., & Williams, J. C. (1981). Developmental cycle of Coxiella burnetii: Structure and morphogenesis of vegetative and sporogenic differentiations. *Journal of Bacteriology*, *147*(3), 1063–1076.

McDonough, J. A., Newton, H. J., Klum, S., Swiss, R., Agaisse, H., & Roy, C. R. (2013). Host pathways important for *Coxiella burnetii* infection revealed by genome-wide RNA interference screening. *MBio*, *4*(1), 1–13.

Meconi, S., Capo, C., Remacle-Bonnet, M., Pommier, G., Raoult, D., & Mege, J. L. (2001). Activation of protein tyrosine kinases by *Coxiella burnetii:* Role in actin cytoskeleton reorganization and bacterial phagocytosis. *Infection and Immunity*, *69*(4), 2520–2526.

Meconi, Sonia, Jacomo, V., Boquet, P., Raoult, D., Mege, J. L., & Capo, C. (1998). *Coxiella burnetii* induces reorganization of the actin cytoskeleton in human monocytes. *Infection and Immunity*, *66*(11), 5527–5533.

Medzhitov, R., & Janeway C., J. (2000). Advances in immunology: Innate immunity. In I. R. Mackay & F. S. Rosen (Eds.), *New England Journal of Medicine* (Vol. 343, Issue 5, pp. 338–344). Massachusetts Medical Society .

Medzhitov, Ruslan, & Janeway, C. A. (2002). Decoding the patterns of self and nonself by the innate immune system. In *Science* (Vol. 296, Issue 5566, pp. 298–300). Science.

Melenotte, C., Caputo, A., Bechah, Y., Lepidi, H., Terras, J., Kowalczewska, M., Di Pinto, F., Nappez, C., Raoult, D., & Brégeon, F. (2019). The hypervirulent *Coxiella burnetii* Guiana strain compared in silico, in vitro and in vivo to the Nine Mile and the German strain. *Clinical Microbiology and Infection*, *25*(9), 1155.e1-1155.e8.

Mesmin, B., Bigay, J., Polidori, J., Jamecna, D., Lacas-Gervais, S., & Antonny, B. (2017). Sterol transfer, PI4P consumption, and control of membrane lipid order by endogenous OSBP . *The EMBO Journal*, *36*(21), 3156–3174.

Metters, G., Norville, I. H., Titball, R. W., & Hemsley, C. M. (2019). From cell culture to cynomolgus macaque: Infection models show lineage-specific virulence potential of Coxiella burnetii. In *Journal of Medical Microbiology* (Vol. 68, Issue 10, pp. 1419–1430). Microbiology Society.

Milazzo, A., Hall, R., Storm, P. A., Harris, R. J., Winslow, W., & Marmion, B. P. (2001). Sexually transmitted Q fever. *Clinical Infectious Diseases*, *33*(3), 399–402.

Millar, J. A., Beare, P. A., Moses, A. S., Martens, C. A., Heinzen, R. A., & Raghavan, R. (2017). Wholegenome sequence of *Coxiella burnetii* Nine Mile RSA439 (phase II, clone 4), a laboratory workhorse strain. *Genome Announcements*, *5*(23).

Miller, H. K., Priestley, R. A., & Kersh, G. J. (2020). Transmission of *Coxiella burnetii* by ingestion in mice. *Epidemiology and Infection*, *148*.

Mittal, E., Skowyra, M. L., Uwase, G., Tinaztepe, E., Mehra, A., Köster, S., Hanson, P. I., & Philips, J. A. (2018). *Mycobacterium tuberculosis* type VII secretion system effectors differentially impact the ESCRT endomembrane damage response. *MBio*, *9*(6).

Moffatt, J. H., Newton, P., & Newton, H. J. (2015). *Coxiella burnetii*: Turning hostility into a home. *Cellular Microbiology*, *17*(5), 621–631.

Mogensen, T. H. (2009). Pathogen recognition and inflammatory signaling in innate immune defenses. In *Clinical Microbiology Reviews* (Vol. 22, Issue 2, pp. 240–273). American Society for Microbiology (ASM).

Morgan, J. K., Luedtke, B. E., & Shaw, E. I. (2010). Polar localization of the *Coxiella burnetii* type IVB secretion system. *FEMS Microbiology Letters*, *305*(2), 177–183.

Morguet, A. J., Jansen, A., Raoult, D., & Schneider, T. (2007). Late relapse of Q fever endocarditis [4]. In *Clinical Research in Cardiology* (Vol. 96, Issue 7, pp. 519–521). Clin Res Cardiol.

Mulye, M., Samanta, D., Winfree, S., Heinzen, R. A., & Gilk, S. D. (2017). Elevated cholesterol in the *Coxiella burnetii* intracellular niche is bacteriolytic. *MBio*, *8*(1).

Mulye, M., Zapata, B., & Gilk, S. D. (2018). Altering lipid droplet homeostasis affects *Coxiella burnetii* intracellular growth. *PLoS ONE*, *13*(2), e0192215.

Nachmias, N., Zusman, T., & Segal, G. (2019). Study of *Legionella* effector domains revealed novel and prevalent phosphatidylinositol 3-phosphate binding domains. *Infection and Immunity*, *87*(6).

Nagai, H., Cambronne, E. D., Kagan, J. C., Amor, J. C., Kahn, R. A., & Roy, C. R. (2005). A C-terminal translocation signal required for Dot/Icm-dependent delivery of the *Legionella* RalF protein to host cells. *Proceedings of the National Academy of Sciences of the United States of America*, *102*(3), 826–831.

Nagai, H., & Kubori, T. (2011). Type IVB secretion systems of *Legionella* and other gram-negative bacteria. In *Frontiers in Microbiology* (Vol. 2, Issue JUNE). Frontiers Research Foundation.

Nagamatsu, K., Kuwae, A., Konaka, T., Nagai, S., Yoshida, S., Eguchi, M., Watanabe, M., Mimuro, H., Koyasu, S., & Abe, A. (2009). *Bordetella* evades the host immune system by inducing IL-10 through a type III effector, BopN. *Journal of Experimental Medicine*, *206*(13), 3073–3088.

Nagashima, S., Tábara, L. C., Tilokani, L., Paupe, V., Anand, H., Pogson, J. H., Zunino, R., McBride, H. M., & Prudent, J. (2020). Golgi-derived PI(4)P-containing vesicles drive late steps of mitochondrial division. *Science*, *367*(6484), 1366–1371.

Nagata, S. (2018). Apoptosis and Clearance of Apoptotic Cells. *Annual Review of Immunology*, *36*(1), 489–517.

Netea, M. G., Balkwill, F., Chonchol, M., Cominelli, F., Donath, M. Y., Giamarellos-Bourboulis,

E. J., Golenbock, D., Gresnigt, M. S., Heneka, M. T., Hoffman, H. M., Hotchkiss, R., Joosten, L. A. B., Kastner, D. L., Korte, M., Latz, E., Libby, P., Mandrup-Poulsen, T., Mantovani, A., Mills, K. H. G., … Dinarello, C. A. (2017). A guiding map for inflammation. In *Nature Immunology* (Vol. 18, Issue 8, pp. 826–831). Nature Publishing Group.

Newton, H. J., Kohler, L. J., McDonough, J. A., Temoche-Diaz, M., Crabill, E., Hartland, E. L., & Roy, C. R. (2014). A Screen of *Coxiella burnetii* Mutants Reveals Important Roles for Dot/Icm Effectors and Host Autophagy in Vacuole Biogenesis. *PLoS Pathogens*, *10*(7).

Newton, H. J., McDonough, J. A., & Roy, C. R. (2013). Effector Protein Translocation by the *Coxiella burnetii* Dot/Icm Type IV Secretion System Requires Endocytic Maturation of the Pathogen-Occupied Vacuole. *PLoS ONE*, *8*(1).

Newton, P., Latomanski, E. A., & Newton, H. J. (2016). Applying fluorescence resonance energy transfer (FRET) to examine effector translocation efficiency by *Coxiella burnetii* during siRNA silencing. *Journal of Visualized Experiments*, *2016*(113).

Newton, P., Thomas, D. R., Reed, S. C. O., Lau, N., Xu, B., Ong, S. Y., Pasricha, S., Madhamshettiwar, P. B., Edgington-Mitchell, L. E., Simpson, K. J., Roy, C. R., & Newton, H. J. (2020). Lysosomal degradation products induce *Coxiella burnetii* virulence. *Proceedings of the National Academy of Sciences of the United States of America*, *117*(12), 6801–6810.

Ning, Z., Yu, S. R., Quan, Y. G., & Xue, Z. (1992). Molecular characterization of cloned variants of *Coxiella burnetii* isolated in China. *Acta Virologica*, *36*(2), 173–183.

Noah, D. L., Huebner, K. D., Darling, R. G., & Waeckerle, J. F. (2002). The history and threat of biological warfare and terrorism. *Emergency Medicine Clinics of North America*, *20*(2), 255–271.

Noroy, C., Lefrançois, T., & Meyer, D. F. (2019). Searching algorithm for type IV effector proteins (S4TE) 2.0: Improved tools for type IV effector prediction, analysis and comparison in proteobacteria. *PLoS Computational Biology*, *15*(3), 301150.

Norris, F. A., Wilson, M. P., Wallis, T. S., Galyov, E. E., & Majerus, P. W. (1998). SopB, a protein required for virulence of *Salmonella dublin*, is an inositol phosphate phosphatase. *Proceedings of the National Academy of Sciences of the United States of America*, *95*(24), 14057–14059.

Norville, I. H., Hartley, M. G., Martinez, E., Cantet, F., Bonazzi, M., & Atkins, T. P. (2014). *Galleria mellonella* as an alternative model of *Coxiella burnetii* infection. *Microbiology (United Kingdom)*, *160*(PART 6), 1175–1181.

Nusinovici, S., Frössling, J., Widgren, S., Beaudeau, F., & Lindberg, A. (2015). Q fever infection in dairy cattle herds: Increased risk with high wind speed and low precipitation. *Epidemiology and Infection*, *143*(15), 3316–3326.

Nusinovici, S., Hoch, T., Brahim, M. L., Joly, A., & Beaudeau, F. (2017). The Effect of Wind on

Coxiella burnetii Transmission Between Cattle Herds: a Mechanistic Approach. *Transboundary and Emerging Diseases*, *64*(2), 585–592.

O'Neill, L. A. J., & Bowie, A. G. (2007). The family of five: TIR-domain-containing adaptors in Toll-like receptor signalling. In *Nature Reviews Immunology* (Vol. 7, Issue 5, pp. 353–364). Nat Rev Immunol.

Ochoa-Repáraz, J., Sentissi, J., Trunkle, T., Riccardi, C., & Pascual, D. W. (2007). Attenuated *Coxiella burnetii* phase II causes a febrile response in gamma interferon knockout and toll-like receptor 2 knockout mice and protects against reinfection. *Infection and Immunity*, *75*(12), 5845–5858.

Omsland, A., Cockrell, D. C., Howe, D., Fischer, E. R., Virtaneva, K., Sturdevant, D. E., Porcella, S. F., & Heinzen, R. A. (2009). Host cell-free growth of the Q fever bacterium *Coxiella burnetii. Proceedings of the National Academy of Sciences of the United States of America*, *106*(11), 4430–4434.

Oyston, P. C. F., & Davies, C. (2011). Q fever: The neglected biothreat agent. *Journal of Medical Microbiology*, *60*(1), 9–21.

Pan, X., Lührmann, A., Satoh, A., Laskowski-Arce, M. A., & Roy, C. R. (2008). Ankyrin repeat proteins comprise a diverse family of bacterial type IV effectors. *Science*, *320*(5883), 1651–1654.

Pareja, M. E. M., Bongiovanni, A., Lafont, F., & Colombo, M. I. (2017). Alterations of the *Coxiella burnetii* replicative vacuole membrane integrity and interplay with the autophagy pathway. *Frontiers in Cellular and Infection Microbiology*, *7*(APR), 112.

Park, D., Chetrit, D., Hu, B., Roy, C. R., & Liu, J. (2020). Analysis of Dot/Icm type IVB secretion system subassemblies by cryoelectron tomography reveals conformational changes induced by DotB binding. *MBio*, *11*(1).

Paz, I., Sachse, M., Dupont, N., Mounier, J., Cederfur, C., Enninga, J., Leffler, H., Poirier, F., Prevost, M. C., Lafont, F., & Sansonetti, P. (2010). Galectin-3, a marker for vacuole lysis by invasive pathogens. *Cellular Microbiology*, *12*(4), 530–544.

Peabody, C. R., Chung, Y. J., Yen, M. R., Vidal-Ingigliardi, D., Pugsley, A. P., & Saier, M. H. (2003). Type II protein secretion and its relationship to bacterial type IV pili and archaeal flagella. In *Microbiology* (Vol. 149, Issue 11, pp. 3051–3072). Society for General Microbiology.

Pearson, T., Hornstra, H. M., Sahl, J. W., Schaack, S., Schupp, J. M., Beckstrom-Sternberg, S. M., O'Neill, M. W., Priestley, R. A., Champion, M. D., Beckstrom-Sternberg, J. S., Kersh, G. J., Samuel, J. E., Massung, R. F., & Keim, P. (2013). When outgroups fail; Phylogenomics of rooting the emerging pathogen, *Coxiella burnetii*. *Systematic Biology*, *62*(5), 752–762.

Pemberton, J. G., & Balla, T. (2019). Polyphosphoinositide-Binding Domains: Insights from

Peripheral Membrane and Lipid-Transfer Proteins. In *Advances in Experimental Medicine and Biology* (Vol. 1111, pp. 77–137). Springer.

Peña-Blanco, A., & García-Sáez, A. J. (2018). Bax, Bak and beyond — mitochondrial performance in apoptosis. In *FEBS Journal* (Vol. 285, Issue 3, pp. 416–431). Blackwell Publishing Ltd.

Philip, C. B. (1948). Comments on the Name of the Q Fever Organism. *Public Health Reports (1896-1970)*, *63*(2), 58.

Picas, L., Viaud, J., Schauer, K., Vanni, S., Hnia, K., Fraisier, V., Roux, A., Bassereau, P., Gaits-Iacovoni, F., Payrastre, B., Laporte, J., Manneville, J. B., & Goud, B. (2014). BIN1/M-Amphiphysin2 induces clustering of phosphoinositides to recruit its downstream partner dynamin. *Nature Communications*, *5*(1), 1–12.

Piñero, A., Barandika, J. F., García-Pérez, A. L., & Hurtado, A. (2015). Genetic diversity and variation over time of *Coxiella burnetii* genotypes in dairy cattle and the farm environment. *Infection, Genetics and Evolution*, *31*, 231–235.

Piper, R. C., & Katzmann, D. J. (2007). Biogenesis and function of multivesicular bodies. *Annual Review of Cell and Developmental Biology*, *23*(1), 519–547.

Pizarro-Cerdá, J., & Cossart, P. (2006). Bacterial adhesion and entry into host cells. In *Cell* (Vol. 124, Issue 4, pp. 715–727). Elsevier.

Pizarro-Cerdá, J., Kühbacher, A., & Cossart, P. (2015). Phosphoinositides and host-pathogen interactions. *Biochimica et Biophysica Acta - Molecular and Cell Biology of Lipids*, *1851*(6), 911–918.

Poltorak, A., He, X., Smirnova, I., Liu, M. Y., Van Huffel, C., Du, X., Birdwell, D., Alejos, E., Silva, M., Galanos, C., Freudenberg, M., Ricciardi-Castagnoli, P., Layton, B., & Beutler, B. (1998). Defective LPS signaling in C3H/HeJ and C57BL/10ScCr mice: Mutations in Tlr4 gene. *Science*, *282*(5396), 2085–2088.

Posor, Y., Eichhorn-Gruenig, M., Puchkov, D., Schöneberg, J., Ullrich, A., Lampe, A., Müller, R., Zarbakhsh, S., Gulluni, F., Hirsch, E., Krauss, M., Schultz, C., Schmoranzer, J., Noé, F., & Haucke, V. (2013). Spatiotemporal control of endocytosis by phosphatidylinositol-3,4- bisphosphate. *Nature*, *499*(7457), 233–237.

Prokop, A., Gouin, E., Villiers, V., Nahori, M. A., Vincentelli, R., Duval, M., Cossart, P., & Dussurget, O. (2017). Orfx, a nucleomodulin required for *Listeria monocytogenes* virulence. *MBio*, *8*(5), 1–17.

Qiu, J., & Luo, Z. Q. (2017). *Legionella* and *Coxiella* effectors: Strength in diversity and activity. *Nature Reviews Microbiology*, *15*(10), 591–605.

Quaglio, G. L., Demotes-Mainard, J., & Loddenkemper, R. (2012). Emerging and re-emerging infectious diseases: A continuous challenge for Europe. In *European Respiratory Journal* (Vol. 40, Issue 6, pp. 1312–1314). European Respiratory Society.

Qualmann, B., Koch, D., & Kessels, M. M. (2011). Let's go bananas: Revisiting the endocytic BAR code. In *EMBO Journal* (Vol. 30, Issue 17, pp. 3501–3515). EMBO J.

Radulovic, M., Schink, K. O., Wenzel, E. M., Nähse, V., Bongiovanni, A., Lafont, F., & Stenmark, H. (2018). ESCRT -mediated lysosome repair precedes lysophagy and promotes cell survival . *The EMBO Journal*, *37*(21).

Ragaz, C., Pietsch, H., Urwyler, S., Tiaden, A., Weber, S. S., & Hilbi, H. (2008). The *Legionella pneumophila* phosphatidylinositol-4 phosphate-binding type IV substrate SidC recruits endoplasmic reticulum vesicles to a replication-permissive vacuole. *Cellular Microbiology*, *10*(12), 2416–2433.

Ramamurthi, K. S., Clapham, K. R., & Losick, R. (2006). Peptide anchoring spore coat assembly to the outer forespore membrane in Bacillus subtilis. *Molecular Microbiology*, *62*(6), 1547–1557.

Ramel, D., Lagarrigue, F., Pons, V., Mounier, J., Dupuis-Coronas, S., Chicanne, G., Sansonetti, P. J., Gaits-Iacovoni, F., Tronchère, H., & Payrastre, B. (2011). *Shigella flexneri* infection generates the lipid PI5P to alter endocytosis and prevent termination of EGFR signaling. *Science Signaling*, *4*(191), 1–10.

Rocha, N., Kuijl, C., Van Der Kant, R., Janssen, L., Houben, D., Janssen, H., Zwart, W., & Neefjes, J. (2009). Cholesterol sensor ORP1L contacts the ER protein VAP to control Rab7-RILP-p150Glued and late endosome positioning. *Journal of Cell Biology*, *185*(7), 1209–1225.

Rodolakis, A. (2009). Q fever in dairy animals. *Annals of the New York Academy of Sciences*, *1166*(1), 90–93.

Rodríguez-Escudero, M., Cid, V. J., Molina, M., Schulze-Luehrmann, J., Lührmann, A., & Rodríguez-Escudero, I. (2016). Studying *Coxiella burnetii* type IV substrates in the yeast saccharomyces cerevisiae: Focus on subcellular localization and protein aggregation. *PLoS ONE*, *11*(1), e0148032.

Roest, H. I. J., Tilburg, J. J. H. C., Van Der Hoek, W., Vellema, P., Van Zijderveld, F. G., Klaassen, C. H. W., & Raoult, D. (2011). The Q fever epidemic in the Netherlands: History, onset, response and reflection. *Epidemiology and Infection*, *139*(1), 1–12.

Rohde, H. M., Cheong, F. Y., Konrad, G., Paiha, K., Mayinger, P., & Boehmelt, G. (2003). The Human Phosphatidylinositol Phosphatase SAC1 Interacts with the Coatomer I Complex. *Journal of Biological Chemistry*, *278*(52), 52689–52699.

Rolain, J. M., Lambert, F., & Raoult, D. (2005). Activity of telithromycin against thirteen new isolates of *C. burnetii* including three resistant to doxycycline. *Annals of the New York Academy of Sciences*, *1063*, 252–256.

Rolhion, N., Furniss, R. C. D., Grabe, G., Ryan, A., Liu, M., Matthews, S. A., & Holden, D. W. (2016). Inhibition of Nuclear Transport of NF-κB p65 by the *Salmonella* Type III Secretion

System Effector SpvD. *PLoS Pathogens*, *12*(5), e1005653.

Romano, P. S., Gutierrez, M. G., Berón, W., Rabinovitch, M., & Colombo, M. I. (2007). The autophagic pathway is actively modulated by phase II *Coxiella burnetii* to efficiently replicate in the host cell. *Cellular Microbiology*, *9*(4), 891–909.

Rosales, E. M., Aguilera, M. O., Salinas, R. P., Carminati, S. A., Colombo, M. I., Martinez-Quiles, N., & Berón, W. (2012). Cortactin is involved in the entry of *Coxiella burnetii* into non-phagocytic cells. *PLoS ONE*, *7*(6), e39348.

Rothmeier, E., Pfaffinger, G., Hoffmann, C., Harrison, C. F., Grabmayr, H., Repnik, U., Hannemann, M., Wölke, S., Bausch, A., Griffiths, G., Müller-Taubenberger, A., Itzen, A., & Hilbi, H. (2013). Activation of Ran GTPase by a *Legionella* Effector Promotes Microtubule Polymerization, Pathogen Vacuole Motility and Infection. *PLoS Pathogens*, *9*(9), e1003598.

Rühl, S., Shkarina, K., Demarco, B., Heilig, R., Santos, J. C., & Broz, P. (2018). ESCRT-dependent membrane repair negatively regulates pyroptosis downstream of GSDMD activation. *Science*, *362*(6417), 956–960.

Ruiz, S., & Wolfe, D. N. (2014). Vaccination against Q fever for biodefense and public health indications. *Frontiers in Microbiology*, *5*(DEC).

Salamon, R. S., & Backer, J. M. (2013). Phosphatidylinositol-3,4,5-trisphosphate: Tool of choice for class I PI 3-kinases. *BioEssays*, *35*(7), 602–611.

Saliba, A. E., Vonkova, I., & Gavin, A. C. (2015). The systematic analysis of protein-lipid interactions comes of age. In *Nature Reviews Molecular Cell Biology* (Vol. 16, Issue 12, pp. 753–761). Nature Publishing Group.

Salinas, R. P., Flores, R. M. O., Distel, J. S., Aguilera, M. O., Colombo, M. I., & Berón, W. (2015). *Coxiella burnetii* phagocytosis is regulated by gtpases of the rho family and the rhoa effectors mdia1 and ROCK. *PLoS ONE*, *10*(12), e0145211.

Salomon, D., Guo, Y., Kinch, L. N., Grishin, N. V., Gardner, K. H., & Orth, K. (2013). Effectors of animal and plant pathogens use a common domain to bind host phosphoinositides. *Nature Communications*, *4*(1), 1–10.

Samanta, D., Clemente, T. M., Schuler, B. E., & Gilk, S. D. (2019). *Coxiella burnetii* Type 4B Secretion System dependent manipulation of endolysosomal maturation is required for bacterial growth. *PLoS Pathogens*, *15*(12), e1007855.

Samanta, D., Mulye, M., Clemente, T. M., Justis, A. V., & Gilk, S. D. (2017). Manipulation of host cholesterol by obligate intracellular bacteria. *Frontiers in Cellular and Infection Microbiology*, *7*(MAY), 1–14.

Samuel, J. E., Frazier, M. E., & Mallavia, L. P. (1985). Correlation of plasmid type and disease caused by *Coxiella burnetii*. *Infection and Immunity*, *49*(3), 775–779.

Sarkes, D., & Rameh, L. E. (2010). A novel HPLC-based approach makes possible the spatial

characterization of cellular PtdIns5P and other phosphoinositides. *Biochemical Journal*, *428*(3), 375–384.

Schäfer, W., Eckart, R. A., Schmid, B., Cagköylü, H., Hof, K., Muller, Y. A., Amin, B., & Lührmann, A. (2017). Nuclear trafficking of the anti-apoptotic *Coxiella burnetii* effector protein AnkG requires binding to p32 and Importin-α1. *Cellular Microbiology*, *19*(1), e12634.

Schmidt, O., & Teis, D. (2012). The ESCRT machinery. In *Current Biology* (Vol. 22, Issue 4, p. R116). Cell Press.

Schoebel, S., Blankenfeldt, W., Goody, R. S., & Itzen, A. (2010). High-affinity binding of phosphatidylinositol 4-phosphate by *Legionella pneumophila* DrrA. *EMBO Reports*, *11*(8), 598–604.

Schroeder, G. N., & Hilbi, H. (2008). Molecular pathogenesis of *Shigella* spp.: Controlling host cell signaling, invasion, and death by type III secretion. In *Clinical Microbiology Reviews* (Vol. 21, Issue 1, pp. 134–156). American Society for Microbiology (ASM).

Schwandner, R., Dziarski, R., Wesche, H., Rothe, M., & Kirschning, C. J. (1999). Peptidoglycan- and lipoteichoic acid-induced cell activation is mediated by Toll-like receptor 2. *Journal of Biological Chemistry*, *274*(25), 17406–17409.

Seshadri, R., Paulsen, I. T., Eisen, J. A., Read, T. D., Nelson, K. E., Nelson, W. C., Ward, N. L., Tettelin, H., Davidsen, T. M., Beanan, M. J., Deboy, R. T., Daugherty, S. C., Brinkac, L. M., Madupu, R., Dodson, R. J., Khouri, H. M., Lee, K. H., Carty, H. A., Scanlan, D., … Heidelberg, J. F. (2003). Complete genome sequence of the Q-fever pathogen *Coxiella burnetii*. *Proceedings of the National Academy of Sciences of the United States of America*, *100*(9), 5455–5460.

Sexton, J. A., & Vogel, J. P. (2002). Type IVB secretion by intracellular pathogens. In *Traffic* (Vol. 3, Issue 3, pp. 178–185).

Shannon, J. G., Howe, D., & Heinzen, R. A. (2005). Virulent *Coxiella burnetii* does not activate human dendritic cells: Role of lipopolysaccharide as a shielding molecule. *Proceedings of the National Academy of Sciences of the United States of America*, *102*(24), 8722–8727.

Shepard, C. C. (1947). An outbreak of q fever in a Chicago packing house. *American Journal of Epidemiology*, *46*(2), 185–192.

Siadous, F. A., Cantet, F., Van Schaik, E., Burette, M., Allombert, J., Lakhani, A., Bonaventure, B., Goujon, C., Samuel, J., Bonazzi, M., & Martinez, E. (2020). *Coxiella* effector protein CvpF subverts RAB26-dependent autophagy to promote vacuole biogenesis and virulence. *Autophagy*, 1–17.

Simons, K., & Vaz, W. L. C. (2004). Model systems, lipid rafts, and cell membranes. In *Annual Review of Biophysics and Biomolecular Structure* (Vol. 33, pp. 269–295). Annu Rev

Biophys Biomol Struct.

Singer, A. U., Rohde, J. R., Lam, R., Skarina, T., Kagan, O., DiLeo, R., Chirgadze, N. Y., Cuff, M. E., Joachimiak, A., Tyers, M., Sansonetti, P. J., Parsot, C., & Savchenko, A. (2008). Structure of the *Shigella* T3SS effector IpaH defines a new class of E3 ubiquitin ligases. *Nature Structural and Molecular Biology*, *15*(12), 1293–1301.

Skowyra, M. L., Schlesinger, P. H., Naismith, T. V., & Hanson, P. I. (2018). Triggered recruitment of ESCRT machinery promotes endolysosomal repair. *Science*, *360*(6384).

Smith, C. B., Evavold, C., & Kersh, G. J. (2019). The Effect of pH on Antibiotic Efficacy against *Coxiella burnetii* in Axenic Media. *Scientific Reports*, *9*(1), 1–9.

Somerharju, P. (1979). Subcellular localization of three degeneration-associated phospholipids in cultured hamster fibroblasts (BHK21 cells). *Biochimica et Biophysica Acta (BBA)/Lipids and Lipid Metabolism*, *574*(3), 461–470.

Steinert, M., Hentschel, U., & Hacker, J. (2000). Symbiosis and pathogenesis: Evolution of the microbe-host interaction. In *Naturwissenschaften* (Vol. 87, Issue 1). Springer-Verlag.

Stephen, S., & Achyutha Rao, K. N. (1979). Coxiellosis in reptiles of South Kanara district, Karnataka. *Indian Journal of Medical Research*, *70*(6), 937–941.

Stewart, M. (2007). Molecular mechanism of the nuclear protein import cycle. In *Nature Reviews Molecular Cell Biology* (Vol. 8, Issue 3, pp. 195–208). Nature Publishing Group.

Stüven, E., Porat, A., Shimron, F., Fass, E., Kaloyanova, D., Brügger, B., Wieland, F. T., Elazar, Z., & Helms, J. B. (2003). Intra-Golgi Protein Transport Depends on a Cholesterol Balance in the Lipid Membrane. *Journal of Biological Chemistry*, *278*(52), 53112–53122.

Sun, Y., Thapa, N., Hedman, A. C., & Anderson, R. A. (2013). Phosphatidylinositol 4,5-bisphosphate: Targeted production and signaling. In *BioEssays* (Vol. 35, Issue 6, pp. 513–522). Bioessays.

Swart, A. L., Steiner, B., Gomez-Valero, L., Schütz, S., Hannemann, M., Janning, P., Irminger, M., Rothmeier, E., Buchrieser, C., Itzen, A., Panse, V. G., & Hilbi, H. (2020). Divergent evolution of *Legionella* RCC1 repeat effectors defines the range of ran gtpase cycle targets. *MBio*, *11*(2).

Tamura, T., Yanai, H., Savitsky, D., & Taniguchi, T. (2008). The IRF family transcription factors in immunity and oncogenesis. In *Annual Review of Immunology* (Vol. 26, pp. 535–584). Annu Rev Immunol.

Tan, X., Thapa, N., Choi, S., & Anderson, R. A. (2015). Emerging roles of PtdIns(4,5)P2 - beyond the plasma membrane. *Journal of Cell Science*, *128*(22), 4047–4056.

Thiele, D., & Willems, H. (1994). Is plasmid based differentiation of *Coxiella burnetii* in “acute” and “chronic” isolates still valid? *European Journal of Epidemiology*, *10*(4), 427–434.

Tissot-Dupont, H., Amadei, M. A., Nezri, M., & Raoult, D. (2004). Wind in November, Q fever in December. *Emerging Infectious Diseases*, *10*(7), 1264–1269.

Tissot-Dupont, H., & Raoult, D. (2008). Q Fever. In *Infectious Disease Clinics of North America* (Vol. 22, Issue 3, pp. 505–514). Elsevier.

Topping, N. H., Shepard, C. C., & Irons, J. V. (1947). Q fever in the united states: Epidemiologic studies of an outbreak among stock handlers and slaughterhouse workers. *Journal of the American Medical Association*, *133*(12), 813–815.

Toulabi, L., Wu, X., Cheng, Y., & Mao, Y. (2013). Identification and structural characterization of a *Legionella* phosphoinositide phosphatase. *Journal of Biological Chemistry*, *288*(34), 24518–24527.

Valková, D., & Kazár, J. (1995). A new plasmid (QpDV) common to *Coxiella burnetii* isolates associated with acute and chronic Q fever. *FEMS Microbiology Letters*, *125*(2–3), 275–280.

van der Meer-Janssen, Y. P. M., van Galen, J., Batenburg, J. J., & Helms, J. B. (2010). Lipids in host-pathogen interactions: Pathogens exploit the complexity of the host cell lipidome. *Progress in Lipid Research*, *49*(1), 1–26.

Van Meer, G., Voelker, D. R., & Feigenson, G. W. (2008). Membrane lipids: Where they are and how they behave. *Nature Reviews Molecular Cell Biology*, *9*(2), 112–124.

van Schaik, E. J., Case, E. D., Martinez, E., Bonazzi, M., & Samuel, J. E. (2017). The SCID mouse model for identifying virulence determinants in *Coxiella burnetii. Frontiers in Cellular and Infection Microbiology*, *7*(FEB), 1–10.

Van Schaik, E. J., Chen, C., Mertens, K., Weber, M. M., & Samuel, J. E. (2013). Molecular pathogenesis of the obligate intracellular bacterium *Coxiella burnetii.* In *Nature Reviews Microbiology* (Vol. 11, Issue 8, pp. 561–573). NIH Public Access.

Van Wijk, M. J., Hogema, B. M., Maas, D. W., & Bokhorst, A. G. (2011). A Q fever outbreak in the Netherlands: Consequences for tissue banking. *Transfusion Medicine and Hemotherapy*, *38*(6), 357–364.

Vanderburg, S., Rubach, M. P., Halliday, J. E. B., Cleaveland, S., Reddy, E. A., & Crump, J. A. (2014). Epidemiology of *Coxiella burnetii* Infection in Africa: A OneHealth Systematic Review. *PLoS Neglected Tropical Diseases*, *8*(4).

Vanlandingham, P. A., & Ceresa, B. P. (2009). Rab7 regulates late endocytic trafficking downstream of multivesicular body biogenesis and cargo sequestration. *Journal of Biological Chemistry*, *284*(18), 12110–12124.

Várnai, P., Gulyás, G., Tóth, D. J., Sohn, M., Sengupta, N., & Balla, T. (2017). Quantifying lipid changes in various membrane compartments using lipid binding protein domains. In *Cell Calcium* (Vol. 64, pp. 72–82). Elsevier Ltd.

Vázquez, C. L., & Colombo, M. I. (2010). *Coxiella burnetii* modulates Beclin 1 and Bcl-2, preventing host cell apoptosis to generate a persistent bacterial infection. *Cell Death and Differentiation*, *17*(3), 421–438.

Vergne, I., Chua, J., Lee, H. H., Lucas, M., Belisle, J., & Deretic, V. (2005). Mechanism of phagolysosome biogenesis block by viable *Mycobacterium tuberculosis*. *Proceedings of the National Academy of Sciences of the United States of America*, *102*(11), 4033–4038.

Viaud, J., Boal, F., Tronchère, H., Gaits-Iacovoni, F., & Payrastre, B. (2014). Phosphatidylinositol 5-phosphate: A nuclear stress lipid and a tuner of membranes and cytoskeleton dynamics. In *BioEssays* (Vol. 36, Issue 3, pp. 260–272). Bioessays.

Viaud, J., Lagarrigue, F., Ramel, D., Allart, S., Chicanne, G., Ceccato, L., Courilleau, D., Xuereb, J. M., Pertz, O., Payrastre, B., & Gaits-Iacovoni, F. (2014). Phosphatidylinositol 5-phosphate regulates invasion through binding and activation of Tiam1. *Nature Communications*, *5*(1), 1–17.

Viaud, J., & Payrastre, B. (2015). Les phosphoinositides : Ces lipides qui coordonnent la dynamique cellulaire. *Medecine/Sciences*, *31*(11), 996–1005.

Vicinanza, M., Korolchuk, V. I., Ashkenazi, A., Puri, C., Menzies, F. M., Clarke, J. H., & Rubinsztein, D. C. (2015). PI(5)P regulates autophagosome biogenesis. *Molecular Cell*, *57*(2), 219–234.

Vincent, C. D., Friedman, J. R., Jeong, K. C., Buford, E. C., Miller, J. L., & Vogel, J. P. (2006). Identification of the core transmembrane complex of the *Legionella* Dot/Icm type IV secretion system. *Molecular Microbiology*, *62*(5), 1278–1291.

Vogel, J. P., Andrews, H. L., Wong, S. K., & Isberg, R. R. (1998). Conjugative transfer by the virulence system of *Legionella pneumophila*. *Science*, *279*(5352), 873–876.

Voth, D. E., Broederdorf, L. J., & Graham, J. G. (2012). Bacterial Type IV secretion systems: Versatile virulence machines. In *Future Microbiology* (Vol. 7, Issue 2, pp. 241–257). NIH Public Access.

Voth, D. E., & Heinzen, R. A. (2007). Lounging in a lysosome: The intracellular lifestyle of *Coxiella burnetii.* In *Cellular Microbiology* (Vol. 9, Issue 4, pp. 829–840). Cell Microbiol.

Voth, D. E., & Heinzen, R. A. (2009a). Sustained activation of Akt and Erk1/2 is required for *Coxiella burnetii* antiapoptotic activity. *Infection and Immunity*, *77*(1), 205–213.

Voth, D. E., & Heinzen, R. A. (2009b). *Coxiella* type IV secretion and cellular microbiology. In *Current Opinion in Microbiology* (Vol. 12, Issue 1, pp. 74–80).

Voth, D. E., Howe, D., Beare, P. A., Vogel, J. P., Unsworth, N., Samuel, J. E., & Heinzen, R. A. (2009). The *Coxiella burnetii* ankyrin repeat domain-containing protein family is heterogeneous, with C-terminal truncations that influence Dot/Icm-mediated secretion. *Journal of Bacteriology*, *191*(13), 4232–4242.

Voth, D. E., Howe, D., & Heinzen, R. A. (2007). *Coxiella burnetii* inhibits apoptosis in human THP-1 cells and monkey primary alveolar macrophages. *Infection and Immunity*, *75*(9), 4263–4271.

Votteler, J., & Sundquist, W. I. (2013). Virus budding and the ESCRT pathway. In *Cell Host*

and Microbe (Vol. 14, Issue 3, pp. 232–241). Cell Press.

Waag, D. M., Byrne, W. R., Estep, J., Gibbs, P., Pitt, M. L., & Banfield, C. M. (1999). Evaluation of cynomolgus (Macaca fascicularis) and rhesus (Macaca mulatta) monkeys as experimental models of acute Q fever after aerosol exposure to phase-I *Coxiella burnetii*. *Laboratory Animal Science*, *49*(6), 634–638.

Waag, D. M., England, M. J., Bolt, C. R., & Williams, J. C. (2008). Low-dose priming before vaccination with the phase I chloroform-methanol residue vaccine against Q fever enhances humoral and cellular immune responses to *Coxiella burnetii*. *Clinical and Vaccine Immunology*, *15*(10), 1505–1512.

Watt, S. A., Kular, G., Fleming, I. N., Downes, C. P., & Lucocq, J. M. (2002). Subcellular localization of phosphatidylinositol 4,5-bisphosphate using the pleckstrin homology domain of phospholipase C δ1. *Biochemical Journal*, *363*(3), 657–666.

Weber, D. J., & Rutala, W. A. (2001). Risks and prevention of nosocomial transmission of rare zoonotic diseases. *Clinical Infectious Diseases*, *32*(3), 446–456.

Weber, M. M., Chen, C., Rowin, K., Mertens, K., Galvan, G., Zhi, H., Dealing, C. M., Roman, V. A., Banga, S., Tan, Y., Luo, Z. Q., & Samuel, J. E. (2013). Identification of *Coxiella burnetii* type IV secretion substrates required for intracellular replication and Coxiella-containing vacuole formation. *Journal of Bacteriology*, *195*(17), 3914–3924.

Weber, M. M., Faris, R., McLachlan, J., Tellez, A., Wright, W. U., Galvan, G., Luo, Z. Q., & Samuel, J. E. (2016). Modulation of the host transcriptome by *Coxiella burnetii* nuclear effector Cbu1314. *Microbes and Infection*, *18*(5), 336–345.

Weber, M. M., Faris, R., Van Schaik, E. J., McLachlan, J. T., Wright, W. U., Tellez, A., Roman, V. A., Rowin, K., Case, E. D. R., Luo, Z. Q., & Samuel, J. E. (2016). The type IV secretion system effector protein cira stimulates the GTPase activity of RhoA and is required for virulence in a mouse model of *Coxiella burnetii* infection. *Infection and Immunity*, *84*(9), 2524–2533.

Weber, M. M., Faris, R., van Schaik, E. J., & Samuel, J. E. (2018). Identification and characterization of arginine finger-like motifs, and endosome-lysosome basolateral sorting signals within the *Coxiella burnetii* type IV secreted effector protein CirA. *Microbes and Infection*, *20*(5), 302–307.

Weber, S. S., Ragaz, C., & Hilbi, H. (2009). Pathogen trafficking pathways and host phosphoinositide metabolism. In *Molecular Microbiology* (Vol. 71, Issue 6, pp. 1341–1352). Mol Microbiol.

Weigele, B. A., Orchard, R. C., Jimenez, A., Cox, G. W., & Alto, N. M. (2017). A systematic exploration of the interactions between bacterial effector proteins and host cell membranes. *Nature Communications*, *8*(1).

Weisburg, W. G., Dobson, M. E., Samuel, J. E., Dasch, G. A., Mallavia, L. P., Baca, O.,

Mandelco, L., Sechrest, J. E., Weiss, E., & Woese, C. R. (1989). Phylogenetic diversity of the Rickettsiae. *Journal of Bacteriology*, *171*(8), 4202–4206.

Whitman, W. B., Coleman, D. C., & Wiebe, W. J. (1998). Prokaryotes: The unseen majority. In *Proceedings of the National Academy of Sciences of the United States of America* (Vol. 95, Issue 12, pp. 6578–6583). National Academy of Sciences.

Wiener-Well, Y., Fink, D., Schlesinger, Y., Raveh, D., Rudensky, B., & Yinnon, A. M. (2010). Q fever endocarditis; not always expected. *Clinical Microbiology and Infection*, *16*(4), 359–362.

Willems, H., Ritter, M., Jäger, C., & Thiele, D. (1997). Plasmid-homologous sequences in the chromosome of plasmidless *Coxiella burnetii* scurry Q217. *Journal of Bacteriology*, *179*(10), 3293–3297.

Wills, R. C., Goulden, B. D., & Hammond, G. R. V. (2018). Genetically encoded lipid biosensors. *Molecular Biology of the Cell*, *29*(13), 1526–1532.

Winchell, C. G., Dragan, A. L., Brann, K. R., Onyilagha, F. I., Kurten, R. C., & Voth, D. E. (2018). *Coxiella burnetii* subverts p62/sequestosome 1 and activates Nrf2 signaling in human macrophages. *Infection and Immunity*, *86*(5).

Wine, E., Ossa, J. C., Gray-Owen, S. D., & Sherman, P. M. (2010). Adherent-invasive *Escherichia coli* target the epithelial barrier. *Gut Microbes*, *1*(2), 80–84.

Wynn, T. A., Chawla, A., & Pollard, J. W. (2013). Macrophage biology in development, homeostasis and disease. In *Nature* (Vol. 496, Issue 7446, pp. 445–455). NIH Public Access.

Xia, Z. Bin, Meng, F. R., Fang, Y. X., Wu, X., Zhang, C. W., Liu, Y., Liu, D., Li, G. Q., Feng, F. B., & Qiu, H. Y. (2018). Inhibition of NF-κB signaling pathway induces apoptosis and suppresses proliferation and angiogenesis of human fibroblast-like synovial cells in rheumatoid arthritis. *Medicine (United States)*, *97*(23), e10920.

Xie, J., Erneux, C., & Pirson, I. (2013). How does SHIP1/2 balance PtdIns(3,4)P2 and does it signal independently of its phosphatase activity? *BioEssays*, *35*(8), 733–743.

Yamaji, T., & Hanada, K. (2015). Sphingolipid Metabolism and Interorganellar Transport: Localization of Sphingolipid Enzymes and Lipid Transfer Proteins. *Traffic*, *16*(2), 101–122.

Yang, S. T., Kreutzberger, A. J. B., Lee, J., Kiessling, V., & Tamm, L. K. (2016). The role of cholesterol in membrane fusion. *Chemistry and Physics of Lipids*, *199*, 136–143.

Yeung, T., Heit, B., Dubuisson, J. F., Fairn, G. D., Chiu, B., Inman, R., Kapus, A., Swanson, M., & Grinstein, S. (2009). Contribution of phosphatidylserine to membrane surface charge and protein targeting during phagosome maturation. *Journal of Cell Biology*, *185*(5), 917–928.

Yu, L., Chen, Y., & Tooze, S. A. (2018). Autophagy pathway: Cellular and molecular

mechanisms. In *Autophagy* (Vol. 14, Issue 2, pp. 207–215). Taylor and Francis Inc.

Zamboni, D. S., Campos, M. A., Torrecilhas, A. C. T., Kiss, K., Samuel, J. E., Golenbock, D. T., Lauw, F. N., Roy, C. R., Almeida, I. C., & Gazzinelli, R. T. (2004). Stimulation of Toll-like receptor 2 by *Coxiella burnetii* is required for macrophage production of pro-inflammatory cytokines and resistance to infection. *Journal of Biological Chemistry*, *279*(52), 54405–54415.

Zamboni, D. S., McGrath, S., Rabinovitch, M., & Roy, C. R. (2003). *Coxiella burnetii* express type IV secretion system proteins that function similarly to components of the *Legionella pneumophila* Dot/Icm system. *Molecular Microbiology*, *49*(4), 965–976.

Zusman, T., Aloni, G., Halperin, E., Kotzer, H., Degtyar, E., Feldman, M., & Segal, G. (2007). The response regulator PmrA is a major regulator of the Dot/Icm type IV secretion system in *Legionella pneumophila* and *Coxiella burnetii*. *Molecular Microbiology*, *63*(5), 1508–1523.

Zusman, T., Yerushalmi, G., & Segal, G. (2003). Functional similarities between the icm/dot pathogenesis systems of *Coxiella burnetii* and *Legionella pneumophila*. *Infection and Immunity*, *71*(7), 3714–3723.

Appendix 1

***Coxiella* effector protein CvpF subverts RAB26-dependent autophagy to promote vacuole biogenesis and virulence**

Siadous FA, Cantet F, Van Schaik E, Burette M, Allombert J, Lahkani A, Bonaventure B, Goujon C, Samuel J, Bonazzi M, Martinez E. Autophagy 2020 Mar1 ;1-17

AUTOPHAGY
https://doi.org/10.1080/15548627.2020.1728098

Taylor & Francis
Taylor & Francis Group

RESEARCH PAPER

OPEN ACCESS Check for updates

Coxiella effector protein CvpF subverts RAB26-dependent autophagy to promote vacuole biogenesis and virulence

Fernande Ayenoue Siadous[a], Franck Cantet[a], Erin Van Schaik[b], Mélanie Burette[a], Julie Allombert[a], Anissa Lakhani[a], Boris Bonaventure[a], Caroline Goujon[a], James Samuel[b], Matteo Bonazzi[a], and Eric Martinez[a]

[a]Institut de Recherche en Infectiologie de Montpellier (IRIM) UMR 9004 CNRS, Université de Montpellier, Montpellier, France; [b]Department of Microbial and Molecular Pathogenesis, Texas A&M Health Science Center College of Medicine, Bryan, TX, USA

ABSTRACT

Coxiella burnetii, the etiological agent of the zoonosis Q fever, replicates inside host cells within a large vacuole displaying autolysosomal characteristics. The development of this compartment is mediated by bacterial effectors, which interfere with a number of host membrane trafficking pathways. By screening a *Coxiella* transposon mutant library, we observed that transposon insertions in *cbu0626* led to intracellular replication and vacuole biogenesis defects. Here, we demonstrate that CBU0626 is a novel member of the *Coxiella* vacuolar protein (Cvp) family of effector proteins, which is translocated by the Dot/Icm secretion system and localizes to vesicles with autolysosomal features as well as *Coxiella*-containing vacuoles (CCVs). We thus renamed this effector CvpF for *Coxiella* vacuolar protein F. CvpF specifically interacts with the host small GTPase RAB26, leading to the recruitment of the autophagosomal marker MAP1LC3B/LC3B (microtubule associated protein 1 light chain 3 beta) to CCVs. Importantly, *cvpF*::Tn mutants were highly attenuated compared to wild-type bacteria in the SCID mouse model of infection, highlighting the importance of CvpF for *Coxiella* virulence. These results suggest that CvpF manipulates endosomal trafficking and macroautophagy/autophagy induction for optimal *C. burnetii* vacuole biogenesis.

Abbreviations: ACCM: acidified citrate cystein medium; AP: adaptor related protein complex; CCV: *Coxiella*-containing vacuole; Cvp: *Coxiella* vacuolar protein; GDI: guanosine nucleotide dissociation inhibitor; GDF: GDI dissociation factor; GEF: guanine exchange factor; LAMP1: lysosomal associated membrane protein 1; MAP1LC3B/LC3B: microtubule associated protein 1 light chain 3 beta; MTORC1: mechanistic target of rapamycin kinase MTOR complex 1; PBS: phosphate-buffered saline; PMA: phorbol myristate acetate; SQSTM1/p62: sequestosome 1; WT: wild-type.

ARTICLE HISTORY
Received 7 June 2019
Revised 28 January 2020
Accepted 4 February 2020

KEYWORDS
Autophagy; *Coxiella burnetii*; effector protein; LC3B; RAB GTPase

Introduction

Coxiella burnetii is the causative agent of animal coxiellosis and human Q fever, considered as one of the most relevant reemerging zoonosis in Europe [1]. The symptoms of Q fever range from fatigue, long-lasting fever, and hepatitis in the acute form of the disease, to severe endocarditis in its chronic form [2]. Upon internalization by phagocytic and non-phagocytic cells, *Coxiella* remains in endosomes that progress in the endocytic pathway. Endosomal acidification triggers the activation of a defect in organelle trafficking genes/intracellular multiplication (Dot/Icm) type 4 secretion system (T4SS) and the translocation of bacterial effectors, which are essential for the biogenesis of the *Coxiella*-containing vacuole (CCV) [3–5]. Bioinformatics analysis and secretion assays using either *Legionella* [6] or *Coxiella* [7] have identified approximately 143 candidate *Coxiella* effectors [8]. However, very few host cell partners have been identified [9,10], and the role of *Coxiella* effectors in CCV biogenesis remains poorly characterized. *Coxiella* vacuolar proteins (Cvps) constitute a class of effectors that localize to endosomal compartments and CCVs in cells infected with wild type *Coxiella*. These effectors play an important role in *Coxiella* vacuole biogenesis, as the mutation of their corresponding genes leads to smaller CCVs [11]. CvpA interacts with adaptor related protein complex 2 (AP2) and clathrin [10]. CvpB (or Cig2) interacts with cellular lipids phosphatidylinositol 3-phosphate (PtdIns3P) and phosphatidylserine (PS) and interferes with PIKFYVE (phosphoinositide kinase, FYVE-type zinc finger containing) activity to promote autophagy-mediated homotypic fusion of CCVs [12]. The functions of CvpC, CvpD, and CvpE remain undetermined. Besides CvpB, additional effector proteins manipulate the autophagy machinery for optimal vacuole biogenesis: effectors CpeB and CpeL colocalize with the autophagosomal marker LC3B [13,14] and mutants of the effector proteins CBU0513, and Cig57 display decreased presence of LC3B at their respective vacuoles [15,16].

Macroautophagy (hereafter termed autophagy) is a highly conserved eukaryotic process used by cells to recycle and degrade cargos, such as damaged organelles and misfolded proteins, in order to acquire nutrients during periods of

CONTACT Eric Martinez eric.martinez@irim.cnrs.fr; Matteo Bonazzi matteo.bonazzi@irim.cnrs.fr Institut de Recherche en Infectiologie de Montpellier (IRIM) UMR 9004 CNRS, Université de Montpellier, Montpellier, France
Supplemental data for this article can be accessed here.

deprivation. It can also act as a cell defense mechanism capable of targeting invading pathogens for degradation. The mechanistic target of rapamycin kinase complex 1 (MTORC1) mediates the nutrient-sensing and regulatory functions of lysosomes. Under normal conditions, phosphorylated MTOR (mechanistic target of rapamycin kinase) localizes to the lysosome surface and downregulates autophagy. Upon starvation or treatment with the MTOR inhibitor torin1, MTOR is inactivated and delocalizes to the cytosol, which triggers a signaling cascade leading to autophagy. RAB GTPases, the key regulators of vesicular sorting and trafficking in the endocytic and secretory pathways, could regulate autophagy membrane dynamics. While RAB1, RAB5, RAB7, RAB9A, RAB11, RAB23, RAB32 and RAB33B act at different stages of autophagosome formation, RAB7, RAB8B and RAB24 participate in autophagosome maturation [17]. Recently, additional RAB GTPases, such as RAB26 and RAB37, have also been shown to participate in the autophagy process [18–21]. RAB GTPases shuttle between a cytosolic inactive GDP-bound state and a membrane-anchored active GTP-bound state. Once inserted into the membranes, these proteins can interact with other partner proteins to mediate vesicular trafficking and maturation events. Their central role in membrane dynamics and immunity made them ideal targets for intracellular bacterial pathogens, which divert their function for the development of optimal intracellular niches [22–24]. In the context of *Coxiella* infections, inhibiting the function or expression of RAB1, RAB5, RAB7, and RAB24 affects the vacuole biogenesis and impairs intracellular replication [12,25–29].

Multi-parametric phenotypic analysis of a *Coxiella* transposon library revealed that transposon insertions in the gene *cbu0626* affect *Coxiella* vacuole biogenesis and intracellular replication [30]. Here, we demonstrate that CBU0626 is a new *Coxiella* vacuolar effector protein interacting with RAB26 to trigger LC3B recruitment at CCVs. Decreased LC3B recruitment at CCVs in cells challenged with *cbu0626* mutants is associated with altered replication *in vitro* and *in vivo*, suggesting that diversion of autophagy by this effector is crucial for *Coxiella* virulence.

Results

CvpF is a Dot/Icm vacuolar effector protein required for LC3B recruitment to CCVs and for Coxiella virulence *in vivo*

Our phenotypic screen of a *Coxiella* transposon mutant library identified a significant number of genes encoding candidate *Coxiella* effector proteins with a role in CCV biogenesis [30]. Among these, the mutant *Tn248* with a transposon insertion in the gene *cbu0626* displayed a severe replication defect in epithelial cells [30]. Bioinformatics analysis indicated that *cbu0626* is likely part of a PmrA-regulated operon, together with *cbu0625* (also known as *cig17*) [31], and possesses a C-terminal E-Block motif found in type 4-secreted effectors [32] (Figure S1A). Southern blot analysis confirmed that transposon insertion in the genome of *Tn248* is unique and occurs in the gene *cbu0626* (Figure S1B). Complementation of the *cbu0626::Tn* mutation in *Tn248* by the introduction of the full *cbu0625-cbu0626* operon under the control of the endogenous PmrA promoter (*Tn248* Comp.) restored the expression of the full *cbu0626* mRNA (Figure S1C and D). We validated CBU0626 translocation by transforming either a control *Coxiella* transposon mutant (*WT*) or a T4SS-defective *dotA*::Tn mutant with a β-lactamase-*cbu0626* fusion construct and comparing the secretion of CBU0626 with that of the previously reported effector protein CvpB [12], using the β-lactamase secretion assay. We verified the expression of all β-lactamase-tagged constructs by western blot (Figure S1E). CBU0626 secretion was comparable with that of CvpB after 24, 48, and 72 h of infection by the control *Coxiella* strain (Figure S1F). The absence of detectable secretion of either protein by the T4SS-defective *dotA*::Tn mutant indicated that CBU0626 is indeed a Dot/Icm secreted protein. Of note, T4SS-dependent translocation was still functional in the *Tn248* mutant strain (Figure S1F).

To determine the subcellular localization and targets of CBU0626, we transfected U2OS cells infected with *WT Coxiella Tn1832* for 4 d with a plasmid coding for mCherry-tagged CBU0626 (mCh-CBU0626, Figure 1A). The *Coxiella* effector colocalized with the lysosomal marker LAMP1 at CCVs, indicating that CBU0626 is a newly identified member of the Cvp family of *Coxiella* effector proteins. We, thus, renamed this protein CvpF for *Coxiella* vacuolar protein F. Next, we used our implemented image analysis algorithm [33] to validate the replication phenotypes previously observed with the *cvpF*::Tn mutant in our transposon library [30]. U2OS and PMA-treated THP-1 cells infected for 6 d with either the control *Coxiella* mutant *Tn1832* (*WT*). We fixed and processed the *cvpF*::Tn transposon mutant or the complemented *cvpF* transposon mutant (*cvpF*::Tn Comp.) for immunofluorescence and quantitative PCR. Automated image analysis indicated that *cvpF* transposon mutant generated smaller CCVs and colonies in U2OS and THP1 cells, respectively (Figure 1B,D), and replicated less efficiently than *WT* bacterium (Figure 1C,E). Interestingly, in ACCM-2 axenic media, replication of the *cvpF*::Tn mutant was similar to *WT Coxiella*, the T4SS-defective *dotA*::Tn mutant and the *cvpF*::Tn complemented strain (Figure 1F), indicating that transposon insertion in *cvpF* only affects intracellular development of the bacterium.

We, then, investigated the *in vivo* relevance of CvpF using the recently developed SCID mice model [34]. Mice challenged via the IP route either with the control *Coxiella* strain NMII, the *cvpF*::Tn mutant, the complemented *cvpF*::Tn strain and the *dotA*::Tn mutant, were culled at 14 d post-infection and we assessed bacterial genome equivalents (GE) in the spleen, as well as splenomegaly (Figure 1G,H). In agreement with the observations on cultured cells, the number of *cvpF*::Tn mutant GE in the spleen of infected animals was significantly lower than those found for the *WT* bacterium and complementation of the *cvpF*::Tn mutant partially restored this replication defect (Figure 1G). The splenomegaly induced by the *cvpF*::Tn mutant was also much lower than the one provoked by *WT* bacterium (Figure 1H), strongly suggesting that the virulence of the *cvpF*::Tn

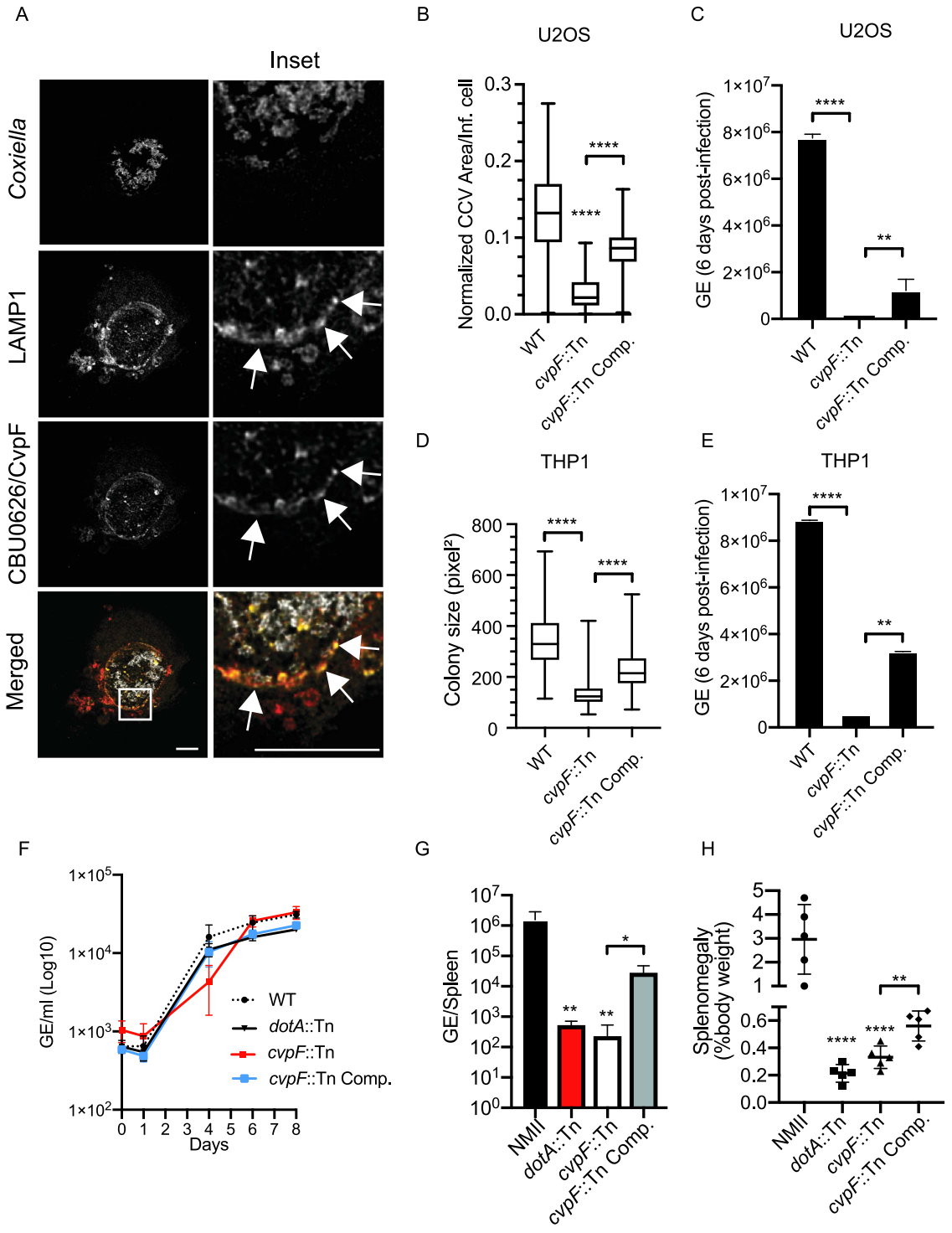

Figure 1. CvpF is a Dot/Icm T4BSS vacuolar effector protein important for *Coxiella* intracellular growth, CCV biogenesis, and virulence. (A) U2OS cells were infected with *Coxiella WT* GFP (gray) and transfected with pLVX-mCherry-CBU0626/CvpF (red) 4 d post-infection. We fixed cells 12 h post-transfection and labeled with an anti-LAMP1 antibody (green). White arrows indicate discrete regions of the *Coxiella* vacuole where CvpF and LAMP1 colocalize. (B) U2OS cells were challenged for 6 d either with *Coxiella WT* GFP (*WT*), *cvpF*::Tn mutant, or the complemented *cvpF*::Tn strain (*cvpF*::Tn Comp.). CCV area for each strain was determined using the Cell Profiler software. (C) U2OS cells were challenged as in B, and Genome Equivalents (GE) were determined by quantitative PCR (D) PMA-treated THP1 cells were challenged for 6 d either with *Coxiella WT* GFP (*WT*), *cvpF*::Tn mutant, or the complemented *cvpF*::Tn strain (*cvpF*::Tn Comp.) The colony area for each strain was determined using the Cell Profiler software. (E) THP1 cells were challenged as in D and Genome Equivalents (GE) were determined by quantitative PCR. (F) *Coxiella WT* GFP (*WT*), *dotA*::Tn mutant, *cvpF*::Tn mutant and the complemented *cvpF*::Tn strain (*cvpF*::Tn Comp.) were grown for 8 d in ACCM-2 and Genome Equivalents (GE)/ml were determined by Pico Green assay. (G) Genome Equivalents (GE) calculated using TaqMan real-time PCR with DNA purified from infected spleens of 5 SCID mice per group on day 14 after challenge with 1×10^6 GE equivalents of the strains shown. (H) Splenomegaly calculated as spleen weight as a percentage of total body weight at the time of necropsy on day 14 after infection with 1×10^6 GE equivalents of the strains listed in the figure legend. Values are mean ± SD from 3 independent experiments (n.s. = non-significant, **** = $P < 0.0001$, ** = $P < 0.0021$, * = $P < 0.033$, one-way ANOVA, Sidak's multiple comparison test). Scale bars: 10 µm.

mutant is severely attenuated *in vivo* and could be partially restored using the *cvpF*::Tn-complemented strain.

As CvpF appears to be important for CCV biogenesis, we investigated whether the absence of CvpF affects typical CCVs markers. More than 80% of vacuoles generated by *WT Coxiella, cvpF*::Tn and *cvpF*::Tn Comp. strains were positive for the acidification marker LysoTracker and the lysosomal/late endosomal protein LAMP1 (Figure 2A,B). However, 15.77 ± 6.8% of CCVs generated by the *cvpF*::Tn mutant was positive for LC3B (Figure 2C,D), while 93.56 ± 3.4% of CCVs generated by *WT Coxiella* and 70.13 ± 10.2% of CCVs generated by the *cvpF*::Tn-complemented strain were positive for LC3B (Figure 2C,D). Colocalization analysis between LAMP1 and LC3B on CCVs generated by *WT, cvpF*::Tn, and *cvpF*::Tn complemented strains (Figure 2E) showed that significantly less LC3B is found on CCVs generated by the *cvpF*::Tn mutant, strongly suggesting that CvpF plays a role in the recruitment of this autophagosomal marker on CCVs.

Ectopically expressed CvpF localizes to vesicular structures with autolysosomal features

The defective vacuole biogenesis phenotype observed with the *cvpF* transposon mutants, accompanied by the loss of LC3B at CCVs, suggested a role for this bacterial effector in re-routing autophagy components to the forming CCV. We, thus, further investigated CvpF localization in cells overexpressing either mCherry- or HA-tagged versions of the effector protein. CvpF was excluded from the Golgi complex either labeled by an anti-GM130 antibody or by expression of GFP-tagged M6PR (mannose-6-phosphate receptor, cation dependent) (Figure S2), whereas we observed partial colocalization of CvpF with markers of the endosomal sorting complex required for transport (ESCRT) complex (GFP-TSG101, GFP-VPS4A and FLAG-CHMP4B) (Figure S2). Conversely, CvpF signal overlapped with the lysosomal marker LAMP1, but also with the early endosomal and autophagosomal markers phosphatidylinositol 3-phosphate (PtdIns3P) probe 2xFYVE-GFP and LC3B (Figure 3A). Importantly, all compartments labeled by CvpF displayed a clustered perinuclear localization (Figure 3A), as opposed to cells expressing either the HA or the mCherry tags alone (Figure S3).

To understand how CvpF is targeted to host cell membranes, we carried out a mutational analysis of this *Coxiella* effector protein. We transfected U2OS cells with mCherry- or HA-tagged versions of incremental deletions either from the N-terminal or the C-terminal of CvpF, and we assessed the localization of the bacterial effector fragments, with respect to 2xFYVE-GFP, LC3B, and LAMP1 (Figure 3B,C). The deletion of the first 370 amino acids did not affect CvpF localization nor the formation of perinuclear clusters of CvpF-labeled compartments (Figure 3B). Conversely, $CvpF_{500\text{-}695}$ failed to localize at cellular membranes and remained diffused in the cytoplasm (Figure 3B). Accordingly, the expression of $CvpF_{500\text{-}695}$ also failed to reposition cellular compartments to the perinuclear area (Figure 3B). Deletion of the last 195 amino acids ($CvpF_{1\text{-}500}$) did not affect membrane targeting of CvpF; however, the localization with LAMP1- and LC3B-positive vesicles was lost, together with the effect on the perinuclear positioning of these two markers. Of note, $CvpF_{1\text{-}500}$ still localized at PtdIns3P-positive structures, which retained the perinuclear localization. Further C-terminal deletions of CvpF resulted in a loss of membrane localization and the cytoplasmic redistribution of membrane markers. This result indicated that the membrane-binding domain (MBD) of CvpF is located between amino acids 370 and 500 and that the C-terminal domain of CvpF (effector domain, ED) may play a role either in the re-routing of early endosomes to autophagosomes or the maturation of autophagosomes to autolysosomes (Figure 3C).

Bioinformatics analysis of the CvpF MBD revealed the presence of one [DERQ]XXX[LI] and 2 YXXΦ endocytic sorting motifs (Figure S4A), involved in the interaction with clathrin adaptor complexes. We, thus, generated di-leucine and tyrosine mutants to validate the functionality of these motifs. The di-leucine LLAA mutant, and the Y440A mutant, failed to affect the membrane targeting and perinuclear localization of CvpF, whereas the Y425A mutation sufficiently displaced CvpF to the cytoplasm with concomitant loss of LAMP1 and LC3B repositioning (Figure S4B and C). Accordingly, Tyr425 is required for CvpF localization at the CCV (Figure S4D). These observations suggest that Tyr425 could be part of a functional endocytic sorting motif. To date, however, we could not detect any interaction or co-localization between CvpF and adaptor complexes or clathrin (data not shown).

CvpF stimulates LC3B-II formation

Several studies have shown that *Coxiella* stimulates the formation of LC3B-II in a T4SS-dependent manner during infection [15,35,36]. To determine whether the secretion of CvpF participates in the formation of LC3B-II, we infected U2OS cells either with the *WT* GFP *Coxiella* strain (*Tn1832*), the *cvpF*::Tn mutant, or the complemented *cvpF*::Tn mutant (*cvpF*::Tn Comp.). Given the intracellular replication defect of the *cvpF*::Tn mutant *Tn248*, and to rule out the possibility that LC3B-II increase is dependent on the bacterial load, we also infected cells with an excess of *cvpF*::Tn mutant (*cvpF*::Tn x10) (Figure 4A). We observed an increase in LC3B-II levels for cells infected with *WT Coxiella* and the complemented *cvpF*::Tn mutant, in the presence of bafilomycin A_1. We observed no LC3B-II increase for cells infected with the *cvpF*::Tn mutant (Figure 4A). Next, we infected the cells as in Figure 4A and starved for 3 h to determine whether the LC3B-II increase observed with *WT Coxiella* and the complemented *cvpF*::Tn mutant was not due to a blockade of the autophagy flux. We analyzed levels of SQSTM1/p62 (sequestosome 1) by western blot, which revealed that upon starvation, SQSTM1 is degraded for all conditions, indicating that CvpF does not block the starvation-induced autophagy flux but stimulates the formation of LC3B-II (Figure 4B).

The vacuolar localization of CvpF, together with the decreased presence of LC3B on CCVs generated by *cvpF*::Tn mutants prompted us to investigate the role of CvpF in autophagosome dynamics further. We probed the individual role of CvpF on LC3B-II increase in transfected cells. We analyzed the autophagy flux by western blotting on U2OS cells expressing

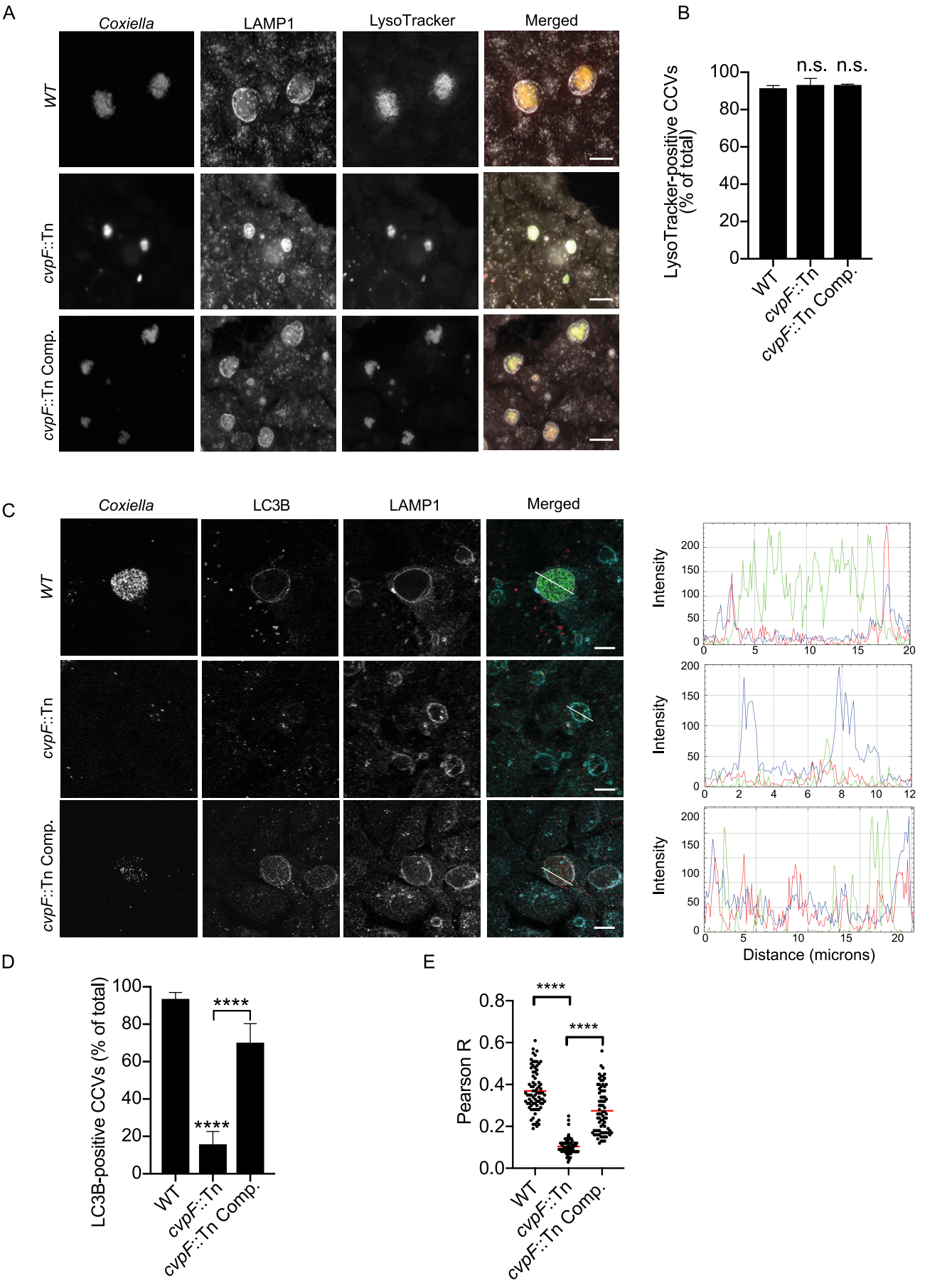
A
Coxiella
LAMP1
LysoTracker
Merged
WT
cvpF::Tn
cvpF::Tn Comp.
B
LysoTracker-positive CCVs (% of total)
n.s. n.s.
WT
cvpF::Tn
cvpF::Tn Comp.
C
Coxiella
LC3B
LAMP1
Merged
WT
cvpF::Tn
cvpF::Tn Comp.
Intensity
Distance (microns)
D
LC3B-positive CCVs (% of total)
****
****
WT
cvpF::Tn
cvpF::Tn Comp.
E
Pearson R
****
****
WT
cvpF::Tn
cvpF::Tn Comp.

HA, HA-CvpF, or HA-CvpF^{Y425A} (Figure 4C). When bafilomycin A_1 blocks the autophagy flux, we observed a marked increase in LC3B-II and SQSTM1 in cells expressing CvpF and HA-CvpF^{Y425A} compared to cells expressing HA, with wild type CvpF having the greatest effect on SQSTM1 levels, indicating that CvpF stimulates the autophagy flux and that its membrane localization participates in this process (Figure 4C).

Next, we co-transfected HA-CvpF and HA-CvpF^{Y425A} with the tandem-fluorescent probe TF-LC3. This probe consists of an LC3B linked to GFP and RFP. Since acidic conditions quench GFP fluorescence, this probe labels autophagosomes in green and red, while autolysosomes appear only red. In transfected cells, HA-CvpF localizes to clustered vesicles, only displaying red fluorescence corresponding to autolysosomes (Figure S5A). Conversely, CvpF^{Y425A} displayed a diffuse localization, and transfected cells displayed non-acidified autophagosomes similarly to HA-transfected cells (Figure S5A). Upon addition of bafilomycin A_1, CvpF was still found present on clustered vesicles, but these were GFP- and RFP-positive (Figure S5B). In bafilomycin A_1-treated cells, HA and HA-CvpF^{Y425A} _ transfected cells displayed non-acidified autophagosomes similarly to the mock-treated condition (Figure S5B). CvpF-dependent clustering of vesicles rendered the scoring of LC3B-positive puncta impossible. Of note, vesicular swelling and clustering triggered by overexpression of LAMP1-Flag did not affect the TF-LC3 probe signal in the presence or absence of bafilomycin A_1, indicating that CvpF alone can stimulate the formation of autophagosomes and autolysosomes. Furthermore, its membrane localization seems critical to act on this endosomal system.

Finally, to rule out the possibility that CvpF stimulates autophagy by inhibiting MTORC1, we stained U2OS cells transfected with HA, HA-CvpF, or HA-CvpF^{Y425A} for MTOR and we labeled lysosomes with LysoTracker (Figure S6A). The expression of CvpF or CvpF^{Y425A} did not affect the localization of MTOR on lysosomes, indicating that CvpF does not alter MTORC1 activity to stimulate autophagy.

CvpF interacts with the autophagy-related RAB GTPase RAB26

Yeast two-hybrid screening identified the small GTPase RAB26 as a candidate interactor of CvpF. Of note, RAB26 has been previously involved in lysosomal positioning [37], autophagosome maturation [18,19], and vesicle-mediated secretion of adrenergic receptors [38]. We, thus, validated the interaction using a co-immunoprecipitation approach on U2OS cells co-expressing HA-CvpF and GFP-RAB26 (Figure 5A). The lack of interaction in cells co-expressing HA-CvpF together with GFP-tagged versions of RAB5, RAB7, RAB9, RAB11, or RAB37 (the closest homolog of RAB26 with 54% amino acid identity), indicated that the CvpF-RAB26 interaction is specific (Figure 5A). In agreement with the interactomics analysis, fluorescence microscopy indicated that CvpF and RAB26 localize at the same cellular compartments, and that expression of CvpF increases membrane targeting of RAB26 (Figure 5B). Of note, we still observed interactions in cells co-expressing CvpF^{Y425A} and RAB26, indicating that the membrane targeting of CvpF is not required for the interaction with RAB26 (Fig. S6B). However, ectopically expressed CvpF^{Y425A} does not alter GFP-RAB26 distribution in cells, indicating that the interaction of CvpF with membranes is required to relocalize RAB26 (Figure S6C). Further analysis using the CvpF truncations revealed that the domain 370–695 of CvpF is sufficient to relocalize RAB26 onto vesicles (Figure S7).

To investigate whether CvpF binds preferentially to active or inactive forms of RAB26, we generated GFP-tagged dominant-negative (GFP-RAB26^{T77N}), dominant-positive (GFP-RAB26^{Q123L}) and guanosine-free (GFP-RAB26^{N177I}) versions of RAB26. We co-expressed these constructs in U2OS cells, in combination with HA-CvpF for the co-immunoprecipitation assay or mCherry-CvpF, to investigate the respective intracellular localization of the two proteins. Interactomics analysis indicated that CvpF preferentially binds to inactive RAB26 (Figure 5C), which we confirmed by fluorescence microscopy. Indeed, co-expression of either GFP-RAB26^{T77N} or GFP-RAB26^{N177I} with mCherry-CvpF resulted in the membrane targeting of the small GTPase, conversely, we observed little or no overlapping between mCherry-CvpF and GFP-RAB26^{Q123L} (Figure 5D). Together, these observations suggest that CvpF might act as a guanosine exchange factor (GEF) or GDI displacement factor (GDF), anchoring and/or activating RAB26 on either early endosomal or pre-autophagosomal structures.

CvpF triggers the recruitment of RAB26 to CCVs

CvpF localization at CCVs (Figure 1A) and its interaction with RAB26 (Figure 5A) suggested that the small GTPase might be recruited at CCVs and be involved in vacuole biogenesis. To test whether RAB26 recruitment at CCVs is CvpF-dependent, we infected U2OS cells with *WT Coxiella*, *cvpF*::Tn or *cvpF*::Tn Comp. and transfected with a plasmid expressing GFP-RAB26 (Figure 6A). Indeed, GFP-RAB26

Figure 2. CvpF participates in LC3B recruitment to CCVs but not in their acidification. (A) U2OS cells were infected with either *Coxiella WT* GFP (top panels), *cvpF*::Tn (middle panels) or the complemented *cvpF*::Tn strain (*cvpF*::Tn Comp., bottom panels) (green) for 6 d, fixed and stained with anti-LAMP1 (pseudo-colored gray) and LysoTracker (red). (B) U2OS cells were infected as in A, and the presence of the LysoTracker probe in CCVs was scored for at least 80 cells. (C) U2OS cells were infected with either *Coxiella WT* GFP (top panels), *cvpF*::Tn (middle panels), or the complemented *cvpF*::Tn strain (*cvpF*::Tn Comp., bottom panels) for 6 d, fixed and stained with anti-LAMP1 (pseudo-colored cyan) and anti-LC3B (red). The white line in the merged image indicates the position of the profile line used for the analysis of intensity distribution. Fluorescence intensity plotting of GFP (green), LC3B (red), and LAMP1 (blue) signals are shown on the right for each strain. (D) U2OS cells were infected as in C and the presence of LC3B on CCVs was scored for at least 80 cells. Values are mean ± SD from 3 independent experiments (n.s. = non-significant, **** = $P < 0.0001$, one-way ANOVA, Dunnett's multiple comparison test). Scale bars: 10 µm. (E) Pearson's correlation coefficient between LC3B and LAMP1 signals in images acquired in C (**** = $P < 0.0001$, one-way ANOVA, Sidak's multiple comparison test).

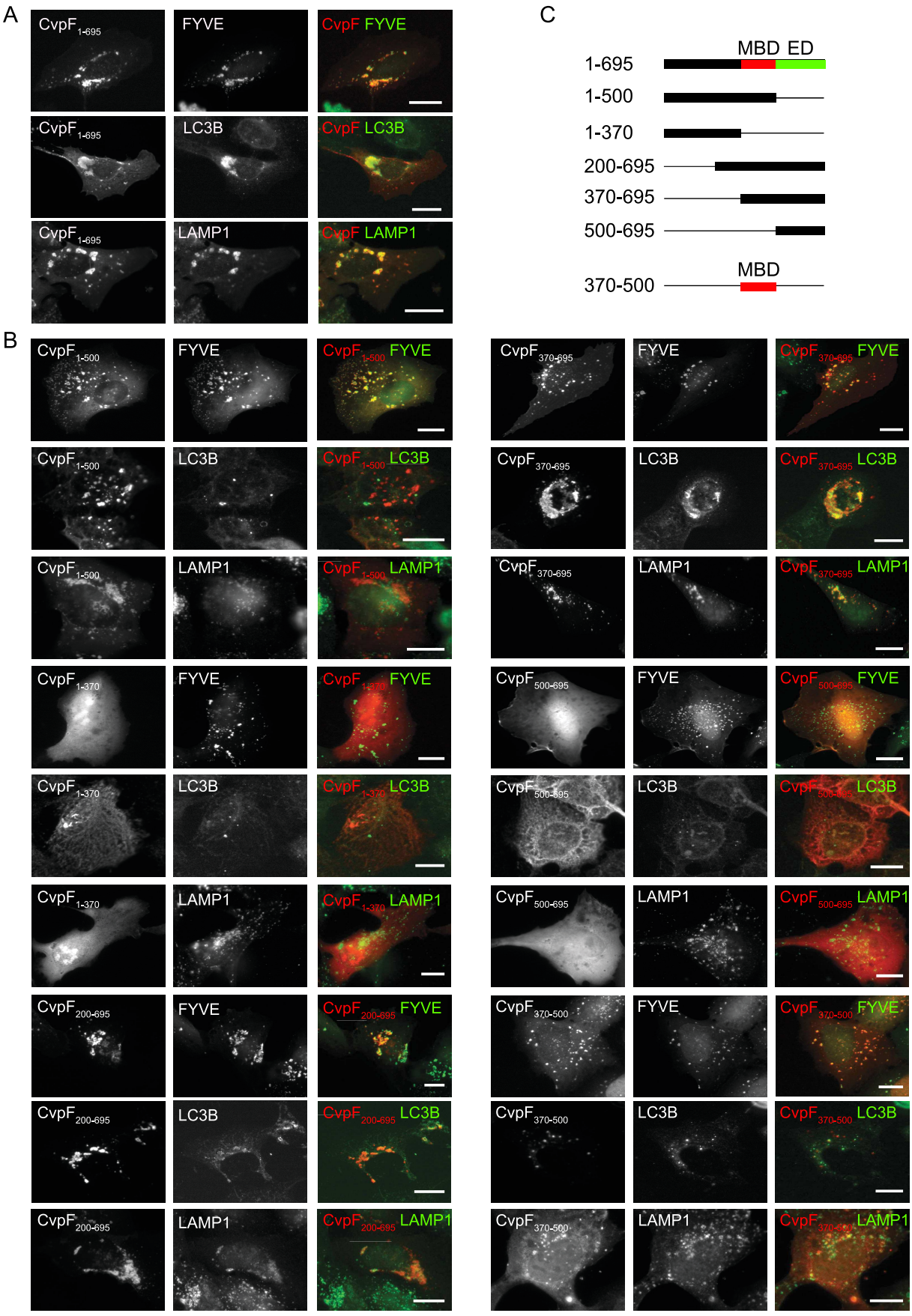

Figure 3. Ectopically expressed CvpF localizes to vesicles with autolysosomal features. (A) U2OS or U2OS GFP-FYVE cells were transfected with pLVX-mCherry-CvpF or pRK5-HA-CvpF (red). Cells were fixed and labeled either with anti-LC3B, or anti-LAMP1 antibodies (green). HA-CvpF was labeled with an anti-HA antibody (red). (B) U2OS or U2OS GFP-FYVE cells were transiently transfected with plasmids pLVX-mCherry or pRK5-HA fused to $CvpF_{1-500}$, $CvpF_{1-370}$, $CvpF_{200-695}$, $CvpF_{370-695}$, $CvpF_{500-695}$, or $CvpF_{370-500}$ (red). Cells were fixed and labeled either with anti-LC3B or anti-LAMP1 antibodies (green). HA-tagged constructs were labeled with anti-HA antibody (red). (C) Schematic representation of CvpF fragments used in A and B. MBD: membrane-binding domain, ED: effector domain. Scale bars: 10 μm.

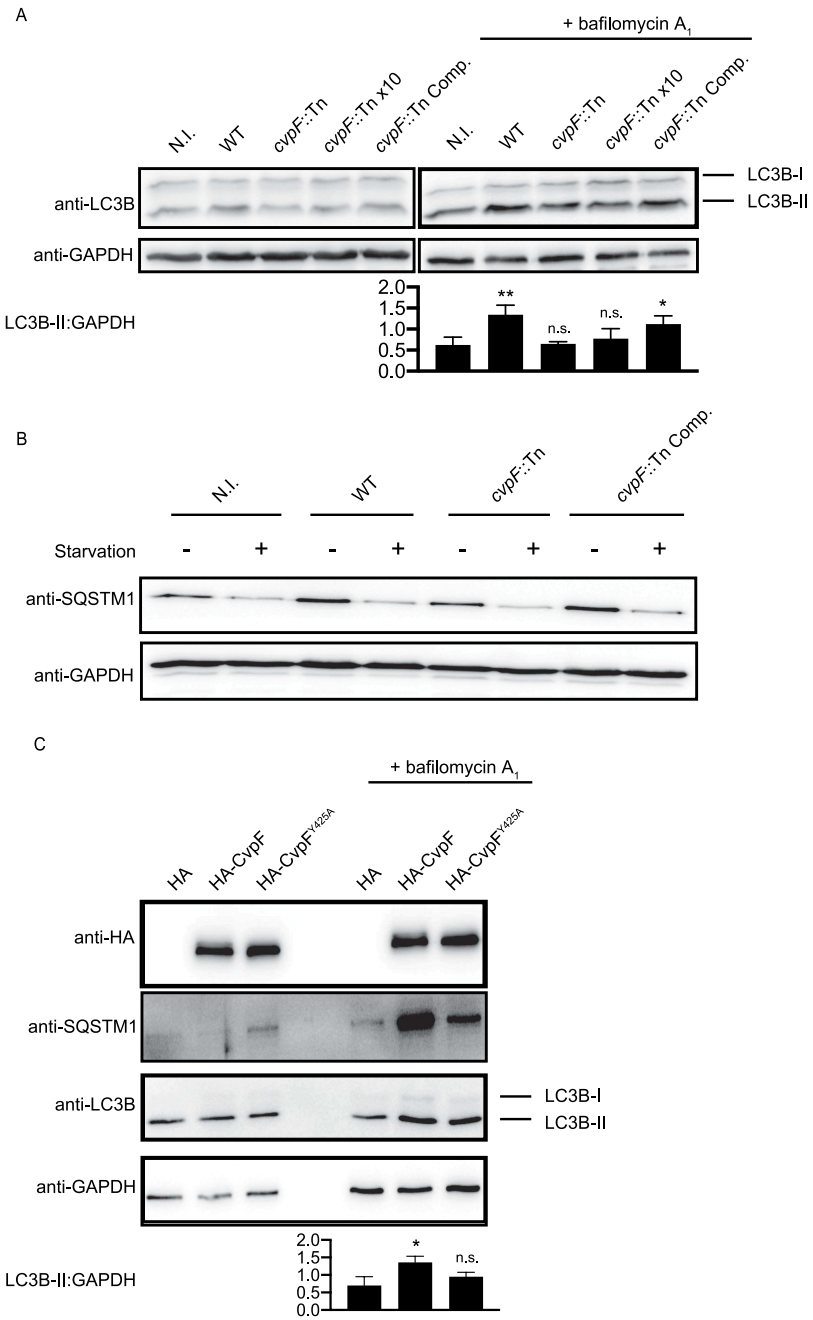

Figure 4. CvpF stimulates the formation of LC3B-II. (A) Immunoblot of lysates from U2OS cells left uninfected (N.I.) or infected with *Coxiella WT* GFP (*WT*), *cvpF*::Tn, 10 times *cvpF*::Tn (*cvpF*::Tn x10) or the complemented *cvpF*::Tn strain (*cvpF*::Tn Comp.) for 72 h in complete media. Bafilomycin A_1 (25 nM) was added to the media 3 h before lysis. Immunoblots were probed with antibodies against LC3B and GAPDH. The signal ratio of LC3B-II versus GAPDH is indicated for samples treated with bafilomycin A_1. (B) Immunoblot of lysates from U2OS cells left uninfected (N.I.) or infected with *Coxiella WT* GFP (*WT*), *cvpF*::Tn, or the complemented *cvpF*::Tn strain (*cvpF*::Tn Comp.) for 72 h in complete media. Starvation was triggered by incubation of cells in HBSS for 3 h before lysis. Immunoblots were probed with antibodies against SQSTM1 and GAPDH. (C) Immunoblot of lysates from U2OS cells transfected with pRK5-HA, pRK5-HA-CvpF or pRK5-HA-$CvpF^{Y425A}$ mock-treated or treated with 25 nM bafilomycin A_1 for 1 h. The signal ratio of LC3B-II versus GAPDH is indicated for samples treated with bafilomycin A_1. Values are mean ± SD from 3 independent experiments (n.s. = non-significant, ** = $P < 0.0021$, * = $P < 0.0033$, one-way ANOVA, Dunnett's multiple comparison test).

became recruited on 75.4 ± 2.72% of CCVs generated by *WT Coxiella* and 66.9 ± 6.12% of CCVs generated by *cvpF*::Tn Comp. strains but only 23.23 ± 3.78% of CCVs generated by *cvpF*::Tn mutants were positive for RAB26 (Figure 6B). Colocalization analysis between LAMP1 and RAB26 on CCVs generated by *WT*, *cvpF*::Tn and *cvpF*::Tn complemented strains (Figure 6C) indicated that CvpF stimulates the presence of RAB26 at the CCV.

Inhibition of RAB26 activity alters LC3B recruitment to CCVs and CCV development

Active RAB26 has been shown to interact with ATG16L1 [18,19], which is key for LC3B anchoring to membranes. We, thus, determined the requirement of active RAB26 for CCV biogenesis and investigated the presence of the LC3B autophagy marker on CCVs in cells expressing GFP, GFP-RAB26, GFP-$RAB26^{T77N}$, GFP-$RAB26^{Q123L}$, and GFP-$RAB26^{N177I}$. The LC3B

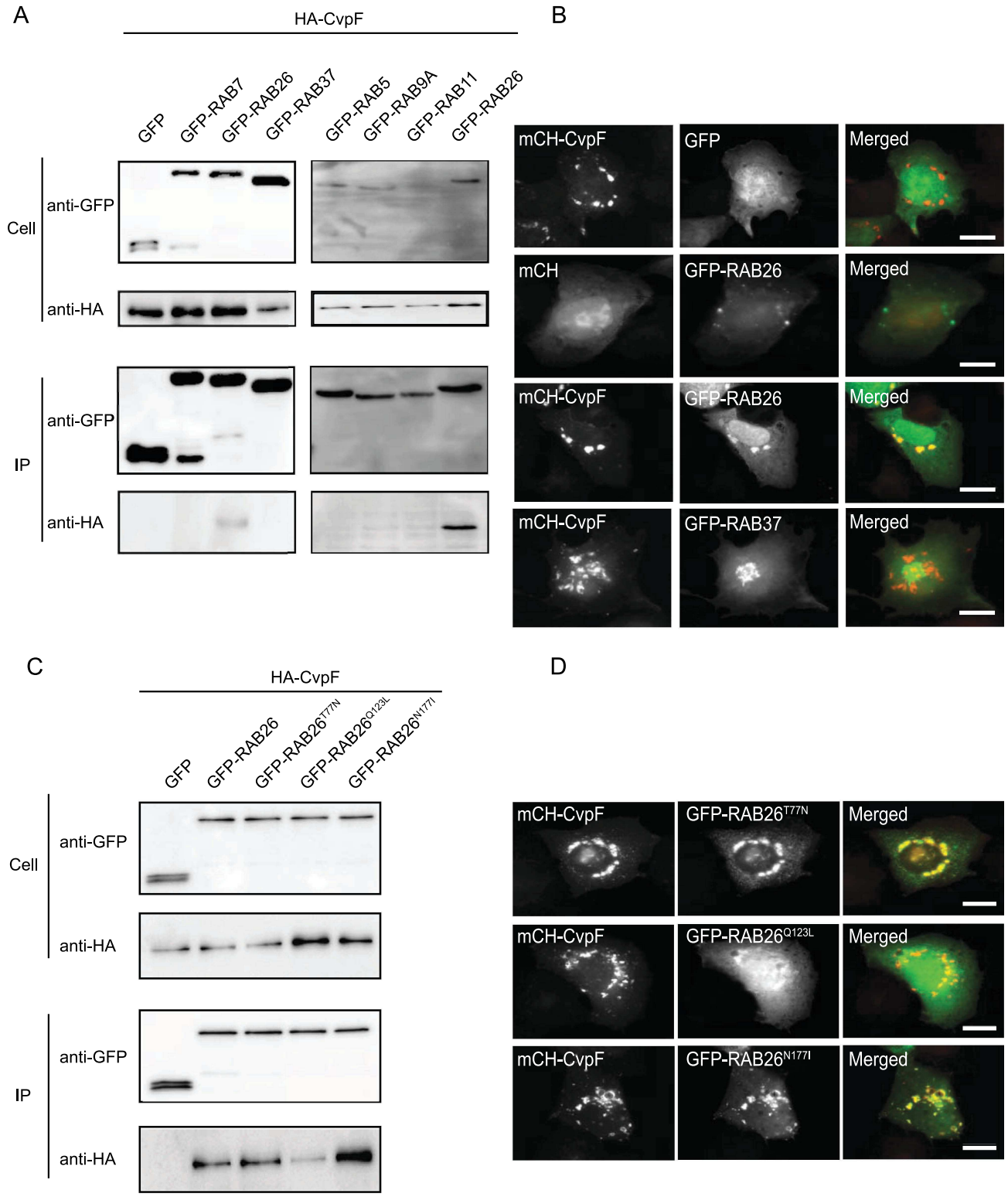

Figure 5. CvpF interacts specifically with RAB26. (A) A co-immunoprecipitation assay using U2OS cells co-transfected with pRK5-HA-CvpF and pLVX-GFP, pLVX-GFP-RAB5, peGFP-RAB7, peGFP-RAB9, pLVX-GFP-RAB11, pLVX-GFP-RAB26, pLVX-GFP-RAB37. RAB GTPases and CvpF were detected using anti-GFP and anti-HA antibodies, respectively. (B) U2OS cells were transfected with pLVX-mCherry or pLVX-mCherry-CvpF (red) and pLVX-GFP, pLVX-GFP-RAB26 or pLVX-GFP-RAB37 (green). (C) A co-immunoprecipitation assay using U2OS cells co-transfected with pRK5-HA-CvpF and pLVX-GFP, pLVX-GFP-RAB26, pLVX-GFP-RAB26^{T77N}, pLVX-GFP-RAB26^{Q123L}, pLVX-GFP-RAB26^{N177I}. The RAB GTPases and CvpF were detected using anti-GFP and anti-HA antibodies, respectively. (D) U2OS cells were transiently transfected with pLVX-mCherry-CvpF (red) and pLVX-GFP-RAB26^{T77N}, pLVX-GFP-RAB26^{Q123L} or pLVX-GFP-RAB26^{N177I} (green). Scale bars: 10 μm.

signal on CCVs generated by *Coxiella* NMII became much reduced in cells transfected with the inactive forms of RAB26 (GFP-RAB26^{T77N} and GFP-RAB26^{N177I}) compared to cells expressing either RAB26 wild type (GFP-RAB26) or active RAB26 (GFP-RAB26^{Q123L}) (Figure 7A). Of note, loss of LC3B was accompanied by a reduction in the size of CCVs (Figure 7B).

To confirm the importance of RAB26 for CCV development, we inhibited endogenous RAB26 expression using the

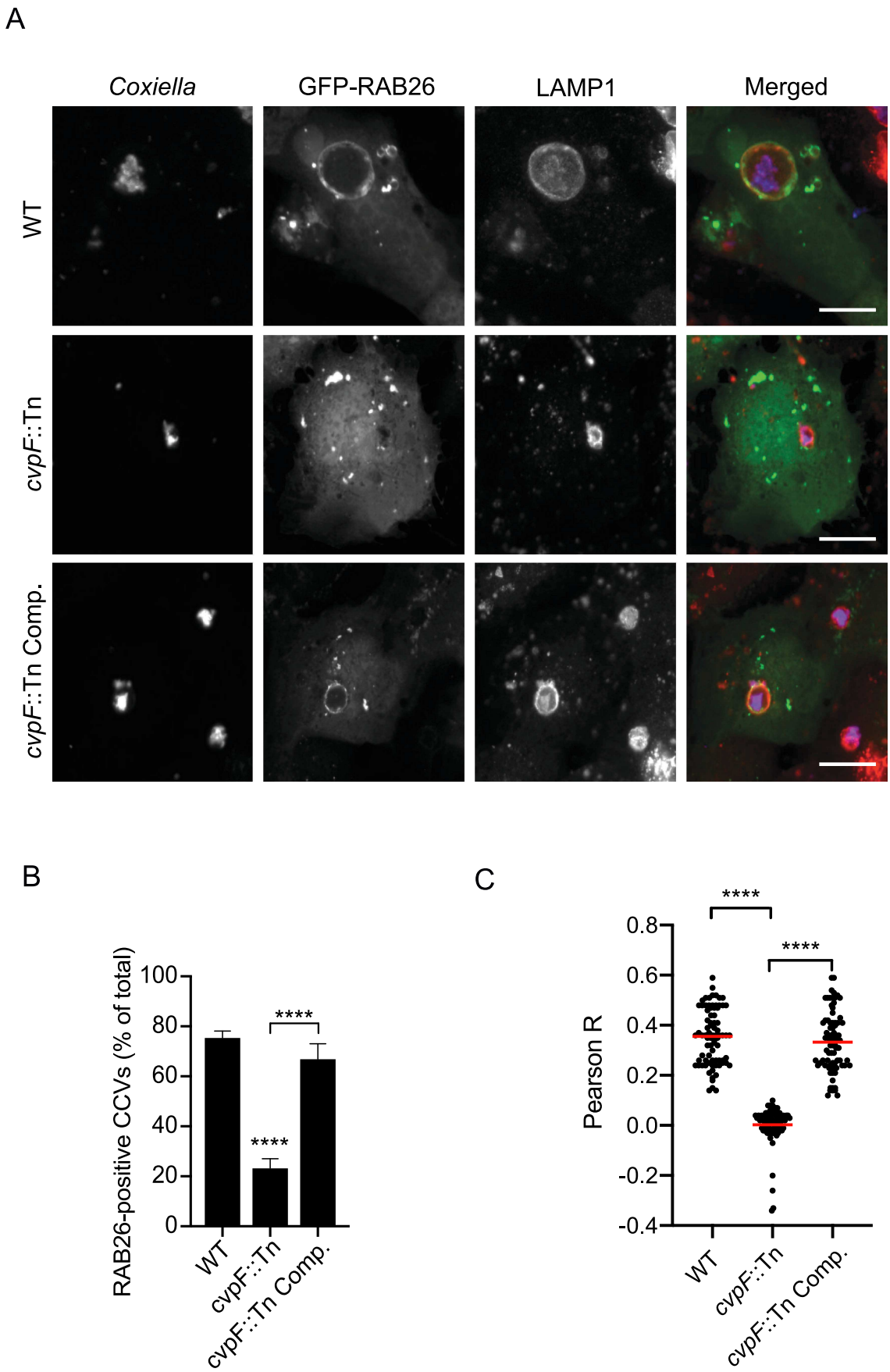

Figure 6. CvpF stimulates the recruitment of RAB26 to CCVs. (A) U2OS cells were infected with either *Coxiella WT* GFP (*WT*, top panels), *cvpF*::Tn (middle panels), or the complemented *cvpF*::Tn strain (*cvpF*::Tn Comp., bottom panels) and transfected with pLVX-GFP-RAB26 (green) 4 d post-infection. We fixed cells 12 h post-transfection and stained with anti-LAMP1 (red) and anti-*Coxiella* (blue) antibodies. (B) U2OS cells were infected, as in A, and the presence of RAB26 on CCVs was scored for at least 80 cells per condition. Values are mean ± SD from 3 independent experiments (n.s. = non-significant, **** = $P < 0.0001$, one-way ANOVA, Bonferroni's multiple comparison test). Scale bars: 10 µm. (C) Pearson's correlation coefficient between RAB26 and LAMP1 signals in images acquired in A (**** = $P < 0.0001$, one-way ANOVA, Sidak's multiple comparison test).

CRISPR-Cas9 genome editing system. We used three RAB26-targeting guides, and guide 5 was the most efficient in decreasing RAB26 expression (Figure 7C). We infected U2OS cells treated with either non-targeting guides or RAB26-targeting guide 5 with *WT Coxiella*, and we determined the CCV area and Genome Equivalents (GE). We observed a marked decrease in CCV area (Figure 7D), as well as bacterial replication (Figure 7E) in cells deficient in RAB26 expression, indicating that RAB26-mediated autophagy is key to the development of CCVs.

Co-expression of RAB26 with CvpF stimulates the formation of LC3B-II

To determine whether the interaction between CvpF and RAB26 stimulates the recruitment of LC3B onto vesicles, we transfected U2OS cells with HA-CvpF, in combination with either GFP, GFP-RAB26, GFP-RAB26^{T77N}, GFP-RAB26^{Q123L}, or GFP-RAB26^{N177I}. While the co-expression of RAB26 wild type and RAB26^{Q123L} with CvpF led to an increase of the LC3B signal onto vesicles, the concomitant expression of the dominant-negative and guanosine-free forms of RAB26 with CvpF led to a moderate increase of the LC3B signal (Figure 8). These observations indicate that active RAB26 can stimulate the recruitment of LC3B onto vesicles and that CvpF could activate RAB26 to trigger the recruitment of LC3B onto vesicles.

Discussion

Coxiella-containing vacuoles (CCVs) are unique compartments with autolysosomal features. Key to the generation of CCVs is the secretion of bacterial effectors that divert host cell mechanisms to shape an adequate environment for bacterial replication. Here, we identified a new *Coxiella* effector protein important for vacuole biogenesis and replication of the bacterium in epithelial and myeloid cell lines. As recent studies have highlighted, the fact that defective vacuole biogenesis impacts *Coxiella* virulence in insect and mammalian models of infection [12,34,39], we, thus, investigated the *in vivo* relevance of CvpF using the recently developed SCID mouse model. This model is capable of assessing two traits relevant to virulence, such as the ability to cause splenomegaly (a surrogate for inflammation) and the ability to replicate within the spleen (replication defect). The *cvpF*::Tn mutant was severely attenuated for both virulence readouts, and we found even less GE in the spleens than in the *dotA*::Tn mutant. We hypothesize that this is a result of the impaired vacuole synthesis, but it could be due to the ability of the *cvpF*::Tn mutant to secrete proteins, which may alert the innate immune system. In agreement with the *in vitro* observations, the complemented strain was able to partially rescue the ability of *cvpF*::Tn to replicate within the spleen and marginally increased the amount of splenomegaly.

Stimulation of autophagy leads to increased CCV size, suggesting that autophagy provides nutrients and membranes to the expanding CCV [28]. It has been shown that infection of cultured myeloid and epithelial cells with *Coxiella* wild type leads to increased lipidation of LC3B [35,40] and that this lipidation is dependent on the secretion of bacterial effectors [15,36]. Besides lipidation of LC3B, secretion of bacterial effectors via the T4SS is required for the acquisition of autophagosomes and autophagosomal markers to the CCV [12,35,39,40]. Here, we showed how the secreted effector CvpF diverts RAB26-dependent autophagy to favor the generation of *Coxiella*-containing vacuoles *in vitro*, and the virulence of the bacterium *in vivo*. Indeed, most of CCVs generated by the *cvpF*::Tn mutant are devoid of the autophagosomal marker LC3B, suggesting that CvpF could favor CCV biogenesis by manipulating autophagy. Interestingly, SQSTM1 levels are stabilized during *Coxiella* infections [40,41], and SQSTM1 is recruited to CCVs in a T4SS-dependent but LC3B-independent manner. We showed here an increase of steady-state levels of LC3B-II and SQSTM1 in cells infected with *WT Coxiella* and the *cvpF*::Tn complemented strains compared to cells infected with the *cvpF*::Tn mutant or in uninfected cells. This observation is similar to what is observed in HeLa cells infected with the *cig57*::Tn mutant [15]. Indeed, *Coxiella* effector Cig57 has been shown to influence autophagy via clathrin recruitment to CCVs, as *cig57*::Tn mutant CCVs display decreased levels of clathrin and LC3B [15,42]. However, contrary to CvpF, Cig57 alone was not capable of inducing LC3B lipidation [15]. This observation raises the possibility that CvpF and Cig57 could be functionally linked through the recruitment of host cell proteins RAB26 and clathrin, respectively, to CCVs.

Cells expressing HA-CvpF show decreased steady-state levels of SQSTM1 but unaltered levels of steady-state LC3B-II. The increased levels of SQSTM1 and LC3B-II in the presence of bafilomycin A_1 suggest that ectopically expressed CvpF could stimulate the degradation of SQSTM1 and the lipidation of LC3B-II. However, in the context of infection, multiple effectors are translocated that could counteract some of CvpF actions (i.e., SQSTM1 degradation, stimulation of SQSTM1 transcription). The fact that cells infected with the *cvpF*::Tn mutant display less SQSTM1 compared to cells infected with the *WT* strain could be the result of other *Coxiella* effectors. Overall, ectopically expressed CvpF stimulates the formation of LC3B-II but also the degradation of SQSTM1, suggesting that CvpF would be involved in the formation of autolysosomes, but other effectors could stabilize SQSTM1 during infection.

Several studies have shown that mature autophagosomes are recruited to the CCV [39,40] and that another effector protein, CvpB/Cig2, is important to recruit LC3B to CCVs and to maintain the CCV in an autolysosomal stage of maturation [35,39]. This is achieved via the CvpB-dependent stabilization of phosphatidylinositol 3-phosphate at CCVs [12]. Interestingly, in *cvpB*/*cig2*::Tn mutants, LC3B lipidation, and SQSTM1 levels are increased. This raises the possibility that *Coxiella* effectors may act in sequence to modify the lipid and protein signature of the CCV, and to alter the physiological behavior of the endosomal network. In this case, effectors such as CvpB and Cig57 would initiate CCV maturation events, and CvpF could then stimulate the autophagy flux to provide membranes and nutrients to expand CCVs and permit optimal *Coxiella* replication.

Ectopic expression showed that CvpF has a strong capacity to remodel the endosomal network by clustering early

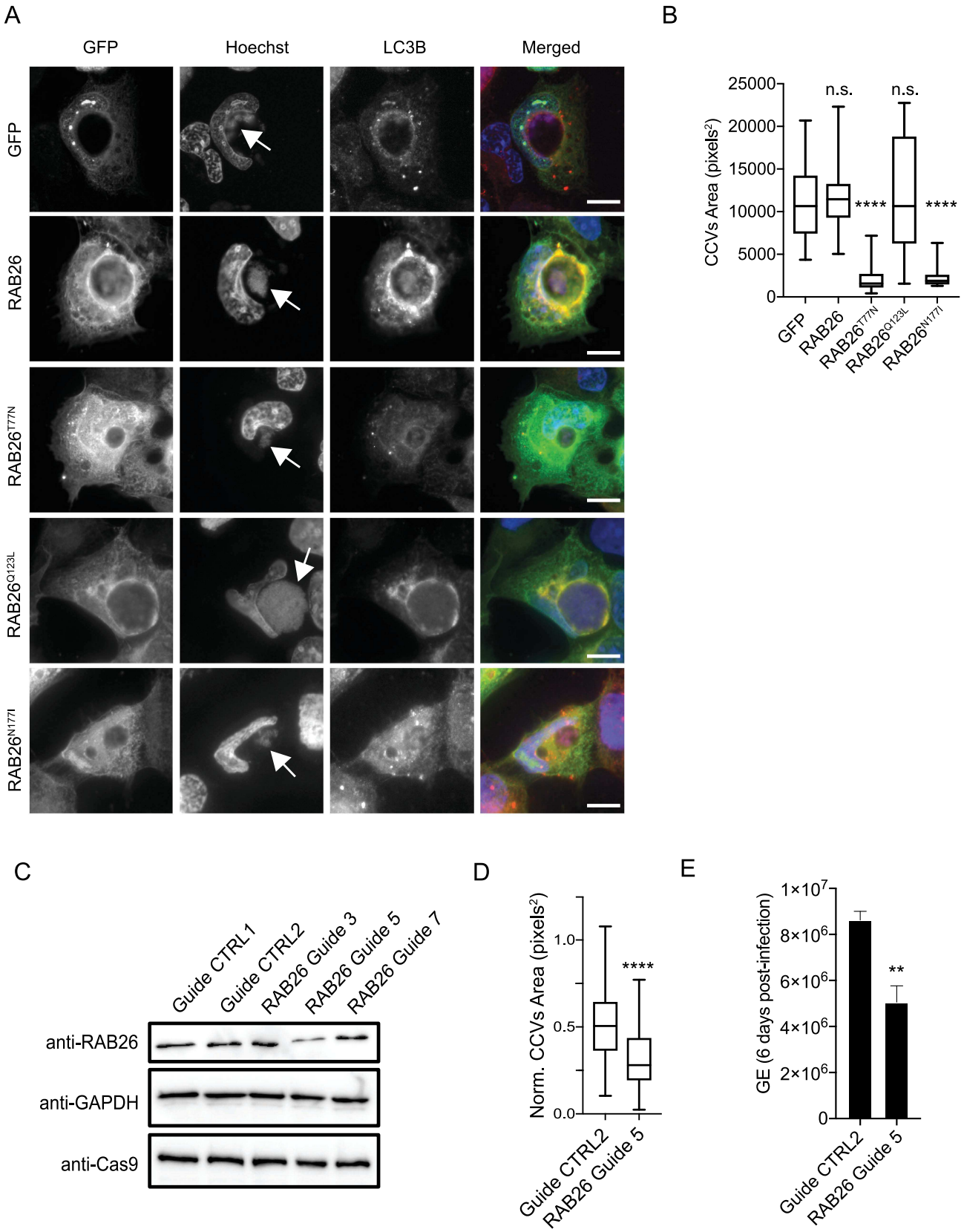

Figure 7. RAB26 activity is essential for CCV biogenesis. (A) U2OS cells infected with *Coxiella* NMII were transfected with pLVX-GFP, pLVX-GFP-RAB26, pLVX-GFP-RAB26^{T77N}, pLVX-GFP-RAB26^{Q123L} or pLVX-GFP-RAB26^{N177I} (green) 2 d post-infection. We fixed cells 24 h post-transfection and stained with anti-LC3B (red) and stained DNA using Hoechst 33,258 (blue). White arrows indicate *Coxiella* colonies. (B) Cells were treated as in A, and the CCV area was measured for at least 100 cells per condition. Values are mean ± SD from 3 independent experiments (n.s. = non-significant, **** = P < 0.0001, one-way ANOVA, Dunnett's multiple comparison test). (C) Immunoblot of lysates from U2OS Cas9 cells expressing non-targeting guides (Guide CTRL1 and guide CTRL2) or RAB26-targeting guides (RAB26 Guide 3, 5 and 7). Immunoblots were probed with antibodies against RAB26, GAPDH and Cas9. (D) U2OS Cas9 cells expressing the non-targeting guide CTRL2 or the RAB26-targeting guide 5 were challenged for 6 d with *Coxiella WT* GFP (*WT*). The normalized CCV area for each condition was determined using the Cell Profiler software. (E) U2OS cells were challenged as in D and Genome Equivalents (GE) were determined by quantitative PCR. Values are mean ± SD from 3 independent experiments (n. s. = non-significant, **** = P < 0.0001, ** = P < 0.001, unpaired t test). Scale bars: 10 µm.

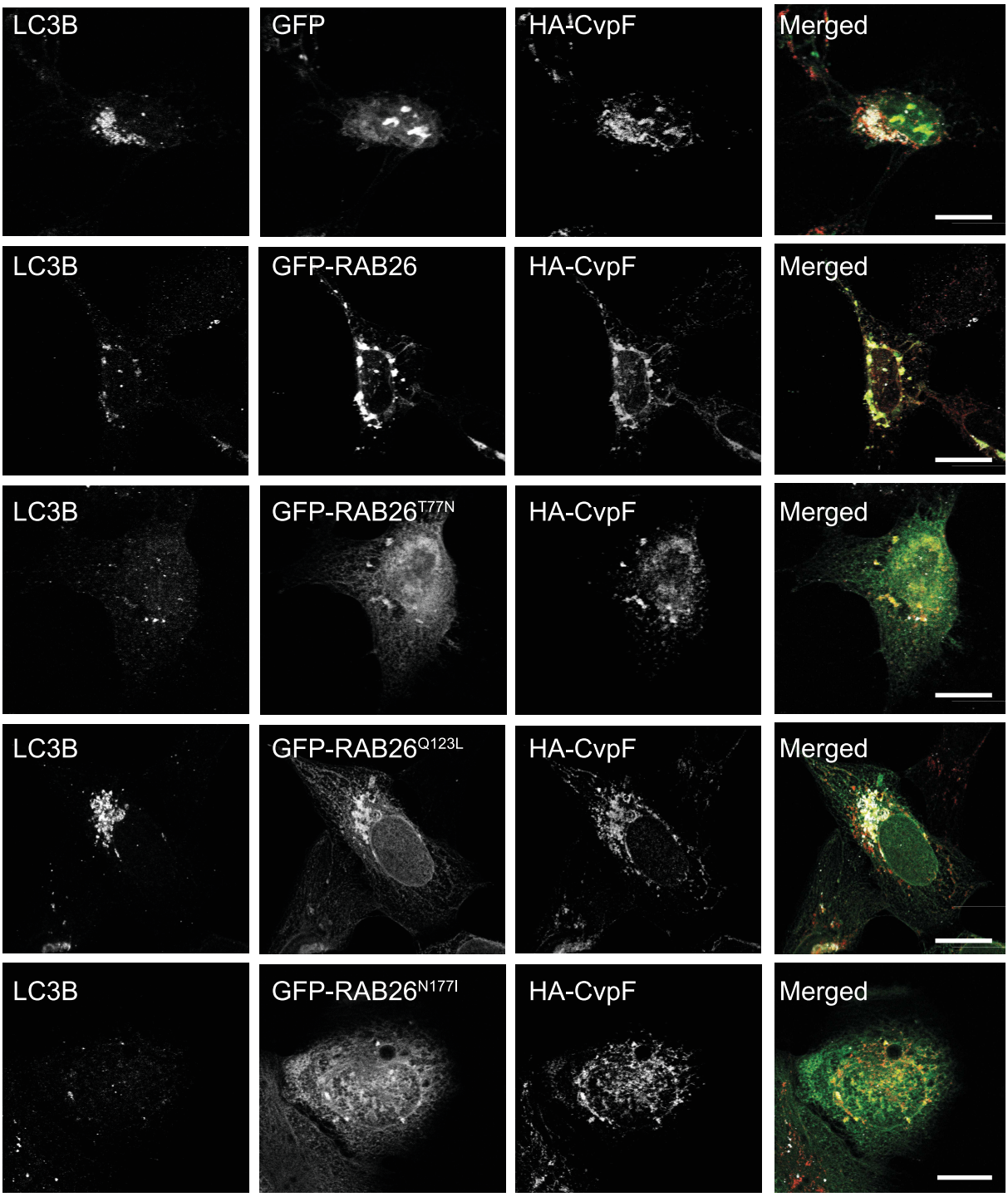

Figure 8. Co-expression of CvpF and RAB26 stimulates the formation of LC3B-positive endosomes. U2OS cells were transfected with pLVX-GFP, pLVX-GFP-RAB26, pLVX-GFP-RAB26^{T77N}, pLVX-GFP-RAB26^{Q123L}, or pLVX-GFP-RAB26^{N177I} (green) and pRK5-HA or pRK5-HA-CvpF. Cells were fixed and stained with anti-LC3B (red) and anti-HA (blue). Scale bars: 10 μm.

and late endosomal vesicles, as well as autophagosomal structures in the perinuclear area of transfected cells. Of note, the dynein-dependent movement of autophagosomes is used in cells to promote their efficient encounter with lysosomes [43], a mechanism that could be used by CvpF to drive transport and maturation of vesicles toward an autolysosomal state. Interestingly, CvpF possesses an internal motif that corresponds to a putative eukaryotic-like endocytic sorting motif that could interact with adaptor complexes (APs), similar to the vacuolar effector CvpA [10]. Indeed, mutation of a critical tyrosine residue in this motif led to the complete relocalization of CvpF to the cytosol of transfected cells. Furthermore, this tyrosine could also be part of an extended LC3-interacting region (LIR) motif

(xx[WFY]xx[LIV]) [44]. However, direct interaction of CvpF with APs and LC3B still needs to be experimentally demonstrated.

Several RAB GTPases have been shown to decorate the CCV (RAB1 [29], RAB7 [26], and RAB24 [28]), all of them being important for its biogenesis. Importantly, CvpF is the first *Coxiella* effector protein to interact with RAB GTPases. Specific interaction of CvpF with RAB26 recruits the small GTPase to CCVs and RAB26-depletion, or inactivation decreases LC3B recruitment at CCVs, which is accompanied by a strong reduction in CCVs size, indicating that active RAB26 and RAB26-dependent stimulation of autophagy favor the development of CCVs. Accordingly, RAB26 participates in the transport of lysosomes to perinuclear regions [37] and autophagy [18,19], as its active form is capable of interacting with ATG16L1 to stimulate LC3B lipidation.

Intracellular pathogens commonly manipulate RAB GTPases for the establishment of their replicative niche [24]. For example, *Legionella pneumophila* secretes at least 7 effectors targeting the RAB GTPase RAB1 for the development of its vacuole [45,46]. CvpF preferentially interacts with the inactive form of RAB26 and stimulates its presence on endosomal vesicles, suggesting that CvpF may act either as a GDI Dissociation Factor (GDF) or Guanine Exchange Factor (GEF) for RAB26. This hypothesis remains to be experimentally validated. Interestingly, CvpF still localizes with inactive RAB26 in the perinuclear area, suggesting that the CvpF-dependent endosomal relocation does not rely on RAB26 activity.

Thus, in this study, we identified the first *Coxiella* effector protein capable of interacting with an autophagy-related RAB GTPase to stimulate the autophagy flux. With a repertoire of more than 130 effector proteins, *Coxiella* could possess additional RAB-modifying proteins that could favor its development in mammalian hosts. CvpF could open the way for the characterization of novel RAB-targeting effectors.

Material and methods

Bacterial strains, cell lines, and growth conditions

Strains used in this study are listed in Supplementary Table 1. *Coxiella burnetii* strains were grown in ACCM-2 [47] supplemented with kanamycin (Sigma-Aldrich, K1377; 340 µg/ml) or chloramphenicol (Sigma-Aldrich, C0378; 3 µg/ml), as appropriate in a humidified atmosphere of 5% CO_2 and 2.5% O_2 at 37°C. U2OS (ATCC, HTB-96), U2OS mCherry, U2OS GFP-FYVE (kindly provided by Dr. Tassula Proikas-Cezanne, Eberhard Karls University Tübingen, Germany), U2OS Cas9, and HEK293T (ATCC, CRL-11268) cell lines were routinely maintained in DMEM with GlutaMAX (GIBCO, 61965–026) containing 10% fetal calf serum (FCS; Sigma-Aldrich, F7524) and THP-1 (ATCC, TIB-202) cells were routinely maintained in RPMI with GlutaMAX (GIBCO, 61,870–010) containing 10% FCS. All cells were grown in a humidified atmosphere of 5% CO_2 at 37°C. THP-1 cells were differentiated into macrophages by treatment with 25 ng/ml phorbol myristate acetate (PMA, Sigma-Aldrich, P8134) for 24 h. Cell growth medium was supplemented with 600 µg/ml of geneticin G418 (Gibco, 10131035), 10 µg/ml of blasticidin (InvivoGen, ant-bl-05) and/or 1 µg/ml of puromycin (Sigma-Aldrich, P8833) as appropriate.

Antibodies and reagents

Hoechst 33258 (94403), anti-mouse (12–349), and anti-rabbit (-12–348) HRP-conjugated antibodies, rabbit anti-LC3B (L8918), rabbit anti-LAMP1 (L1418), mouse anti-GAPDH (G8795), mouse anti-Flag (F1804) and bafilomycin A_1 (B1793) were purchased from Sigma-Aldrich. Rabbit monoclonal anti-GOLGA2/GM130 (ab52649) and rabbit polyclonal anti-RAB26 (ab187151) were purchased from AbCam. Mouse monoclonal anti-beta-lactamase (MA1-20370) was from ThermoFisher Scientific. Mouse anti-LC3B (ALX-803-080-C100) was from Enzo Life Sciences. Rabbit anti-HA (sc-7392) was from Santa Cruz Biotechnology, and mouse anti-HA (66006-1-lg) was from Proteintech. Rabbit polyclonal anti-SQSTM1/p62 (GTX100685) was from GeneTex. Phalloidin coupled to Alexa Fluor 647 (A22287) and LysoTracker Red (L7528) were purchased from Life technologies. Rabbit anti-GFP (PABG1-20) was from Chromotek. Rabbit anti-MTOR (2983S) was from Cell Signaling Technology. Mouse anti-Cas9 (844302) was from BioLegend. Rabbit anti-*Coxiella* NMII antibodies [30] were generated by Covalab. Mouse and rabbit IgG conjugated to Alexa Fluor 488 (A-11029 and A-11008), 555 (A-21147 and A-21429), or 647 (A-21239 and A-21245), as well as Prolong Gold antifade mounting reagent (P36930) were purchased from Invitrogen. Paraformaldehyde (15700) was provided by Electron Microscopy Sciences, PA.

Plasmids

Plasmids and primers used in this study are listed in Supplementary Tables 2 and 3, respectively. DNA sequences were amplified by PCR using Phusion polymerase (New England Biolabs, M0530L) and gene-specific primers (Sigma-Aldrich). All site-directed mutagenesis was performed by PCR overlap extension with the mentioned primer pairs.

Complementation in *C. burnetii*

The operon comprising *cbu0625* promoter (600 nt upstream *cbu0625* start codon), *cbu0625*, and *cbu0626/cvpF* was amplified from *Coxiella* RSA439 NMII genomic DNA using Prom-0625-NheI-Fw and CvpF-XhoI-Rv and cloned into pUCR6K-miniTn7-Kan (kindly provided by Prof. Robert Heinzen, Rocky Mountain Laboratories, MT, USA) to generate Mini-Tn7-Kan-prom625-0625-0626. Preparation of electrocompetent *Coxiella cvpF*::Tn was performed as described in [33] and the bacteria were electroporated with an equimolar amount of Mini-Tn7-Kan-prom625-0625-0626 (carrying the transposon prom625-0625-0626) and pTnS2 (carrying the Tn7 transposase, kindly provided by Prof. Robert Heinzen) plasmids prior to selection and amplification in ACCM-2 containing appropriate antibiotics.

Lentivirus production and stable cell line engineering

To produce lentiviral particles, HEK293T cells were cotransfected with an HIV-1 based genome coding plasmid (pLentiCas9-Blast [Addgene, 47948], pLentiGuide-Puro [Addgene, 68463], or pLVX-mCherry-C1 [Clontech, 632561]), pCMV-dR8.91 (HIV-1 GagPol, kindly provided by Dr. Antoine Gross, IRIM UMR9004 CNRS, Montpellier, France) and pMD.G (VSV-G, kindly provided by Dr. Antoine Gross, IRIM UMR9004 CNRS, Montpellier, France) at a ratio of 1:1:0.5, respectively. The medium was replaced after 6 h, and viral particles were harvested 42 h later, filtered on 0.45-µm filters (Clearline, 146561), and directly used to transduce U2OS target cells. After 4 to 6 h, the transduction medium was replaced with fresh DMEM containing 10% FCS, and the relevant antibiotics were added 48 h later to select transduced U2OS Cas9 and U2OS mCherry cells.

Reverse transcription and PCR

Coxiella strains *Tn1832* (*WT), Tn248*, or *Tn248* Comp. were grown for 7 d in 5 ml of ACCM-2 containing the appropriate antibiotics. Bacteria were centrifuged for 30 min at 21,000 × g at 4°C and total RNA was extracted using the RNA easy kit (Qiagen, 74104) or the Direct-zol RNA miniprep kit (Zymo Research, R2051), according to the manufacturer's recommendations. DNA was further removed using DNase I (New England Biolabs, M0303S). 1 µg of total RNA was used for reverse transcription using the High Capacity cDNA reverse transcription kit (Applied Biosystems, 4368814) or the SuperScript VILO cDNA synthesis kit (Invitrogen, 11754–050) according to the manufacturer's recommendations. Gene-specific primers (Supplementary Table 3) were used to amplify the cDNA corresponding to *ompA* (*cbu1260), cbu0625*, and *cbu0626*/*cvpF*.

Real-time PCR

Lightcycler 480 SYBR Green I master mix (Thermo Fisher Scientific, 4887352001) was used for real-time PCR and readouts was acquired on a Lightcycler480 real-time system (Roche) according to the manufacturer's instructions. The relative levels of transcripts were calculated by the ΔΔCT threshold cycle (CT) method using *dotA* as the internal control. The relative levels of mRNA from the *WT* samples were adjusted to 1 and served as the basal control value. Each experiment was done in biological triplicate. For the calibration curve construction, aliquots of the plasmid pCR2.1::*dotA* (Provided by Dr. Robert Heinzen, 8×10^{10} copies/µl) in dilutions ranging from 8×10^{2} to 8×10^{9} copy numbers were applied. Three replicative runs of a *dotA* real-time PCR for all samples were performed. For the standard curves, the threshold cycle (Cq) values were calculated using the Lightcycler480 Software (Roche).

Immunofluorescence staining

Cells were either fixed in 3% paraformaldehyde in PBS (ThermoFisher Scientific, 14190–094) at room temperature for 30 min, or in methanol/acetone (1:1) at −20°C for 5 min. Samples were rinsed in PBS and incubated in BSS (0.5% BSA (Sigma-Aldrich, A2058), 50 mM NH_4Cl in PBS pH 7.4) or FBS (5% fetal bovine serum [Sigma-Aldrich, F7524] in PBS pH 7.4) blocking solutions. Primary and secondary antibodies were diluted in the respective blocking solutions and used for immunofluorescence staining.

Co-immunoprecipitation

U2OS cells were transfected with equimolar amounts of plasmids expressing GFP- and HA-tagged constructs. After 24 h, cells were trypsinized, washed twice in PBS and incubated in the co-IP buffer (20 mM Tris-HCl pH 7.6, 200 mM NaCl, 0.5 mM EDTA, 1% IGEPAL CA-630 [Sigma-Aldrich, I8896], Complete protease inhibitor [Roche, 11836170001]) on ice for 30 min. Following a 10-min spin at 21,000 x g at 4°C, cell lysates were incubated with magnetic GFP-trap beads (Chromotek, gtma-20) for 1 h at 4°C on a roller. Beads were washed thrice with co-IP buffer, and proteins were collected in Laemmli buffer.

Beta-lactamase translocation assay

For *C. burnetii* effector translocation assays, cells were cultured in black, clear-bottomed, 96-well plates (Greiner Bio-One, 655,090), and infected with the appropriate *C. burnetii* strain (MOI of 100) for 24, 48, and 72 h. *C. burnetii* expressing β-lactamase alone was used as a negative control; *C. burnetii* expressing β-Lactamase-tagged CvpB was used as a positive control. Cell monolayers were loaded with the fluorescent substrate CCF4/AM (LiveBLAzer-FRET B/G loading kit; Invitrogen, K1095) in a solution containing 15 mM probenecid (Sigma-Aldrich, P36400). Cells were incubated in the dark for 1 h at room temperature and imaged using an EVOS inverted fluorescence microscope (ThermoFisher Scientific, UK). Images were acquired using a DAPI and GFP filter cubes. The image analysis software CellProfiler (Broad Institute, MA) was used to segment and identify all cells in the sample (GFP) and positive cells (DAPI) and to calculate the intensity of fluorescence in each channel. The percentage of positive cells versus the total number of cells was then calculated and used to evaluate effector translocation.

Microscopy and image analysis

Samples were imaged with a Zeiss Axio Imager Z1 epifluorescence microscope (Carl Zeiss, Germany) connected to a CoolSNAP HQ^2 CCD camera (Teledyne Photometrics, Tucson, AZ). Images were acquired with 40x oil immersion objectives and processed with Metamorph (Molecular Devices, San Jose, CA). High throughput image acquisition was performed on an epifluorescence automated microscope (Cellomics, ThermoFisher Scientific, Pittsburgh, PA) equipped with a 20X objective. Image analysis was performed using the CellProfiler 3.0 software, as previously

described (Martinez *et al*., 2015). Briefly, Hoechst 33258 (Sigma-Aldrich, 94403) staining, cytoplasmic mCherry fluorescence produced by U2OS mCherry cells and LAMP1 labeling were used to identify nucleus, cytoplasm, and lysosomal/late endosomal compartments, respectively. The GFP signal was used to identify *C. burnetii* colonies, and CCVs were segmented based on the LAMP1 antibody labeling and GFP fluorescence, respectively. After sorting non-infected and infected cells, a morphometrical analysis was carried out over a population of at least 200 objects (CCVs and/or *C. burnetii* colonies) per condition. Confocal microscopy was performed using a TCS SP8 HyVolution microscope (Leica, Germany) connected to a DFC9000 sCMOS camera or an SP5-SMD microscope (Leica, Germany). Images were acquired with 63x oil immersion objectives and processed with LAS-AF (Leica, Germany). Fluorescence was measured using Fiji analysis software (version 2.0.0) and the Multicolor line profile plot macro (University of Leicester). LC3B and RAB26 recruitment at CCVs were scored as follow: The mean ± confidence interval (CI) Pearson's correlation coefficient between LAMP1 and the cellular marker of interest (LC3B or RAB26) was calculated using Icy analysis software from triplicate experiments representing a total of at least 80 CCVs per condition (*WT*, *cvpF*::Tn, *cvpF*::Tn Comp.). The mean + positive CI calculated from cells infected with the *cvpF*::Tn mutant was then taken as a threshold to calculate the percentage of CCVs positive for either marker.

Animal experiments

SCID (C.B-17/LcrHsd-*Prkdc*^{scid}) mice were handled and infected, as previously described [34]. All animal procedures were done in compliance with Texas A&M University IACUC (AUP#2016-0370). DNA was purified from infected organs, and primers and probe for IS1111 were used to determine Genome Equivalents (GE) using TaqMan real-time PCR.

Statistical analysis

Statistical analyses of data were performed using Prism software (GraphPad, San Diego, CA). For experiments requiring statistical analysis, an adapted statistical test was performed, as described in the corresponding figure legends.

Acknowledgments

This work was supported by the French National Research Agency (ANR; ANR-14-CE14-0012-01, project AttaQ) and by the ERA-NET Infect-ERA (ANR-13-IFEC-0003, project EUGENPATH). FAS is the recipient of a fellowship from the Agence Nationale Bourses Gabon (ANBG). We acknowledge the imaging facility MRI, member of the national infrastructure France-BioImaging supported by the French National Research Agency (ANR-10-INBS-04, «Investments for the future»). We thank Dr. Martine Biard-Piechaczyk, Dr. Lucile Espert, and Dr. Fabien Blanchet (IRIM CNRS UMR9004 Montpellier, France) for scientific advice and sharing material.

Disclosure statement

No potential conflict of interest was reported by the authors.

Funding

This work was supported by the Agence Nationale de la Recherche [ANR-13-IFEC-0003];Agence Nationale de la Recherche [ANR-14-CE14-0012-01];Agence Nationale de la Recherche [ANR-10-INBS-04].

ORCID

Erin Van Schaik http://orcid.org/0000-0003-2536-0857
Mélanie Burette http://orcid.org/0000-0001-5751-2208
Caroline Goujon http://orcid.org/0000-0001-8571-1108
Matteo Bonazzi http://orcid.org/0000-0001-5499-8759

References

[1] Quaglio GL, Demotes-Mainard J, Loddenkemper R. Emerging and re-emerging infectious diseases: a continuous challenge for Europe. Eur Respir J. 2012;40:1312–1314.
[2] Waag DM, Fritz DL. Q fever. Biodefense Res Methodol Anim Model. Second Ed. 2012; 12:179–196.
[3] Moffatt JH, Newton P, Newton HJ. *Coxiella burnetii*: turning hostility into a home. Cell Microbiol. 2015;17:621–631.
[4] Lührmann A, Newton HJ, Bonazzi M. Beginning to understand the role of the type IV secretion system effector proteins in *Coxiella burnetii* pathogenesis. Curr Top Microbiol Immunol. 2017;413:243–268.
[5] Voth DE, Heinzen RA. Lounging in a lysosome: the intracellular lifestyle of *Coxiella burnetii*. Cell Microbiol. 2007;9:829–840.
[6] Carey KL, Newton HJ, Lührmann A, et al. The *Coxiella burnetii* Dot/Icm system delivers a unique repertoire of type IV effectors into host cells and is required for intracellular replication. PLoS Pathog. 2011;7(5):e1002056.
[7] Newton HJ, McDonough JA, Roy CR. Effector protein translocation by the *Coxiella burnetii* Dot/Icm type iv secretion system requires endocytic maturation of the pathogen-occupied vacuole. PLoS One. 2013;8:e54566.
[8] Larson CL, Martinez E, Beare PA, et al. Right on Q: genetics begin to unravel *Coxiella burnetii* host cell interactions. Future Microbiol. 2016;11:919–939.
[9] Lührmann A, Nogueira CV, Carey KL, et al. Inhibition of pathogen-induced apoptosis by a *Coxiella burnetii* type IV effector protein. Proc Natl Acad Sci U S A. 2010;107:18997–19001.
[10] Larson CL, Beare PA, Howe D, et al. *Coxiella burnetii* effector protein subverts clathrin mediated vesicular trafficking for pathogen vacuole biogenesis. Proc Natl Acad Sci U S A. 2013;110:E4770–9.
[11] Larson CL, Beare PA, Voth DE, et al. *Coxiella burnetii* effector proteins that localize to the parasitophorous vacuole membrane promote intracellular replication. Infect Immun. 2015;83:661–670.
[12] Martinez E, Allombert J, Cantet F, et al. *Coxiella burnetii* effector CvpB modulates phosphoinositide metabolism for optimal vacuole development. Proc Natl Acad Sci U S A. 2016;113:E3260–9.
[13] Voth DE, Beare PA, Howe D, et al. The *Coxiella burnetii* cryptic plasmid is enriched in genes encoding type IV secretion system substrates. J Bacteriol. 2011;193:1493–1503.
[14] Maturana P, Graham JG, Sharma UM, et al. Refining the plasmid-encoded type IV secretion system substrate repertoire of *Coxiella burnetii*. J Bacteriol. 2013;195:3269–3276.
[15] Latomanski EA, Newton HJ. Interaction between autophagic vesicles and the *Coxiella*-containing vacuole requires CLTC (clathrin heavy chain). Autophagy. 2018;14:1710–1725.
[16] Crabill E, Schofield WB, Newton HJ, et al. Dot/Icm-translocated proteins important for biogenesis of the *Coxiella burnetii*-containing vacuole identified by screening of an effector mutant sublibrary. Infect Immun. 2018;86:e00758–17.
[17] Ao X, Zou L, Wu Y. Regulation of autophagy by the Rab GTPase network. Cell Death Differ. 2014;21:348–358.
[18] Binotti B, Pavlos NJ, Riedel D, et al. The GTPase RaB26 links synaptic vesicles to the autophagy pathway. Elife. 2014;2015:1–23.

[19] Dong W, He B, Qian H, et al. RAB26-dependent autophagy protects adherens junctional integrity in acute lung injury. Autophagy. 2018;14:1677–1692.
[20] Song Y, Shang D, Cheng H, et al. The small GTPase RAB37 functions as an organizer for autophagosome biogenesis. Autophagy. 2018;14:727–729.
[21] Sheng Y, Song Y, Li Z, et al. RAB37 interacts directly with ATG5 and promotes autophagosome formation via regulating ATG5-12-16 complex assembly. Cell Death Differ. 2018;25:918–934.
[22] Spanò S, Galán JE. Taking control: hijacking of RAB GTPases by intracellular bacterial pathogens. Small GTPases. 2018;9:182–191.
[23] Stein MP, Müller MP, Wandinger-Ness A. Bacterial pathogens commandeer RAB GTPases to establish intracellular niches. Traffic. 2012;13:1565–1588.
[24] Martinez E, Siadous FA, Bonazzi M. Tiny architects: biogenesis of intracellular replicative niches by bacterial pathogens. FEMS Microbiol Rev. 2018;42:425–447.
[25] McDonough JAJ, Newton HJHHJ, Klum S, et al. Host pathways important for *Coxiella burnetii* infection revealed by genome-wide RNA interference screening. MBio. 2013;4:e00606–12.
[26] Berón W, Gutierrez MG, Rabinovitch M, et al. *Coxiella burnetii* localizes in a Rab7-labeled compartment with autophagic characteristics. Infect Immun. 2002;70:5816–5821.
[27] Romano PS, Gutierrez MG, Berón W, et al. The autophagic pathway is actively modulated by phase II *Coxiella burnetii* to efficiently replicate in the host cell. Cell Microbiol. 2007;9:891–909.
[28] Gutierrez MG, Vázquez CL, Munafó DB, et al. Autophagy induction favours the generation and maturation of the *Coxiella*-replicative vacuoles. Cell Microbiol. 2005;7:981–993.
[29] Campoy EM, Martín Zoppino FC, Colombo MI. The early secretory pathway contributes to the growth of the *Coxiella*-replicative niche. Infect Immun. 2011;79:402–413.
[30] Martinez E, Cantet F, Fava L, et al. Identification of OmpA, a *Coxiella burnetii* protein involved in host cell invasion, by multi-phenotypic high-content screening. PLoS Pathog. 2014;10:e1004013.
[31] Zusman T, Aloni G, Halperin E, et al. The response regulator PmrA is a major regulator of the icm/dot type IV secretion system in *Legionella pneumophila* and *Coxiella burnetii*. Mol Microbiol. 2007;63:1508–1523.
[32] Lifshitz Z, Burstein D, Peeri M, et al. Computational modeling and experimental validation of the *Legionella* and *Coxiella* virulence-related type-IVB secretion signal. Proc Natl Acad Sci U S A. 2013;110:E707–15.
[33] Martinez E, Cantet F, Bonazzi M. Generation and multi-phenotypic high-content screening of *Coxiella burnetii* transposon mutants. J Vis Exp. 2015;2015:4–6.
[34] van Schaik EJ, Case ED, Martinez E, et al. The SCID mouse model for identifying virulence determinants in *Coxiella burnetii*. Front Cell Infect Microbiol. 2017;7:25.
[35] Newton HJ, Kohler LJ, McDonough JA, et al. A screen of *Coxiella burnetii* mutants reveals important roles for Dot/Icm effectors and host autophagy in vacuole biogenesis. PLoS Pathog. 2014;10(7):e1004286.
[36] Larson CL, Sandoz KM, Cockrell DC, et al. Noncanonical Inhibition of mTORC1 by *Coxiella burnetii* promotes replication within a phagolysosome-like vacuole. MBio. 2019;10(1):e02816–18.
[37] Jin RU, Mills JC. RAB26 coordinates lysosome traffic and mitochondrial localization. J Cell Sci. 2014;127:1018–1032.
[38] Lambert NA, Lan T-H, Li C, et al. Rab26 modulates the cell surface transport of α 2 -adrenergic receptors from the golgi. J Biol Chem. 2012;287:42784–42794.
[39] Kohler LJ, Reed SR, Sarraf SA, et al. Effector protein *cig2* decreases host tolerance of infection by directing constitutive fusion of autophagosomes with the *Coxiella*-containing vacuole. MBio. 2016;7:1–14.
[40] Winchell CG, Graham JG, Kurten RC, et al. *Coxiella burnetii* type IV secretion-dependent recruitment of macrophage autophagosomes. Infect Immun. 2014;82:2229–2238.
[41] Winchell CG, Dragan AL, Brann KR, et al. *Coxiella burnetii* subverts p62/sequestosome 1 and activates Nrf2 signaling in human macrophages. Infect Immun. 2018;86:e00608–17.
[42] Latomanski EA, Newton P, Khoo CA, et al. The effector Cig57 hijacks FCHO-mediated vesicular trafficking to facilitate intracellular replication of *Coxiella burnetii*. PLoS Pathog. 2016;12(12):e1006101.
[43] Kimura S, Noda T, Yoshimori T. Dynein-dependent movement of autophagosomes mediates efficient encounters with lysosomes. Cell Struct Funct. 2008;33:109–122.
[44] Kalvari I, Tsompanis S, Mulakkal NC, et al. iLIR: a web resource for prediction of Atg8-family interacting proteins. Autophagy. 2014;10:913–925.
[45] Goody RS, Itzen A. Modulation of small Gtpases by *Legionella*. Curr Top Microbiol Immunol. 2013;376:117–133.
[46] Wang Z, McCloskey A, Cheng S, et al. Regulation of the small GTPase Rab1 function by a bacterial glucosyltransferase. Cell Discov. 2018;4:53.
[47] Omsland A, Beare PA, Hill J, et al. Isolation from animal tissue and genetic transformation of *Coxiella burnetii* are facilitated by an improved axenic growth medium. Appl Environ Microbiol. 2011;77:3720–3725.

Appendix 2

The secreted protein kinase CstK from *Coxiella burnetii* influences vacuole development and interacts with the GTPase-activating host protein TBC1D5

Martinez E, Huc-Brandt S, Brelle S, Allombert J, Cantet F, Gannoun-Zaki L, Burette M, Martin M, Letourneur F, Bonazzi M, Molle V. J Biol Chem 2020 May 22;295(21):7391-7403.

JBC Papers in Press. Published on April 17, 2020 as Manuscript RA119.010112
The latest version is at https://www.jbc.org/cgi/doi/10.1074/jbc.RA119.010112

The secreted protein kinase CstK from *Coxiella burnetii* influences vacuole development and interacts with the GTPase-activating host protein TBC1D5

Eric Martinez[1,#], Sylvaine Huc-Brandt[2,#], Solène Brelle[2], Julie Allombert[1], Franck Cantet[1], Laila Gannoun-Zaki[2], Mélanie Burette[1], Marianne Martin[2], François Letourneur[2], Matteo Bonazzi[1,*] and Virginie Molle[2,*]

[1]IRIM, CNRS, Université de Montpellier, Montpellier, France
[2]Laboratory of Pathogen Host Interactions, Université de Montpellier, CNRS, UMR 5235, Montpellier, France

Running title: *CstK affects C. burnetii vacuole biogenesis*

[*]**Corresponding author:**
VM: Tel: (+33) 4 67 14 47 25, E-mail: virginie.molle@umontpellier.fr
MB: Tel: (+33) 4 34 35 94 59, E-mail: matteo.bonazzi@irim.cnrs.fr

[#] Both authors contributed equally to this manuscript
Keywords: *Coxiella burnetii*, secreted kinase, phosphorylation, serine/threonine/tyrosine protein kinase, parasitophorous vacuole, host substrates, Q fever, bacterial effector, virulence factor

The authors declare that they have no conflicts of interest with the contents of this article.

ABSTRACT

The intracellular bacterial pathogen *Coxiella burnetii* is the etiological agent of the emerging zoonosis Q fever. Crucial to its pathogenesis is type 4b secretion system (T4SS)-mediated secretion of bacterial effectors into host cells that subvert host cell membrane trafficking, leading to the biogenesis of a parasitophorous vacuole for intracellular replication. The characterization of prokaryotic Serine/Threonine Protein Kinases (STPKs) in bacterial pathogens is emerging as an important strategy to better understand host-pathogen interactions. In this study, we investigated CstK (for *Coxiella* ser/thr Kinase), a protein kinase identified in *C. burnetii* by *in silico* analysis. We demonstrate that this putative protein kinase undergoes autophosphorylation on Thr and Tyr residues, and phosphorylates a classical eukaryotic protein kinase substrate *in vitro*. This dual Thr-Tyr kinase activity is also observed for a eukaryotic dual-specificity Tyr phosphorylation-regulated kinase class. We found that CstK is translocated during infections and localizes to *Coxiella*-containing vacuoles (CCVs). Moreover, a CstK- overexpressing *C. burnetii* strain displayed a severe CCV development phenotype, suggesting that CstK fine-tunes CCV biogenesis during the infection. Protein-protein interaction experiments identified the Rab7 GTPase-activating protein (GAP) TBC1D5 as a candidate CstK-specific target, suggesting a role for this host GAP in *Coxiella* infections. Indeed, CstK colocalized with TBC1D5 in non-infected cells, and TBC1D5 was recruited to CCVs in infected cells. Accordingly, TBC1D5 depletion from infected cells significantly affected CCV development. Our results indicate that CstK functions as a bacterial effector protein that interacts with the host protein TBC1D5 during vacuole biogenesis and intracellular replication.

Signal transduction is an essential and universal function that allows all cells, from prokaryotes to eukaryotes, to translate environmental signals to adaptive changes. By this mechanism, extracellular inputs propagate through complex signaling networks whose activity is often regulated by reversible protein phosphorylation. Signaling mediated by Serine/Threonine/Tyrosine protein phosphorylation has been extensively studied in eukaryotes, however, its relevance in prokaryotes has only begun to be appreciated. The recent discovery that bacteria also use Ser/Thr/Tyr kinase-based signaling pathways has opened new perspectives to study environmental adaptation, especially in the case of bacterial pathogens, with respect to host infection (1). Thus, advances in genetic strategies and genome sequencing have revealed the existence of "eukaryotic-like" serine/threonine protein kinases (STPKs) and phosphatases in a number of prokaryotic organisms

(2), including pathogens such as, *Streptococcus* spp. (3-6), *Mycobacteria* (7-12), *Yersinia* spp. (13,14), *Listeria monocytogenes* (15,16), *Pseudomonas aeruginosa* (17), *Enterococcus faecalis* (18) or *Staphylococcus aureus* (19,20). Consequently, the study of STPKs in human bacterial pathogens is emerging as an important strategy to better understand host-pathogen interactions and develop new, targeted antimicrobial therapies. However, if on one hand it is clear that STPKs and phosphatases regulate important functions in bacterial pathogens, their signal transduction mechanism remains ill-defined and restricted to a limited number of microbes.

Importantly, STPKs expressed by pathogenic bacteria can either act as key regulators of important microbial processes, or be translocated by secretion systems to interact with host substrates, thereby subverting essential host functions including the immune response, cell shape and integrity (21). Phosphorylation of host substrates has been demonstrated for some bacterial STPKs, whereas others seem to require their kinase activity but their phosphorylated substrates remain to be identified (21). Therefore, biochemical mechanisms of these pathogen-directed targeted perturbations in the host cell-signaling network are being actively investigated and STPKs are proving to be molecular switches that play key roles in host-pathogen interactions (21).

Among emerging human pathogens, *Coxiella burnetii* is a highly infectious bacterium, responsible for the zoonosis Q fever, a debilitating flu-like disease leading to large outbreaks with a severe health and economic burden (22-24). The efficiency of infections by *C. burnetii* is likely associated with the remarkable capacity of this bacterium to adapt to environmental as well as intracellular stress. Indeed, outside the host, *C. burnetii* generates pseudo-spores that facilitate its airborne dissemination. *C. burnetii* has developed a unique adaptation to the host, being the only bacterium that thrives in an acidic compartment containing active lysosomal enzymes. Upon host cell invasion, bacteria reside within membrane-bound compartments that passively traffic through the endocytic maturation pathway, progressively acquiring early and late endocytic markers such as Rab5 and Rab7, respectively (25). Fusion of *Coxiella*-containing vacuoles (CCVs) with late endosomes and lysosomes is accompanied by the acidification of the endosomal environment, which is required to activate the translocation of bacterial effector proteins by a Dot/Icm Type 4b Secretion System (T4SS) (26). Some of these effectors modulate important signaling pathways of infected cells, including apoptosis and inflammasome activation (27-29), whereas others are essential for the development of the intracellular replicative niche. Among these CvpB and CvpF have been recently implicated in the manipulation of autophagy for optimal vacuole development (30-33). *C. burnetii* genome analysis revealed a close homology to the facultative intracellular pathogen *Legionella pneumophila*, in particular at the level of Dot/Icm core genes (34). *In silico* analysis identified over 100 candidate effector proteins encoded in the *C. burnetii* genome, some of which have been validated for secretion using either *C. burnetii* or *L. pneumophila* as a surrogate model (26,35,36).
In this study, we investigated the candidate effector CBU_0175, which encodes a unique putative *Coxiella* Ser/Thr kinase (CstK). We demonstrated CstK translocation by *C. burnetii* during infection and we reported its localization at CCVs. *In vitro* kinase assays revealed that CstK undergoes autophosphorylation on Thr and Tyr residues, and displays a 'bona fide' kinase activity towards a test substrate of eukaryotic protein kinases. Furthermore, the identification of the Rab7 GTP-activating protein (GAP) TBC1D5 as a CstK interactor suggests that this protein might be involved during infection to facilitate CCVs biogenesis. Indeed, TBC1D5 is actively recruited at CCVs during *Coxiella* infections and TBC1D5-targeting siRNAs significantly affect CCVs development. Our data provide the first evidence that a *C. burnetii* secreted kinase might control host cell infection.

RESULTS

Coxiella burnetii genome encodes a single putative protein kinase. *In silico* analysis of the virulent *C. burnetii* strain RSA493 NMI genome revealed only one gene encoding a putative Serine/Threonine Protein Kinase (STPK). To date, no STPKs have been characterized in this organism. This gene was named *cstK* for *C. burnetii* serine threonine Kinase and encodes a 246 amino acids protein with an estimated molecular mass of 31 kDa. The gene coding for *cstK* is flanked by genes CBU_0174 (which encodes an hypothetical protein) and CBU_0176, a gene coding for the serine protease domain-containing protein degP.1. Of note, these genes are not part of an operon (Fig. 1A). InterProScan analysis of CstK revealed the presence of most of the essential amino acids and sequence subdomains characterizing the Hanks family of eukaryotic-like protein kinases (37). CstK shares a common eukaryotic protein kinases

superfamily fold with two lobes and a Gly-rich loop. These include the central core of the catalytic domain, and the invariant lysine residue in the consensus motif within subdomain II, which is usually involved in the phosphate transfer reaction and required for the autophosphorylating activity of eukaryotic STPKs (Fig. 1A) (37-39). The activation loop in the catalytic domain is particularly short in CstK, and the DFG motif is substituted by a GLG motif. Interestingly, the transmembrane domain usually present in classical prokaryotic STPKs is lacking in CstK, thus it is a so-called cytoplasmic STPK.

CstK is a Dot/Icm effector protein. Bioinformatics analysis using the prediction software S4TE 2.0 (40) indicated that CstK harbors features corresponding to secreted effector proteins, including a promoter motif typically found in effector proteins from intra-vacuolar bacterial pathogens, suggesting that CstK is indeed a *Coxiella* effector protein (Fig. 1A). Consistently, previous studies by Chen and colleagues have shown that CstK is secreted in a T4SS-dependent manner by the surrogate host *L. pneumophila*, albeit with low efficiency (36). In order to validate CstK secretion in *C. burnetii*, we engineered plasmids encoding, either CstK or CvpB (a known *C. burnetii* effector protein) (30), fused to Beta-Lactamase (BLAM) and expressed in wt *Coxiella Tn1832* (a *C. burnetii* transposon mutant expressing GFP and that phenocopies wild-type *C. burnetii*) or the Dot/Icm-defective *dotA*::Tn mutant, also expressing GFP. By means of a BLAM secretion assay, we could observe that BLAM-CstK was secreted by wt *Coxiella* at 48 and 72 hours, but not at 24 hours post-infection (Fig. 1B). Secretion of BLAM-CvpB or BLAM-CstK was not detectable in cells infected with the *dotA*::Tn strain, indicating that both CvpB and CstK are *C. burnetii* Dot/Icm substrates (Fig. 1B). Next, the intracellular localization of Cstk was investigated by ectopically expressing HA-tagged CstK either in non-infected or wt *C. burnetii*-infected U2OS cells. In non-infected cells, CstK localized at intracellular compartments that were negative for the lysosomal marker LAMP1, whereas it was recruited at CCVs (as revealed by the co-localization with LAMP1) in infected cells (Fig. 1C).

CstK displays autokinase and protein kinase activities. To determine whether CstK is a functional protein kinase, this protein was overproduced in *E. coli* and purified as a recombinant protein fused to glutathione *S*-transferase (GST) tag. The purified tagged CstK protein (Fig. 2A, upper panel) was then assayed for autokinase activity in presence of the phosphate donor [γ-^{33}P]ATP. As shown in Fig. 2A (lower panel), CstK incorporated radioactive phosphate from [γ-^{33}P]ATP, generating a radioactive signal corresponding to the expected size of the protein isoform, strongly suggesting that this kinase undergoes autophosphorylation. To confirm CstK autophosphorylation and exclude that contaminant kinase activities from *E. coli* extracts might phosphorylate CstK, we mutated the conserved Lys55 residue present in subdomain II into CstK by site-directed mutagenesis. Indeed protein sequence analysis revealed that Lys55 in CstK is similarly positioned as a conserved Lys residue usually involved in the phosphotransfer reaction and also required for the autophosphorylating activity of eukaryotic-like STPKs (37,38). Thus, Lys55 was substituted by a Met residue, the mutated form of CstK, CstK_K55M, was purified as described above (Fig. 2A, upper panel) and it was then tested for autophosphorylation in presence of [γ-^{33}P]ATP. As expected, no radioactive signal could be detected (Fig. 2A, lower panel), thus establishing that CstK displayed autophosphorylation activity. A kinetic analysis of CstK phosphorylation was next performed to determine the initial CstK phosphorylation rate (Fig. 2B). Incorporation of γ-phosphate occurred rapidly, reaching about 50% of its maximum rate within 5 min of reaction. This autokinase activity was dependent on bivalent cations such as Mg^{2+} and Mn^{2+} in the range of 5mM, thus in correlation with concentrations required for canonical STPK activity, as shown in Fig. 2C, and abolished by addition of 20 mM EDTA chelating all the divalent cations available (data not shown).

The recombinant CstK protein was further characterized by studying its ability to phosphorylate exogenous proteins and was thus assayed for *in vitro* phosphorylation of the general eukaryotic protein kinase substrate, myelin basic protein (MBP), in the presence of [γ-^{33}P]ATP. MBP is a commonly used substrate for both Ser/Thr and Tyr kinases. A radiolabeled signal at the expected 18-kDa molecular mass of MBP was detected, thus demonstrating that CstK phosphorylates protein substrates such as MBP (Fig. 2A). As expected, the CstK_K55M mutant did not phosphorylated MBP. Altogether, these data indicate that *in vitro*, CstK possesses intrinsic autophosphorylation activity and displays kinase functions for exogenous substrates.

Identification of CstK autophosphorylation sites. To determine the specificity of this kinase, we next identified its autophosphorylation sites. A mass

spectrometry approach was used since this technique allows precise characterization of post-translational modifications including phosphorylation (41,42). NanoLC/nanospray/ tandem mass spectrometry (LC-ESI/MS/MS) was applied for the identification of phosphorylated peptides and for localization of phosphorylation sites in CstK. This approach led to 97% of sequence coverage, while the remaining residues uncovered that did not include Ser, Thr or Tyr residues.

As detailed in Table 3, analysis of tryptic digests allowed the characterization of three phosphorylation sites in CstK. Surprisingly, unlike classical Ser/Thr or Tyr kinases, CstK was phosphorylated on two Tyr residues (Y14 and Y209), in addition to one Thr site (T232). Since protein sequence analysis did not reveal a classical activation loop in this kinase, the contribution of T232, Y14 and Y209 to CstK kinase activity was individually assessed. Hence, these residues were mutated either to phenylalanine to replace tyrosine residues or alanine to replace threonine residue, generating the single mutants CstK_Y14F, CstK_Y209F, and CstK_T232A as well as the CstK_Y14F/Y209F/T232A triple mutant (CstK_FFA). Next, *in vitro* kinase assays with [γ-^{33}P]ATP were carried out and revealed that maximum loss in CstK autophosphorylation activity was observed in the CstK_Y14F mutant (Fig. 2D), suggesting that this site is central for CstK activation. In contrast, the CstK_Y209F mutant exhibited a slight hyperphosphorylation, which might indicate that Y209 only plays an accessory role in controlling CstK autophosphorylation (Fig. 2D). Finally, the CstK_T232A mutant showed a reduced CstK phosphorylation and displayed diminished kinase activity towards the exogenous substrate MBP (Fig. 2D). Note that mutating all three autophosphorylation sites fully abrogated CstK kinase activity (Fig. 2D). These results indicate that Y14 and T232 are the major phosphorylation sites in CstK and strongly suggest that CstK might be a dual specificity (Thr/Tyr) kinase.

CstK activity and phosphorylated state affect its intracellular localization.

Next, we ectopically expressed HA-tagged CstK, CstK_K55M and CstK_FFA derivatives in non-infected and *C. burnetii* infected U2OS cells, to investigate its intracellular localization. CstK mainly localized at vesicular compartments in non-infected cells, and accumulated at CCVs upon *C. burnetii* infection, suggesting an active role in the biogenesis of this compartment (Fig. 1C). Interestingly, the inactive CstK_K55M mutant localized at vesicular structures positive for the lysosomal marker LAMP1 but not at CCVs while the non-phosphorylated CstK_FFA displayed a diffuse localization in the cytosol of transfected cells (Fig. 2E). Overall, these data suggest that the kinase activity and phosphorylated state of CstK play an important role in its localization in cells.

CstK regulates vacuole development and C. burnetii replication within infected cells. As a first step towards the understanding of CstK functions in the course of infection, and to appreciate the extent to which this kinase is required for growth and viability of *C. burnetii*, we attempted to inactivate the corresponding chromosomal gene. Unfortunately, after several attempts we were unable to generate a null mutant suggesting that *cstK* might be essential. However, we had previously isolated a *C. burnetii* mutant (*Tn2496*) carrying a transposon insertion allowing GFP expression at position 156783, 32 bp upstream of the starting codon of *cstK* (43) (Fig. 1A). To determine the effect of this transposon insertion on *cstK* gene expression, we assessed the expression level of *cstK* mRNA from wt *C. burnetii* and *Tn2496* strains. Surprisingly, *cstK* expression was significantly upregulated in the mutant strain, suggesting that the transposon insertion may have released a transcriptional negative regulation (Fig. 3A). This suggested that a putative transcriptional regulator might bind the *cstK* promoter and control its activity during host invasion.

We next examined the effects of CstK overexpression on *C. burnetii* infections by challenging Vero cells either with wt *C. burnetii*, the Dot/Icm-defective *dotA*::Tn mutant or the *Tn2496* mutant. Intracellular growth of the CstK overexpressing strain was significantly reduced over 7 days of infection with an intermediate phenotype between wt and the *dotA*::Tn mutant (Fig. 3B). Accordingly, multiparametric phenotypic profile analysis of the *Tn2496* mutant indicated that this strain exhibited a major defect in CCV development as compared to wt *C. burnetii* (Fig. 3C & D). To further investigate the effects of CstK overexpression on *C. burnetii* infections, GFP-expressing *C. burnetii* were transformed with plasmids expressing HA-tagged wt CstK or its corresponding mutants (CstK_K55M and CstK_FFA) under the control of an IPTG promoter. U2OS cells expressing cytoplasmic mCherry were challenged with the three *C. burnetii* strains in the presence or absence of IPTG. After 6 days of infection, cells were fixed, labelled with Hoechst and anti-LAMP1 antibody to visualize host cells nuclei and CCVs respectively, and

processed for automated image analysis. In all cases, the overexpression of CstK was detrimental for CCVs biogenesis and bacterial replication (Fig. 3E). Next, U2OS cells were challenged either with wt *C. burnetii,* the GFP-expressing *Tn2496* mutant strain or a combination of the two for 6 days (Fig. 3F). Cells were then fixed and labelled with an anti-*C. burnetii* antibody to label both bacteria strains and incubated with Hoechst to visualize host cells nuclei (Fig. 3F). Automated image analysis was then used to determine the effects of CstK overexpression on the replication of wt bacteria, in trans. Co-infections resulted in a significant increase in the size of *Tn2496* colonies, indicating that wt *C. burnetii* can partially restore the growth of the CstK-overexpressing strain (Fig. 3G). However, a significant decrease in the size of bacterial colonies labelled by the anti-*C. burnetii* antibodies indicated that CstK-overexpression has a detrimental effect in trans, on the development of wt bacteria (Fig. 3G). Of note, vacuoles harboring wt or mutant colonies alone were never observed in co-infection experiments. Therefore, we concluded that CstK participates in the formation of the *C. burnetii* replicative vacuole, and that its expression must be finely tuned for optimal intracellular replication.

CstK specifically interacts with host cell proteins. Since CstK is a secreted protein, we assume that this kinase would interfere with host cell signal transduction pathways to subvert host cell defenses to the benefit of the bacteria. To identify host cell proteins that could interact with CstK, we made use of the model amoeba *Dictyostelium discoideum*. *D. discoideum* is a eukaryotic professional phagocyte amenable to genetic and biochemical studies. Lysate from cells overexpressing CstK tagged with a C-terminal FLAG epitope (CstK-FLAG) was incubated with beads coupled to an anti-FLAG antibody. Beads were extensively washed, and bound proteins were separated by SDS-PAGE before mass-spectrometry analysis. Among the putative interactants of CstK identified by this approach, some were discarded on the basis of their intracellular localization while other retained candidates were mostly involved in the endocytic pathway (Table S1). Among these, the Rab GAP/TBC domain-containing protein, DDB_G0280253 (UniProtKB - Q54VM3**),** is a 136.4 kDa protein homologous to mammalian TBC1D5 (http://dictybase.org), a GTPase-activating protein (GAP) for Rab7a and Rab7b (44-46) that acts as a molecular switch between the endosomal and the autophagy pathway (47). Given the recently reported implication of TBC1D5 in the biogenesis of *L. pneumophila*-containing vacuoles (48) and the role of autophagy in the biogenesis of CCVs (25,31,49), we aimed at validating the interaction between human TBC1D5 (Hs-TBC1D5) and CstK in HEK-293T cells. Cells co-expressing Hs-TBC1D5-GFP and HA-CstK or CstK mutants were used for immunoprecipitation using anti-HA beads. Wild-type and CstK derivatives were detected as co-immunoprecipitated in presence of Hs-TBC1D5-GFP, thus confirming that Hs-TBC1D5 is a bona fide CstK interactant (Fig. 4A). Significantly higher levels of TBC1D5 were co-immunoprecipitated by the CstK mutants suggesting that the interaction might be increased in the absence of phosphorylation turn-over of the kinase (Fig 4A, lower panel). Interestingly, the interaction is not dependent on the phosphorylation status of CstK as the K55M mutant or the triple FFA mutant are still able to interact. Other candidates identified by mass spectrometry are currently being investigated.

TBC1D5 is recruited at CCVs and regulates their biogenesis. Given its recently reported role in the development of *L. pneumophila*-containing vacuoles, we investigated the localization of TBC1D5 in U2OS cells infected either with wt *C. burnetii*, the CstK-overexpressing strain *Tn2496* or the Dot/Icm-defective mutant *dotA*::Tn. Consistently with previous studies demonstrating a role in the activation of Rab7a and b, TBC1D5 seems to accumulate specifically at CCVs in a Dot/Icm-independent manner as the eukaryotic protein was found at CCVs generated by all *C. burnetii* (wt, the *Tn2496* and the *dotA*::Tn Fig. 4B and Supplementary Fig.1). Next, we used siRNA to deplete cells of TBC1D5 prior to *C. burnetii* infection, to investigate a possible role in CCVs development and intracellular bacterial replication. Indeed, vacuole development was significantly reduced in cells exposed to Hs-TBC1D5-targeted siRNAs as opposed to cells treated with non-targeting siRNA oligonucleotides (Fig. 4C).

TBC1D5 is not phosphorylated in vitro by recombinant CstK. We assessed whether CstK might phosphorylate the recombinant Hs-TBC1D5. Despite the *in silico* prediction of several Ser/Thr and Tyr phosphorylatable residues in Hs-TBC1D5, we failed to detect Hs-TBC1D5 phosphorylation using several *in vitro* kinases assays (Supplementary Fig.2). In addition, Hs-TBC1D5 phosphorylation status was also investigated upon transfection with CstK or its inactive derivative (K55M) followed by Hs-TBC1D5 immunoprecipitation. No

phosphorylation could be detected in our experimental conditions.

DISCUSSION

Bacterial Ser/Thr/Tyr kinases expressed by pathogenic bacteria can either act as key regulators of important microbial processes, or be translocated by secretion systems to interact with host substrates, thereby our results provide the first biochemical analysis of the secreted *C. burnetii* kinase CstK and its involvement in the process of infection and CCVs development. Importantly, CstK presents important differences as compared to classical Ser/Thr kinases. In particular, we provided evidence that CstK is a dual kinase able to autophosphorylate on Thr and Tyr residues. Moreover, the observation that a transposon insertion 32 bp upstream of the *cstK* starting codon leads to an increase in the levels of *cstK* mRNAs was indicative of the presence of a negative transcriptional regulation of gene expression, suggesting a fine tuning of the levels of CstK. Indeed, the *Tn2496* mutant displays a severe CCV biogenesis defect when used to challenge U2OS cells, highlighting the importance of regulating *cstK* expression during *C. burnetii* infections. Accordingly, inducing the expression of wt CstK in wt *C. burnetii* severely impairs CCVs development and bacterial replication. Co-infection experiments demonstrated that CstK overexpression can also act in trans, by perturbing the intracellular replication of wt *C. burnetii*. The identification of candidate eukaryotic interactors of CstK further corroborated a role of the bacterial kinase in subverting host functions during infection. Here we confirmed that CstK interacts with TBC1D5, but we failed to detect phosphorylation of the eukaryotic target by CstK. Though we cannot exclude that TBC1D5 is a genuine CstK substrate *in vivo* as the lack of phosphorylation of host interactors of bacterial STPKs is not uncommon. Interaction between STPKs and host proteins might as well perturb protein interaction networks at play in host cells (21). Indeed, the induced overexpression of CstK mutants lacking kinase activity in wt *C. burnetii* impaired CCVs development to the same extent as the overexpression of wt CstK. The biochemical mechanisms of these pathogen-directed targeted perturbations of host cell-signaling networks are being actively investigated. Regardless, siRNA depletion of TBC1D5 in *C. burnetii*-infected cells points at a role of the eukaryotic protein in CCVs development. In mammals, TBC1D5 was suggested to function as a molecular switch between endosomal and autophagy pathways. Indeed TBC1D5 associates the retromer VPS29 subunit involved in endosomal trafficking, and upon autophagy induction, the autophagy ubiquitin-like protein LC3 can displace VPS29, thus orienting TBC1D5 functions towards autophagy instead of endosomal functions (47). It is thus tempting to propose that CstK might interfere with this tight regulation between TBC1D5, LC3 and VPS29, and redirect TBC1D5 functions to support efficient *C. burnetii* intracellular replication. Further work will need to be carried out to decipher how CstK recognizes these host substrates and how they participate in the establishment of *C. burnetii* parasitophorous vacuoles. Another perspective of this work is the opening of a new field of investigation for future drug development to fight this pathogen. Because CstK seems to be essential, specific inhibitors of this kinase preventing *C. burnetii* growth would be extremely useful for the development of new therapies.

EXPERIMENTAL PROCEDURES

Bacterial strains and growth conditions. Bacterial strains and plasmids are described in Table 1. Strains used for cloning and expression of recombinant proteins were *Escherichia coli* TOP10 (Invitrogen) and *E. coli* BL21 (DE3)Star (Stratagene), respectively. *E. coli* cells were grown and maintained at 25 °C in LB medium supplemented with 100 µg/ml ampicillin when required. *Coxiella burnetii* RSA439 NMII and transposon mutants *Tn1832*, *Tn2496*, and *dotA::Tn* were grown in ACCM-2 (45) supplemented with chloramphenicol (3 mg/ml) in a humidified atmosphere of 5% CO2 and 2.5% O2 at 37 °C.

Cloning, expression and purification of CstK derivatives. The *cstK (CBU_0175)* gene was amplified by PCR using *Coxiella burnetii* RSA439 NMII chromosomal DNA as a template with the primers listed in Table 2 containing a *Bam*HI and *Hind*III restriction site, respectively. The corresponding amplified product was digested with *Bam*HI and *Hind*III, and ligated into the bacterial pGEX(M) plasmid, that includes a N-terminal GST-tag, thus generating pGEX(M)_*cstK*. pGEX(M)_*cstK* derivatives harboring different mutations were generated by using the QuikChange Site-Directed Mutagenesis Kit (Stratagene, La Jolla, CA), and resulted in the construction of plasmids detailed in Table 2. For overexpression assays, *cstK* and its derivatives were cloned in the pJA-LACO-4xHA vector (30) using *Kpn*I and *Bam*HI restriction sites. All constructs were verified by DNA sequencing.

Transformed *E. coli* BL21 Star cells with pGEX(M)_*cstK* derivatives were grown at 16 °C in LB medium containing 1 g/liter of glucose and 100 µg/ml of ampicillin and protein synthesis induced with 0.5 mM IPTG overnight. Bacteria were disrupted by sonication (Branson, digital sonifier) and centrifuged at 14,000 rpm for 25 min. Purifications of the GST-tagged recombinants were performed as described by the manufacturer (GE Healthcare). *cstK* coding sequence was also optimized for mammalian cell expression (GenScript), amplified by PCR and cloned into pDXA-3C (50) containing a FLAG-tag for C-terminal fusion. After sequencing, the plasmid was linearized by the restriction enzyme *Sca*I and transfected in *D. discoideum* as described (51). Clone selection was made with 10 mg/ml of G418, and protein expression was assayed by Western blot analysis of *D. discoideum* crude extract with an anti-FLAG rabbit polyclonal antibody (GenScript, USA). For ectopic expression assays, *cstK, cstK_K55M* and *cstK_FFA* with optimized codons (IDT) were cloned in pRK5-HA using the primer pair CstKopt-BamHI-Fw/CstKopt-EcoRI-Rv.

Cloning, expression and purification of TBC1D5 derivatives. The *D. discoideum* GFP-tagged TBC1D5 was previously generated (48). Cells were grown at 22 °C in HL5 medium as previously described (51). Human TBC1D5 coding sequence was obtained from the hORFeome v8.1 (ORF 2659, Q92609, fully-sequenced cloned human ORFs in Gateway Entry clones ready for transfer to Gateway-compatible expression vectors). HsTBC1D5 coding sequence has been recombined into pEGFP-N1 RfC Destination vector by GateWay reaction (MGC Platform Montpellier) thus generating pEGFP-N1_HsTBC1D5 coding for HsTBC1D5 with a C-terminal GFP Tag. pmCH_Hs-TBC1D5-mCherry has been generated by the same method (MGC Platform Montpellier).

RNA extraction and quantitative RT-PCR (qRT-PCR). Fifty ml of *C. burnetii* culture was harvested, resuspended in 600 µL of RNA protect reagent (Qiagen) and incubated 5 min at room temperature. Bacteria were centrifuged and resuspended in 200 µl TE (10 mM Tris-HCl, 1 mM EDTA, pH 8) containing 1 mg/ml lysozyme. Bacterial suspension was incubated at room temperature for 5 min and bacteria were disrupted by vigorous vortexing for 10 sec every 2 min. 700 µl of RLT buffer from RNA easy kit (Qiagen), were added to the bacterial suspension and disruption was completed by vortexing vigorously. RNA was purified with the RNA easy kit according to manufacturer's instructions. DNA was further removed using DNAse I (Invitrogen). cDNA was produced using Superscript III reverse transcriptase (Invitrogen). Controls without reverse transcriptase were done on each RNA sample to rule out possible DNA contamination. Quantitative real-time PCR was performed using LightCycler 480 SYBR Green I Master (Roche) and a 480 light cycler instrument (Roche). PCR conditions were as follows: 3 min denaturation at 98 °C, 45 cycles of 98 °C for 5 sec, 60 °C for 10 sec and 72 °C for 10 sec. The *dotA* gene was used as internal control. The sequences of primers used for qRT-PCR are listed in Table 2. The expression level of *cstK* in the wild type strain was set at 100 and the expression levels of *cstK* in the *Tn2496* mutant were normalized to the wild type levels.

In vitro kinase assays. *In vitro* phosphorylation was performed with 4 µg of wild-type CstK or CstK derivatives in 20 µl of buffer P (25 mM Tris-HCl, pH 7.0; 1 mM DTT; 5 mM $MnCl_2$; 1 mM EDTA; 50 µM ATP) with 200 µCi ml^{-1} (65 nM) [γ-^{33}P]ATP (PerkinElmer, ref: NEG 602H250UC, 3000 Ci $mmol^{-1}$) for 30 min at 37 °C. For substrate phosphorylation, 4 µg of MBP (Myelin Basic Protein) (Sigma) and 4 µg of CstK were used. Each reaction mixture was stopped by addition of an equal volume of Laemmli buffer and the mixture was heated at 100 °C for 5 min. After electrophoresis, gels were soaked in 16% TCA for 10 min at 90 °C, and dried. Radioactive proteins were visualized by autoradiography using direct exposure to films.

Mass spectrometry analysis. For mass spectrometry analysis, CstK was phosphorylated as described above, except that [γ-^{33}P]ATP was replaced with 5 mM cold ATP. Subsequent mass spectrometry analyses were performed as previously reported (52,53). Briefly, samples were submitted to trypsin digestion and analyzed using an Ultimate 3000 nano-RSLC (Thermo Scientific, San Jose California) coupled on line with a quadrupole-orbitrap Q Exactive HF mass spectrometer via a nano-electrospray ionization source (Thermo Scientific, San Jose California). Samples were injected and loaded on a C18 Acclaim PepMap100 trap-column (Thermo Scientific) and separated on a C18 Acclaim Pepmap100 nano-column (Thermo Scientific). MS data were acquired in a data dependent strategy selecting the fragmentation events based on the 20 most abundant precursor ions in the survey scan (350-1600 Th). The resolution of the survey scan was 60,000 at m/z 200 Th and for MS/MS scan the resolution was set to 15,000 at m/z 200 Th.

Peptides selected for MS/MS acquisition were then placed on an exclusion list for 30s using the dynamic exclusion mode to limit duplicate spectra. Data files were then analyzed with Proteome Discover 2.2 using the SEQUEST HT algorithm against the Uniprot *Dictyostelium discoideum* to which was included the sequence of CstK.

C. burnetii infections. U2OS epithelial cells were challenged either with *Coxiella burnetii* RSA439 NMII, the transposon mutants *Tn1832*, *dotA*::Tn or *Tn2496* as previously described (38,49). For co-infection experiments, cells were challenged with a 1:1 ratio of *Coxiella burnetii* RSA439 NMII and *Tn2496* transposon mutant. For gene silencing, U2OS cells were seeded at 2,000 cells per well in black, clear-bottomed, 96-well plates in triplicate and transfected with siRNA oligonucleotides 24 h later by using the RNAiMAX transfection reagent (Thermo Fisher Scientific) according to the manufacturer's recommendations. At 24 h post transfection, cells were challenged with *C. burnetii* (MOI of 100) and further incubated for 5 d. Cells were then fixed and processed for immunofluorescence. Where appropriate, anti-LAMP1 antibodies were used to label lysosomes and CCVs as previously described (54). Samples were imaged with a Zeiss Axio Imager Z1 epifluorescence microscope (Carl Zeiss, Germany) connected to a CoolSNAP HQ^2 CCD camera (Teledyne Photometrics, Tucson, AZ). Images were acquired with 40x oil immersion objectives and processed with Metamorph (Molecular Devices, San Jose, CA). For phenotypic screening, samples were imaged with an ArrayScan VTI Live epifluorescence automated microscope (Cellomics) equipped with an ORCA-ER CCD camera (Hamamatsu). 25 fields per well were acquired for image analysis. ImageJ and ICY software were used for image analysis and quantifications. Phenotypic profiles (expressed as z-scores) were calculated using CellProfiler, from triplicate experiments as previously described (54) following median based normalization of 96-well plates. Plates effects were corrected by the median value across wells that are annotated as control.

Beta-lactamase translocation assay. Effector proteins translocation assays were performed as previously described (30). Briefly, *Coxiella burnetii Tn1832* (wt) and *dotA*::Tn were transformed either with pXDC-Blam (negative control), pXDC-Blam-CvpB (positive control) or pXDC-Blam-CstK. Each strain was used to infect U2OS epithelial cells. After 24, 48 or 72 hours of infection, cells were loaded with the fluorescent substrate CCF4/AM (LiveBLAzer-FRET B/G loading kit; Invitrogen) in HBSS (20 mM HEPES pH 7.3) containing 15 mM probenecid (Sigma). Cells were incubated in the dark for 1 h at room temperature and imaged using an EVOS inverted fluorescence microscope. Images were acquired using DAPI and GFP filter cubes. The image analysis software CellProfiler was used to segment and identify all cells in the sample (GFP), positive cells (DAPI) and to calculate the intensity of fluorescence in each channel. The percentage of positive cells versus the total number of infected cells was then calculated and used to evaluate effector translocation.

Immunoprecipitation from D. discoideum lysates. For immunoprecipitation assays, $2x10^7$ cells were lysed in lysis buffer (50 mM Tris-HCl pH 7.5, 300 mM NaCl, 0.5% NP40, protease inhibitors (Roche)) and cleared by centrifugation for 15 min at 14 000 rpm in a microfuge. Lysate supernatants were incubated overnight at 4 °C with anti-flag monoclonal antibody coated on agarose beads (Genscript). The beads were then washed five times in wash buffer (50 mM Tris-HCl pH 7.5, 300 mM NaCl, 0.1% NP40) and once in PBS. Bound proteins were migrated on SDS-PAGE and analyzed by LC-MS/MS.

Cell culture, heterologous expression and anti-HA immunoprecipitation. HEK-293T cells were grown in DMEM (Gibco) containing 10% (vol/vol) FBS, 1% glutamax (Gibco, 200 mM stock), 0.5% Penicillin/Streptomycin (Gibco, 10000 U/mL stock) and maintained under standard conditions at 37 °C in a humidified atmosphere containing 5% CO2. Cells were transiently transfected using the jetPEI Transfection Reagent (Polyplus-Transfection Inc.) to express either Hs-TBC1D5-GFP, CstK_HA derivatives, or each CstK derivatives with TBC1D5_GFP protein. Cells were used 24h after transfection for immunoprecipitation assay. Transfected cells were washed two times in cold PBS and lysed in lysis buffer (50 mM Tris, 150 mM NaCl, 0.5 mM EDTA, 0.5 % NP40, protease and phosphatases inhibitors (Roche)). Cleared lysate (950 µL, approximately 1 mg total proteins) were incubated with anti HA magnetic Beads (Pierce) for 30 min at room temperature under gentle rotation. The beads were washed three times in lysis buffer, boiled in 2X Laemmli sample buffer and loaded on ExpressPlus™ PAGE Gels (GenScript). The eluted proteins were visualized by Western Blotting with the following antibodies: anti-HA from Chromotek, anti-GFP from Torrey Pines, donkey anti-rat or anti-rabbit from Jackson ImmunoResearch.

Densitometry.
Regions of Interest (ROIs) were obtained from each band of interest and the intensity was measured using ImageLab (From Biorad). For each band, the same ROI was used for background calculation and removal from areas adjacent to each band.

DATA AVAILABILITY STATEMENT

All the data are contained in this manuscript.

ACKNOWLEDGMENTS

We wish to thank the Montpellier RIO imaging facility at the University of Montpellier, member of the national infrastructure France-BioImaging, that is supported by the French National Research Agency (ANR-10-INBS-04, «Investments for the future»). We acknowledge the contribution of the Protein Science Facility of the SFR Biosciences (UMS3444/CNRS, US8/Inserm, ENS de Lyon, UCBL), especially Frédéric DELOLME and Adeline PAGE who performed the mass spectrometry analysis. This work was supported by grants from the ATIP/AVENIR Program for V.M. and M.B., the Region Occitanie for S. B., a Marie Curie CIG to E.M. (grant n. 293731), the Agence Nationale de la Recherche (ANR) Grant ANR-14-CE14-0012-01 (project AttaQ) to M.B.

CONFLICT OF INTEREST

The authors declare that they have no conflicts of interest with the contents of this article.

REFERENCES

1. Stancik, I. A., Sestak, M. S., Ji, B., Axelson-Fisk, M., Franjevic, D., Jers, C., Domazet-Loso, T., and Mijakovic, I. (2018) Serine/Threonine Protein Kinases from Bacteria, Archaea and Eukarya Share a Common Evolutionary Origin Deeply Rooted in the Tree of Life. *J Mol Biol* **430**, 27-32
2. Janczarek, M., Vinardell, J. M., Lipa, P., and Karas, M. (2018) Hanks-Type Serine/Threonine Protein Kinases and Phosphatases in Bacteria: Roles in Signaling and Adaptation to Various Environments. *Int J Mol Sci* **19**
3. Rajagopal, L., Clancy, A., and Rubens, C. E. (2003) A eukaryotic type serine/threonine kinase and phosphatase in *Streptococcus agalactiae* reversibly phosphorylate an inorganic pyrophosphatase and affect growth, cell segregation, and virulence. *J Biol Chem* **278**, 14429-14441
4. Hussain, H., Branny, P., and Allan, E. (2006) A eukaryotic-type serine/threonine protein kinase is required for biofilm formation, genetic competence, and acid resistance in *Streptococcus mutans*. *J Bacteriol* **188**, 1628-1632
5. Echenique, J., Kadioglu, A., Romao, S., Andrew, P. W., and Trombe, M. C. (2004) Protein serine/threonine kinase StkP positively controls virulence and competence in *Streptococcus pneumoniae*. *Infect Immun* **72**, 2434-2437
6. Jin, H., and Pancholi, V. (2006) Identification and biochemical characterization of a eukaryotic-type serine/threonine kinase and its cognate phosphatase in *Streptococcus pyogenes*: their biological functions and substrate identification. *J Mol Biol* **357**, 1351-1372
7. Av-Gay, Y., and Everett, M. (2000) The eukaryotic-like Ser/Thr protein kinases of *Mycobacterium tuberculosis*. *Trends Microbiol* **8**, 238-244
8. Chaba, R., Raje, M., and Chakraborti, P. K. (2002) Evidence that a eukaryotic-type serine/threonine protein kinase from *Mycobacterium tuberculosis* regulates morphological changes associated with cell division. *Eur J Biochem* **269**, 1078-1085
9. Wehenkel, A., Bellinzoni, M., Grana, M., Duran, R., Villarino, A., Fernandez, P., Andre-Leroux, G., England, P., Takiff, H., Cervenansky, C., Cole, S. T., and Alzari, P. M. (2008) Mycobacterial Ser/Thr protein kinases and phosphatases: physiological roles and therapeutic potential. *Biochim Biophys Acta* **1784**, 193-202
10. Molle, V., and Kremer, L. (2010) Division and cell envelope regulation by Ser/Thr phosphorylation: *Mycobacterium* shows the way. *Mol Microbiol* **75**, 1064-1077
11. Alber, T. (2009) Signaling mechanisms of the *Mycobacterium tuberculosis* receptor Ser/Thr protein kinases. *Curr Opin Struct Biol* **19**, 650-657

12. Greenstein, A. E., Grundner, C., Echols, N., Gay, L. M., Lombana, T. N., Miecskowski, C. A., Pullen, K. E., Sung, P. Y., and Alber, T. (2005) Structure/function studies of Ser/Thr and Tyr protein phosphorylation in *Mycobacterium tuberculosis*. *J Mol Microbiol Biotechnol* **9**, 167-181
13. Galyov, E. E., Hakansson, S., Forsberg, A., and Wolf-Watz, H. (1993) A secreted protein kinase of *Yersinia pseudotuberculosis* is an indispensable virulence determinant. *Nature* **361**, 730-732
14. Hakansson, S., Galyov, E. E., Rosqvist, R., and Wolf-Watz, H. (1996) The Yersinia YpkA Ser/Thr kinase is translocated and subsequently targeted to the inner surface of the HeLa cell plasma membrane. *Mol Microbiol* **20**, 593-603
15. Archambaud, C., Gouin, E., Pizarro-Cerda, J., Cossart, P., and Dussurget, O. (2005) Translation elongation factor EF-Tu is a target for Stp, a serine-threonine phosphatase involved in virulence of *Listeria monocytogenes*. *Mol Microbiol* **56**, 383-396
16. Lima, A., Duran, R., Schujman, G. E., Marchissio, M. J., Portela, M. M., Obal, G., Pritsch, O., de Mendoza, D., and Cervenansky, C. (2011) Serine/threonine protein kinase PrkA of the human pathogen *Listeria monocytogenes*: biochemical characterization and identification of interacting partners through proteomic approaches. *J Proteomics* **74**, 1720-1734
17. Wang, J., Li, C., Yang, H., Mushegian, A., and Jin, S. (1998) A novel serine/threonine protein kinase homologue of *Pseudomonas aeruginosa* is specifically inducible within the host infection site and is required for full virulence in neutropenic mice. *J Bacteriol* **180**, 6764-6768
18. Kristich, C. J., Wells, C. L., and Dunny, G. M. (2007) A eukaryotic-type Ser/Thr kinase in *Enterococcus faecalis* mediates antimicrobial resistance and intestinal persistence. *Proc Natl Acad Sci U S A* **104**, 3508-3513
19. Beltramini, A. M., Mukhopadhyay, C. D., and Pancholi, V. (2009) Modulation of cell wall structure and antimicrobial susceptibility by a *Staphylococcus aureus* eukaryote-like serine/threonine kinase and phosphatase. *Infect Immun* **77**, 1406-1416
20. Truong-Bolduc, Q. C., Ding, Y., and Hooper, D. C. (2008) Posttranslational modification influences the effects of MgrA on norA expression in *Staphylococcus aureus*. *J Bacteriol* **190**, 7375-7381
21. Canova, M. J., and Molle, V. (2014) Bacterial serine/threonine protein kinases in host-pathogen interactions. *J Biol Chem* **289**, 9473-9479
22. Kazar, J. (2005) *Coxiella burnetii* infection. *Ann N Y Acad Sci* **1063**, 105-114
23. Arricau-Bouvery, N., and Rodolakis, A. (2005) Is Q fever an emerging or re-emerging zoonosis? *Vet Res* **36**, 327-349
24. Madariaga, M. G., Rezai, K., Trenholme, G. M., and Weinstein, R. A. (2003) Q fever: a biological weapon in your backyard. *Lancet Infect Dis* **3**, 709-721
25. Beron, W., Gutierrez, M. G., Rabinovitch, M., and Colombo, M. I. (2002) *Coxiella burnetii* localizes in a Rab7-labeled compartment with autophagic characteristics. *Infect Immun* **70**, 5816-5821
26. Newton, H. J., McDonough, J. A., and Roy, C. R. (2013) Effector protein translocation by the *Coxiella burnetii* Dot/Icm type IV secretion system requires endocytic maturation of the pathogen-occupied vacuole. *PLoS One* **8**, e54566
27. Luhrmann, A., Nogueira, C. V., Carey, K. L., and Roy, C. R. (2010) Inhibition of pathogen-induced apoptosis by a *Coxiella burnetii* type IV effector protein. *Proc Natl Acad Sci U S A* **107**, 18997-19001
28. Klingenbeck, L., Eckart, R. A., Berens, C., and Luhrmann, A. (2013) The *Coxiella burnetii* type IV secretion system substrate CaeB inhibits intrinsic apoptosis at the mitochondrial level. *Cell Microbiol* **15**, 675-687
29. Cunha, L. D., Ribeiro, J. M., Fernandes, T. D., Massis, L. M., Khoo, C. A., Moffatt, J. H., Newton, H. J., Roy, C. R., and Zamboni, D. S. (2015) Inhibition of inflammasome activation by *Coxiella burnetii* type IV secretion system effector IcaA. *Nat Commun* **6**, 10205
30. Martinez, E., Allombert, J., Cantet, F., Lakhani, A., Yandrapalli, N., Neyret, A., Norville, I. H., Favard, C., Muriaux, D., and Bonazzi, M. (2016) *Coxiella burnetii* effector CvpB modulates phosphoinositide metabolism for optimal vacuole development. *Proc Natl Acad Sci U S A* **113**, E3260-3269
31. Siadous, F. A., Cantet, F., Van Schaik, E., Burette, M., Allombert, J., Lakhani, A., Bonaventure, B., Goujon, C., Samuel, J., Bonazzi, M., and Martinez, E. (2020) Coxiella effector protein CvpF subverts RAB26-dependent autophagy to promote vacuole biogenesis and virulence. *Autophagy*, 1-17

32. Newton, H. J., Kohler, L. J., McDonough, J. A., Temoche-Diaz, M., Crabill, E., Hartland, E. L., and Roy, C. R. (2014) A screen of *Coxiella burnetii* mutants reveals important roles for Dot/Icm effectors and host autophagy in vacuole biogenesis. *PLoS Pathog* **10**, e1004286
33. Latomanski, E. A., Newton, P., Khoo, C. A., and Newton, H. J. (2016) The Effector Cig57 Hijacks FCHO-Mediated Vesicular Trafficking to Facilitate Intracellular Replication of *Coxiella burnetii*. *PLoS Pathog* **12**, e1006101
34. Vogel, J. P. (2004) Turning a tiger into a house cat: using *Legionella pneumophila* to study *Coxiella burnetii*. *Trends Microbiol* **12**, 103-105
35. Carey, K. L., Newton, H. J., Luhrmann, A., and Roy, C. R. (2011) The *Coxiella burnetii* Dot/Icm system delivers a unique repertoire of type IV effectors into host cells and is required for intracellular replication. *PLoS Pathog* **7**, e1002056
36. Chen, C., Banga, S., Mertens, K., Weber, M. M., Gorbaslieva, I., Tan, Y., Luo, Z. Q., and Samuel, J. E. (2010) Large-scale identification and translocation of type IV secretion substrates by *Coxiella burnetii*. *Proc Natl Acad Sci U S A* **107**, 21755-21760
37. Hanks, S. K., and Hunter, T. (1995) Protein kinases 6. The eukaryotic protein kinase superfamily: kinase (catalytic) domain structure and classification. *Faseb J* **9**, 576-596
38. Hanks, S. K., Quinn, A. M., and Hunter, T. (1988) The protein kinase family: conserved features and deduced phylogeny of the catalytic domains. *Science* **241**, 42-52
39. Carrera, A. C., Alexandrov, K., and Roberts, T. M. (1993) The conserved lysine of the catalytic domain of protein kinases is actively involved in the phosphotransfer reaction and not required for anchoring ATP. *Proc Natl Acad Sci U S A* **90**, 442-446
40. Noroy, C., Lefrancois, T., and Meyer, D. F. (2019) Searching Algorithm for Type IV Effector proteins (S4TE) 2.0: improved tools for type IV effector prediction, analysis and comparison. *bioRxiv*
41. Fiuza, M., Canova, M. J., Zanella-Cleon, I., Becchi, M., Cozzone, A. J., Mateos, L. M., Kremer, L., Gil, J. A., and Molle, V. (2008) From the characterization of the four serine/threonine protein kinases (PknA/B/G/L) of *Corynebacterium glutamicum* toward the role of PknA and PknB in cell division. *J Biol Chem* **283**, 18099-18112
42. Molle, V., Leiba, J., Zanella-Cleon, I., Becchi, M., and Kremer, L. (2010) An improved method to unravel phosphoacceptors in Ser/Thr protein kinase-phosphorylated substrates. *Proteomics* **10**, 3910-3915
43. Martinez, E., Cantet, F., Fava, L., Norville, I., and Bonazzi, M. (2014) Identification of OmpA, a *Coxiella burnetii* protein involved in host cell invasion, by multi-phenotypic high-content screening. *PLoS Pathog* **10**, e1004013
44. Borg Distefano, M., Hofstad Haugen, L., Wang, Y., Perdreau-Dahl, H., Kjos, I., Jia, D., Morth, J. P., Neefjes, J., Bakke, O., and Progida, C. (2018) TBC1D5 controls the GTPase cycle of Rab7b. *Journal of cell science* **131**
45. Seaman, M. N. J., Mukadam, A. S., and Breusegem, S. Y. (2018) Inhibition of TBC1D5 activates Rab7a and can enhance the function of the retromer cargo-selective complex. *Journal of cell science* **131**
46. Sun, M., Luong, G., Plastikwala, F., and Sun, Y. (2020) Control of Rab7a activity and localization through endosomal type Igamma PIP 5-kinase is required for endosome maturation and lysosome function. *FASEB J* **34**, 2730-2748
47. Popovic, D., and Dikic, I. (2014) TBC1D5 and the AP2 complex regulate ATG9 trafficking and initiation of autophagy. *EMBO reports* **15**, 392-401
48. Barlocher, K., Hutter, C. A. J., Swart, A. L., Steiner, B., Welin, A., Hohl, M., Letourneur, F., Seeger, M. A., and Hilbi, H. (2017) Structural insights into *Legionella* RidL-Vps29 retromer subunit interaction reveal displacement of the regulator TBC1D5. *Nat Commun* **8**, 1543
49. McDonough, J. A., Newton, H. J., Klum, S., Swiss, R., Agaisse, H., and Roy, C. R. (2013) Host pathways important for *Coxiella burnetii* infection revealed by genome-wide RNA interference screening. *mBio* **4**, e00606-00612
50. Manstein, D. J., Schuster, H. P., Morandini, P., and Hunt, D. M. (1995) Cloning vectors for the production of proteins in *Dictyostelium discoideum*. *Gene* **162**, 129-134
51. Alibaud, L., Cosson, P., and Benghezal, M. (2003) *Dictyostelium discoideum* transformation by oscillating electric field electroporation. *BioTechniques* **35**, 78-80, 82-73

52. Brelle, S., Baronian, G., Huc-Brandt, S., Zaki, L. G., Cohen-Gonsaud, M., Bischoff, M., and Molle, V. (2016) Phosphorylation-mediated regulation of the *Staphylococcus aureus* secreted tyrosine phosphatase PtpA. *Biochem Biophys Res Commun* **469**, 619-625
53. Baronian, G., Ginda, K., Berry, L., Cohen-Gonsaud, M., Zakrzewska-Czerwinska, J., Jakimowicz, D., and Molle, V. (2015) Phosphorylation of *Mycobacterium tuberculosis* ParB participates in regulating the ParABS chromosome segregation system. *PLoS One* **10**, e0119907
54. Martinez, E., Cantet, F., and Bonazzi, M. (2015) Generation and multi-phenotypic high-content screening of *Coxiella burnetii* transposon mutants. *Journal of visualized experiments : JoVE*, e52851
55. Beare, P. A., Sandoz, K. M., Omsland, A., Rockey, D. D., and Heinzen, R. A. (2011) Advances in genetic manipulation of obligate intracellular bacterial pathogens. *Frontiers in microbiology* **2**, 97
56. Molle, V., Kremer, L., Girard-Blanc, C., Besra, G. S., Cozzone, A. J., and Prost, J. F. (2003) An FHA phosphoprotein recognition domain mediates protein EmbR phosphorylation by PknH, a Ser/Thr protein kinase from *Mycobacterium tuberculosis*. *Biochemistry* **42**, 15300-15309
57. Charpentier, E., Anton, A. I., Barry, P., Alfonso, B., Fang, Y., and Novick, R. P. (2004) Novel cassette-based shuttle vector system for gram-positive bacteria. *Appl Environ Microbiol* **70**, 6076-6085

FIGURE LEGENDS

Figure 1. ***CstK is a Dot/Icm effector protein*** **(A)** Schematic representation of CstK. A conserved promoter-binding domain is predicted between aa -227 and -213 (*Apm*) and the transposon insertion site for *Tn2496* is indicated. The kinase domain is predicted between aa 26 and 174 and is shown in red. The conserved lysine residue is indicated, and the phosphorylated sites are indicated by an asterisk. **(B)** BLAM secretion assay. U2OS cells were infected for 24, 48, or 72h (black, grey and white bars, respectively) with wt *C. burnetii* or the *dotA*::Tn mutant transformed with vectors expressing Beta-Lactamase alone (BLAM, negative control), BLAM-CvpB (positive control) or BLAM-CstK. Protein translocation was probed using the CCF-4 substrate. The average percentage of cells positive for cleaved CCF-4 as compared to the total number of cells was assessed. Values are mean ± SD from 3 independent experiments. ns = non-significant; *** = P<0.0001, one-way ANOVA, Dunnett's multiple comparison test. CstK localization. **(C)** U2OS cells ectopically expressing HA-tagged CstK (red) were either left untreated (top panels) or challenged with wt *C. burnetii* expressing GFP (green) for 3 days. Lysosomal compartments were labelled using anti-LAMP1 antibodies (blue). Scale bars 10 µm.

Figure 2. (A) Biochemical characterization of CstK. Recombinant CstK derivatives were overproduced, purified on glutathione-Sepharose 4B matrix and submitted to gel electrophoresis and stained with Coomassie Blue (upper panel). *In vitro* phosphorylation assays were performed with [γ-^{33}P]ATP for 30 min and the eukaryotic substrate myelin basic protein (MBP) when required. Proteins were analyzed by SDS-PAGE, and radioactive bands were revealed by autoradiography (lower panel). The upper bands illustrate the autokinase activity of CstK, and the lower bands represent phosphorylated MBP. Standard proteins of known molecular masses were run in parallel. **(B)** A kinetic analysis was performed by incubation of CstK with [γ-^{33}P]ATP over different times. Proteins were analyzed by SDS-PAGE, and radioactive bands were revealed by autoradiography. **(C)** Effects of cations on autokinase activity of CstK. Purified CstK protein was subjected to *in vitro* autophosphorylation assays in the presence of 50 µM ATP [γ-^{33}P]ATP and 5 mM of Mg^{2+} or Mn^{2+}. Phosphoproteins were separated by SDS-PAGE and then revealed by autoradiography. **(D)** *In vitro* phosphorylation of CstK mutant derivatives. The mutated variants CstK_Y14F (harboring a Tyr to Phe substitution at Y14), CstK_Y209F (harboring a Tyr to Phe substitution at Y209), CstK_T232A (harboring a Thr to Ala substitution at T232), or CstK_Y14F/Y209F/T232A (harboring all three substitutions) were incubated in presence of [γ-^{33}P]ATP with or without the eukaryotic substrate myelin basic protein (MBP). Samples were separated by SDS-PAGE, stained with Coomassie Blue (upper panel), and visualized by autoradiography (lower panel). The upper bands illustrate the autokinase activity of CstK, and the lower bands represent phosphorylated MBP. Standard proteins of known molecular masses were run in parallel (kDa lane). **(E)** U2OS cells ectopically expressing either HA-tagged CstK_K55M or CstK_FFA (red) were challenged with wt *C. burnetii* expressing GFP (green) for 3 days. Lysosomal compartments were labelled using anti-LAMP1 antibodies (blue). Scale bars 10 µm. Inset magnification scale bars 4 µm.

Figure 3. CstK regulates vacuole development and *C. burnetii* replication within infected cells. **(A)** Expression of *cstk* was measured by qRT-PCR from cultures of either wt *C. burnetii* or the *Tn2496* mutant strain. Values are means ± SEM of 4 independent experiments. ***, $p < 0.001$, unpaired t-test. **(B)** Vero cells were challenged either with wt *C. burnetii*, the *dotA*::Tn mutant or the *Tn2496* mutant strains, all expressing GFP. Intracellular replication was monitored over 7 days of infection by monitoring the GFP fluorescence using a microplate reader. Values are mean ± SD from 3 independent experiments. **(C)** U2OS cells were challenged either with wt *C. burnetii* or the *Tn2496* mutant strain, both expressing GFP (green). 7 days post-infection, cells were fixed and labelled with an anti-LAMP1 antibody (red) and Hoechst (blue) to visualize CCVs and host cell nuclei, respectively. Scale bars 10 µm. **(D)** An average of 50000 cells were automatically imaged and analyzed from triplicate experiments for each condition illustrated in **C**, and the phenotypic profile of the *Tn2496* mutant was compared to that of wt *C. burnetii* and expressed as z-scores over 15 independent features. **(E)** GFP-expressing *C. burnetii* transformed with plasmids encoding either wt CstK, the K55M or the FFA mutants, all under the regulation of an IPTG-inducible promoters were used to infect U2OS cells for 6 days, in the presence or absence of IPTG. Cells were then fixed and labelled as in **C**, and an average of 50000 cells were automatically imaged and analyzed for each condition. The mean size of *C. burnetii* colonies and CCVs was calculated (red bars). **(F)** U2OS cells were challenged either with wt *C. burnetii*, the GFP-expressing mutant *Tn2496* or a combination of the two strains for 6 days. Cells were then fixed and labelled with anti-*C. burnetii* antibodies (anti-NMII) to label both strains. **(G)** An average of 50000 cells were automatically imaged and analyzed for each condition illustrated in **F** and the mean size of *C. burnetii* colonies was calculated (red bars). n.s., non-significant; ****, $p < 0.0001$, one-way ANOVA, Dunnett's multiple comparison test.

Figure 4. CstK interacts with TBC1D5. (A) The interaction between CstK and the human TBC1D5 has been confirmed after cotransfection of HEK-293T cells to express each HA-tagged CstK derivatives with GFP-tagged Hs-TBC1D5. Cells have been lysed and HA-tagged CstK derivatives have been trapped on anti-HA magnetic beads (Pierce). Beads were washed, eluted by boiling, and bound proteins were revealed by Western blot analysis. Anti-HA antibody confirms the immunoprecipitation of CstK derivatives. For the densitometry graph, Regions of Interest (ROIs) were obtained from each band of interest and the intensity was measured **(B)** Hs_TBC1D5 localization during infection was monitored in U2OS cells expressing mCherry-tagged Hs-TBC1D5 (red) challenged for 4 days either with wt *C. burnetii*, the Dot/Icm-defective *dotA*::Tn mutant or the CstK-overexpressing mutant *Tn2496*, all expressing GFP (green). Lysosomal compartments were labelled with anti-LAMP1 antibodies (blue). Scale bars 10 µm. Inset magnification scale bars 4 µm **(C)** The role of TBC1D5 in *C. burnetii* infections was investigated using siRNA to deplete Hs-TBC1D5 in U2OS prior to challenge with GFP-expressing wt *C. burnetii*. The size of CCVs was automatically calculated over an average of 150000 cells per condition. Red bars indicate medians. ***, $p < 0.0001$; **, $p < 0.001$; *, $p < 0.01$; one-way ANOVA, Dunnett's multiple comparison test. Scale bars 10 µm.

TABLES

Table 1. Strains and plasmids used in this study

Strains or Plasmids	Genotype or Description [a]	Source or Reference
***Escherichia coli* strains**		
E. coli TOP10	*E. coli* derivative ultra-competent cells used to general cloning; F- mcrA D(*mrr-hsd*RMS-*mcr*BC) f80*dlac*ZÄM15 D *lac*X74 *end*A1 *rec*A1*ara*D139 D (*ara*, *leu*)7697 *gal*U *gal*K *rps*L *nup*G - *ton*A	Invitrogen
E. coli BL21(DE3)Star	F2 *ompT hsdSB*(rB2 mB2) *gal dcm* (DE3); used to express recombinant proteins in *E. coli*	Stratagene
***Coxiella burnetii* strains**		
Coxiella burnetii RSA439 NMII	Wild type (wt) *Coxiella burnetii* RSA439 NMII non-fluorescent	(55)
Coxiella burnetii Tn2496	*Coxiella burnetii* RSA439 NMII carrying an Himar1-CAT-GFP cassette 32 bp upstream of CBU_0175, expressing GFP	This study
Coxiella burnetii Tn1832	*Coxiella burnetii* RSA439 NMII carrying an Himar1-CAT-GFP cassette in the intergenic region between CBU_1847b and CBU_1849, expressing GFP	(43)
Coxiella burnetii Tn292	*Coxiella burnetii* RSA439 NMII carrying an Himar1-CAT-GFP cassette in CBU_1648 (*dotA*), expressing GFP	(43)
Plasmids		
pGEX(M)	pGEX with a 321-bp *Eco*RI/*Bam*HI fragment from pET19b introducing a *Hind*III site in the pGEX polylinker	(56)
pGEX(M)_*cstK*	pGEX(M) derivative used to express GST-tagged fusion of CstK (Amp^R)	This study
pGEX(M)_*cstK_K55M*	pGEX(M) derivative used to express GST-tagged fusion of CstK_K55M (Amp^R)	This study
pGEX(M)_*cstK_Y14F*	pGEX(M) derivative used to express GST-tagged fusion of CstK_Y14F (Amp^R)	This study
pGEX(M)_*cstK_Y209F*	pGEX(M) derivative used to express GST-tagged fusion of CstK_Y209F (Amp^R)	This study

pGEX(M)_*cstK_T232A*	pGEX(M) derivative used to express GST-tagged fusion of CstK_T232A (Amp^R)	This study
pGEX(M)_*cstK_Y14F/Y209F/T232A*	pGEX(M) derivative used to express GST-tagged fusion of CstK_Y14F/Y209F/T232A (Amp^R)	This study
peGFPN1	Vector used for mammalian expression of C-terminal GFP-tagged fusion proteins	Addgene
peGFPN1_Hs-TBC1D5-GFP	peGFP-N1 derivative used to express C-terminal GFP-tagged fusion of Hs_TBC1D5 for mammalian expression	This study
pmCH_Hs-TBC1D5-mCherry	pmCH derivative used to express C-terminal mCherry-tagged fusion of Hs_TBC1D5 for mammalian expression	This study
pRK5_HA_*cstK*opt	pRK5_HA derivative used to express N-terminal HA-tagged fusion of CstK codon-optimized for mammalian expression	This study
pRK5_HA_*cstK_K55M*opt	pRK5_HA derivative used to express N-terminal HA-tagged fusion of *cstK_K55M* codon-optimized for mammalian expression	This study
pRK5_HA_*cstK_FFA*opt	pRK5_HA derivative used to express N-terminal HA-tagged fusion of *cstK_FFA* codon-optimized for mammalian expression	This study
pXDC61K-Blam	Vector with IPTG-inducible expression of Beta-Lactamase (Blam)	(57)
pXDC61K-Blam-*cvpB*	pXDC61K-Blam derivative used to express Blam-tagged fusion of CvpB	This study
pXDC61K-Blam-*cstK*	pXDC61K-Blam derivative used to express Blam-tagged fusion of CstK	This study
pJA-LACO-4xHA	Vector with IPTG-inducible expression of 4xHA-tagged proteins	(30)
pJA-LACO-4xHA-*cstK*	Vector with IPTG-inducible expression of 4xHA-tagged *cstK*	This study
pJA-LACO-4xHA-*cstK_K55M*	Vector with IPTG-inducible expression of 4xHA-tagged *cstK_K55M*	This study
pJA-LACO-4xHA-*cstK_FFA*	Vector with IPTG-inducible expression of 4xHA-tagged *cstK_FFA*	This study
***Dictyostelium discoideum* plasmids**		
pDXA-3C_*cstK-FLAG*	vector for overexpression of CstK with a C-terminal Flag tag in *D. discoideum*	This study
pDXA-3C_*DdTBC1D5-myc*	vector for expression of myc-DdTBC1D5 in *D. discoideum*	This study

Table 2. Primers used in this study

Primers	5' to 3' Sequence[a, b]
NtermCstK	TATGGATCCTTAATGGCTTATATGAGGCTTAGT (*BamHI*)
CtermCstK	TATAAGCTTTTAATCCCATTCAATATTTTC (*Hind*III)
RvCstK K55M	ATAAAAGAG**CAT**CGCCGCTCG
FwCstKY14F	CTTAGTGTGGCTGACTTT**TTT**GATTTGAAGAAGGGCAAG
FwCstKY209F	GGGGCGACGGGCTATCGC**TTC**TGTAACCCTCACATAAAG
FwCstKT232A	CATTCGTGAACAGTTTAAT**GCT**GCGGGCCATTTGCGATTAC
CstKopt-BamHI-Fw	GAAGGATCCCTGATGGCGTATATGCGTCTGAG
CstKopt-EcoRI-Rv	CTTGAATTCTTAGTCCCACTCGATGTTTTCCAGATG
CstK-KpnI-Fw	AGGGGTACCTTAATGGCTTATATGAGGCTTAGT
CstK-BamHI-Rv	AGGGGATCCTAATTAATCCCATTCAATATTTTCTAA
CvpB-KpnI-Fw	GATGGTACCAGCAGACAGCCATCATTG
CvpB-KpnI-Fw	GATGGTACCAGCAGACAGCCATCATTG

RT-PCR PRIMERS

DotA-F	GCTCCCAGCATTCATCCAGT
DotA-R	GGCACTTAACCAGCCCTCAT
CstK-F	GGCAAGGTATTAGGGCGGAA
CstK-R	GGGATTCTCACCATTGGCCT

[a] Restriction sites are underlined and specified into brackets.
[b] Mutagenized codons are shown in bold.

Table 3. Phosphoacceptors identified after phosphorylation of *C. burnetii* CstK. Sequences of the phosphorylated peptides identified in CstK as determined by mass spectrometry following tryptic digestion are indicated, and phosphorylated residues (pT or pY) are shown in bold.

Phosphorylated tryptic peptide sequence of CstK	**Number of detected phosphate groups LC/MS/MS**	**Phosphorylated residue(s)**
[8-18] LSVADF**pY**DLKK	**1**	**Y14**
[228-237] EQFN**pT**AGHLR	**1**	**T232**
[209-215] **pY**CNPHIK	**1**	**Y209**

Figure 1

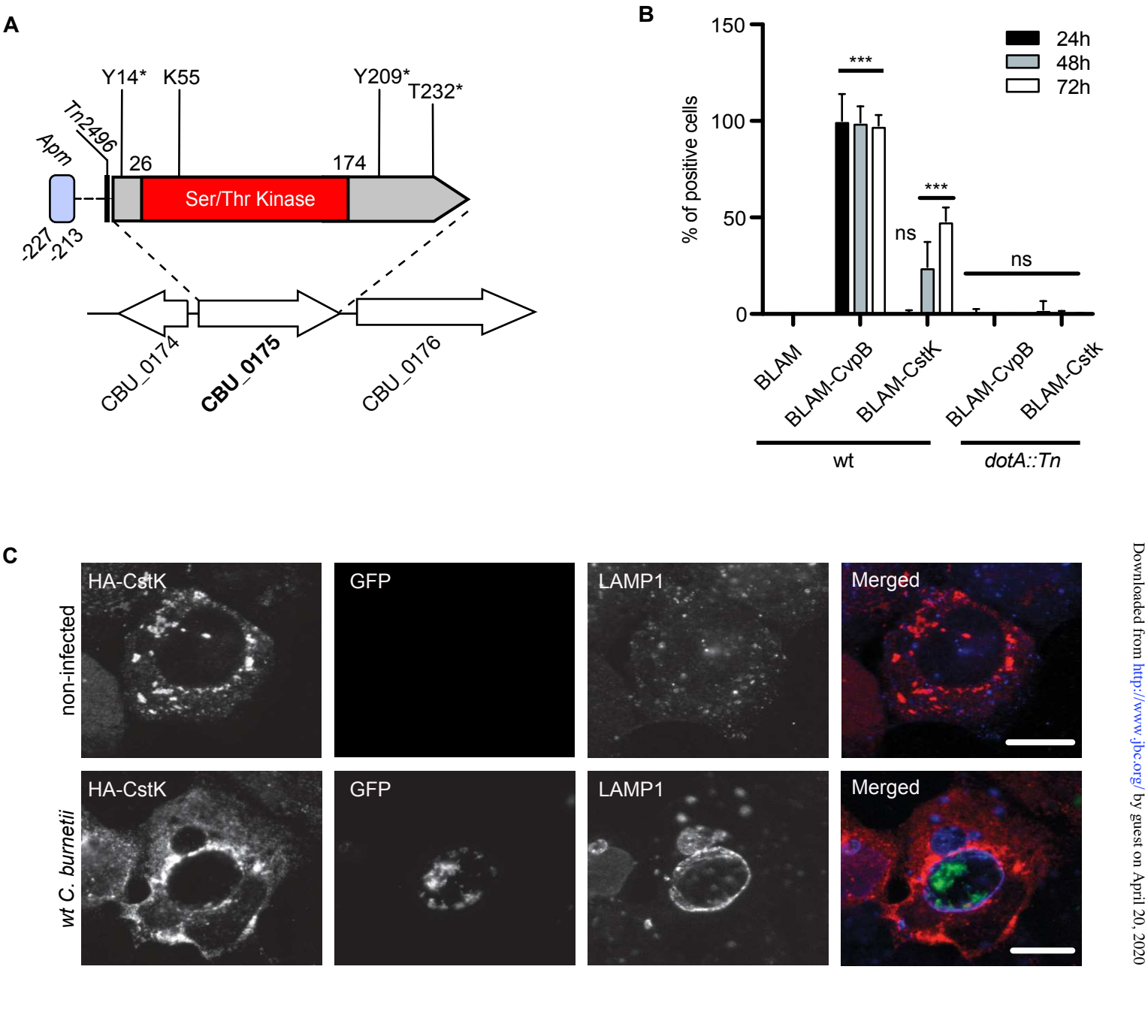

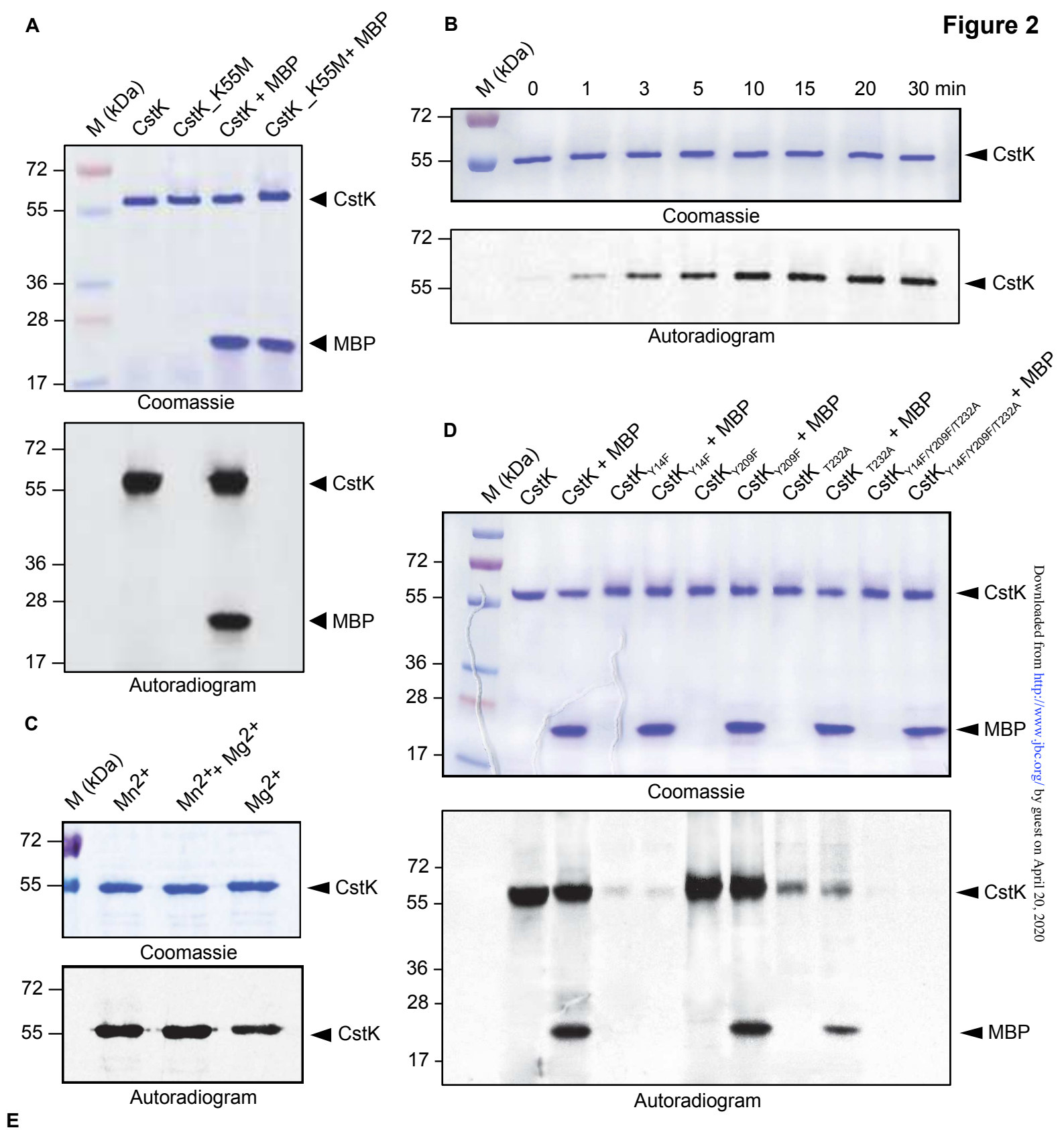

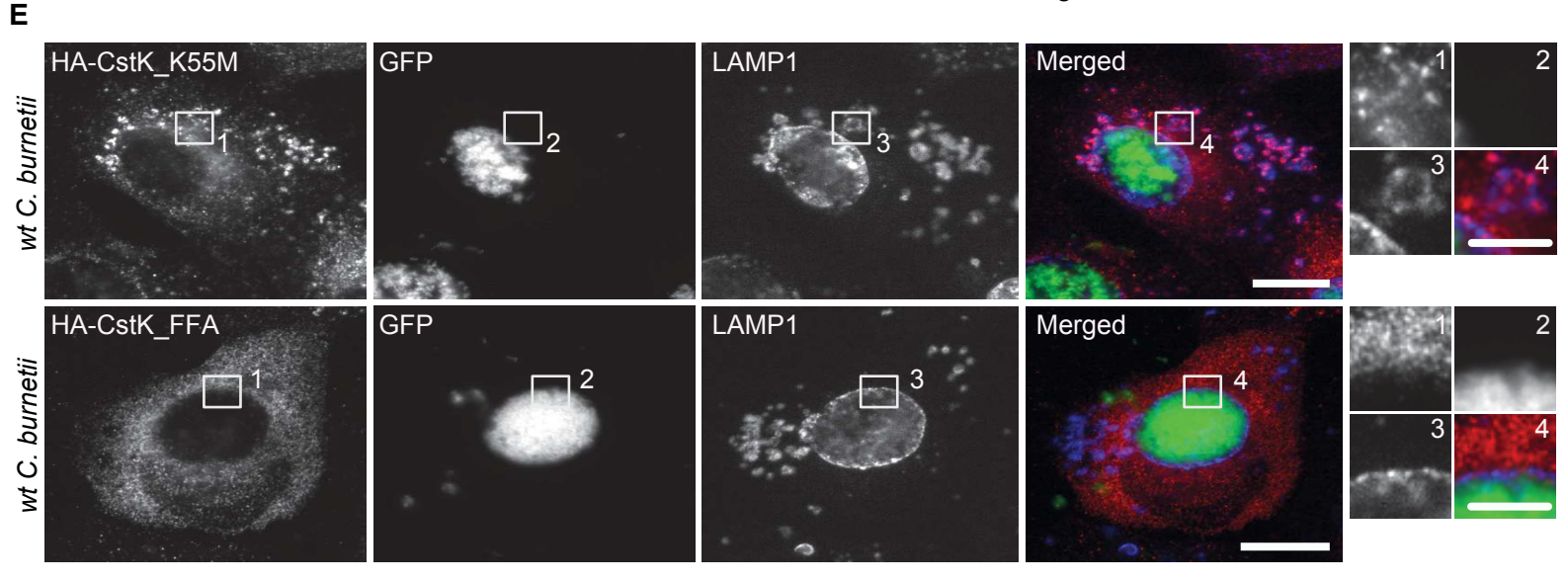

Figure 3

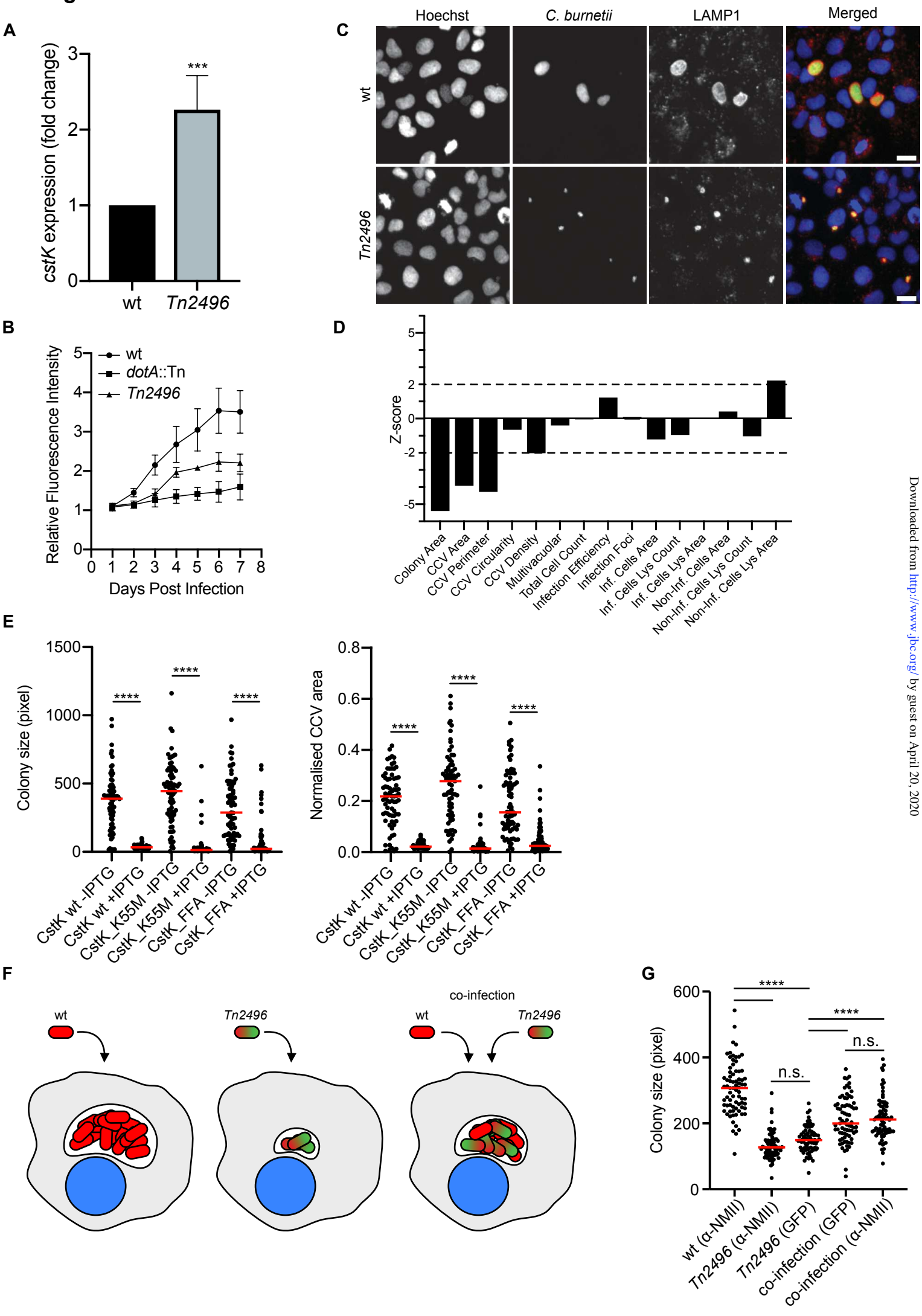

Figure 4

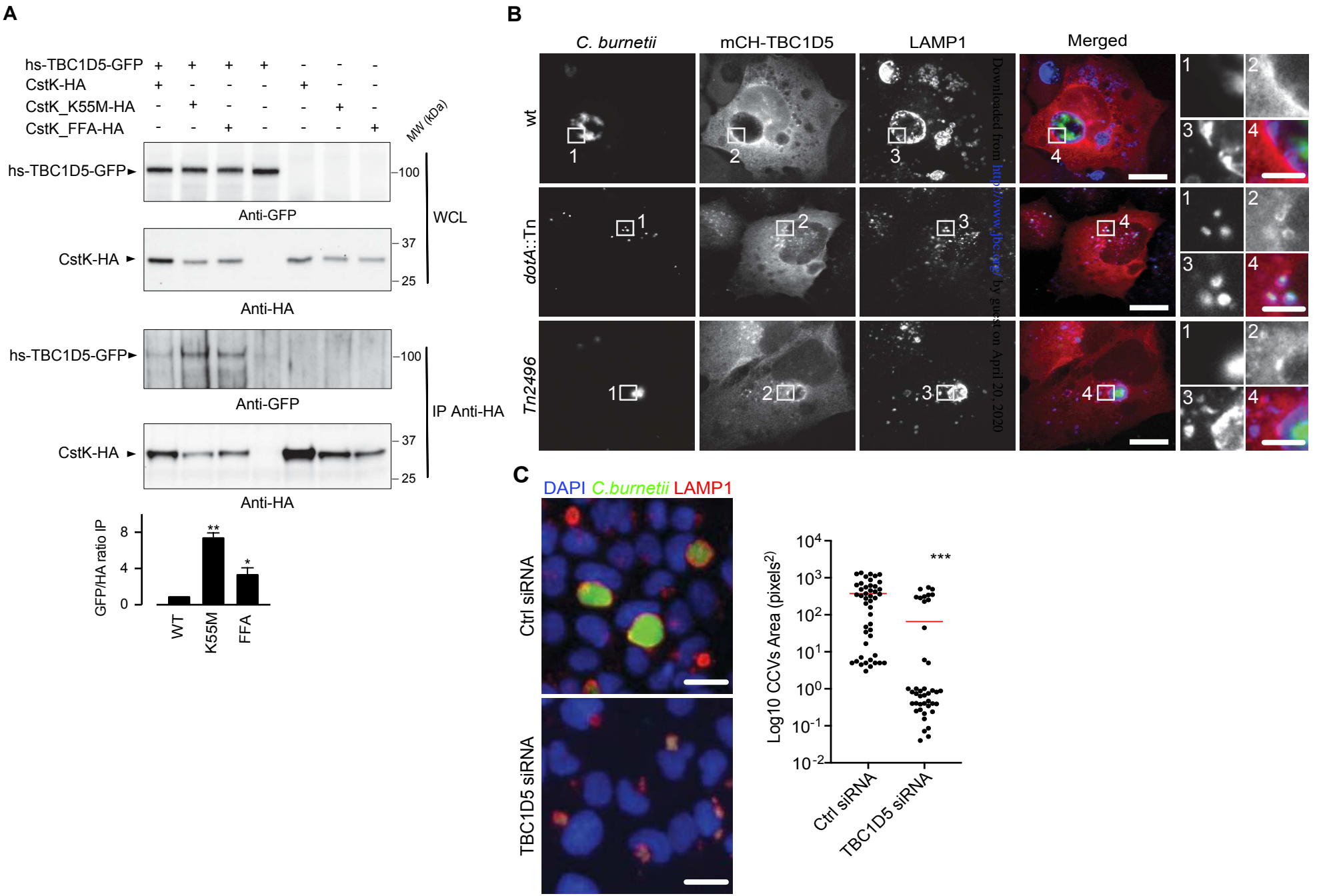
A
hs-TBC1D5-GFP + + + + - - -
CstK-HA + - - - + - -
CstK_K55M-HA - + - - - + -
CstK_FFA-HA - - + - - - +
MW (kDa)
hs-TBC1D5-GFP
100
Anti-GFP
CstK-HA
37
25
WCL
Anti-HA
hs-TBC1D5-GFP
100
Anti-GFP
IP Anti-HA
CstK-HA
37
25
Anti-HA
GFP/HA ratio IP
8
4
0
**
*
WT
K55M
FFA
B
C. burnetii
mCH-TBC1D5
LAMP1
Merged
wt
dotA::Tn
Tn2496
1
2
3
4
Downloaded from http://www.jbc.org/ by guest on April 20, 2020
C
DAPI C.burnetii LAMP1
Ctrl siRNA
TBC1D5 siRNA
Log10 CCVs Area (pixels2)
10^4
10^3
10^2
10^1
10^0
10^-1
10^-2
***
Ctrl siRNA
TBC1D5 siRNA

Intracellular replication and persistence strategies of the Q fever pathogen *Coxiella burnetii*

Coxiella burnetii is the causative agent of human Q Fever, considered as one of the most relevant re-emerging zoonosis in Europe. *C. burnetii* infects humans through the inhalation of contaminated aerosols, causing epidemics with serious economic and health consequences. Following internalisation, *C. burnetii* subverts host cell functions to inhibit the innate immune response and generate a replicative niche called CCV (*Coxiella*-containing vacuole) characterised by a unique protein and lipid composition. My thesis project focuses on the study of the host/pathogen interactions underlying the persistence and intracellular replication of *C. burnetii*.

First, the function of the effector protein NopA was discovered showing how this protein inhibits the innate immune response in infected cells. The results obtained during my PhD have shown that NopA interacts with Ran and triggers an imbalance in its nucleocytoplasmic gradient, thereby perturbing the nuclear import of eukaryotic proteins and the expression of pro-inflammatory cytokines. In parallel, the role of lipid metabolism in the establishment of the CCV was investigated. By using a wide array of lipid probes and confocal microscopy, the lipid signature of CCVs was determined and revealed that PI(4)P and LBPA are actively subverted by *C. burnetii* during infection. Lipid pulldown assays then led to the identification of *C. burnetii* candidate effector proteins interacting with host cell lipids. One of them, CBU0635, is a putative phosphoinositide phosphatase that diverts the secretory pathway to the forming *Coxiella*-containing vacuole while CBU2007 manipulates lysobisphosphatidic acid metabolism to recruit the ESCRT machinery and block the biogenesis of multivesicular bodies. These results help to better understand intracellular replication and persistence strategies of *C. burnetii* and could allow the development of new antimicrobials and the therapeutic repurposing of *C. burnetii* proteins.

Keywords: host-pathogen interactions, *Coxiella burnetii*, innate immunity, lipid metabolism, type IV secretion system

Etude de la réplication intracellulaire et de la persistance de *Coxiella burnetii*, agent pathogène de la fièvre Q

Coxiella burnetii est la bactérie responsable de la fièvre Q, une maladie considérée comme l'une des zoonoses réémergentes les plus préoccupantes en Europe. *C. burnetii* infecte les humains par inhalation d'aérosols contaminés, causant des épidémies avec de lourdes conséquences économiques et sanitaires. A la suite de l'invasion, *C. burnetii* détourne les fonctions de la cellule hôte pour inhiber la réponse immunitaire innée et générer une niche réplicative appelée CCV (*Coxiella*-containing vacuole) d'une composition protéique et lipidique unique. Mon projet de thèse se focalise sur l'étude des interactions hôte/pathogène permettant la persistance et la réplication intracellulaire de *C. burnetii.*

Tout d'abord, nous avons démontré comment la protéine effectrice bactérienne NopA inhibe la réponse immunitaire innée des cellules infectées. Les résultats obtenus au cours de ma thèse ont montré que NopA interagit avec Ran et déséquilibre son gradient nucléocytoplasmique, perturbant ainsi l'importation nucléaire de protéines eucaryotes et l'expression de cytokines pro-inflammatoires. En parallèle, le rôle du métabolisme des lipides dans la biogenèse de la CCV a été étudié. En utilisant un large éventail de sondes liant les lipides et de la microscopie confocale, la signature lipidique des CCVs a été mise en évidence, révélant que le PI(4)P et le LBPA sont activement recrutés à la CCV par *C. burnetii* au cours de l'infection. La coprécipitation des protéines de *C. burnetii* avec des lipides eucaryotes a ensuite conduit à l'identification de candidats effecteurs liant les lipides. Parmi ceux-ci, CBU0635 pourrait être une phosphatase des lipides qui détourne la voie sécrétoire vers la CCV tandis que CBU2007 manipule le métabolisme de l'acide lysobisphosphatidique pour recruter la machinerie ESCRT et bloquer la biogenèse des corps vésiculaires. Ces résultats permettent donc une meilleure compréhension des stratégies de réplication et de persistance de *C. burnetii* et pourraient à terme être utilisés dans le développement de nouveaux antimicrobiens et dans l'utilisation à des fins thérapeutiques de protéines de *C. burnetii*.

Mots clés: interactions hôte-pathogène, *Coxiella burnetii*, immunité innée, métabolisme des lipides, système de sécrétion de type IV